



Abbas, Hamera (2006) *Controllable growth of polyoxometalate based building blocks: towards the construction of clusters, arrays and nanostructures*. PhD thesis.

<http://theses.gla.ac.uk/6269/>

Copyright and moral rights for this thesis are retained by the author

A copy can be downloaded for personal non-commercial research or study, without prior permission or charge

This thesis cannot be reproduced or quoted extensively from without first obtaining permission in writing from the Author

The content must not be changed in any way or sold commercially in any format or medium without the formal permission of the Author

When referring to this work, full bibliographic details including the author, title, awarding institution and date of the thesis must be given

**Controllable Growth of Polyoxometalate Based Building
Blocks: Towards the Construction of Clusters, Arrays and
Nanostructures.**



UNIVERSITY
of
GLASGOW

Hamera Abbas

A thesis submitted to the University of Glasgow
for the degree of Doctor of Philosophy

Department of Chemistry



*“When you want something, all the universe conspires in helping
you to achieve it.”*

The Alchemist

Paulo Coelho

I would like to dedicate this thesis to my family. Their prayers, understanding and patience have not gone unnoticed or unappreciated. Thank you all for your support. You have made this possible.

ACKNOWLEDGMENTS

There are so many people that I would love to thank individually but space doesn't permit this so if I don't mention you especially it's not because I don't care!

Thanks to:

My supervisor **Prof. Lee Cronin**, for his support, advice and enthusiasm over the past three years. I know I haven't been the easiest PhD student to work with, mainly due to my rather pessimistic views about my work among many other things. Thanks for keeping me motivated!

Dr. De-Liang Long and **Dr. Eric Burkholder** for crystallography work and project advice. **Dr. Paul Kögerler** for DFT studies and input on papers. **Dr. Jesus de la Fuente** for his friendship, project advice and microscopy work. **Dr. Nikolaj Gadegaard** for all the SEM work. **Dr. Alexandra Pickering** for her friendship, help and advice at the start of my PhD.

Geoff and **Chris** - for help in countless things, **Phil** - for being on my side (sometimes), **Carsten** - for your technical expertise (end note- need I say any more?) to discussions on Ag-related work (you can't avoid the nanoworld any longer!) and for checking through my thesis so thoroughly and **Graham** - for his endless supply of triangle things which you seem to make out of almost anything (how do you do that?). Thanks also to **Liz** for all her help with the mass spec. stuff and to my project student **Andrew** for his contributions to this thesis.

Nicola for just being you- sparkly pink shoes, the bumble-bee outfit, the shoe shopping, the latest developments in the department, the list is endless. **Louise**, I can't imagine what the last three years would have been like without you. Thanks for being there through the good and the bad times; although we managed to remedy the bad times pretty well with coffee, cake, chocolate and shoes!

All the **Cronin Group** members past and present. The past three years have been very memorable!

Sharon- your support over the past *seven* years is something I'll always be grateful for.

Above all I would like to thank all my family and friends and especially my little sister **Mariam**. This has been a long journey which has been an endurable one only through your constant support, encouragement and love.

TABLE OF CONTENTS

1	INTRODUCTION	1
1.1	Polyoxometalates: Structure, Bonding and Synthesis.....	1
1.2	Synthesis of High Nuclearity Polyoxometalate Clusters in ‘One-Pot’	4
1.2.1	Molybdates.....	4
1.2.2	Tungstates	9
1.2.3	Vanadates	11
1.3	Designing and Understanding Polyoxometalate Clusters.....	12
1.3.1	Structural Features of Functional Polyoxometalates.....	13
1.3.2	Organic-Inorganic Hybrid Polyoxometalate Materials.....	16
1.3.2.1	Functionalised Polyoxometalates.....	17
1.3.2.2	Non-coordinating Organic Composites.....	18
1.3.2.3	Construction of Hybrid Arrays via Coordinative Organic-Metal Composites.....	20
1.4	Functional Nanomaterials	23
1.4.1	‘Top-down’ vs. ‘Bottom-up’	24
1.4.2	Nanostructures: Synthesis and Application	25
1.5	Outlook.....	29
2	AIMS.....	30
3	RESULTS AND DISCUSSION	32
3.1	The Formation of {Ag(Mo ₈ O ₂₆)Ag} Synthons and β-[Mo ₈ O ₂₆] ⁴⁻	32
3.1.1	Structure Analysis of β-[Mo ₈ O ₂₆] ⁴⁻	33
3.1.2	The Influence of Silver(I) on [Mo ₆ O ₁₉] ²⁻ , α- and β-[Mo ₈ O ₂₆] ⁴⁻	35
3.1.3	The Formation of β-[Mo ₈ O ₂₆] ⁴⁻	44
3.2	Structural Influence by Cation and Solvent.....	47
3.2.1	From Monomer to Chain.....	47
3.2.2	Monomeric Clusters	50
3.2.3	One-dimensional Arrays and Chains	53
3.2.4	Two-dimensional Arrays.....	62
3.2.5	Argentophilic Interactions.....	68
3.2.5.1	Ag...Ag Interactions in One-Dimensional Arrays.....	68
3.2.5.2	Density Functional Theory Studies.....	72

3.3	Solvent Assisted Arrays	75
3.3.1	Acetonitrile Arrays	75
3.3.2	DMSO Arrays	86
3.4	Surface Studies	94
3.4.1	Growth of Nanorods and Spherulites	94
3.4.2	Growth of Silver Nanostructures	100
3.4.3	Microscopy Studies on Other Ag-Mo Polyoxometalates	110
3.5	Potassium Polyoxomolybdate Clusters	115
4	CONCLUSIONS AND FUTURE WORK	124
4.1	Formation of {Ag(Mo ₈ O ₂₆)Ag} Synthons and β-[Mo ₈ O ₂₆] ⁴⁻	124
4.2	Structural Influence by Cation and Solvent	125
4.3	Solvent Assisted Arrays	128
4.4	Silver Based Nanostructures	129
4.5	Potassium Polyoxometalate Clusters	131
5	EXPERIMENTAL	132
5.1	Materials	132
5.2	Instrumentation	132
5.3	Synthesis	133
5.3.1	((<i>n</i> -C ₄ H ₉) ₄ N) ₂ Mo ₆ O ₁₉ (1)	133
5.3.2	((<i>n</i> -C ₇ H ₁₅) ₄ N) ₂ Mo ₆ O ₁₉ (2)	134
5.3.3	(Ph ₄ P) ₂ Mo ₆ O ₁₉ ·2CH ₃ CN (3)	134
5.3.4	((<i>n</i> -C ₄ H ₉) ₄ N) _{2n} [Ag ₂ Mo ₈ O ₂₆] _n (4)	135
5.3.5	α-((<i>n</i> -C ₄ H ₉) ₄ N) ₄ Mo ₈ O ₂₆ (5)	135
5.3.6	((<i>n</i> -C ₄ H ₉) ₄ N) _{2n} [Ag ₂ Mo ₈ O ₂₆ (CH ₃ CN) ₂] _n ·2CH ₃ CN (6)	136
5.3.7	β-((<i>n</i> -C ₄ H ₉) ₄ N) ₃ KMo ₈ O ₂₆ ·2H ₂ O (7)	136
5.3.8	((<i>n</i> -C ₄ H ₉) ₄ N) _{2n} [Ag ₂ Mo ₈ O ₂₆] _n (4c)	137
5.3.9	((<i>n</i> -C ₄ H ₉) ₄ N) _{2n} [KAg(CH ₃ CN) ₂ Mo ₈ O ₂₆] _n (8)	137
5.3.10	(Ph ₄ P) ₂ [Ag ₂ (DMSO) ₄ (Mo ₈ O ₂₆)] (9)	137
5.3.11	(Ph ₄ P) ₂ [Ag ₂ (CH ₃ CN) ₂ Mo ₈ O ₂₆] _n ·2CH ₃ CN (10)	138
5.3.12	((<i>n</i> -C ₄ H ₉) ₄ N) _{2n} [Ag ₂ (CH ₃ CN) ₂ Mo ₈ O ₂₆] _n (11)	138
5.3.13	[Ag(C ₇ H ₁₂ O ₂ N)] _{2n} [(Ag(CH ₃ CN)) ₂ Mo ₈ O ₂₆] _n ·2CH ₃ CN (12)	139
5.3.14	(Ph ₄ P) _{2n} [Ag ₂ (DMF) ₂ Mo ₈ O ₂₆] _n ·2DMF (13)	139
5.3.15	(H ₂ NMe ₂) _{2n} [Ag ₂ (DMF) ₂ Mo ₈ O ₂₆] _n ·2DMF (14)	140

5.3.16	$((n\text{-C}_4\text{H}_9)_4\text{N})_{2n}[\text{Ag}_2(\text{DMSO})_2\text{Mo}_8\text{O}_{26}]_n$ (15)	140
5.3.17	$(\text{HDMF})_n[\text{Ag}_3(\text{DMF})_4\text{Mo}_8\text{O}_{26}]_n$ (16)	140
5.3.18	$[(\text{Ag}(\text{DMF}))_2(\text{Ag}(\text{DMF})_2)_2\text{Mo}_8\text{O}_{26}]_n$ (17)	141
5.3.19	$[(\text{Ag}_2(\text{CH}_3\text{CN})_3)(\text{Ag}(\text{CH}_3\text{CN})_2)\text{AgMo}_8\text{O}_{26}]_n$ (18)	141
5.3.20	$[\text{Ag}_4(\text{DMSO})_6(\text{OC}(\text{CH}_3)_2)_2\text{Mo}_8\text{O}_{26}]_n$ (21)	142
5.3.21	$[\text{Ag}_4(\text{DMSO})_8\text{Mo}_8\text{O}_{26}]_n$ (22)	143
5.3.22	$((n\text{-C}_4\text{H}_9)_4\text{N})_{2n}[\text{K}_2(\text{DMSO})_3\text{Mo}_8\text{O}_{26}]_n$ (23)	144
5.3.23	$((n\text{-C}_4\text{H}_9)_4\text{N})_n(\text{H}_2\text{NMe}_2)_n[\text{K}_2(\text{DMF})\text{Mo}_8\text{O}_{26}]_n \cdot \text{DMF}$ (24)	144
5.4	Surface Studies	145
5.4.1	Substrate Preparation of $((n\text{-C}_4\text{H}_9)_4\text{N})_{2n}[\text{Ag}_2\text{Mo}_8\text{O}_{26}]_n$ (4b) Crystals.....	145
5.4.2	Substrate Preparation of $((n\text{-C}_4\text{H}_9)_4\text{N})_{2n}[\text{Ag}_2\text{Mo}_8\text{O}_{26}]_n$ (4b) Crystals.....	145
5.4.3	Substrate Preparation of $((n\text{-C}_4\text{H}_9)_4\text{N})_{2n}[\text{Ag}_2\text{Mo}_8\text{O}_{26}]_n$ (4b) Powder Material.	146
5.4.4	TEM and SAED preparation of $((n\text{-C}_4\text{H}_9)_4\text{N})_{2n}[\text{Ag}_2\text{Mo}_8\text{O}_{26}]_n$ (4b) Powder Material.	147
5.4.5	Additional Silver to $((n\text{-C}_4\text{H}_9)_4\text{N})_{2n}[\text{Ag}_2\text{Mo}_8\text{O}_{26}]_n$ (4b) Crystal Solution..	147
5.4.6	Additional Silver to $((n\text{-C}_4\text{H}_9)_4\text{N})_{2n}[\text{Ag}_2\text{Mo}_8\text{O}_{26}]_n$ (4b) Powder Solution.	148
5.4.7	Silver(I) Fluoride Control Test.....	148
5.4.8	Substrate Preparation of $((n\text{-C}_4\text{H}_9)_4\text{N})_{2n}[\text{Ag}_2(\text{DMSO})_2\text{Mo}_8\text{O}_{26}]_n$ (15)	149
5.4.9	Substrate Preparation of $[\text{Ag}(\text{C}_7\text{H}_{12}\text{O}_2\text{N})]_{2n}[(\text{Ag}(\text{CH}_3\text{CN}))_2\text{Mo}_8\text{O}_{26}]_n \cdot 2\text{CH}_3\text{CN}$ (12)	149
6	CRYSTALLOGRAPHIC DATA	150
6.1	X-ray Summary Table.....	151
6.2	Crystal data for $((n\text{-C}_4\text{H}_9)_4\text{N})_{2n}[\text{Ag}_2\text{Mo}_8\text{O}_{26}]_n$ (4a/b/c)	153
6.3	Crystal data for $(n\text{-C}_4\text{H}_9)_4\text{N})_{2n}[\text{Ag}_2(\text{CH}_3\text{CN})_2\text{Mo}_8\text{O}_{26}]_n \cdot 2\text{CH}_3\text{CN}$ (6)	159
6.4	Crystal data for $((n\text{-C}_4\text{H}_9)_4\text{N})_{2n}[\text{KMo}_8\text{O}_{26}\text{Ag}(\text{CH}_3\text{CN})_2]_n$ (8)	170
6.5	Crystal data for $(\text{Ph}_4\text{P})_2[\text{Ag}_2(\text{CH}_3\text{CN})_2\text{Mo}_8\text{O}_{26}] \cdot 2\text{CH}_3\text{CN}$ (10)	178
6.6	Crystal data for $((n\text{-C}_4\text{H}_9)_4\text{N})_{2n}[\text{Ag}_2(\text{CH}_3\text{CN})_2\text{Mo}_8\text{O}_{26}]_n$ (11)	183
6.7	Crystal data for $[\text{Ag}(\text{C}_7\text{H}_{12}\text{O}_2\text{N})(\text{CH}_3\text{CN})]_{2n}[(\text{Ag}(\text{CH}_3\text{CN}))_2\text{Mo}_8\text{O}_{26}]_n \cdot 2\text{CH}_3\text{CN}$ (12)	188
6.8	Crystal data for $(\text{Ph}_4\text{P})_{2n}[\text{Ag}_2(\text{DMF})_2\text{Mo}_8\text{O}_{26}]_n \cdot 2\text{DMF}$ (13)	193
6.9	Crystal data for $(\text{H}_2\text{NMe}_2)_{2n}[\text{Ag}_2(\text{DMF})_2\text{Mo}_8\text{O}_{26}]_n \cdot 2\text{DMF}$ (14)	199
6.10	Crystal data for $((n\text{-C}_4\text{H}_9)_4\text{N})_{2n}[\text{Ag}_2(\text{DMSO})_2\text{Mo}_8\text{O}_{26}]_n$ (15)	203

6.11	Crystal data for $(\text{HDMF})_n[\text{Ag}_3(\text{DMF})_4\text{Mo}_8\text{O}_{26}]_n$ (16)	211
6.12	Crystal data for $[(\text{Ag}(\text{DMF}))_2(\text{Ag}(\text{DMF})_2)_2\text{Mo}_8\text{O}_{26}]_n$ (17)	216
6.13	Crystal data for $[(\text{Ag}(\text{CH}_3\text{CN})_3)_2(\text{Ag}(\text{CH}_3\text{CN})_2)\text{AgMo}_8\text{O}_{26}]_n$ (18)	221
6.14	Crystal data for $[(\text{Ag}(\text{CH}_3\text{CN}))_2(\text{Ag}(\text{CH}_3\text{CN})_2)_2\text{Mo}_8\text{O}_{26}]_n$ (19)	227
6.15	Crystal data for $[(\text{Ag}(\text{CH}_3\text{CN})_2)_2\text{Ag}_2\text{Mo}_8\text{O}_{26}]_n$ (20)	231
6.16	Crystal data for $[\text{Ag}_4(\text{DMSO})_6(\text{OC}(\text{CH}_3)_2)_2\text{Mo}_8\text{O}_{26}]_n$ (21)	235
6.17	Crystal data for $[\text{Ag}_4(\text{DMSO})_8\text{Mo}_8\text{O}_{26}]_n$ (22)	240
6.18	Crystal data for $((n\text{-C}_4\text{H}_9)_4\text{N})_{2n}[\text{K}_2(\text{DMSO})_3\text{Mo}_8\text{O}_{26}]_n$ (23)	245
6.19	Crystal data for $((n\text{-C}_4\text{H}_9)_4\text{N})_n(\text{H}_2\text{NMe}_2)_n[\text{K}_2(\text{DMF})\text{Mo}_8\text{O}_{26}]_n \cdot \text{DMF}$ (24)	254
7	SUPPLEMENTARY DATA	262
7.1	Mass Spectrum for $[\text{Mo}^{\text{VI}}\text{Mo}^{\text{V}}\text{O}_6]^{1-}$	262
7.2	EDX Data for Wire Material.....	263
7.3	EDX Data for Wires/Fibres Obtained from Powder Material	264
7.4	EDX Data for $((n\text{-C}_4\text{H}_9)_4\text{N})_{2n}[\text{Ag}_2(\text{DMSO})_2\text{Mo}_8\text{O}_{26}]_n$ (15)	265
8	REFERENCES	266

PUBLICATIONS

- Molecular Computers – Tomorrow’s Technology?
H. Abbas and L. Cronin, *Education in Chemistry* **2007**, *44*, 16.
- Confined Electron Transfer Reactions within a Molecular Metal Oxide ‘Trojan Horse’.
D. -L. Long, H. Abbas, P. Kögerler and L. Cronin, *Angew. Chem. In. Ed.* **2005**, *44*, 3415.
- Controllable Growth of Chains and Grids from Polyoxomolybdate Building Blocks Linked by Silver(I) Dimers.
H. Abbas, A. L. Pickering, D. -L. Long, P. Kögerler, and L. Cronin, *Chem. Eur. J.* **2005**, *11*, 11071.
- A High Nuclearity ‘Celtic-Ring’ Isopolyoxotungstate: $[\text{H}_{12}\text{W}_{36}\text{O}_{120}]^{12-}$.
D. -L. Long, H. Abbas, P. Kögerler, and L. Cronin, *J. Am. Chem. Soc.* **2004**, *126*, 13880.
- Pentadecadentate Chelating Ligands as Building Blocks for an $\{\text{Fe}_6\}$ Cage with 12 Exo-coordinated Sodium Cations.
G. J. T. Cooper, H. Abbas, D. -L. Long, P. Kögerler, L. Cronin, *Inorg. Chem.* **2004**, *43*, 7266.

ABBREVIATIONS

POM(s)	Polyoxometalate(s)
M	Transition metal/ secondary metal
TBA	Tetra- <i>n</i> -butylammonium
TPA	Tetra- <i>n</i> -propylammonium
Ph	Phenyl
Me	Methyl
DMSO	Dimethyl sulfoxide
DMF	<i>N, N'</i> - dimethylformamide
EDX	Energy Dispersive X-ray
SEM	Scanning Electron Microscope
SAED	Selective Area Electron Diffraction
TEM	Transmission Electron Microscopy
MS	Mass Spectrometry
UV	Ultra Violet
FT-IR	Fourier Transform Infrared Spectroscopy
<i>m/z</i>	mass/charge ratio

ABSTRACT

The work presented in this thesis describes routes to the controlled growth of small polyoxometalate clusters achieved by utilising a range of organic counterions in conjunction with electrophilic Ag(I) ions. The subsequent isolation of a new building block; $\{\text{Ag}(\beta\text{-Mo}_8\text{O}_{26})\text{Ag}\}$ has demonstrated how subtle control can be achieved through the use of bulky and flexible counterions and by solvent. The assembly of these building blocks has been further probed by using mass spectrometry to gain insight into the solution chemistry and through which the presence of Ag-Mo based fragments have been identified as well as other important intermediate molybdate species.

Within most structures the electrophilic ions form $\{\text{Ag}_2\}$ dimer groups that link together β -octamolybdate anions to produce a family of structurally related architectures ranging from isolated units, one- and two-dimensional architectures. Each of the architectures contain $\{\text{Ag}(\beta\text{-Mo}_8\text{O}_{26})\text{Ag}\}$ based building blocks that can be controlled in their self-assembly by cation and solvent interaction in the solid state. This set of architectures differ in the coordination modes of the linker $\{\text{Ag}_2\}$ groups and in the nature of the Ag...Ag interactions that are present in most structures. Furthermore, the isolation of polymeric structures exclusively through solvent ligation has yielded one- and two-dimensional architectures where acetonitrile molecules in particular have formed pseudo cations around the $\{\text{Ag}(\beta\text{-Mo}_8\text{O}_{26})\text{Ag}\}$ based building blocks. The above synthetic strategy was also extended to other metals to yield some additional structures.

Several of the silver polyoxomolybdate compounds have been further investigated on silicon substrates using Scanning Electron Microscope (SEM), and in some instances with Energy Dispersive X-ray (EDX), Transmission Electron Microscopy (TEM) and Selective Area Electron Diffraction (SAED). These techniques have revealed the growth of nanostructures on multiple length scales. Knowledge of the molecular architecture has given a unique understanding of the assembly of these nanostructures including various one-dimensional assemblies (nanorods and nanowires), that have been obtained through different, efficient and inexpensive synthetic methods. The structures have been identified

and a hypothetical mechanism for the growth of Ag(0) based nanowires has been correlated to the partial oxidation of methanol and the reduction of Ag(I).

1 INTRODUCTION

Polyoxometalates constitute a class of compounds that have had continuing and widespread interest in inorganic chemistry. Their structural versatility and unique properties have made them subject to vast research,¹ in well-established areas. Their unrivalled versatility has been shown by the continuous growth of this field, which in recent years has extended into new areas interfacing with various scientific disciplines.

1.1 Polyoxometalates: Structure, Bonding and Synthesis

Polyoxometalates are inorganic metal-oxide anions that contain individual MO_x units ($M = \text{V, Mo, W}$), that can aggregate to form a range of clusters with low to high nuclearities, ranging from 2 to 368 metal atoms in a single molecule. The versatile nature of polyoxometalates originates from the ability to polymerise these MO_x units to form highly symmetrical clusters. Tungsten and molybdenum for reasons of property tunability dominate many of the polyoxometalate (POM) based structures characterised.² Their stability and rich redox chemistry allow them to be part of a class of inorganic compounds that display semi-conducting, magnetic, thermal and photochemical properties.³⁻⁵

These d^0 anionic clusters use octahedral shaped building blocks in their construction. Consequently, it is easier to describe the structure and bonding of POMs by replacing this metal-oxide building block with a polyhedron where the metal ion resides at the centre with oxygen ligands at the vertices (Figure 1).⁶

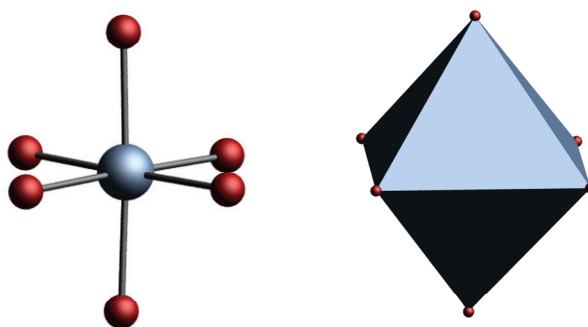


Figure 1 Bond and polyhedral representation of the MO_6 octahedron where $M = \text{Mo}$ or W . M : blue, O : red.

Connection of the polyhedra can occur either through corner or edge sharing modes (Figure 2) or a combination of both. Subsequently it is easy to see how the assembly of new cluster types can be achieved without limitations being placed on how the polyhedra can be interlinked.

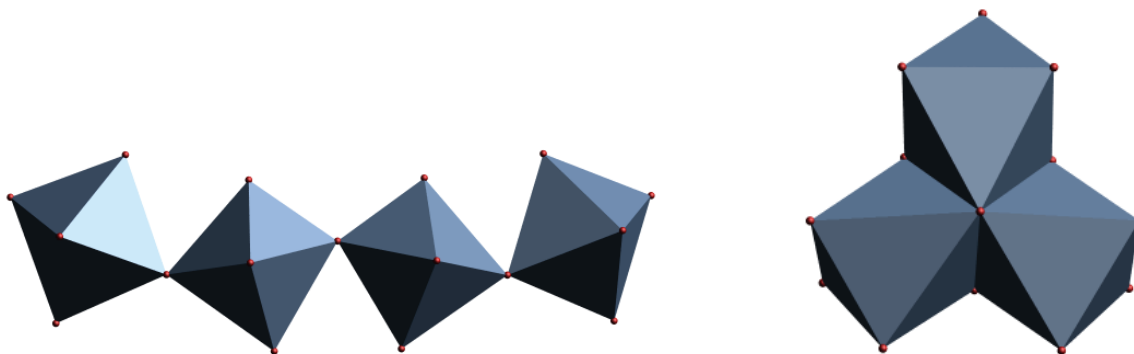


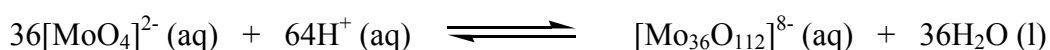
Figure 2 Example of corner (*LHS*) and edge sharing (*RHS*) where $M = \text{Mo}$ or W . M : blue, O : red.

A number of reasons govern why molybdenum and tungsten form polyoxoanions more readily than other transition metals including: the accessibility of empty d orbitals for metal-oxygen π bonding, ionic radius and charge.¹ These metals also display $M\text{-O-M}$ bridging interactions which are of moderate strength and strong $M=\text{O}$ terminal bonds, that are more nucleophilic/basic and offer further sites of polymerisation. Thus, various oxygen types exist within each cluster including bridging (O_b) and terminal (O_t) oxygen atoms.

The most common synthetic approach to producing POM clusters is through ‘one-pot’ reaction conditions which has the distinct advantage of removing step-by-step syntheses to generate complex compounds. The combination of the various precursors and their

inclusion and the various reaction parameters can influence the overall architecture of the polyoxoanion generated.

Using acidic conditions, elimination of water causes polymerisation of the mononuclear oxo anions e.g. $[\text{MO}_4]^{2-}$ (M= Mo or W) of the early transition metals. In addition to this, changes to acid type, pH level, temperature, solvent (aqueous or non-aqueous systems), use of a ligand, heteroatom or reducing agent, all play a role in the assembly of new clusters. Adjusting the pH to a specific level can give rise to POMs with different nuclearities and the $[\text{MoO}_4]^{2-}$ anion is a prime example of this with larger nuclearity clusters forming as the acidity of the solution changes (Scheme 1). Thus, under these reaction conditions, manipulation of a few synthetic parameters can produce the most unusual and complex clusters that vary from one another through differences in synthesis or structure assembly.



Scheme 1 Polymerisation of $[\text{MoO}_4]^{2-}$ through a condensation process.

A structural hierarchy exists in POM chemistry but in general can be broadly split into three classes:

i) Isopolyanions which consist exclusively of early transition metal-oxide building blocks and no other internal heteroatom. Examples of such clusters include the well known octahedral Lindqvist anion $[\text{M}_6\text{O}_{19}]^{2-}$, (Figure 3). This anion is frequently used as a precursor to generate larger POM species and can often be found as a side product in many syntheses partly due to its high stability.

ii) Heteropolyanions that contain one or more heteroatoms and can serve as templates for the assembly of the individual metal-oxide building blocks. This class of POM clusters contains a large number of the most commonly synthesised structures. One such example is the Keggin anion, so named after J. F. Keggin who was successful in fully characterising the cluster.⁷ The anion contains twelve transition metal atoms and one other central heteroatom and can be represented by the general formula $[\text{XM}_{12}\text{O}_{40}]^{n-}$, where X can be a main group element such as boron, silicon, and phosphorus to name a few. These hetero-ions

will form a XO_4 tetrahedron around which tungsten, molybdenum and even niobium metal-oxide octahedra will arrange to form a cluster with ideally tetrahedral symmetry. The Wells-Dawson cluster (Figure 3) can be described as two halves of a Keggin cluster with two tetrahedral hetero-ions trapped inside a cage-like structure. As such the general formula for the anion is $[\text{M}_{18}\text{O}_{54}(\text{XO}_4)_2]^{n-}$, where XO_4 can be represented by main group oxo-ions e.g. SO_4^{2-} , PO_4^{3-} . It is also possible to produce lacunary derivatives of both the Keggin and Dawson clusters where a skeletal MO_6 octahedra can be omitted producing single or multiple vacancies that can be filled by other main group or transition metal ions.

iii) Molybdenum-blue and brown reduced species. Reduced molybdenum blue solutions were first observed by Scheele in 1783.⁸ Müller and co-workers however, were able to conduct a more systematic exploration of this class of compounds to yield clusters of nanoscale dimensions which will be discussed in more detail later (section 1.2.1).

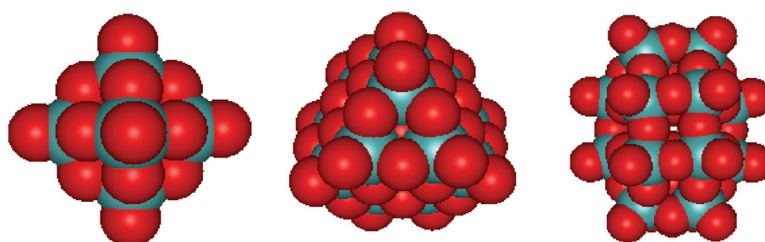


Figure 3 Space filled representations from left to right of the Lindqvist (O_h), Keggin (T_d), and Dawson, (D_{3d}) clusters. Mo: green, O: red.

1.2 Synthesis of High Nuclearity Polyoxometalate Clusters in ‘One-Pot’

1.2.1 Molybdates

Most POM chemistry exposure has come from its renowned ability to produce clusters of astounding proportions. Through the virtue of self-assembly we have seen structures that are unrivalled in their architectural composition, and whose size and dimensions can compete with proteins on a macromolecular scale (Figure 4).^{9,10}

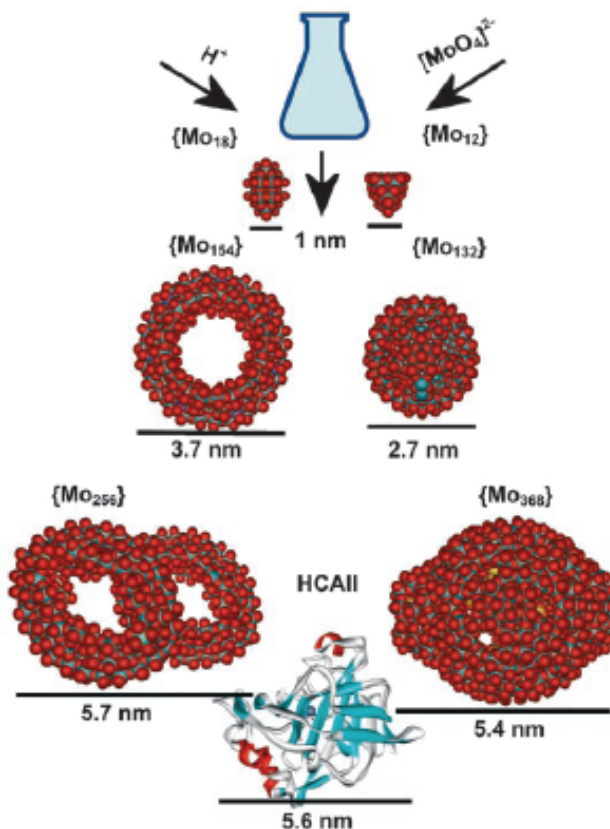


Figure 4 Demonstration of the dimensions of various POM clusters with respect to the protein Human Carbonic Anhydrase II. Mo: green, O: red.⁹

Müller and co-workers have isolated some of the largest known polyoxomolybdates which are often referred to as the ‘giant-wheel’ type architectures.^{8,11} In this respect the field of POM chemistry and its ability to form such structures has always been impressive and unparalleled when we think of how the molecules in question are synthesised using ‘one-pot’ conditions.

To understand their assembly is more complicated and is easier to comprehend when we think of the individual mononuclear polyhedra as building blocks in the construction of larger clusters. In addition to this, smaller low nuclearity POM clusters can also be used as fragments in the assembly of larger high nuclearity clusters. Figure 5 demonstrates the self-assembly of a star-like object starting with a building block that has 5-fold symmetry which can combine with another type of building block. When these bigger building blocks combine a molecular sphere is produced that is only 2.7 nm wide.

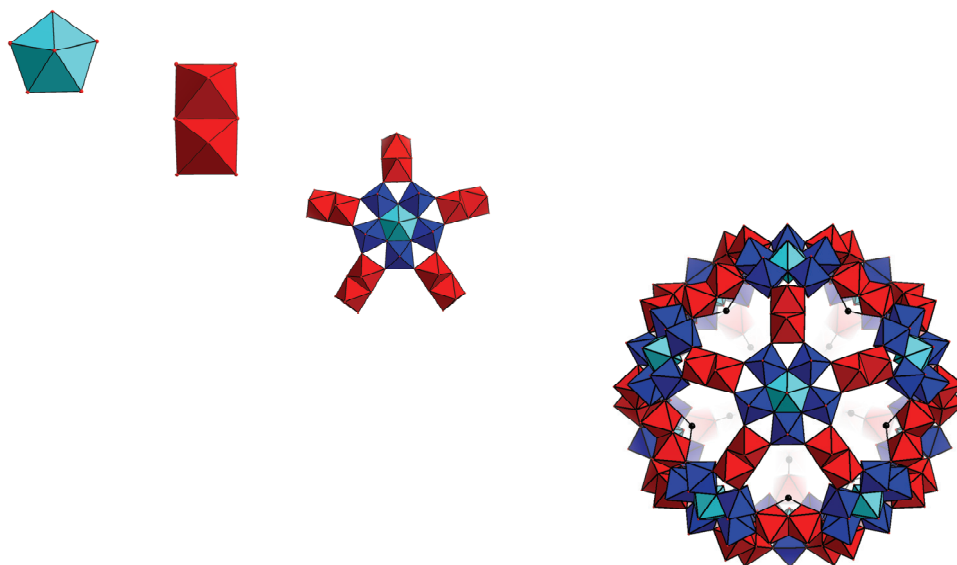


Figure 5 Molecular growth from a basic $\{\text{MoO}_7\}$ building block to the final structure; a molecular sphere.

Remarkably the novelty of the ‘giant-wheel’ structures is not only limited to their nuclearity and dimension but also due to the fact that they can be produced using relatively simple reaction conditions. Simple acidification of an aqueous solution and addition of reducing agent and other hetero atoms has been enough to isolate these clusters.

Müller and co-workers were able to synthesise the much cited $\{\text{Mo}_{132}\}$ ‘ball’ through the generation of different nuclearity molybdenum-oxide fragments in solution.^{12,13} The cluster with the overall formula of $[\text{Mo}^{\text{VI}}_{72}\text{Mo}^{\text{V}}_{60}\text{O}_{372}(\text{MeCO}_2)_{30}(\text{H}_2\text{O})_{72}]^{42-}$ is made up of two types of building blocks: 12 pentagonal $\{(\text{Mo})\text{Mo}_5\}$ and 30 $\{\text{Mo}^{\text{V}}_2\}$ units. The latter can be seen as the linking component; the pentagonal units however, are responsible for the overall spherical shape of the cluster (Figure 6).

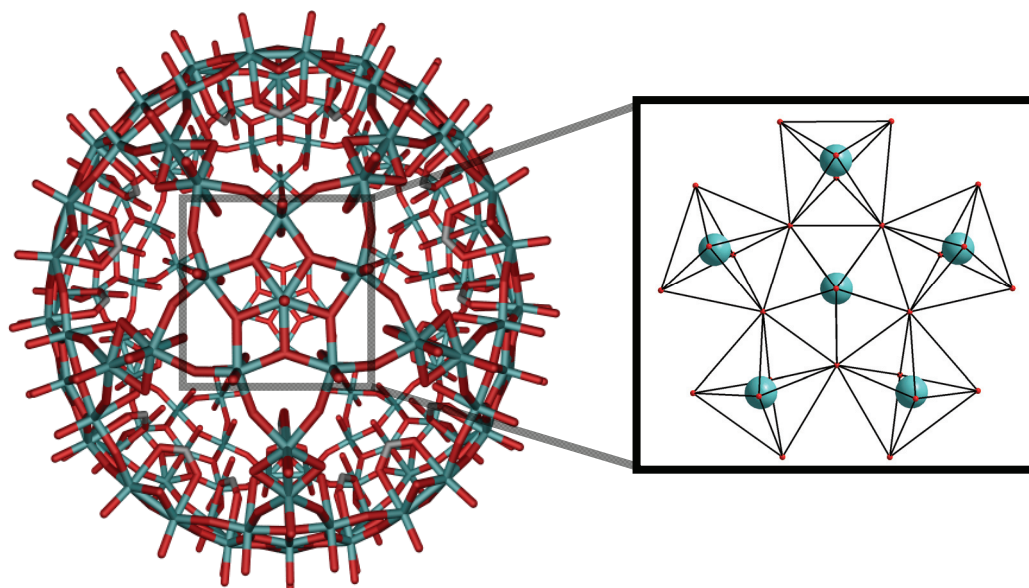


Figure 6 $\{Mo_{132}\}$ wheel with expanded view of the pentagonal unit represented by open face polyhedra. Mo: green, O: red, C: grey.

In 1995 Müller *et al.* were able to isolate a mixed valent diamagnetic compound, $[Mo_{154}O_{462}H_{14}(H_2O)_{70}]^{14-}$ constructed using three individual building blocks (Figure 7) to create the first wheel shaped cluster.¹⁴

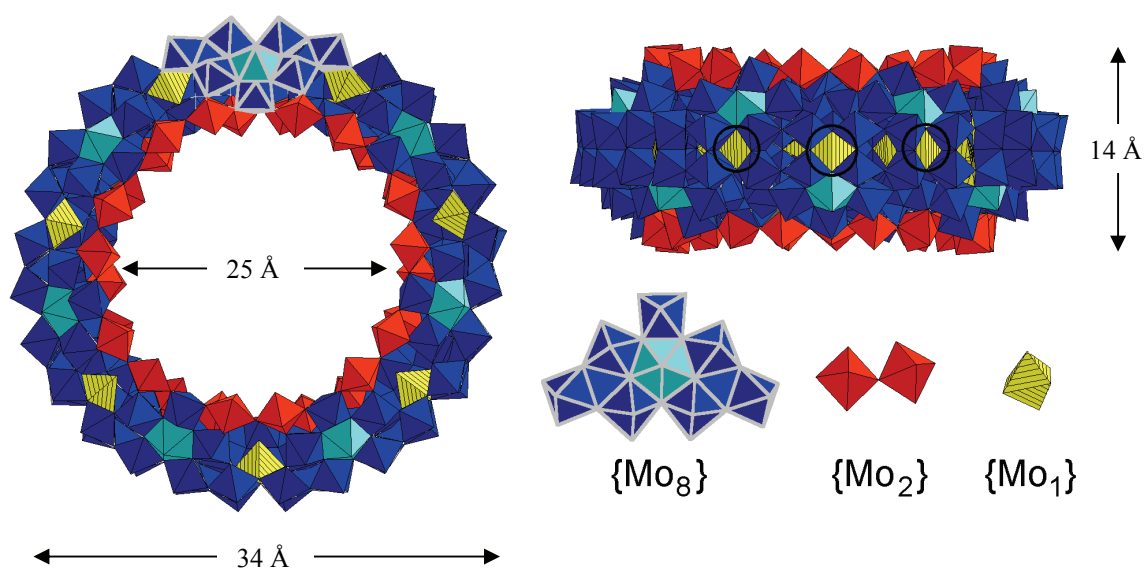


Figure 7 A polyhedral representation of $\{Mo_{154}\}$ cluster constructed using $\{Mo_1\}$ (yellow hatched polyhedra), $\{Mo_2\}$ (red polyhedra), and $\{Mo_8\}$ (blue polyhedra) fragments.¹⁵

The wheel can be simplified to two rings; an inner and outer ring. The inner ring is made of $\{\text{Mo}_2\}$ units which are fused to the neighbouring $\{\text{Mo}_8\}$ units which form the outer ring. Closer inspection of the $\{\text{Mo}_8\}$ fragment reveals a pentagonal unit of the form $\{(\text{Mo})\text{Mo}_5\}$ to which two further $\{\text{MoO}_6\}$ units are fused to each side *via* corner sharing modes, bringing the total to eight molybdenum centres. In addition to the high nuclearity of the cluster, the $\{\text{Mo}_{154}\}$ has generated much interest due its dimensions, with an inner diameter spanning 25 Å with a thickness of 14 Å and an outer diameter of approximately 34 Å rendering the cluster a nanoscopic molecule.⁶

The discovery of $[(\text{MoO}_3)_{176}(\text{H}_2\text{O})_{80}\text{H}_{32}]$ and $[\text{Mo}_{248}\text{O}_{720}(\text{H}_2\text{O})_{128}]^{16-}$ saw the ‘giant-wheel’ chemistry move in a new direction.^{16,17} Müller and co-workers isolation of $\{\text{Mo}_{176}\}$ and the discovery of $\{\text{Mo}_{248}\}$ gave an insight to the solution chemistry and the assembly of the molybdenum-oxide fragments in solution. A simple synthetic modification i.e. the use of ascorbic acid as a reducing agent, initiates the molecular growth of $\{\text{Mo}_{174}\}$ to $\{\text{Mo}_{248}\}$. The latter is comprised of one $\{\text{Mo}_{174}\}$ central cluster to which two $[\text{Mo}_{36}\text{O}_{96}(\text{H}_2\text{O})_{24}]$ clusters are fused in a ‘hub-cap’ fashion (Figure 8).

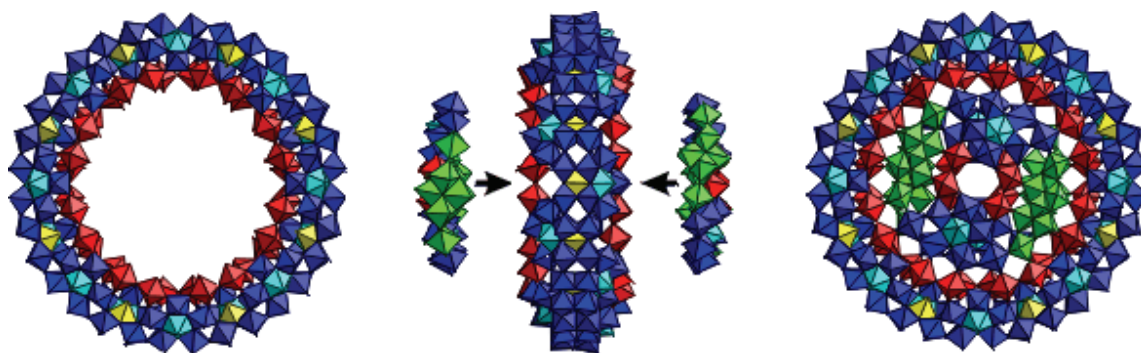


Figure 8 Polyhedral representation of $\{\text{Mo}_{176}\}$ (*LHS*), the attachment of two $\{\text{Mo}_{36}\}$ groups (*centre*) and the completed $\{\text{Mo}_{248}\}$ cluster (*RHS*).

Perhaps the most famous and largest cluster to be isolated to date is a cluster that contains 368 individual molybdenum centres, $[\text{H}_x\text{Mo}_{368}\text{O}_{1032}(\text{H}_2\text{O})(\text{SO}_4)_{48}]^{48-}$.¹⁸ The cluster is once again comprised of $\{(\text{Mo})\text{Mo}_5\}$ units adding curvature to the structure in addition to the $\{\text{Mo}_1\}$ and $\{\text{Mo}_2\}$ linking units and is often described as a ‘lemon’ or ‘hedgehog’ shaped cluster (Figure 9).

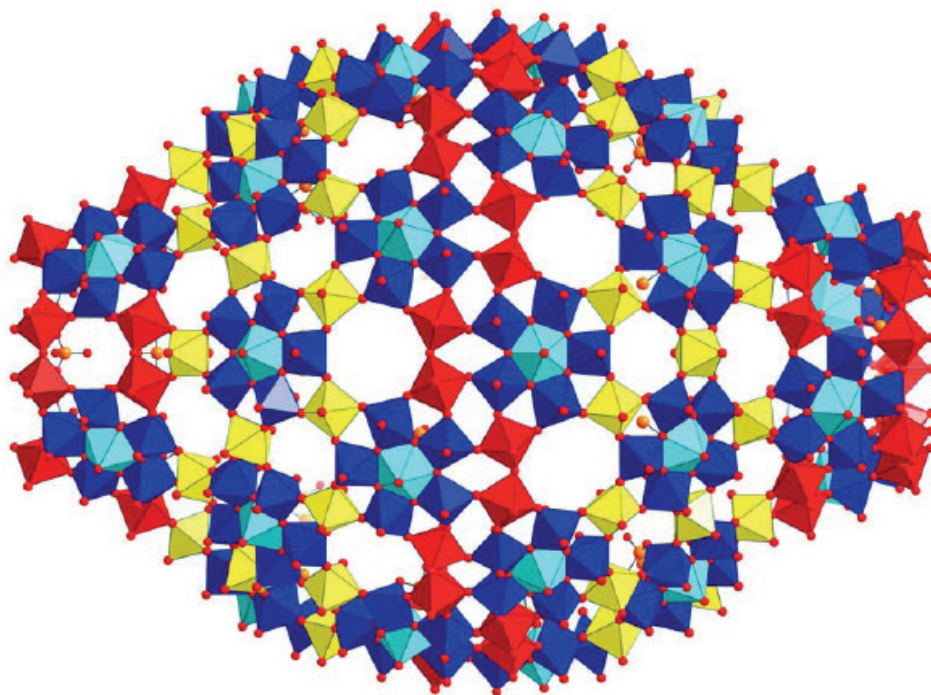


Figure 9 A polyhedral representation of $\{\text{Mo}_{368}\}$ cluster constructed using $\{\text{Mo}_1\}$ (yellow polyhedra), $\{\text{Mo}_2\}$ (red polyhedra), and $\{(\text{Mo})\text{Mo}_5\}$ (blue polyhedra) fragments.¹⁵

The importance in understanding how the individual fragments assemble in solution should not be overlooked. However, understanding the mechanism involved in the construction of such molecules is limited. In the assembly of the ‘giant-wheel’ architectures the $\{(\text{Mo})\text{Mo}_5\}$ pentagonal unit is a vital component that gives these architectures their spherical or ring shape qualities, highlighting that detailed knowledge of the fragments that aggregate and favour the assembly of structures within the ‘giant wheel’ domain is important.¹⁹ Furthermore, it appears that the intrinsic properties of the simple building blocks ($\{(\text{Mo})\text{Mo}_5\}$, $\{\text{Mo}_2\}$, and $\{\text{Mo}_1\}$) in solution facilitate the growth of these clusters.

1.2.2 Tungstates

High nuclearity polyoxotungstates in contrast to molybdates are more likely to be formed *via* lacunary fragments of the more common Keggin cluster which can exist as five

different skeletal isomers.⁶ The basic oxygen ions present at the vacant sites are highly attractive for binding of secondary transition metals including lanthanides.²⁰

The cyclic cluster $[\text{Ln}_{16}\text{As}_{12}\text{W}_{148}\text{O}_{524}(\text{H}_2\text{O})_{36}]^{76-}$ discovered by Pope and co-workers, was and remains one of the largest polyoxotungstates to date.²¹ The cluster is composed of lacunary $[\text{AsW}_9\text{O}_{34}]^{9-}$ and $[\text{W}_5\text{O}_{18}]^{6-}$ ions that are connected by Ln(III) cations (Figure 10).

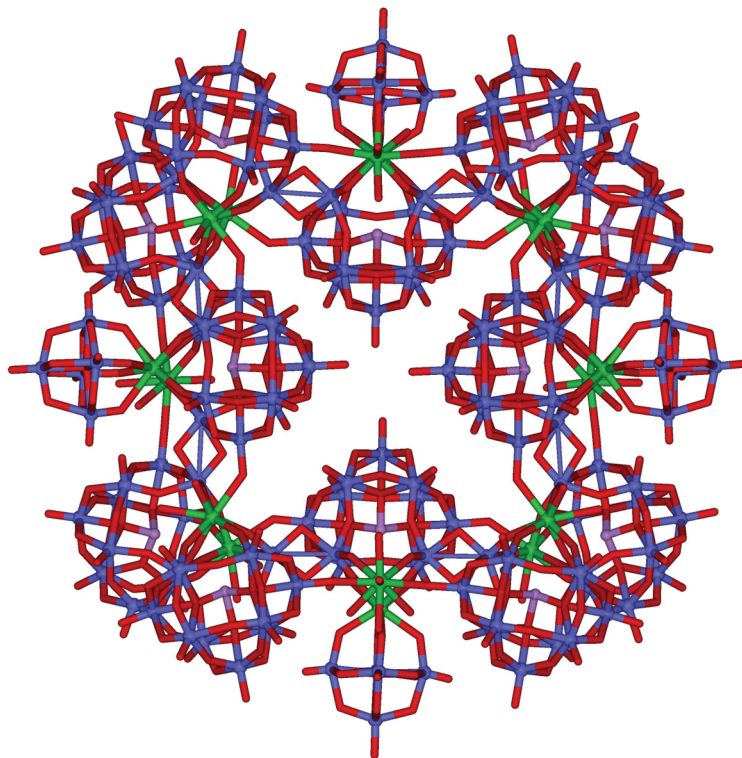


Figure 10 The cyclic $\{\text{W}_{148}\}$ cluster. W: blue, O: red, As: purple, Ln: green.

Cronin *et al.* have discovered the largest isopolytungstate to date $(\text{TEAH})_9\text{Na}_2\{\text{K}[\text{H}_{12}\text{W}_{36}\text{O}_{120}]\}\cdot 25\text{H}_2\text{O}$ (TEAH = protonated triethanolamine).²² Synthesised under ‘one-pot’ reaction conditions the initial aqueous tungstate solution was acidified and reduced in the presence of the organic compound triethanolamine. The organic counterion appears to have some influence in producing a compound with C_{3v} symmetry by ‘imprinting’ its own three-fold symmetry²³ onto the cluster giving it a Celtic-ring type appearance. The cluster itself is comprised of three $\{\text{W}_{11}\}$ subunits which are bridged together by three $\{\text{W}_1\}$ groups creating an inner $\{\text{W}_6\text{O}_6\}$ moiety (Figure 11). Due to the framework of the cluster the inner cavity radius is estimated to be *ca.* 2.8 Å and is

suitable for complexing some Group I and II metal ions and NH_4^+ , similar to the 18-crown-6 ether. For instance, potassium can coordinate to six oxygen atoms *via* ligation of the corner oxygen atoms of the $\{\text{W}_6\text{O}_6\}$ moiety.

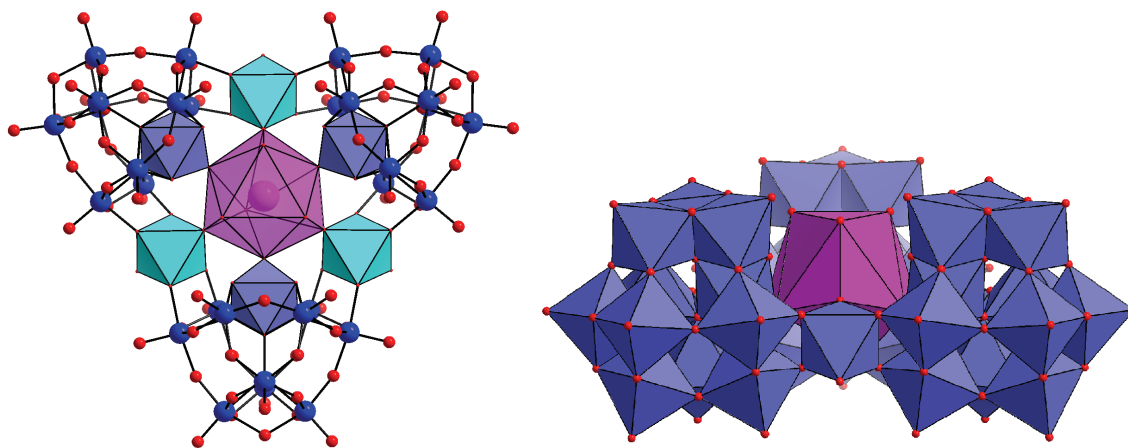


Figure 11 Ball and stick (*LHS*) and polyhedral representation (*RHS*) of the $\{\text{W}_{36}\}$ cluster. W: blue, O: red, K: purple, $\{\text{W}_1\}$ bridging units: cyan.

1.2.3 Vanadates

Polyoxovanadates represent an important subclass of metal-oxide based clusters. Vanadium has numerous oxidation states and is also known to exhibit a variety of coordination geometries and for this reason can structurally exert more flexibility and shows a common tendency to form clusters with shell and cage like topologies.^{6,24} Many of these clusters are comprised of octahedral VO_6 , pyramidal VO_5 and tetrahedral VO_4 units with vanadium in the V(IV) and V(V) oxidation states.^{25,26} Clusters that contain mixed valence species ($\text{V}^{\text{IV/V}}$) are highly attractive for magnetic studies and this arises from the full or partial delocalisation of the single 3d electrons of the vanadium ions over both valence types or the complete localisation over the paramagnetic ions.^{27,28} Polyoxovanadates are almost always synthesised under aqueous or hydrothermal conditions which may limit the isolation of different cluster types.²⁹

One of the largest polyoxovanadates isolated to date is the $[\text{V}_{34}\text{O}_{82}]^{10-}$.³⁰ The cluster can be described as a sheath with two identical halves that are related by a 90° rotation. The sheath itself is constructed by 30 tetragonal VO_5 units with a central V_4O_4 cube (Figure 12).

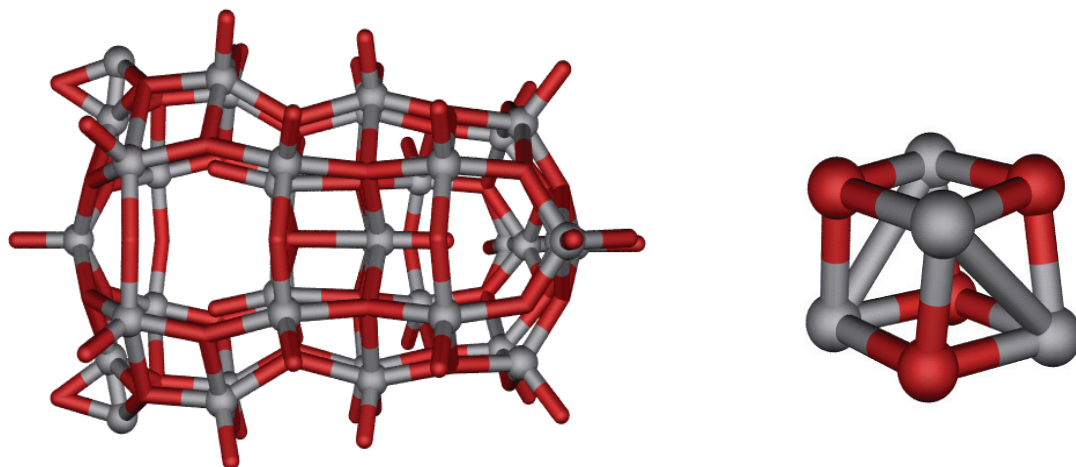


Figure 12 The $\{\text{V}_{34}\}$ cluster (*LHS*) and the V_4O_4 cube (*RHS*). V: grey, O: red.

1.3 Designing and Understanding Polyoxometalate Clusters

Polyoxometalate clusters have been the subject of an immense number of studies due to their attractive electronic and molecular properties that give rise to a variety of applications in many fields including catalysis,³¹⁻³³ magnetism,³⁴⁻³⁶ medicinal chemistry,³⁷ and materials science.^{38,39}

However, the most frequently found POM synthesis methods employ ‘one-pot’ reaction conditions to create structures of phenomenal diversity such as we have already discussed (section 1.2). The variable reaction parameters can be easily manipulated and offer a straight-forward route to new POM architectures, albeit through a rather serendipitous approach. The disadvantage of such experimental conditions is that there is little understanding of the complex mechanism involved in the formation of such clusters in solution.⁴⁰ Furthermore, the structures that fall into the domain of high nuclearity clusters

offer architectures with unparalleled structural beauty, but their functionality is often very limited.

Thus the current focus in POM chemistry can be categorised in two ways:

- To produce POMs with greater functionality taking advantage of their unique physical properties which include organisation in all dimensions and on surfaces.
- To understand and manipulate the self-assembly process that underpins the formation of POM clusters to create complexes with greater functionality.

The latter is of particular interest as this could be a fundamental route towards designing nanoscopic clusters with pre-determined structure and function.⁴¹

1.3.1 Structural Features of Functional Polyoxometalates

Numerous publications exist that exemplify the unique structural and physical components offered by POM frameworks, leading to compounds that exhibit key functional properties. Often many of these structures will contain additional components that enhance the physical properties of the POM cluster. In this respect, the POM framework provides a ‘foundation’ for the binding of external or internal components as will be discussed.

Derivatives of POM clusters can have amplified magnetic properties *via* incorporation of paramagnetic centres. For this reason, lacuna derivatives of the most stable heteropoly Keggin ion, $[XM_{12}O_{40}]^{n-}$ have been extensively researched, where studies have shown that replacing a core metal ion can result in a significant change in properties of the heteropolyanion.⁴²

Of particular interest is the diamagnetic trivacant Keggin ion, $[XW_9O_{34}]^{n-}$. The three vacant sites have been shown to act as ligands that permit the inclusion of isolated magnetic clusters of various nuclearity.⁴³ Two trivacant clusters can encapsulate tetranuclear $\{M_4O_{12}\}$ units creating a ‘sandwich’ type arrangement (Figure 13). Magnetically active

clusters have been isolated where the $\{M_4O_{12}\}$ sub-unit can be made up of the following transition metals: nickel, cobalt, copper and manganese. Mono and trivalent derivatives of Wells-Dawson type clusters have also been extensively researched with paramagnetic 3d ions.⁴⁴

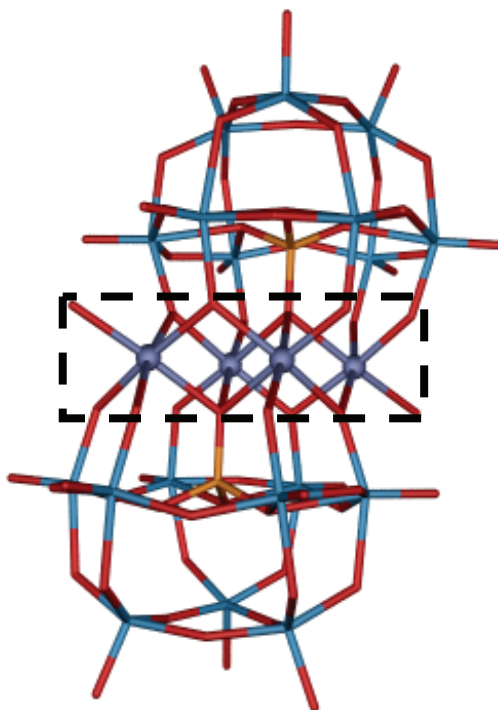


Figure 13 Example of a sandwich type complex where two tungsten based lacuna fragments are linked by a central belt of cobalt ions. W: blue, O: red, Co: purple, P: orange.

The application of transition metal substituted lacuna also extends to catalysis; a prominent area of research within POM chemistry. Again, several key structural features make them attractive for use in catalysis; the oxo (O^{2-}) ligands bound to the d^0 W(VI) atoms are oxidatively resistant, the skeletal tungsten atoms can be substituted for catalytically active transition metals, they are rigid and thermally robust.^{45,46} Such structural attributes makes them valuable for application in both homogenous and heterogeneous catalysis.⁴⁷ Titanium and ruthenium substituted lacuna of the Dawson and Keggin type clusters have been synthesised and probed for their catalytic properties.⁴⁸⁻⁵²

In addition to external modifications, either through loss of skeletal tungsten ions or addition *via* surface oxygen atoms, internal structural modifications can also be made. This was recently demonstrated by the isolation of a thermochromic Dawson-type mixed-valent

polyoxomolybdate $[\text{Mo}_{18}\text{O}_{54}(\text{SO}_3)_2]^{n-}$ that possesses unusual electronic properties.⁵³ Two pyramidal sulfite ions are encapsulated within the Dawson framework creating a short unusual S...S interaction between the lone pairs of the two anions. Upon heat activation there is partial electron loss from the sulfur atoms to the cluster shell resulting in a fully reversible colour change of the crystalline material from yellow to red on going from 77 K to 500 K (Figure 14).

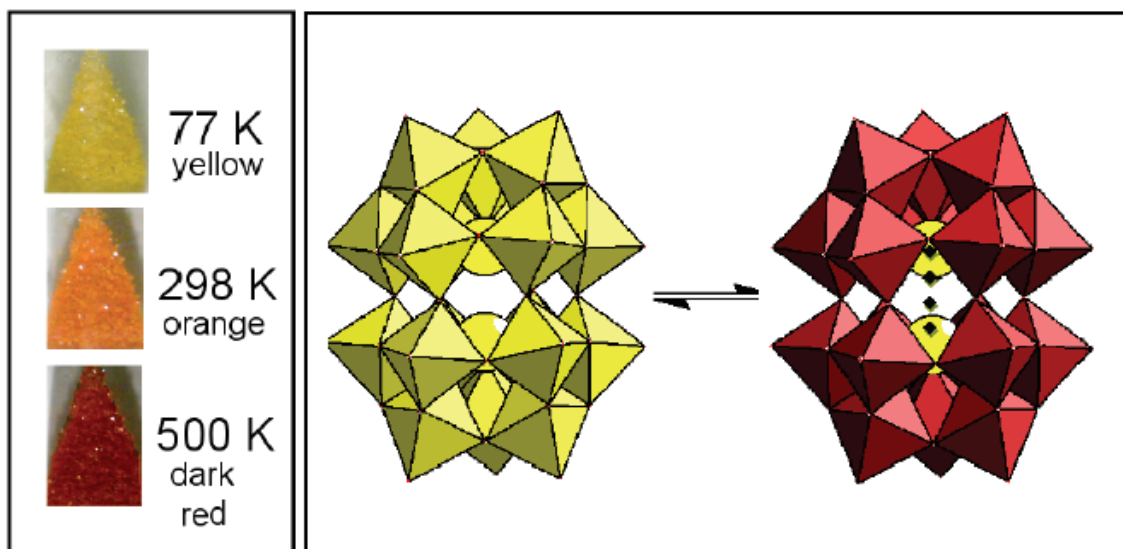


Figure 14 Photographs of crystals of the thermochromic cluster (*LHS*) and polyhedral representation of the sulfite Dawson with movement of electrons from the centre of the cluster to the surface (*RHS*).

A similar tungsten based cluster has been made that can also change colour when heated.⁵⁴ Encased inside the tungsten-oxygen metal cage are two sulfite atoms arranged in a very precise environment. Exposure to heat can cause a chemical reaction to occur resulting in a structural and electronic rearrangement of the encased atoms, which can be observed through a colour change of the molecule from white to blue and back again (Figure 15). The two sulfite atoms are releasing two electrons to the cluster shell upon activation by the heat source.

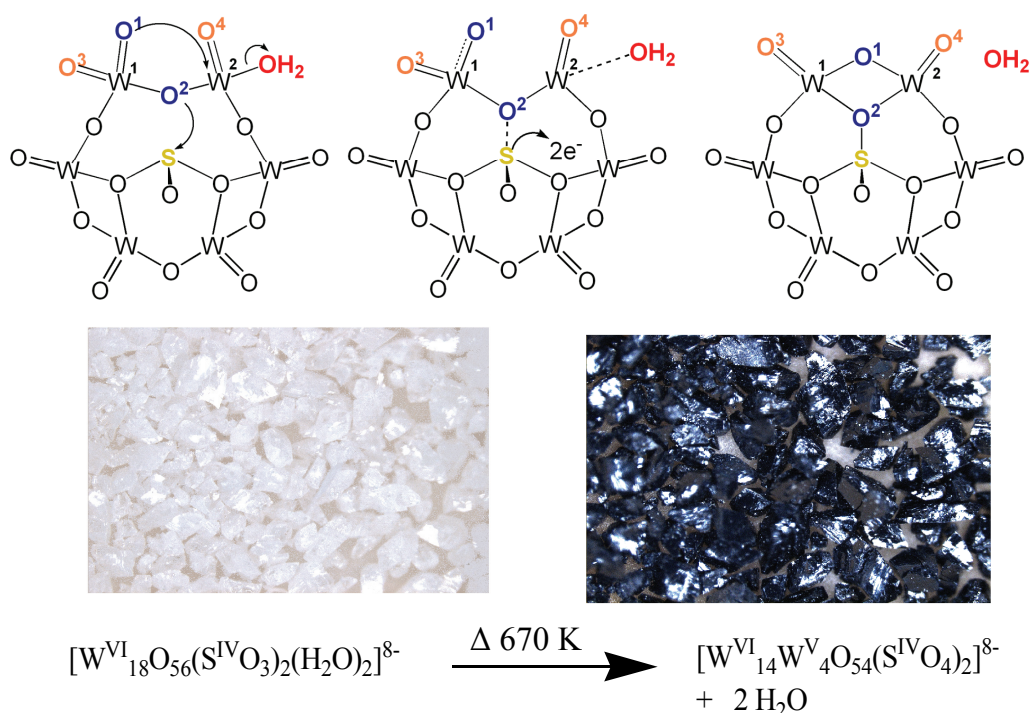


Figure 15 Scheme illustrating the proposed reaction mechanism (top). Photographs of the crystals of the reactant (white, *LHS*) and the product (blue, *RHS*) along with the reaction equation (bottom).

1.3.2 Organic-Inorganic Hybrid Polyoxometalate Materials

Organic-inorganic hybrid composites are also of immense interest for a number of reasons. In addition to the synergetic properties such as electrical, magnetic and optical properties,⁵⁵ these hybrid materials can also serve as good models towards understanding the molecular growth process that occurs in POM chemistry. Needless to say, the latter is a field that remains undeveloped and much of the interest in hybrid POMs comes from producing clusters which display the many physical properties attributed to such complexes. As such, the contemporary interest in this class of compounds is overwhelming but equally can be divided into the more highly researched subclasses and will be discussed in the following sections.

1.3.2.1 *Functionalised Polyoxometalates*

Tethering organic molecules to the ends of POM clusters can be perceived as ‘value-adding’ components.⁵⁶ In addition to this, the possibility of rationally designing such compounds in a bid to gain control over the individual building blocks in solution could also be achieved. The use of aromatic molecules is a common theme with this particular subclass of compounds and in particular organo-imido derivatives are greatly favoured.^{57,58} This mainly extends from the stability between the imido-metal to nitrogen linkage and the delocalisation of organic π -electrons on the POM cluster.⁵⁹ Small molybdates such as $[\text{Mo}_6\text{O}_{19}]^{2-}$ serve as good ‘anchors’ for these types of derivatisations and one group has also shown how the electronic properties of a bound phenanthroline ligand has been considerably modified through intramolecular charge transfer.⁶⁰

It has also been possible to derivatise tungsten based POMs where removal of one or more of the core metal ions will increase the negative charge on the heteropolyanion which in turn is localised on the oxygen atoms of the lacuna. These oxygen atoms are highly nucleophilic and are more reactive towards electrophilic molecules allowing the binding of organosilyl and organophosphoryl groups.⁶¹⁻⁶³

Aside from the possible physical properties, these compounds are also prime candidates to understand and gain control over reactive binding sites present on the cluster. Modifying the surface of the clusters with organic compounds gives a degree of control because it is easier to predict the connectivity and hence the final product.⁶⁴ The nitrogen donor atoms present on organoimido derivatised clusters should be attractive towards the binding of various transition metals resulting in the isolation of interesting functional architectures.⁶⁵ Peng and co-workers have managed to isolate such a complex recently, where Fe^{2+} can be bound to the bis(terpyridine) ligand *via* the three donor nitrogen atoms to give $[\text{Mo}_{12}\text{O}_{36}\text{N}_8\text{C}_{50}\text{H}_{36}\text{Fe}]^{2-}$ (Figure 16).⁵⁹

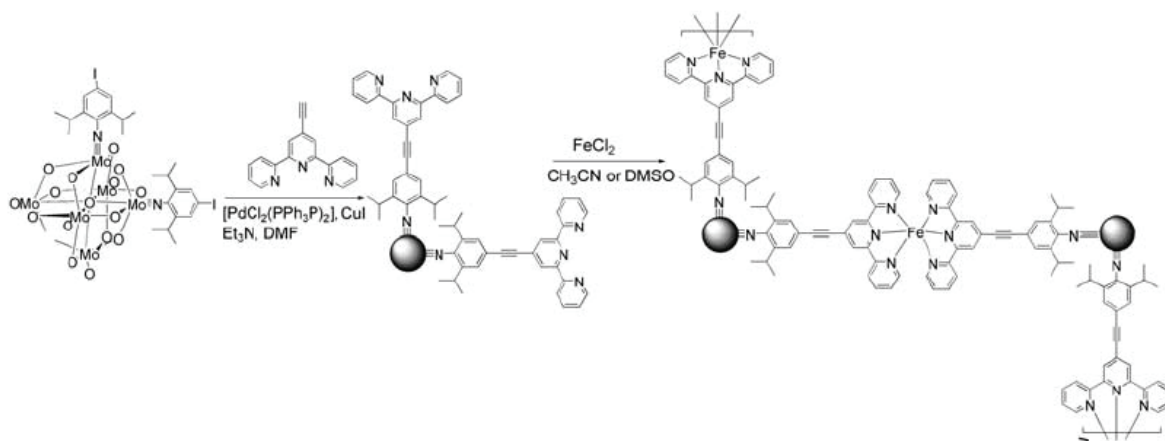


Figure 16 Synthesis of a functionalised POM and subsequent coordination to iron(II) ions to produce a hybrid polymer.⁵⁹

1.3.2.2 Non-coordinating Organic Composites

Within the realm of POM chemistry, additional organic components can also play important roles as templates and hosts or can be used for their charge compensating properties. Finding the right organic molecule to match the right polyoxoanion is difficult,⁶⁶ but can result in architectures with numerous nuclearity and structural diversity and can also provide an insight into solution chemistry. In the latter point researchers can begin to understand how the reactive building blocks can form under various synthetic conditions, where previously they were masked by ‘one-pot’ conditions.

The isolation of a new structure type, $[\text{H}_2\text{Mo}_{16}\text{O}_{52}]^{10-}$ by virtue of the cations used to encapsulate or ‘shrink-wrap’ this cluster, exemplifies the previous point.⁶⁷ Protonated hexamethylenetetramine (HMTA) counterions have managed to limit the reorganisation of this complex into other well-known structure types or more highly symmetrical clusters allowing access to a more diverse set of $\{\text{Mo}_{16}\}$ cluster-based building blocks (Figure 17). Furthermore, the building block character of this anion exhibit significant nucleophilicity, demonstrated when di-valent electrophilic transition metal cations M^{2+} ($\text{M} = \text{Fe}, \text{Mn}, \text{Co}$) are added to solutions of this cluster, resulting in a family of isostructural compounds.⁶⁸

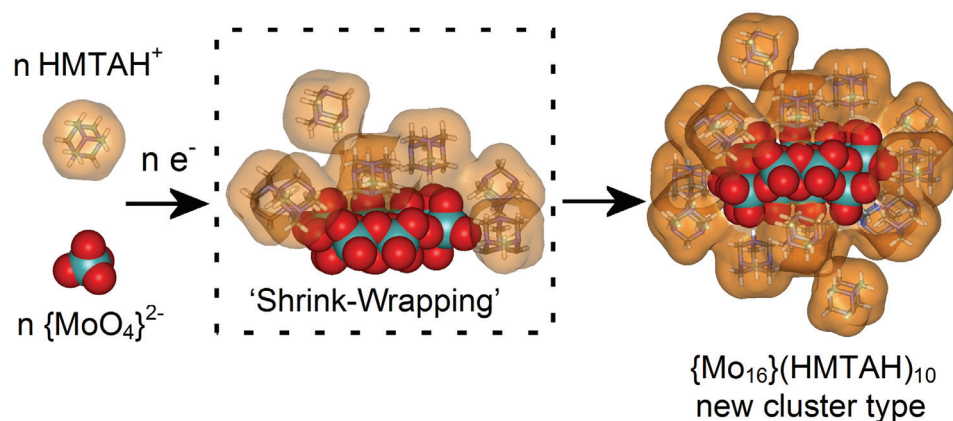


Figure 17 An illustration of the ‘shrink-wrapping’ process that allows the isolation of the new $\{ \text{Mo}_{16} \}$ cluster using protonated HMTA. Mo: green, O: red, counterions: orange.

Keller and co-workers recently reported an example of a host-guest complex in which eight phenanthroline ligands and six copper(I) centres self-assembled to form two bowl shaped cavities.⁶⁹ Inside these cavities can reside two heteropoly Keggin ions to form $[\text{Cu}_6(4,7\text{-phenanthroline})_8(\text{MeCN})_4]_2\text{PM}_{12}\text{O}_{40}$ ($M = \text{Mo}$ or W , Figure 18). The bowls open in opposite directions and the depth of the cavity created by the bowl is such that it cannot fully accommodate the cluster but that there are still significant host-guest interactions.

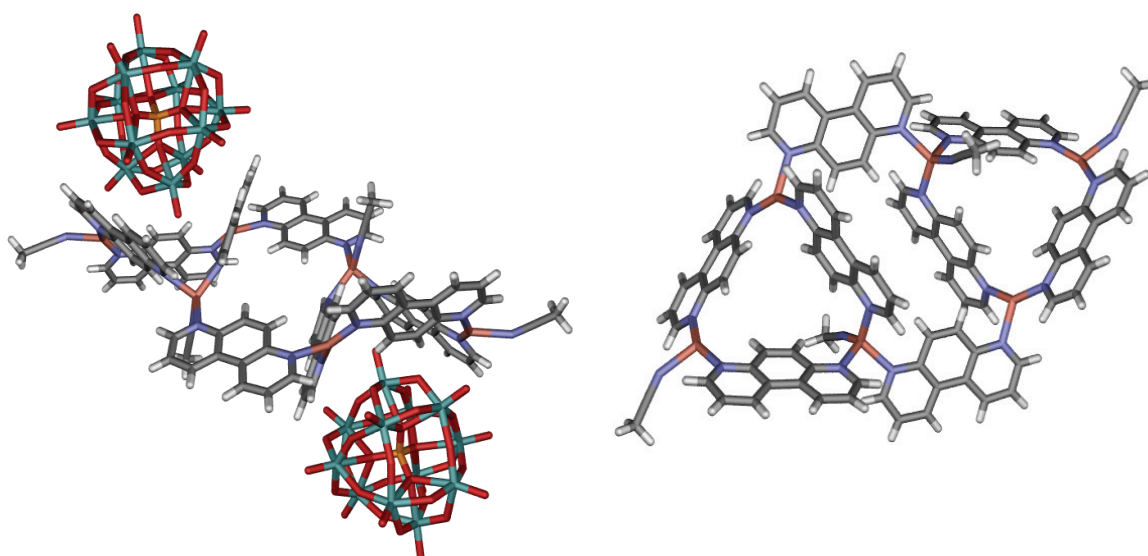


Figure 18 Ball and stick representation of the two POM anions sitting in the bowl-shaped cavities (*LHS*) and the complex cation (*RHS*). Mo: green, O: red, Cu: pink, N: blue, C: grey, H: white.

The group have also reported a structure which uses a phosphotungstate ion, $[\text{PW}_{12}\text{O}_{40}]^{3-}$ as a non-coordinating anionic template.⁷⁰ At the time of publication, the structure was one of the largest non-coordinating anions within a coordination polymer, the result of which lead to the formation of a three-dimensional Cu(I)-4,4'-bipyridine (bpy) network to form $[\text{Cu}(\text{MeCN})_4]_3\text{PW}_{12}\text{O}_{40}\cdot 2\text{C}_6\text{H}_5\text{CN}$.

More commonly organic cations provide necessary charge compensation properties when creating POM structures. In doing so it is also possible to influence the growth of the POM into a zero, one, two or three dimensional network. Such influences are clearly determined by the size, flexibility/rigidity⁷¹⁻⁷³ with respect to the counterion used and are also dependent on other external conditions such as the inclusion of solvent molecules and/or other main group or transition metals.⁷⁴

1.3.2.3 Construction of Hybrid Arrays via Coordinative Organic-Metal Composites

One of the most popular domains of POM chemistry is in the construction of inorganic-organic hybrid arrays. These can be constructed in a number of ways and as discussed in the previous section the outcome or the architectural disposition of the final product is very much dependent on the additional synthetic components used in the synthesis.

The structure-directing influences that carefully chosen organic molecules can exert over POM building blocks provides researchers with the ability to achieve the 'subtle' control measures and predictability that is needed in rational design.⁷⁵ Creating such hybrid materials also opens the door to synthesising POMs under non-aqueous conditions, where previously using water as a solvent often limited the structures that could be isolated.

The inclusion of secondary transition metals, rare-earth metals, and main group metals, can serve as inorganic ligands that can bridge and link POM clusters into chains and networks.⁷⁶⁻⁸⁰ In addition to this, many groups utilise coordinative organic composites that can readily bind to other transition metals and can act as extended bridging ligands, spacers or can complete the coordination geometry requirements around the metal ion.

Unlike the syntheses of large high nuclearity POMs, a degree of control can be achieved because the coordinative organic compound will have well-defined binding sites and their favourability towards coordinating with the POM or other transition metals can also be predicted. In a similar way, POMs can be seen as inorganic multi-dentate ligands that can readily bind to secondary transition metals. The advantage of generating or using small metal-oxide clusters is that they have well-defined binding sites, their oxidation states are known, as well as their solubility preferences.

A more rational approach therefore to producing POM clusters may allow the design of larger architectures with more functionality. It also provides the opportunity to establish what factors govern the self-assembly of POM fragments or synthons to produce structures of a given dimensionality.

For instance, in isolated clusters quite often the use of a capping ligand that only contains binding sites on one side will lead to a closed ‘environment’ restricting its growth in the opposite direction. Organic ligands of this type are ethylenediamine (en), 2, 2’-bi-pyridine and phenanthroline, where coordination is exclusive to one secondary metal and no other linking atoms (e.g. to an oxygen of the subsequent POM, Figure 19).⁸¹⁻⁸³ Bulky complex cations can also suffice in limiting the growth of POM fragments.⁸⁴

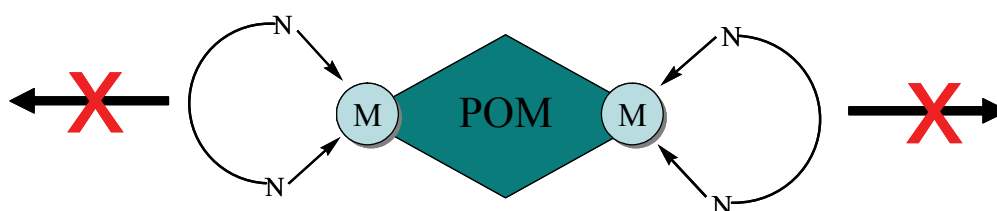


Figure 19 Illustration of how a capped unit is limited in its growth in any direction. M = secondary metal.

Wang and co-workers have shown how nickel and cobalt can decorate the surface of heteropolymolybdates *via* coordination of the terminal oxygen atoms.⁸⁵ These fragments are then capped by the ‘enclosing’ ligands, 2,2’-bipyridine (bpy) or phenanthroline to create isolated clusters such as $[\text{PMo}^{\text{VI}}_8\text{Mo}^{\text{V}}_2\text{V}^{\text{IV}}_8\text{O}_{44}\{\text{Co}-(2,2'\text{-bpy})_2(\text{H}_2\text{O})\}_4]^{3+}$ (Figure 20).

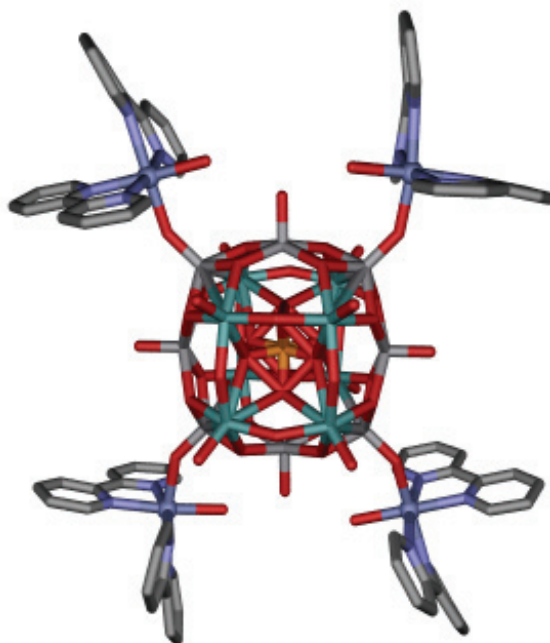


Figure 20 An isolated Keggin unit capped by cobalt and 2,2'-bpy units. Mo: green, O: red, P: orange, Co: purple spheres, C: grey, N: blue.

To encourage growth in a one-dimensional direction, the use of non-enclosing ligands are of particular use as well as the use of metals that can bind to many centres.^{86,87,88} Organic compounds such as ethylenediamine which can also form capping ligands, can exert a degree of flexibility allowing rotation around the carbon atom. This can lead to a bidentate ligand that can coordinate to two metal centres acting as a linker and can encourage the POM fragments to grow out in multiple directions.^{77,89} In the same way the rigid 4,4'-bpy ligand can also bridge together POM fragments (Figure 21).⁹⁰

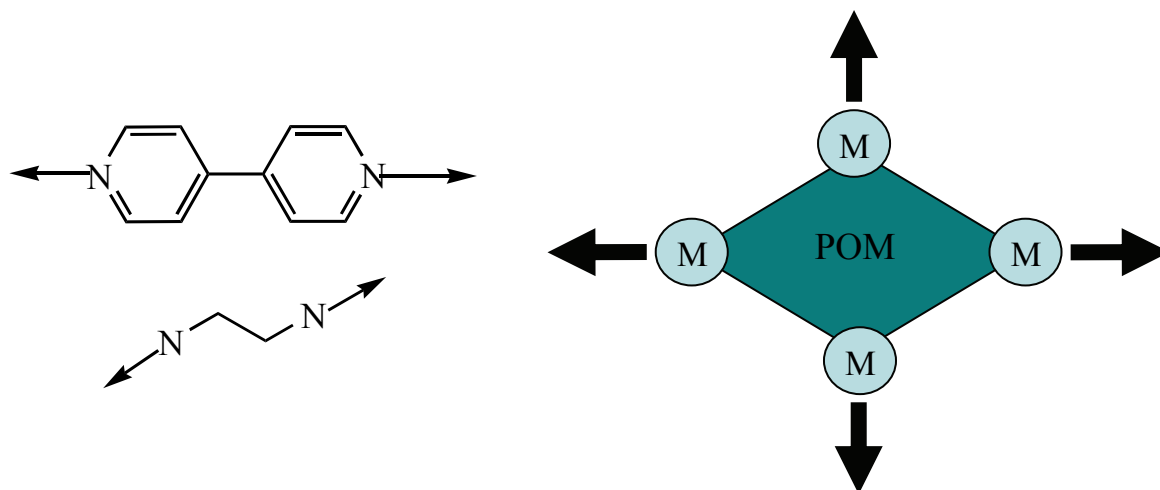


Figure 21 Illustration of how bi-dentate ligands and the binding of multiple metal centres can help POM fragments grow in any direction. M = secondary metal.

Yang *et al.* recently published a one-dimensional vanadate chain $[\text{Ni}(2,2'\text{-bpy})_3]_2[\{\text{Ni}(\text{en})_2\}\text{As}_6\text{V}_{15}\text{O}_{42}(\text{H}_2\text{O})]\cdot 9.5\text{H}_2\text{O}$.⁹¹ The structure is comprised of $\{\text{As}_6\text{V}_{12}\}$ clusters that are linked together by $[\text{Ni}(\text{en})_2]^{2+}$ bridges to form a chain. In addition to these there are two $[\text{Ni}(2,2'\text{-bpy})_3]_2$ complex cations that form a layer of cations in between the chains in a A-B-A-B fashion. These bulky counterions restrict the growth of the POM fragment in any other direction.

Two- and three-dimensional structures can be obtained in a similar manner to one-dimensional chains. The exception is that the higher dimensional structures will bind more secondary metals to the POM precursor or cluster that is generated in the reaction. Multiple coordination on the different faces of a given cluster can encourage the growth of a POM fragment into a two- or three-dimensional array.⁹²⁻⁹⁷

1.4 Functional Nanomaterials

POM chemistry has a great propensity to extend into unfamiliar realms of chemistry, interfacing with some of the most diverse areas of science. Scientists have continued to exploit POMs for their numerous properties, both physical and structural and this has been a key influence in moving towards the ‘nanoworld’.

Designing both fundamental and technologically interesting materials is a challenge that can be met at the interface of chemistry and materials science. The idea that small numbers of molecules or molecular clusters can be used in the formation of nano-structured scaffolding or as active components in molecular electronics is a fascinating prospect. Supramolecular and polyoxometalate (POM) chemistry in particular have been making many advances in this field with many published structures offering properties that are available at the nano-scale level.^{9,98}

1.4.1 ‘Top-down’ vs. ‘Bottom-up’

What has been achieved to date in the area of technology has been through the efforts of the man-made ‘top-down’ approach, where molecules are assembled onto surfaces to meet the demands of producing powerful computational devices.⁹⁹ This technique allows the miniaturisation of silicon-based chips, but will not be able to address the impending issue of down-sizing electronic components to atomic magnitudes.¹⁰⁰

These limitations in nanotechnology have provided opportunities for the molecular chemist. Using the ‘top-down’ approach, electrical engineers have used careful planning to map components onto surfaces to construct computer parts like processors. Through the ‘bottom-up’ approach using self-assembly researchers hope to build circuits by assembling chemically synthesised molecular-scale components.¹⁰¹ This type of self-assembly also allows researchers to exert control over dimension and fundamental properties as well as composition. However, it will require using a combination of planning and pattern formation to grow the molecular fragments in an organised pre-determined way and will most likely need to access new principles that will allow researchers to organise molecular components in the same way as the ‘top-down’ approach.¹⁰²

1.4.2 Nanostructures: Synthesis and Application

The challenge of producing functional materials has placed a large demand on researchers to construct new materials through controlled measures. As such, researchers have complied using the ‘bottom-up’ approach where knowledge at the molecular level can offer scope as to how materials can be modified at the nano-scale end to generate materials that can be used in molecular and nano-electronics.^{103,104}

The outcome of this has resulted in many groups looking at the fabrication of nanostructured materials, in particular one-dimensional nanowires. This class of materials can display many properties including optical, photophysical and electron transfer which can be attributed to the focussed flow of electrons in one direction.¹⁰⁵ Further, their shape and size make them ideal interconnects for use in integrated systems and other functional devices.¹⁰⁶⁻¹⁰⁸ Electronic devices can therefore be conceived through the manufacturing of nanowires with enhanced physical properties.

There are numerous techniques that can be used to synthesise nanowires.¹⁰⁹ Among the more sophisticated techniques is electrodeposition. Penner and co-workers use this method to synthesise one-dimensional molybdenum(0) wires in a controlled and uniform manner.¹¹⁰ The group prepares the wires through a two-step procedure which firstly involves using a ‘step-edge’ decoration method (Figure 22) where molybdenum oxide wires are deposited. Preparation in this way can help control the growth of the wires in one direction. Reduction of the molybdenum oxide wires to molybdenum(0) is achieved by heating the sample in hydrogen gas at 500 °C. The wires are then removed using a graphite electrode surface and tested for their conductivity and mechanical resilience.

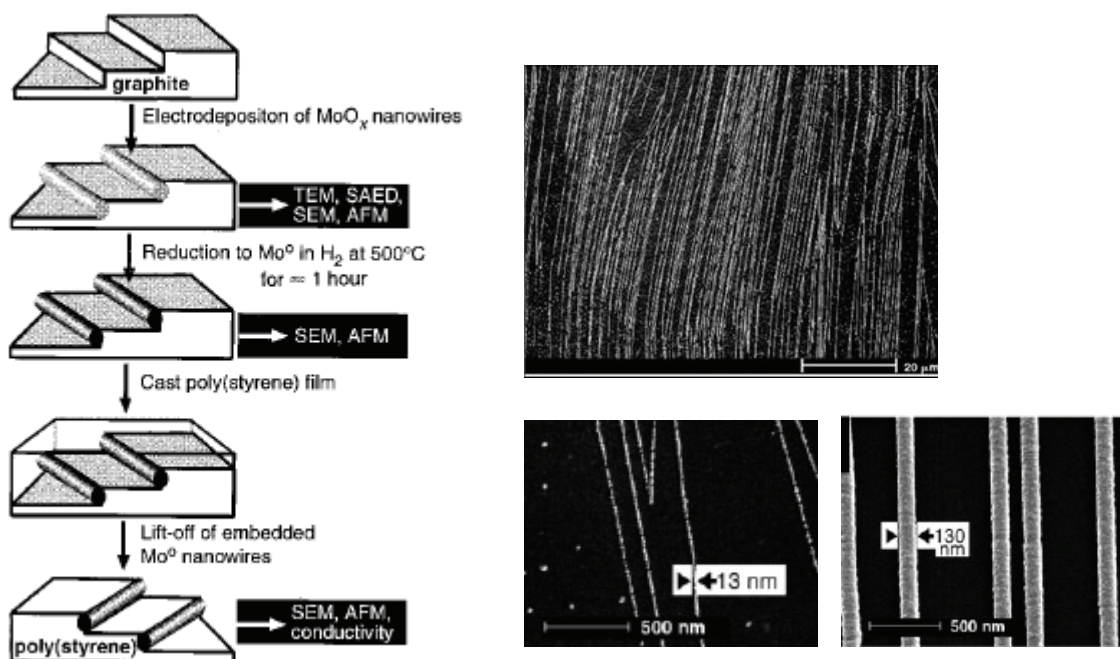


Figure 22 An illustration of step-edge decoration procedure used in the synthesis of Mo⁰ nanowires (LHS) and SEM images of graphite surfaces following the electrodeposition of MoO_x nanowires (RHS).¹¹⁰

Template assisted growth of nanowires is perhaps one of the most common techniques used, where the range of templates can extend from zeolites, carbon and peptide nanotubes, to name a few.¹¹¹⁻¹¹³ A simplified explanation of this method would be to think of it as filling cylindrical holes with a given material.¹¹⁴ The wires can then be grown by a number of methods such as electrochemical or photochemical reduction. Kim and co-workers reported the synthesis of ultra-thin silver nanowires using organic nanotubes some years ago.¹¹⁵ The templates are self-assembled calix[4]hydroquinone nanotubes (CHQ) inside which silver nanowires can grow up to micrometer length scales in ambient aqueous conditions (Figure 23).

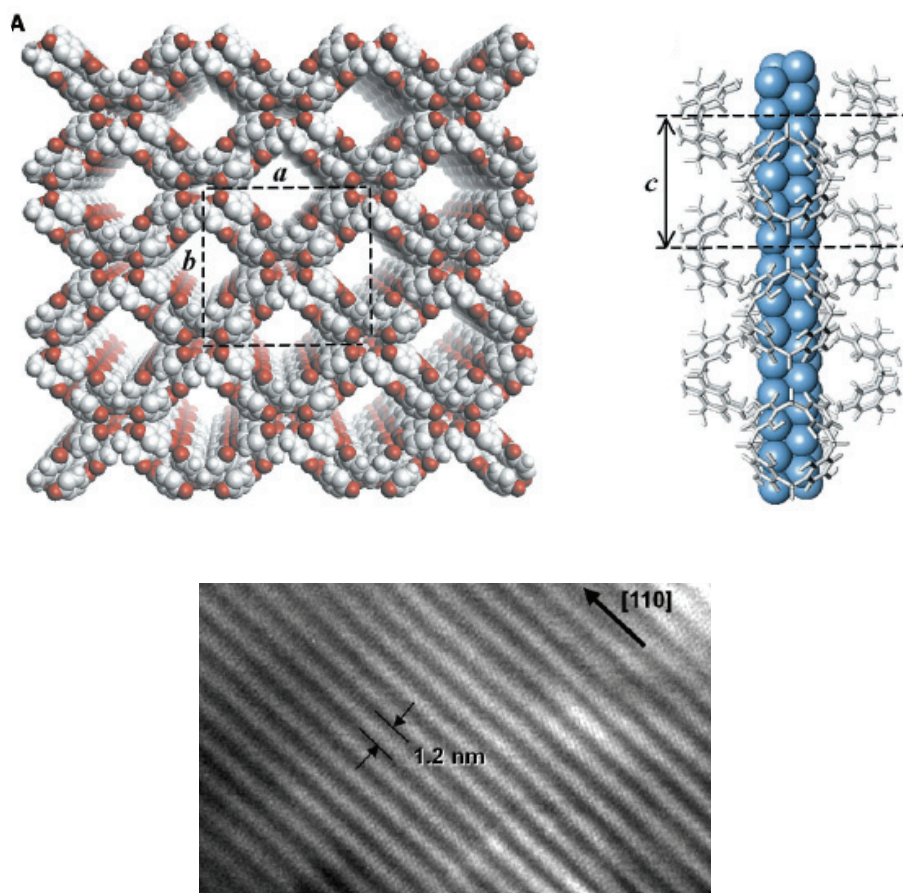


Figure 23 The organic nanotube template (top, *LHS*) and blue space-filled representation of the silver nanowire inside the CHQ nanotube (top, *RHS*) and image of the nanowire arrays (bottom).¹¹⁵

While these methods produce nanowires using controlled measures, these procedures are not simple and inexpensive. Solution-phase synthesis has the distinct advantage of being a cost-effective and straight-forward method and remains an interesting field for the exploration of nanowires.^{116,117} However, a major drawback of this method is that it is not always possible to produce uniform nanowires with well-defined shapes and sizes and growth of the nanowires in one direction is also a limiting factor (Figure 24).

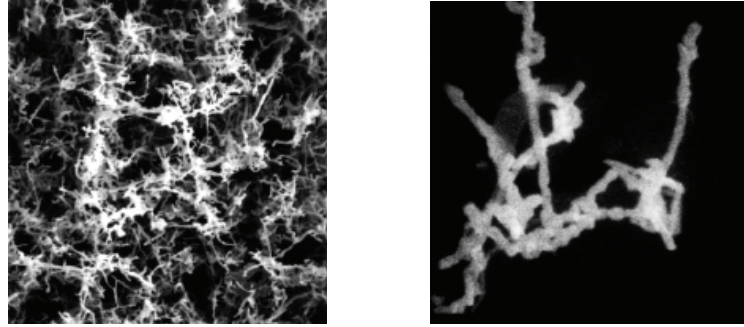


Figure 24 SEM micrographs of nanowires grown from solution.¹¹⁷

The success and perhaps one of the biggest obstacles of nanowire technology relies in being able to assemble these one-dimensional materials and integrate them into nanoelectronics. Establishing routes towards the synthesis of nanowires in a predictable and reproducible way has allowed researchers to move onto the next phase which is to incorporate these structures into functional devices to produce transistors, light-emitting diodes and logic gates.¹¹⁸ Although this area is still under extensive research some advancements have been made by the likes of Lieber and co-workers who have managed to create an integrated nano-circuit using photolithographic techniques (Figure 25).¹¹⁹

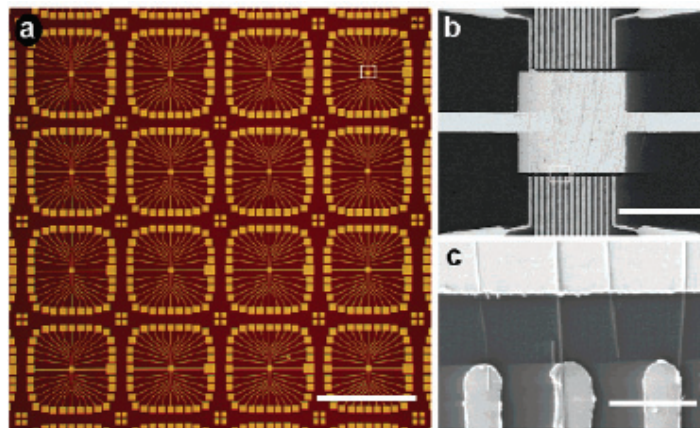


Figure 25 Optical micrograph of integrated metal electrode arrays deposited on top of a patterned parallel nanowire array created by photolithography.¹¹⁹

1.5 Outlook

“I can hardly doubt that when we have some control of the arrangement of things on a small scale we will get an enormously greater range of possible properties that substances can have.”¹²⁰

The current interest in polyoxometalates (POMs) lies in synthesising functional clusters that can also be exploited for their diverse properties. However, the self-assembly process that underpins the formation of many complex POM structures is little understood, and predicting the outcome from ‘one-pot’ strategies is difficult when knowledge of the reactive building blocks in solution is limited. Evidently the drive in understanding and gaining control of reactive building blocks has grown with many research groups taking an active interest in this area of POM chemistry. Nonetheless, efforts to control the reactive synthons can be hampered when control in crystal engineering is difficult to obtain where even subtle changes in synthetic conditions can result in different structures. Rational design of clusters offers a route to producing structures that can have conceivable uses within many areas of chemistry and in particular the nanoworld where there is a significant demand for the miniaturisation of devices; a challenge that could be answered by bottom-up self-assembly.

2 AIMS

Most frequently polyoxometalate synthesis methods employ ‘one-pot’ reaction conditions to create structures of diversity and with a wide range of nuclearity. However, details of the complex formation mechanisms remain scarce, and as such the manipulation of some of the many reaction parameters often represent a straight-forward, but rather serendipitous route to new polyoxometalate architectures. One potential avenue of investigation that may allow the design of larger architectures based on clusters uses polyoxometalate building blocks as synthons. This is because the ability to assemble large cluster systems from smaller known building blocks could be a direct way to systematically control the overall cluster architecture and properties, and thus might form the basis to work towards the growth of nanoscopic clusters of pre-determined structure and function.

The major problem with this approach lies in establishing routes to produce reactive building blocks present in solution, in significant concentrations, and can be reliably utilised in the formation of larger architectures, without re-organising to other unknown fragments. Such limitations may be circumvented by adopting an approach that kinetically stabilises the building block in solution, thereby effectively preventing its reorganisation to other structure types. In order to create materials with enhanced physical properties, a degree of control and understanding of the individual building blocks is required.

These challenges have formed the basis of the investigation which are:

- i) to use a small well-known polyoxometalate to create molybdenum based building blocks or reactive synthons in solution through the use of additional transition metals like silver(I).
- ii) to produce synthons or building blocks through reproducible routes and which can be easily controlled to construct new architectures.
- iii) to gain insight into the molecular growth process as a way to achieve controllable molecular growth through various methods i.e. structure elucidation and solution studies.

-
- iv) investigate the effects that counterion and solvent could have in the isolation of new organic-inorganic clusters.
 - v) to produce multi-functional materials that can exploit the potential properties of the new polyoxometalate clusters.

The construction of polyoxometalate clusters by these methods will hopefully allow the growth of this class of materials on multiple length scales. In doing so it could also provide a route to producing structures that can be used in a number of ways, in particular in the area of materials and nanochemistry. Thus, it is hoped that the clusters can be used not just for their physical properties such as conductivity, redox, magnetic and so on, but also for their size and dimensionality.

3 RESULTS AND DISCUSSION

3.1 The Formation of $\{\text{Ag}(\text{Mo}_8\text{O}_{26})\text{Ag}\}$ Synthons and $\beta\text{-}[\text{Mo}_8\text{O}_{26}]^{4-}$

The predictability that is needed to design complexes can often be influenced by factors such as solvent interaction, presence of a counterion and the nature of both the metal and ligand used. Using ligands with well defined binding sites makes achieving control over the self-assembly process more straightforward and like multi-dentate organic ligands, POMs can take on a similar persona binding readily to secondary transition metals.⁹¹ The advantage of generating or using small metal-oxide clusters is that they have well-defined binding sites, their oxidation states are known, as well as their solubility preferences.

To explore the possibility of creating hybrid materials, the small well-known hexamolybdate anion $[\text{Mo}_6\text{O}_{19}]^{2-}$ was employed under various reaction conditions. The anion can be synthesised with relative ease using various organic counterions and as such is highly soluble in a number of organic solvents. The cluster is formed under highly acidic conditions where the acidification of an aqueous sodium molybdate solution to pH 2 will yield $[\text{Mo}_6\text{O}_{19}]^{2-}$ anions. The organic cation of choice can then be added and the resulting precipitate extracted and re-crystallised to give the final product in good purity.

The overall cluster geometry is octahedral, where each metal bears one terminal oxygen atom and shares an additional four μ_2 -oxygen atoms with adjacent metal centres providing a metal-oxide composite with well-known binding sites. Several secondary transition metals such as copper, cobalt and nickel are known to bind to the terminal oxygen atoms or form complex counterions around the anion.^{121,122} The exploration of the coordination chemistry of this anion and POMs in general with silver is one that is still being established but holds attractive possibilities with respect to producing functional silver-POM architectures. As a transition metal silver(I) is one of the most versatile, displaying a range of geometries and forming between two to six coordination bonds, both making it a prime candidate to act as a linker of polyoxoanions. In addition to this, silver offers many key

chemical and physical properties that make these materials ideal candidates for applications ranging from catalysis, luminescence and conductivity.¹²³⁻¹²⁵

Using $[\text{Mo}_6\text{O}_{19}]^{2-}$ with various organic counterions in the presence of silver and under non-aqueous conditions offers a route to producing functional hybrid materials. However, the repeated formation of β -octamolybdate from hexamolybdate within our structures opened an area of investigation that may allow us to understand the complex cluster formation and rearrangement mechanism occurring in solution; an understanding that is often limited within solution POM chemistry.

To gain a deeper insight into this formation mechanism and to increase our knowledge of the solution chemistry of the above reaction, a series of experiments were carried out. In doing so, these studies also offered an insight into the building block strategy which could be employed within this work. These experiments involved taking various precursors of polyoxomolybdates and complexing them with silver(I) salts. Within this section of studies tetra-*n*-butylammonium (TBA) salts of the POM clusters were used, as these are the simplest compounds to synthesise and allow a degree of control over the products isolated.

3.1.1 Structure Analysis of β - $[\text{Mo}_8\text{O}_{26}]^{4-}$

The well established β -octamolybdate cluster (β - $[\text{Mo}_8\text{O}_{26}]^{4-}$), has binding sites that can be considered as reactive points on the cluster. To our knowledge and what has been observed thus far is that these reactive sites are the terminal and not the bridging oxygen atoms within our structures. Within POMs the terminal oxygen atoms are known to be weakly basic or nucleophilic due to the higher electron density and so are highly attractive towards electrophilic metal centres such as Co, Ni, Mn, to name a few. Figure 26 illustrates the most typical binding sites of β - $[\text{Mo}_8\text{O}_{26}]^{4-}$ to which secondary transition metals can coordinate.^{79,121}

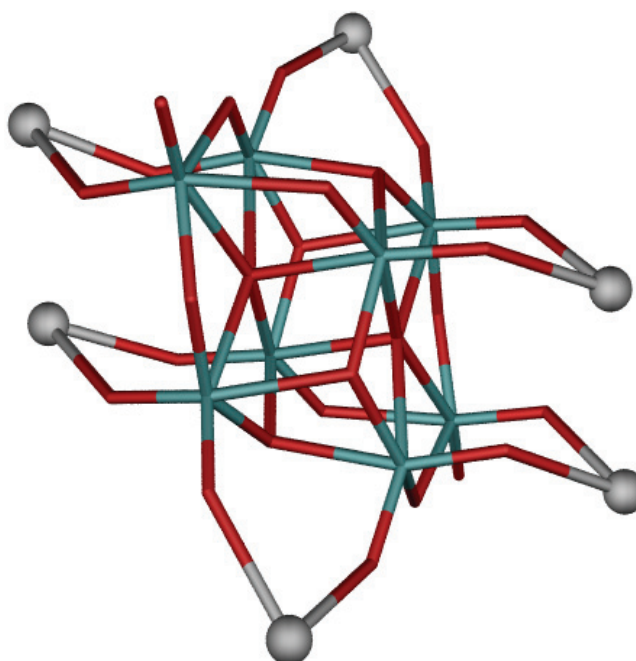


Figure 26 Representation of a β -[Mo₈O₂₆]⁴⁺ cluster with preferred binding sites. Mo: green, O: red, typical coordination modes: grey spheres.

The cluster can be described as a rhombohedral cluster which is made up of two sets of {Mo₄O₁₃} units (Figure 27), each of the sets being assembled from four distorted, corner- and edge-sharing MoO₆ octahedra with seven terminal Mo=O groups. Four of these terminal groups can form square {O₄} arrangements that represent preferred, multidentate coordination sites for electrophilic metal centres. It is also evident that opposite faces of the cluster provide similar coordination environments; hence two {O₄} coordination sites are present per cluster, leading to the formation of {M₂Mo₈O₂₆} units, (M = transition metal).

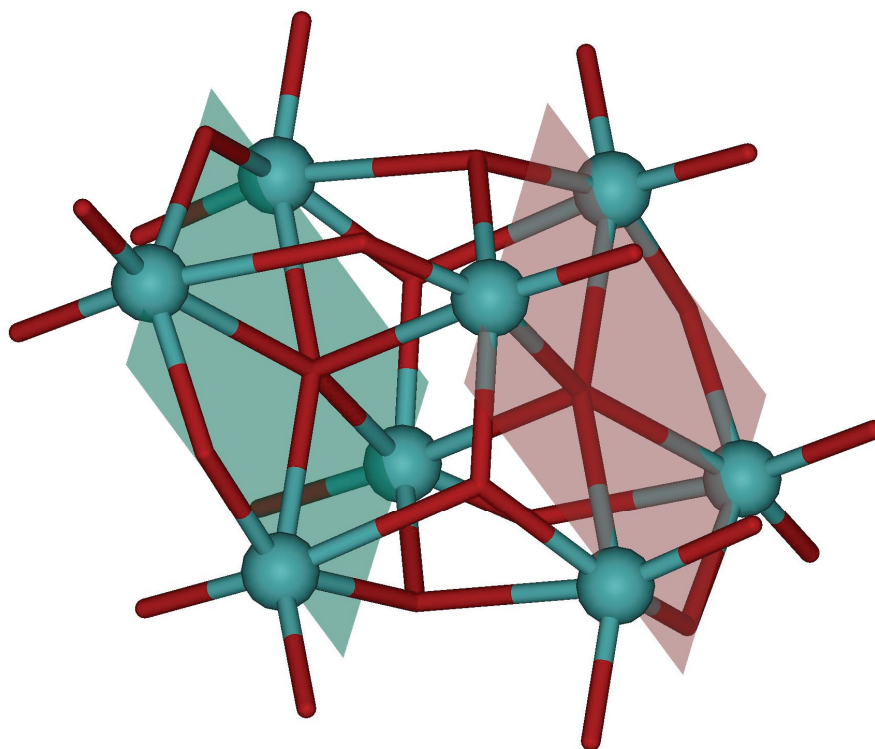


Figure 27 A β - $[\text{Mo}_8\text{O}_{26}]^{4+}$ cluster with the two $\{\text{Mo}_4\text{O}_{13}\}$ units highlighted by a green or red plane. Mo: green spheres, O: red.

3.1.2 The Influence of Silver(I) on $[\text{Mo}_6\text{O}_{19}]^{2-}$, α - and β - $[\text{Mo}_8\text{O}_{26}]^{4-}$

The isolation of a whole family of structurally related compounds by similar syntheses, established the role of silver with the well-known Lindqvist-type polyoxomolybdate, $[\text{Mo}_6\text{O}_{19}]^{2-}$. What has been repeatedly observed is the influence the transition metal can have in converting the precursor, hexamolybdate, $[\text{Mo}_6\text{O}_{19}]^{2-}$ to forming only one out of a possible seven isomers of the octamolybdate cluster, $[\text{Mo}_8\text{O}_{26}]^{4-}$; the beta isomer. The reaction of silver with $[\text{Mo}_6\text{O}_{19}]^{2-}$, regardless of the counterion used, will form structures where the core framework contains $\{\text{Ag}(\text{Mo}_8)\text{Ag}\}$ building blocks. The nature of the silver linker groups and the silver coordination environments in these structures suggest that the building blocks in solution are not individual $\{\text{Ag}_2\}$ and $\{\text{Mo}_8\}$ groups, but are most likely $[\text{Ag}^{\text{I}}\text{-Mo}_8^{\text{VI}}\text{O}_{26}\text{-Ag}^{\text{I}}]$ -type synthons (Figure 28) or fragments of this synthon and will be discussed in more detail later.

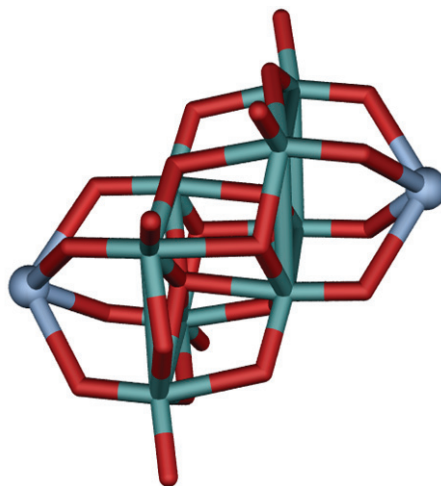


Figure 28 A β - $\{\text{Mo}_8\text{O}_{26}\}$ fragment coordinated to two silver(I) ions. Mo: green, Ag: light blue spheres, O: red.

Previously it has been reported, that the reaction between $((n\text{-C}_4\text{H}_9)_4\text{N})_2\text{Mo}_6\text{O}_{19}$ (**1**) and silver(I) fluoride results in the isolation of a one-dimensional chain of the form $((n\text{-C}_4\text{H}_9)_4\text{N})_{2n}[\text{Ag}_2\text{Mo}_8\text{O}_{26}]_n$ (**4**^{*}, Figure 29).¹²⁶

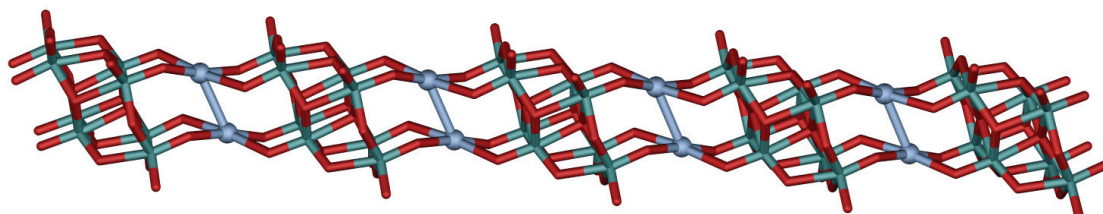


Figure 29 Linking of β - $\{\text{Mo}_8\text{O}_{26}\}$ fragments by silver(I) dimers in **4**. Mo: green, Ag: light blue spheres, O: red (hydrogen atoms and cations removed for clarity).

A detailed account of this structure will be given in the next section (section 3.2.1). However, the most important structural feature of this chain is the linking of β - $\{\text{Mo}_8\text{O}_{26}\}$ fragments by silver(I) dimers (Figure 30). Each Ag(I) ion coordinates to two oxo positions of each $\{\text{O}_4\}$ group to form a virtually planar $\{\text{O}_2\text{AgO}_2\}$ bridging motif (Ag-O distances range between 2.270(17) and 2.414(15) Å, O-Ag-O angles between 81.18(5) and 173.61(5)° for minimum *cis* and maximum *trans* values respectively).

^{*} Compound **4** can be synthesised by two different routes; one which was discovered by Pickering (**4a**) and one developed later (**4b**).

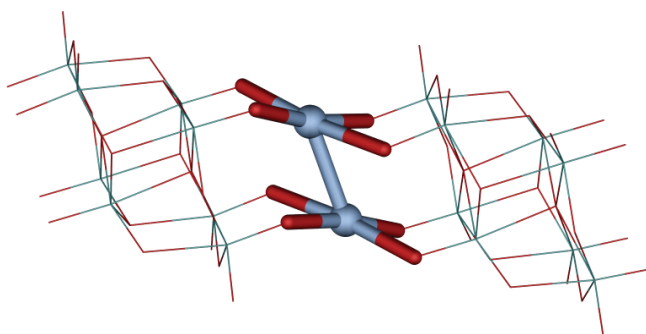


Figure 30 Silver(I) coordination geometry to the oxygen atoms of two $\{\text{Mo}_8\}$ clusters. Mo: green, Ag: light blue spheres, O: red.

Further evidence supporting the presence of Ag-Mo POM fragments was found by using Cryospray Mass Spectrometry (CSMS) to examine reaction mixtures of $[\text{Mo}_6\text{O}_{19}]^{2-}$ and Ag(I) salts in acetonitrile or acetonitrile/ methanol mixtures.

Analysis of a reaction mixture of $((n\text{-C}_4\text{H}_9)_4\text{N})_2\text{Mo}_6\text{O}_{19}$ (**1**) and silver(I) fluoride in acetonitrile shows a peak at $m/z = 1122.63$ that corresponds to the $[\text{Mo}_6\text{O}_{19}]^{2-}$ anion and one TBA cation. The same experiment also shows some interesting speciation of dimolybdate $[\text{Mo}_2\text{O}_7]^{2-}$ which may be an intermediate in the reaction of $\{\text{Mo}_6\}$ to $\{\text{Mo}_8\}$, the specifics of this reaction will be discussed in more detail later (section 3.1.3). The cluster contains molybdenum ions in two different oxidation states where $[\text{Mo}^{\text{VI}}\text{Mo}^{\text{V}}\text{O}_6]^{1-}$ was seen at $m/z = 285.75$. The simulated and observed spectra for both these species show considerable matches (supplementary data section 7.1). In addition to this a peak at $m/z = 699.46$ is observed which corresponds to a $[\text{AgMo}_4\text{O}_{13}]^{1-}$ fragment. This fragment is exactly one half of the $[\text{Ag}_2\text{Mo}_8\text{O}_{26}]^{2-}$ synthon which is thought to be produced in solution and used in the construction of the Ag-Mo POMs. The same peak at $m/z = 699.43$ was observed when $((n\text{-C}_7\text{H}_{15})_4\text{N})_2\text{Mo}_6\text{O}_{19}$ (**2**) was reacted with silver(I) tetrafluoroborate. Further, the experimental spectrum matches the simulated and observed CSMS spectrum for $[\text{AgMo}_4\text{O}_{13}]^{1-}$ (Figure 31) with both spectra showing Gaussian distribution.

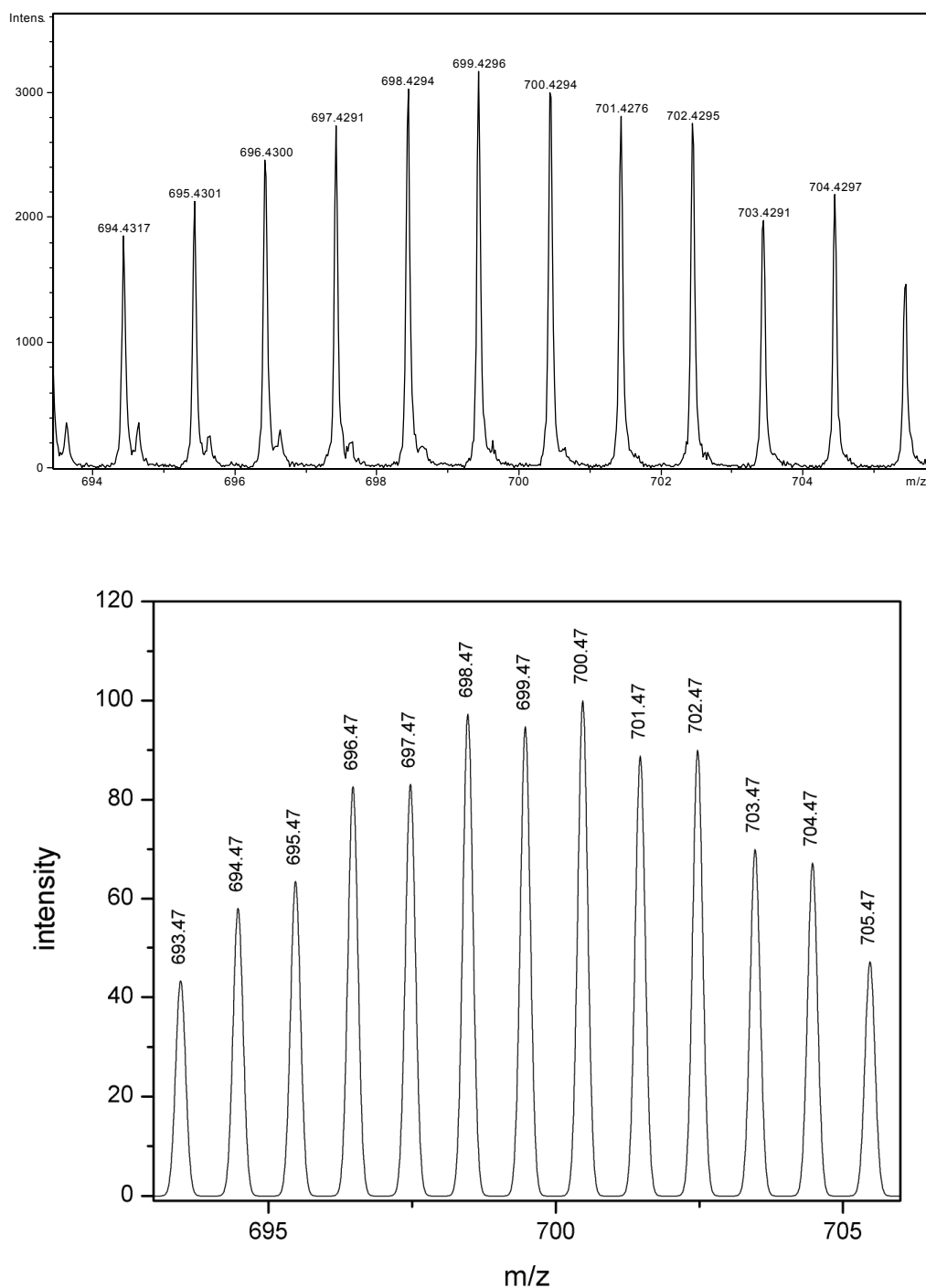


Figure 31 Observed cryospray mass spectrum for $[\text{AgMo}_4\text{O}_{13}]^{1-}$ (top) at $-40\text{ }^\circ\text{C}$ and simulated spectrum (bottom).

A peak at $m/z = 410.64$ from the same reaction can be correlated to a $[\text{AgMo}_2\text{O}_7]^{1-}$ fragment and again the simulated spectrum matches the observed CSMS spectrum (Figure 32). The isolation of this cluster in the solid state has been reported by Gatehouse and Leverett in the form of $\text{Ag}_2\text{Mo}_2\text{O}_7$ clusters linked in a chain like formation.¹²⁷

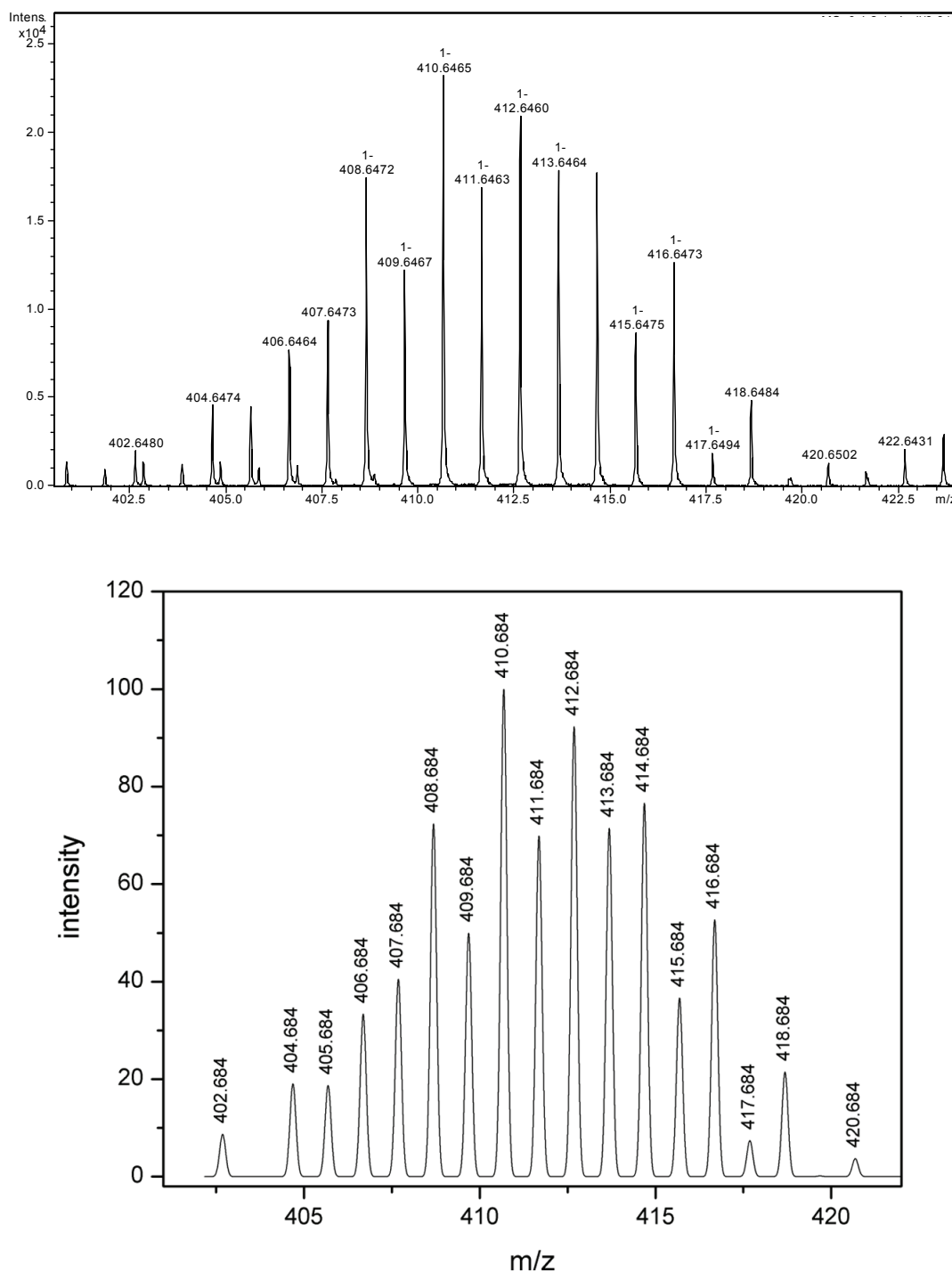
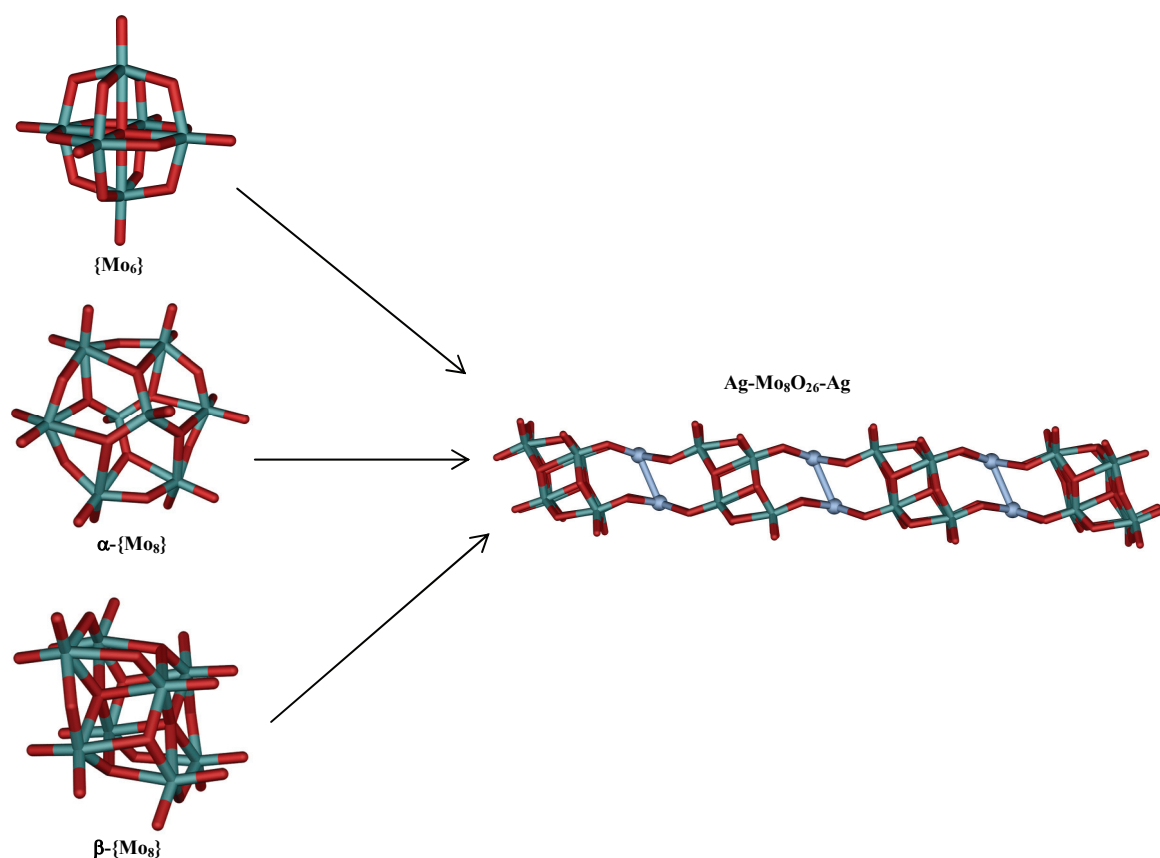


Figure 32 Observed cryospray mass spectrum for $[\text{AgMo}_2\text{O}_7]^{1-}$ (top) at -40°C and simulated spectrum (bottom).

To explore the formation of Ag-Mo POM synthons in solution, further experiments were carried out that were not exclusive to $[\text{Mo}_6\text{O}_{19}]^{2-}$. The experiments used two isomers of $\{\text{Mo}_8\}$; the alpha and beta form that were subsequently reacted with silver salts. The various POM precursors, in particular $\beta\text{-}\{\text{Mo}_8\}$ showed that the resulting structures all

contain the same $\{\text{Ag}(\text{Mo}_8)\text{Ag}\}_\infty$ backbone as in **4**, thus suggesting the formation of Ag-Mo POM synthons in solution (Scheme 2).



Scheme 2 The different polyoxomolybdate precursors which can react with silver to form the $\{\text{Ag}(\text{Mo}_8\text{O}_{26})\text{Ag}\}_\infty$ backbone.

The cluster $\alpha\text{-}((n\text{-C}_4\text{H}_9)_4\text{N})_4\text{Mo}_8\text{O}_{26}$ (**5**) can be obtained in the same way as $(n\text{-C}_4\text{H}_9)_4\text{N})_2\text{Mo}_6\text{O}_{19}$ (**1**), but at a higher pH of *ca.* 4.5, compared with a pH of *ca.* 2.0 for $\{\text{Mo}_6\}$. It has been possible to force the alpha isomer of the octamolybdate cluster, $\alpha\text{-}\{\text{Mo}_8\}$, to form a one-dimensional chain with a $\{\text{Ag}(\text{Mo}_8)\text{Ag}\}$ backbone reminiscent of **4**. The complexation of silver(I) tetrafluoroborate with $\alpha\text{-}((n\text{-C}_4\text{H}_9)_4\text{N})_4\text{Mo}_8\text{O}_{26}$ (**5**) in acetonitrile can yield a chain of the composition $((n\text{-C}_4\text{H}_9)_4\text{N})_{2n}[\text{Ag}_2(\text{CH}_3\text{CN})_2\text{Mo}_8\text{O}_{26}]_n \cdot 2\text{CH}_3\text{CN}$ (**6**). Similarities between the two compounds extend to forming a chain that contains the same backbone framework of $\beta\text{-}\{\text{Mo}_8\}$ fragments linked by silver(I) dimers. In addition to this, complex **6** also coordinates two acetonitrile molecules to all silver(I) sites within the chain (Figure 33). There are two additional acetonitrile solvent molecules within the crystal lattice bringing the total to four

acetonitrile molecules within the asymmetric unit. The remaining asymmetric unit contains two TBA counterions, two silver(I) ions which are not crystallographically equivalent, and two halves of a $\{\text{Mo}_8\}$ cluster.

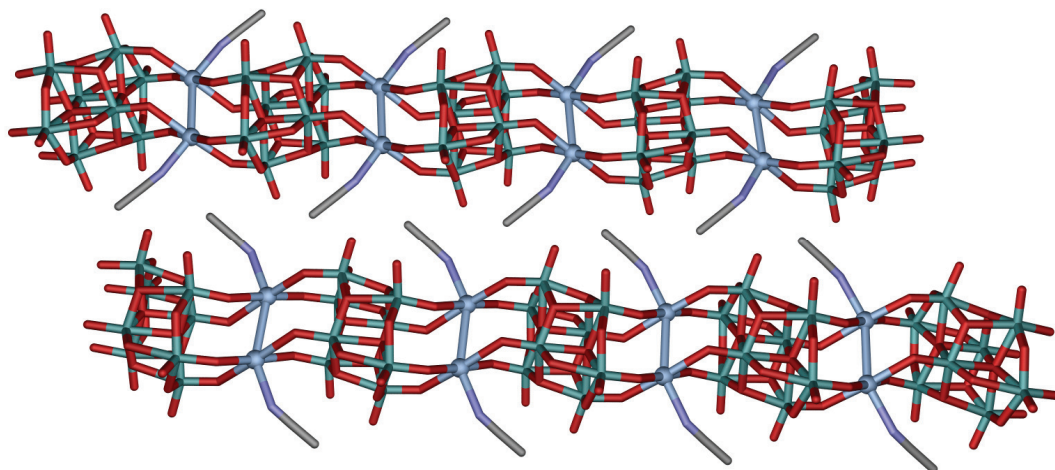


Figure 33 View along the crystallographic a axis of chain 1 (top) and chain 2 (bottom) in **6**. Mo: green, Ag: light blue spheres, O: red, C: grey, N: blue (hydrogen atoms, solvent molecules and cations removed for clarity).

Compound **6** contains two crystallographically unique polymeric chains that run parallel to one another (*intra*-layer distance of 4.875 Å along the crystallographic c axis, *inter*-layer distance of 15.259 Å along the crystallographic b axis, Figure 34). Between each layer of polymers are two layers that contain acetonitrile solvent molecules and TBA counterions. This packing arrangement allows the polymers in one layer to pack closer together as there are no solvent or cation molecules between the chains but rather van der Waals interactions. Hence, the relatively short *intra*-layer distance is primarily due to the A-B-B-A arrangement, where A refers to the layer of polymers and B to the layer of solvent molecules and TBA counterions. With no hydrogen-bonding network present in the crystal lattice, the cation and solvent interactions are minimal with only van der Waals interactions to the oxygen atoms of the POM cluster.

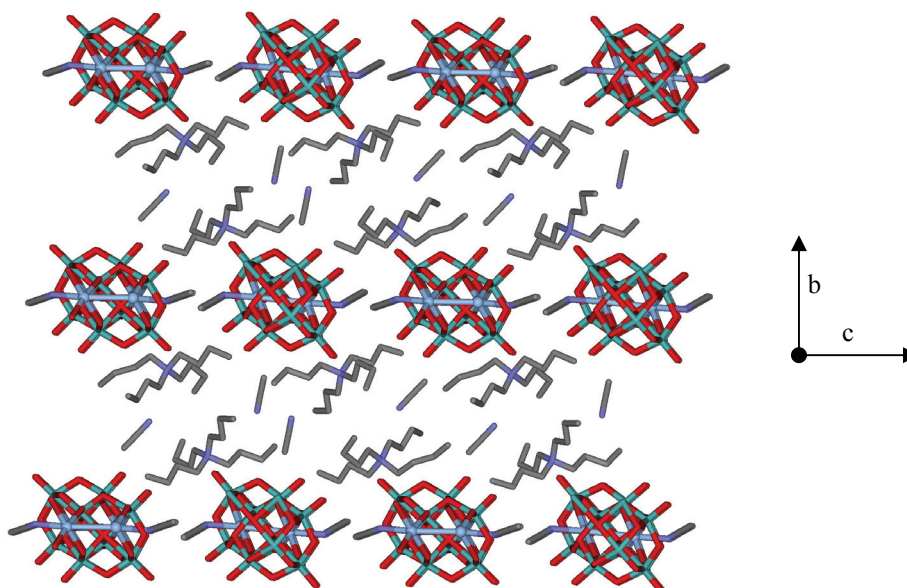


Figure 34 View along the crystallographic *a* axis of **6**. Mo: green, Ag: light blue spheres, O: red, C: grey, N: blue (hydrogen atoms removed for clarity).

The silver(I) ion geometries are similar to those found in **4** with both silver(I) centres displaying distorted square planar geometry (O-Ag-O angles between $72.15(16)^\circ$ to $177.59(17)^\circ$ and $76.08(16)^\circ$ to $177.29(17)^\circ$ for chains 1 and 2 respectively with minimum *cis* and maximum *trans* values for bond angles). The bond distances to oxygen atoms lie within expected ranges (Ag-O distances from 2.396(5) to 2.505(5) Å, and 2.360(5) to 2.444(5) Å for chain 1 and 2 respectively).

The beta isomer of octamolybdate can be made by using α - $((n\text{-C}_4\text{H}_9)_4\text{N})_4\text{Mo}_8\text{O}_{26}$ (**5**) and adding a saturated solution of KBr to form the complex β - $((n\text{-C}_4\text{H}_9)_4\text{N})_3\text{KMo}_8\text{O}_{26}\cdot 2\text{H}_2\text{O}$ (**7**), thereby substituting one of the TBA counterions for potassium and causing the structural rearrangement of the alpha isomer to the beta form. Thus, the KBr solution is necessary for the structural rearrangement.

When **7** was reacted with silver(I) nitrate, complex $((n\text{-C}_4\text{H}_9)_4\text{N})_{2n}[\text{Ag}_2\text{Mo}_8\text{O}_{26}]_n$ (**4c**) was produced, demonstrating that it is also possible to use the building block found in the final product as a precursor in solution and that the synthesis of these chain compounds is not exclusive to $\{\text{Mo}_6\}$ and α - $\{\text{Mo}_8\}$ but can be achieved directly by introducing β - $\{\text{Mo}_8\}$ as a starting material.

In addition to the isolation of **4c**, on occasion a different type of chain can also be isolated. The one-dimensional chain $((n\text{-C}_4\text{H}_9)_4\text{N})_{2n}[\text{KMo}_8\text{O}_{26}\text{Ag}(\text{CH}_3\text{CN})_2]_n$ (**8**) does not consist of the same $\{\text{Ag}(\text{Mo}_8)\text{Ag}\}$ backbone, but instead potassium is associated with the $\beta\text{-}\{\text{Mo}_8\}$ fragments, linking the clusters in a one-dimensional array (Figure 35). The asymmetric unit contains one $\{\text{Mo}_8\}$ cluster to which one potassium and one silver atom is coordinated and there are two further acetonitrile molecules coordinating to each silver position. Finally there are two TBA counterions for charge balance.

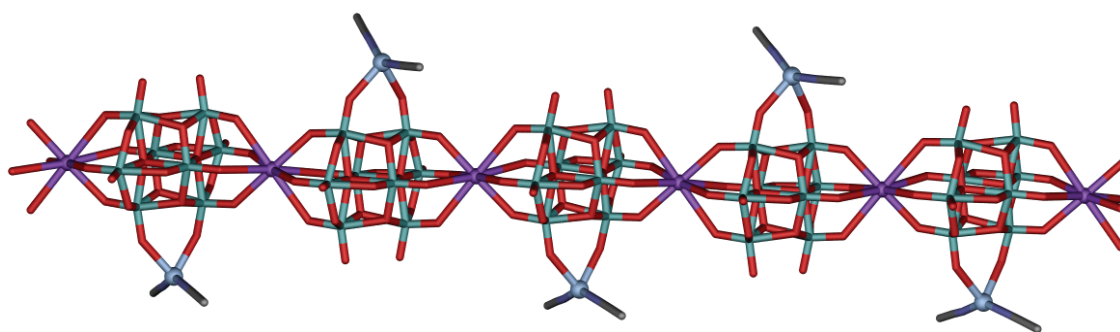


Figure 35 View along the crystallographic c axis of **8**. Mo: green, Ag: light blue spheres, K: purple spheres, O: red, C: grey, N: blue (hydrogen atoms and counterions removed for clarity).

The TBA counterions facilitate the growth of the individual $\{\text{K-Mo}_8\text{-Ag}\}$ building blocks into a one-dimensional chain by nearly encapsulating each individual chain; thus preventing the chains from aligning in close proximity to one another as seen in **6** (Figure 36). The $\text{Ag}(\text{CH}_3\text{CN})_2$ moieties are bound to two surface oxygen atoms of $\{\text{Mo}_8\}$ (Ag-O distances of 2.412(4) and 2.430(4) Å and O-Ag-O angle of 76.25(11)°) and can be found on alternating faces of each $\{\text{Mo}_8\}$ cluster, so that when viewed along the crystallographic c axis they appear in an isotactic fashion (Figure 35). The potassium ion associates with the $\{\text{O}_4\}$ square planar group of two $\{\text{Mo}_8\}$ clusters with an overall square pyramidal geometry (K-O distances between 2.667(3)-3.141(3) Å and O-K-O angles between 57.59(8) and 176.70(8)° for minimum *cis* and maximum *trans* values respectively).

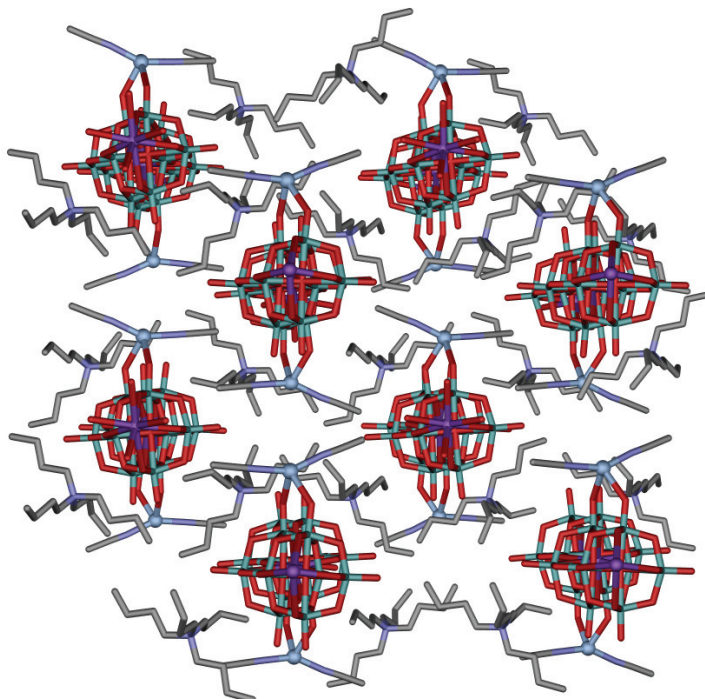


Figure 36 View along the crystallographic *c* axis of **8**. Mo: green, Ag: light blue spheres, K: purple spheres, O: red, C: grey, N: blue (hydrogen atoms removed for clarity).

The two products, **8** and **4c** can be obtained through very similar reaction conditions. Although complex **8** was first isolated through the same synthesis as **4c**, subsequent reactions have shown that the reaction time between the starting materials may be enough to favour one product over another. It appears that to encourage a complete rearrangement and displacement of the potassium ions requires longer reaction times and hence favours the formation of **4c**, and as such a shorter time produces **8**. The source of the potassium ions can be found in the precursor material as a counterion used to form β - $\{\text{Mo}_8\}$ from α - $\{\text{Mo}_8\}$ as discussed previously.

3.1.3 The Formation of β - $[\text{Mo}_8\text{O}_{26}]^{4-}$

The mechanism that forms the β - $\{\text{Mo}_8\}$ fragment in solution remains elusive. What is clearly evident is that the reaction of $\{\text{Mo}_6\}$ or α - $\{\text{Mo}_8\}$ with silver results in a structural re-arrangement of the cluster in order to form $\{\text{Mo}_8\}$ in its beta isomer.

Among the suggested mechanisms is one that involves the decomposition of the $\{\text{Mo}_6\}$ cluster in solution to produce di-molybdate ions, $[\text{Mo}_2\text{O}_7]^{2-}$, which can then re-assemble to form $\beta\text{-}[\text{Mo}_8\text{O}_{26}]^{4-}$.¹²⁸ This suggested mechanism is one that has been derived by the reverse reaction through the formation of $\{\text{Mo}_6\}$ via $\alpha\text{-}[\text{Mo}_8\text{O}_{26}]^{4-}$.¹²⁹

This mechanism is possible if water is present in the reaction giving rise to the following schemes:



This equation can be broken down further to the following to account for the $[\text{Mo}_2\text{O}_7]^{2-}$ ions in solution and builds upon the mass spectroscopy information from section 3.1.2:



Which can be added and reduced to:



To fully comprehend the solution chemistry of $\{\text{Mo}_6\}$ and $\{\text{Mo}_8\}$ would require studies that extend to analysing the spectroscopic results and reaction kinetics that occur during the synthesis of $\beta\text{-}\{\text{Mo}_8\}$. However, there are a number of published structures that reinforce the idea of producing the uncommon di-molybdate ions in addition to Peng and co-workers findings.¹²⁹ The initial discovery of the ion was through degradation of the $\alpha\text{-}[\text{Mo}_8\text{O}_{26}]^{4-}$ cluster by addition of a base.¹³⁰ Klemperer *et al.* put forward some ideas with regards to the stability of the $[\text{Mo}_2\text{O}_7]^{2-}$ ion which appears to be influenced by the nature of the counterion. Their research also suggests that when a non-aqueous solution of $\{\text{Mo}_2\}$ is acidified, characteristic absorptions of $\alpha\text{-}[\text{Mo}_8\text{O}_{26}]^{4-}$ and of $[\text{Mo}_6\text{O}_{19}]^{2-}$ are observed suggesting that $\{\text{Mo}_2\}$, $\{\text{Mo}_6\}$ and $\{\text{Mo}_8\}$ exist in a proton-dependent equilibrium. Dance and co-workers also confirm the isolation of the $\{\text{Mo}_2\}$ ion through a similar methodology.¹³¹ In addition to these findings, a recent publication of a hybrid structure

gives further support to the ability of both β -[Mo₈O₂₆]⁴⁻ and of [Mo₆O₁₉]²⁻ to co-exist in a highly pH dependent solution.¹³²

3.2 Structural Influence by Cation and Solvent

3.2.1 From Monomer to Chain

The $\{\text{Ag}(\text{Mo}_8\text{O}_{26})\text{Ag}\}$ building block was isolated by utilising rigid, bulky cations and solvent molecules. Pickering *et al.* isolated the compound $(\text{Ph}_4\text{P})_2[\text{Ag}_2(\text{DMSO})_4\text{Mo}_8\text{O}_{26}]$ (**9**) by virtue of the bulky tetra-phenylphosphonium (Ph_4P^+) counterion and the capping of the $\{\text{Ag}(\text{Mo}_8)\text{Ag}\}$ synthon by dimethylsulfoxide (DMSO) molecules.¹²⁶ The introduction of the sterically demanding Ph_4P^+ cation and the strongly coordinating DMSO, results in a crystal lattice that is comprised of ‘monomeric’ $\{\text{Ag}(\text{Mo}_8)\text{Ag}\}$ anions (Figure 37).

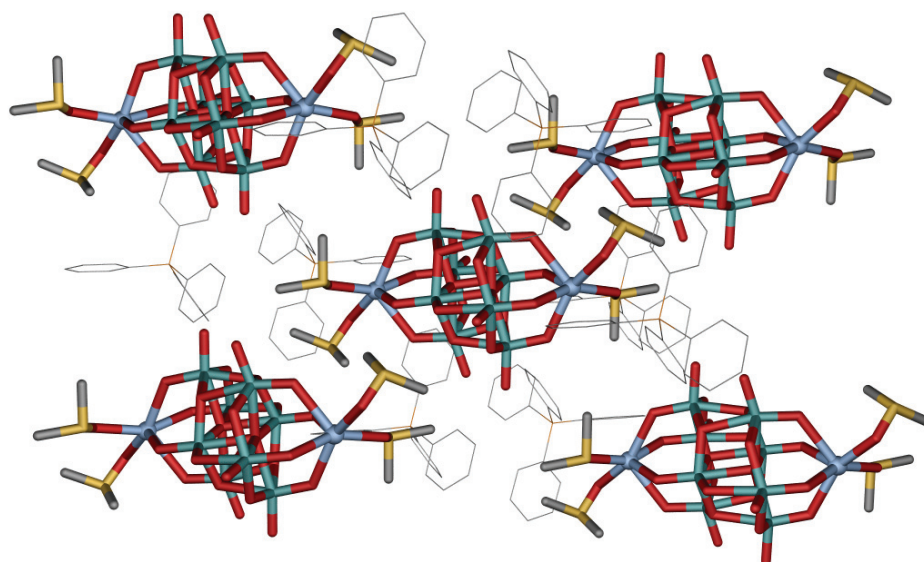


Figure 37 Packing arrangement of **9**. Mo: green, Ag: light blue spheres, C: grey, P: orange, S: yellow (hydrogen atoms removed for clarity).

Reacting two equivalents of silver(I) nitrate with one equivalent of $(\text{Ph}_4\text{P})_2\text{Mo}_6\text{O}_{19}$ in a methanol/DMSO solution yielded colourless block crystals of **9**. Containing two Ag(I) ions, the $\{\text{Ag}(\text{Mo}_8)\text{Ag}\}$ unit is the common component seen in the structures that have already been described. Each silver ion binds or interacts with one square $\{\text{O}_4\}$ face of the $\beta\text{-}[\text{Mo}_8\text{O}_{26}]^{4-}$ anion (Ag-O distances within the range of 2.355(2) to 2.624(2) Å with O-Ag-O angles between 76.99(6) and 155.52(7)° for minimum *cis* and maximum *trans* values

respectively and an inter unit Ag...Ag distance of 7.893 Å). The coordination environment of each silver centre is a distorted octahedron and is completed by further coordination of two DMSO molecules *via* the oxygen atom (Figure 38).

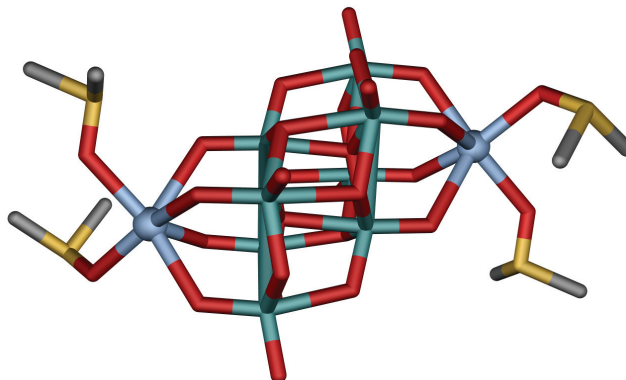


Figure 38 The isolated cluster in **9**. Mo: green, Ag: light blue spheres, C: grey, S: yellow (hydrogen atoms and counterions removed for clarity).

Cluster **9** has an overall charge of -2 and is balanced with two Ph_4P^+ counterions. The DMSO molecules at either end of the molecular unit in effect cap the reactive Ag(I) sites and together with the counterion prevent polymerisation and results in the formation of isolated units. These initial results were supported after further investigations produced various other architectures based on the same building block obtained through variation of the reacting components and counterions.

When the counterion in the precursor material is substituted for a more flexible compound such as tetra-*n*-butylammonium (TBA), the formation of polymeric chains based on the $\{\text{Ag}(\text{Mo}_8)\text{Ag}\}$ synthon can be observed. Pickering *et al.* were able to demonstrate that when $((n\text{-C}_4\text{H}_9)_4\text{N})_2\text{Mo}_6\text{O}_{19}$ is reacted with silver(I) fluoride in an acetonitrile/methanol mixture, a unique one-dimensional chain structure of the composition $((n\text{-C}_4\text{H}_9)_4\text{N})_{2n}[\text{Ag}_2\text{Mo}_8\text{O}_{26}]_n$ (**4**, Figure 39) can be formed.¹²⁶ Comparison of **9** with **4** shows that both compounds are made up of the same building block $\{\text{Ag}(\text{Mo}_8)\text{Ag}\}$.

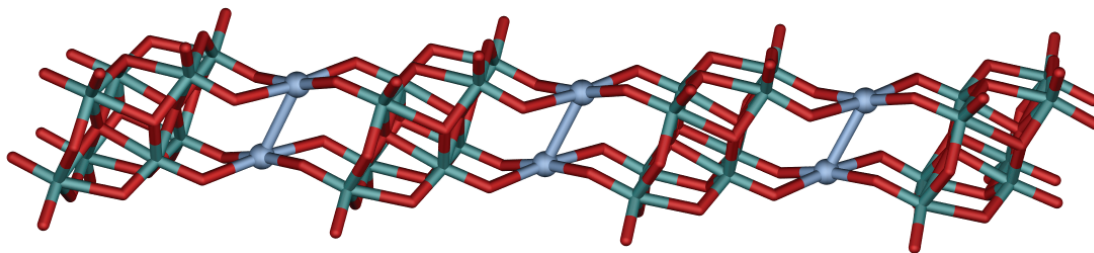


Figure 39 Chain structure of **4**. Mo: green, Ag: light blue spheres, O: red (counterions removed for clarity).

In **4**, the flexible TBA cations nearly completely wrap around the linear chain of linked $[\text{Ag}^{\text{I}}\text{Mo}^{\text{VI}}_8\text{O}_{26}\text{Ag}^{\text{I}}]^{2-}$ units and thereby allow growth in one-dimension only (Figure 40). In the solid state these chains are packed to a network of co-linear, organic ‘tunnels’ that accommodate the polymeric $\{\text{Ag}_2\text{Mo}_8\text{O}_{26}\}_\infty$ anions. All the octamolybdate fragments are identically oriented whereby all $\{\text{O}_4\}$ groups are coplanar, face each other and are linked *via* two Ag(I) centres with an almost square planar geometry. Interestingly, this Ag(I) coordination mode results in Ag...Ag contacts (2.853(4) Å) which are shorter than the sum of the van der Waals radii of two silver(I) ions (3.44 Å),¹³³ suggesting significant silver(I)-silver(I) interactions.

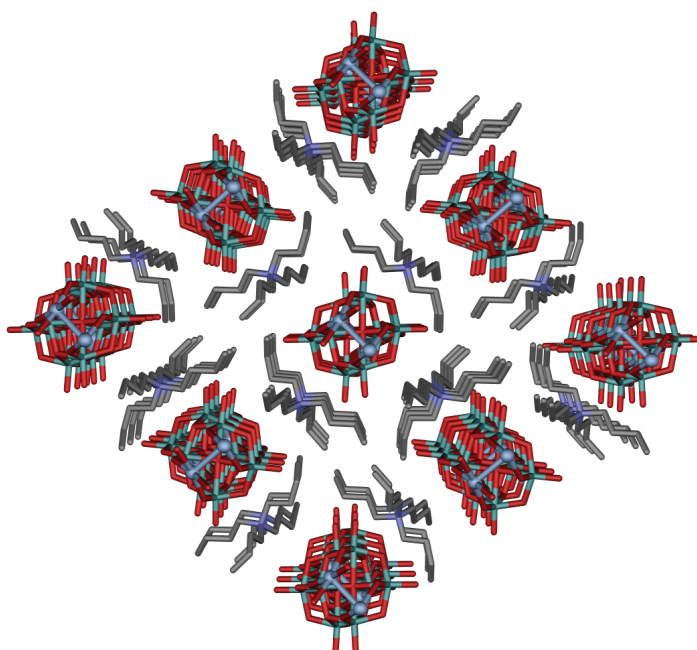


Figure 40 Packing diagram of **4** along the crystallographic *a* axis. Mo: green, Ag: light blue spheres, C: grey, N: blue (hydrogen atoms removed for clarity).

The $\{\text{O}_2\text{AgO}_2\}$ bridging moiety has been observed previously when Gouzerh *et al.* published the first Ag-POM cluster (Figure 41), where the $\{\text{O}_2\text{AgO}_2\}$ bridging moiety holds two $\{\text{Mo}_5\}$ clusters together.¹³⁴ The cluster was also isolated using TBA cations and the NO groups at either end of the cluster as well as the OMe groups appear to be unfavourable towards the binding of Ag(I).

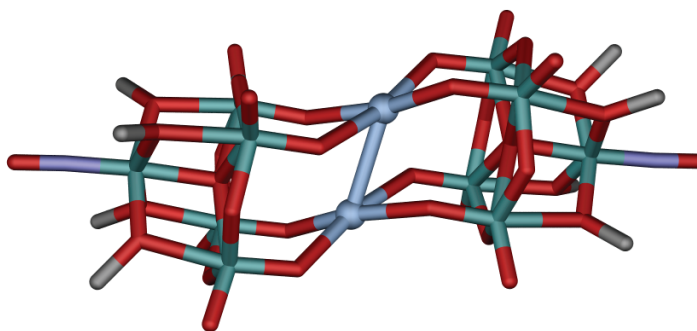


Figure 41 The first example of a Ag linked POM: $((n\text{-C}_4\text{H}_9)_4\text{N})_4[\text{Ag}_2\{\text{Mo}_5\text{O}_{13}(\text{OMe})_4(\text{NO})\}_2]$.¹³⁴ Mo: green, Ag: light blue spheres, C: grey, N: blue (hydrogen atoms and counterions removed for clarity).

3.2.2 Monomeric Clusters

Isolating the monomeric building block that is generated in-situ when forming the polymer **4** demonstrated the subtle control both solvent and counterion can have. This led to the idea that the growth of the individual building blocks into a one-dimensional polymer could probably be influenced by exchanging the counterion (Figure 42).

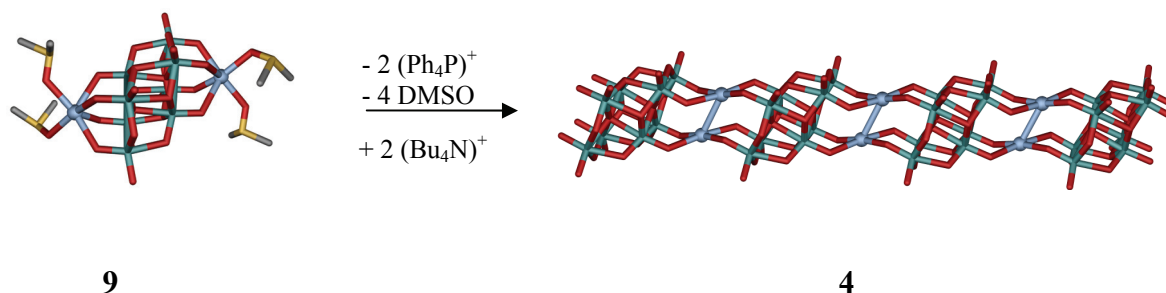


Figure 42 Hypothetical illustration of the molecular growth from the isolated unit **9** into the 1D polymer **4**. Mo: green, Ag: light blue spheres, C: grey, S: yellow (hydrogen atoms and cations removed for clarity).

A stoichiometric amount of the isolated monomer $(\text{Ph}_4\text{P})_2[\text{Ag}_2(\text{DMSO})_2\text{Mo}_8\text{O}_{26}]$ (**9**) was reacted with $((n\text{-C}_4\text{H}_9)_4\text{N})\text{BF}_4$ to displace the rigid bulky Ph_4P^+ counterions within the complex. As in **4** the flexible aliphatic TBA cation has the ability to almost wrap itself around the one-dimensional polymer and cause restricted growth of the $\{\text{Ag}(\text{Mo}_8\text{O}_{26})\text{Ag}\}$ building block into a one-dimensional structure.

The original syntheses of the one-dimensional polymer as already discussed previously used solvent mixtures of both acetonitrile and methanol. In the same way many of the synthetic conditions were retained in order to promote the growth of the isolated unit into polymer **4**. An optimum reaction time of one week allowed the fragments to reassemble in solution and further give the system sufficient time to undergo the growth process to self-assemble into the one-dimensional polymer.

Upon crystallisation however, it was discovered that a new isolated unit, $(\text{Ph}_4\text{P})_2[\text{Ag}_2(\text{CH}_3\text{CN})_2\text{Mo}_8\text{O}_{26}] \cdot 2\text{CH}_3\text{CN}$ (**10**) had been synthesised with substitution of the DMSO ligands present in the precursor with acetonitrile. The silver(I) ions cap the two square faces of the β - $\{\text{Mo}_8\}$ cluster (Ag-O distances ranging from 2.321(4)-2.678(4) Å and O-Ag-O angles between 71.74(14) and 117.19(14)° for minimum *cis* and maximum *trans* values respectively). The coordination requirements of the silver(I) ions are completed by the acetonitrile ligands (N-Ag-O bond angles between 84.47(18) and 155.73(18)°) which create a heavily distorted square pyramidal geometry around the silver. Thus, at each end of the octamolybdate cluster is one silver(I) ion with an acetonitrile ‘arm’ pointing either up or down (Figure 43).

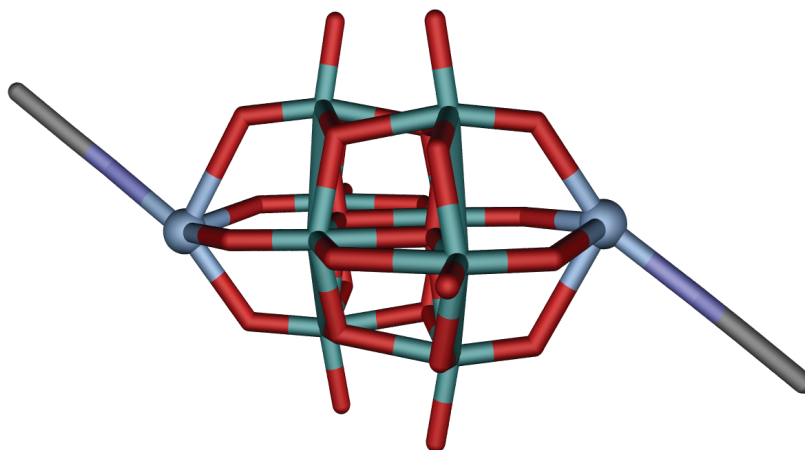


Figure 43 (Ph₄P)₂[Ag₂(CH₃CN)₂(Mo₈O₂₆)]·2CH₃CN (**10**). Mo: green, Ag: light blue spheres, C: grey, N: blue (hydrogen atoms, solvent molecules and cations removed for clarity).

The *trans* position of the arms (to one another, within one cluster) can be attributed to the close proximity of the neighbouring cluster where the arm will point in the opposite direction, again in a *trans* orientation (*intra*-layer distance of 3.647 Å, Figure 44). In addition to this, cations and solvent molecules can also be found positioned close to the arms of the cluster. Thus, the steric requirements of the arms require them to be positioned in this way.

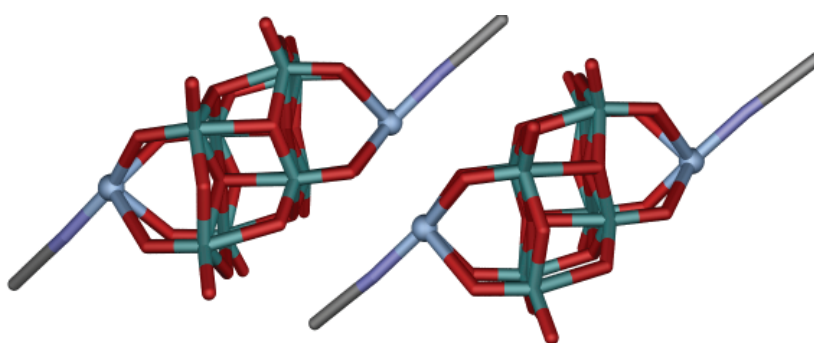


Figure 44 View along the crystallographic *a* axis of **10**. Mo: green, Ag: light blue spheres, O: red, C: grey, N: blue (hydrogen atoms and counterions removed for clarity).

The -4 charge of the {Mo₈} cluster is counterbalanced by not only the two silver(I) ions but also by the two bulky Ph₄P⁺ counterions. Their presence hinders the silver ions on either face of the β-{Mo₈} cluster from approaching too closely and forming short Ag...Ag contacts (intra unit Ag...Ag distance of 3.647 Å, significantly longer than the sum of the

van der Waals radii of two silver(I) ions). Figure 45 illustrates the sequential packing of cluster-cation-cluster forming layers along the crystallographic a axis. In addition to this, solvent acetonitrile molecules provide further stability to the crystal lattice through van der Waals interactions.

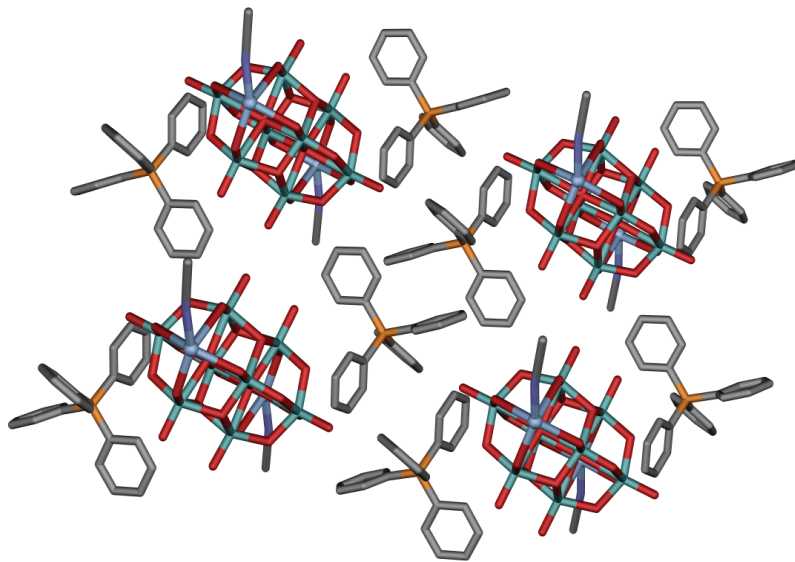


Figure 45 View of **10** along the a axis. Mo: green, Ag: light blue spheres, C: grey, P: orange, N: blue (hydrogen atoms and solvent molecules removed for clarity).

Isolated POM clusters that contain silver often include organic components that have the ability to cap the silvers and prevent further coordination and growth in any direction. The DMSO and acetonitrile molecules that cap the $\{\text{Ag}(\text{Mo}_8)\text{Ag}\}$ synthon in **9** and **10** respectively and in conjunction with the encapsulating cations also prevent further growth. Similar ‘capping’ effects have been studied by Wang *et al.*,¹³⁵ where 2,2’-bipyridine effectively caps Ag(I) ions coordinated to a tungsten based POM. By this means the organic molecules are able to stop cluster growth and produce a monomeric unit rather than a polymeric chain.

3.2.3 One-dimensional Arrays and Chains

As discussed with compound **4**, the direction of growth of the $\{\text{Ag}(\text{Mo}_8)\text{Ag}\}$ synthon can be influenced in a number of ways. The compound $((n\text{-C}_4\text{H}_9)_4\text{N})_{2n}[\text{Ag}_2(\text{CH}_3\text{CN})_2\text{Mo}_8\text{O}_{26}]_n$ (**11**) is an analogue of **4** as both compounds are based on linear arrays of $\{\text{Ag}(\text{Mo}_8)\text{Ag}\}$

building blocks, and the formation of compound **11** is facilitated by the encapsulating ability of the flexible TBA cation. The exception here is that additional acetonitrile ligands coordinate to all Ag(I) positions in compound **11** (Figure 46), similar to the situation found in **6**.

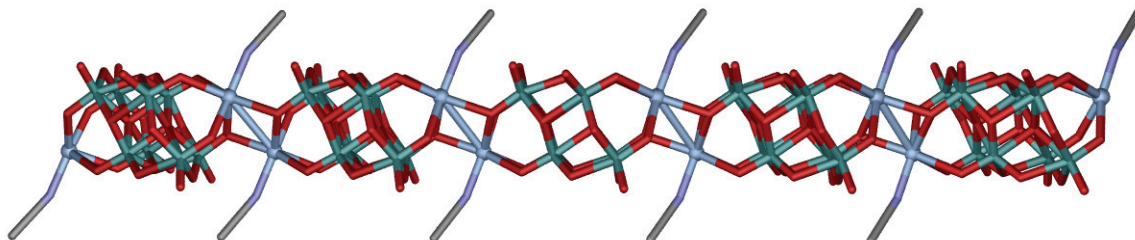


Figure 46 Fragment of **11** along the crystallographic *a* axis. Mo: green, Ag: light blue spheres, O: red, N: blue, C: grey (counterions and hydrogen atoms removed for clarity).

The $\{\text{Ag}_2\}$ bridging groups in the $\{\text{Ag}(\text{Mo}_8)\text{Ag}\}_\infty$ array are characterised by a shift in the Ag centres (relative to the situation found in **4**) so that each Ag(I) ion features a terminal acetonitrile ligand and now caps one $\{\text{Mo}_8\}\text{-O}_4$ group, i.e. chelated in a tetradentate fashion (Ag-O distances in the range of 2.393(2)-2.574(3) Å, O-Ag-O angles between 77.26(8) and 115.58(8)° for minimum *cis* and maximum *trans* values respectively and Ag...Ag distance of 3.454 Å). In addition to this there are also weak Ag-O interactions to the neighbouring $\{\text{Mo}_8\}$ fragment *via* one oxo position of the adjacent $\{\text{O}_4\}$ group (Ag...O distance of 2.630 Å). The TBA counterions, although still surrounding the anionic polymer, are slightly displaced from the polymer (i.e. the channels incorporating the cluster strands in **11** are approximately 1.82 Å wider than in **4** due to the steric requirements of the acetonitrile ligands, Figure 47).

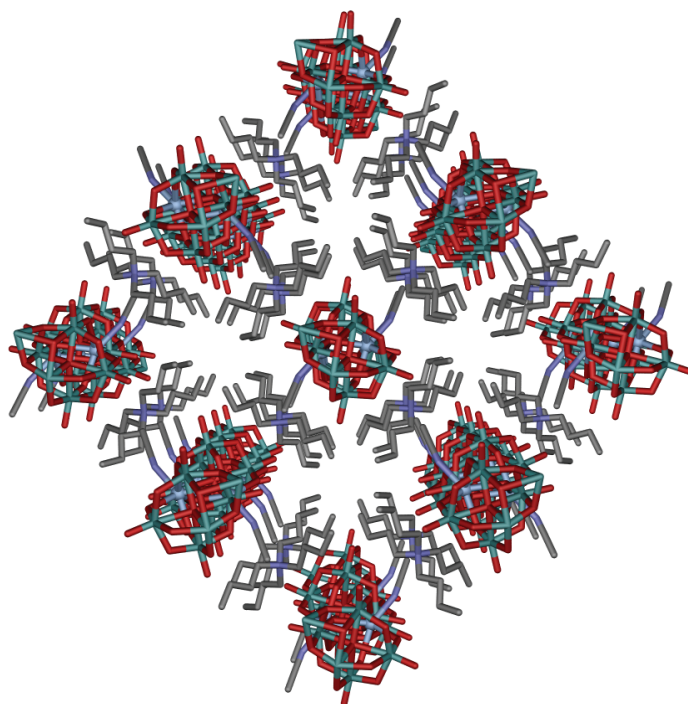


Figure 47 View along the crystallographic *a* axis of **11**. Mo: green, Ag: light blue spheres, O: red, N: blue, C: grey (hydrogen atoms removed for clarity).

Complexation of $((n\text{-C}_4\text{H}_9)_4\text{N})_2\text{Mo}_6\text{O}_{19}$ and silver(I) nitrate with the addition of 2,6-pyridine di-methanol in a 1:2:2 ratio respectively results in the formation of a one-dimensional array separated by complex aromatic cations. It has been possible to displace the TBA counterion from the $\{\text{Mo}_6\}$ precursor by using 2,6-pyridine di-methanol to yield the structure $[\text{Ag}(\text{C}_7\text{H}_{12}\text{O}_2\text{N})(\text{CH}_3\text{CN})]_{2n}[(\text{Ag}(\text{CH}_3\text{CN}))_2\text{Mo}_8\text{O}_{26}]_n \cdot 2\text{CH}_3\text{CN}$ (**12**). The asymmetric unit consists of one half of a $\{\text{Mo}_8\}$ cluster bound to one silver(I) ion with one coordinated acetonitrile molecule, one 2,6-pyridine di-methanol complex cation as well as one acetonitrile solvent molecule.

The isolated units of **12** are arranged or held in a one-dimensional array through weak Ag...Ag interactions (Ag...Ag distance of 3.181(6) Å). The silver(I) ions displaying ‘T’ geometry (Figure 48) are complexed to two oxygen atoms adjacent to one another on the $\{\text{Mo}_8\}$ cluster, and to the nitrogen from a coordinating acetonitrile molecule (Ag-O distances of 2.510(3) and 2.346(2) Å with O-Ag-O bond angles of 78.59(8)°).

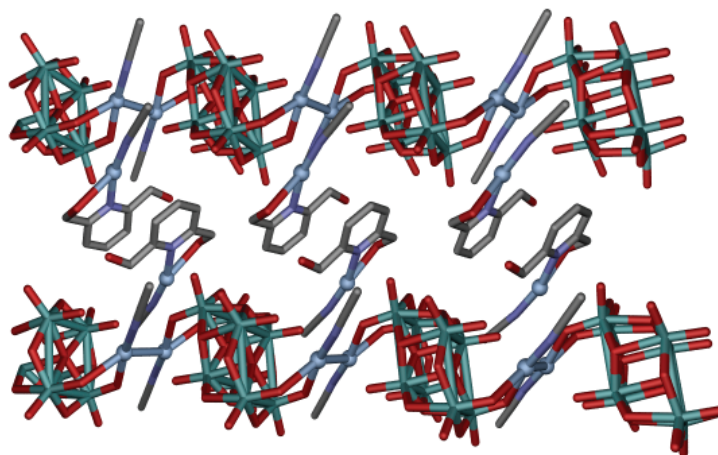


Figure 48 Fragment of **12** along the crystallographic *a* axis. Mo: green, Ag: light blue spheres, O: red, C: grey, N: blue (hydrogen atoms and solvent molecules removed for clarity).

The structure is reinforced by interactions between the silver(I) ions (which are crystallographically equivalent) and to the remaining terminal oxygen atoms on the same face of the cluster (Ag...O distance of 2.765 and 2.799 Å, Figure 49).

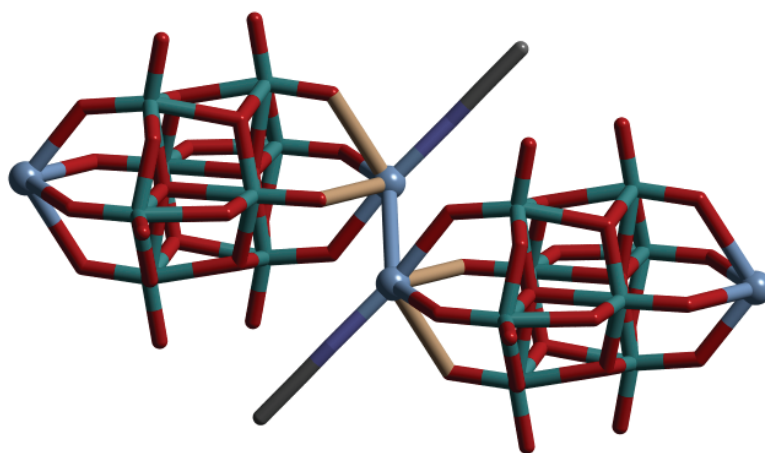


Figure 49 Ag...O interactions shown in pale pink between Ag(I) and remaining terminal oxygen atoms of the cluster. Mo: green, Ag: light blue spheres, O: red, N: blue, C: grey (hydrogen atoms and solvent molecules removed for clarity).

The 2,6-pyridine di-methanol complex counterions have the ability to promote the growth of the building blocks into a one-dimensional array. The nitrogen of the pyridine and the oxygen on one of the CH₂OH arms is coordinating to a third crystallographically different silver(I) ion which further coordinates to an acetonitrile molecule forming an extended

'tail' on the counterion ($\text{N-Ag-N} = 166.60(11)^\circ$). The cations are stacked in pairs but not directly above one another so that when viewed down the crystallographic a axis they are 'off centre' (Figure 50). Hence, there may also be π - π interactions and the complex cation provides support to the crystal lattice through hydrogen bonding interactions. As illustrated in Figure 50, the cations form layers parallel to the layer of polymers along the crystallographic b axis (*intra*-layer and *inter*-layer distance between polymers is 3.340 Å and 12.115Å respectively), consequently meaning that the one-dimensional arrays are separated not completely by the cations, but rather by the 'tail' on the cation and the coordinated acetonitrile molecules.

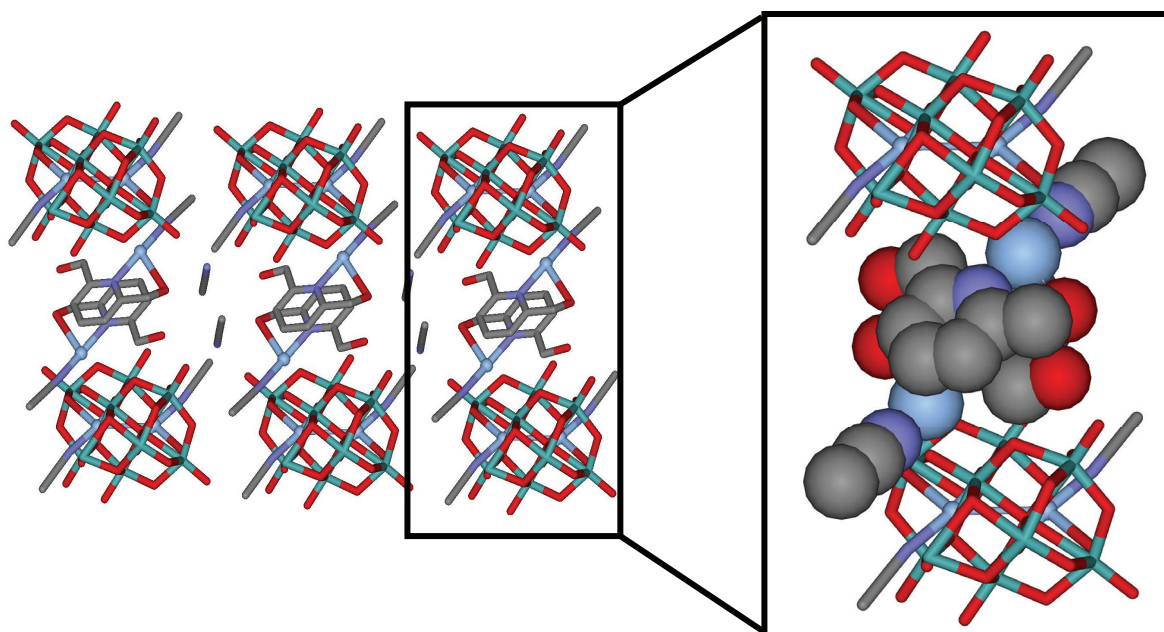


Figure 50 View along the crystallographic a axis of the cluster-cation packing in **12**. Inset: space-filled representation of cation to illustrate the effect of the $\text{Ag-(N}\equiv\text{C-CH}_3$) 'tail'. Mo: green, Ag: light blue spheres, O: red, N: blue, C: grey (hydrogen atoms removed for clarity).

The space-filling representation (Figure 50, inset) provides a better idea of the interactions between the complex counter ion and the POM cluster. The extended 'tail' on the counterion may be responsible for the silver(I) ions only forming weak interactions and thus the $\{\text{Ag}(\text{Mo}_8)\text{Ag}\}$ building blocks remain as isolated units. The 'tails' on the complex counterions are positioned very closely to the remaining terminal oxygen atoms of the cluster, which only form weak interactions to the silver(I) ions which are coordinated to the cluster. This may also be why the silver(I) ions are prevented from forming formal bonds to the terminal oxygen atoms of the POM. The acetonitrile molecules coordinated to

the silver(I) ions within the cluster may also prevent the ions from approaching each other too closely and forming significant Ag...Ag interactions.

Non-capping solvent molecules have also been instrumental in the growth of the $\{\text{Ag}(\text{Mo}_8)\text{Ag}\}$ synthon in the presence of the bulky Ph_4P^+ counterion. Crystallisation of $(\text{Ph}_4\text{P})_2\text{Mo}_6\text{O}_{19}$ with silver(I) nitrate from *N,N*-dimethylformamide (DMF) leads to the formation of $[\text{Mo}_8\text{O}_{26}]^{4-}$ capped by silver(I) dimers on either side, forming a chain with the composition $(\text{Ph}_4\text{P})_{2n}[\text{Ag}_2(\text{DMF})_2\text{Mo}_8\text{O}_{26}]_n \cdot 2\text{DMF}$ (**13**). The asymmetric unit contains one half of an $\{\text{Mo}_8\}$ cluster, one silver(I) ion, one Ph_4P^+ counterion and one coordinated and one non-coordinated DMF molecule.

The silver atoms link two $[\text{Mo}_8\text{O}_{26}]^{4-}$ units through two oxo positions of each $\{\text{O}_4\}$ group to form a virtually planar $\{\text{O}_2\text{AgO}_2\}$ bridging group, analogous to **4** and **6** (Ag-O distances ranging from 2.406(4)-2.489(4) Å and O-Ag-O angles between 73.87(12) and 177.65(3)° for minimum *cis* and maximum *trans* values respectively). The structure is further stabilised by interactions to the adjacent silver atom and to the oxygen atom of a DMF molecule (Ag...Ag distance of 3.130(9) Å and Ag-O distance of 2.398(5) Å). As such, the silver dimers exist in a distorted square pyramidal environment (Figure 51).

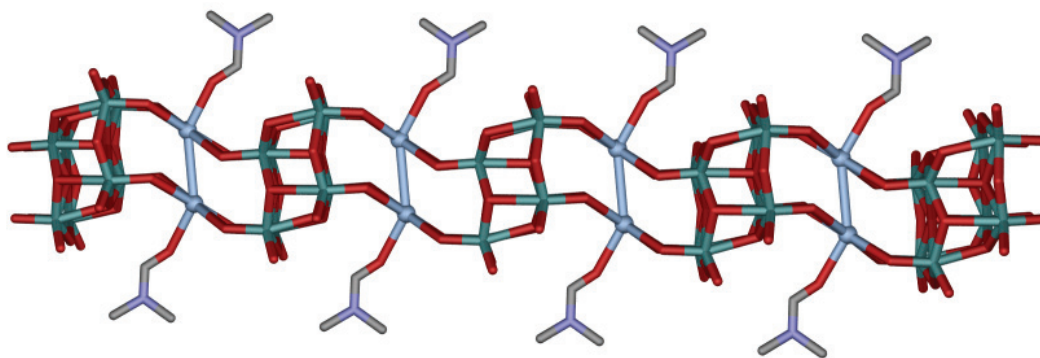


Figure 51 View of the polymeric chain found in **13** along the crystallographic *b* axis. Mo: green, Ag: light blue spheres, O: red, N: blue, C: grey (counterions, hydrogen atoms and solvent molecules removed for clarity).

Each monomeric cluster unit has a charge of -2 which is balanced by two Ph_4P^+ ions. These cations are bulky and exclude interactions with other chains, thus preventing cross-linking into a two-dimensional network (Figure 52). Previously we discussed the unit

(Ph₄P)₂[Ag₂(DMSO)₄Mo₈O₂₆] (**9**), where the use of the bulky Ph₄P⁺ cation and the capping of the silver(I) ions by additional DMSO ligands allowed the isolation of this unit. In **13** however, the DMF does not act as a capping unit but as ‘spacers’, creating a void between the bulky counterions and allow the {Ag(Mo₈)Ag} synthon to extend in one direction forming chains which was not possible in **9** and in structure **10**.

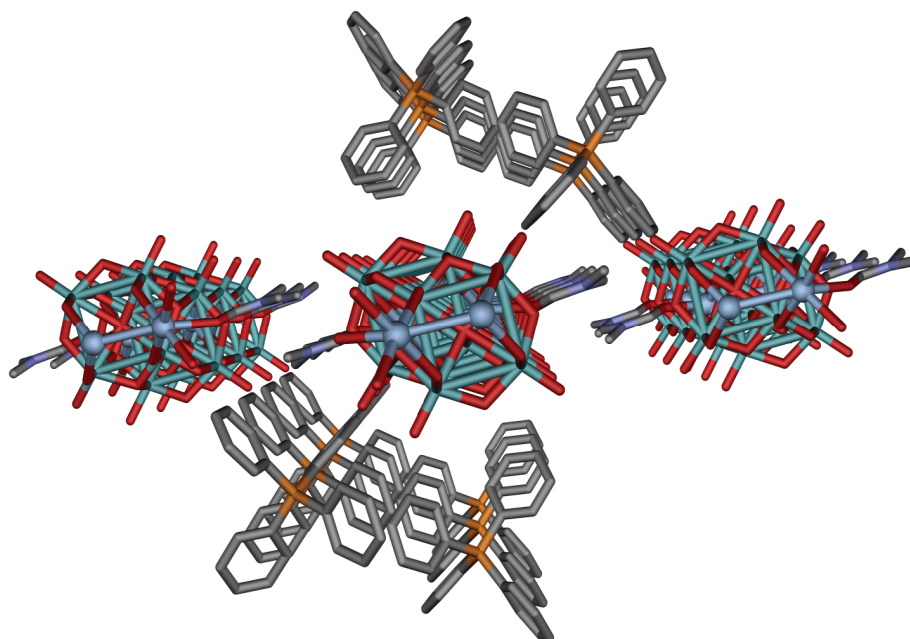


Figure 52 View of the polymeric chain in **13** along the crystallographic *b* axis. Mo: green, Ag: light blue spheres, O: red, N: blue, C: grey, P: orange (hydrogen atoms and solvent molecules removed for clarity).

The Ph₄P⁺ cation no longer has the ability to cause restricted growth of the synthon as in complex **13**, so there is not complete encapsulation by the cation. In addition, the presence of solvent DMF molecules in the crystal lattice further prevents the counterion from approaching the {Ag(Mo₈)Ag} synthon.

It is possible to form architectures from the {Ag(Mo₈)Ag} synthons without the inclusion of the original organic counterion from the {Mo₆} precursor. To the best of our knowledge the constraints of the Ag-Mo POM structures in the solid-state do not allow the inclusion of large bulky cations such as tetra-*n*-hexylammonium, ((*n*-C₆H₁₃)₄N). Hence the charge is either balanced by incorporating extra silver(I) ions or as in compound (H₂NMe₂)_{2n}[Ag₂(DMF)₂Mo₈O₂₆]_n·2DMF (**14**) by protonated dimethylamine, a

decomposition product of the solvent DMF can be found interspersed between the chains. Mixing two equivalents of silver(I) nitrate with one equivalent of $((n\text{-C}_6\text{H}_{13})_4\text{N})_2\text{Mo}_6\text{O}_{19}$ in DMF, produces the one-dimensional structure **14**. The asymmetric unit contains again one half of an $\{\text{Mo}_8\}$ cluster, one silver(I) ion, two DMF molecules one of which is coordinated to the Ag in the Ag-POM framework and one protonated dimethylamine cation.

The chain structure of **14** is made up of $\beta\text{-}\{\text{Mo}_8\}$ building blocks which are linked by the $\{\text{Ag}_2\}$ dimers to give a one-dimensional chain. Each silver ion coordinates to two oxygen atoms of the square $\{\text{O}_4\}$ arrangement of one $\beta\text{-}\{\text{Mo}_8\}$ unit (the Ag-O distances range from 2.461(5)-2.492(5) Å and the O-Ag-O angles range between 74.36(15) and 174.99(14)° for minimum *cis* and maximum *trans* values respectively, Figure 53). The silver ions with distorted square pyramidal geometry are crystallographically equivalent (Ag...Ag distance of 3.020(10) Å) and each ion further coordinates to a solvent DMF molecule (the Ag-O{DMF} distance is 2.491(4) Å).

Again the counterions and the coordinated DMF molecules prevent the chains from cross-linking and forming a two-dimensional network. The chain is comparable to **4** and even more so to **13**. The slightly shorter Ag...Ag interactions could be attributable to the direction in which the coordinated DMF ligands are arranged in complex **14**, where the DMF ligands appear to be pointing in a *trans* oriented arrangement when compared to **13** where the ligands are in the plane.

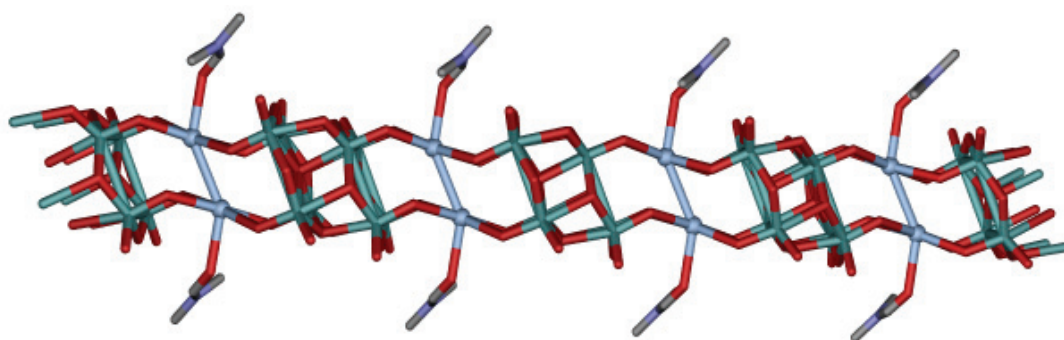


Figure 53 Illustration of the polymeric chain in **14** linked *via* two Ag(I) ions to each $\{\text{Mo}_8\text{O}_{26}\}$ fragment. Mo: green, Ag: light blue spheres, C: grey, N: blue (counterions, solvent molecules and hydrogen atoms removed for clarity).

Protonated dimethylamine counterions and solvent DMF molecules (Figure 54) are arranged between the cations and provide stability to the crystal lattice by forming hydrogen-bonding contacts to a bridging oxygen of the $\{\text{Mo}_8\}$ cluster, to the oxygen of the coordinated DMF and the solvent DMF molecule (N-H...O distances range from 2.680 to 3.019 Å).

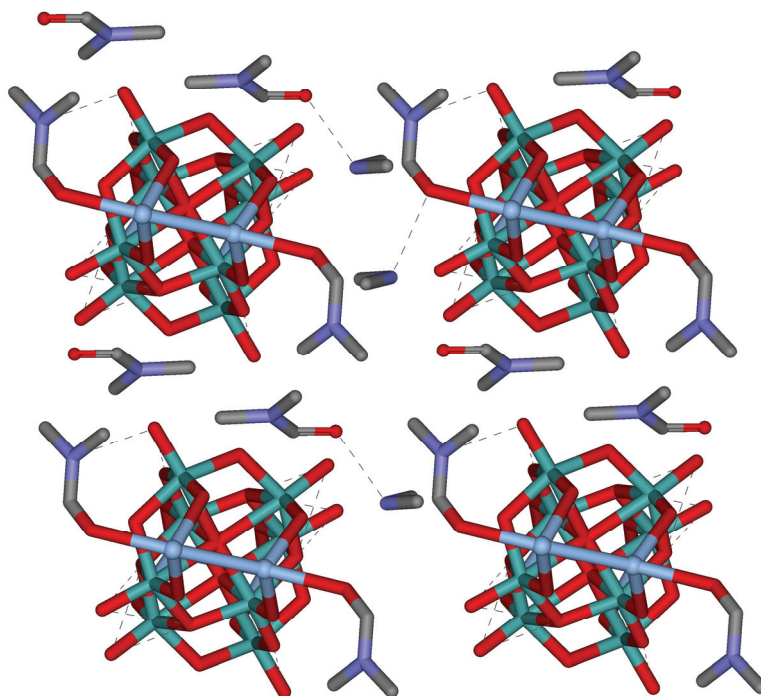


Figure 54 View of hydrogen bonding interactions between counterions, solvent molecules and the chains in **14**. Mo: green, Ag: light blue spheres, C: grey, N: blue (hydrogen atoms removed for clarity).

There is no evidence of an interaction between the chains which extend along the a axis (selected *inter-chain* distances range from 3.699–8.307 Å when measured from the coordinated DMF molecules and terminal oxygen atoms on the cluster).

In each of the complexes presented in this section, the isolation of the one-dimensional structures is facilitated by either the counterion or solvent, or a combination of the two. Thus, the restricted growth of the building blocks in only one direction forms polymers which will align along only one axis and the space between each chain is consequently filled by cations or solvent molecules which act as spacers and therefore prevent cross-linking into a two-dimensional array (Figure 55).

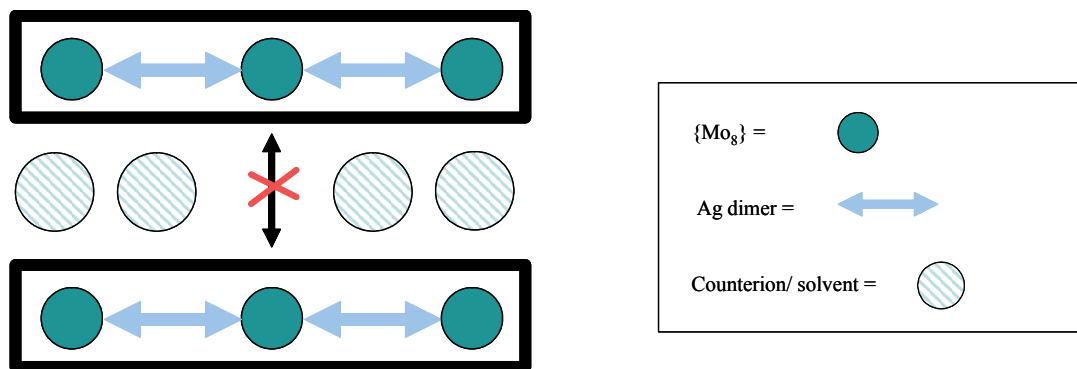


Figure 55 Illustration of the counterion induced growth or inhibition and the resulting formation of a $\{\text{Ag}(\text{Mo}_8)\text{Ag}\}_\infty$ chain.

3.2.4 Two-dimensional Arrays

The flexible TBA cation can also facilitate the growth of one-dimensional chains into a two-dimensional array. Using a methanol/DMSO solution, the complexation of one equivalent of silver(I) fluoride to two equivalents of $((n\text{-C}_4\text{H}_9)_4\text{N})_2\text{Mo}_6\text{O}_{19}$ yielded colourless block crystals on diffusion with ethanol to give $((n\text{-C}_4\text{H}_9)_4\text{N})_{2n}[\text{Ag}_2(\text{DMSO})_2\text{Mo}_8\text{O}_{26}]_n$ (**15**). The asymmetric unit contains two halves of a $\{\text{Mo}_8\}$ cluster to which each is coordinated one silver atom (and which are crystallographically different to one another), two DMSO molecules and two TBA counterions.

Compound **15** is of special interest as it contains two types of chains (*a* and *b*) of $\{\text{Ag}(\text{Mo}_8)\text{Ag}\}_\infty$ building blocks with different silver linking groups that cross-over in alternatively packed layers, whereby the angle between the chains of neighbouring layers equals to approximately 86° (Figure 56).

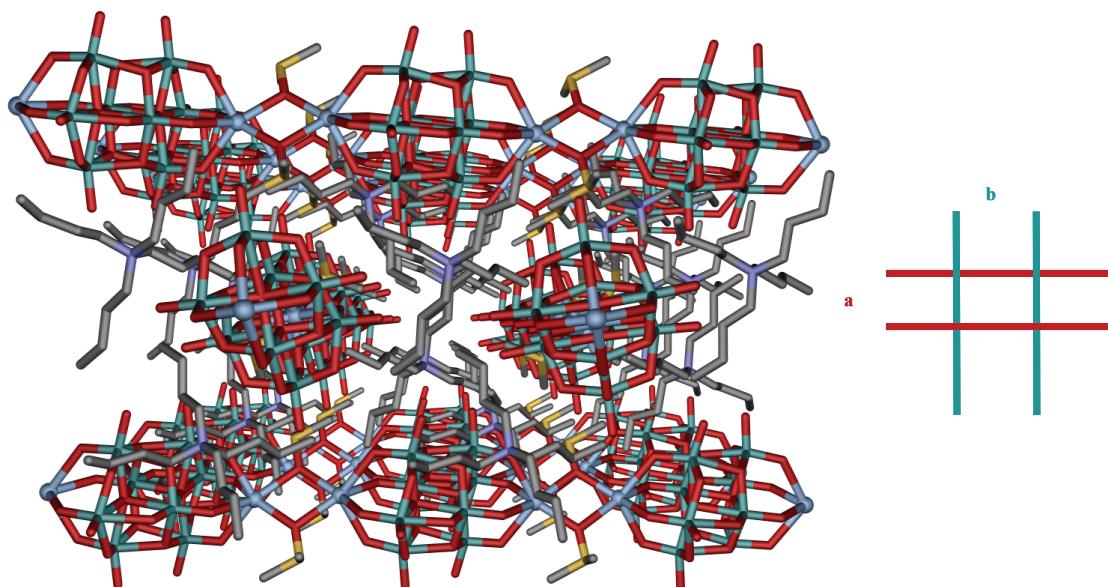


Figure 56 The two-dimensional arrangement of the chains in **15**. Mo: green, Ag: light blue spheres, S: yellow, O: red, C: grey, N: blue (hydrogen atoms removed for clarity).

In both types of chains the silver positions are not directly bridging the $\{\text{Mo}_8\}$ units, but each silver centre is coordinated to only one $\{\text{Mo}_8\}$ cluster. Neighbouring silver centres are then linked *via* two DMSO ligands to form $(\text{O}_4)\text{Ag}(\mu_2\text{-DMSO})_2\text{Ag}(\text{O}_4)$ bridges between the adjoining $\{\text{Mo}_8\}$ fragments (Figure 57). The two chain types differ in the bridging mode of the DMSO ligands: in *a*-type chains, both Ag(I) positions coordinate to the μ_2 -oxo centres of the DMSO molecules (Ag- μ_2 -O(SC₂H₆) distances are 2.366(3)/2.493(3) Å, with a Ag...Ag distance of 3.889(6) Å). In *b*-type chains, the Ag...Ag distance is widened (Ag...Ag distance of 4.848(6) Å) due to the bidentate bridging mode of the two DMSO ligands *via* the oxygen and sulfur position of each molecule (Ag- μ_2 -O(SC₂H₆) distances of 2.514 Å and Ag- μ_2 -S(OC₂H₆) 2.462 Å).

In addition, while in chains of type *a* the silver positions cap all four oxo positions of an $\{\text{O}_4\}$ group (Ag-O distances between 2.480(3) and 2.564(3) Å and O-Ag-O lengths between 73.73(11) to 146.37(10)° for minimum *cis* values and maximum *trans* values respectively), the silver centres in type *b*-chains coordinate to only two of the four oxo positions (Ag-O distances of 2.364(3) and 2.394(3) Å, and O-Ag-O lengths between 77.53(15) to 142.37(19)° for minimum *cis* values and maximum *trans* values respectively).

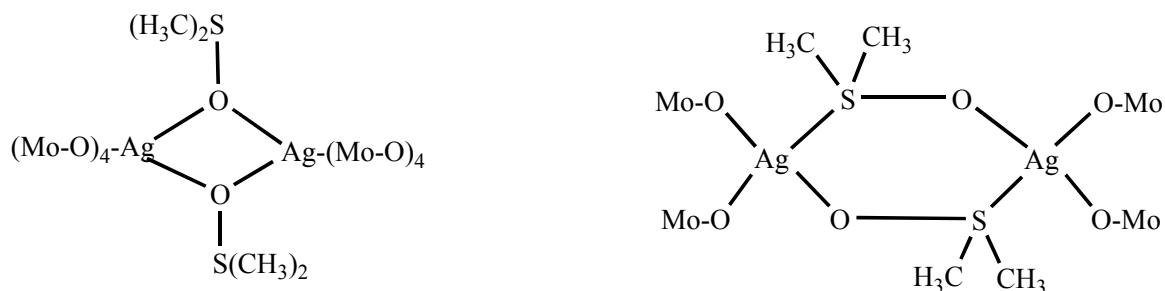


Figure 57 The two types of bridging modes in **15**; type *a* (LHS) and type *b* (RHS).

If the steric shielding ability of the organic cations is reduced, this ‘insulation’ can partly be disrupted and the electrophilic polyoxomolybdate chains can be interlinked, illustrating the versatility of using counterions as a route to new cluster-based networks. When for example the TBA cations in the reaction system are replaced with less bulky tetra-*n*-propylammonium ($(n\text{-C}_3\text{H}_7)_4\text{N}$), TPA) cations, compound $(\text{HDMF})_n[\text{Ag}_3(\text{DMF})_4\text{Mo}_8\text{O}_{26}]_n$ (**16**) with a planar infinite grid structure of $\{\text{Ag}(\text{Mo}_8)\text{Ag}\}_\infty$ strands (Figure 58) results in the presence of protonated DMF. In this case the TPA cations are *not* incorporated into the compound but are replaced by protonated DMF (HDMF^+) cations and additional silver(I) ions. Here neighbouring $\{\text{Mo}_8\}$ fragments in each strand are linked *via* two $\text{Ag}(\text{DMF})$ groups that each bridge two oxo positions of a $\{\text{Mo}_8\}\text{-O}_4$ group with two oxo-positions of the $\{\text{O}_4\}$ group of a neighbouring $\{\text{Mo}_8\}$ group, forming a virtually planar $\{\text{O}_2\text{AgO}_2\}$ bridging motif similar to that in **4**, but resulting in a slightly longer $\text{Ag}\dots\text{Ag}$ interaction ($\text{Ag}\dots\text{Ag}$ distance of 3.148(6) Å).

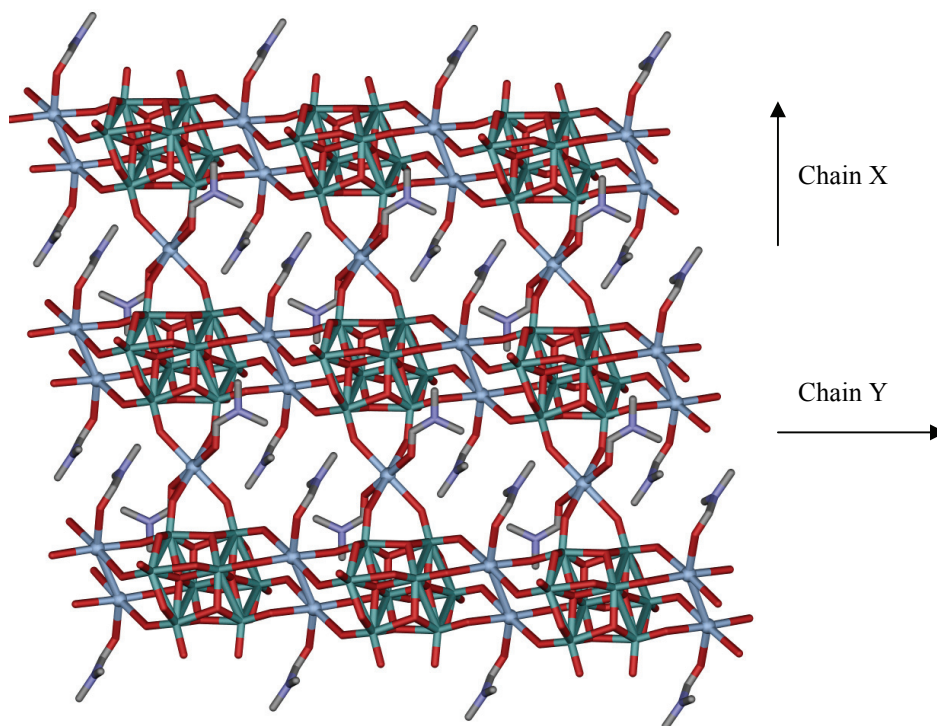


Figure 58 View along the crystallographic c axis of **16**. Mo: green, Ag: light blue spheres, O: red, C: grey, N: blue (hydrogen atoms and counterions removed for clarity).

Due to the absence of encapsulating TBA cations, additional $[\text{Ag}(\text{DMF})_2]^+$ ions now coordinate to terminal $\text{Mo}=\text{O}$ groups perpendicular to the chain direction and interlink neighbouring Y chains (closest *inter-chain* distance is 7.279 Å) via $\{\text{Mo}_8\}-(\text{O})_2-\text{Ag}(\text{DMF})_2-(\text{O})_2-\{\text{Mo}_8\}$ bridging motifs to form a planar two-dimensional grid of parallel chains. The silver in the $[\text{Ag}(\text{DMF})_2]^+$ group also displays octahedral geometry (Ag-O distances between 2.327(3) and 2.460(2) Å, O-Ag-O angles between 73.45(8) and 180.00°, for minimum *cis* and maximum *trans* values respectively, Figure 59).

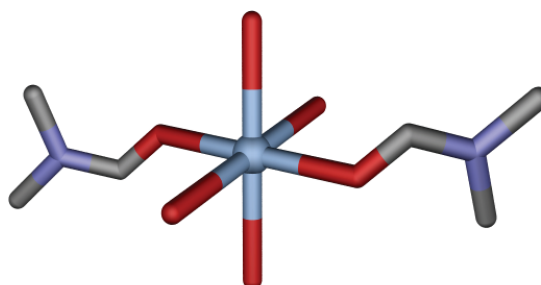


Figure 59 The $[\text{Ag}(\text{DMF})_2]^+$ linker group found in **16**. Mo: green, Ag: light blue spheres, O: red, C: grey, N: blue (hydrogen atoms and counterions removed for clarity).

Thus, chain Y which is reminiscent of chains found in the other chain-type structures can be connected above and below by the binding of additional silver(I) ions (Figure 60), which results in the formation of chain X.

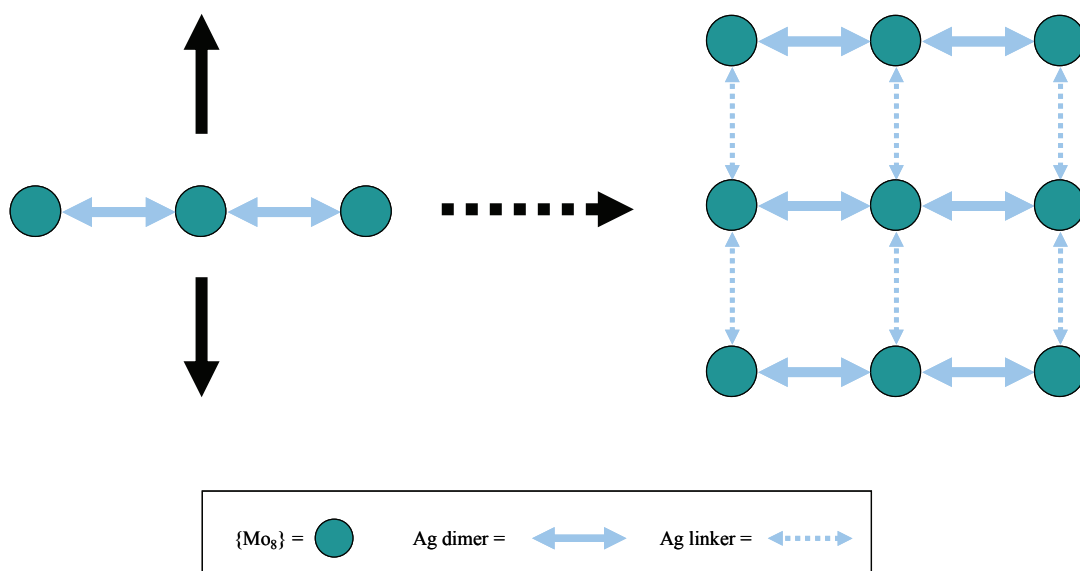


Figure 60 Illustration of how the $\{Ag(Mo_8)Ag\}_\infty$ chain structure can grow to form a two-dimensional network that grows in opposite directions.

It can be seen what remarkable effect substituting the counterion in the precursor material can have on directing the growth of the $\{Ag(Mo_8)Ag\}$ synthon. To complete the comprehensive study involving the interaction of the counterion with the solvent DMF, the experimental strategy was extended to using even larger aliphatic amines. Tetra-*n*-heptylammonium ($(n-C_7H_{15})_4N$) was reacted with sodium molybdate to give $((n-C_7H_{15})_4N)_2Mo_6O_{19}$ (**2**). When **2** is reacted with silver(I) nitrate (1:2 equivalents respectively) in DMF, another two-dimensional network was isolated of the form $[(Ag(DMF))_2(Ag(DMF)_2)_2Mo_8O_{26}]_n$ (**17**, Figure 61).

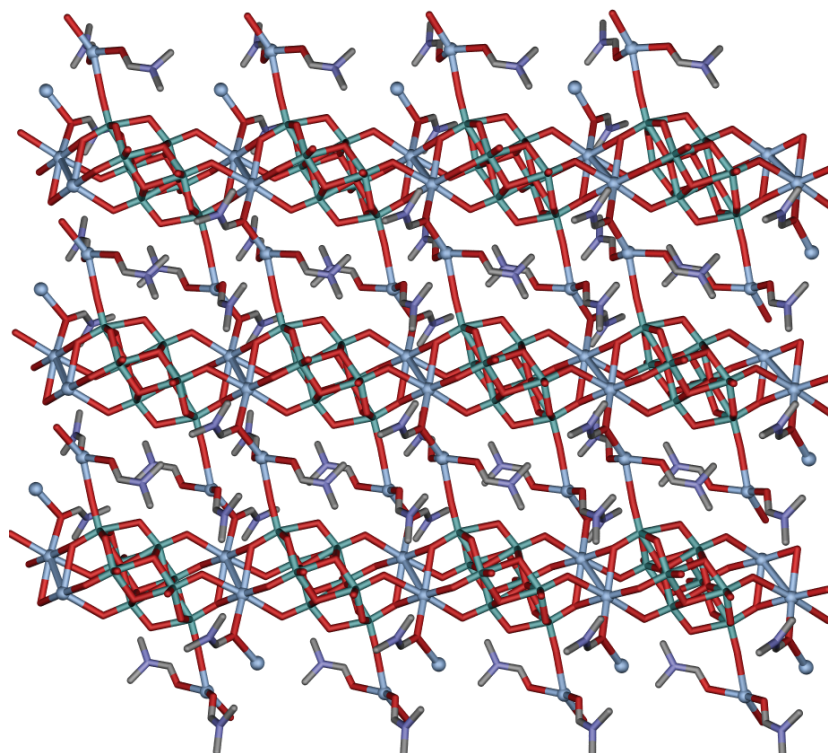


Figure 61 View along the crystallographic *c* axis of **17**. Mo: green, Ag: light blue spheres, O: red, C: grey, N: blue (hydrogen atoms and counterions removed for clarity).

Structurally this network is similar to **16** with a few exceptions. Again the $\{\text{Ag}(\text{Mo}_8)\text{Ag}\}$ synthons are arranged in a chain formation similar to **4** and in **16** (Ag-O distances range between 2.399(2) and 2.592(2) Å and O-Ag-O angles between 72.52(8) and 176.85(8)° for minimum *cis* and maximum *trans* values respectively) but in addition and different to **16** is the coordination of two further Ag(I) ions. As with **16**, the binding of additional DMF ligands on the silver dimer units have decreased the Ag...Ag interaction (Ag...Ag distance of 3.0549(5) Å).

In **16** two Ag ions with octahedral geometry each bind to two free terminal M=O atoms on adjacent faces. In **17** however, the two Ag(I) ions with distorted square planar geometry only bind to one free terminal M=O atom each. Again these Ag(I) ions periodically cross-link the chains into a two-dimensional network and the additional ligands on these silver linker units (Figure 62) are two DMF molecules. Further, coordination to the O_t are not to the same M=O moieties as in **16** (the Ag-O distances are between 2.302(3)-2.531(2) Å and O-Ag-O angles are between 80.80(9) and 146.29(8)° for minimum *cis* and maximum *trans* values respectively).

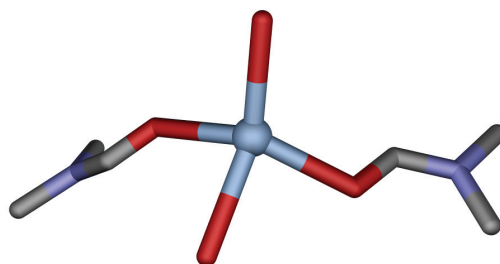


Figure 62 The ‘linker’ unit in **17**. Mo: green, Ag: light blue spheres, O: red, C: grey, N: blue (hydrogen atoms removed for clarity).

3.2.5 Argentophilic Interactions

Metalphilic interactions amongst d^{10} metals remains an elusive area in particular for Cu(I) and Ag(I). Aurophilic interactions are well documented in the literature but the less common ligand-unsupported argentophilic interactions are not so well known. However in recent years a number of publications have reported strong evidence to support that weak attractive interactions do exist for both Cu(I) and Ag(I) in the absence of a bridging ligand.¹³⁶

Within our work we have observed a number of interesting factors that influence and contribute to the structural outcome of selected compounds. These involve the ligand-unsupported assembly of the $\{\text{Ag}(\text{Mo}_8)\text{Ag}\}$ synthon in a linear array as seen in all the structures discussed in section 3.1 and 3.2 with the exception of **9** and **15**, the latter which is involved in ligand supported interactions. In addition to this, we have also reported the degree of interaction between the silver(I) centres and the reasons governing the strength of these interactions of selected structures.

3.2.5.1 *Ag...Ag Interactions in One-Dimensional Arrays*

The interaction of the Ag...Ag ions within selected compounds is of particular interest when we compare the coordination environments and the strength of those interactions.

Within these structures the assembly of the $\{\text{Ag}(\text{Mo}_8)\text{Ag}\}$ synthon can result in linear arrays which can be divided into two distinct types (Figure 63). Type *a* are those structures in which one silver ion is bound to two different $\{\text{Mo}_8\}$ clusters and interacts with a similarly coordinated silver ion. In type *b* on the other hand, one silver ion is bound to only one $\{\text{Mo}_8\}$ fragment and interacts weakly with the neighbouring silver-POM cluster, either through $\text{Ag}\dots\text{Ag}$ interactions and/or through $\text{Ag}\dots\text{O}$ interactions.

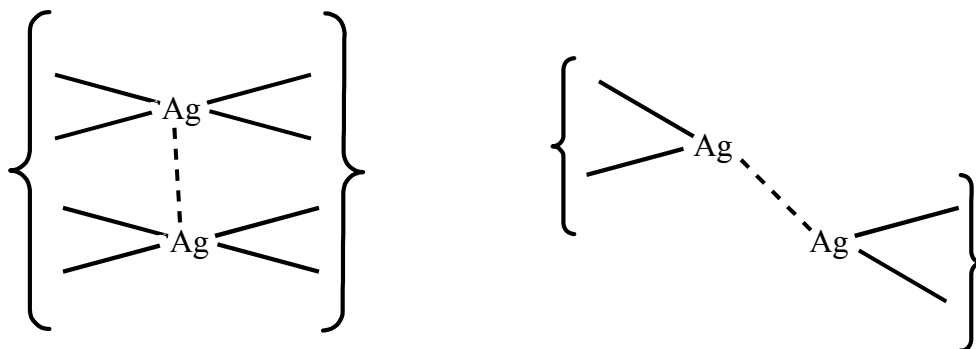


Figure 63 The Ag coordination environments in type *a* (LHS) and type *b* (RHS) structures.

The latter is interesting as the interactions, in particular the $\text{Ag}\dots\text{Ag}$ interactions, are instrumental in holding the synthons in a one-dimensional array. However, the degree of these interactions can be influenced by a number of factors given that they do not form bonds with the terminal oxygen atoms of the subsequent POM as in type *a* structures. Compounds **10**, **11** and **12** fall into the type *b* category, and share a number of similarities but also show some distinct differences.

In each of the structures the $\{\text{Ag}(\text{Mo}_8)\text{Ag}\}$ synthons are held in a linear mode and consequently dictate whether the synthons form one-dimensional arrays or isolated clusters based on the strength of these interactions. In addition to this, each silver site is further coordinated to an acetonitrile molecule (Table 1). Thus, the differences in the strength of the $\text{Ag}\dots\text{Ag}$ interactions are due to a combination of the particular oxo-environments and counterion influence.

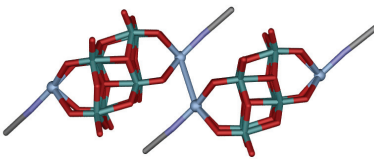
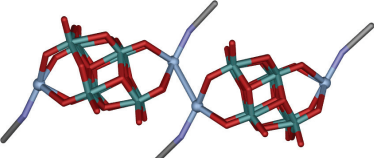
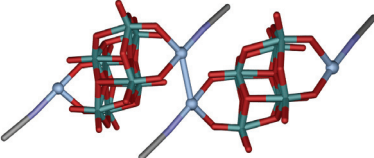
Compound	Structure	Ag...Ag (Å)	All Ag...O (Å)	Comment
10		3.647	2.792	Isolated cluster Bulky cations Solvent molecules 2 coordinate Ag
11		3.454	2.630	1D array Flexible cations No solvent molecules 3 coordinate Ag
12		3.181	2.824 5.163	1D array Planar/linear cations Solvent molecules 2 coordinate Ag

Table 1 Comparison of the Ag coordination environments in **10**, **11** and **12**.

Compound **10**, which is principally composed of isolated clusters, can be seen to some extent to form a one-dimensional array (Figure 64). Each of the clusters arrange in a linear array which has been made possible not by the weak Ag...Ag interaction but by the weak Ag...O interaction (Table 1). However, in compound **11**, the Ag...Ag and Ag...O interactions are shorter and the combination of these two interactions are important to the overall assembly of the synthons. In compound **12**, the scenario is different and here the significantly shorter Ag...Ag interaction (when compared with **10** and **11**) is important in the linear arrangement of the {Ag(Mo₈)Ag} synthon. The question of interest here is, why then do the synthons remain as isolated clusters in **10** but form ‘stronger’ Ag...Ag interactions in **11** and **12**. The answer may lie in the surrounding environment of the silver ions.

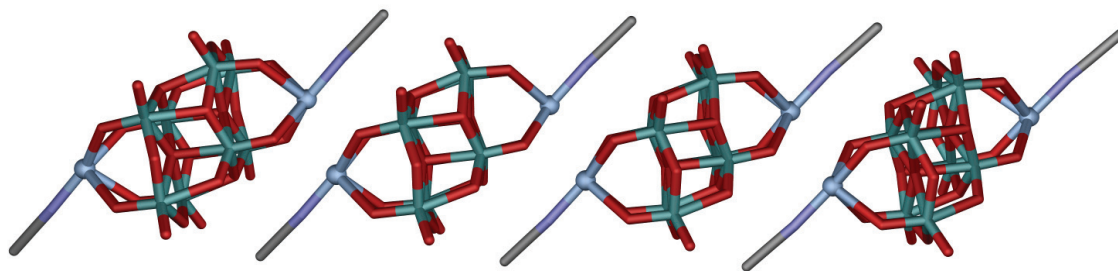


Figure 64 View along the crystallographic *a* axis of **10**. Mo: green, Ag: light blue spheres, O: red, C: grey, N: blue (hydrogen atoms and counterions removed for clarity).

Comparison of all three structures shows a gradual change in Ag...Ag and Ag...O interactions, which appear to be influenced by counterion and solvent molecules. The bulky cations in compound **10** and acetonitrile molecules form a number of weak interactions with the synthons, causing encapsulation and keeping the silver ions at a distance larger than the sum of their van der Waals radii (3.4 Å). In compound **11**, the TBA counterions are more flexible and the space created between the coordinated acetonitrile molecules allows the synthons to approach more closely than in **10**, and consequently form interactions that are stronger (Table 1). However, in **12** the positioning of the synthons is such that the silver ions cannot form interactions with the terminal oxygen atoms of the subsequent POM, which may be caused by the weak interactions to the complex counterion. The Ag...Ag interaction however is stronger and is instrumental in holding the synthons together in a one-dimensional array.

Type *a* compounds contain virtually planar {O₂AgO₂} bridging motifs as seen in structures **4**, **6**, **13**, and **14**, which are notably similar to Gouzerhs' structure.¹³⁴ The bridging motif can also be seen in the chain structures of **16** and **17**, which consequently form two-dimensional networks due to the absence of a restricting cation. However the longer Ag...Ag interactions in **6**, **13** and **14** can be attributed to the presence of terminal ligands on the silver centres. Comparing selected published Ag-POMs, the general trend appears to be that most Ag...Ag interactions are between small POM clusters. This is clearly visible when we compare the structures that contain metalophilic interactions which are mainly observed with {Mo₈} and {Mo₆} such as the ones published by Cronin *et al.*,¹³⁷ Lu *et al.*,¹²⁸ and Wang *et al.*⁹² In these papers the silver ions display most commonly

coordination numbers of four and five and correspondingly have various coordination geometries.

Within the Ag-Mo POM clusters discussed in 3.1 and 3.2, the subtle interplay between the various types of interactions, counterion and solvent inclusion, highlight the ways in which the synthons can be held in a given structure, and ultimately how to gain control over their arrangement.

3.2.5.2 *Density Functional Theory Studies*

To probe the nature of the Ag...Ag contacts, comparative Density Functional Theory (DFT) calculations were performed,^{138,139} the results of which indicate significant bonding interactions between the silver centres. DFT calculations were performed of selected structures from sections 3.1 and 3.2. The molecular growth of the network architectures *via* the connection of β - $\{\text{Mo}_8\}$ -based building blocks by silver(I) ions in the series **1–4** (Table 2), coincides with a gradual evolution of coordination modes of the silver(I) centres with respect to the relevant oxo ligands of the adjoined $\{\text{Mo}_8\}$ fragments, exemplified by the shortening of the Ag...Ag distances within the $\{\text{Ag}_2\}$ linker groups from 4.848(6) Å in **15** to 2.853(4) Å in **4**.

Within the geometric boundaries of the series **1–4**, both the Mulliken overlap integrals and the atomic partial charges are primarily correlated with the coordination environment of the individual silver positions and, to a lesser degree, the Ag...Ag distance. These parameters are summarised with geometrical parameters of the silver coordination environments in Table 2. In a first approximation, the findings can be explained using a simple (electrostatic) crystal field model, according to which Ag(4d) electron density is repelled by the surrounding electronegative ligand positions and is stabilised between the silver centres if significant Ag(4d)-Ag(4d) overlap is achieved; the partial atomic net charge correspondingly decreases with an increase in bonding overlap. Hence, the maximal Ag-Ag overlap and the minimal partial charges for silver are observed for **16**, in which the silver positions are ligated by $\{\text{Mo}_8\}$ -oxo groups in a nearly square-planar geometry.

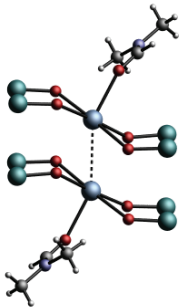
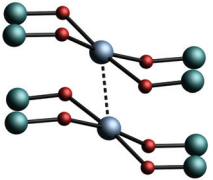
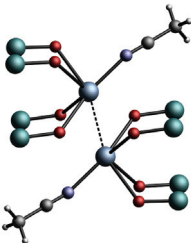
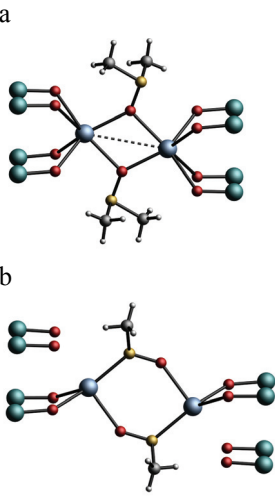
Compound (real compound code)	4 (16)	1 (4)	2(11)	3 (15)
Coordination environment of {Ag ₂ } ¹				
Ag-O({Mo ₈ }) (average, Å)	2.413(3)	2.343(2) ²	2.536(2)	<i>a</i> : 2.555(3), <i>b</i> : 2.375(3)
Ag...Ag (Å)	3.147(6)	2.853(4)	3.454(6)	<i>a</i> : 3.889(6), <i>b</i> : 4.848(6)
Ag-L (Å)	2.442(3) (L = DMF)	–	2.236(3) (L = MeCN)	<i>a</i> : 2.366(3)/2.495(3) [O] <i>b</i> : 2.462(3) [S] / 2.514(2) [O] (L = DMSO)
partial Ag charge	0.123	0.144	0.089	<i>a</i> : 0.080, <i>b</i> : –0.03 ³
Ag-Ag Mulliken overlap population	0.296	0.203	0.049	<i>a</i> : 0.046, <i>b</i> : 0.020
{Mo ₈ }...{Mo ₈ } (Å) ⁴	6.835	6.644	7.509	<i>a</i> : 9.976, <i>b</i> : 11.612

Table 2 Comparison of the local Ag coordination environments in 1–4 and selected geometrical and electronic parameters. ¹Mo: green, Ag: light blue, O: red, C: grey, H: white, N: blue, S: yellow. Ag-O contacts < 3.0 Å are shown. Ag...Ag contacts (< 4.0 Å) are represented by dotted black lines. ²Based on equatorial Ag-O bonds; the average including the long Ag-O bonds (2.835 and 2.913 Å) increases the average to 2.511 Å. ³Using the same basis sets and functionals, this net charge falls in the typical range (0.01 to –0.04) for discrete Ag⁺ complexes of oxo ligands, e.g. the Ag⁺ positions in **9**. ⁴Closest intra-chain Mo...Mo distances between neighbouring {Mo₈} groups.

The coordination is completed by an apical DMF ligand that is *trans*-oriented to the neighbouring silver position ($\gamma(\text{O}[\text{DMF}]-\text{Ag}-\text{Ag})$ angle of 154°). Despite a shorter Ag...Ag

contact and slightly lower average Ag-O({Mo₈}) distances, the Ag-Ag overlap is smaller for **4** due to the relative close distance of each silver position to two oxo ligands of the neighbouring silver centre (2.84 and 2.91 Å, respectively) and due to the absence of a terminal ligand. In **11** the Ag-Ag overlap is further decreased, as the average Ag-O({Mo₈}) and the Ag...Ag distance widens. For **15** the Ag-Ag overlap and especially the partial charges decrease for both types of chains, most probably as a result of the large increase in the Ag...Ag distance which is ligand supported.

3.3 Solvent Assisted Arrays

The influence of counterion and solvent has been well established in the structures discussed previously. The subtle control that can be employed in these syntheses can direct the synthons into producing structures of a particular dimensionality. We were able to explore this set of parameters further when we isolated several structures whereby the solvent in particular was instrumental in holding these structures together. Within these compounds no organic counterions can be found which is most likely to due to the size of the amine which is too small or too large to associate with the $\{\text{Ag}(\text{Mo}_8)\text{Ag}\}$ synthon.

3.3.1 Acetonitrile Arrays

It has been discussed previously that the steric constraints of the $\{\text{Ag}(\text{Mo}_8)\text{Ag}\}$ synthons thus far has not allowed the inclusion of large or very small aliphatic counterions. In the same way the use of tetra-*n*-heptylammonium ($((n\text{-C}_7\text{H}_{15})_4\text{N})$) as a counterion to $[\text{Mo}_6\text{O}_{19}]^{2-}$ has isolated a truly unique one-dimensional chain that differs from the one-dimensional arrays mentioned earlier. It is not surprising that the large counterion is not seen in any of the structures isolated when even the starting material $((n\text{-C}_7\text{H}_{15})_4\text{N})_2\text{Mo}_6\text{O}_{19}$ was initially difficult to prepare. This was mainly due to the large aliphatic counterion which increased the organic nature of the material, making it difficult to isolate the product from the aqueous mother liquor. Re-crystallising the material was a further challenge as all traces of water had to be removed by heating the viscous material which appeared to be both hydrophobic and hydrophilic in appearance.

The complex $[(\text{Ag}(\text{CH}_3\text{CN})_3)_2(\text{Ag}(\text{CH}_3\text{CN})_2)\text{AgMo}_8\text{O}_{26}]_n$ (**18**) can be prepared by reacting silver(I) tetrafluoroborate with $((n\text{-C}_7\text{H}_{15})_4\text{N})_2\text{Mo}_6\text{O}_{19}$ in acetonitrile. There are a number of interesting structural features that separate this chain from the other one-dimensional polymers. The asymmetric unit of **18** contains two halves of a $\{\text{Mo}_8\}$ cluster, four crystallographically different Ag(I) ions and eight acetonitrile molecules. The significant difference observed in this chain is the absence of the $\{\text{Ag}_2\}$ dimers that are often vital in holding the $\{\text{Ag}(\text{Mo}_8)\text{Ag}\}$ synthons in a one-dimensional arrangement (Figure 65).

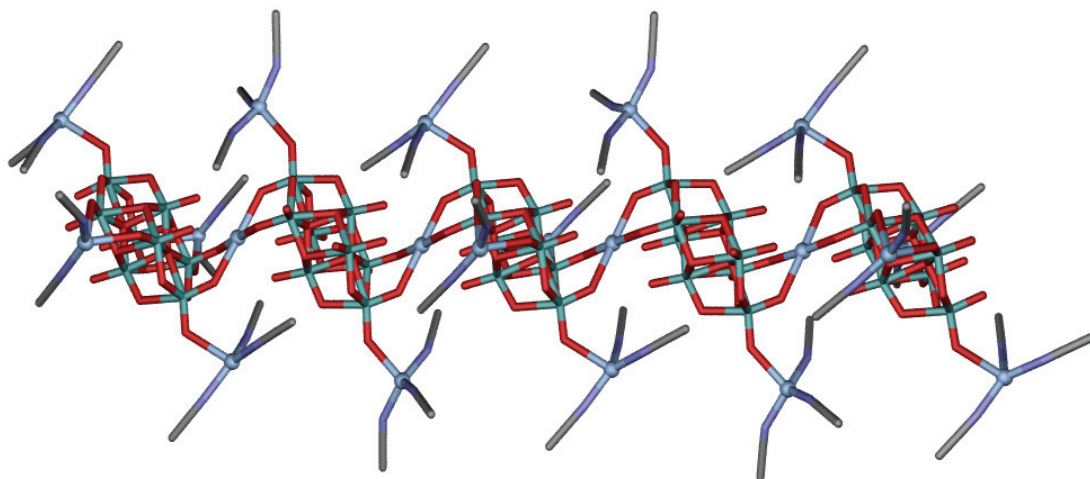


Figure 65 The chain structure of **18**. Mo: green, Ag: light blue spheres, O: red, C: grey, N: blue (hydrogen atoms removed for clarity).

Instead one silver(I) ion is present which can be considered to have either almost linear geometry or square planar geometry if two long range Ag...O interactions are taken into account. Consequently the linking of the $\{\text{Mo}_8\}$ clusters can be seen as $\{\text{OAgO}\}$ (Ag-O distances of 2.395(2) and 2.437(2) Å and O-Ag-O angle of 177.13(8)°) or alternatively $\{\text{O}_2\text{AgO}_2\}$ bridging motifs (Ag-O distances between 2.395(2)-2.509 Å, O-Ag-O angles between 73.57(7) and 177.13(8)° for minimum *cis* and maximum *trans* values respectively, Figure 66). The sum of the van der Waals radii of Ag and O is 3.20 Å,¹⁴⁰ implying that the proximity of O1 and O15 are such that they can be considered to have interactions with Ag1.

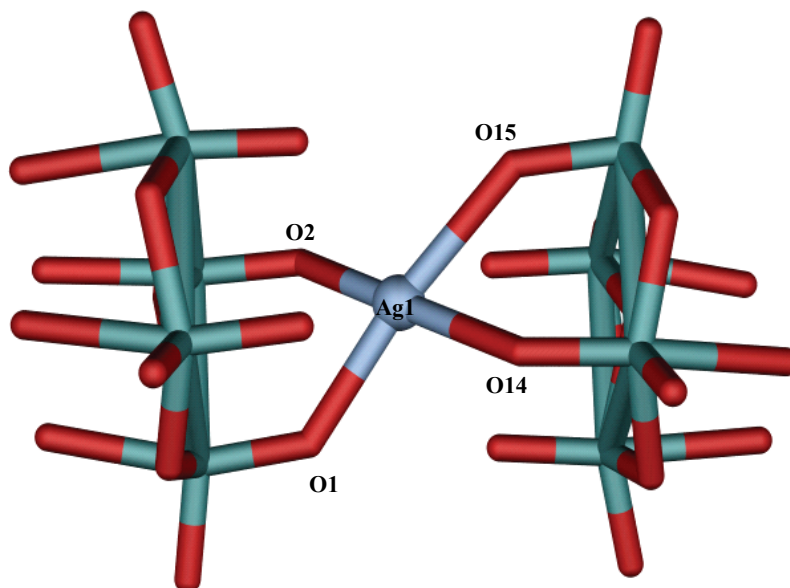


Figure 66 The square planar bridging motif in **18**. Mo: green, Ag: light blue sphere, O: red.

In addition to the bridging silver centre there are three other Ag(I) ions that associate with various M=O atoms of the $\{\text{Mo}_8\}$ cluster through long range coordination interactions which are vital to the stability of the structure. Two silver(I) ions feature similar coordination environments but differ in their particular Ag-O distances resulting in slightly different geometries around the metal centres. Both Ag3 and Ag4 are bound to three acetonitrile molecules with weak interactions to the terminal surface oxygen atoms of the cluster (Figure 67). However, these ions are not found on the same cluster but are coordinated alternatively to Ag1 (Figure 65). Both these ions do not form formal bonds to the terminal oxygen atoms but rather weak interactions (Ag3-O17 distance of 2.590(2) Å and Ag4-O10 distance of 2.701 Å). Both of these can be considered significant in terms of the influence they have on the overall geometry of the two silver ions which have coordination numbers of three but do not form ‘T’ shaped coordination environments.

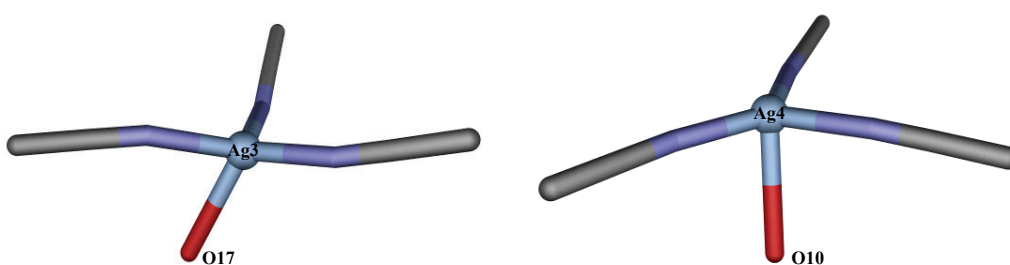


Figure 67 The coordination environments around Ag3 (*LHS*) and Ag4 (*RHS*). Ag: light blue spheres, O: red, C: grey, N: blue (hydrogen atoms removed for clarity).

It is generally known that in fully oxidised polyoxomolybdates, the terminal oxygen atoms are weakly basic and strongly electronegative. The high local electrodensity results in attractive interactions with secondary transition metals such as silver(I). The interaction between Ag3 and O17 pulls the Ag(I) ion out of the plane, thereby creating an intermediate coordination environment between trigonal planar and tetrahedral in order to increase the Ag-O orbital overlap (see table 3 of selected bond angles).

N3-Ag3-N5	119.02(12)	N6-Ag4-N8	131.25(12)
N3-Ag3-N4	110.64(12)	N6-Ag4-N7	122.31(12)
N5-Ag3-N4	121.18(13)	N8-Ag4-N7	105.79(12)
N3-Ag3-O17	119.55(11)	N6-Ag4-O10	81.94
N4-Ag3-O17	102.78(10)	N7-Ag4-O10	84.87
N5-Ag3-O17	79.01(10)	N8-Ag4-O10	111.84

Table 3 Selected bond angles [°] for compound **18**.

The coordination environment around Ag4 however is more consistent with trigonal planar geometry although the N-Ag-N bond angles vary considerably from 120°. The differences in O-Ag-N bond angles between Ag3 and Ag4 can be explained by the different Ag...O interactions between Ag3-O17 and Ag4-O10. The interaction between Ag3-O17 is stronger when compared to Ag4-O10 and therefore results in a further displacement of Ag3 from the trigonal plane.

The fourth silver(I) coordination environment can be found on the same cluster as Ag4 but on the adjacent face of the {Mo₈} cluster. Here Ag2 is weakly interacting with two terminal oxygen atoms (Ag-O distances of 2.532(2) and 2.546(2) Å and O-Ag-O angle of 71.07(7)° for minimum *cis* and maximum *trans* values respectively). Further, Ag2 is coordinating two acetonitrile molecules (Ag-N distances of 2.167(3) and 2.173(3) Å and N-Ag-O angles between 93.05(10) and 115.48(10)°). The coordination environment around the Ag2 ion is such that the linear arrangement is bent inwards rather than out of the plane; again indicating a considerable interaction between the electronegative oxygen atoms and the electropositive silver ion (Figure 68).

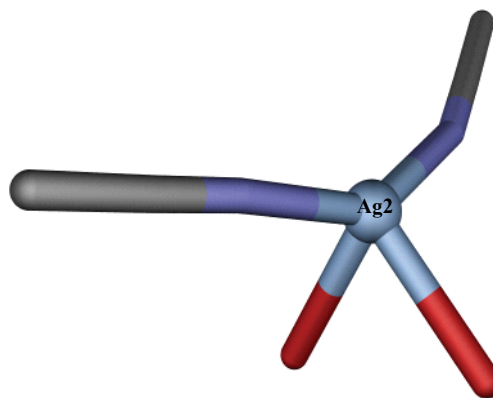


Figure 68 The coordination environment around Ag2. Ag: light blue spheres, O: red, C: grey, N: blue (hydrogen atoms removed for clarity).

The versatility of the Ag-POM reaction system is further demonstrated by the fact that two more structures can be isolated from the same system that yielded **18**. This highlights that controlling the $\{\text{Ag}(\text{Mo}_8)\text{Ag}\}$ synthon in the presence of a large counterion and a solution with a high concentration of acetonitrile is vital to allow the control of the overall structure.

Both of the additional compounds represent the different ways in which the $\{\text{Ag}(\text{Mo}_8)\text{Ag}\}$ synthon can be arranged under the above reaction conditions. Compounds $[(\text{Ag}(\text{CH}_3\text{CN}))_2(\text{Ag}(\text{CH}_3\text{CN})_2)_2\text{Mo}_8\text{O}_{26}]_n$ (**19**) and $[(\text{Ag}(\text{CH}_3\text{CN})_2)_2\text{Ag}_2\text{Mo}_8\text{O}_{26}]_n$ (**20**) are both two-dimensional arrays that differ in the arrangement of the $\{\text{Ag}(\text{Mo}_8)\text{Ag}\}$ synthons and as in **18** each synthon has a number of $\text{Ag}(\text{CH}_3\text{CN})_x$ ($x = 1, 2$ or 3) groups associated with it for charge compensation.

The asymmetric unit of compound **19** shows that there are two crystallographically different silver(I) ions, one half of a $\{\text{Mo}_8\}$ cluster and three acetonitrile molecules. Two Ag1 ions are each bound to one square $\{\text{O}_4\}$ face of the $\{\text{Mo}_8\}$ and are held in a tetradentate mode by formal and long range Ag-O bonds (Ag-O distances of 2.420(3) to 2.715 Å and O-Ag-O angles between 73.13(10) and 114.05° for minimum *cis* and maximum *trans* values respectively) and a weak interaction to a bridging oxygen of a neighbouring cluster (Ag-O distances of 2.715 Å). This type of interaction to bridging oxygen atoms is unusual within this set of clusters. Furthermore, the Ag1 centre coordinates one acetonitrile molecule (Ag-N distance of 2.334(4) Å, Figure 69).

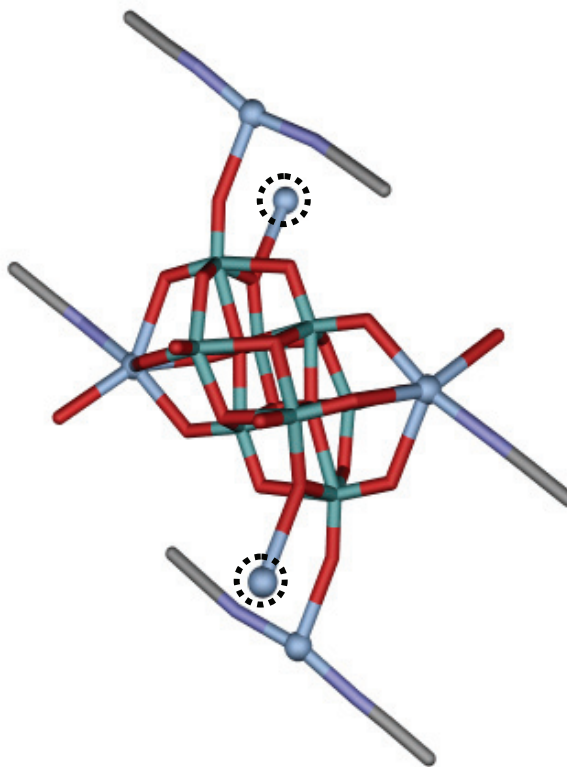


Figure 69 View of the repeating unit in **19** with the Ag of a neighbouring cluster, coordinating to a bridging O highlighted by a dashed circle. Mo: green, Ag: light blue spheres, O: red, C: grey, N: blue (hydrogen atoms removed for clarity).

The remaining two crystallographically equivalent silver ions (Ag2) form interactions with a terminal oxygen atom. This $\text{Ag}(\text{CH}_3\text{CN})_2$ moiety is next to the bridging oxygen atom of Ag1. Thus, the two-dimensional array (Figure 70) is solely formed and stabilised *via* the interactions between Ag1 and the bridging oxygen.

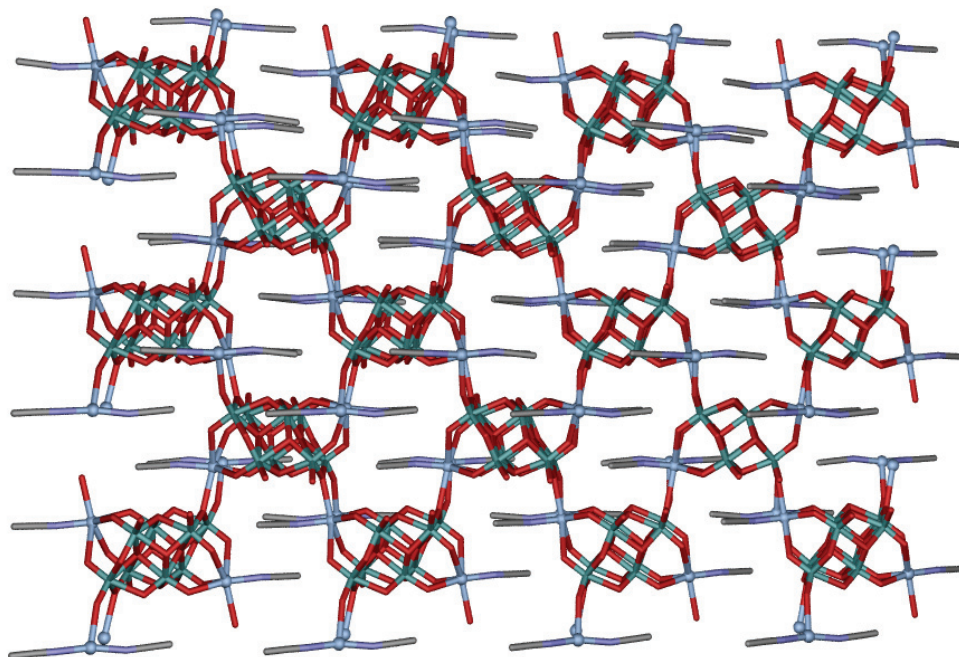


Figure 70 View along the crystallographic *a* axis of **19**. Mo: green, Ag: light blue spheres, O: red, C: grey, N: blue (hydrogen atoms removed for clarity).

Compound **20** is different from **18** and **19**, but shows similar features to $(\text{HDMF})_n[\text{Ag}_3(\text{DMF})_4\text{Mo}_8\text{O}_{26}]_n$ (**16**) and $[(\text{Ag}(\text{DMF}))_2(\text{Ag}(\text{DMF})_2)_2\text{Mo}_8\text{O}_{26}]_n$ (**17**) discussed earlier (section 3.2.4). The asymmetric unit once again contains two crystallographically different silver(I) ions to which one of the acetonitrile molecules are bound and half a $\{\text{Mo}_8\}$ cluster. The main difference between this cluster and **18** and **19**, is the presence of the $\{\text{O}_2\text{AgO}_2\}$ bridging mode which can be found in **16** and **17** (Ag-O distance between 2.377(3) to 2.527(3) Å and O-Ag-O angles between 73.59(10) and 174.48(9)° for minimum *cis* and maximum *trans* values respectively, Figure 71). The chain structure within **20** is held in place by the $\{\text{Ag}_2\}$ dimers and further reinforced by Ag...Ag interactions (Ag...Ag distance of 3.018(7) Å).

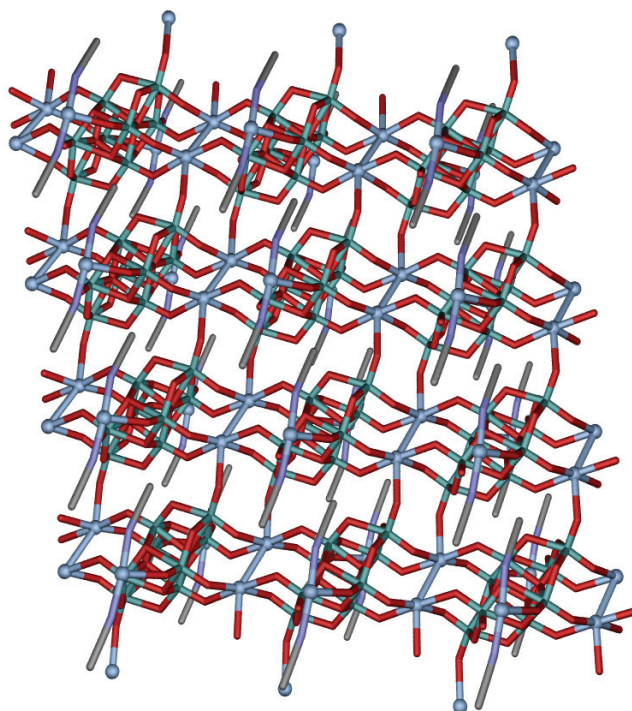


Figure 71 View along the crystallographic *c* axis of **20**. Mo: green, Ag: light blue spheres, O: red, C: grey, N: blue (hydrogen atoms removed for clarity).

Two $\text{Ag}(\text{CH}_3\text{CN})_2$ groups interact with a terminal oxygen atom on the adjacent face of the $\{\text{Mo}_8\}$ cluster (Ag...O distance of 2.624 Å, Ag-N distances is 2.136(4) and 2.147(4) Å, Figure 72).

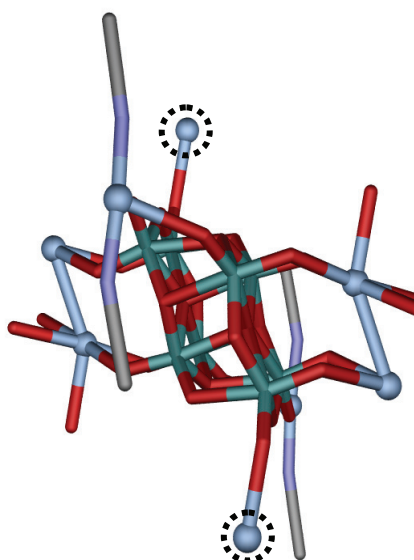


Figure 72 View of the repeating unit in **20** with the linking Ag ion of a neighbouring Ag dimer highlighted by a dashed circle. Mo: green, Ag: light blue spheres, O: red, C: grey, N: blue (hydrogen atoms removed for clarity).

The silver dimer that is found in the chain structure of this **20** is responsible for extending this chain into a two-dimensional array. Unlike the two-dimensional nets presented earlier, this chain does not use additional silver ions to link the chains. Instead the Ag dimers are linked by a bridging μ_2 -oxygen atom coordinating to a neighbouring $\{\text{Mo}_8\}$ cluster perpendicular to the direction of the principal chain (Ag...O distance of 2.527(3) Å, Figure 73).

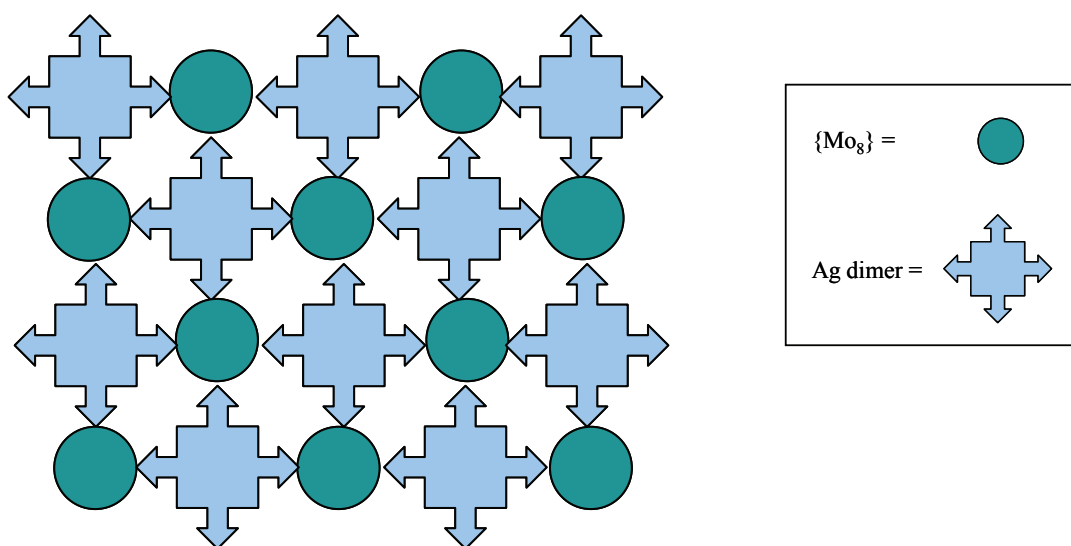


Figure 73 Illustration of how the Ag dimers link the $\{\text{Mo}_8\}$ units into a two-dimensional array.

In all three compounds the presence of the $\text{Ag}(\text{CH}_3\text{CN})_x$ group is interesting and as with other counterions seem to have a degree of control over the self-assembly of the $\{\text{Ag}(\text{Mo}_8)\text{Ag}\}$ building blocks in solution. Figure 74 shows the resulting encapsulation that can be achieved by these groups in **18**, where each Ag ion coordinates to one or two terminal $\text{Mo}=\text{O}$ groups in a way which allows the $\{\text{Ag}(\text{Mo}_8)\text{Ag}\}$ building blocks to grow in only one direction. These groups are present on all faces of the $\{\text{Mo}_8\}$ cluster with the exception of the side that is free to combine the Ag-Mo synthons into a one-dimensional array i.e. the side that is coordinated to the square planar silver ion.

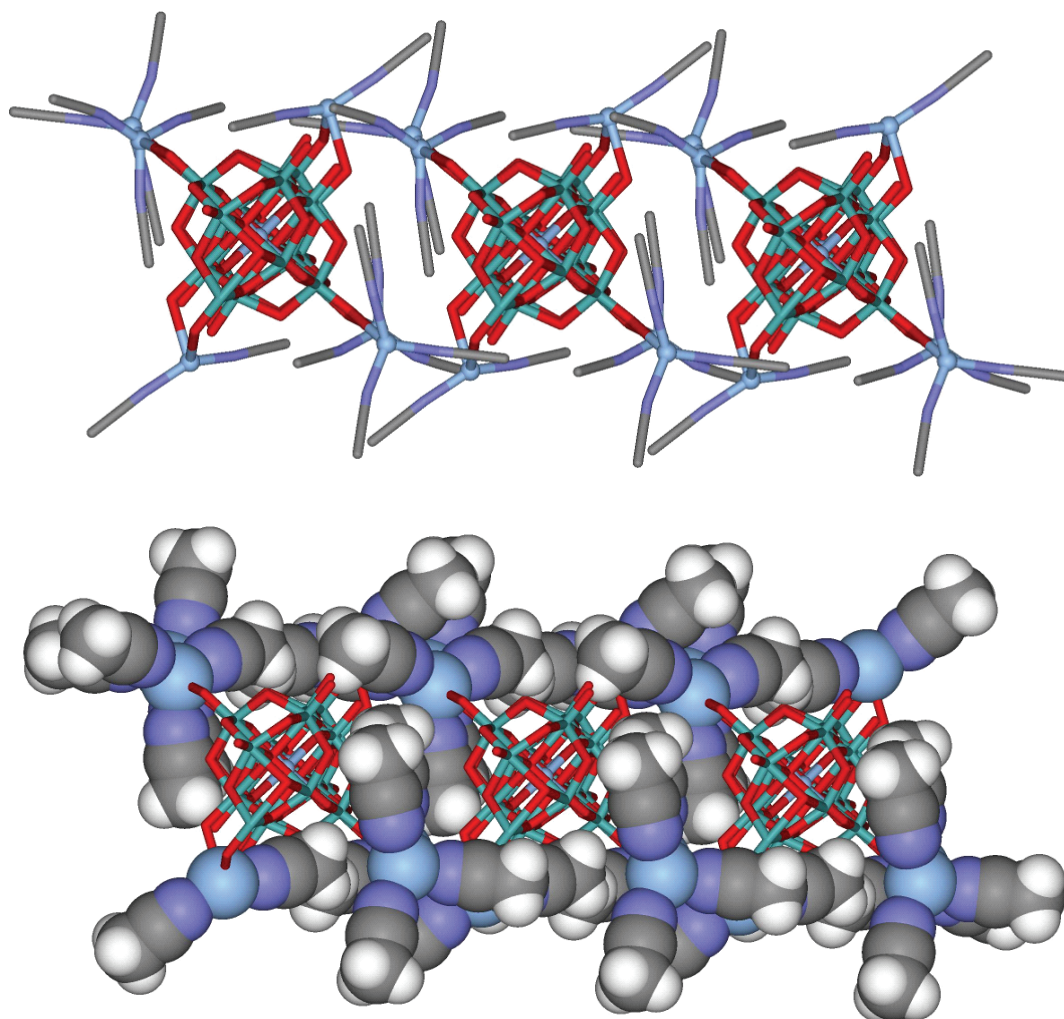


Figure 74 View along one axis of **18** (top) with space-filling representation of the $\text{Ag}(\text{CH}_3\text{CN})_x$ groups where $x = 2$ or 3 (bottom). Mo: green, Ag: light blue spheres, O: red, C: grey, N: blue, H: white.

In compounds **19** and **20** however, these shielding groups are present on only two sides of the synthon, almost as if two parallel brick walls of a given width and length had been placed at either side of the anions; thus allowing the growth of the synthons in two directions. In **19**, the two-dimensional arrays will pack very closely together, creating chains that are parallel to one another when viewed down the crystallographic b axis. As such the acetonitrile ‘branches’ that create the ‘wall’ (Figure 75) are arranged closely together and at an angle between one layer and the next (shortest *inter*-layer distance between two acetonitrile ‘branches’ is 6.886 Å). Remarkably, no hydrogen bonding contacts exist within **19**.

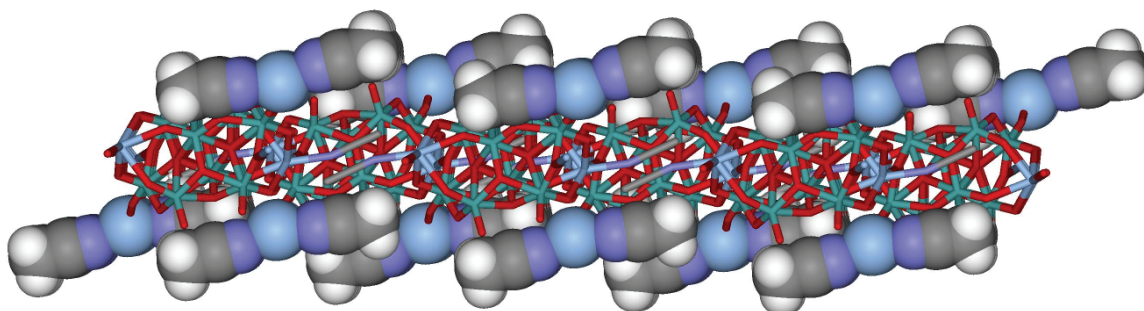


Figure 75 Side view of **19** with space-filling representation of the $\text{Ag}(\text{CH}_3\text{CN})_x$ groups where $x = 1$ or 2 . Mo: green, Ag: light blue spheres, O: red, C: grey, N: blue, H: white.

In a similar way **20**, contains layers of the two-dimensional arrays that run parallel along the crystallographic b axis. The acetonitrile ‘branches’ create a ‘wall’ around the $\{\text{Ag}(\text{Mo}_8)\text{Ag}\}$ array (Figure 76).

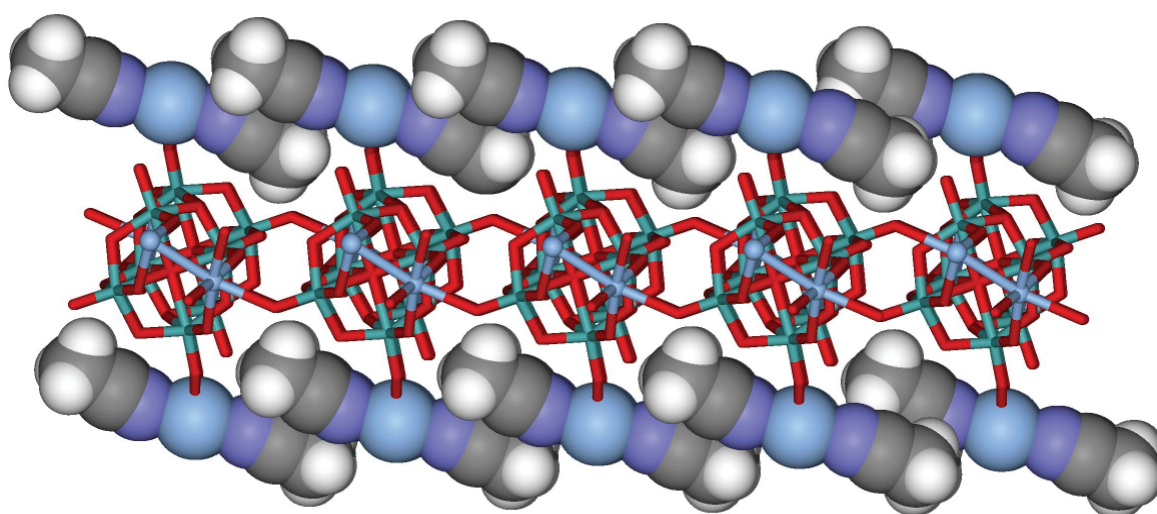


Figure 76 Side view of **20** with space-filling representation of the $\text{Ag}(\text{CH}_3\text{CN})_x$ groups and ball and stick representation where $x = 2$. Mo: green, Ag: light blue spheres, O: red, C: grey, N: blue, H: white.

These branches also pack in between one another (*inter*-layer distance between two acetonitrile branches of two neighbouring layers is 8.886 Å, Figure 77) and feature van der Waals interactions between the nitrogen of one layer to a bridging oxygen on a $\{\text{Mo}_8\}$ cluster of the neighbouring layer (NH...O distance of 2.966 Å).

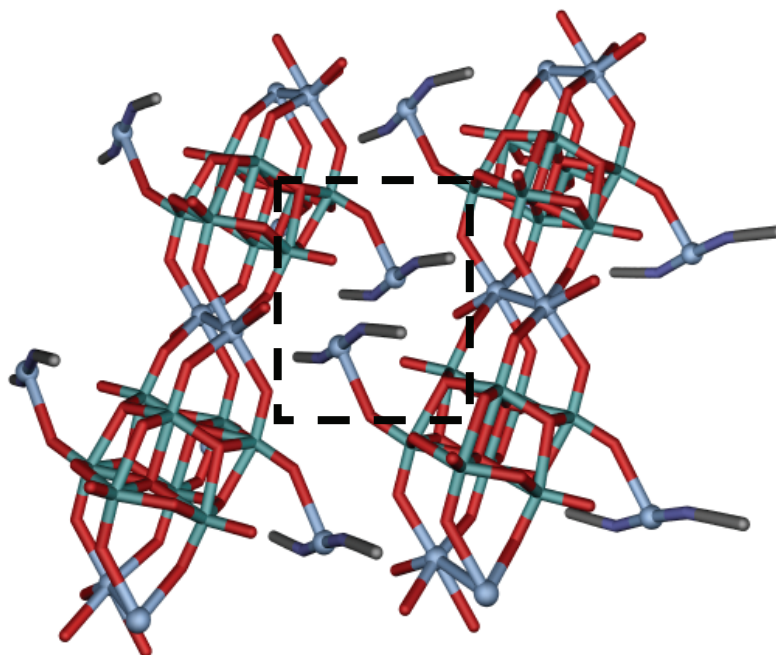


Figure 77 Side view of **20** with the interpenetrating $\text{Ag}(\text{CH}_3\text{CN})_x$ groups between one layer and the next (highlighted by the dashed black box) where $x = 2$. Mo: green, Ag: light blue spheres, O: red, C: grey, N: blue (hydrogen atoms removed for clarity).

3.3.2 DMSO Arrays

Studies with DMSO revealed that in the absence of a restricting counterion this solvent can exert a vital control over the arrangement of the $\{\text{Ag}(\text{Mo}_8)\text{Ag}\}$ building blocks where DMSO plays an important role in pillaring the building blocks. However, due to the intrinsic instability of these systems, full characterisation is still a challenge.

The reaction of two equivalents of silver(I) nitrate with one equivalent of $((n\text{-C}_5\text{H}_{11})_4\text{N})_2\text{Mo}_6\text{O}_{19}$ in a methanol/DMSO mixture yielded colourless crystals with the formula $[\text{Ag}_4(\text{DMSO})_6(\text{OC}(\text{CH}_3)_2)_2\text{Mo}_8\text{O}_{26}]$ (**21**).

Each $\{\text{Mo}_8\text{O}_{26}\}$ unit coordinates to four Ag atoms linking it into an array. Two distinct coordination environments exist for these Ag atoms; Ag1 and Ag2 (Figure 78), where each forms a number of formal and weak Ag-O bonds. The Ag1 centre interacts with the square

{O₄} coordination environment of the {Mo₈} cluster, *via* interactions of varying lengths (Table 4). In the same way Ag₂ interacts weakly with one oxygen atom of the {Mo₈} cluster to form one formal Ag-O bond.

Ag-POM Interactions				Ag-Ligand Interactions			
Ag-O		O-Ag-O		Ag-O		O-Ag-O	
Ag1-O5	2.599(4)	O5-Ag1-O6	73.53(11)	Ag1-O1	2.449(3)	O1-Ag1-O2	76.05(11)
Ag1-O6	2.518(3)	O5-Ag1-O8	112.02	Ag1-O2	2.523(3)	O1-Ag1-O3	82.42(14)
Ag1-O8	2.644	O5-Ag1-O16	71.51	Ag1-O3	2.501(4)	O2-Ag1-O3	81.05(12)
Ag1-O16	2.612	O6-Ag1-O8	71.55				
		O6-Ag1-O16	110.76	Ag2-O1	2.423(3)	O1-Ag2-O2	75.45(12)
Ag2-O9	2.618	O8-Ag1-O16	69.62	Ag2-O2	2.579(4)	O1-Ag2-O3	85.88(13)
Ag2-O13	2.329(3)			Ag2-O3	2.364(4)	O2-Ag2-O3	82.52(12)
		O9-Ag2-O13	74.20	Ag2-O4	2.472(4)		

Table 4 Bond lengths [Å] and angles [°] for the two silver(I) ion environments in **21**.

Each silver(I) ion coordinates to three DMSO molecules *via* the oxygen atoms, resulting in similar bond lengths and distances (Table 4). In addition to this, Ag₂ further coordinates to a molecule of acetone, again through the oxygen atom. As a result of the steric bulk the Ag...Ag interaction is relatively weak (Ag...Ag distance of 3.280 Å and Ag1-O(DMSO)-Ag2 average of 83.10(11)°) and in this instance is ligand supported by the three bridging DMSO molecules (Figure 78).

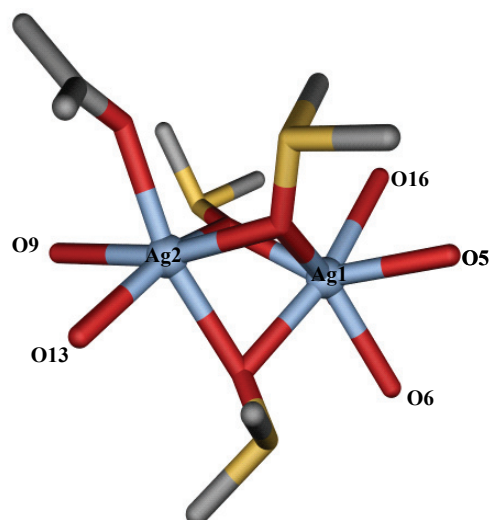


Figure 78 View of the coordination environments of Ag1 and Ag2 within **21**. Ag: light blue spheres, S: yellow, O: red, C: grey (hydrogen atoms removed for clarity and only selected oxygen atoms labelled).

The $\{\text{Ag}(\text{Mo}_8)\text{Ag}\}$ units form a one-dimensional polymer *via* coordination to the μ_2 -oxo centres of the DMSO ligands to form $(\text{O})\text{Ag}1(\mu_2\text{-dmsO})_3\text{Ag}2(\text{O})$ bridges, similar to the bridging modes observed in $((n\text{-C}_4\text{H}_9)_4\text{N})_{2n}[\text{Ag}_2(\text{DMSO})_2\text{Mo}_8\text{O}_{26}]_n$ (**15**). The assembly of the $\{\text{Ag}(\text{Mo}_8)\text{Ag}\}$ units is such that each alternating cluster is in a different position to the subsequent cluster, giving an A-B-A-B arrangement to the $\{\text{Mo}_8\}$ cluster of this building block (Figure 79).

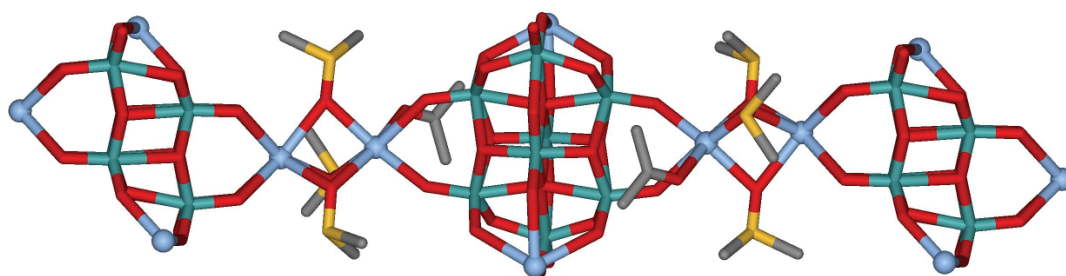


Figure 79 Fragment of one chain in **21** showing the A-B-A arrangement of the $\{\text{Mo}_8\}$ cluster within the $\{\text{Ag}(\text{Mo}_8)\text{Ag}\}$ unit. Mo: green, Ag: light blue spheres, S: yellow, O: red, C: grey (hydrogen atoms removed for clarity).

The absence of a bulky organic counterion enables the units to cross-link without any steric restraint and as a result the compound self-assembles into a two-dimensional array. This array is different to the other two-dimensional structures encountered so far (with the

exception of **19**), which all have a series of parallel chains which are linked into a network. In this case however, both axes of the network are equivalent forming two sets of parallel chains which run perpendicular to one another and are cross-linked by the Ag(DMSO) linkages to form **21** (Figure 80).

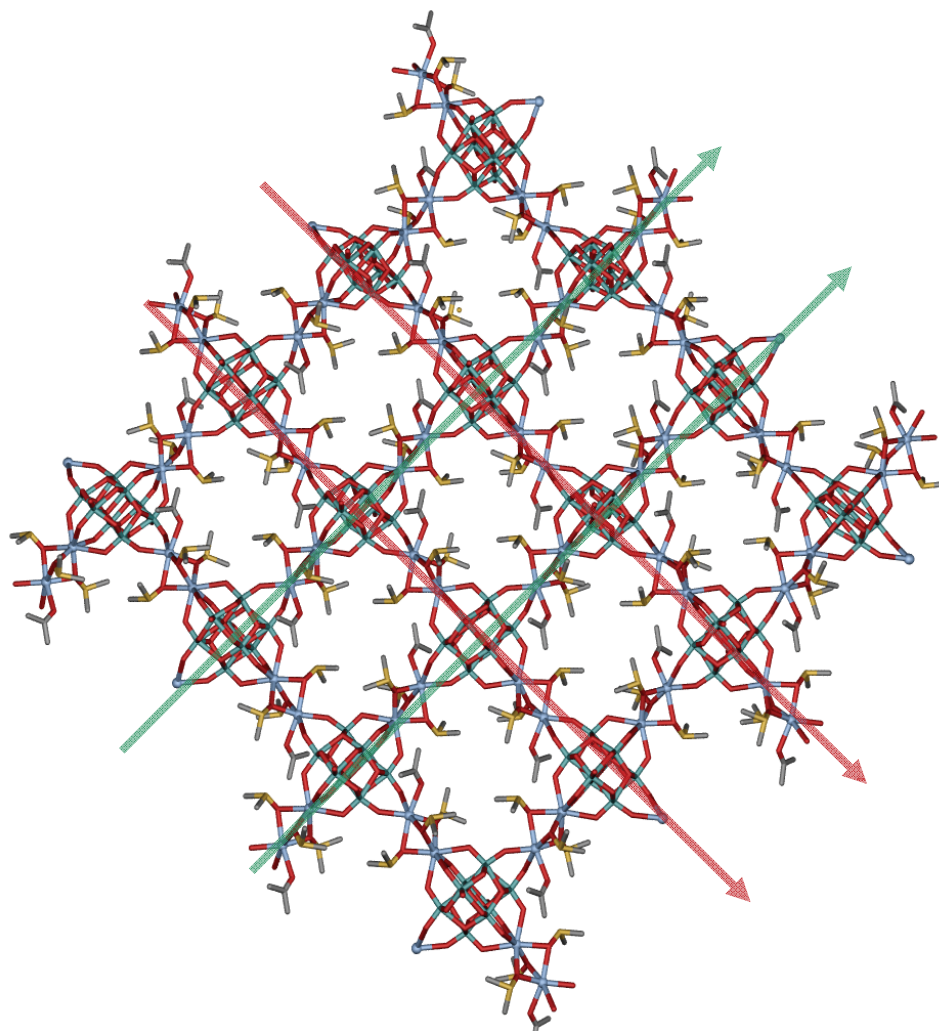


Figure 80 View along the crystallographic a axis of **21** and highlighting the chains which run parallel and perpendicular to one another with red and green arrows. Mo: green, Ag: light blue spheres, S: yellow, O: red, C: grey (hydrogen atoms removed for clarity).

The two-dimensional layers pack closely along the crystallographic c or b axis (closest *intra*-layer distance of 3.147 Å between neighbouring DMSO molecules). Again there are more similarities to structure **15**, where the formation of the isolated one-dimensional chains was facilitated by the TBA counterions. As discussed in section 3.2.4, the chains in **15** formed a two-dimensional array creating an interweaved effect. However, as there is no organic counterion present in **21**, the chain structures are able to directly interlink into a

true two-dimensional array *via* the bridging DMSO ligands. This linking mode however, was not feasible in **15** due to the steric bulk of the organic counterions. Despite the slightly different arrangement of the individual $\{\text{Ag}(\text{Mo}_8)\text{Ag}\}$ units within the polymers of **21**, the overall arrangement is similar to the interweaved arrangements of the chains in **15** (Figure 89).

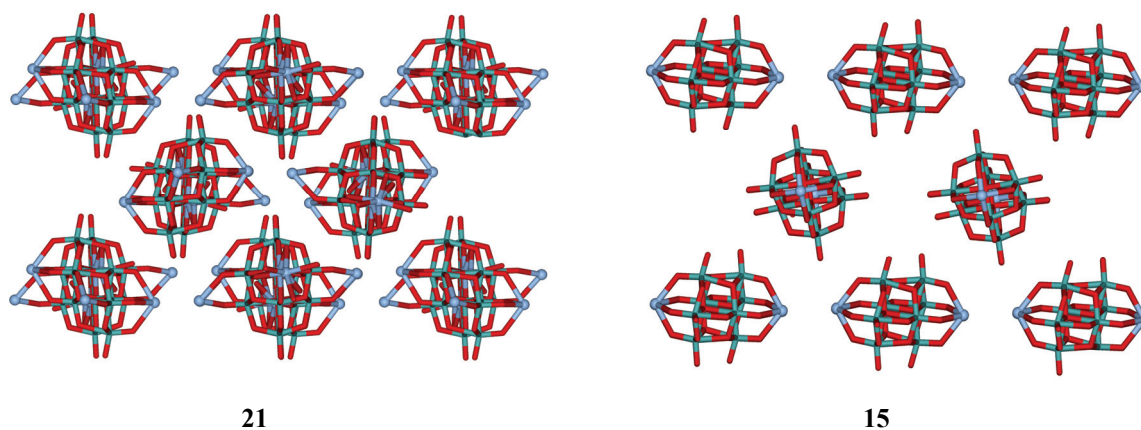


Figure 89 Comparative view of **21** (LHS) and **15** (RHS). Mo: green, Ag: light blue spheres, O: red (hydrogen atoms, DMSO and acetone ligands and counterions removed for clarity).

What is interesting is that in the original synthesis no acetone was present in the mother liquor, but rather the diffusion of this solvent as a method of crystallisation resulted in its inclusion within **21**. However, attempts to repeat this structure have been a challenge when even slight modifications to the original synthesis had been made (on this basis, collecting a full and complete analytical data set is still pending). The attempt to facilitate the synthesis of **21** by adding a small volume of acetone to the reaction mixture, resulted in the formation of colourless crystals which were suitable for single crystal X-ray analysis. Inspection of the structure revealed that **22** forms a two-dimensional array with the formula $[\text{Ag}_4(\text{DMSO})_8\text{Mo}_8\text{O}_{26}]$ (**22**). The asymmetric unit of this cluster consists of two crystallographically independent silver(I) ions (Ag1, Ag2) with similar geometry, half an $\{\text{Mo}_8\}$ fragment, and four coordinated DMSO molecules, but notably no molecules of acetone.

However, unlike the other chain-like structures and the two-dimensional arrays discussed previously, the $\{\text{Ag}(\text{Mo}_8)\text{Ag}\}$ synthons in **22** do not link together to form a chain arrangement that can extend both above and below generating a two-dimensional array.

Instead the structure represents a prime example of how solvent molecules are not only incorporated into the structure but also ‘pillar’ the Ag-Mo POM fragments providing essential support to the overall network. The {Ag(Mo₈)Ag} synthons are able to arrange themselves and extend into a two-dimensional network via the μ_2 -oxo and μ_2 -sulfur centres of the DMSO molecules (Figure 90). Due to the steric requirements of the synthon the inclusion of the tetra-*n*-pentylammonium ((*n*-C₅H₁₁)₄N)⁺ counterion is not possible. Instead two additional silver(I) ions coordinate to the cluster and thereby balance the charge.

There are two crystallographically different silver ions where Ag1 is bound to one oxygen atom of a [Mo₈O₂₆]⁴⁻ and interacts with two other oxo atoms. In addition to this, Ag1 further coordinates to a bridging oxo atom of a DMSO molecule and to the oxo atom of another DMSO ligand. Thus, the Ag1 centre has a heavily distorted square pyramidal geometry (O-Ag-O angles between 74.15(7) and 151.89(9)° for minimum *cis* and maximum *trans* values respectively and Ag-O bond distances between 2.296(3) and 2.581(2) Å). In addition to this, one of the DMSO molecules is further coordinated to another silver ion (Ag2) through a μ_2 -sulfur bond. This silver forms part of the ‘linker’ unit that connects the Ag-Mo POM unit together in a two-dimensional array. The silver also has distorted square pyramidal geometry, and on closer inspection is actually coordinating to a total number of four DMSO molecules (Figure 90, inset) either through Ag-O bonds or Ag-S bonds (O-Ag-S angles between 76.96(6) and 119.56(6)° with Ag-O bond distances of 2.343(2) to 2.449(2) Å and Ag-S bond distances of 2.628(9) and 2.807(9) Å).

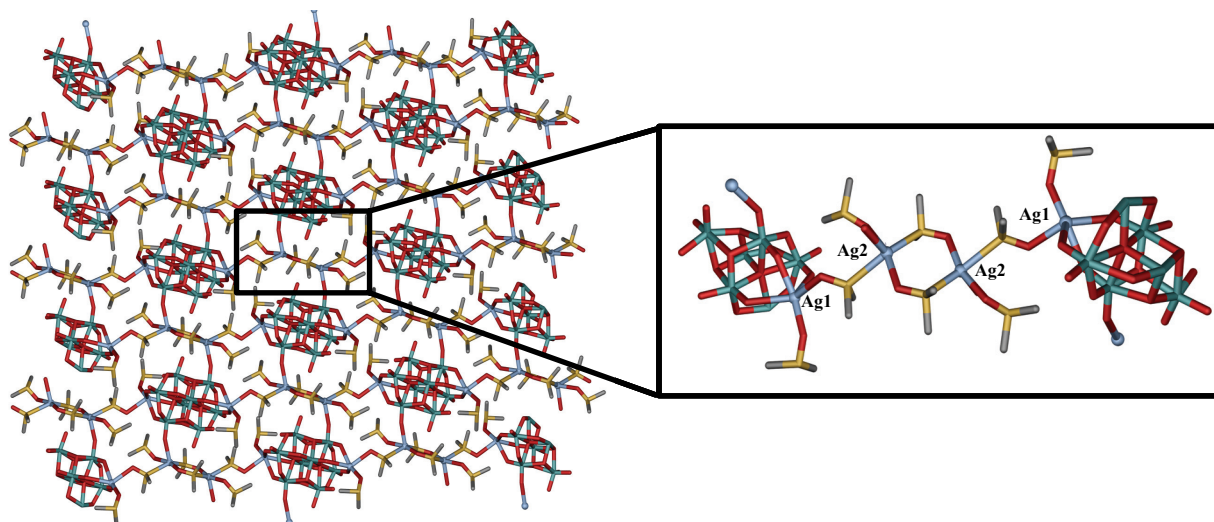


Figure 90 View along the crystallographic b axis of **22**. Inset: expanded view of the ‘linker’ unit. Mo: green, Ag: light blue spheres, S: yellow, O: red, C: grey (hydrogen atoms removed for clarity).

Peng and co-workers, in a similar way to **22**, were able to link β - $\{\text{Mo}_8\text{O}_{26}\}$ fragments into a one-dimensional chain via Ag-organic moieties.¹⁴¹ There are no Ag...Ag interactions, however there are considerable $\text{Ag}^{\text{I}}-\pi$ interactions between the silver(I) ions and the aromatic phenazine ligand used. Hill *et al.* published a silver hetero-POM that consists of two $[\text{PV}_2\text{Mo}_{10}\text{O}_{40}]^{-5}$ clusters that are bridged together by silver(I) ions.¹⁴² Extended arrays of hetero-tungstate POMs have also been linked together via silver-organic moieties¹⁴⁰ and by additional -Ag-POM-Ag- linkages.¹⁴³

Compound **22** can be isolated from a number of different procedures with only slight variation in solvent mixture and silver salt ratio or change in the counterion of the starting material. These experimental comparisons indicate that perhaps **22** is more stable than **21** and consequently its formation is less susceptible to slight changes in synthetic conditions.

A 2:1 equivalent of silver(I) nitrate to $((n\text{-C}_3\text{H}_7)_4\text{N})_2\text{Mo}_6\text{O}_{19}$ in a methanol/DMSO mixture, yields **22** by diffusion of diethyl ether over a period of three weeks. Similarly, a 2:1 equivalent of silver(I) nitrate to $((n\text{-C}_6\text{H}_{13})_4\text{N})_2\text{Mo}_6\text{O}_{19}$ or $((n\text{-C}_7\text{H}_{15})_4\text{N})_2\text{Mo}_6\text{O}_{19}$ in DMSO will also give **22** by diffusion of ethanol over two weeks. The latter methods provide crystals in good yield unlike the original method of using TPA which takes a long time and produces a poor yield.

By comparison, a 2:1 equivalent of silver(I) nitrate to $((n\text{-C}_5\text{H}_{11})_4\text{N})_2\text{Mo}_6\text{O}_{19}$ in a DMSO solution and diffusion by acetone over two months gave **21** on only one occasion in a very poor yield. The exact same experimental set up, with the exception that the silver to $\{\text{Mo}_6\}$ ratio was changed to 3:1 gave **22** in a poor yield. In an attempt to reproduce **21** and as already discussed, the deliberate addition of acetone to the original synthesis of **21**, produces a greater yield and faster crystallisation time of 10 days to give yet again **22**. A summary of the experimental set ups can be found in table 5.

Ratio of Ag:Mo ₆	Counterion of $[\text{Mo}_6\text{O}_{19}]^{2-}$			
	$((n\text{-C}_3\text{H}_7)_4\text{N})$	$((n\text{-C}_5\text{H}_{11})_4\text{N})$	$((n\text{-C}_6\text{H}_{13})_4\text{N})$	$((n\text{-C}_7\text{H}_{15})_4\text{N})$
2:1	22	22	22	22
		21		
3:1		22		

Table 5 A summary of the experimental set ups for **22** (colour coded by a red box) and **21** (colour coded by a green box).

Thus, the repeated isolation of **22** even in the presence of acetone under various conditions implies that the stability of this compound and perhaps kinetics of formation are greater than that of **21** and may also explain why it is harder to retrieve the original cluster **21**.

3.4 Surface Studies

Studies of compound $((n\text{-C}_4\text{H}_9)_4\text{N})_{2n}[\text{Ag}_2\text{Mo}_8\text{O}_{26}]_n$, (**4**) deposited on a silicon substrate were discovered to yield some unusual structures. Indeed, such structures may even be considered to form through a series of self-assembly processes from the molecular to the nanoscale level and beyond. It is interesting to note these structures appear to be composed of Ag^0 -based nanostructures from which the synthesis of silver wires of nano dimensions under ambient conditions have been discovered.¹²⁶ The growth of the silver wires appears to be facilitated by the deposition of crystalline material of **4** on a silicon substrate after 30 days. These results also demonstrate how the molecular aspects of **4** can be combined with the nanoscale level, signifying the possibility of these materials bridging the molecular with the nanoscale and beyond.⁹⁸

Investigation of this phenomenon has been limited to growth on silicon substrates and several studies aimed at elucidating the growth mechanism have been undertaken using a variety of approaches including Scanning Electron Microscopy (SEM). However, interpretations are hampered by the fact that some of the structures are not always observed reproducibly, whilst others are seen in every experiment. The observation of these structures at the various time intervals will be discussed in more detail and any logical assumptions that can be made from the experiments will be highlighted throughout the discussion.

3.4.1 Growth of Nanorods and Spherulites

Nanoscale molybdenum and tungsten based oxides are particularly interesting because of their numerous interesting physical and electronic properties. There are strong surface acid sites in the +5/+6 oxidation states and the metal-oxide double bonds are particularly important for the use of this class of materials in the catalytic industry and also as sensor materials.¹⁴⁴ In addition to this, low dimensional nanomaterials also have many features that can be used in a wide range of applications dependent upon their shape and size. In particular one-dimensional nanowires can be used as interconnects in electronic circuits, as

well as optical and sensing devices.¹⁴⁵ Much focus has been placed upon the controlled growth of these materials on the nanoscale level using novel and convenient methods.^{146,147} Thus, the various Ag-Mo based oxide compounds isolated and discussed in the previous chapters present a whole set of materials with potential use as functional materials where the growth of the individual building blocks can be controlled by cation and solvent interaction.

The self-assembly of silver octamolybdate anions in solution are assisted by the use of organic cations to isolate molybdenum oxide polymeric architectures. In one instance, we see the growth of the $\{\text{Ag}(\text{Mo}_8\text{O}_{26})\text{Ag}\}$ building blocks into a one-dimensional polymer $((n\text{-C}_4\text{H}_9)_4\text{N})_{2n}[\text{Ag}_2\text{Mo}_8\text{O}_{26}]_n$, **4**) or array $((n\text{-C}_4\text{H}_9)_4\text{N})_{2n}[\text{Ag}_2(\text{CH}_3\text{CN})\text{Mo}_8\text{O}_{26}]_n$, **11**) facilitated by the ‘wrapping’ action of the TBA counter ion (Figure 91). These chains are packed to a network of co-linear, organic ‘tunnels’ that accommodate the polymeric $\{\text{Ag}_2\text{Mo}_8\text{O}_{26}\}_\infty$ anions. In addition to this, Ag...Ag interactions as discussed in section 3.2 also play an instrumental role with compound **4** displaying a short metalphilic interaction of 2.853(4) Å and for comparison, **11** with a much longer interaction of 3.454(6) Å.

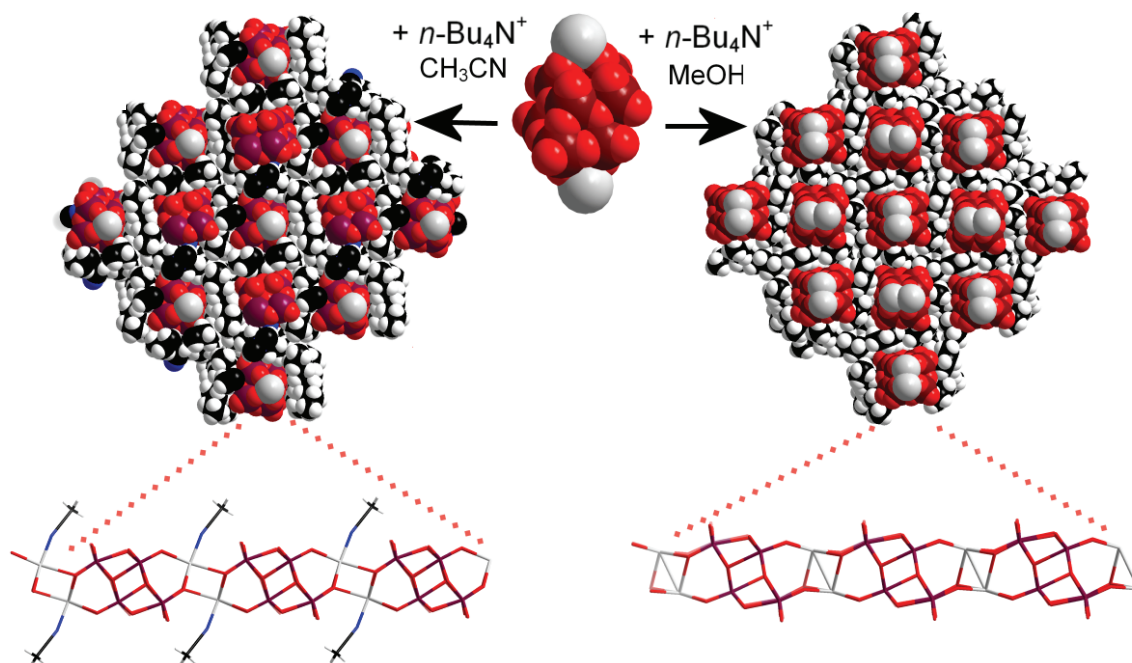


Figure 91 Space-filling packing representations, seen along the direction of the polymers, comparing the structures of compounds **4** (RHS) and **11** (LHS) and demonstrating the growth of the $\{\text{Ag}(\text{Mo}_8)\text{Ag}\}$ unit (centre) to 1D **4** (RHS) and **11** (LHS). Stick representations of each 1D architecture are shown below in perpendicular views. Mo: brown, O: red, Ag: grey, C: black, N: blue, H: white.

The idea that this compound could be used for its conductive or catalytic properties was a key influence in looking at compound **4** on surfaces. Crystals of **4** were suspended in a methanol solution and deposited onto a silicon substrate which shows rod-like structures all over the surface from deposition of ‘fresh’ (i.e. un-matured - here defined as 1-3 days old) solution (Figure 92).

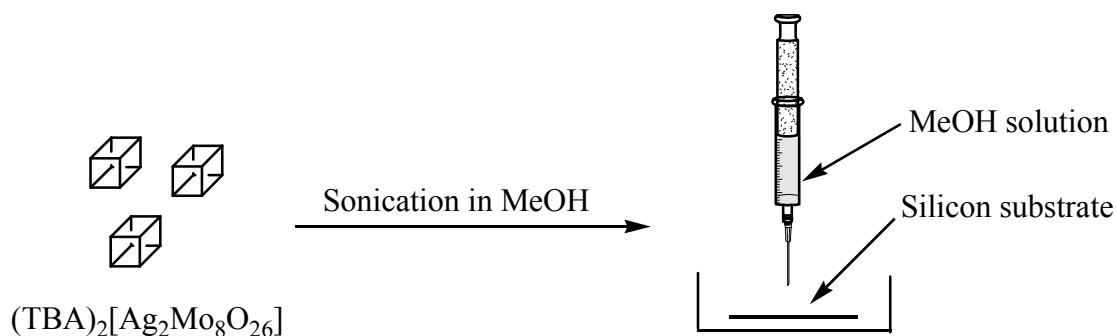


Figure 92 Illustration of the sonication process of $(n\text{-C}_4\text{H}_9)_4\text{N})_{2n}[\text{Ag}_2\text{Mo}_8\text{O}_{26}]_n$, (**4**) in methanol and its deposition onto a silicon substrate.

Examination of the surface using SEM reveals crystals of the polymeric architecture which are shown to be rod-like structures that are approximately 1 μm in diameter (Figure 93, top RHS). Energy Dispersive X-ray (EDX) carried out on the rod-like structures indicates a similar composition to compound **4** (Ag:Mo:O ratios: experimental = 1:4:12.5, theoretical = 1:4:13).¹²⁶ This strongly indicates that the rods observed have the same composition as for **4** which is highlighted by the insolubility of this compound in methanol without coercion from other sources such as heat (assumption 1: sonication produces micro-crystals of **4**). This assumption combined with observations of the crystal form using SEM indicates strongly that the rods observed also have the same structure as **4** (assumption 2: rods have same structure as **4**).

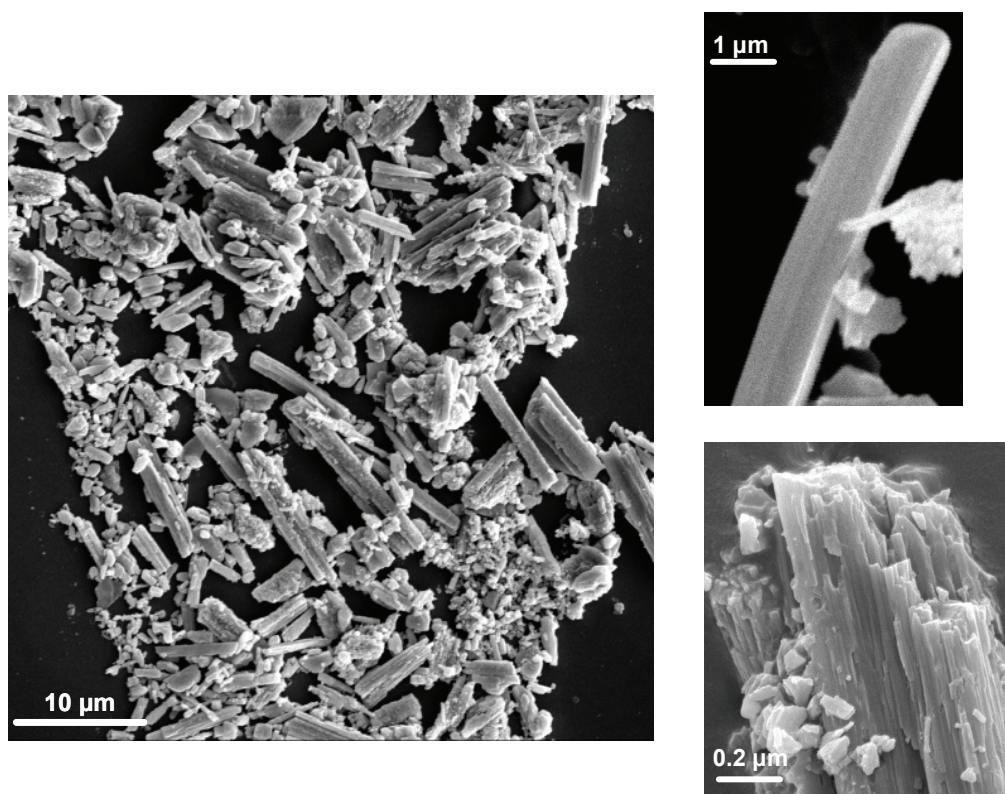


Figure 93 SEM image of nanorods of **4** (LHS) with magnified image of a nanorod (top, RHS) and the layering of crystalline material to form the nanorods (bottom, RHS).¹²⁶

The SEM images of the nanorods and microcrystals (Figure 93, bottom RHS) show how layers and layers of crystalline material can arrange on top of one another to form a microcrystal (Figure 93, top RHS). Based on the knowledge of the crystal structure of compound **4** where the building blocks assemble into the polymer and then into a packed array in the presence of the TBA cations (Figure 94), a hypothesis can be made with regards to the nanorod structure. Highlighted in figure 94 is the growth of the nanorods along the crystallographic a axis, an assumption based on the crystal structure of **4**, where the polymer grows along the a axis with the crystal morphology of the nanorod.

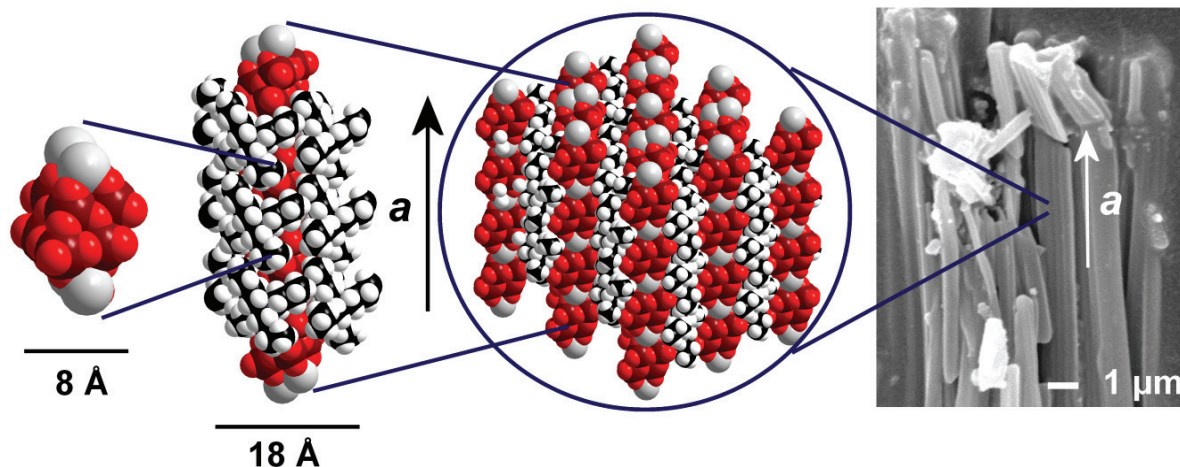


Figure 94 Space-filling representations of **4** containing the $\{\text{Ag}(\text{Mo}_8)\text{Ag}\}$ building block and the growth of the fragment into linear chains ‘wrapped’ by the TBA cations and the arrangement of the packed array (LHS). A SEM image of microcrystals of **4** is shown with the crystallographic a axis parallel to the direction of the polymer (RHS). Mo: brown, O: red, Ag: grey, C: black, H: white.

In addition to this, micro-rods can be seen to aggregate into spherulites, where the rods begin to ‘extend’ and grow in a radial fashion on the surface increasing the surface area covered to eventually form spherulites (Figure 95). The formation of similar structures has been previously observed where CuO nanoribbon strips which all point to a common centre, align perpendicular to a spherical surface to form ‘dandelions’ or microspheres.¹⁴⁸

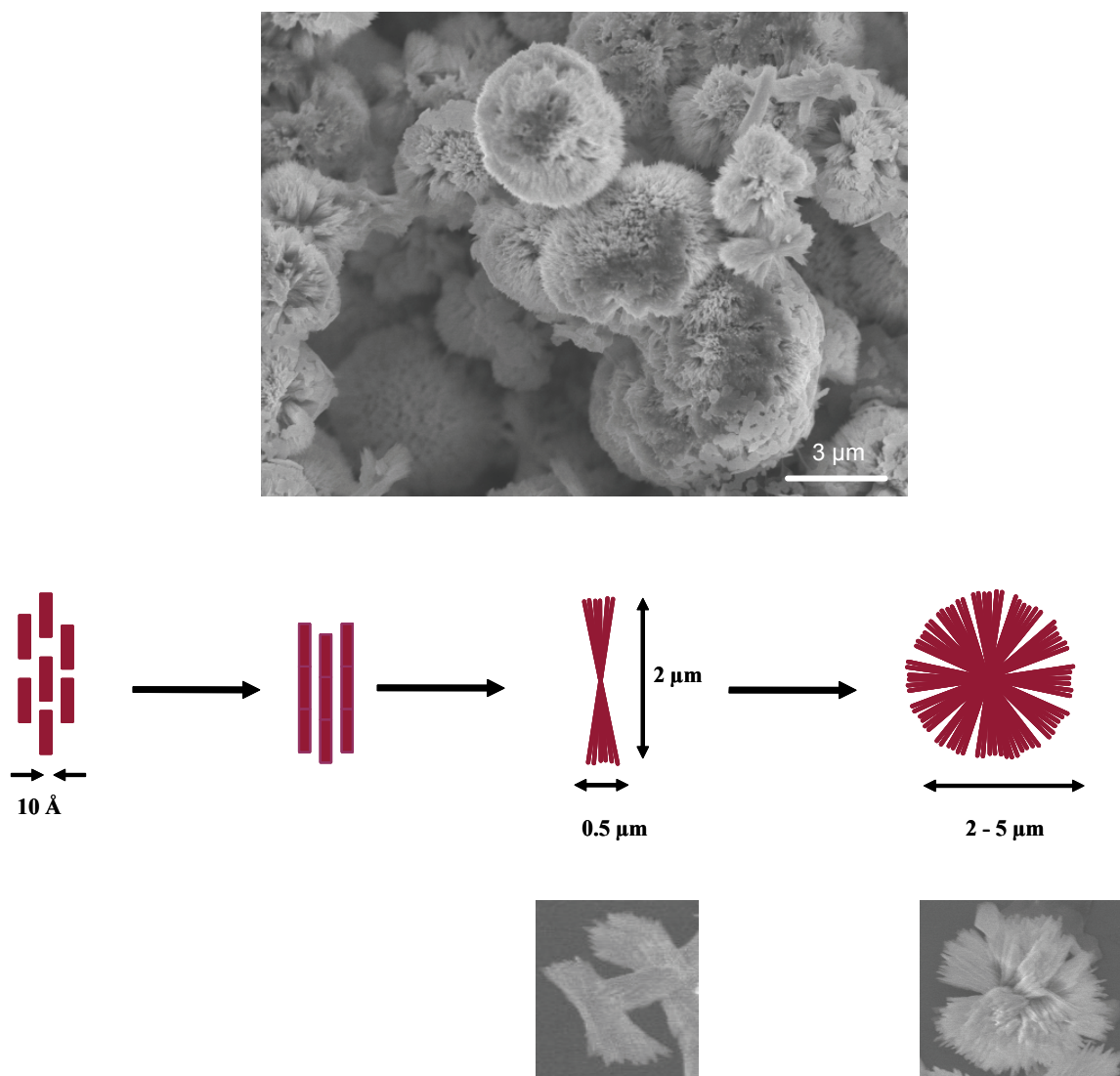


Figure 95 SEM image of full spherulite formation from a seven day old solution (top)¹²⁶ and illustration of the growth of the spherulites from the alignment of the rod-like crystals (bottom).

However, unlike the CuO structures the spherulites observed from the methanol solution of **4** are not hollow but rather have a flat ‘base’ and a centre from which the crystals align themselves and grow out from in a radial manner (Figure 96). At first the growth of the spherulites was attributed to imperfections along the surface caused by scratched grooves which provided a nucleation point for crystal growth.¹²⁶ However, similar structures have also been found on un-scratched surfaces, confirming that a scratched surface is not always necessary for growth of these structures but can help to act as a point of localisation for the crystals and hence nucleation.

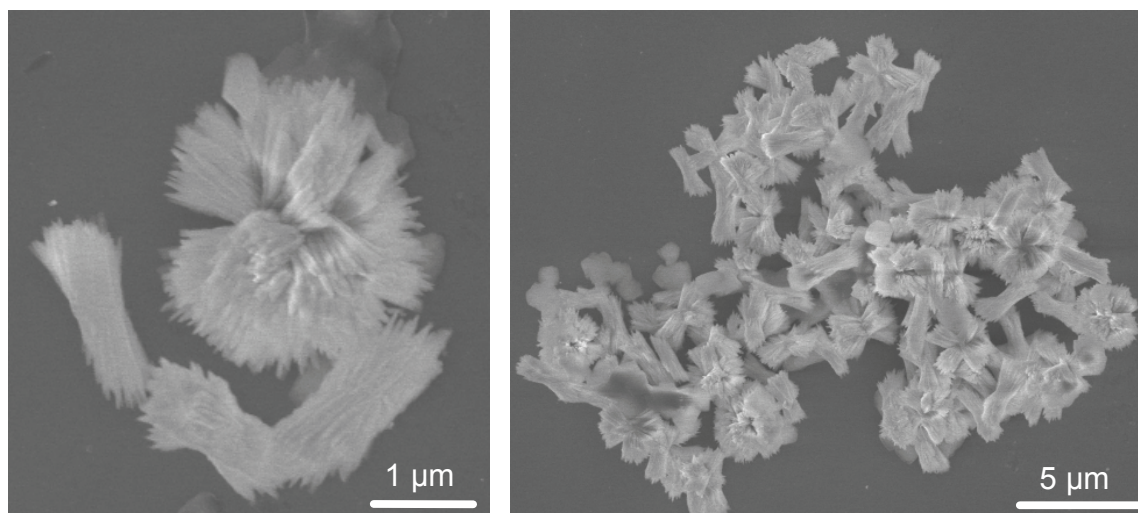


Figure 96 SEM image of partial growth of the spherulites from the alignment of the rod-like crystals.

The structures are typically formed when the methanol solution is left to stand at room temperature exposed to a minimum amount of light over a period of 7-10 days. The diameters range from 2-5 μm and EDX analysis shows the spherulites to be mainly composed of silver and oxygen with a low molybdenum ratio ($\text{Ag:Mo:O} = 1.2:1:2$).

3.4.2 Growth of Silver Nanostructures

The maturation of the original solution over time yielded results of a more interesting nature, where the growth of silver wires was observed. Typically, the wires form after the original methanol solution containing crystals of **4** is left for a period of approximately one month. Since we assume that the rods that give rise to these Ag-based structures are composed of $((n\text{-C}_4\text{H}_9)_4\text{N})_{2n}[\text{Ag}_2\text{Mo}_8\text{O}_{26}]_n$ (**4**) then some conclusions and assumptions can be made:

- The untypical short Ag...Ag interaction within **4** is possible due to the multi-oxo ligand donor set. This can be explained by a simple (electrostatic) crystal field model, according to which Ag(4d) electron density is repelled by the surrounding electronegative ligand positions and is stabilised between the Ag centres if significant Ag(4d)-Ag(4d) overlap is achieved.¹³⁷

- For the growth of the silver nanowires three possible scenarios could exist:
 - a) The Ag^{I} ions migrate to the surface of the crystal and are reduced to Ag^0 .
 - b) The Ag^{I} ions are reduced to Ag^0 which migrate to the surface of the crystal.
 - c) Ag can combine at the exposed sites of the crystal – this is dependent upon crystal decomposition to account for the free silver in the solution.
- The Ag nanostructures are growing from the crystals *via* the ‘tunnels’ created by the TBA cations which allow the growth of the wires in one direction. If Ag was not coming from the crystals then it would be more likely to form structures that are less directed i.e. not one-dimensional.
- SEM studies have shown that the rods from **4** are stable to electron irradiation and do not change as a function of time under the SEM.

We have previously reported that the wires are seen to grow from the spherulites (Figure 97, top) but in most instances the wires can be observed to grow in bundles with random orientation all over the silicon substrate (Figure 97, bottom). The wires also appear to be stable to the electron beam displaying no signs of further decomposition and grow in a non-uniform manner with diameters of approximately 50 nm.¹²⁶ EDX analysis has shown the wires to have a high silver and very low oxygen content with no presence of molybdenum (Ag:Mo:O = 53:0:14), confirming that the wires are mainly composed of Ag(0) (supplementary data section 7.2).

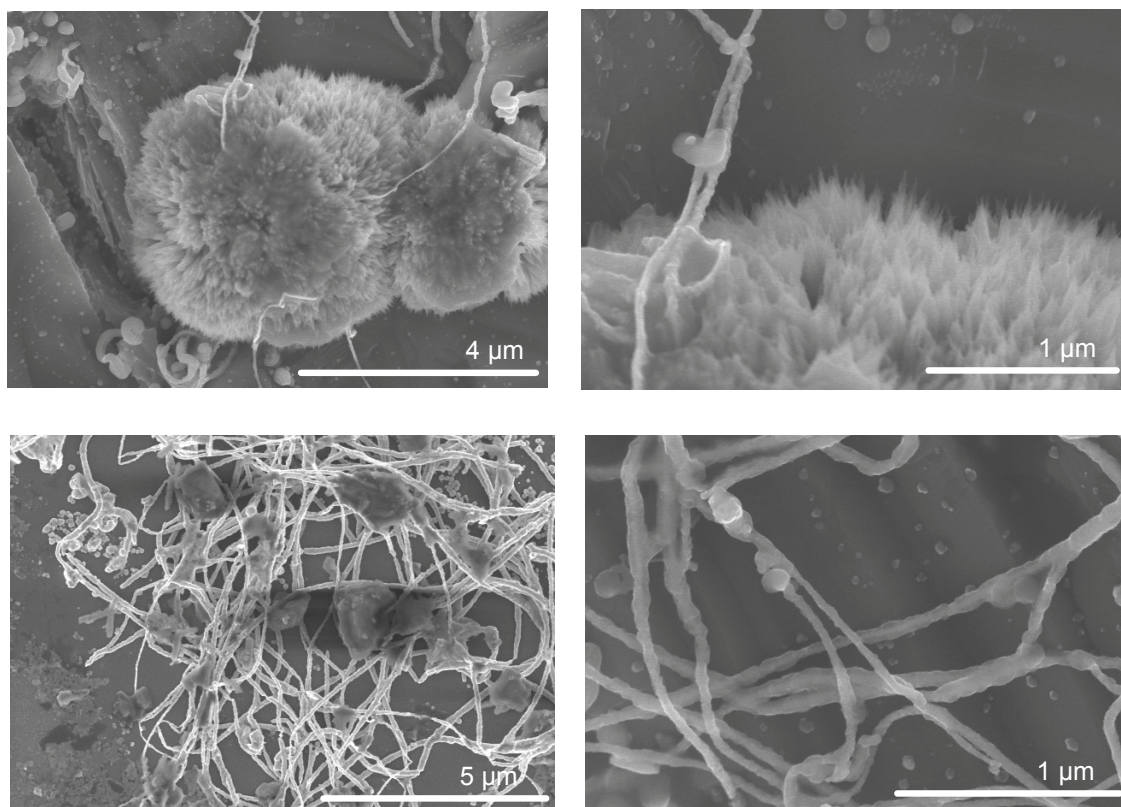


Figure 97 SEM images of wires growing from a spherulite (top), and bundles of the wires (bottom), all grown from a one month old solution.¹²⁶

SEM images of five month old methanol solutions show many crystals and growth of wires from these crystals (Figure 98, top). The crystals also align or grow against one another to produce even bigger crystals (Figure 98, bottom).

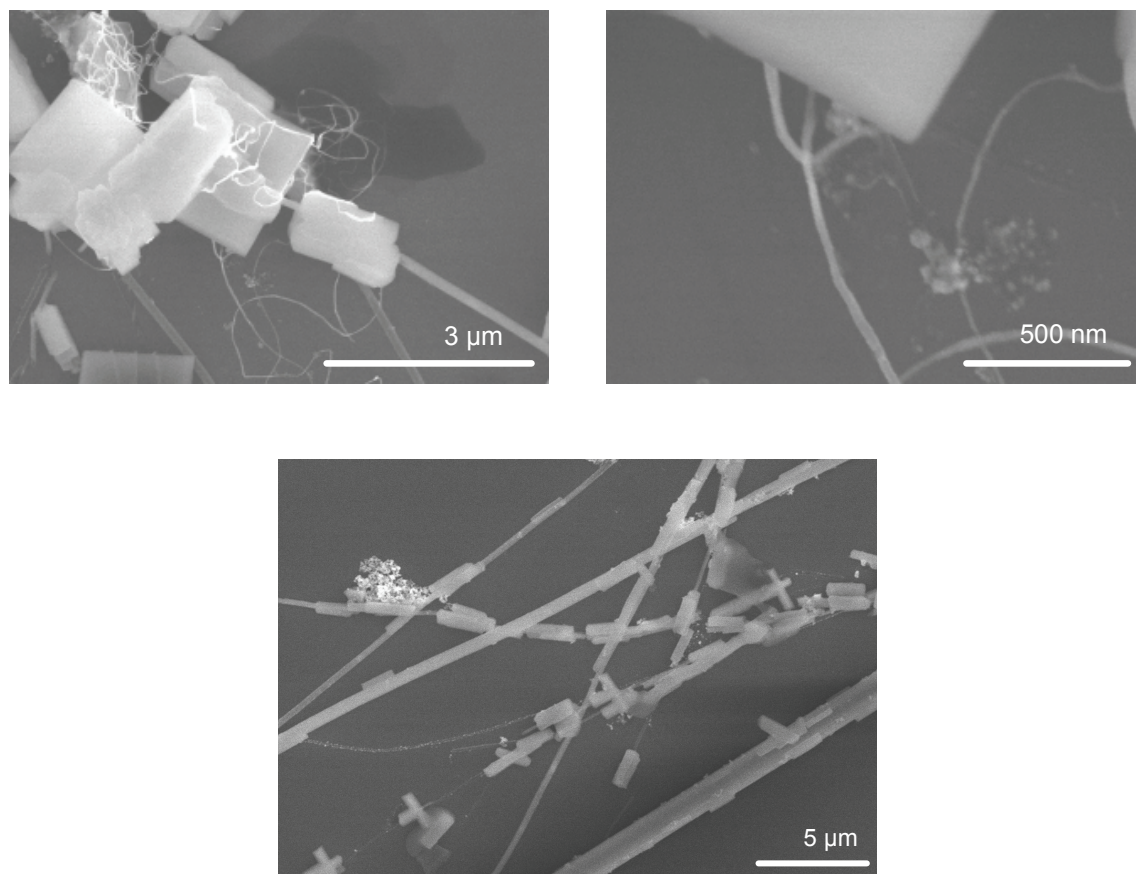


Figure 98 SEM image of wires growing from crystals obtained from a five month old solution (top, *LHS*) and a magnified image of the same sample with a wire growing from one face of the crystal (top, *RHS*). SEM image of crystals aligning against one another to produce bigger crystals (bottom).

One hypothesis can be suggested to understand the growth of the wires within this system which involves reduction and oxidation processes of Ag^+ and methanol respectively. The process is one that also involves the formation of formaldehyde from methanol using silver as an oxidant and which has been reported on a number of occasions.^{149,150}

The model is based on the redox potentials^{151,152} of Ag^+ and methanol:

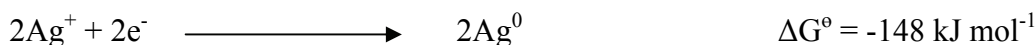
$$\Delta G^\circ = -n F E^\circ$$

$$E^\circ \text{ for } \text{Ag}^+/\text{Ag} = 0.77 \text{ V}$$

$$E^\circ \text{ for } \text{CH}_3\text{OH}/\text{H}_2\text{C}=\text{O} = -0.5 \text{ V}$$

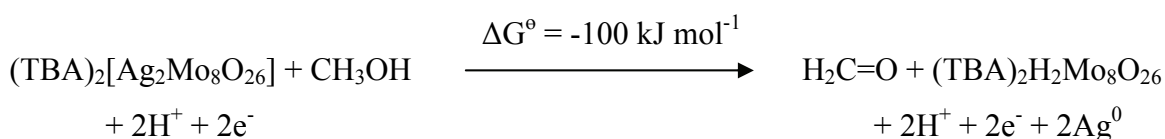
$$\Delta G^\circ \text{ for } \text{Ag}^+ = -1 \times 96485 \text{ C mol}^{-1} \times 0.77 \text{ V} = -74 \text{ kJ mol}^{-1}$$

$$\Delta G^\circ \text{ for } \text{CH}_3\text{OH} = 1 \times 96485 \text{ C mol}^{-1} \times 0.5 \text{ V} = 48 \text{ kJ mol}^{-1}$$



$\Delta G^\circ = -100 \text{ kJ mol}^{-1}$ (an upper estimate for this reaction when Ag^+ is in an oxo environment).

Evaluation of the half reactions with the reactions below indicates that the negative value favours the reactions and will release energy. It also suggests that the reaction is spontaneous and does not require initiation by other external factors such as light.



The above mechanism is a working hypothesis that can be used to explain the formation of the Ag^0 wires and relies on the production of formaldehyde from methanol.

Below is a theoretical evaluation for the maximum silver wire growth from a crystal. The calculations suggest that a reasonable amount of Ag^0 can be produced from a crystal to give wires of substantial length:

$$\begin{aligned} \text{Dimensions of crystal} &= 5 \mu\text{m} \times 2 \mu\text{m} \times 2 \mu\text{m} \\ &= 5 \times 10^{-6} \text{ m} \times 2 \times 10^{-6} \text{ m} \times 2 \times 10^{-6} \text{ m} \end{aligned}$$

$$V_{\text{crystal}} = 5 \times 10^{-6} \text{ m} \times 2 \times 10^{-6} \text{ m} \times 2 \times 10^{-6} \text{ m} = 2 \times 10^{-17} \text{ m}^3$$

$$V_{\text{u.c.}} = 2713.4 \text{ \AA}^3 = 2.713 \times 10^{-27} \text{ m}^3 \quad \text{u.c.} = \text{unit cell}$$

For $((n\text{-C}_4\text{H}_9)_4\text{N})_{2n}[\text{Ag}_2\text{Mo}_8\text{O}_{26}]_n$ (4) = 4 Ag ions per unit cell

$$V_{\text{crystal}} / V_{\text{u.c}} = 2 \times 10^{-17} \text{ m}^3 / 2.713 \times 10^{-27} \text{ m}^3 = 7.37 \times 10^9$$

$$\begin{aligned} \text{No. of silver ions in crystal} &= 7.37 \times 10^9 \times 4 \\ &= \sim 3 \times 10^{10} \end{aligned}$$

$$\text{Avogadro's constant} = 6.022 \times 10^{23} \text{ mol}^{-1}$$

$$\begin{aligned} \text{No. of silver ions in crystal} &= 3 \times 10^{10} / 6.022 \times 10^{23} \text{ mol}^{-1} \\ &= 5 \times 10^{-14} \text{ mol} \end{aligned}$$

$$\text{Formula weight of Ag: } 107.86 \text{ g mol}^{-1}$$

$$M_{\text{Ag}} = 5 \times 10^{-14} \text{ mol} \times 107.86 \text{ g mol}^{-1} = \sim 5.39 \times 10^{-12} \text{ g}$$

$$d_{\text{Ag}} = 10.5 \text{ g cm}^3$$

$$M_{\text{Ag}} / d_{\text{Ag}} = V_{\text{Ag}} = \sim 5 \times 10^{-13} \text{ cm}^3 = 5 \times 10^8 \text{ nm}^3$$

Based on a nanowire with a radius of 25 nm and diameter of 50 nm:

$$V = \pi r^2 h$$

$$h = V / \pi r^2$$

$$h = 5 \times 10^8 \text{ nm}^3 / \pi 625 \text{ nm}^2 = \sim 254 \times 10^3 \text{ nm} = \sim \mathbf{254 \mu m}$$

Therefore the maximum length of silver wire that can be produced from a crystal with a dimension of 5 μm x 2 μm x 2 μm is approximately 254 μm .

To establish the growth mechanism of the wires and to optimise the synthesis, further experiments were carried out which included the growth of wire-like structures from powder material of **4** and the addition of extra silver and will be discussed in the following sections.

Growth of Wires from Powder Material of $((n\text{-C}_4\text{H}_9)_4\text{N})_{2n}[\text{Ag}_2\text{Mo}_8\text{O}_{26}]_n$ (4b)

The synthesis of compound **4** can occur in two ways: either from ether diffusion, directly into the reaction mixture of $((n\text{-C}_4\text{H}_9)\text{N})_2\text{Mo}_6\text{O}_{19}$ and silver(I) fluoride to give **4a** or through the extraction of a white powder material which can be recrystallised to give the same compound (**4b**). The latter procedure gives a higher yield and better purity and can also be used to produce wires/fibres on smaller time scales of approximately 10 days. However, the quality of the wires isolated from this method is greatly reduced, and SEM images have shown the wires to be more disjointed in their assembly (Figure 99). It is also possible to see the formation of structures that appear to be partial spherulites but more crystalline in nature.

The appearance of the disjointed nanostructures can be directly related back to the original starting material and correlates well with the idea of this particular system being one of mass transfer. Here the powder material is made of smaller crystals which contain much less silver when compared with single crystals of **4** but have increased surface area. The silver wires which are disjointed, short and poor quality in their appearance are a direct result of rapid growth of the wires from the smaller crystals.

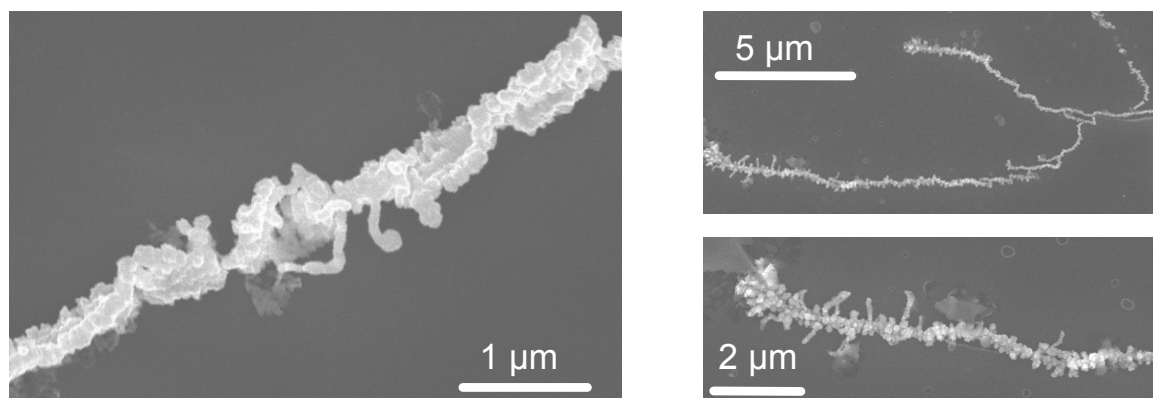


Figure 99 SEM images of Ag wires grown from powder material of **4**.

Transmission Electron Microscopy (TEM) and Selective Area Electron Diffraction (SAED) have also shown these wires to be Ag(0) coated in a layer of molybdenum oxide (Figure 100). The sharp peaks can be indexed to (111), (002), (220) for Ag(0) and (200) for MoO_3 . Thus, the SAED diffraction pattern reveals two different materials, one which

indicates poly crystalline material of Ag(0) and another of the molybdenum oxide species; MoO₃. Similar SAED patterns have been seen before by a number of groups for silver nanostructures.^{117,153} EDX analysis has also shown that these wires are composed of silver (supplementary data section 7.3).

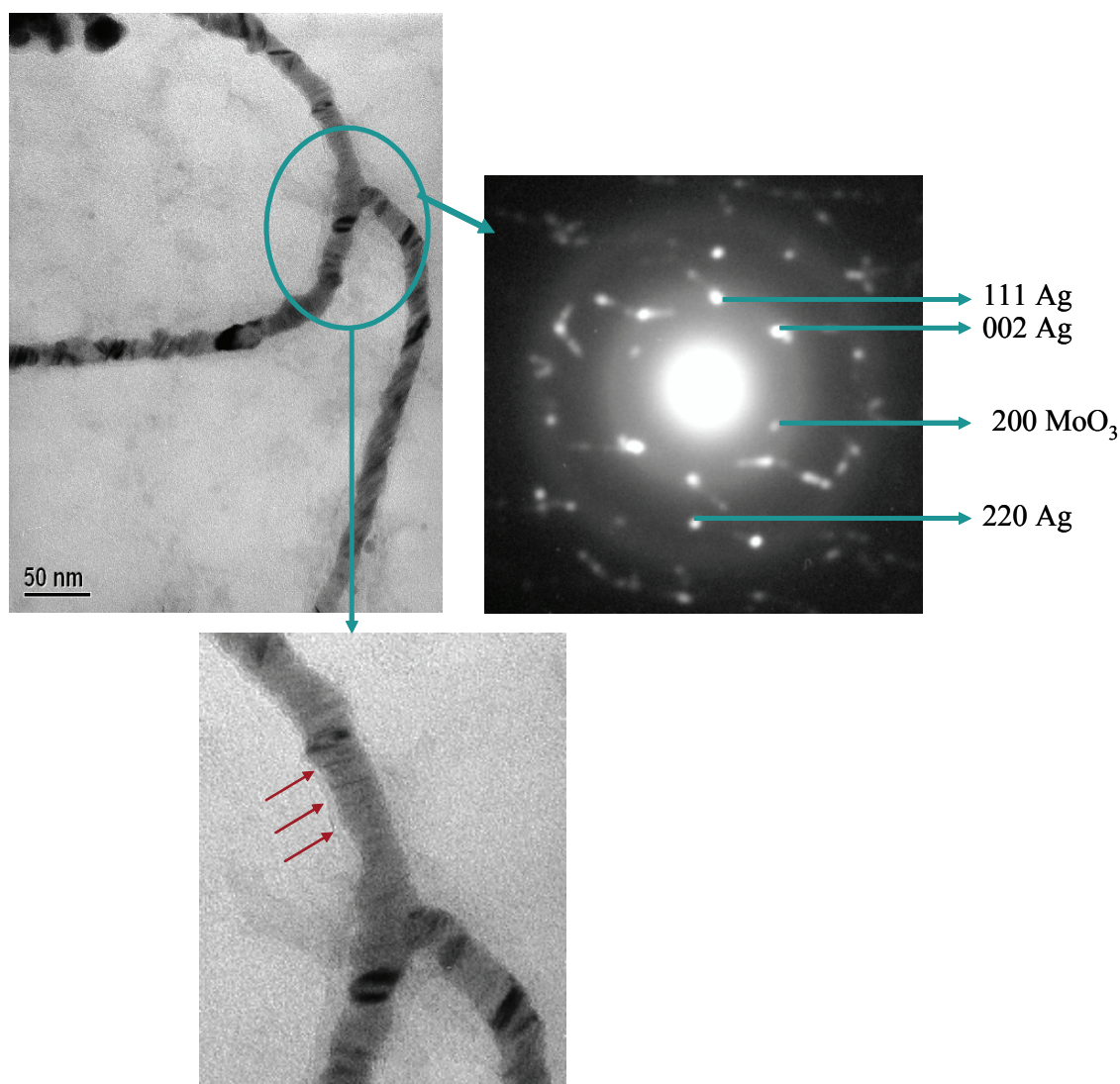


Figure 100 TEM image (top, *LHS*) and SAED pattern of the wires (top, *RHS*) with an expanded view of the nanowires and the thin layer of molybdenum oxide highlighted by the red arrows (bottom).

Addition of Silver(I) Fluoride

Interesting results were also obtained when the original method used to prepare the wires was modified by adding additional silver in the form of silver(I) fluoride. These

preliminary studies were carried out on samples prepared with crystals or powder of **4**, and the results presented are still being investigated.

In the initial procedure the wires were produced from a solution containing suspended crystals of **4** after a period of one month. In this new procedure, additional silver(I) fluoride was added to a solution prepared in the same way as before. The results were the formation of many bundles of wires all over the silicon substrate from only a 10 day old solution (Figure 111, LHS), a marked decrease in the time it takes to produce such wires.

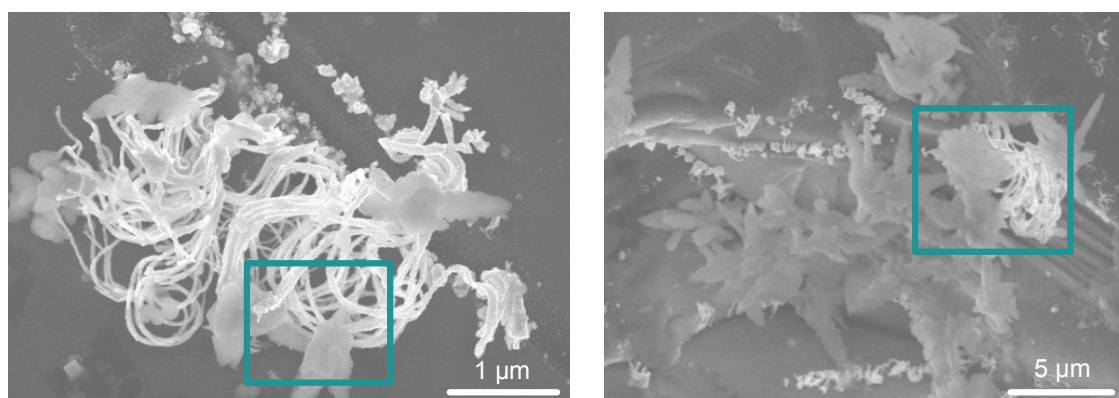


Figure 111 SEM images of bundles of wires growing from microcrystals (highlighted by green box) from a 10 day old solution with additional silver.

These findings suggest a number of things related to how the wires are grown within this set-up and perhaps give an insight into the growth of the wires in the original procedure. What can be observed from the SEM images is the presence of microcrystals and the growth of the wires from these (Figure 111, green box), suggesting that perhaps the crystals are of compound **4** and that free labile silver in the methanol solution is able to increase the reaction rate in solution and thus the rate at which the wires grow. A control set-up of silver(I) fluoride in methanol left for 10 days shows crystals on a silicon substrate with flake like morphology (Table 6) and indicates that the crystals in the additional silver set up are most likely to be of compound **4**.

The silver wires grown from a ‘matured’ solution of **4**, can be observed to come from the spherulite structures or microcrystals (Figure 112). Within these examples however, the silver nanostructures have controlled growth in one orientation due to the organic ‘tunnels’

and thus spatial control is given by limiting mass transfer of silver which migrates to the surface *via* the ‘tunnels’.

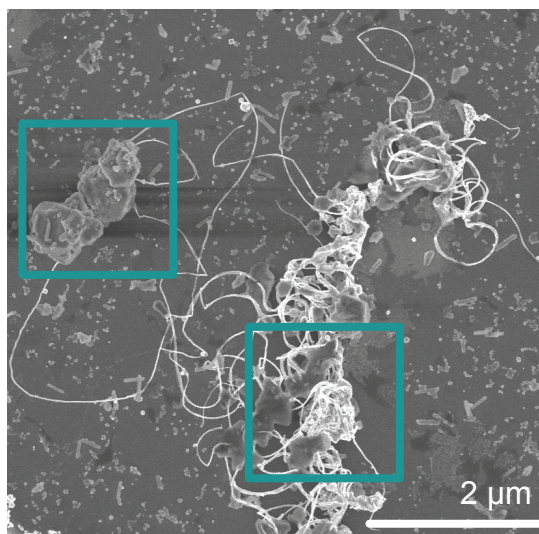


Figure 112 SEM images of bundles of wires growing from microcrystals (highlighted by green box).¹²⁶

Additional silver was also added to a methanol solution containing powder material of **4** with preliminary results showing microcrystals on the silicon substrate. What is also interesting is the growth of nanostructures from the microcrystals (Figure 113). There is a possibility that these nanostructures are composed of silver and the growth could be most likely attributed to the extrusion of silver from the crystal. These assumptions can be made based on the growth of the nanostructures which come from only one face of the crystal and highlight the influence the organic ‘tunnels’ have and that the silver most likely does not come from excess silver in solution. Had the excess silver contributed to the growth from the crystal then multiple growths should be observed from the crystal and not from only two points (Figure 113, RHS).

This is a key observation where SEM images capture the initial growth process of the silver nanostructures from the crystals. Examples of extrusion from bulk material have been noted previously by several groups through different methods. Barsoum and Farber reported the unusual physical phenomenon of the extrusion of gallium whiskers from bulk Cr_2GaN samples under high temperatures.¹⁵⁴ Edward *et al.* and Banhart *et al.* have also reported the extrusion of nanomaterials using templates.^{155,156}

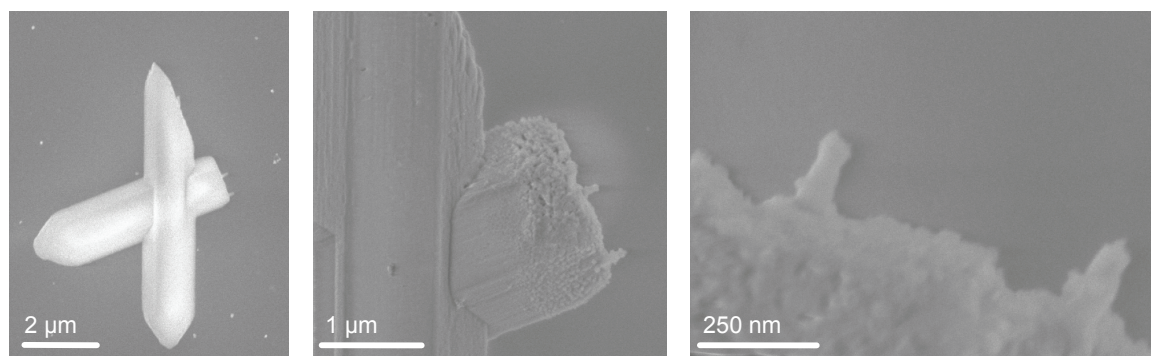


Figure 113 SEM image of a crystal (*LHS*) with gradual magnification of the nanostructures (*centre* and *RHS*) growing from the crystal.

3.4.3 Microscopy Studies on Other Ag-Mo Polyoxometalates

SEM studies were also carried out on two other Ag-Mo POM compounds: $((n\text{-C}_4\text{H}_9)_4\text{N})_{2n}[\text{Ag}_2(\text{DMSO})_2\text{Mo}_8\text{O}_{26}]_n$ (**15**) and $[\text{Ag}(\text{C}_7\text{H}_{12}\text{O}_2\text{N})(\text{CH}_3\text{CN})]_{2n}[(\text{Ag}(\text{CH}_3\text{CN}))_2\text{Mo}_8\text{O}_{26}]_n \cdot 2\text{CH}_3\text{CN}$ (**12**). Compound **15** as discussed in section 3.2.4 is made of up interweaved chains isolated by TBA cations where the $\{\text{Ag}(\text{Mo}_8)\text{Ag}\}$ building blocks are linked together by μ_2 -oxo DMSO bridges. Unlike **4**, crystals of **15** were not suspended in a methanol solution but rather grown directly onto a silicon substrate. Using normal methods of crystallisation, a co-solvent was diffused into a vial of the reaction mixture which also contained a silicon substrate to produce **15**. The crystals were grown over a period of 60 days. The SEM image of the sample shows what looks to be a crystal that has decomposed over time (Figure 114), and a silver wire growing from the top of this crystal. EDX analysis confirms that the wire is composed of silver and the surrounding crystal to be composed of molybdenum and oxygen with no silver (supplementary data section 7.4).

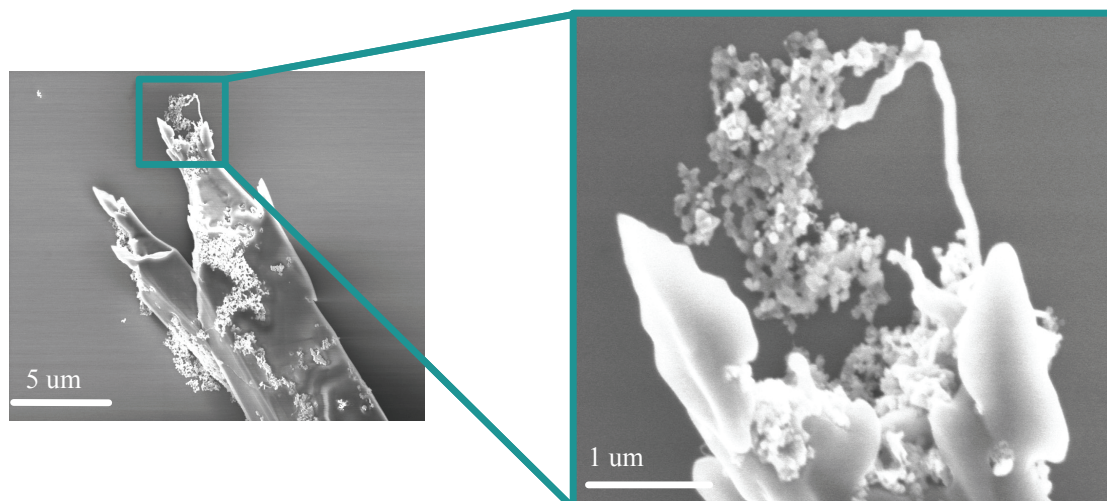


Figure 114 SEM image of a crystal (*LHS*) with magnification of the silver nanostructure (*RHS*) growing from the crystal.

Preliminary surface work was also carried out on complex **12**, a one-dimensional array of $\{\text{Ag}(\text{Mo}_8)\text{Ag}\}$ synthons held together by long $\text{Ag}\dots\text{Ag}$ interactions. Placed interstitially around the chains are aromatic complex cations, where 2,6-pyridine-di-methanol is complexed to one $\text{Ag}(\text{I})$ ion at the nitrogen position. Here the idea was to compare one form of polymer without TBA cations with **4** which does contain TBA cations. The solutions were made by suspending crystals of **12** in methanol. The ‘fresh’ solution was then deposited onto a silicon substrate. Initial results have shown the assembly of fibrous material that appears to grow out from a common point (Figure 115, *LHS*), to produce a larger microstructure that is more fibrous in its appearance (Figure 115, *RHS*). Although the structures are not growing out in a complete spherical manner, their appearance and the idea of growing from a common point is similar to the spherulites observed in **4**.

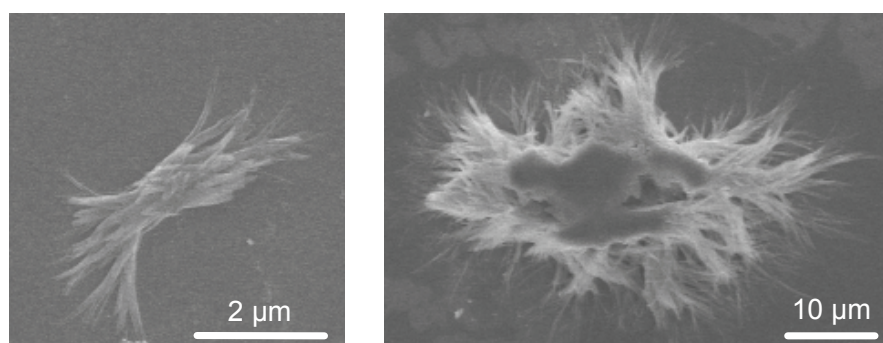


Figure 115 SEM image of the fibrous material aligning (*LHS*) and growing out to a larger fibrous nanostructure (*RHS*).

The silicon substrates were also prepared by creating imperfections along the plate to produce indentations, and a point of nucleation for the crystals to grow, a method used by Pickering in the earlier studies of 4. Again preliminary results have shown the growth of wire-like structures from the indentations (Figure 116).

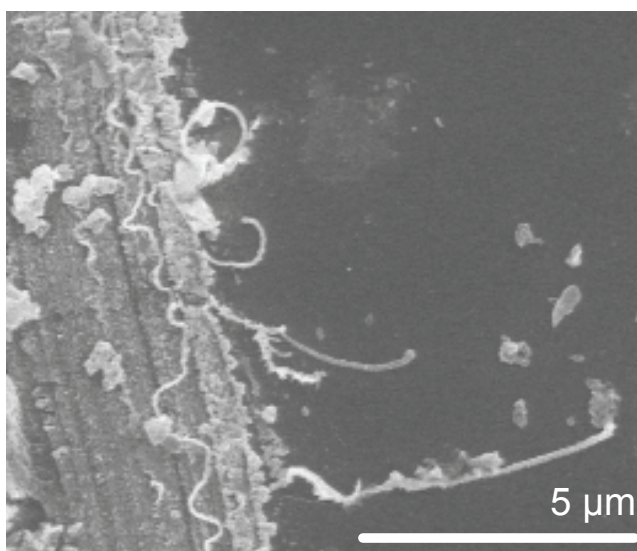
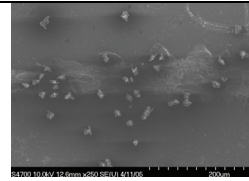
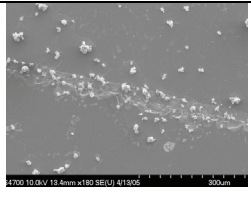
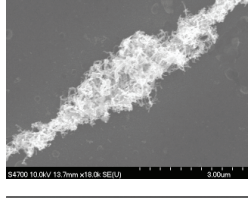
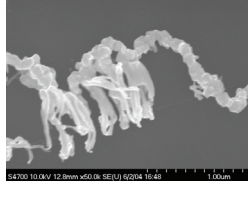
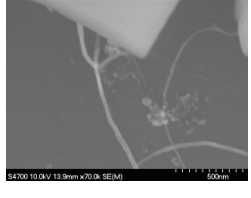
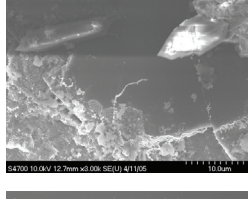
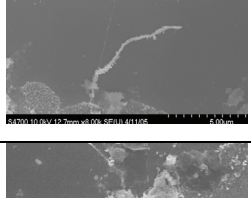
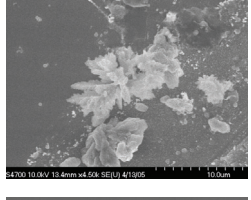
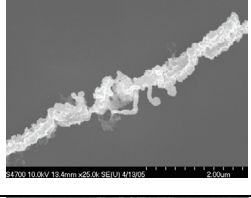
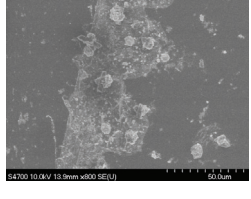


Figure 116 SEM image of the wire-like structures growing from the indentations.

The investigations into 15 and 12 are currently on-going and as such their analysis remains in-complete and so any initial conclusions that can be drawn from the SEM images is for only speculative comparison to the work done with 4.

The many results presented and discussed throughout section 3.4 can be summarised in table 6:

Experimental Set-up (Section 5)	Age of solution (approx. days)	Description	EDX/ TEM/ SAED	Picture
5.4.1	10	Crystals / rods	-----	

	20	Crystals	-----	
	30	Bundles of wires	EDX	 
	40	Crystals	-----	-----
5.4.2	150	Wires growing from crystals	-----	
5.4.3	10	Poor quality wires and rods	EDX	 
	20	Spherulites	-----	
		Poor quality wires	-----	
	30	Crystals	-----	

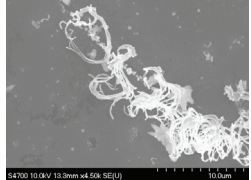
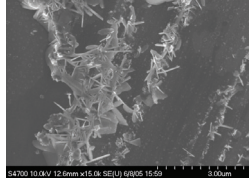
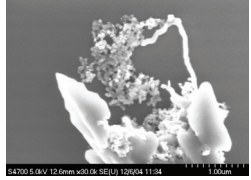
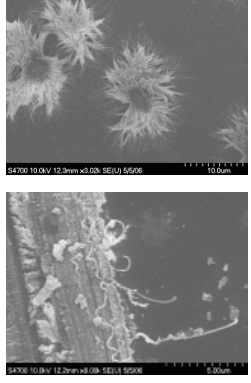
	40	Crystals	----	----
5.4.4	----	Fibres	TEM/ SAED	
5.4.5	10	Wires/ fibres	----	
5.4.6	10	Crystals and wires	----	
5.4.7	12	Crystals with flake like appearance	----	
5.4.8	60	Crystals and wires	EDX	
5.4.9	15	Spherulites and fibres	----	

Table 6 Tabulated summary of microscopy results with corresponding experimental codes.

3.5 Potassium Polyoxomolybdate Clusters

Using the d^{10} transition metal silver has proved to be successful in isolating a whole family of structurally related compounds. Extending this strategy towards other POM clusters and transition metals therefore seemed to be the next logical step. Many attempts were made to react $((n\text{-C}_4\text{H}_9)_4\text{N})_2\text{Mo}_6\text{O}_{19}$ (**1**) with other transition metals such as iron, copper and lanthanides. However, under these reaction conditions the $\{\text{Mo}_6\}$ cluster proved to be stable and un-reactive and only the starting material was recovered.

Within the published literature there have been no accounts to date of POM clusters containing gold. It seemed therefore an interesting choice for extending the strategy used in the previous syntheses by substituting silver for gold, with the idea of generating iso-structural or similar compounds as the ones obtained with silver.

At first gold(I) iodide was used and due to its insolubility it was suspended in DMSO or DMF and subsequently added to a solution of $((n\text{-C}_4\text{H}_9)_4\text{N})_2\text{Mo}_6\text{O}_{19}$ (**1**) in DMSO or DMF. The results were limited with only crystals of the starting material forming even though a colour change had been identified during the course of the reaction. This may be partly due to the insolubility of the gold(I) iodide or the un-reactive nature of the starting material $\{\text{Mo}_6\}$ which was also observed with the other transition metals. Thus, another gold salt, hydrogen tetrachloroaurate, $\text{HAuCl}_4 \cdot 3\text{H}_2\text{O}$ was employed to solve the issue of solubility. As a protonated, highly hygroscopic species, this gold compound is very soluble in water and in other non-aqueous coordinating solvents such as DMF and DMSO. It was also thought that as a ‘soft’ metal, the gold ions would be attractive towards the ‘soft’ and polarisable sulphur atoms within the DMSO solvent molecules.

However, the outcome was once again a large volume of yellow crystals of **1** which can be attributed to the un-reactive nature of both the gold salt and of **1** under these reaction conditions. Alternatively it could also be due to the increased number of protons in solution which favours the starting material **1**. As already discussed, **1** is produced under highly acidic conditions, which rarely proved to be a problem in the silver based reactions. With this in mind organic bases were used to remove the excess protons in the reaction

mixture when using DMF and DMSO, however, the result was once again the isolation of **1**.

Having very little success in using $\{\text{Mo}_6\}$ as a precursor the next step was to then use $\beta\text{-}\{\text{Mo}_8\}$. The compound $\beta\text{-}((n\text{-C}_4\text{H}_9)_4\text{N})_3\text{KMo}_8\text{O}_{26}\cdot 2\text{H}_2\text{O}$ (**7**) was reacted with both gold(I) iodide and hydrogen tetrachloroaurate. On using hydrogen tetrachloroaurate, yellow crystals were formed that were identified as **1**. The octamolybdate cluster is formed at a higher pH than hexamolybdate and the presence of excess protons in solution may be enough to convert $\beta\text{-}\{\text{Mo}_8\}$ into $\{\text{Mo}_6\}$, the reverse of which has been demonstrated in reactions with silver.

Gold(I) iodide when reacted with **7** produced some new architectures which interestingly enough did not contain gold. Instead, the potassium ion that is used to counterbalance the charge of the Mo-starting material can be seen to interact with a number of terminal oxygen atoms on $\beta\text{-}\{\text{Mo}_8\}$, to produce two new architectures that are comparable to two of the Ag-Mo POMs discussed previously. The isolation of both has been facilitated by the TBA counterion in the starting material.

When gold(I) iodide was suspended in DMSO and added to a DMSO solution of **7**, the result was the isolation of a two-dimensional array that contained two types of chains $((n\text{-C}_4\text{H}_9)_4\text{N})_{2n}[\text{K}_2(\text{DMSO})_3\text{Mo}_8\text{O}_{26}]_n$ (**23**). The asymmetric unit contains two halves of a $\{\text{Mo}_8\}$ cluster to which each is coordinated one potassium atom (and which are crystallographically different to one another), three DMSO molecules and two TBA counterions.

What is especially interesting is that the chains are similar to the chains found in $((n\text{-C}_4\text{H}_9)_4\text{N})_{2n}[\text{Ag}_2(\text{DMSO})_3\text{Mo}_8\text{O}_{26}]_n$ (**15**) and have the same arrangement, creating interweaved chains (Figure 117). The difference is that the $\{\text{Mo}_8\}$ clusters that are linked by silver(I) in **15**, are linked here by potassium ions, whereby the angle between the chains of neighbouring layers equals to approximately 73° .

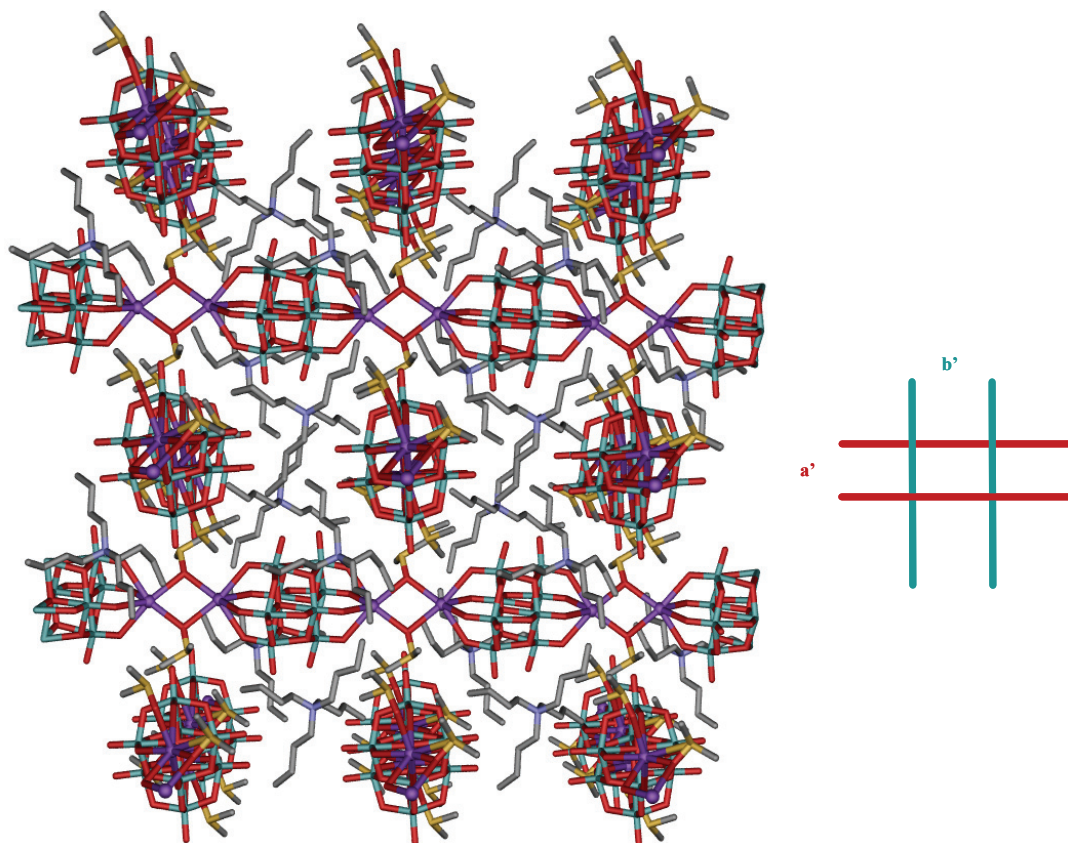


Figure 117 View of **23** along the crystallographic b axis. Inset shows a simplified schematic of the 2D array. Mo: green, K: purple spheres, S: yellow, O: red, C: grey, N: blue (hydrogen atoms removed for clarity).

In both types of chains the potassium positions are not directly bridging the $\{\text{Mo}_8\}$ units, but each potassium centre is coordinated to only one $\{\text{Mo}_8\}$ cluster and as in **15**, DMSO ligands act as bridges linking the $\{\text{Mo}_8\}$ clusters together. As in **15** there are two different chain types with similar bridging modes of the DMSO ligands creating a' -type and b' -type chains (Figure 117, inset).

The a' -type chains have identical bridging modes as found in a -type chains in **15** (Figure 118). Neighbouring potassium centres are linked *via* two DMSO ligands to form $(\text{O}_4)\text{K}(\mu_2\text{-DMSO})_2\text{K}(\text{O}_4)$ bridges between the adjoining $\{\text{Mo}_8\}$ fragments (Figure 118). Both potassium ions coordinate to the μ_2 -oxo centres of the DMSO molecules (the $\text{K}-\mu_2\text{O}(\text{SC}_2\text{H}_6)$ distances are nearly equivalent 2.702(3)/2.753(3) Å, with a $\text{K}\dots\text{K}$ distance of 4.331(2) Å and $\text{O}-\text{K}-\text{O}$ angle of 105.11(11)°). The coordination to the terminal oxygen atoms of the $\{\text{Mo}_8\}$ cluster is to the square $\{\text{O}_4\}$ moieties, thereby creating a tetradentate

arrangement (K-O distances between 2.746(3) and 2.784(3) Å and O-K-O angles of 65.85(9) and 105.16(9)° for minimum *cis* and maximum *trans* values respectively).

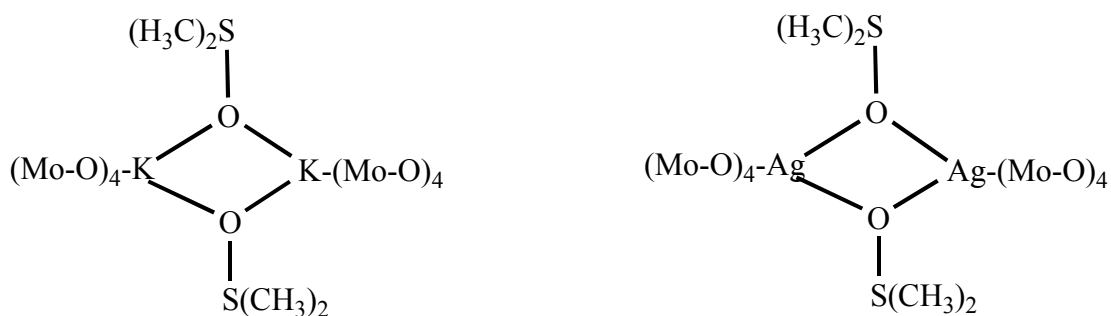


Figure 118 Representation of the similar bridging modes in **23** type *a'* chains (*LHS*) and **15** type *a* chains (*RHS*).

In *b'*-type chains the same bridging mode as in *a'*-type chains within **23** can be found, with regards to the μ_2 -oxo bridges of DMSO. However, their coordination to the terminal oxygen atoms of {Mo₈} is the same as seen in the *b*-type chains in **15** (Figure 119). Unlike the *b*-type chains of **15** where the {Ag(Mo₈)Ag} clusters are bridged through the sulfur and oxo atoms within DMSO, here the potassium ions are linked in the same way as in *a'*-type chains (the K- μ_2 -O(SC₂H₆) distances are nearly equivalent 2.752(3)/2.767(3) Å, with a K...K distance of 4.457(2) Å and O-K-O angle of 107.70(11)° for minimum *cis* and maximum *trans* values respectively). The exception is that while in chains of type *a'* the potassium positions cap all four oxo positions of an {O₄} group, the potassium centres in type *b'*-chains coordinate to only two of the four oxo positions (K-O distances of 2.808(3) and 2.832(3) Å, O-K-O angle of 68.72(9)°), the same as the silver(I) ion in *b*-type chains in **15**. There are also interactions to the remaining two terminal oxygen atoms of {Mo₈} (K-O distances of 2.930(3) and 3.049(3) Å, O-K-O angles between 61.37(8) and 97.51(9)°). There is one further DMSO ligand bound to the potassium ion in *b'*-type chains that is not a bridging ligand (K-O distances of 2.930(3) Å).

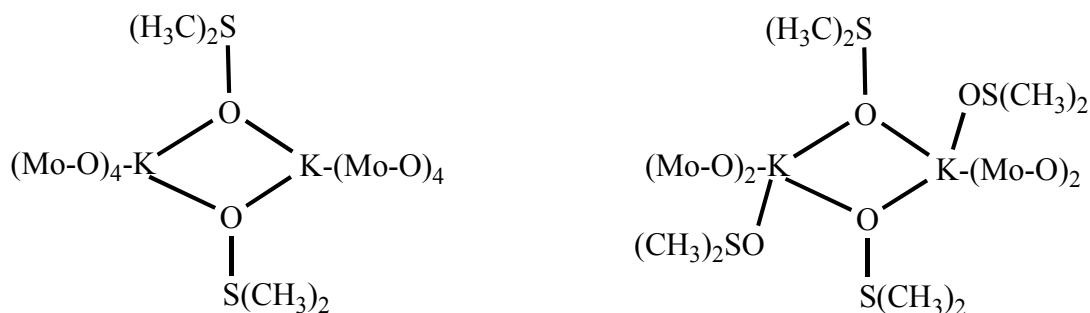


Figure 119 The two types of bridging modes in **23** type *a'* (*LHS*) and type *b'* (*RHS*) chains.

As has been demonstrated repeatedly with previous structures and comparatively with **15**, TBA cations have prevented the chains from cross linking into a two-dimensional network. However, this was not the case with $((n\text{-C}_4\text{H}_9)_4\text{N})_n(\text{H}_2\text{NMe}_2)_n[\text{K}_2(\text{DMF})\text{Mo}_8\text{O}_{26}]_n \cdot \text{DMF}$ (**24**) which is the only example of a two-dimensional network that contains TBA cations. This has never been observed in the Ag-Mo based POMs that form the two-dimensional networks and arrays discussed in section 3.2. This may be due to the change in secondary metal ion or more likely due to only *one* TBA cation being present in each unit cell and one small cation in the form of protonated dimethylamine. The asymmetric unit of **24** therefore contains one $\{\text{Mo}_8\}$ cluster, two potassium ions to which one is coordinated a DMF molecule, one TBA cation, one dimethylamine cation and one solvent DMF molecule.

A 2:1 equivalent of gold(I) iodide to $\beta\text{-}((n\text{-C}_4\text{H}_9)_4\text{N})_3\text{KMo}_8\text{O}_{26} \cdot 2\text{H}_2\text{O}$ in DMF yielded a network, where the arrangement of the $\{\text{K}(\text{Mo}_8)\text{K}\}$ repeating unit is similar to the $\{\text{Ag}(\text{Mo}_8)\text{Ag}\}$ synthon arrangement in $[\text{Ag}_4(\text{DMSO})_6(\text{OC}(\text{CH}_3)_2)_2\text{Mo}_8\text{O}_{26}]_n$ (**21**).

Each $\{\text{Mo}_8\text{O}_{26}\}$ unit has four potassium atoms linking it into an array. Two distinct coordination environments exist for these potassium atoms; K1 and K2 (Figure 120), where each has the same number of associations to the oxygen atoms of the $\{\text{Mo}_8\}$ cluster. K1 coordinates to the square $\{\text{O}_4\}$ group of one $\{\text{Mo}_8\}$ cluster, and to two further oxygen atoms of the subsequent cluster (K-O distances are between 2.621(12) and 2.870(13) Å and O-K-O angles between 65.10(3) and 156.30(4)° for minimum *cis* and maximum *trans* values respectively). In addition to this the coordination sphere of K1 is completed by one DMF ligand which reinforces the structure through hydrogen bonding to the nearby protonated dimethylamine cation (K-O distance of 2.993 Å, N-H...O distance of 2.712 Å).

The same cation also has hydrogen bonding interactions to the solvent DMF molecule within the lattice (N-H...O distance of 2.732 Å).

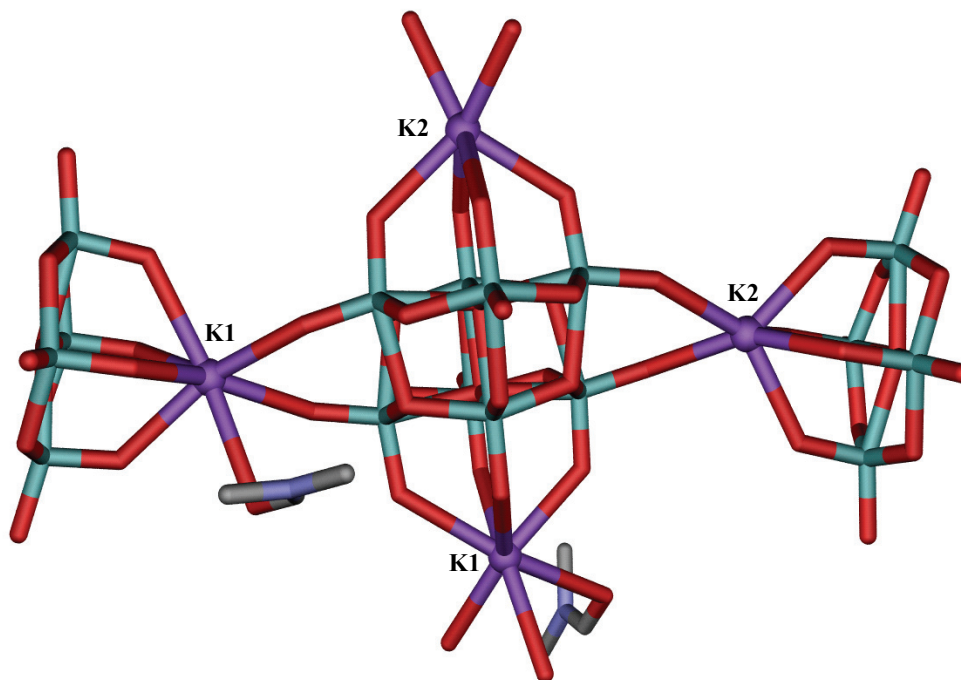


Figure 120 The coordination environments of K1 and K2 in **24**. Mo: green, K: purple spheres, O: red, C: grey, N: blue (hydrogen atoms and counterions removed for clarity).

In the same way K2 interacts with the square $\{O_4\}$ group of one $\{Mo_8\}$ cluster, and to two of the subsequent cluster (K-O distances are between 2.642(12) and 2.788(11) Å and O-K-O angles between 67.90(4) and 150.80(4)° for minimum *cis* and maximum *trans* values respectively). There is no additional DMF ligand bound at the K2 position, giving it a different coordination environment to K1.

Where as in compound **21** the μ_2 -oxo centres of the DMSO ligands helped to bridge the $\{Ag(Mo_8)Ag\}$ units into chains and then cross-link them into a two-dimensional network, a different arrangement is found in **24**. Here the solvent molecules have no linking action and the potassium ions connect the $\{Mo_8\}$ clusters into two sets which run parallel and perpendicular to one another (Figure 121).

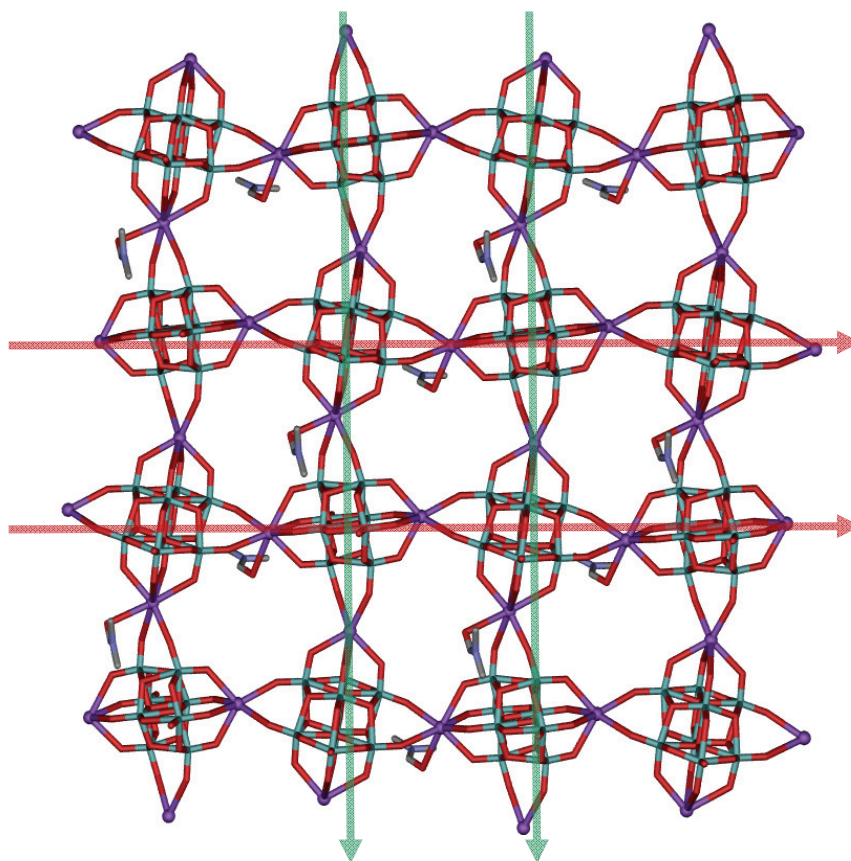


Figure 121 View along the crystallographic a axis of **24** highlighting the two perpendicular sets of chains by red and green arrows. Mo: green, K: purple spheres, O: red, C: grey, N: blue (hydrogen atoms and counterions removed for clarity).

However, as discussed for **21**, the arrangement of the chains is such that each alternating $\{\text{Mo}_8\}$ cluster is in a different position to the subsequent cluster, giving an A-B-A-B arrangement (Figure 122) and an array in which each axis of the network is equivalent and forms chains parallel and perpendicular to one another which then cross-link to form **24**.

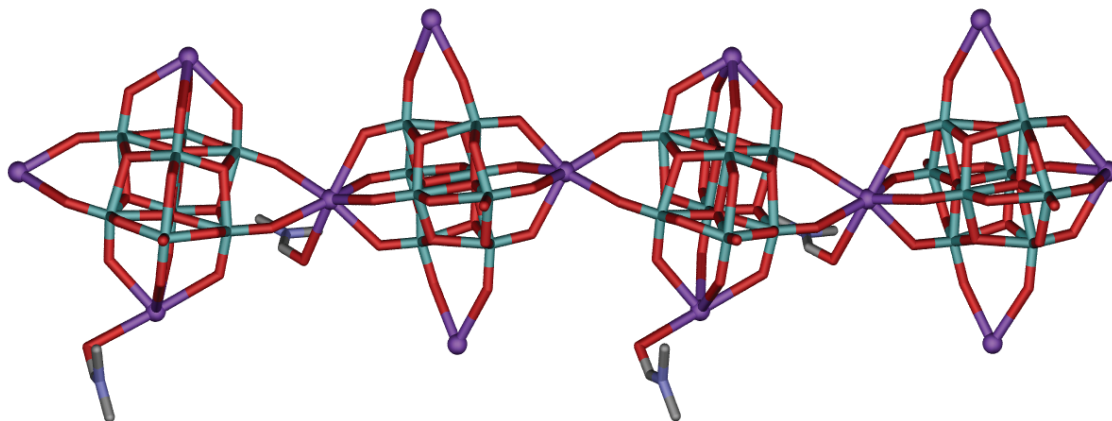


Figure 122 View of the chain structure in **24** along the crystallographic *c* axis. Mo: green, K: purple spheres, O: red, C: grey, N: blue (hydrogen atoms and counterions removed for clarity).

Previously, the absence of restricting counterions was attributed to the growth of two-dimensional networks. However, **24** is an exception as it contains two types of cations that act as spacers between each layer of anions, creating an A-B-A-B arrangement of cations and POMs (Figure 123). Thus, the two-dimensional layers cannot pack closely together along the crystallographic *b* axis (closest *intra*-layer distance of 11.704 Å between neighbouring K₂ ions). As a result, the inclusion of a bulky cation results in the restriction of the network in one direction but allowing the chains of the {K(Mo₈)K} building blocks to grow along the *a* and *c* axis into a two-dimensional network.

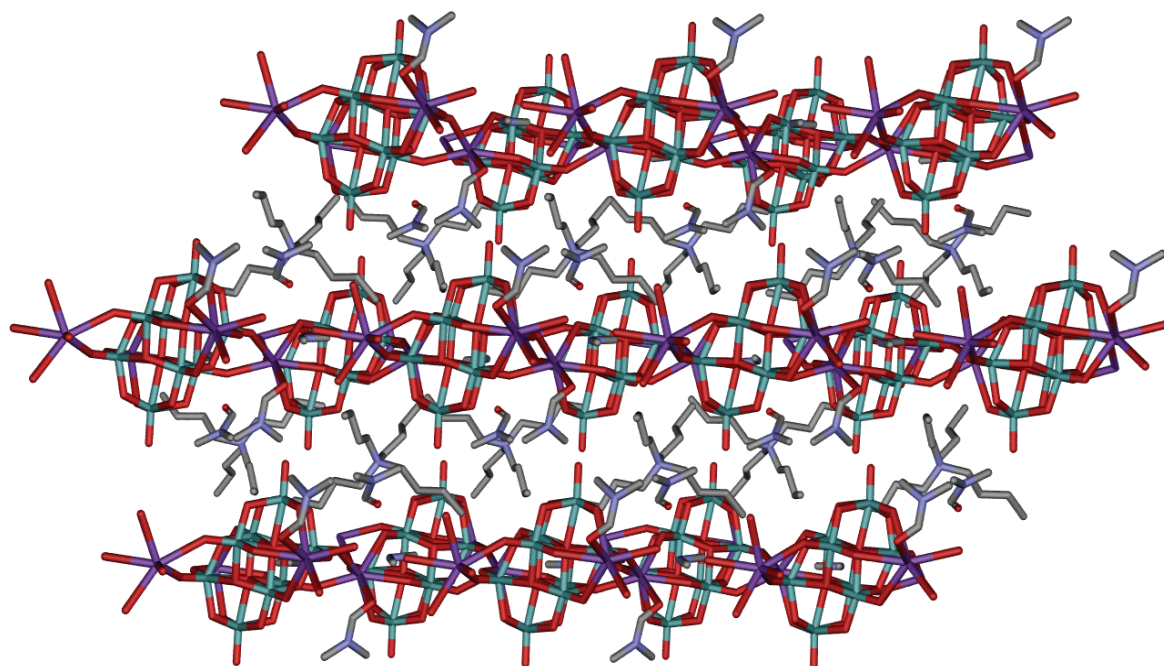


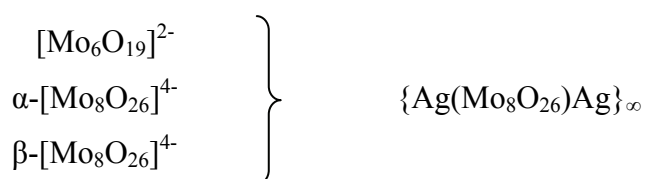
Figure 123 The packing arrangement of **24**. Mo: green, K: purple spheres, O: red, C: grey, N: blue (hydrogen atoms removed for clarity).

4 CONCLUSIONS AND FUTURE WORK

The structural influence of polyoxomolybdates has been investigated with silver(I) salts in various non-aqueous solvent systems. This work demonstrates a strategy to control the molecular growth process from $[\text{Ag}(\text{Mo}_8\text{O}_{26})\text{Ag}]^{2-}$ isolated clusters to one- and two-dimensional polyoxometalate (POM) architectures, in which the choice of cation and solvent represent a crucial factor. In addition to this, some of these compounds have been further investigated using several microscopy based techniques.

4.1 Formation of $\{\text{Ag}(\text{Mo}_8\text{O}_{26})\text{Ag}\}$ Synthons and $\beta\text{-}[\text{Mo}_8\text{O}_{26}]^{4-}$

A number of experiments were carried out to establish the formation of silver polyoxomolybdate fragments in solution. The reaction of silver with various POM precursors has resulted in the formation of compounds with similar structural features (Scheme 3). Thus, structure elucidation as well as confirmation by mass spectrometry indicates that Ag-Mo POM fragments are being produced and provide greater detail of the mechanism that underpins the formation of these clusters in solution.



Scheme 3 The different polyoxomolybdate precursors which can react with silver to form the $\{\text{Ag}(\text{Mo}_8\text{O}_{26})\text{Ag}\}_\infty$ backbone.

The initial studies carried out using mass spectrometry with the Ag-Mo based systems have provided a basis to understand the breakdown of $\{\text{Mo}_6\}$ to $\{\text{Mo}_8\}$ *via* the $\{\text{Mo}_2\}$ clusters, something which previously remained speculative. Further studies therefore, will continue to analyse the reaction mixtures by mass spectrometry to gain detailed knowledge of the solution chemistry, as this could be a fundamental route to achieving further

controllable growth of POM building blocks. These findings could be used to make new structure types and subsequently be extended or applied to other POM based systems.

4.2 Structural Influence by Cation and Solvent

The controllable molecular growth of a well-established Ag-Mo POM based building block has been achieved, through cation and solvent interaction (Figure 124). A general overview of the structures (Table 7) reveals that to form isolated clusters requires the use of a bulky counterion such as Ph_4P^+ . Using such a counterion can ‘shield’ the $\{\text{Ag}(\text{Mo}_8)\text{Ag}\}$ synthon as in $(\text{Ph}_4\text{P})_2[\text{Ag}_2(\text{DMSO})_2\text{Mo}_8\text{O}_{26}]$ (**9**) and $(\text{Ph}_4\text{P})_2[\text{Ag}_2(\text{CH}_3\text{CN})_2\text{Mo}_8\text{O}_{26}]$ (**10**) along with capping solvent molecules which prevent the polymerisation of the molecular building blocks. However, the one-dimensional chain $(\text{Ph}_4\text{P})_{2n}[\text{Ag}_2(\text{DMF})_2\text{Mo}_8\text{O}_{26}]_n \cdot 2\text{DMF}$ (**13**) is formed in the presence of the same counterion but the solvent molecules act as ‘spacers’ and allow the growth of the synthons in one direction, thus forming a chain.

The formation of one-dimensional structures is directed by flexible $(n\text{-C}_4\text{H}_9)_4\text{N}^+$ cations, or as in some instances counterions which do not surround the synthons but still allow its growth in only one direction. Again, either cation as seen in structures $((n\text{-C}_4\text{H}_9)_4\text{N})_{2n}[\text{Ag}_2\text{Mo}_8\text{O}_{26}]_n$ (**4**) and $((n\text{-C}_4\text{H}_9)_4\text{N})_{2n}[\text{Ag}_2(\text{CH}_3\text{CN})_2\text{Mo}_8\text{O}_{26}]_n$ (**11**) or a combination of cation and solvent molecules as in $[\text{Ag}(\text{C}_7\text{H}_{12}\text{O}_2\text{N})(\text{CH}_3\text{CN})]_{2n}[(\text{Ag}(\text{CH}_3\text{CN}))_2\text{Mo}_8\text{O}_{26}]_n \cdot 2\text{CH}_3\text{CN}$ (**12**), $(\text{Ph}_4\text{P})_{2n}[\text{Ag}_2(\text{DMF})_2\text{Mo}_8\text{O}_{26}]_n \cdot 2\text{DMF}$ (**13**), $(\text{H}_2\text{NMe}_2)_{2n}[\text{Ag}_2(\text{DMF})_2\text{Mo}_8\text{O}_{26}]_n \cdot 2\text{DMF}$ (**14**) and $((n\text{-C}_4\text{H}_9)_4\text{N})_{2n}[\text{Ag}_2(\text{DMSO})_2\text{Mo}_8\text{O}_{26}]_n$ (**15**) can influence the formation of one-dimensional chains and arrays.

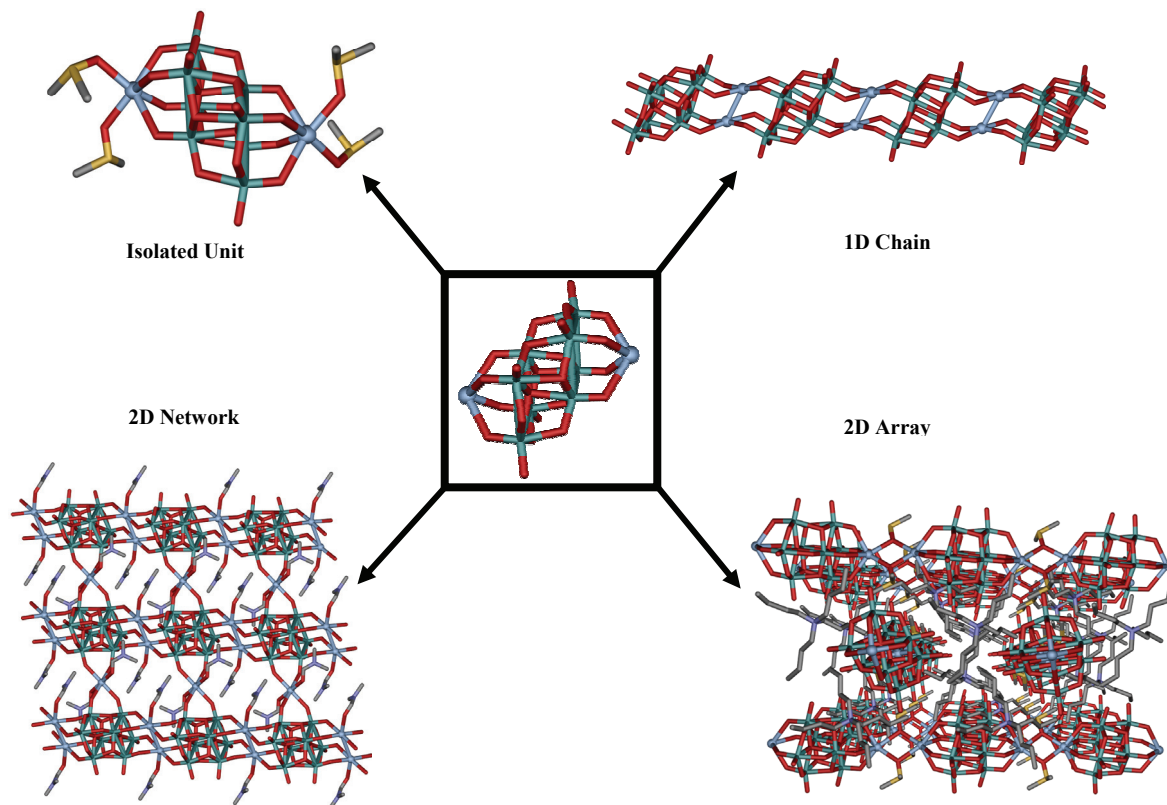


Figure 124 The molecular growth from isolated unit to polymeric architectures of 1D chains, 2D arrays and 2D networks from small molecular building blocks based upon the silver substituted polyoxometalate cluster synthon, $\{\text{Ag}(\text{Mo}_8\text{O}_{26})\text{Ag}\}$ (*centre*).

The use of smaller $(n\text{-C}_3\text{H}_7)_4\text{N}^+$ cations or very large aliphatic cations e.g. $(n\text{-C}_x\text{H}_{2x+1})_4\text{N}$ (where $x = 5, 6, \text{ or } 7$) favours the formation of two-dimensional networks. Within these structures additional silver(I) ions that are coordinated by the oxygen atoms located along the side of the $\{\text{Mo}_8\}$ cluster link the polymer chains into a two-dimensional silver(I) coordination network as seen in $(\text{HDMF})_n[\text{Ag}_3(\text{DMF})_4\text{Mo}_8\text{O}_{26}]_n$ (**16**) and $[\text{Ag}_2(\text{DMF})_2\text{Ag}_2(\text{DMF})_4\text{Mo}_8\text{O}_{26}]_n$ (**17**).

Solvent or ligand ^[a] ↓ Cation ^[b] →	Ph ₄ P	(<i>n</i> -C ₃ H ₇) ₄ N	(<i>n</i> -C ₄ H ₉) ₄ N	(<i>n</i> -C _{<i>x</i>} H _{2<i>x</i>+1}) ₄ N <i>x</i> = 5, 6, 7
DMF	1D Chain	2D Net	1D Chain ^[c]	1D Chain 2D Net
DMSO	Isolated cluster	2D Net	1D Chains in 2D array	2D Net
CH ₃ CN	Isolated cluster	----	1D Chains	1D Chain 2D Arrays

Table 7 Some of the experimental set-ups used to produce the various structures. [a] Solvent in which reaction is carried out and can also act as a ligand or as solvent molecules in the final structure. [b] Cation that is present in the precursor {Mo₆}. [c] Lu *et al.* published¹²⁸ the same structure using different reaction conditions.

In addition to the influence counterion and solvent can have on the overall structure, various interactions in the form of Ag...Ag, Ag...O and hydrogen bonding have also been important. In particular the distance of the Ag...Ag interactions within each structure can be influenced by a number of factors and can also play an instrumental role along with Ag...O interactions in the assembly of the {Ag(Mo₈)Ag} building blocks. These have been important in a number of structures but most notably for **10**, **11** and **12** where a combination of these interactions help to stabilise the structures.

Thus, these reactions represent examples for control of the self-assembly processes of functional materials, which is of great interest in many areas of chemistry. Influencing the growth of the {Ag(Mo₈)Ag} synthon is attained easily with respect to the counterion used. In isolating these Ag-POM architectures, insight can be gained into how silver and its inclusion into octamolybdate structures can influence the formation of a cluster.

This information can be incorporated into further studies to make clusters with improved functionality. Therefore, further work will look at new ways of gaining control over the {Ag(Mo₈)Ag} building blocks to make new architectures with enhanced physical and

chemical properties. In producing such compounds, research within this area could extend to using these compounds for catalysis and electronic studies. Other work will also look to expanding this strategy to small tungsten based systems.

Given the versatile electronic properties of POMs, these processes might become relevant e.g. the production of spacers of specific dimensionality for use as conducting interconnectors in nanoscale electronic devices, or as e-beam resists. Future work will therefore concentrate on extending this molecular growth strategy to other POM-based structures, and to investigate their physical properties for potential applications.

4.3 Solvent Assisted Arrays

In the absence of counterions, solvent molecules have also been fundamental in influencing or pillaring the growth of the $\{\text{Ag}(\text{Mo}_8)\text{Ag}\}$ building blocks into one- or two-dimensional arrays.

The isolation of multiple acetonitrile supported arrays from the same reaction conditions indicates the instability of these structures in acetonitrile and the support offered to the structures by the solvent molecules. Subtle differences in synthesis may influence the outcome of the end product, which by in large produces compound $[(\text{Ag}(\text{CH}_3\text{CN})_3)_2(\text{Ag}(\text{CH}_3\text{CN}))_2\text{AgMo}_8\text{O}_{26}]$ (**18**).

Further work therefore will look at improving upon the existing syntheses to optimise reproducibility and yield of **18**, as well as $[(\text{Ag}(\text{CH}_3\text{CN}))_2(\text{Ag}(\text{CH}_3\text{CN})_2)_2\text{Mo}_8\text{O}_{26}]_n$ (**19**) and $[(\text{Ag}(\text{CH}_3\text{CN})_2)_2\text{Ag}_2\text{Mo}_8\text{O}_{26}]_n$ (**20**). These compounds, and in particular **18** represent materials that could be used as gas storage materials, an attractive application for metal organic frameworks.^{157,158} The Ag(I) ions offer points on the cluster that can be used to bind gas e.g. hydrogen and thus act as potential gas storage materials. In order to do this however the acetonitrile molecules will have to be removed, as such future studies of these compounds will also look at removing the acetonitrile molecules through TGA and DSC to

leave the Ag(I) ions ‘exposed’ (Figure 125) and active for uptake of gases. Mass spectrometry studies may also provide essential information about the reaction mixtures.

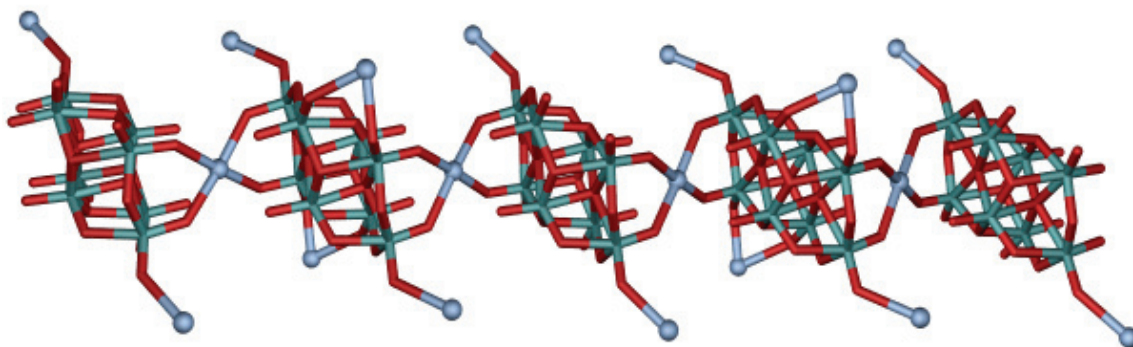


Figure 125 View the chain structure of **18** with loss of all acetonitrile ligands and ‘exposed’ Ag ions. Mo: green, Ag: light blue spheres, O: red (carbon, nitrogen and hydrogen atoms removed).

Full structure analysis and optimised synthesis for the two-dimensional network $[\text{Ag}_4(\text{DMSO})_6(\text{OC}(\text{CH}_3)_2)_2\text{Mo}_8\text{O}_{26}]_n$ (**21**) will be carried out and if possible mass spectrometry may also provide further insight about this compound. The DMSO supported arrays also provide interesting materials for catalysis and future work will also look at TGA and DSC studies on these compounds.

4.4 Silver Based Nanostructures

The growth of nanostructures from clusters that use molecular based building blocks has been accomplished through a simple synthetic strategy which is dependent upon time. The growth of these nanostructures on multiple length scales *via* silver polyoxomolybdate based compounds illustrates the control which can be achieved at the molecular level and which can subsequently produce silver based materials including Ag^0 wires. SEM studies have shown $((n\text{-C}_4\text{H}_9)_4\text{N})_{2n}[\text{Ag}_2\text{Mo}_8\text{O}_{26}]_n$ (**4**) to be a versatile material and its crystal composition key to the growth of the nanowires (Figure 126) with the likelihood of the TBA cations encouraging this growth. These findings will continue to stimulate further research into the synthesis of the wires with emphasis on achieving controlled growth in a uniform manner.

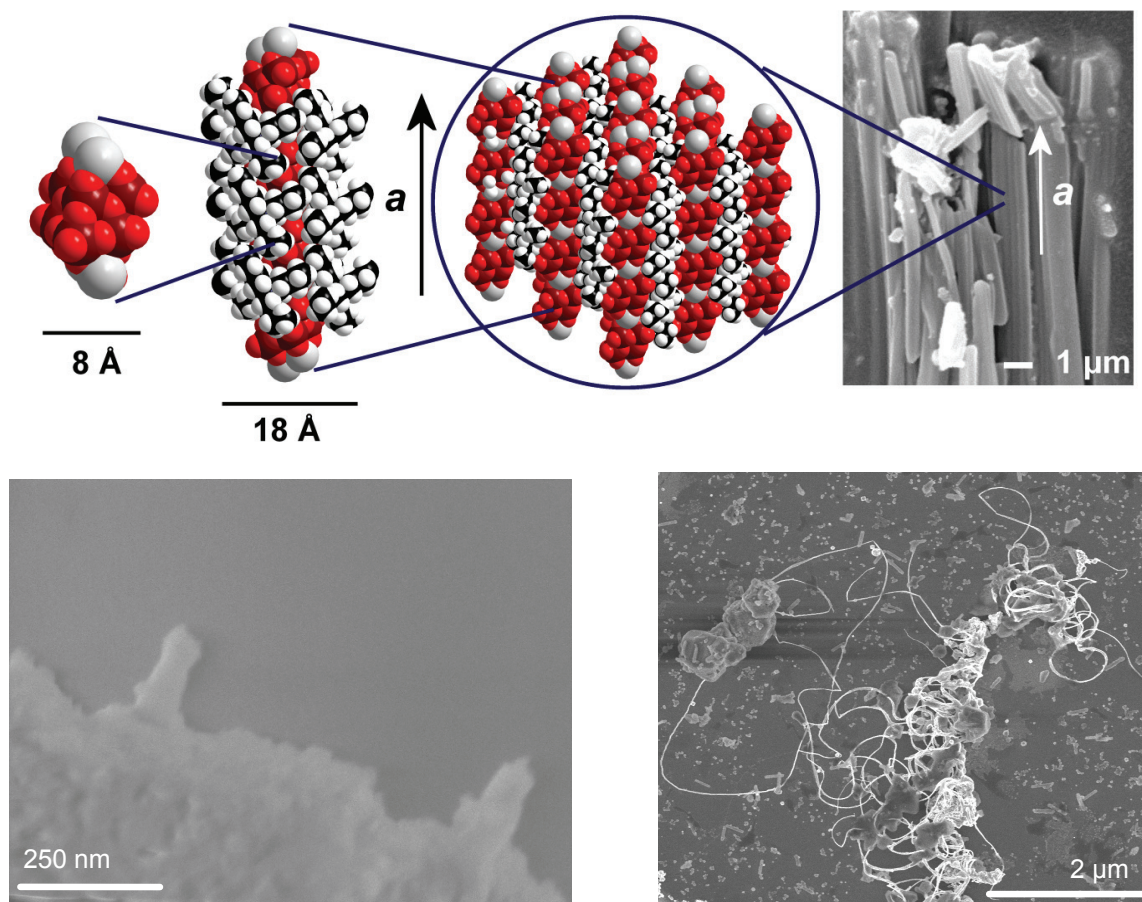


Figure 126 A summary of the possible key growth processes starting from the $\{\text{Ag}(\text{Mo}_8)\text{Ag}\}$ building block which grows into the polymer then nanorods (top), followed by the initial growth of nanowires from a crystal (bottom, *LHS*) and the end point of this process with nanowires of a given length (bottom, *RHS*). Mo: brown, O: red, Ag: grey, C: black, H: white.

Studies will also be carried out to identify the physical properties i.e. conductance measurements of the silver nanowires and other prospective properties such as catalysis. Ongoing research will also continue to understand the mechanism of growth of the wires by establishing the oxidation of methanol to formaldehyde and the reduction of Ag^{I} to Ag^{0} .

Gaining a deeper understanding of the mechanism will provide new alternatives that can be used to grow the wires in greater yield and optimised time. It could also extend the research of this material into new areas of science including self-assembled monolayers (SAMs), a technique which can combine current lithographic techniques (or printing of molecules onto surfaces) with self-assembly. Lithography can be used to pattern surfaces with organic molecules to create a self-assembled monolayer where these molecules act as

‘homing beacons’ directing or encouraging other and what could be highly functional molecules to self-assemble or ‘anchor’ at these points.

These ideas could be used in combination with the work described in this thesis where chemistry meets at the interface of materials science to *conceptually* design a new type of micro-electronic circuit using POMs. What has been established by the work presented here is not just the interaction and control that can be gained over Ag-Mo fragments by cation and solvent molecules, but also the affinity of the POM fragments for the organic cation. These cations represent the ‘homing beacons’ that can be placed onto surfaces using lithography and which can direct the Ag-Mo clusters into position. Thus, gaining the organised self-assembly that is needed for micro-electronic circuits and answering the issue of downsizing electronic components to atomic magnitudes. The wires that are produced from the Ag-Mo clusters would provide the essential circuitry that is needed within such systems.

4.5 Potassium Polyoxometalate Clusters

The inclusion of gold within hexa and octamolybdate systems has proven to be unsuccessful but has resulted in the formation of two new K-Mo based POM clusters. As with the Ag-Mo based POM clusters discussed throughout sections 3.1-3.3, where cation and solvent interaction are important in influencing the overall structure, the same can be said here where structures $((n\text{-C}_4\text{H}_9)_4\text{N})_{2n}[\text{K}_2(\text{DMSO})_3\text{Mo}_8\text{O}_{26}]_n$ (**23**) and $((n\text{-C}_4\text{H}_9)_4\text{N})_n(\text{H}_2\text{NMe}_2)_n[\text{K}_2(\text{DMF})\text{Mo}_8\text{O}_{26}]_n \cdot \text{DMF}$ (**24**) have been influenced by the tetra-*n*-butylammonium cations.

Future work will continue to explore the inclusion of gold within small polyoxomolybdate clusters and analyse the solution chemistry of the reaction systems to gain a better understanding of the reactive building blocks.

5 EXPERIMENTAL

5.1 Materials

All reagents and chemicals were supplied by *Aldrich Chemical Company Ltd.*, *Fisher Chemicals*, and *Lancaster Chemicals Ltd.* and used without further purification. Solvents were supplied by *Fisher Chemicals*.

5.2 Instrumentation

For analytical and spectroscopic techniques the following were used:

Fourier Transform Infrared (FT-IR) Spectroscopy: IR services within the Department of Chemistry, University of Glasgow. Data collected using the Jasco FT-IR-410 spectrometer. Wave numbers (ν) in cm^{-1} ; intensities denoted as vs = very strong, s = strong, m = medium, w = weak, b = broad.

Microanalysis: Microanalysis services within the Department of Chemistry, University of Glasgow. EA 1110 CHNS, CE-440 Elemental Analyser.

pH Measurements: Hanna Instruments HI 9025C microcomputer pH meter (HI 1230 pH electrode).

Mass Spectrometry: Mass spectrometry data collected using a Bruker microTOFQ microspray in negative ion mode at $-40\text{ }^{\circ}\text{C}$.

Single Crystal X-Ray Diffraction: Crystal data collected using X-ray services within the Department of Chemistry, University of Glasgow. Data were measured at $150(2)\text{ K}$ unless

stated otherwise on a Nonius Kappa CCD diffractometer (λ ($\text{MoK}\alpha$) = 0.71073 Å) graphite monochromator or Bruker Apex II (λ ($\text{MoK}\alpha$) = 0.71073 Å) graphite monochromator.

Scanning Electron Microscopy (SEM): SEM services within the Department of Engineering, University of Glasgow. SEM images obtained using field emission SEM (Hitachi, S4700) operated at an acceleration voltage of 10 kV.

Transmission Electron Microscopy (TEM)/ Selected Area Electron Diffraction (SAED): TEM and SEM services in the Laboratory of Glyconanotechnology, Seville, Spain. TEM and SAED information obtained using a Philips CM200 microscope working at 200 kV.

5.3 Synthesis

5.3.1 $((n\text{-C}_4\text{H}_9)_4\text{N})_2\text{Mo}_6\text{O}_{19}$ (1)

$\text{Na}_2\text{MoO}_4 \cdot 2\text{H}_2\text{O}$ (2.4 g, 9.9 mmol) was dissolved in water (50 mL, approximate pH = 8.5-9.0) and to this was added concentrated HCl (37 %) until pH decreased to approximately pH 2. Then $(n\text{-C}_4\text{H}_9)_4\text{NBr}$ (1.06 g, 3.3 mmol) in water (10 mL) was added to the above solution dropwise. A white/cream precipitate was formed which when left to stir at room temperature for approximately one hour became yellow. The precipitate was collected and dried for a short period of time in a desiccator and recrystallised from a minimum amount of acetonitrile to yield yellow block crystals when left open to the air. Yield: 2.7g (1.98 mmol, 60.18 %). $\text{C}_{32}\text{H}_{72}\text{N}_2\text{Mo}_6\text{O}_{19}$ - found (calc.) %: C 28.09 (28.17), H 5.34 (5.32), N 2.10 (2.05); I.R. (KBr) ν/cm^{-1} : 3442 (b), 2962 (s), 2874 (s), 1470 (s), 1380 (s), 1177 (w), 1107 (w), 956 (vs), 880 (w), 797 (vs).

The above synthesis can be substituted for the following counterions: $(n\text{-C}_5\text{H}_{11})_4\text{NBr}$ (1.25g), $(n\text{-C}_6\text{H}_{13})_4\text{NBr}$ (1.35g), $(n\text{-C}_3\text{H}_7)_4\text{NBr}$ (0.88g, not possible to recrystallise from acetonitrile, instead powder is used as precursor material).

E.A. found (calc.) %:

$((n\text{-C}_3\text{H}_7)_4\text{N})_2\text{Mo}_6\text{O}_{19}$ - C 23.15 (23.02), H 4.10 (4.07), N 2.02 (2.24).

$((n\text{-C}_5\text{H}_{11})_4\text{N})_2\text{Mo}_6\text{O}_{19}$ - C 32.54 (32.53), H 6.09 (6.00), N 2.00 (1.90).

$((n\text{-C}_6\text{H}_{13})_4\text{N})_2\text{Mo}_6\text{O}_{19}$ - C 36.26 (36.28), H 6.64 (6.60), N 1.86 (1.76).

5.3.2 $((n\text{-C}_7\text{H}_{15})_4\text{N})_2\text{Mo}_6\text{O}_{19}$ (2)

Na_2MoO_4 (2.04 g, 9.9 mmol) was dissolved in water (50 mL, approximate pH = 8.5-9.0) and to this was added concentrated HCl (37 %) until pH decreased to approximately pH 2. Then $(n\text{-C}_7\text{H}_{15})_4\text{NBr}$ (1.62 g, 3.3 mmol) in water (20 mL) and acetonitrile (10 mL) was added to the above solution dropwise. A yellow viscous/sticky substance was formed when left to stir for four hours. After this time the water was decanted and fresh water added. The yellow residue was sonicated for 10-15 minutes and then heated till it became more opaque. The water was again decanted and the yellow residue recrystallised from a minimum amount of acetonitrile to yield yellow needle crystals when left at 0 °C. Yield: 1.93g (1.13 mmol, 34.36 %). $\text{C}_{56}\text{H}_{120}\text{N}_2\text{Mo}_6\text{O}_{19}$ - found (calc.) %: C 38.94 (39.54), H 7.04 (7.11), N 1.76 (1.65); I.R. (KBr) ν/cm^{-1} : 3432 (b), 2927 (vs), 2857 (vs), 1912 (w), 1482 (s), 1379 (m), 1119 (w), 957 (vs), 798 (vs), 726 (s).

5.3.3 $(\text{Ph}_4\text{P})_2\text{Mo}_6\text{O}_{19}\cdot 2\text{CH}_3\text{CN}$ (3)

$\text{Na}_2\text{MoO}_4\cdot 2\text{H}_2\text{O}$ (2.0 g, 9.9 mmol) was dissolved in water (50 mL, approximate pH = 8.5-9.0) and to this was added concentrated HCl (37 %) until pH decreased to approximately pH 2. Then $(\text{Ph}_4\text{P})\text{Br}$ (1.16 g, 2.77 mmol) in acetonitrile (10 mL) was added to the above solution dropwise. A white/cream precipitate was formed which when left to stir at room temperature for approximately one hour eventually became yellow. The precipitate was collected and dried for a short period of time in a dessicator and recrystallised from a minimum amount of acetonitrile to yield yellow block crystals when left open to air. Yield 2.40g (1.46 mmol, 52.88 %). $\text{C}_{52}\text{H}_{46}\text{P}_2\text{N}_2\text{Mo}_6\text{O}_{19}$ - found (calc.) %: C 38.14 (38.07), H 2.77 (2.83), N 1.74 (1.71); I.R. (KBr) ν/cm^{-1} : 3437 (b), 2929 (w), 2251 (w), 1584 (w), 1482 (w), 1436 (w), 1313 (w), 1163 (w), 1108 (w), 997 (s), 956 (vs), 799 (vs), 721 (s), 687 (s).

5.3.4 $((n\text{-C}_4\text{H}_9)_4\text{N})_{2n}[\text{Ag}_2\text{Mo}_8\text{O}_{26}]_n$ (**4**)

Route 1 (**4a**)¹²⁶:

Silver(I) fluoride (28 mg, 0.22 mmol) suspended in methanol (3 mL) by sonication, was added to a solution of $((n\text{-C}_4\text{H}_9)_4\text{N})_2\text{Mo}_6\text{O}_{19}$ (150 mg, 0.11 mmol) in acetonitrile (4 mL). When left to stir overnight at room temperature, a cloudy white solution is formed. Filtration of this solution affords a clear colourless solution. Diffusion of diethyl ether yielded colourless rectangular crystals over two days which were suitable for single crystal X-ray diffraction. Yield: 107 mg (0.057 mmol, 68 %). $\text{C}_{32}\text{H}_{72}\text{Ag}_2\text{Mo}_8\text{N}_2\text{O}_{26}$ - found (calc.) %: C 20.53 (20.39), H 3.78 (3.85), N 1.53 (1.48); I.R. (KBr) ν/cm^{-1} : 2960 (w), 2873 (w), 1481 (m), 1376 (w), 1153 (w), 1106 (w), 1025 (m), 952 (s), 921 (s), 890 (s), 867 (s), 817 (s), 705 (s), 647 (m).

Route 2 (**4b**):

Silver(I) fluoride (28 mg, 0.22 mmol) suspended in methanol (3 mL) by sonication was added to a solution of $((n\text{-C}_4\text{H}_9)_4\text{N})_2\text{Mo}_6\text{O}_{19}$ (150 mg, 0.11 mmol) in acetonitrile (4 mL) and left to stir overnight at room temperature. After this time a colourless solution is formed with some grey precipitate which is filtered off. Diethyl ether is added to the remaining solution to precipitate a white/cream powder. The powder is collected on a sinter and left to dry in air overnight. The powder is then suspended in acetonitrile which produces a cloudy brown solution which is filtered through micro-fibre filter paper to yield a clear colourless solution and crystallised by diffusion of diethyl ether. After 3-4 days large colourless block crystals are formed of $((n\text{-C}_4\text{H}_9)_4\text{N})_{2n}[\text{Ag}_2\text{Mo}_8\text{O}_{26}]_n$ (**4a**), which were checked by single crystal X-ray diffraction. Yield: 40 mg (0.02 mmol, 18.92 %). $\text{C}_{32}\text{H}_{72}\text{Ag}_2\text{Mo}_8\text{N}_2\text{O}_{26}$ - found (calc.) %: C 20.37 (20.39), H 3.84 (3.85), N 1.56 (1.48); I.R. (KBr) ν/cm^{-1} : 3437 (b), 2961 (w), 1482 (m), 1379 (w), 955 (s), 924 (vs), 896 (vs), 870 (vs), 822 (s), 712 (s).

5.3.5 $\alpha\text{-}((n\text{-C}_4\text{H}_9)_4\text{N})_4\text{Mo}_8\text{O}_{26}$ (**5**)

The method published by Filowitz *et al.*¹⁵⁹ is similar to the procedure used below:

Na_2MoO_4 (1.064 g, 5.17 mmol) was dissolved in 3 mL water (approximate pH is 8.5-9.0) and to this was added 1 mL of 6M HCl (37 %) until pH decreased to approximately pH 4.5. Then $(n\text{-C}_4\text{H}_9)_4\text{NBr}$ (0.80 g, 0.79 mmol) was added to the above solution and the resulting precipitate was filtered off and washed successively with water, ethanol, acetone and diethyl ether. The white precipitate is recrystallised by dissolving 1.05 g of the crude product in 10 mL of acetonitrile at 25 °C and cooling the solution to 0 °C. Large clear colourless, block shaped crystals are obtained overnight and lose their transparency upon drying *in vacuo*. Yield: 570 mg (0.27 mmol, 33.3 %). $\text{C}_{64}\text{H}_{144}\text{Mo}_8\text{N}_4\text{O}_{26}$ - found (calc.) %: C 35.65 (35.70), H 6.82 (6.74.), N 2.69 (2.60); I.R. (KBr) ν/cm^{-1} : 3466 (b), 2942 (s), 2869 (s), 1827 (w), 1638 (s), 1380 (s), 1154 (w), 915 (s), 912 (s), 799 (s), 653 (s).

5.3.6 $((n\text{-C}_4\text{H}_9)_4\text{N})_{2n}[\text{Ag}_2\text{Mo}_8\text{O}_{26}(\text{CH}_3\text{CN})_2]_n \cdot 2\text{CH}_3\text{CN}$ (6)

Silver(I) tetrafluoroborate (47 mg, 0.24 mmol) in acetonitrile (2 mL) was added to a solution of $\alpha\text{-}((n\text{-C}_4\text{H}_9)_4\text{N})_4\text{Mo}_8\text{O}_{26}$ (200 mg, 0.09 mmol) in acetonitrile (5 mL). Upon stirring for 24 hours a cloudy grey solution is formed. Centrifugation of this solution yields a clear colourless solution, from which colourless needles were obtained through diffusion of diethyl ether for 10 days. The crystals were suitable for single crystal X-ray diffraction and dried under vacuum. Yield: 111 mg (0.06 mmol, 65.21 %). $\text{C}_{40}\text{H}_{84}\text{Ag}_2\text{Mo}_8\text{N}_6\text{O}_{26}$ - found (calc.) %: C 21.94 (23.45), H 3.83 (4.13.), N 2.73 (4.10) (shows loss of two acetonitrile solvent molecules); I.R. (KBr) ν/cm^{-1} : 3465 (b), 2962 (s), 2873 (s), 1621 (m), 1481 (s), 1379 (m), 946 (s), 903 (s), 710 (s), 657 (s).

5.3.7 $\beta\text{-}((n\text{-C}_4\text{H}_9)_4\text{N})_3\text{KMo}_8\text{O}_{26} \cdot 2\text{H}_2\text{O}$ (7)

The method published by Filowitz *et al.*¹⁵⁹ is similar to the procedure used below:

A saturated solution of KBr (100 mg, 0.84 mmol) in 0.18 mL water was added to a solution of $\alpha\text{-}((n\text{-C}_4\text{H}_9)_4\text{N})_4\text{Mo}_8\text{O}_{26}$ (0.38 mg, 0.18 mmol) in 10 mL of acetonitrile and the resulting precipitate was filtered off immediately. The clear filtrate was left to crystallise for 24 hours at 0 °C to give white, needle shaped crystals which were dried under vacuum

upon collection. Yield: 126.5 mg (0.06 mmol, 36.09 %). $C_{48}H_{112}Mo_8N_3KO_{28}$ - found (calc.) %: C 28.44 (29.03), H 5.31 (5.68), N 2.16 (2.12); I.R. (KBr) ν/cm^{-1} : 3464 (b), 2961 (s), 2872 (s), 1639 (m), 1482 (s), 1379 (m), 941 (s), 912 (s), 806 (s), 713 (s), 663 (s).

5.3.8 $((n-C_4H_9)_4N)_{2n}[Ag_2Mo_8O_{26}]_n$ (**4c**)

Silver(I) nitrate (12.5 mg, 0.077 mmol) in acetonitrile (2 mL) was added to a solution of β - $((n-C_4H_9)_4N)_3KMo_8O_{26}\cdot 2H_2O$ (73 mg, 0.037 mmol) in acetonitrile (5 mL). Upon stirring for four days a cloudy grey solution is formed with precipitate. Centrifugation of this solution yields a clear colourless solution, from which colourless block crystals were obtained through diffusion of diethyl ether for seven days. Unit cell check revealed compound **4a**. Yield: 10.8 mg (0.0057 mmol, 6.8 %). $C_{32}H_{72}Ag_2Mo_8N_2O_{26}$ - found (calc.) %: C 20.86 (20.39), H 3.95 (3.85), N 1.66 (1.48); I.R. (KBr) ν/cm^{-1} : 2960 (m), 2873 (m), 1630 (w), 1481 (m), 1379 (w), 1152 (w), 942 (s), 916 (s), 899(s), 718 (s), 662 (s), 553 (m).

5.3.9 $((n-C_4H_9)_4N)_{2n}[KAg(CH_3CN)_2Mo_8O_{26}]_n$ (**8**)

Silver(I) nitrate (13 mg, 0.074 mmol) in acetonitrile (2 mL) was added dropwise to a solution of β - $((n-C_4H_9)_4N)_3KMo_8O_{26}\cdot 2H_2O$ (73 mg, 0.037 mmol) in acetonitrile (5 mL). The solution was left to stir overnight after which time a colourless solution had formed with some white precipitate. Filtration of this solution yields a clear colourless solution, from which colourless needle crystals were obtained through diffusion of diethyl ether over five days and were suitable for single crystal X-ray diffraction. Yield: 7 mg (0.004 mmol, 10.0 %). $C_{36}H_{78}AgKMo_8N_4O_{26}$ - found (calc.) %: C 21.29 (22.78), H 3.92 (4.14), N 2.13 (2.95) (shows loss of one acetonitrile molecule); I.R. (KBr) ν/cm^{-1} : 3434 (b), 2960 (m), 1482 (m), 1378 (w), 943 (s), 920 (s), 898 (m), 843 (s), 716 (s).

5.3.10 $(Ph_4P)_2[Ag_2(DMSO)_4(Mo_8O_{26})]^{126}$ (**9**)

Silver(I) nitrate (22 mg, 0.13 mmol) in methanol (2 mL) was added to a solution of $(Ph_4P)_2Mo_6O_{19}\cdot 2CH_3CN$ (100 mg, 0.06 mmol) in DMSO (5 mL) and stirred for 24 hours at

room temperature. Filtration yielded a clear, pale yellow solution, from which colorless block crystals were obtained by diffusion of diethyl ether over five days and were suitable for single crystal X-ray diffraction. Yield: 10 mg (0.004 mmol, 6.86 %). $C_{56}H_{64}Ag_2Mo_8O_{30}P_2S_4$ - found (calc.) %: C 28.32 (28.13), H 2.43 (2.69); I.R. (KBr): ν/cm^{-1} : 3058 (w), 3014 (w), 1714 (m), 1481 (m), 1431 (s), 1402 (m), 1309 (m), 1166 (m), 1106 (s), 1012 (s), 933 (s), 910 (s), 887 (s), 831 (s), 759 (m).

5.3.11 $(Ph_4P)_2[Ag_2(CH_3CN)_2Mo_8O_{26}] \cdot 2CH_3CN$ (10)

Silver(I) nitrate (22 mg, 0.13 mmol) in methanol (2 mL) was added to a solution of $(Ph_4P)_2Mo_6O_{19} \cdot 2CH_3CN$ (100 mg, 0.06 mmol) in DMSO (5 mL) and stirred for 24 hours at room temperature. Filtration yielded a clear, pale yellow solution to which diethyl ether was added to precipitate a grey powder which was then collected by filtration. To a solution of this powder (50 mg, 0.02 mmol) in acetonitrile (6 mL) was added $(n-C_4H_9)_4NBF_4$ (6.7 mg, 0.02 mmol). Upon stirring at room temperature (one week) a cloudy grey/black solution had formed. Filtration yielded a clear colourless solution from which colourless crystals were obtained when left open to the air overnight. Crystallisation of the remaining solution by diffusion of diethyl ether over two days resulted in colourless rectangular crystals which were suitable for single crystal X-ray diffraction. Yield: 22 mg (0.098 mmol, 47 %). $C_{56}H_{52}Ag_2Mo_8N_4O_{26}P_2$ - found (calc.) %: C 29.95 (29.99), H 2.31 (2.34), N 2.55 (2.50); I.R. (KBr) ν/cm^{-1} : 3448 (b), 3059 (m), 2927 (m), 1584 (m), 1482 (m), 1438 (s), 1316 (m), 1189 (m), 1109 (s), 997 (m), 945 (s), 904 (s).

5.3.12 $((n-C_4H_9)_4N)_2n[Ag_2(CH_3CN)_2Mo_8O_{26}]_n$ (11)

Silver(I) nitrate (19 mg, 0.11 mmol) in water (1 mL) was added to a solution of $((n-C_4H_9)_4N)_2Mo_6O_{19}$ (75 mg, 0.055 mmol) in acetonitrile (5 mL) with tri-hydroxy methyl-aminomethane (13 mg, 0.11 mmol) and stirred for four hours at room temperature. Filtration yielded a clear colourless solution from which colourless block crystals were obtained by evaporation over 24 hours and were suitable for single crystal X-ray diffraction. Yield: 38 mg (0.019 mmol, 47 %). $C_{36}H_{78}Ag_2Mo_8N_4O_{26}$ - elemental analysis

showed decomposition to compound **4a**; I.R. (KBr) ν/cm^{-1} : 3433 (w), 2959 (s), 2872 (m), 1481 (s), 1378 (m), 870 (s), 821 (s).

5.3.13 $[\text{Ag}(\text{C}_7\text{H}_{12}\text{O}_2\text{N})]_{2n}[(\text{Ag}(\text{CH}_3\text{CN}))_2\text{Mo}_8\text{O}_{26}]_n \cdot 2\text{CH}_3\text{CN}$ (**12**)

A solution of silver(I) nitrate (38 mg, 0.22 mmol) and 2,6-pyridine di-methanol (30 mg, 0.22 mmol) in water (2 mL) was added dropwise to a solution of $((n\text{-C}_4\text{H}_9)_4\text{N})_2\text{Mo}_6\text{O}_{19}$ (75 mg, 0.055 mmol) in acetonitrile (5 mL). Upon stirring for four hours at room temperature a clear colourless solution forms with white precipitate. Filtration yields a clear colourless solution. Crystallisation of this solution by diffusion of ethanol over three days afforded colourless block crystals suitable for single crystal X-ray diffraction. Yield: 32 mg (0.013 mmol, 27 %). $\text{C}_{26}\text{H}_{36}\text{Ag}_4\text{Mo}_8\text{N}_8\text{O}_{30}$ - found (calc.) %: C 12.82 (14.59), H 1.47 (1.69), N 3.96 (5.24) (shows loss of two acetonitrile molecules); I.R. (KBr) ν/cm^{-1} : 3425 (b), 2929 (w), 1603 (w), 1578 (w), 1443 (w), 1361 (w), 1066 (s), 936 (s), 896 (s), 828 (s), 794 (w), 715 (s).

5.3.14 $(\text{Ph}_4\text{P})_{2n}[\text{Ag}_2(\text{DMF})_2\text{Mo}_8\text{O}_{26}]_n \cdot 2\text{DMF}$ (**13**)

Silver (I) nitrate (33 mg, 0.19 mmol) was dissolved in DMF (2 mL) and added dropwise to a solution of $(\text{Ph}_4\text{P})_2\text{Mo}_6\text{O}_{19} \cdot 2\text{CH}_3\text{CN}$ (150 mg, 0.09 mmol) in DMF (5 mL) under stirring. The mixture was covered, and left for 20 hours to stir at room temperature. After this time the solution was still transparent yellow. Colourless needle crystals were successfully grown by diffusion of diethyl ether or ethanol over three days and were suitable for single crystal X-ray diffraction. Yield: 48 mg (0.02 mmol, 22.15 %). $\text{C}_{60}\text{H}_{68}\text{Ag}_2\text{Mo}_8\text{N}_4\text{O}_{30}\text{P}_2$ - found (calc.) %: C 29.82 (30.40), H 2.58 (2.89), N 1.92 (2.36); I.R. (KBr) ν/cm^{-1} : 3436 (b), 3062 (m), 2924 (m), 1655 (s), 1584 (m), 1484 (m), 1438 (s), 1381 (s), 1107 (s), 997 (s), 947 (s), 826 (s), 723 (s), 527 (s).

5.3.15 $(\text{H}_2\text{NMe}_2)_{2n}[\text{Ag}_2(\text{DMF})_2\text{Mo}_8\text{O}_{26}]_n \cdot 2\text{DMF}$ (14)

Silver(I) nitrate (34 mg, 0.20 mmol) was dissolved in DMF (2 mL) and added dropwise to a solution of $((n\text{-C}_6\text{H}_{13})_4\text{N})_2\text{Mo}_6\text{O}_{19}$ (159 mg, 0.10 mmol) in DMF (5 mL) under stirring. The mixture was covered and left for 20 hours to stir at room temperature, after which time the solution was still transparent yellow. Colourless block crystals were successfully grown by diffusion of diethyl ether over 20 days, which were suitable for single crystal X-ray diffraction. Yield: 17 mg (0.010 mmol, 9.5 %). $\text{C}_{16}\text{H}_{44}\text{Ag}_2\text{Mo}_8\text{N}_6\text{O}_{30}$ - found (calc.) %: C 10.83 (10.78), H 2.43 (2.48), N 4.56 (4.71); I.R. (KBr) ν/cm^{-1} : 3441 (b), 2926 (m), 1654 (s), 1386 (s), 1259 (s), 1104 (s), 946 (s), 915 (s), 846 (m), 709 (s), 664 (s), 561 (s), 525 (s), 415 (s).

5.3.16 $((n\text{-C}_4\text{H}_9)_4\text{N})_{2n}[\text{Ag}_2(\text{DMSO})_2\text{Mo}_8\text{O}_{26}]_n$ (15)

Silver(I) fluoride (3 mg, 0.024 mmol) suspended in methanol (1 mL) by sonication, was added dropwise to a solution of $((n\text{-C}_4\text{H}_9)_4\text{N})_2\text{Mo}_6\text{O}_{19}$ (75 mg, 0.055 mmol) in DMSO (3 mL) and stirred for five hours at room temperature. After this time a clear yellow solution had formed. Colourless block single crystals were obtained by diffusion of ethanol into the solution over two weeks. The crystals were suitable for single crystal X-ray diffraction. Yield: 10 mg (0.005 mmol, 12.0 %). $\text{C}_{36}\text{H}_{84}\text{Ag}_2\text{Mo}_8\text{N}_2\text{O}_{28}\text{S}_2$ - found (calc.) %: C 21.34 (21.19), H 4.05 (4.15), N 1.46 (1.37); I.R. (KBr) ν/cm^{-1} : 3435 (m), 2961 (s), 2872 (s), 1633 (w), 1480 (s), 1378 (m), 1151 (w), 1003 (m), 943 (s), 835 (s).

5.3.17 $(\text{HDMF})_n[\text{Ag}_3(\text{DMF})_4\text{Mo}_8\text{O}_{26}]_n$ (16)

Silver(I) nitrate (22 mg, 0.13 mmol) was dissolved in methanol (3 mL) was added to a solution of $((n\text{-C}_3\text{H}_7)_4\text{N})_2\text{Mo}_6\text{O}_{19}$ (80 mg, 0.06 mmol) in DMF (6 mL) and stirred for 24 hours at room temperature. Filtration yielded a clear yellow solution, from which colourless block crystals were obtained by diffusion of acetone over three weeks, which were suitable for single crystal X-ray diffraction. Yield: 6 mg (0.003 mmol, 7 %). $\text{C}_{15}\text{H}_{36}\text{Ag}_3\text{Mo}_8\text{N}_5\text{O}_{31}$ - found (calc.) %: C 9.84 (9.62), H 2.00 (1.94), N 3.28 (3.74); I.R.

(KBr) ν/cm^{-1} : 3427 (m), 2924 (m), 1648 (s), 1413 (w), 1382 (m), 1254 (w), 1101 (m), 942 (s), 902 (s), 841 (m).

5.3.18 $[(\text{Ag}(\text{DMF}))_2(\text{Ag}(\text{DMF})_2)_2\text{Mo}_8\text{O}_{26}]_n$ (17)

Silver(I) nitrate (34 mg, 0.20 mmol) suspended in DMF (2 mL) and added to dropwise to a solution of $((n\text{-C}_7\text{H}_{15})_4\text{N})_2\text{Mo}_6\text{O}_{19}$ (148 mg, 0.09 mmol) in DMF (5 mL). The solution was left to stir overnight after which time a yellow solution had formed with some brown precipitate. Filtration of this solution yields a clear yellow solution, from which colourless block crystals were obtained through diffusion of diethyl ether for five days and were suitable for single crystal X-ray diffraction. Yield: 11 mg (0.01 mmol, 6.16 %). $\text{C}_{18}\text{H}_{42}\text{Ag}_4\text{Mo}_8\text{N}_6\text{O}_{32}$ - found (calc.) %: C 8.72 (10.53), H 1.83 (2.06), N 3.53 (4.09) (shows loss of one DMF molecule); I.R. (KBr) ν/cm^{-1} : 3433(b), 2924(w), 2873(s), 1656 (vs), 1414 (w), 1384 (w), 1252 (w), 1107 (m), 947 (vs), 905 (vs), 842 (m), 714 (s).

5.3.19 $[(\text{Ag}(\text{CH}_3\text{CN})_3)_2(\text{Ag}(\text{CH}_3\text{CN})_2)\text{Ag}\text{Mo}_8\text{O}_{26}]_n$ (18)



Silver(I) tetrafluoroborate (39 mg, 0.20 mmol) suspended in acetonitrile (2 mL) was added dropwise to a solution of $((n\text{-C}_7\text{H}_{15})_4\text{N})_2\text{Mo}_6\text{O}_{19}$ (170 mg, 0.10 mmol) in acetonitrile (5 mL). Upon stirring for 24 hours a cloudy yellow solution is formed. Filtration of this solution yields a clear yellow solution from which colourless block crystals were obtained through diffusion of diethyl ether for four days and were suitable for single crystal X-ray diffraction. For compound **18**: Yield: 10 mg (0.01 mmol, 5.15 %). $\text{C}_{16}\text{H}_{24}\text{Ag}_4\text{Mo}_8\text{N}_8\text{O}_{26}$ - found (calc.) %: C 6.27 (9.89), H 0.82 (1.24), N 3.50 (5.77) (shows loss of three acetonitrile molecules); I.R. (KBr) ν/cm^{-1} : 3467 (b), 2251 (w), 1612 (m), 1402 (w), 948 (vs), 910 (vs), 847 (s), 713 (s), 665 (s).

Attempt	C	H	N
1	6.65 7.04	0.82 0.84	3.49 3.77
2 a	6.08 6.46	0.81 0.83	3.39 3.61
b	6.59 6.21	0.85 0.79	3.71 3.38
3	7.65 7.63	0.84 0.83	4.11 4.15
4	5.74 5.94	0.62 0.68	3.08 3.15

Attempt 1 and 2 match microanalysis for **18** but when three acetonitrile molecules are lost.

Attempt 3 matches microanalysis for **19**.

Attempt 4 matches microanalysis for **20**.

5.3.20 $[\text{Ag}_4(\text{DMSO})_6(\text{OC}(\text{CH}_3)_2)_2\text{Mo}_8\text{O}_{26}]_n$ (**21**)

Silver(I) nitrate (23 mg, 0.14 mmol) in DMSO (2 mL) was added dropwise to a solution of $((n\text{-C}_5\text{H}_{11})_4\text{N})_2\text{Mo}_6\text{O}_{19}$ (102 mg, 0.069 mmol) in DMSO (5 mL). The mixture was covered, and left for 48 hours to stir at room temperature. After this time the solution was still transparent yellow. Colourless block crystals were grown by diffusion of acetone over two months. The crystals were suitable for single crystal X-ray diffraction. Yield: 2 mg (0.0009 mmol, 1.32 %).[†]

[†] The reproducibility of **21** has been discussed in section 3.3.2. As such a full analysis is pending.

5.3.21 $[\text{Ag}_4(\text{DMSO})_8\text{Mo}_8\text{O}_{26}]_n$ (**22**)

Route 1:

Silver(I) nitrate (23 mg, 0.14 mmol) in DMSO (2 mL) was added dropwise to a solution of $((n\text{-C}_5\text{H}_{11})_4\text{N})_2\text{Mo}_6\text{O}_{19}$ (102 mg, 0.069 mmol) in DMSO (5 mL) and then acetone was added (0.01 mL). The mixture was covered, and left for 48 hours to stir at room temperature. After this time the solution was still transparent yellow. Large colourless block crystals were successfully grown by diffusion of ethanol over 10 days. The crystals were suitable for single crystal X-ray diffraction. Yield: 48 mg (0.02 mmol, 31.02 %). $\text{C}_{16}\text{H}_{48}\text{Ag}_4\text{Mo}_8\text{O}_{34}\text{S}_8$ - found (calc.) %: C 8.59 (8.59), H 2.17 (2.16); I.R. (KBr) ν/cm^{-1} : 3432 (b), 2996 (m), 1634 (m), 1435 (m), 1402 (m), 1311 (m), 1026 (s), 944 (s), 914 (s), 841 (s), 711 (s).

Route 2:

Silver(I) nitrate (22 mg, 0.13 mmol) in methanol (3 mL) was added dropwise to a solution of $((n\text{-C}_3\text{H}_7)_4\text{N})_2\text{Mo}_6\text{O}_{19}$ (80 mg, 0.063 mmol) in DMSO (6 mL). The solution was covered and left for 24 hours to stir at room temperature. After this time the solution was yellow and had produced some white precipitate. This was filtered to give a clear yellow solution. Colourless block crystals were successfully grown by diffusion of diethyl ether over three weeks which were suitable for single crystal X-ray diffraction. Yield: 11 mg (0.005 mmol, 4 %). $\text{C}_{16}\text{H}_{48}\text{Ag}_4\text{Mo}_8\text{O}_{34}\text{S}_8$ - found (calc.) %: C 8.60 (8.59), H 1.96 (2.16); I.R. (KBr) ν/cm^{-1} : 3436 (b), 2996 (m), 1621 (m), 1402 (m), 1313 (m), 1026 (s), 952 (s), 907 (s), 839 (s), 707 (s).

The $((n\text{-C}_3\text{H}_7)_4\text{N})_2\text{Mo}_6\text{O}_{19}$ starting material can be substituted for $((n\text{-C}_6\text{H}_{13})_4\text{N})_2\text{Mo}_6\text{O}_{19}$ and $((n\text{-C}_7\text{H}_{15})_4\text{N})_2\text{Mo}_6\text{O}_{19}$ in the same silver to $\{\text{Mo}_6\}$ ratio. Diffusion of ethanol will afford colourless crystals of **19** suitable for single crystal X-ray diffraction over two weeks.

Route 3:

Silver(I) nitrate (35 mg, 0.21 mmol) in DMSO (2 mL) was added dropwise to a solution of $((n\text{-C}_5\text{H}_{11})_4\text{N})_2\text{Mo}_6\text{O}_{19}$ (100 mg, 0.068 mmol) in DMSO (5 mL). The mixture was covered, and left for 20 hours to stir at room temperature. After this time the solution was still transparent yellow. Colourless block crystals were successfully grown by diffusion of

acetone over 10 days. The crystals were suitable for single crystal X-ray diffraction. Yield: 8 mg (0.005 mmol, 7.4 %). $C_{16}H_{48}Ag_4Mo_8O_{34}S_8$ - found (calc.) %: C 8.66 (8.59), H 2.13 (2.16); I.R. (KBr) ν/cm^{-1} : 3434 (b), 2999 (m), 2916 (w), 1624 (m), 1435 (m), 1403 (m), 1314 (m), 1025 (s), 946 (s), 919 (s), 842 (s), 714 (s).

5.3.22 $((n-C_4H_9)_4N)_2n[K_2(DMSO)_3Mo_8O_{26}]_n$ (23)

Gold(I) iodide (33 mg, 0.103 mmol) in DMSO (1 mL) was added dropwise to a solution of $\beta-((n-C_4H_9)_4N)_3KMo_8O_{26}\cdot 2H_2O$ (100 mg, 0.050 mmol) in DMSO (5 mL) and left to stir for 20 hours at room temperature. The resulting clear yellow solution was left to crystallise by diffusion of ethanol. Colourless block crystals suitable for single crystal X-ray diffraction were obtained after 14 days. Yield: 40 mg (0.02 mmol, 40.4 %). $C_{38}H_{90}K_2Mo_8N_2O_{29}S_3$ - found (calc.) %: C 23.11 (23.04), H 4.61 (4.58), N 1.50 (1.41); I.R. (KBr) ν/cm^{-1} : 3436 (w), 2961(s), 2873 (s), 1634 (w), 1480 (s), 1380 (s), 1150 (s), 1031 (s), 935 (s), 845 (s).

5.3.23 $((n-C_4H_9)_4N)_n(H_2NMe_2)_n[K_2(DMF)Mo_8O_{26}]_n\cdot DMF$ (24)

Gold(I) iodide (33 mg, 0.103 mmol) suspended by sonication in DMF (2 mL) and added dropwise to a solution of $\beta-((n-C_4H_9)_4N)_3KMo_8O_{26}\cdot 2H_2O$ (100 mg, 0.050 mmol) in DMF (5 mL) and left to stir overnight at room temperature. After this time a golden yellow solution had formed with a small amount of brown precipitate. The solution was filtered and the resulting clear yellow solution was left to crystallise by diffusion of diethyl ether. Two crystal morphologies are found to form but the dominant form are colourless block crystals, were obtained after seven days and were suitable for single crystal X-ray diffraction. Yield: 15.4 mg (0.01 mmol, 18.03 %). $C_{24}H_{58}K_2Mo_8N_4O_{28}$ - found (calc.) %: C 17.53 (16.99), H 3.55 (3.45), N 3.30 (3.30); I.R. (KBr) ν/cm^{-1} : 3436 (w), 2961 (s), 2873 (s), 1634 (w), 1480 (s), 1380 (s), 1150 (s), 1031 (s), 935 (s), 845 (s).

5.4 Surface Studies

5.4.1 Substrate Preparation of $((n\text{-C}_4\text{H}_9)_4\text{N})_{2n}[\text{Ag}_2\text{Mo}_8\text{O}_{26}]_n$ (**4b**) Crystals.

1 mg of **4b** crystals suspended in 1 mL methanol and sonicated for 15 minutes. The solution was then left to sit in a cupboard (minimum exposure to light)[‡] at room temperature. The silicon substrates were cleaned and prepared by sonicating them in ethanol for 20 minutes. After x days (where $x = 10, 20, 30$ or 40 days), 10 μL of the solution is loaded onto a silicon substrate and left to dry at 4 °C for approximately one week. After this time the silicon substrates were investigated by SEM.

1. 10 day old solution deposited onto substrate.

Result: crystals and rods.

2. 20 day old solution deposited onto substrate.

Result: crystals.

3. 30 day old solution deposited onto substrate.

Result: bundles of wires.

4. 40 day old solution deposited onto substrate.

Result: crystals.

5.4.2 Substrate Preparation of $((n\text{-C}_4\text{H}_9)_4\text{N})_{2n}[\text{Ag}_2\text{Mo}_8\text{O}_{26}]_n$ (**4b**) Crystals.

1 mg of **4b** crystals suspended in 1 mL methanol and sonicated for 15 minutes. The solution was then left to sit in a cupboard (minimum exposure to light) at room temperature. The silicon substrates were cleaned and prepared by sonicating them in ethanol for 20 minutes. After 150 days, 10 μL of the solution is deposited onto a silicon

[‡] The minimum exposure to light refers to the partial exposure of solutions to normal laboratory light and is the most common set-up in the microscopy experiments unless otherwise stated.

substrate and left to dry at 4 °C for approximately one week. After this time the silicon substrates were investigated by SEM.

Result: cubic shaped crystals and wires growing from the crystals.

5.4.3 Substrate Preparation of $((n\text{-C}_4\text{H}_9)_4\text{N})_{2n}[\text{Ag}_2\text{Mo}_8\text{O}_{26}]_n$ (4b) Powder Material.

1 mg of powder (isolated from synthesis 5.3.4- route 2) suspended in 1 mL methanol and sonicated for a few minutes and left to sit in a cupboard (minimum exposure to light) at room temperature. The silicon substrates were cleaned and prepared by sonicating them in ethanol for 20 minutes. After x days (where $x = 10, 20, 30$ or 40 days), 10 μL of the solution is deposited onto a silicon substrate and left to dry at 4 °C for approximately one week. After this time the silicon substrates were investigated by SEM.

1. 10 day old solution deposited onto substrate.

Result: wires and rods.

2. 20 day old solution deposited onto substrate.

Result: spherulites and wires.

3. 30 day old solution deposited onto substrate.

Result: crystals.

4. 40 day old solution deposited onto substrate.

Result: crystals.

5.4.4 TEM and SAED preparation of $((n\text{-C}_4\text{H}_9)_4\text{N})_{2n}[\text{Ag}_2\text{Mo}_8\text{O}_{26}]_n$ (**4b**) Powder Material.

1 mg of powder (isolated from synthesis 5.3.4- route 2) suspended in 1 mL methanol and sonicated for a few minutes and left to sit in a cupboard (minimum exposure to light) at room temperature. After 30 days a single drop of the methanol solution was placed onto a copper grid coated with a carbon film. The grid was left to dry in air for several hours at room temperature and investigated by TEM and SAED.

Result: many wires/fibres with a high composition of silver and coated in molybdenum oxide.

5.4.5 Additional Silver to $((n\text{-C}_4\text{H}_9)_4\text{N})_{2n}[\text{Ag}_2\text{Mo}_8\text{O}_{26}]_n$ (**4b**) Crystal Solution.

2 mg of **4b** crystals suspended in 2 mL methanol and sonicated for 15 minutes. The solution was then split into two:

A - 1 mL of above solution taken and to this another 1 mL of methanol added.

B - 1 mL of above solution taken and to this was added a solution of silver(I) fluoride (0.5 mg in 1 mL methanol).

Both solutions left to sit in the cupboard (minimum exposure to light) at room temperature. The silicon substrates were cleaned and prepared by sonicating them in ethanol for 20 minutes. After 10 days, 10 μL of the solution is deposited onto a silicon substrate and left to dry at 4 $^\circ\text{C}$ for approximately one week. After this time the silicon substrates were investigated by SEM.

Results: A - rod shaped crystals.

B - lots of wires present on the silicon substrate.

5.4.6 Additional Silver to $((n\text{-C}_4\text{H}_9)_4\text{N})_{2n}[\text{Ag}_2\text{Mo}_8\text{O}_{26}]_n$ (4b) Powder Solution.

2 mg of powder (isolated from synthesis 5.3.5) suspended in 2 mL methanol and sonicated for a few minutes. This solution was split into two:

A - 1 mL of above solution taken and to this another 1 mL of methanol added.

B - 1 mL of above solution taken and to this was added a solution of silver(I) fluoride (0.5 mg in 1 mL methanol).

Both solutions were left to sit in a cupboard (minimum exposure to light) at room temperature. The silicon substrates were cleaned and prepared by sonicating them in ethanol for 20 minutes. After 10 days, 10 μL of the solution is deposited onto a silicon substrate and left to dry at 4 $^\circ\text{C}$ for approximately one week. After this time the silicon substrates were investigated by SEM.

Results: A - crystals and some small nanowires.

B - crystal with growth from the tip of the crystal.

5.4.7 Silver(I) Fluoride Control Test

2 mg of silver(I) fluoride suspended in 2 mL methanol and sonicated for two minutes. Solution then taken and split into volumes of 1 mL to which another 1 mL of methanol was added and solution then left to sit in cupboard at room temperature. The silicon substrates were cleaned and prepared by sonicating them in ethanol for 20 minutes. After 12 days, 10 μL of the solution is deposited onto a silicon substrate and left to dry at 4 $^\circ\text{C}$ for approximately one week. After this time the silicon substrates were investigated by SEM.

Result: crystals of 'flake' composition.

5.4.8 Substrate Preparation of $((n\text{-C}_4\text{H}_9)_4\text{N})_{2n}[\text{Ag}_2(\text{DMSO})_2\text{Mo}_8\text{O}_{26}]_n$ (15)

Silver(I) fluoride (3 mg, 0.024 mmol) in methanol (1 mL) was added dropwise to a solution of $((n\text{-C}_4\text{H}_9)_4\text{N})_2\text{Mo}_6\text{O}_{19}$ (75 mg, 0.055 mmol) in DMSO (3 mL). Upon stirring for two hours a clear, pale yellow solution forms. Silicon substrates were cleaned and prepared by sonicating them in ethanol for 20 minutes. The solution is taken and crystallised onto pitted (micro-wells pitted onto silicon surface using a diamond tip pen before cleaning) silicon substrates by diffusion of ethanol. SEM was carried out after 60 days.

Result: crystals seen all over the surface but also what looks to be the growth of a silver wire growing from one of the crystals.

5.4.9 Substrate Preparation of



Two samples prepared with 1 mg of **12** crystals suspended in 1 mL methanol and sonicated for 15 minutes. Some of the silicon substrates were prepared by scratching the surface with a diamond tip pen and all of them cleaned by sonicating them in ethanol for 20 minutes. 8 μL of the solution was deposited onto the silicon substrates and left to dry at 4 °C for 15 days. The silicon substrates were investigated by SEM.

A - solution left to sit (minimum exposure to light) at room temperature.

B - solution exposed to UV short wave light (wavelength = 264 nm) for one night and then left to sit on bench at room temperature.

Results: A - scratched - fibrous spherulite type structures and crystals.

unscratched - fibrous spherulite type structures and crystals.

B - scratched - wires growing from scratch and fibrous spherulite type structures.

unscratched - fibrous spherulite type structures and crystals.

Tabulated summary of all SEM results can be found in section 3.4.3, Table 6.

6 CRYSTALLOGRAPHIC DATA

18 structures are presented in this thesis. Due to the large amounts of tabulated data such as atoms coordinates, anisotropic displacement parameters and hydrogen atom coordinates, only tables with bond length and angles are given in this section. For additional data, the reader is referred to the supplementary data which is deposited with this thesis and can be obtained from the University of Glasgow.

Structures were solved by Patterson or Direct methods with SHELXS-97¹⁶⁰ or SIR-92¹⁶¹ using WinGX¹⁶² routines. Refinement was accomplished by full matrix least-squares on F^2 with SHELXL-97. All non-hydrogen atoms were refined anisotropically except otherwise stated. Hydrogen atoms were placed using standard geometric criteria and refined using a riding model. All data manipulation and presentation were performed using WinGX. Details of interest about the structure refinement are given in the tables.

The following quantities are given in the information for each structure and were calculated as follows:

$$\text{Goodness-of-fit (GooF)} = \{\Sigma[w(F_o^2 - F_c^2)^2] / (n-p)\}^{1/2}$$

$$\text{Weighting scheme } w = [\sigma^2(F_o^2) + (A * P)^2 + B * P]^{-1}$$

$$P = [\max(I_{\text{obs}}, 0) + 2 F_c^2] / 3$$

p = number of parameters, n = number of data. Weighting scheme parameters A and B given for each structure.

$$\text{R-factors: } R1 = \Sigma||F_o| - |F_c|| / \Sigma|F_o| \text{ and } wR2 = \{\Sigma[w(F_o^2 - F_c^2)^2] / \{\Sigma[w(F_o^2)^2]\}\}^{1/2}$$

$R(\text{int}) = \Sigma|F_o^2 - F_c^2 (\text{mean})| / \Sigma[(F_o^2)]$ where both summation involve reflections for which more than one symmetry equivalent is averaged.

Only unique atoms in the asymmetric unit are numbered in the Ortep-style representations. To illustrate the coordination environment of the compounds, these asymmetric units are expanded where appropriate.

6.1 X-ray Summary Table

Code	Crystal System	Space Group	$a/b/c$ / Å	$\alpha/\beta/\gamma$ / °	V / Å ³
4a/b/c $((n\text{-C}_4\text{H}_9)_4\text{N})_{2n}[\text{Ag}_2\text{Mo}_8\text{O}_{26}]_n$	Monoclinic	$P2_1/c$	9.7341(1) 15.9359(4) 17.5362(4)	90 94.042(11) 90	2713.45(10)
6 $((n\text{-C}_4\text{H}_9)_4\text{N})_{2n}$ $[\text{Ag}_2(\text{CH}_3\text{CN})_2\text{Mo}_8\text{O}_{26}]_n \cdot 2\text{CH}_3\text{CN}$	Triclinic	$P-1$	9.4468(19) 15.259(3) 22.59(5)1	93.34(3) 90.25(3) 98.11(3)	3218.1(11)
8 $((n\text{-C}_4\text{H}_9)_4\text{N})_{2n}$ $[\text{KM}_8\text{O}_{26}\text{Ag}(\text{CH}_3\text{CN})_2]_n$	Monoclinic	$P2_1/c$	18.8073(5) 16.4856(3) 20.2432(6)	90 104.491(2) 90	6076.7(3)
10 $(\text{Ph}_4\text{P})_2[\text{Ag}_2(\text{CH}_3\text{CN})_2\text{Mo}_8\text{O}_{26}] \cdot 2\text{CH}_3\text{CN}$	Triclinic	$P-1$	9.7210(3) 11.7984(5) 16.0976(7)	85.561(2) 75.929(2) 68.078(2)	1661.2(11)
11 $((n\text{-C}_4\text{H}_9)_4\text{N})_{2n}$ $[\text{Ag}_2(\text{CH}_3\text{CN})_2\text{Mo}_8\text{O}_{26}]_n$	Monoclinic	$P21/n$	10.4827(3) 16.6484(4) 16.8280(4)	90 93.144(1) 90	2932.41(13)
12 $[\text{Ag}(\text{C}_7\text{H}_{12}\text{O}_2\text{N})(\text{CH}_3\text{CN})]_{2n}$ $[(\text{Ag}(\text{CH}_3\text{CN}))_2\text{Mo}_8\text{O}_{26}]_n \cdot 2\text{CH}_3\text{CN}$	Triclinic	$P-1$	9.6535(3) 10.8471(3) 12.1151(3)	80.068(2) 82.5150(10) 85.153(2)	1236.44(6)
13 $(\text{Ph}_4\text{P})_{2n}[\text{Ag}_2(\text{DMF})_2\text{Mo}_8\text{O}_{26}]_n \cdot 2\text{DMF}$	Monoclinic	$P2_1/n$	17.1720(5) 9.2312(3) 24.0351(5)	90 100.400(2) 90	3747.41(18)
14 $(\text{H}_2\text{NMe}_2)_{2n}[\text{Ag}_2(\text{DMF})_2\text{Mo}_8\text{O}_{26}]_n \cdot 2\text{DMF}$	Triclinic	$P-1$	10.0246(7) 10.5735(7) 11.8724(6)	85.711(4) 65.494(4) 69.821(3)	1071.33(12)
15 $((n\text{-C}_4\text{H}_9)_4\text{N})_{2n}[\text{Ag}_2(\text{DMSO})_2\text{Mo}_8\text{O}_{26}]_n$	Triclinic	$P-1$	12.9182(2) 14.5922(3) 16.9871(3)	76.988(1) 86.366 (1) 83.784(1)	3099.07(10)
16 $(\text{HDMF})_n[\text{Ag}_3(\text{DMF})_4\text{Mo}_8\text{O}_{26}]_n$	Triclinic	$P-1$	9.9458(4) 10.8856(3) 11.7553(5)	62.938(2) 73.481(2) 83.657(2)	1086.31(7)
17 $[(\text{Ag}(\text{DMF}))_2(\text{Ag}(\text{DMF})_2)_2\text{Mo}_8\text{O}_{26}]_n$	Triclinic	$P-1$	10.1101(2) 11.4232(3) 11.5474(3)	63.312(1) 76.600(2) 88.951(1)	1153.43(5)

18 [(Ag(CH ₃ CN) ₃) ₂ (Ag(CH ₃ CN)) ₂ AgMo ₈ O ₂₆] _n	Triclinic	<i>P</i> -1	11.0978(2) 12.7612(3) 15.6460(3)	97.212(2) 97.158(2) 99.247(2)	2145.86(8)
19 [(Ag(CH ₃ CN)) ₂ (Ag(CH ₃ CN)) ₂ Mo ₈ O ₂₆] _n	Monoclinic	<i>P</i> 2 ₁ / <i>n</i>	10.6524(5) 13.4553(6) 13.2691(3)	90 103.579(3) 90	1848.71(13)
20 [(Ag(CH ₃ CN)) ₂ Ag ₂ Mo ₈ O ₂₆] _n	Triclinic	<i>P</i> -1	7.7079(3) 9.8937(4) 11.0988(5)	71.733(2) 75.067(2) 77.256(3)	767.52(6)
21 [Ag ₄ (DMSO) ₆ (OC(CH ₃) ₂) ₂ Mo ₈ O ₂₆] _n	Orthorhombic	<i>Pbca</i>	14.7008(5) 18.6995(7) 19.1703(4)	90 90 90	5269.9(3)
22 [Ag ₄ (DMSO) ₈ Mo ₈ O ₂₆] _n	Triclinic	<i>P</i> -1	10.8053(3) 11.1381(3) 13.3396(3)	97.200(2) 113.4870(10) 108.7740(1)	1333.3(6)
23 ((<i>n</i> -C ₄ H ₉) ₄ N) _{2n} [K ₂ (DMSO) ₃ Mo ₈ O ₂₆] _n	Triclinic	<i>P</i> -1	13.9729(4) 14.1830(5) 17.3775(5)	76.311(2) 86.084(2) 83.630(2)	3322.2(18)
24 ((<i>n</i> -C ₄ H ₉) ₄ N) _n (H ₂ NMe ₂) _n [K ₂ (DMF)Mo ₈ O ₂₆] _n ·DMF	Monoclinic	<i>P</i> 2 ₁	11.7040(4) 15.4744(7) 15.0085(6)	90 111.800(2) 90	2523.83(18)

6.2 Crystal data for $((n\text{-C}_4\text{H}_9)_4\text{N})_{2n}[\text{Ag}_2\text{Mo}_8\text{O}_{26}]_n$ (4a/b/c)

Empirical formula	$\text{C}_{32}\text{H}_{72}\text{Ag}_2\text{Mo}_8\text{N}_2\text{O}_{26}$	
Crystal growth	Diffusion of diethyl ether, 3 days.	
Crystal description	Colourless rectangular blocks.	
Crystal size	$0.4 \times 0.2 \times 0.16 \text{ mm}^3$	
Formula weight	942.09	
Temperature	150 K	
Wavelength	0.71073 Å	
Crystal system	Monoclinic	
Space group	$P2_1/c$	
Unit cell dimensions	$a = 9.7341(1) \text{ Å}$	$\alpha = 90^\circ$
	$b = 15.9359(4) \text{ Å}$	$\beta = 94.0421(11)^\circ$
	$c = 17.5362(4) \text{ Å}$	$\gamma = 90^\circ$
Volume	2713.4 Å^3	
Z	4	
Density (calculated)	2.306 Mg/m^3	
Absorption coefficient	2.566 mm^{-1}	
$F(000)$	1832	
Theta range for data collection	1.73 to 30.07°	
Index ranges	$-13 \leq h \leq 13, -22 \leq k \leq 22, -24 \leq l \leq 24$	
Reflections collected/ unique	44448 / 7937 [$R(\text{int}) = 0.0388$]	
Completeness to theta	30.07° 99.4 %	
Absorption correction	Semi-empirical from equivalents	
Max. and min. transmission	0.499 and 0.424	
Refinement method	Full-matrix least-squares on F^2	
Data / restraints / parameters	7937 / 0 / 316	
Goodness-of-fit on F^2	1.042	
Final R indices [$I > 2\sigma(I)$]	$R1 = 0.0235, wR2 = 0.0556$	
R indices (all data)	$R1 = 0.0295, wR2 = 0.0574$	
Extinction coefficient	None	
Largest diff. peak and hole	0.408 and -1.066 e.Å^{-3}	

Bond lengths [Å] and angles [°]

N(1)-C(5)	1.519(3)	H(8A)-C(8)-H(8C)	109.5
N(1)-C(13)	1.521(3)	H(8B)-C(8)-H(8C)	109.5
N(1)-C(1)	1.523(3)	C(10)-C(9)-N(1)	116.19(19)
N(1)-C(9)	1.526(3)	C(10)-C(9)-H(9A)	108.2
C(1)-C(2)	1.523(3)	N(1)-C(9)-H(9A)	108.2
C(1)-H(1A)	0.97	C(10)-C(9)-H(9B)	108.2
C(1)-H(1B)	0.97	N(1)-C(9)-H(9B)	108.2
C(2)-C(3)	1.524(4)	H(9A)-C(9)-H(9B)	107.4
C(2)-H(2A)	0.97	C(9)-C(10)-C(11)	109.9(2)
C(2)-H(2B)	0.97	C(9)-C(10)-H(10A)	109.7
C(3)-C(4)	1.508(4)	C(11)-C(10)-H(10A)	109.7
C(3)-H(3A)	0.97	C(9)-C(10)-H(10B)	109.7
C(3)-H(3B)	0.97	C(11)-C(10)-H(10B)	109.7
C(4)-H(4A)	0.96	H(10A)-C(10)-H(10B)	108.2
C(4)-H(4B)	0.96	C(12)-C(11)-C(10)	112.6(2)
C(4)-H(4C)	0.96	C(12)-C(11)-H(11A)	109.1
C(5)-C(6)	1.519(3)	C(10)-C(11)-H(11A)	109.1
C(5)-H(5A)	0.97	C(12)-C(11)-H(11B)	109.1
C(5)-H(5B)	0.97	C(10)-C(11)-H(11B)	109.1
C(6)-C(7)	1.524(3)	H(11A)-C(11)-H(11B)	107.8
C(6)-H(6A)	0.97	C(11)-C(12)-H(12A)	109.5
C(6)-H(6B)	0.97	C(11)-C(12)-H(12B)	109.5
C(7)-C(8)	1.524(4)	H(12A)-C(12)-H(12B)	109.5
C(7)-H(7A)	0.97	C(11)-C(12)-H(12C)	109.5
C(7)-H(7B)	0.97	H(12A)-C(12)-H(12C)	109.5
C(8)-H(8A)	0.96	H(12B)-C(12)-H(12C)	109.5
C(8)-H(8B)	0.96	C(14)-C(13)-N(1)	115.45(19)
C(8)-H(8C)	0.96	C(14)-C(13)-H(13A)	108.4
C(9)-C(10)	1.514(3)	N(1)-C(13)-H(13A)	108.4
C(9)-H(9A)	0.97	C(14)-C(13)-H(13B)	108.4
C(9)-H(9B)	0.97	N(1)-C(13)-H(13B)	108.4
C(10)-C(11)	1.534(4)	H(13A)-C(13)-H(13B)	107.5
C(10)-H(10A)	0.97	C(13)-C(14)-C(15)	110.6(2)
C(10)-H(10B)	0.97	C(13)-C(14)-H(14A)	109.5
C(11)-C(12)	1.496(5)	C(15)-C(14)-H(14A)	109.5
C(11)-H(11A)	0.97	C(13)-C(14)-H(14B)	109.5
C(11)-H(11B)	0.97	C(15)-C(14)-H(14B)	109.5

C(12)-H(12A)	0.96	H(14A)-C(14)-H(14B)	108.1
C(12)-H(12B)	0.96	C(16)-C(15)-C(14)	111.6(2)
C(12)-H(12C)	0.96	C(16)-C(15)-H(15A)	109.3
C(13)-C(14)	1.521(3)	C(14)-C(15)-H(15A)	109.3
C(13)-H(13A)	0.97	C(16)-C(15)-H(15B)	109.3
C(13)-H(13B)	0.97	C(14)-C(15)-H(15B)	109.3
C(14)-C(15)	1.530(3)	H(15A)-C(15)-H(15B)	108
C(14)-H(14A)	0.97	C(15)-C(16)-H(16A)	109.5
C(14)-H(14B)	0.97	C(15)-C(16)-H(16B)	109.5
C(15)-C(16)	1.521(4)	H(16A)-C(16)-H(16B)	109.5
C(15)-H(15A)	0.97	C(15)-C(16)-H(16C)	109.5
C(15)-H(15B)	0.97	H(16A)-C(16)-H(16C)	109.5
C(16)-H(16A)	0.96	H(16B)-C(16)-H(16C)	109.5
C(16)-H(16B)	0.96	O(1)-Ag(1)-O(8)#1	171.00(6)
C(16)-H(16C)	0.96	O(1)-Ag(1)-O(2)	81.89(5)
Ag(1)-O(1)	2.2704(17)	O(8)#1-Ag(1)-O(2)	96.92(6)
Ag(1)-O(8)#1	2.2953(17)	O(1)-Ag(1)-O(11)#1	99.02(5)
Ag(1)-O(2)	2.3920(15)	O(8)#1-Ag(1)-O(11)#1	81.18(5)
Ag(1)-O(11)#1	2.4130(15)	O(2)-Ag(1)-O(11)#1	173.61(5)
Ag(1)-Ag(1)#1	2.8531(4)	O(1)-Ag(1)-Ag(1)#1	120.37(4)
Mo(1)-O(2)	1.7035(15)	O(8)#1-Ag(1)-Ag(1)#1	67.93(4)
Mo(1)-O(5)	1.7510(14)	O(2)-Ag(1)-Ag(1)#1	120.52(4)
Mo(1)-O(4)	1.9487(15)	O(11)#1-Ag(1)-Ag(1)#1	64.51(4)
Mo(1)-O(7)	1.9549(15)	O(2)-Mo(1)-O(5)	104.64(7)
Mo(1)-O(13)#2	2.1360(14)	O(2)-Mo(1)-O(4)	101.35(7)
Mo(1)-O(13)	2.3246(14)	O(5)-Mo(1)-O(4)	96.67(7)
Mo(2)-O(3)	1.6871(17)	O(2)-Mo(1)-O(7)	100.47(7)
Mo(2)-O(1)	1.7244(16)	O(5)-Mo(1)-O(7)	96.74(7)
Mo(2)-O(6)	1.8981(15)	O(4)-Mo(1)-O(7)	150.51(6)
Mo(2)-O(4)	2.0075(14)	O(2)-Mo(1)-O(13)#2	98.11(6)
Mo(2)-O(7)#2	2.2917(14)	O(5)-Mo(1)-O(13)#2	157.25(6)
Mo(2)-O(13)#2	2.3364(15)	O(4)-Mo(1)-O(13)#2	78.69(6)
Mo(3)-O(9)	1.6942(16)	O(7)-Mo(1)-O(13)#2	78.80(6)
Mo(3)-O(8)	1.7336(16)	O(2)-Mo(1)-O(13)	173.53(6)
Mo(3)-O(6)	1.9149(16)	O(5)-Mo(1)-O(13)	81.83(6)
Mo(3)-O(10)	1.9289(16)	O(4)-Mo(1)-O(13)	77.83(6)
Mo(3)-O(5)#2	2.2220(15)	O(7)-Mo(1)-O(13)	78.25(6)
Mo(3)-O(13)#2	2.5006(14)	O(13)#2-Mo(1)-O(13)	75.42(6)
Mo(4)-O(12)	1.6922(17)	O(3)-Mo(2)-O(1)	104.63(8)
Mo(4)-O(11)	1.7267(16)	O(3)-Mo(2)-O(6)	102.52(7)

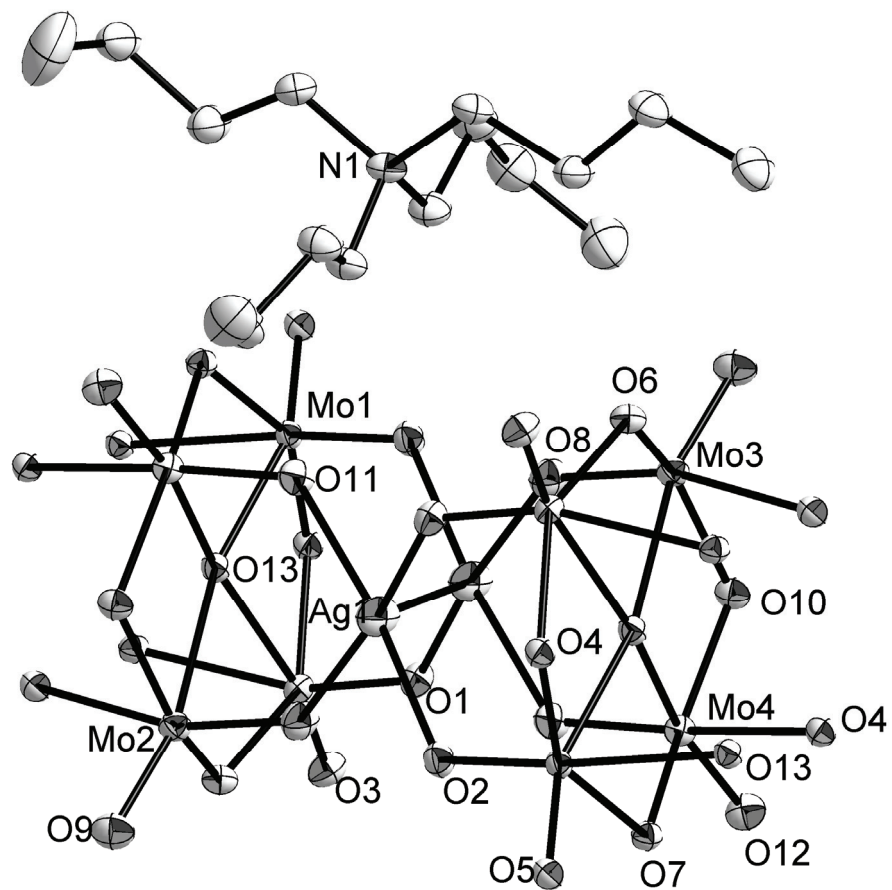
Mo(4)-O(10)	1.8955(15)	O(1)-Mo(2)-O(6)	100.26(7)
Mo(4)-O(7)	2.0136(14)	O(3)-Mo(2)-O(4)	100.98(7)
Mo(4)-O(4)#2	2.2868(14)	O(1)-Mo(2)-O(4)	96.47(7)
Mo(4)-O(13)#2	2.3113(15)	O(6)-Mo(2)-O(4)	146.52(6)
O(4)-Mo(4)#2	2.2868(14)	O(3)-Mo(2)-O(7)#2	91.55(7)
O(5)-Mo(3)#2	2.2220(15)	O(1)-Mo(2)-O(7)#2	161.85(7)
O(7)-Mo(2)#2	2.2917(14)	O(6)-Mo(2)-O(7)#2	83.83(6)
O(8)-Ag(1)#1	2.2953(17)	O(4)-Mo(2)-O(7)#2	72.00(5)
O(11)-Ag(1)#1	2.4130(15)	O(3)-Mo(2)-O(13)#2	163.32(7)
O(13)-Mo(1)#2	2.1360(14)	O(1)-Mo(2)-O(13)#2	91.60(7)
O(13)-Mo(4)#2	2.3113(15)	O(6)-Mo(2)-O(13)#2	77.84(6)
O(13)-Mo(2)#2	2.3364(15)	O(4)-Mo(2)-O(13)#2	72.88(5)
O(13)-Mo(3)#2	2.5006(14)	O(7)#2-Mo(2)-O(13)#2	71.85(5)
		O(9)-Mo(3)-O(8)	104.86(8)
C(5)-N(1)-C(13)	111.24(17)	O(9)-Mo(3)-O(6)	104.70(8)
C(5)-N(1)-C(1)	110.95(18)	O(8)-Mo(3)-O(6)	98.21(8)
C(13)-N(1)-C(1)	107.03(17)	O(9)-Mo(3)-O(10)	103.12(8)
C(5)-N(1)-C(9)	106.79(17)	O(8)-Mo(3)-O(10)	96.11(7)
C(13)-N(1)-C(9)	110.16(18)	O(6)-Mo(3)-O(10)	144.10(6)
C(1)-N(1)-C(9)	110.72(18)	O(9)-Mo(3)-O(5)#2	93.70(7)
C(2)-C(1)-N(1)	114.04(19)	O(8)-Mo(3)-O(5)#2	161.36(7)
C(2)-C(1)-H(1A)	108.7	O(6)-Mo(3)-O(5)#2	78.23(6)
N(1)-C(1)-H(1A)	108.7	O(10)-Mo(3)-O(5)#2	77.76(6)
C(2)-C(1)-H(1B)	108.7	O(9)-Mo(3)-O(13)#2	163.26(7)
N(1)-C(1)-H(1B)	108.7	O(8)-Mo(3)-O(13)#2	91.83(6)
H(1A)-C(1)-H(1B)	107.6	O(6)-Mo(3)-O(13)#2	73.46(6)
C(1)-C(2)-C(3)	111.9(2)	O(10)-Mo(3)-O(13)#2	73.35(6)
C(1)-C(2)-H(2A)	109.2	O(5)#2-Mo(3)-O(13)#2	69.58(5)
C(3)-C(2)-H(2A)	109.2	O(12)-Mo(4)-O(11)	104.95(8)
C(1)-C(2)-H(2B)	109.2	O(12)-Mo(4)-O(10)	102.59(7)
C(3)-C(2)-H(2B)	109.2	O(11)-Mo(4)-O(10)	99.66(7)
H(2A)-C(2)-H(2B)	107.9	O(12)-Mo(4)-O(7)	99.53(7)
C(4)-C(3)-C(2)	114.3(2)	O(11)-Mo(4)-O(7)	96.92(7)
C(4)-C(3)-H(3A)	108.7	O(10)-Mo(4)-O(7)	147.76(6)
C(2)-C(3)-H(3A)	108.7	O(12)-Mo(4)-O(4)#2	91.50(7)
C(4)-C(3)-H(3B)	108.7	O(11)-Mo(4)-O(4)#2	161.69(7)
C(2)-C(3)-H(3B)	108.7	O(10)-Mo(4)-O(4)#2	84.21(6)
H(3A)-C(3)-H(3B)	107.6	O(7)-Mo(4)-O(4)#2	72.00(5)
C(3)-C(4)-H(4A)	109.5	O(12)-Mo(4)-O(13)#2	163.26(7)
C(3)-C(4)-H(4B)	109.5	O(11)-Mo(4)-O(13)#2	91.17(7)

H(4A)-C(4)-H(4B)	109.5	O(10)-Mo(4)-O(13)#2	78.64(6)
C(3)-C(4)-H(4C)	109.5	O(7)-Mo(4)-O(13)#2	73.55(5)
H(4A)-C(4)-H(4C)	109.5	O(4)#2-Mo(4)-O(13)#2	71.92(5)
H(4B)-C(4)-H(4C)	109.5	Mo(2)-O(1)-Ag(1)	133.37(9)
N(1)-C(5)-C(6)	115.39(19)	Mo(1)-O(2)-Ag(1)	125.43(8)
N(1)-C(5)-H(5A)	108.4	Mo(1)-O(4)-Mo(2)	109.58(7)
C(6)-C(5)-H(5A)	108.4	Mo(1)-O(4)-Mo(4)#2	110.00(7)
N(1)-C(5)-H(5B)	108.4	Mo(2)-O(4)-Mo(4)#2	103.79(6)
C(6)-C(5)-H(5B)	108.4	Mo(1)-O(5)-Mo(3)#2	118.37(7)
H(5A)-C(5)-H(5B)	107.5	Mo(2)-O(6)-Mo(3)	118.66(8)
C(5)-C(6)-C(7)	110.9(2)	Mo(1)-O(7)-Mo(4)	108.60(7)
C(5)-C(6)-H(6A)	109.5	Mo(1)-O(7)-Mo(2)#2	110.11(6)
C(7)-C(6)-H(6A)	109.5	Mo(4)-O(7)-Mo(2)#2	103.42(6)
C(5)-C(6)-H(6B)	109.5	Mo(3)-O(8)-Ag(1)#1	135.72(10)
C(7)-C(6)-H(6B)	109.5	Mo(4)-O(10)-Mo(3)	117.63(8)
H(6A)-C(6)-H(6B)	108	Mo(4)-O(11)-Ag(1)#1	129.91(8)
C(6)-C(7)-C(8)	112.3(2)	Mo(1)#2-O(13)-Mo(4)#2	92.80(5)
C(6)-C(7)-H(7A)	109.1	Mo(1)#2-O(13)-Mo(1)	104.58(6)
C(8)-C(7)-H(7A)	109.1	Mo(4)#2-O(13)-Mo(1)	97.10(5)
C(6)-C(7)-H(7B)	109.1	Mo(1)#2-O(13)-Mo(2)#2	92.46(5)
C(8)-C(7)-H(7B)	109.1	Mo(4)#2-O(13)-Mo(2)#2	163.37(7)
H(7A)-C(7)-H(7B)	107.9	Mo(1)-O(13)-Mo(2)#2	96.83(5)
C(7)-C(8)-H(8A)	109.5	Mo(1)#2-O(13)-Mo(3)#2	165.20(7)
C(7)-C(8)-H(8B)	109.5	Mo(4)#2-O(13)-Mo(3)#2	85.59(5)
H(8A)-C(8)-H(8B)	109.5	Mo(1)-O(13)-Mo(3)#2	90.22(5)
C(7)-C(8)-H(8C)	109.5	Mo(2)#2-O(13)-Mo(3)#2	85.31(5)

Symmetry transformations used to generate equivalent atoms:

#1 $-x+2, -y, -z+1$ #2 $-x+1, -y, -z+1$

Ortep style representation of $((n\text{-C}_4\text{H}_9)_4\text{N})_{2n}[\text{Ag}_2\text{Mo}_8\text{O}_{26}]_n$ (**4a/b/c**): thermal ellipsoids at 50% probability, hydrogen atoms are omitted for clarity and carbon atoms are not labelled.



6.3 Crystal data for $(n\text{-C}_4\text{H}_9)_4\text{N})_{2n}[\text{Ag}_2(\text{CH}_3\text{CN})_2\text{Mo}_8\text{O}_{26}]_n \cdot 2\text{CH}_3\text{CN}$ (6)

Empirical formula	$\text{C}_{40}\text{H}_{84}\text{N}_6\text{Ag}_2\text{Mo}_8\text{O}_{26}$	
Crystal growth	Diffusion of diethyl ether, 10 days	
Crystal description	Colourless needle crystals	
Crystal size	$0.20 \times 0.10 \times 0.10 \text{ mm}^3$	
Formula weight	2048.39	
Temperature	90(2) K	
Wavelength	0.71073 Å	
Crystal system	Triclinic	
Space group	$P\bar{1}$	
Unit cell dimensions	$a = 9.4468(19) \text{ Å}$	$\alpha = 93.34(3)^\circ$
	$b = 15.259(3) \text{ Å}$	$\beta = 90.25(3)^\circ$
	$c = 22.591(5) \text{ Å}$	$\gamma = 98.11(3)^\circ$
Volume	$3218.1(11) \text{ Å}^3$	
Z	2	
Density (calculated)	2.114 Mg/m^3	
Absorption coefficient	2.175 mm^{-1}	
$F(000)$	2008	
Theta range for data collection	0.90 to 26.48°	
Index ranges	$-11 \leq h \leq 11, -19 \leq k \leq 19, 0 \leq l \leq 28$	
Reflections collected	22722	
Independent reflections	22722 [R(int) = 0.0000]	
Completeness to theta	26.48° 97.9 %	
Refinement method	Full-matrix least-squares on F^2	
Data / restraints / parameters	22722 / 0 / 752	
Goodness-of-fit on F^2	1.001	
Final R indices [$I > 2\sigma(I)$]	$R1 = 0.0498, wR2 = 0.1066$	
R indices (all data)	$R1 = 0.0925, wR2 = 0.1200$	
Largest diff. peak and hole	1.066 and -1.478 e.Å^{-3}	

Bond lengths [\AA] and angles [$^\circ$]

Ag(1)-O(2)	2.360(5)	O(16)-Mo(5)-Mo(6)	124.43(14)
Ag(1)-O(1)	2.395(5)	O(17)-Mo(5)-Mo(6)	46.53(13)
Ag(1)-O(8)#1	2.418(5)	O(17)#4-Mo(5)-Mo(6)	85.76(12)
Ag(1)-N(1)	2.439(7)	O(18)-Mo(6)-O(19)	104.8(2)
Ag(1)-O(10)#1	2.444(5)	O(18)-Mo(6)-O(20)	102.6(2)
Ag(1)-Ag(1)#1	3.2345(15)	O(19)-Mo(6)-O(20)	101.8(2)
Ag(2)-N(2)	2.367(7)	O(18)-Mo(6)-O(25)#4	100.3(2)
Ag(2)-O(19)#2	2.396(5)	O(19)-Mo(6)-O(25)#4	95.9(2)
Ag(2)-O(23)#2	2.469(5)	O(20)-Mo(6)-O(25)#4	146.2(2)
Ag(2)-O(14)	2.485(5)	O(18)-Mo(6)-O(16)#4	92.4(2)
Ag(2)-O(15)	2.505(5)	O(19)-Mo(6)-O(16)#4	160.2(2)
Ag(2)-Ag(2)#2	3.2281(15)	O(20)-Mo(6)-O(16)#4	83.40(19)
Mo(1)-O(3)	1.715(5)	O(25)#4-Mo(6)-O(16)#4	71.10(18)
Mo(1)-O(1)	1.725(5)	O(18)-Mo(6)-O(17)	163.3(2)
Mo(1)-O(5)	1.926(5)	O(19)-Mo(6)-O(17)	91.3(2)
Mo(1)-O(4)	1.931(5)	O(20)-Mo(6)-O(17)	77.64(18)
Mo(1)-O(9)#3	2.268(5)	O(25)#4-Mo(6)-O(17)	73.35(18)
Mo(1)-O(6)	2.447(5)	O(16)#4-Mo(6)-O(17)	71.01(17)
Mo(2)-O(13)	1.698(5)	O(18)-Mo(6)-Mo(5)	135.27(15)
Mo(2)-O(2)	1.720(5)	O(19)-Mo(6)-Mo(5)	82.68(16)
Mo(2)-O(4)	1.889(5)	O(20)-Mo(6)-Mo(5)	119.23(15)
Mo(2)-O(11)	2.004(5)	O(25)#4-Mo(6)-Mo(5)	35.13(14)
Mo(2)-O(12)	2.312(5)	O(16)#4-Mo(6)-Mo(5)	78.23(12)
Mo(2)-O(6)	2.337(5)	O(17)-Mo(6)-Mo(5)	41.59(12)
Mo(2)-Mo(3)	3.2187(11)	O(22)-Mo(7)-O(23)	104.4(2)
Mo(3)-O(10)	1.711(5)	O(22)-Mo(7)-O(26)	103.5(2)
Mo(3)-O(9)	1.746(5)	O(23)-Mo(7)-O(26)	97.5(2)
Mo(3)-O(12)#3	1.951(5)	O(22)-Mo(7)-O(20)	102.8(2)
Mo(3)-O(11)	1.954(5)	O(23)-Mo(7)-O(20)	98.3(2)
Mo(3)-O(6)	2.163(5)	O(26)-Mo(7)-O(20)	144.7(2)
Mo(3)-O(6)#3	2.331(5)	O(22)-Mo(7)-O(21)	92.4(2)
Mo(3)-Mo(4)	3.2187(12)	O(23)-Mo(7)-O(21)	163.2(2)
Mo(4)-O(7)	1.690(5)	O(26)-Mo(7)-O(21)	78.52(19)
Mo(4)-O(8)	1.727(5)	O(20)-Mo(7)-O(21)	77.26(19)
Mo(4)-O(5)	1.885(5)	O(22)-Mo(7)-O(17)	161.9(2)
Mo(4)-O(12)#3	2.013(5)	O(23)-Mo(7)-O(17)	93.6(2)
Mo(4)-O(6)	2.325(5)	O(26)-Mo(7)-O(17)	74.10(18)

Mo(4)-O(11)#3	2.326(5)	O(20)-Mo(7)-O(17)	73.55(18)
Mo(5)-O(14)	1.710(5)	O(21)-Mo(7)-O(17)	69.56(16)
Mo(5)-O(21)#4	1.747(5)	O(24)-Mo(8)-O(15)	106.3(2)
Mo(5)-O(25)#4	1.949(5)	O(24)-Mo(8)-O(26)	101.8(2)
Mo(5)-O(16)	1.952(5)	O(15)-Mo(8)-O(26)	102.5(2)
Mo(5)-O(17)	2.135(5)	O(24)-Mo(8)-O(16)	100.8(2)
Mo(5)-O(17)#4	2.332(5)	O(15)-Mo(8)-O(16)	95.9(2)
Mo(5)-Mo(6)	3.2144(11)	O(26)-Mo(8)-O(16)	145.4(2)
Mo(6)-O(18)	1.697(5)	O(24)-Mo(8)-O(25)	90.4(2)
Mo(6)-O(19)	1.721(5)	O(15)-Mo(8)-O(25)	160.7(2)
Mo(6)-O(20)	1.891(5)	O(26)-Mo(8)-O(25)	83.07(18)
Mo(6)-O(25)#4	2.014(4)	O(16)-Mo(8)-O(25)	70.82(18)
Mo(6)-O(16)#4	2.302(5)	O(24)-Mo(8)-O(17)	161.0(2)
Mo(6)-O(17)	2.334(5)	O(15)-Mo(8)-O(17)	92.3(2)
Mo(7)-O(22)	1.694(5)	O(26)-Mo(8)-O(17)	77.65(18)
Mo(7)-O(23)	1.728(5)	O(16)-Mo(8)-O(17)	72.53(18)
Mo(7)-O(26)	1.919(5)	O(25)-Mo(8)-O(17)	70.66(17)
Mo(7)-O(20)	1.935(5)	Mo(1)-O(1)-Ag(1)	134.6(3)
Mo(7)-O(21)	2.276(5)	Mo(2)-O(2)-Ag(1)	137.3(3)
Mo(7)-O(17)	2.469(5)	Mo(2)-O(4)-Mo(1)	118.0(2)
Mo(8)-O(24)	1.692(5)	Mo(4)-O(5)-Mo(1)	117.3(2)
Mo(8)-O(15)	1.733(5)	Mo(3)-O(6)-Mo(4)	91.58(17)
Mo(8)-O(26)	1.905(5)	Mo(3)-O(6)-Mo(3)#3	104.73(19)
Mo(8)-O(16)	1.990(5)	Mo(4)-O(6)-Mo(3)#3	98.30(18)
Mo(8)-O(25)	2.333(5)	Mo(3)-O(6)-Mo(2)	91.24(18)
Mo(8)-O(17)	2.336(5)	Mo(4)-O(6)-Mo(2)	162.1(2)
O(6)-Mo(3)#3	2.331(5)	Mo(3)#3-O(6)-Mo(2)	98.06(18)
O(8)-Ag(1)#1	2.417(5)	Mo(3)-O(6)-Mo(1)	163.6(2)
O(9)-Mo(1)#3	2.268(5)	Mo(4)-O(6)-Mo(1)	86.00(16)
O(10)-Ag(1)#1	2.444(5)	Mo(3)#3-O(6)-Mo(1)	91.66(16)
O(11)-Mo(4)#3	2.326(5)	Mo(2)-O(6)-Mo(1)	86.32(15)
O(12)-Mo(3)#3	1.951(5)	Mo(4)-O(8)-Ag(1)#1	137.7(3)
O(12)-Mo(4)#3	2.013(5)	Mo(3)-O(9)-Mo(1)#3	116.7(2)
O(16)-Mo(6)#4	2.302(5)	Mo(3)-O(10)-Ag(1)#1	132.7(3)
O(17)-Mo(5)#4	2.332(5)	Mo(3)-O(11)-Mo(2)	108.8(2)
O(19)-Ag(2)#2	2.396(5)	Mo(3)-O(11)-Mo(4)#3	110.4(2)
O(21)-Mo(5)#4	1.747(5)	Mo(2)-O(11)-Mo(4)#3	103.9(2)
O(23)-Ag(2)#2	2.470(5)	Mo(3)#3-O(12)-Mo(4)#3	108.6(2)
O(25)-Mo(5)#4	1.949(5)	Mo(3)#3-O(12)-Mo(2)	111.3(2)
O(25)-Mo(6)#4	2.014(4)	Mo(4)#3-O(12)-Mo(2)	104.1(2)

N(1)-C(1)	1.137(10)	Mo(5)-O(14)-Ag(2)	133.1(3)
N(2)-C(3)	1.153(10)	Mo(8)-O(15)-Ag(2)	136.5(2)
N(3)-C(9)	1.524(9)	Mo(5)-O(16)-Mo(8)	109.6(2)
N(3)-C(17)	1.526(9)	Mo(5)-O(16)-Mo(6)#4	111.0(2)
N(3)-C(5)	1.528(8)	Mo(8)-O(16)-Mo(6)#4	105.4(2)
N(3)-C(13)	1.538(9)	Mo(5)-O(17)-Mo(5)#4	104.83(18)
N(4)-C(21)	1.517(9)	Mo(5)-O(17)-Mo(6)	91.88(18)
N(4)-C(25)	1.517(8)	Mo(5)#4-O(17)-Mo(6)	97.60(18)
N(4)-C(29)	1.529(8)	Mo(5)-O(17)-Mo(8)	92.06(17)
N(4)-C(33)	1.534(8)	Mo(5)#4-O(17)-Mo(8)	98.33(18)
N(5)-C(37)	1.138(10)	Mo(6)-O(17)-Mo(8)	162.0(2)
N(6)-C(39)	1.139(11)	Mo(5)-O(17)-Mo(7)	163.6(2)
C(1)-C(2)	1.455(12)	Mo(5)#4-O(17)-Mo(7)	91.52(17)
C(2)-H(2A)	0.96	Mo(6)-O(17)-Mo(7)	85.69(15)
C(2)-H(2B)	0.96	Mo(8)-O(17)-Mo(7)	85.61(16)
C(2)-H(2C)	0.96	Mo(6)-O(19)-Ag(2)#2	136.6(3)
C(3)-C(4)	1.471(11)	Mo(6)-O(20)-Mo(7)	117.3(2)
C(4)-H(4A)	0.96	Mo(5)#4-O(21)-Mo(7)	117.0(2)
C(4)-H(4B)	0.96	Mo(7)-O(23)-Ag(2)#2	133.3(2)
C(4)-H(4C)	0.96	Mo(5)#4-O(25)-Mo(6)#4	108.4(2)
C(5)-C(6)	1.535(9)	Mo(5)#4-O(25)-Mo(8)	110.8(2)
C(5)-H(5A)	0.97	Mo(6)#4-O(25)-Mo(8)	103.44(19)
C(5)-H(5B)	0.97	Mo(8)-O(26)-Mo(7)	117.3(2)
C(6)-C(7)	1.516(10)	C(1)-N(1)-Ag(1)	143.5(7)
C(6)-H(6A)	0.97	C(3)-N(2)-Ag(2)	152.7(7)
C(6)-H(6B)	0.97	C(9)-N(3)-C(17)	105.9(5)
C(7)-C(8)	1.524(10)	C(9)-N(3)-C(5)	112.2(6)
C(7)-H(7A)	0.97	C(17)-N(3)-C(5)	110.9(5)
C(7)-H(7B)	0.97	C(9)-N(3)-C(13)	112.2(6)
C(8)-H(8A)	0.96	C(17)-N(3)-C(13)	111.6(5)
C(8)-H(8B)	0.96	C(5)-N(3)-C(13)	104.1(5)
C(8)-H(8C)	0.96	C(21)-N(4)-C(25)	105.8(5)
C(9)-C(10)	1.538(10)	C(21)-N(4)-C(29)	111.2(5)
C(9)-H(9A)	0.97	C(25)-N(4)-C(29)	110.7(5)
C(9)-H(9B)	0.97	C(21)-N(4)-C(33)	111.0(5)
C(10)-C(11)	1.520(10)	C(25)-N(4)-C(33)	110.2(5)
C(10)-H(10A)	0.97	C(29)-N(4)-C(33)	108.0(5)
C(10)-H(10B)	0.97	N(1)-C(1)-C(2)	177.5(10)
C(11)-C(12)	1.512(10)	C(1)-C(2)-H(2A)	109.5
C(11)-H(11A)	0.97	C(1)-C(2)-H(2B)	109.5

C(11)-H(11B)	0.97	H(2A)-C(2)-H(2B)	109.5
C(12)-H(12A)	0.96	C(1)-C(2)-H(2C)	109.5
C(12)-H(12B)	0.96	H(2A)-C(2)-H(2C)	109.5
C(12)-H(12C)	0.96	H(2B)-C(2)-H(2C)	109.5
C(13)-C(14)	1.568(9)	N(2)-C(3)-C(4)	178.6(9)
C(13)-H(13A)	0.97	C(3)-C(4)-H(4A)	109.5
C(13)-H(13B)	0.97	C(3)-C(4)-H(4B)	109.5
C(14)-C(15)	1.535(10)	H(4A)-C(4)-H(4B)	109.5
C(14)-H(14A)	0.97	C(3)-C(4)-H(4C)	109.5
C(14)-H(14B)	0.97	H(4A)-C(4)-H(4C)	109.5
C(15)-C(16)	1.525(9)	H(4B)-C(4)-H(4C)	109.5
C(15)-H(15A)	0.97	N(3)-C(5)-C(6)	116.2(6)
C(15)-H(15B)	0.97	N(3)-C(5)-H(5A)	108.2
C(16)-H(16A)	0.96	C(6)-C(5)-H(5A)	108.2
C(16)-H(16B)	0.96	N(3)-C(5)-H(5B)	108.2
C(16)-H(16C)	0.96	C(6)-C(5)-H(5B)	108.2
C(17)-C(18)	1.534(10)	H(5A)-C(5)-H(5B)	107.4
C(17)-H(17A)	0.97	C(7)-C(6)-C(5)	115.7(6)
C(17)-H(17B)	0.97	C(7)-C(6)-H(6A)	108.4
C(18)-C(19)	1.543(10)	C(5)-C(6)-H(6A)	108.4
C(18)-H(18A)	0.97	C(7)-C(6)-H(6B)	108.4
C(18)-H(18B)	0.97	C(5)-C(6)-H(6B)	108.4
C(19)-C(20)	1.531(10)	H(6A)-C(6)-H(6B)	107.4
C(19)-H(19A)	0.97	C(6)-C(7)-C(8)	112.4(7)
C(19)-H(19B)	0.97	C(6)-C(7)-H(7A)	109.1
C(20)-H(20A)	0.96	C(8)-C(7)-H(7A)	109.1
C(20)-H(20B)	0.96	C(6)-C(7)-H(7B)	109.1
C(20)-H(20C)	0.96	C(8)-C(7)-H(7B)	109.1
C(21)-C(22)	1.513(9)	H(7A)-C(7)-H(7B)	107.9
C(21)-H(21A)	0.97	C(7)-C(8)-H(8A)	109.5
C(21)-H(21B)	0.97	C(7)-C(8)-H(8B)	109.5
C(22)-C(23)	1.516(10)	H(8A)-C(8)-H(8B)	109.5
C(22)-H(22A)	0.97	C(7)-C(8)-H(8C)	109.5
C(22)-H(22B)	0.97	H(8A)-C(8)-H(8C)	109.5
C(23)-C(24)	1.547(10)	H(8B)-C(8)-H(8C)	109.5
C(23)-H(23A)	0.97	N(3)-C(9)-C(10)	116.5(6)
C(23)-H(23B)	0.97	N(3)-C(9)-H(9A)	108.2
C(24)-H(24A)	0.96	C(10)-C(9)-H(9A)	108.2
C(24)-H(24B)	0.96	N(3)-C(9)-H(9B)	108.2
C(24)-H(24C)	0.96	C(10)-C(9)-H(9B)	108.2

C(25)-C(26)	1.514(10)	H(9A)-C(9)-H(9B)	107.3
C(25)-H(25A)	0.97	C(11)-C(10)-C(9)	110.4(6)
C(25)-H(25B)	0.97	C(11)-C(10)-H(10A)	109.6
C(26)-C(27)	1.552(9)	C(9)-C(10)-H(10A)	109.6
C(26)-H(26A)	0.97	C(11)-C(10)-H(10B)	109.6
C(26)-H(26B)	0.97	C(9)-C(10)-H(10B)	109.6
C(27)-C(28)	1.510(10)	H(10A)-C(10)-H(10B)	108.1
C(27)-H(27A)	0.97	C(12)-C(11)-C(10)	112.6(7)
C(27)-H(27B)	0.97	C(12)-C(11)-H(11A)	109.1
C(28)-H(28A)	0.96	C(10)-C(11)-H(11A)	109.1
C(28)-H(28B)	0.96	C(12)-C(11)-H(11B)	109.1
C(28)-H(28C)	0.96	C(10)-C(11)-H(11B)	109.1
C(29)-C(30)	1.506(9)	H(11A)-C(11)-H(11B)	107.8
C(29)-H(29A)	0.97	C(11)-C(12)-H(12A)	109.5
C(29)-H(29B)	0.97	C(11)-C(12)-H(12B)	109.5
C(30)-C(31)	1.536(10)	H(12A)-C(12)-H(12B)	109.5
C(30)-H(30A)	0.97	C(11)-C(12)-H(12C)	109.5
C(30)-H(30B)	0.97	H(12A)-C(12)-H(12C)	109.5
C(31)-C(32)	1.495(10)	H(12B)-C(12)-H(12C)	109.5
C(31)-H(31A)	0.97	N(3)-C(13)-C(14)	113.8(6)
C(31)-H(31B)	0.97	N(3)-C(13)-H(13A)	108.8
C(32)-H(32A)	0.96	C(14)-C(13)-H(13A)	108.8
C(32)-H(32B)	0.96	N(3)-C(13)-H(13B)	108.8
C(32)-H(32C)	0.96	C(14)-C(13)-H(13B)	108.8
C(33)-C(34)	1.510(9)	H(13A)-C(13)-H(13B)	107.7
C(33)-H(33A)	0.97	C(15)-C(14)-C(13)	108.2(6)
C(33)-H(33B)	0.97	C(15)-C(14)-H(14A)	110.1
C(34)-C(35)	1.507(9)	C(13)-C(14)-H(14A)	110.1
C(34)-H(34A)	0.97	C(15)-C(14)-H(14B)	110.1
C(34)-H(34B)	0.97	C(13)-C(14)-H(14B)	110.1
C(35)-C(36)	1.524(10)	H(14A)-C(14)-H(14B)	108.4
C(35)-H(35A)	0.97	C(16)-C(15)-C(14)	110.7(6)
C(35)-H(35B)	0.97	C(16)-C(15)-H(15A)	109.5
C(36)-H(36A)	0.96	C(14)-C(15)-H(15A)	109.5
C(36)-H(36B)	0.96	C(16)-C(15)-H(15B)	109.5
C(36)-H(36C)	0.96	C(14)-C(15)-H(15B)	109.5
C(37)-C(38)	1.466(11)	H(15A)-C(15)-H(15B)	108.1
C(38)-H(38A)	0.96	C(15)-C(16)-H(16A)	109.5
C(38)-H(38B)	0.96	C(15)-C(16)-H(16B)	109.5
C(38)-H(38C)	0.96	H(16A)-C(16)-H(16B)	109.5

C(39)-C(40)	1.464(12)	C(15)-C(16)-H(16C)	109.5
C(40)-H(40A)	0.96	H(16A)-C(16)-H(16C)	109.5
C(40)-H(40B)	0.96	H(16B)-C(16)-H(16C)	109.5
C(40)-H(40C)	0.96	N(3)-C(17)-C(18)	115.9(6)
		N(3)-C(17)-H(17A)	108.3
O(2)-Ag(1)-O(1)	82.52(17)	C(18)-C(17)-H(17A)	108.3
O(2)-Ag(1)-O(8)#1	99.85(17)	N(3)-C(17)-H(17B)	108.3
O(1)-Ag(1)-O(8)#1	177.29(17)	C(18)-C(17)-H(17B)	108.3
O(2)-Ag(1)-N(1)	93.1(2)	H(17A)-C(17)-H(17B)	107.4
O(1)-Ag(1)-N(1)	86.3(2)	C(17)-C(18)-C(19)	109.6(6)
O(8)#1-Ag(1)-N(1)	94.9(2)	C(17)-C(18)-H(18A)	109.7
O(2)-Ag(1)-O(10)#1	174.35(16)	C(19)-C(18)-H(18A)	109.7
O(1)-Ag(1)-O(10)#1	101.47(16)	C(17)-C(18)-H(18B)	109.7
O(8)#1-Ag(1)-O(10)#1	76.08(16)	C(19)-C(18)-H(18B)	109.7
N(1)-Ag(1)-O(10)#1	91.1(2)	H(18A)-C(18)-H(18B)	108.2
O(2)-Ag(1)-Ag(1)#1	108.09(13)	C(20)-C(19)-C(18)	114.8(6)
O(1)-Ag(1)-Ag(1)#1	113.49(12)	C(20)-C(19)-H(19A)	108.6
O(8)#1-Ag(1)-Ag(1)#1	64.60(12)	C(18)-C(19)-H(19A)	108.6
N(1)-Ag(1)-Ag(1)#1	152.23(16)	C(20)-C(19)-H(19B)	108.6
O(10)#1-Ag(1)-Ag(1)#1	66.72(11)	C(18)-C(19)-H(19B)	108.6
N(2)-Ag(2)-O(19)#2	98.3(2)	H(19A)-C(19)-H(19B)	107.6
N(2)-Ag(2)-O(23)#2	82.5(2)	C(19)-C(20)-H(20A)	109.5
O(19)#2-Ag(2)-O(23)#2	79.92(16)	C(19)-C(20)-H(20B)	109.5
N(2)-Ag(2)-O(14)	86.2(2)	H(20A)-C(20)-H(20B)	109.5
O(19)#2-Ag(2)-O(14)	173.48(15)	C(19)-C(20)-H(20C)	109.5
O(23)#2-Ag(2)-O(14)	105.45(16)	H(20A)-C(20)-H(20C)	109.5
N(2)-Ag(2)-O(15)	97.5(2)	H(20B)-C(20)-H(20C)	109.5
O(19)#2-Ag(2)-O(15)	102.45(16)	C(22)-C(21)-N(4)	117.3(6)
O(23)#2-Ag(2)-O(15)	177.59(17)	C(22)-C(21)-H(21A)	108
O(14)-Ag(2)-O(15)	72.15(16)	N(4)-C(21)-H(21A)	108
N(2)-Ag(2)-Ag(2)#2	144.97(17)	C(22)-C(21)-H(21B)	108
O(19)#2-Ag(2)-Ag(2)#2	112.54(11)	N(4)-C(21)-H(21B)	108
O(23)#2-Ag(2)-Ag(2)#2	117.90(12)	H(21A)-C(21)-H(21B)	107.2
O(14)-Ag(2)-Ag(2)#2	61.84(11)	C(21)-C(22)-C(23)	110.5(6)
O(15)-Ag(2)-Ag(2)#2	60.91(12)	C(21)-C(22)-H(22A)	109.5
O(3)-Mo(1)-O(1)	104.4(2)	C(23)-C(22)-H(22A)	109.5
O(3)-Mo(1)-O(5)	103.6(2)	C(21)-C(22)-H(22B)	109.5
O(1)-Mo(1)-O(5)	97.9(2)	C(23)-C(22)-H(22B)	109.5
O(3)-Mo(1)-O(4)	103.2(2)	H(22A)-C(22)-H(22B)	108.1
O(1)-Mo(1)-O(4)	98.0(2)	C(22)-C(23)-C(24)	112.4(6)

O(5)-Mo(1)-O(4)	144.2(2)	C(22)-C(23)-H(23A)	109.1
O(3)-Mo(1)-O(9)#3	91.2(2)	C(24)-C(23)-H(23A)	109.1
O(1)-Mo(1)-O(9)#3	164.4(2)	C(22)-C(23)-H(23B)	109.1
O(5)-Mo(1)-O(9)#3	77.41(19)	C(24)-C(23)-H(23B)	109.1
O(4)-Mo(1)-O(9)#3	78.70(19)	H(23A)-C(23)-H(23B)	107.9
O(3)-Mo(1)-O(6)	161.1(2)	C(23)-C(24)-H(24A)	109.5
O(1)-Mo(1)-O(6)	94.57(19)	C(23)-C(24)-H(24B)	109.5
O(5)-Mo(1)-O(6)	73.58(18)	H(24A)-C(24)-H(24B)	109.5
O(4)-Mo(1)-O(6)	73.38(17)	C(23)-C(24)-H(24C)	109.5
O(9)#3-Mo(1)-O(6)	69.86(16)	H(24A)-C(24)-H(24C)	109.5
O(13)-Mo(2)-O(2)	104.3(2)	H(24B)-C(24)-H(24C)	109.5
O(13)-Mo(2)-O(4)	102.5(2)	C(26)-C(25)-N(4)	116.0(6)
O(2)-Mo(2)-O(4)	100.3(2)	C(26)-C(25)-H(25A)	108.3
O(13)-Mo(2)-O(11)	100.9(2)	N(4)-C(25)-H(25A)	108.3
O(2)-Mo(2)-O(11)	97.4(2)	C(26)-C(25)-H(25B)	108.3
O(4)-Mo(2)-O(11)	145.9(2)	N(4)-C(25)-H(25B)	108.3
O(13)-Mo(2)-O(12)	92.8(2)	H(25A)-C(25)-H(25B)	107.4
O(2)-Mo(2)-O(12)	161.4(2)	C(25)-C(26)-C(27)	110.7(6)
O(4)-Mo(2)-O(12)	82.70(19)	C(25)-C(26)-H(26A)	109.5
O(11)-Mo(2)-O(12)	71.76(18)	C(27)-C(26)-H(26A)	109.5
O(13)-Mo(2)-O(6)	163.5(2)	C(25)-C(26)-H(26B)	109.5
O(2)-Mo(2)-O(6)	91.9(2)	C(27)-C(26)-H(26B)	109.5
O(4)-Mo(2)-O(6)	76.81(18)	H(26A)-C(26)-H(26B)	108.1
O(11)-Mo(2)-O(6)	73.77(18)	C(28)-C(27)-C(26)	114.4(6)
O(12)-Mo(2)-O(6)	70.77(16)	C(28)-C(27)-H(27A)	108.7
O(13)-Mo(2)-Mo(3)	135.70(17)	C(26)-C(27)-H(27A)	108.7
O(2)-Mo(2)-Mo(3)	83.77(17)	C(28)-C(27)-H(27B)	108.7
O(4)-Mo(2)-Mo(3)	119.00(15)	C(26)-C(27)-H(27B)	108.7
O(11)-Mo(2)-Mo(3)	35.08(14)	H(27A)-C(27)-H(27B)	107.6
O(12)-Mo(2)-Mo(3)	78.81(11)	C(27)-C(28)-H(28A)	109.5
O(6)-Mo(2)-Mo(3)	42.21(11)	C(27)-C(28)-H(28B)	109.5
O(10)-Mo(3)-O(9)	105.1(2)	H(28A)-C(28)-H(28B)	109.5
O(10)-Mo(3)-O(12)#3	101.9(2)	C(27)-C(28)-H(28C)	109.5
O(9)-Mo(3)-O(12)#3	97.3(2)	H(28A)-C(28)-H(28C)	109.5
O(10)-Mo(3)-O(11)	101.0(2)	H(28B)-C(28)-H(28C)	109.5
O(9)-Mo(3)-O(11)	95.7(2)	C(30)-C(29)-N(4)	115.5(6)
O(12)#3-Mo(3)-O(11)	149.73(19)	C(30)-C(29)-H(29A)	108.4
O(10)-Mo(3)-O(6)	97.9(2)	N(4)-C(29)-H(29A)	108.4
O(9)-Mo(3)-O(6)	157.0(2)	C(30)-C(29)-H(29B)	108.4
O(12)#3-Mo(3)-O(6)	78.55(19)	N(4)-C(29)-H(29B)	108.4

O(11)-Mo(3)-O(6)	78.83(19)	H(29A)-C(29)-H(29B)	107.5
O(10)-Mo(3)-O(6)#3	173.2(2)	C(29)-C(30)-C(31)	112.2(6)
O(9)-Mo(3)-O(6)#3	81.71(19)	C(29)-C(30)-H(30A)	109.2
O(12)#3-Mo(3)-O(6)#3	77.35(18)	C(31)-C(30)-H(30A)	109.2
O(11)-Mo(3)-O(6)#3	77.63(18)	C(29)-C(30)-H(30B)	109.2
O(6)-Mo(3)-O(6)#3	75.27(19)	C(31)-C(30)-H(30B)	109.2
O(10)-Mo(3)-Mo(2)	89.00(16)	H(30A)-C(30)-H(30B)	107.9
O(9)-Mo(3)-Mo(2)	131.76(16)	C(32)-C(31)-C(30)	112.5(6)
O(12)#3-Mo(3)-Mo(2)	125.09(14)	C(32)-C(31)-H(31A)	109.1
O(11)-Mo(3)-Mo(2)	36.10(14)	C(30)-C(31)-H(31A)	109.1
O(6)-Mo(3)-Mo(2)	46.55(13)	C(32)-C(31)-H(31B)	109.1
O(6)#3-Mo(3)-Mo(2)	86.04(12)	C(30)-C(31)-H(31B)	109.1
O(10)-Mo(3)-Mo(4)	89.31(17)	H(31A)-C(31)-H(31B)	107.8
O(9)-Mo(3)-Mo(4)	133.66(16)	C(31)-C(32)-H(32A)	109.5
O(12)#3-Mo(3)-Mo(4)	36.35(14)	C(31)-C(32)-H(32B)	109.5
O(11)-Mo(3)-Mo(4)	125.05(15)	H(32A)-C(32)-H(32B)	109.5
O(6)-Mo(3)-Mo(4)	46.23(13)	C(31)-C(32)-H(32C)	109.5
O(6)#3-Mo(3)-Mo(4)	86.18(12)	H(32A)-C(32)-H(32C)	109.5
Mo(2)-Mo(3)-Mo(4)	91.36(4)	H(32B)-C(32)-H(32C)	109.5
O(7)-Mo(4)-O(8)	106.0(2)	C(34)-C(33)-N(4)	116.4(6)
O(7)-Mo(4)-O(5)	102.1(2)	C(34)-C(33)-H(33A)	108.2
O(8)-Mo(4)-O(5)	102.2(2)	N(4)-C(33)-H(33A)	108.2
O(7)-Mo(4)-O(12)#3	99.7(2)	C(34)-C(33)-H(33B)	108.2
O(8)-Mo(4)-O(12)#3	96.6(2)	N(4)-C(33)-H(33B)	108.2
O(5)-Mo(4)-O(12)#3	145.8(2)	H(33A)-C(33)-H(33B)	107.3
O(7)-Mo(4)-O(6)	161.0(2)	C(35)-C(34)-C(33)	112.2(6)
O(8)-Mo(4)-O(6)	92.5(2)	C(35)-C(34)-H(34A)	109.2
O(5)-Mo(4)-O(6)	77.32(19)	C(33)-C(34)-H(34A)	109.2
O(12)#3-Mo(4)-O(6)	73.57(17)	C(35)-C(34)-H(34B)	109.2
O(7)-Mo(4)-O(11)#3	90.0(2)	C(33)-C(34)-H(34B)	109.2
O(8)-Mo(4)-O(11)#3	161.6(2)	H(34A)-C(34)-H(34B)	107.9
O(5)-Mo(4)-O(11)#3	82.63(19)	C(34)-C(35)-C(36)	113.5(6)
O(12)#3-Mo(4)-O(11)#3	71.30(18)	C(34)-C(35)-H(35A)	108.9
O(6)-Mo(4)-O(11)#3	71.04(17)	C(36)-C(35)-H(35A)	108.9
O(7)-Mo(4)-Mo(3)	134.68(17)	C(34)-C(35)-H(35B)	108.9
O(8)-Mo(4)-Mo(3)	83.26(17)	C(36)-C(35)-H(35B)	108.9
O(5)-Mo(4)-Mo(3)	119.51(16)	H(35A)-C(35)-H(35B)	107.7
O(12)#3-Mo(4)-Mo(3)	35.07(13)	C(35)-C(36)-H(36A)	109.5
O(6)-Mo(4)-Mo(3)	42.20(11)	C(35)-C(36)-H(36B)	109.5
O(11)#3-Mo(4)-Mo(3)	78.97(12)	H(36A)-C(36)-H(36B)	109.5

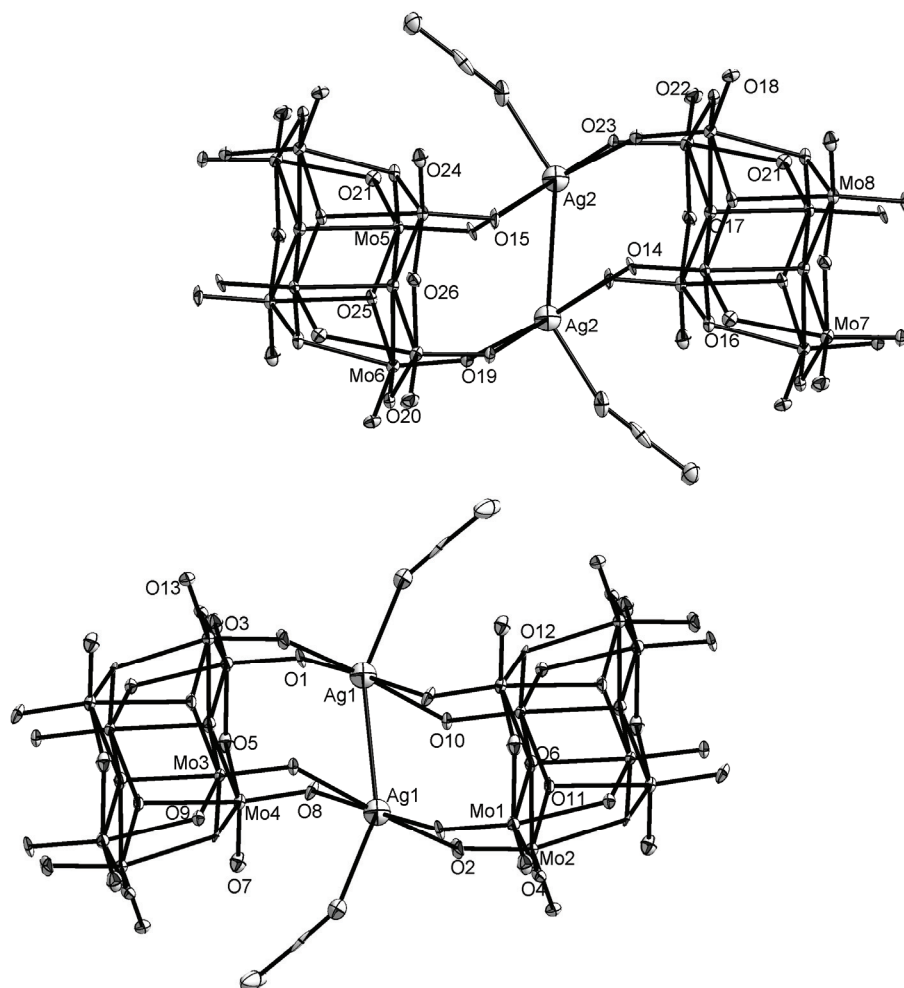
O(14)-Mo(5)-O(21)#4	105.6(2)	C(35)-C(36)-H(36C)	109.5
O(14)-Mo(5)-O(25)#4	101.8(2)	H(36A)-C(36)-H(36C)	109.5
O(21)#4-Mo(5)-O(25)#4	96.1(2)	H(36B)-C(36)-H(36C)	109.5
O(14)-Mo(5)-O(16)	100.8(2)	N(5)-C(37)-C(38)	179.3(9)
O(21)#4-Mo(5)-O(16)	97.1(2)	C(37)-C(38)-H(38A)	109.5
O(25)#4-Mo(5)-O(16)	149.6(2)	C(37)-C(38)-H(38B)	109.5
O(14)-Mo(5)-O(17)	97.3(2)	H(38A)-C(38)-H(38B)	109.5
O(21)#4-Mo(5)-O(17)	157.1(2)	C(37)-C(38)-H(38C)	109.5
O(25)#4-Mo(5)-O(17)	79.31(18)	H(38A)-C(38)-H(38C)	109.5
O(16)-Mo(5)-O(17)	77.93(19)	H(38B)-C(38)-H(38C)	109.5
O(14)-Mo(5)-O(17)#4	172.5(2)	N(6)-C(39)-C(40)	177.6(11)
O(21)#4-Mo(5)-O(17)#4	81.9(2)	C(39)-C(40)-H(40A)	109.5
O(25)#4-Mo(5)-O(17)#4	77.61(18)	C(39)-C(40)-H(40B)	109.5
O(16)-Mo(5)-O(17)#4	77.31(19)	H(40A)-C(40)-H(40B)	109.5
O(17)-Mo(5)-O(17)#4	75.18(19)	C(39)-C(40)-H(40C)	109.5
O(14)-Mo(5)-Mo(6)	89.40(16)	H(40A)-C(40)-H(40C)	109.5
O(21)#4-Mo(5)-Mo(6)	132.54(16)	H(40B)-C(40)-H(40C)	109.5
O(25)#4-Mo(5)-Mo(6)	36.49(13)		

Symmetry transformations used to generate equivalent atoms:

#1 -x,-y+2,-z+1 #2 -x+1,-y+2,-z #3 -x+1,-y+2,-z+1

#4 -x,-y+2,-z

Ortep style representation of $((n\text{-C}_4\text{H}_9)_4\text{N})_{2n}[\text{Ag}_2(\text{CH}_3\text{CN})_2\text{Mo}_8\text{O}_{26}]_n \cdot 2\text{CH}_3\text{CN}$ (**6**): thermal ellipsoids at 50% probability, hydrogen atoms and counterions are omitted for clarity. Carbon, nitrogen and oxygen atoms of acetonitrile not labelled.



6.4 Crystal data for $((n\text{-C}_4\text{H}_9)_4\text{N})_{2n}[\text{KMo}_8\text{O}_{26}\text{Ag}(\text{CH}_3\text{CN})_2]_n$ (8)

Empirical formula	$\text{C}_{36}\text{H}_{78}\text{AgKM}_8\text{O}_{26}\text{N}_4$	
Crystal growth	Diffusion of diethyl ether, 5 days	
Crystal description	Colorless needles crystals	
Crystal size	$0.30 \times 0.10 \times 0.10 \text{ mm}^3$	
Formula weight	1897.51	
Temperature	150(2) K	
Wavelength	0.71073 Å	
Crystal system	Monoclinic	
Space group	$P2_1/c$	
Unit cell dimensions	$a = 18.8073(5) \text{ Å}$	$\alpha = 90^\circ$
	$b = 16.4856(3) \text{ Å}$	$\beta = 104.491(2)^\circ$
	$c = 20.2432(6) \text{ Å}$	$\gamma = 90^\circ$
Volume	$6076.7(3) \text{ Å}^3$	
<i>Z</i>	4	
Density (calculated)	2.074 Mg/m^3	
Absorption coefficient	2.053 mm^{-1}	
<i>F</i> (000)	3728	
Theta range for data collection	1.61 to 25.50°	
Index ranges	$-22 \leq h \leq 22, 0 \leq k \leq 19, 0 \leq l \leq 24$	
Reflections collected/ unique	47429 / 11302 [$R(\text{int}) = 0.0655$]	
Completeness to theta	25.50° 100.0 %	
Absorption correction	Gaussian	
Max. and min. transmission	0.873 and 0.633	
Refinement method	Full-matrix least-squares on F^2	
Data / restraints / parameters	11302 / 0 / 696	
Goodness-of-fit on F^2	1.030	
Final <i>R</i> indices [$I > 2\sigma(I)$]	$R1 = 0.0386, wR2 = 0.0683$	
<i>R</i> indices (all data)	$R1 = 0.0750, wR2 = 0.0762$	
Extinction coefficient	0.000054(10)	
Largest diff. peak and hole	0.65 and -0.71 e.Å ⁻³	

Bond lengths [\AA] and angles [$^\circ$]

Mo(1)-O(22)	1.696(3)	O(19)-Mo(5)-O(7)	103.43(13)
Mo(1)-O(2)	1.706(3)	O(3)-Mo(5)-O(7)	98.61(13)
Mo(1)-O(7)	1.900(3)	O(14)-Mo(5)-O(7)	144.83(14)
Mo(1)-O(13)	2.004(3)	O(19)-Mo(5)-O(15)	91.83(14)
Mo(1)-O(9)	2.344(3)	O(3)-Mo(5)-O(15)	163.06(14)
Mo(1)-O(25)	2.349(3)	O(14)-Mo(5)-O(15)	78.28(12)
Mo(1)-Mo(7)	3.2065(6)	O(7)-Mo(5)-O(15)	77.14(12)
Mo(2)-O(6)	1.693(3)	O(19)-Mo(5)-O(25)	161.06(14)
Mo(2)-O(15)	1.744(3)	O(3)-Mo(5)-O(25)	93.79(13)
Mo(2)-O(9)	1.942(3)	O(14)-Mo(5)-O(25)	73.69(11)
Mo(2)-O(11)	1.961(3)	O(7)-Mo(5)-O(25)	74.29(11)
Mo(2)-O(26)	2.129(3)	O(15)-Mo(5)-O(25)	69.27(10)
Mo(2)-O(25)	2.378(3)	O(8)-Mo(6)-O(17)	105.13(16)
Mo(2)-Mo(8)	3.2021(6)	O(8)-Mo(6)-O(20)	98.69(14)
Mo(2)-Mo(4)	3.2109(6)	O(17)-Mo(6)-O(20)	103.60(13)
Mo(3)-O(10)	1.703(3)	O(8)-Mo(6)-O(21)	97.03(13)
Mo(3)-O(18)	1.708(3)	O(17)-Mo(6)-O(21)	101.62(13)
Mo(3)-O(14)	1.892(3)	O(20)-Mo(6)-O(21)	145.50(14)
Mo(3)-O(12)	1.989(3)	O(8)-Mo(6)-O(23)	163.57(13)
Mo(3)-O(25)	2.300(3)	O(17)-Mo(6)-O(23)	91.28(14)
Mo(3)-O(11)	2.318(3)	O(20)-Mo(6)-O(23)	77.88(12)
Mo(3)-Mo(7)	3.2115(6)	O(21)-Mo(6)-O(23)	78.40(12)
Mo(3)-K#1	4.1026(11)	O(8)-Mo(6)-O(26)	93.58(13)
Mo(4)-O(4)	1.705(3)	O(17)-Mo(6)-O(26)	161.20(13)
Mo(4)-O(16)	1.710(3)	O(20)-Mo(6)-O(26)	74.80(11)
Mo(4)-O(21)	1.887(3)	O(21)-Mo(6)-O(26)	73.72(11)
Mo(4)-O(11)	1.992(3)	O(23)-Mo(6)-O(26)	70.00(10)
Mo(4)-O(26)	2.304(3)	O(1)-Mo(7)-O(23)	105.40(15)
Mo(4)-O(12)	2.321(3)	O(1)-Mo(7)-O(13)	102.11(13)
Mo(4)-K	4.1022(12)	O(23)-Mo(7)-O(13)	95.90(13)
Mo(5)-O(19)	1.703(3)	O(1)-Mo(7)-O(12)	101.37(13)
Mo(5)-O(3)	1.706(3)	O(23)-Mo(7)-O(12)	96.16(13)
Mo(5)-O(14)	1.926(3)	O(13)-Mo(7)-O(12)	149.63(12)
Mo(5)-O(7)	1.927(3)	O(1)-Mo(7)-O(25)	98.79(14)
Mo(5)-O(15)	2.268(3)	O(23)-Mo(7)-O(25)	155.79(13)
Mo(5)-O(25)	2.463(3)	O(13)-Mo(7)-O(25)	79.45(11)
Mo(6)-O(8)	1.706(3)	O(12)-Mo(7)-O(25)	78.15(11)

Mo(6)-O(17)	1.708(3)	O(1)-Mo(7)-O(26)	174.40(13)
Mo(6)-O(20)	1.918(3)	O(23)-Mo(7)-O(26)	80.10(12)
Mo(6)-O(21)	1.934(3)	O(13)-Mo(7)-O(26)	78.05(11)
Mo(6)-O(23)	2.267(3)	O(12)-Mo(7)-O(26)	76.72(11)
Mo(6)-O(26)	2.445(3)	O(25)-Mo(7)-O(26)	75.70(11)
Mo(7)-O(1)	1.688(3)	O(1)-Mo(7)-Mo(1)	90.07(11)
Mo(7)-O(23)	1.754(3)	O(23)-Mo(7)-Mo(1)	132.22(9)
Mo(7)-O(13)	1.943(3)	O(13)-Mo(7)-Mo(1)	36.32(9)
Mo(7)-O(12)	1.966(3)	O(12)-Mo(7)-Mo(1)	125.23(9)
Mo(7)-O(25)	2.130(3)	O(25)-Mo(7)-Mo(1)	47.10(7)
Mo(7)-O(26)	2.385(3)	O(26)-Mo(7)-Mo(1)	86.85(7)
Mo(8)-O(24)	1.693(3)	O(1)-Mo(7)-Mo(3)	90.45(11)
Mo(8)-O(5)	1.715(3)	O(23)-Mo(7)-Mo(3)	132.07(9)
Mo(8)-O(20)	1.905(3)	O(13)-Mo(7)-Mo(3)	125.06(9)
Mo(8)-O(9)	1.999(3)	O(12)-Mo(7)-Mo(3)	35.94(9)
Mo(8)-O(13)	2.351(3)	O(25)-Mo(7)-Mo(3)	45.67(7)
Mo(8)-O(26)	2.355(3)	O(26)-Mo(7)-Mo(3)	84.96(7)
Ag-N(4)	2.125(4)	Mo(1)-Mo(7)-Mo(3)	91.573(15)
Ag-N(3)	2.133(4)	O(24)-Mo(8)-O(5)	105.17(15)
Ag-O(16)	2.412(3)	O(24)-Mo(8)-O(20)	101.46(14)
Ag-O(18)	2.430(3)	O(5)-Mo(8)-O(20)	101.38(15)
K-O(4)	2.667(3)	O(24)-Mo(8)-O(9)	101.34(14)
K-O(10)#2	2.674(3)	O(5)-Mo(8)-O(9)	97.06(14)
K-O(8)	2.742(3)	O(20)-Mo(8)-O(9)	145.62(12)
K-O(3)#2	2.771(3)	O(24)-Mo(8)-O(13)	90.73(13)
K-O(1)#2	3.035(4)	O(5)-Mo(8)-O(13)	161.76(12)
K-O(2)#2	3.038(3)	O(20)-Mo(8)-O(13)	83.72(12)
K-O(6)	3.140(4)	O(9)-Mo(8)-O(13)	70.60(11)
K-O(5)	3.141(3)	O(24)-Mo(8)-O(26)	162.15(14)
K-Mo(3)#2	4.1026(11)	O(5)-Mo(8)-O(26)	92.45(12)
O(1)-K#1	3.035(4)	O(20)-Mo(8)-O(26)	77.29(11)
O(2)-K#1	3.038(3)	O(9)-Mo(8)-O(26)	73.14(10)
O(3)-K#1	2.771(3)	O(13)-Mo(8)-O(26)	71.42(10)
O(10)-K#1	2.674(3)	O(24)-Mo(8)-Mo(2)	136.27(12)
N(1)-C(13)	1.516(6)	O(5)-Mo(8)-Mo(2)	83.71(10)
N(1)-C(5)	1.520(6)	O(20)-Mo(8)-Mo(2)	118.95(9)
N(1)-C(1)	1.525(5)	O(9)-Mo(8)-Mo(2)	35.07(8)
N(1)-C(9)	1.526(6)	O(13)-Mo(8)-Mo(2)	78.56(7)
N(2)-C(21)	1.514(5)	O(26)-Mo(8)-Mo(2)	41.66(7)
N(2)-C(17)	1.521(6)	N(4)-Ag-N(3)	151.87(17)

N(2)-C(29)	1.522(6)	N(4)-Ag-O(16)	104.12(15)
N(2)-C(25)	1.524(5)	N(3)-Ag-O(16)	98.56(14)
N(3)-C(33)	1.116(6)	N(4)-Ag-O(18)	92.86(14)
N(4)-C(35)	1.129(6)	N(3)-Ag-O(18)	108.69(14)
C(1)-C(2)	1.520(7)	O(16)-Ag-O(18)	76.25(11)
C(2)-C(3)	1.546(6)	O(4)-K-O(10)#2	174.30(10)
C(3)-C(4)	1.494(7)	O(4)-K-O(8)	70.71(9)
C(5)-C(6)	1.504(7)	O(10)#2-K-O(8)	114.19(9)
C(6)-C(7)	1.523(7)	O(4)-K-O(3)#2	105.19(10)
C(7)-C(8)	1.510(7)	O(10)#2-K-O(3)#2	69.97(9)
C(9)-C(10)	1.510(6)	O(8)-K-O(3)#2	175.75(9)
C(10)-C(11)	1.524(7)	O(4)-K-O(1)#2	120.01(10)
C(11)-C(12)	1.519(8)	O(10)#2-K-O(1)#2	64.58(9)
C(13)-C(14)	1.512(7)	O(8)-K-O(1)#2	81.49(9)
C(14)-C(15)	1.522(7)	O(3)#2-K-O(1)#2	99.99(10)
C(15)-C(16)	1.516(9)	O(4)-K-O(2)#2	82.53(9)
C(17)-C(18)	1.516(6)	O(10)#2-K-O(2)#2	97.85(9)
C(18)-C(19)	1.544(7)	O(8)-K-O(2)#2	111.56(9)
C(19)-C(20)	1.528(7)	O(3)#2-K-O(2)#2	66.24(9)
C(21)-C(22)	1.510(7)	O(1)#2-K-O(2)#2	59.78(9)
C(22)-C(23)	1.541(6)	O(4)-K-O(6)	63.73(9)
C(23)-C(24)	1.535(6)	O(10)#2-K-O(6)	111.86(9)
C(25)-C(26)	1.526(6)	O(8)-K-O(6)	97.94(9)
C(26)-C(27)	1.535(6)	O(3)#2-K-O(6)	80.90(9)
C(27)-C(28)	1.519(7)	O(1)#2-K-O(6)	175.46(8)
C(29)-C(30)	1.518(6)	O(2)#2-K-O(6)	124.34(9)
C(30)-C(31)	1.523(7)	O(4)-K-O(5)	96.55(9)
C(31)-C(32)	1.532(7)	O(10)#2-K-O(5)	83.38(9)
C(33)-C(34)	1.462(7)	O(8)-K-O(5)	65.18(9)
C(35)-C(36)	1.460(7)	O(3)#2-K-O(5)	117.05(9)
		O(1)#2-K-O(5)	118.40(9)
O(22)-Mo(1)-O(2)	105.43(14)	O(2)#2-K-O(5)	176.70(8)
O(22)-Mo(1)-O(7)	101.44(14)	O(6)-K-O(5)	57.59(8)
O(2)-Mo(1)-O(7)	101.18(15)	O(4)-K-Mo(4)	16.00(6)
O(22)-Mo(1)-O(13)	101.07(14)	O(10)#2-K-Mo(4)	164.77(7)
O(2)-Mo(1)-O(13)	97.18(14)	O(8)-K-Mo(4)	59.28(7)
O(7)-Mo(1)-O(13)	145.84(12)	O(3)#2-K-Mo(4)	116.95(7)
O(22)-Mo(1)-O(9)	90.54(13)	O(1)#2-K-Mo(4)	124.08(6)
O(2)-Mo(1)-O(9)	161.78(12)	O(2)#2-K-Mo(4)	97.38(6)
O(7)-Mo(1)-O(9)	83.76(12)	O(6)-K-Mo(4)	58.70(6)

O(13)-Mo(1)-O(9)	70.67(11)	O(5)-K-Mo(4)	81.40(6)
O(22)-Mo(1)-O(25)	161.84(14)	O(4)-K-Mo(3)#2	161.90(7)
O(2)-Mo(1)-O(25)	92.46(12)	O(10)#2-K-Mo(3)#2	16.10(6)
O(7)-Mo(1)-O(25)	77.57(11)	O(8)-K-Mo(3)#2	124.48(7)
O(13)-Mo(1)-O(25)	73.07(11)	O(3)#2-K-Mo(3)#2	59.34(7)
O(9)-Mo(1)-O(25)	71.30(10)	O(1)#2-K-Mo(3)#2	59.09(6)
O(22)-Mo(1)-Mo(7)	135.97(12)	O(2)#2-K-Mo(3)#2	82.30(6)
O(2)-Mo(1)-Mo(7)	83.86(10)	O(6)-K-Mo(3)#2	118.32(6)
O(7)-Mo(1)-Mo(7)	119.17(8)	O(5)-K-Mo(3)#2	99.13(6)
O(13)-Mo(1)-Mo(7)	35.03(8)	Mo(4)-K-Mo(3)#2	176.09(3)
O(9)-Mo(1)-Mo(7)	78.49(7)	Mo(7)-O(1)-K#1	127.37(15)
O(25)-Mo(1)-Mo(7)	41.61(7)	Mo(1)-O(2)-K#1	131.95(13)
O(6)-Mo(2)-O(15)	104.97(15)	Mo(5)-O(3)-K#1	135.21(17)
O(6)-Mo(2)-O(9)	102.28(13)	Mo(4)-O(4)-K	138.48(15)
O(15)-Mo(2)-O(9)	95.43(13)	Mo(8)-O(5)-K	131.05(14)
O(6)-Mo(2)-O(11)	101.25(13)	Mo(2)-O(6)-K	126.36(14)
O(15)-Mo(2)-O(11)	96.32(13)	Mo(1)-O(7)-Mo(5)	117.41(14)
O(9)-Mo(2)-O(11)	149.92(12)	Mo(6)-O(8)-K	137.31(17)
O(6)-Mo(2)-O(26)	99.18(14)	Mo(2)-O(9)-Mo(8)	108.68(14)
O(15)-Mo(2)-O(26)	155.85(13)	Mo(2)-O(9)-Mo(1)	111.04(13)
O(9)-Mo(2)-O(26)	79.59(11)	Mo(8)-O(9)-Mo(1)	105.08(11)
O(11)-Mo(2)-O(26)	78.39(11)	Mo(3)-O(10)-K#1	138.09(14)
O(6)-Mo(2)-O(25)	174.98(13)	Mo(2)-O(11)-Mo(4)	108.64(14)
O(15)-Mo(2)-O(25)	79.98(12)	Mo(2)-O(11)-Mo(3)	110.49(13)
O(9)-Mo(2)-O(25)	77.85(11)	Mo(4)-O(11)-Mo(3)	103.13(12)
O(11)-Mo(2)-O(25)	77.09(11)	Mo(7)-O(12)-Mo(3)	108.59(14)
O(26)-Mo(2)-O(25)	75.87(11)	Mo(7)-O(12)-Mo(4)	110.86(13)
O(6)-Mo(2)-Mo(8)	90.37(10)	Mo(3)-O(12)-Mo(4)	103.13(12)
O(15)-Mo(2)-Mo(8)	131.68(9)	Mo(7)-O(13)-Mo(1)	108.65(14)
O(9)-Mo(2)-Mo(8)	36.25(9)	Mo(7)-O(13)-Mo(8)	110.98(13)
O(11)-Mo(2)-Mo(8)	125.71(9)	Mo(1)-O(13)-Mo(8)	104.64(11)
O(26)-Mo(2)-Mo(8)	47.33(7)	Mo(3)-O(14)-Mo(5)	116.68(14)
O(25)-Mo(2)-Mo(8)	86.86(7)	Mo(2)-O(15)-Mo(5)	119.17(14)
O(6)-Mo(2)-Mo(4)	90.69(10)	Mo(4)-O(16)-Ag	147.37(18)
O(15)-Mo(2)-Mo(4)	132.30(10)	Mo(3)-O(18)-Ag	140.30(17)
O(9)-Mo(2)-Mo(4)	125.32(9)	Mo(8)-O(20)-Mo(6)	117.25(15)
O(11)-Mo(2)-Mo(4)	36.00(9)	Mo(4)-O(21)-Mo(6)	116.67(14)
O(26)-Mo(2)-Mo(4)	45.79(7)	Mo(7)-O(23)-Mo(6)	118.32(14)
O(25)-Mo(2)-Mo(4)	85.22(7)	Mo(7)-O(25)-Mo(3)	92.85(10)
Mo(8)-Mo(2)-Mo(4)	91.940(15)	Mo(7)-O(25)-Mo(1)	91.29(10)

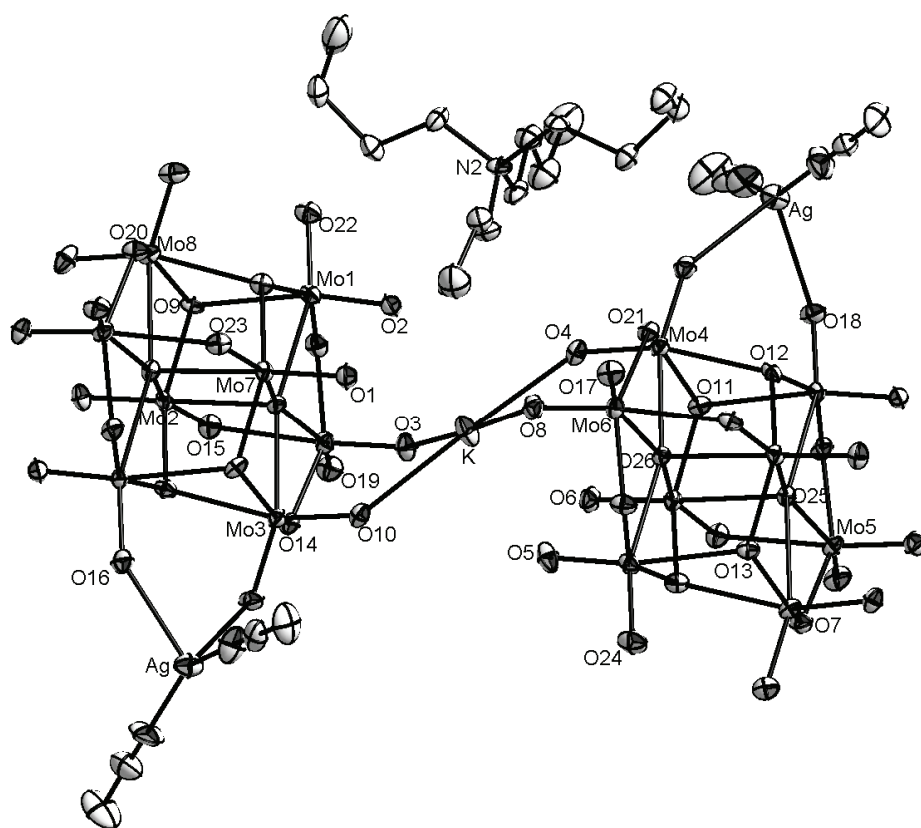
O(10)-Mo(3)-O(18)	104.32(14)	Mo(3)-O(25)-Mo(1)	163.28(16)
O(10)-Mo(3)-O(14)	100.68(14)	Mo(7)-O(25)-Mo(2)	104.30(13)
O(18)-Mo(3)-O(14)	100.43(13)	Mo(3)-O(25)-Mo(2)	97.66(10)
O(10)-Mo(3)-O(12)	97.11(14)	Mo(1)-O(25)-Mo(2)	97.00(10)
O(18)-Mo(3)-O(12)	101.27(13)	Mo(7)-O(25)-Mo(5)	164.09(15)
O(14)-Mo(3)-O(12)	147.45(12)	Mo(3)-O(25)-Mo(5)	86.00(9)
O(10)-Mo(3)-O(25)	92.88(12)	Mo(1)-O(25)-Mo(5)	85.59(9)
O(18)-Mo(3)-O(25)	162.62(14)	Mo(2)-O(25)-Mo(5)	91.57(9)
O(14)-Mo(3)-O(25)	78.33(11)	Mo(2)-O(26)-Mo(4)	92.74(10)
O(12)-Mo(3)-O(25)	73.73(11)	Mo(2)-O(26)-Mo(8)	91.00(10)
O(10)-Mo(3)-O(11)	163.63(12)	Mo(4)-O(26)-Mo(8)	163.47(15)
O(18)-Mo(3)-O(11)	90.35(13)	Mo(2)-O(26)-Mo(7)	104.08(13)
O(14)-Mo(3)-O(11)	83.41(12)	Mo(4)-O(26)-Mo(7)	97.85(10)
O(12)-Mo(3)-O(11)	72.51(11)	Mo(8)-O(26)-Mo(7)	96.84(10)
O(25)-Mo(3)-O(11)	72.28(10)	Mo(2)-O(26)-Mo(6)	164.27(15)
O(10)-Mo(3)-Mo(7)	84.61(10)	Mo(4)-O(26)-Mo(6)	86.40(9)
O(18)-Mo(3)-Mo(7)	136.64(11)	Mo(8)-O(26)-Mo(6)	85.66(9)
O(14)-Mo(3)-Mo(7)	119.80(8)	Mo(7)-O(26)-Mo(6)	91.58(9)
O(12)-Mo(3)-Mo(7)	35.47(8)	C(13)-N(1)-C(5)	107.1(4)
O(25)-Mo(3)-Mo(7)	41.48(7)	C(13)-N(1)-C(1)	111.1(4)
O(11)-Mo(3)-Mo(7)	79.67(7)	C(5)-N(1)-C(1)	110.7(4)
O(10)-Mo(3)-K#1	25.81(9)	C(13)-N(1)-C(9)	111.0(4)
O(18)-Mo(3)-K#1	129.52(11)	C(5)-N(1)-C(9)	110.8(4)
O(14)-Mo(3)-K#1	89.15(9)	C(1)-N(1)-C(9)	106.2(3)
O(12)-Mo(3)-K#1	95.42(9)	C(21)-N(2)-C(17)	111.5(4)
O(25)-Mo(3)-K#1	67.85(8)	C(21)-N(2)-C(29)	105.4(3)
O(11)-Mo(3)-K#1	140.12(7)	C(17)-N(2)-C(29)	111.3(3)
Mo(7)-Mo(3)-K#1	70.34(2)	C(21)-N(2)-C(25)	111.7(3)
O(4)-Mo(4)-O(16)	104.11(14)	C(17)-N(2)-C(25)	105.2(3)
O(4)-Mo(4)-O(21)	100.79(15)	C(29)-N(2)-C(25)	111.9(4)
O(16)-Mo(4)-O(21)	100.65(14)	C(33)-N(3)-Ag	178.5(5)
O(4)-Mo(4)-O(11)	97.27(14)	C(35)-N(4)-Ag	173.6(5)
O(16)-Mo(4)-O(11)	101.17(14)	C(2)-C(1)-N(1)	116.6(4)
O(21)-Mo(4)-O(11)	147.21(12)	C(1)-C(2)-C(3)	109.0(4)
O(4)-Mo(4)-O(26)	93.67(12)	C(4)-C(3)-C(2)	111.9(4)
O(16)-Mo(4)-O(26)	162.05(14)	C(6)-C(5)-N(1)	116.6(4)
O(21)-Mo(4)-O(26)	78.04(11)	C(5)-C(6)-C(7)	109.8(4)
O(11)-Mo(4)-O(26)	73.68(11)	C(8)-C(7)-C(6)	112.8(5)
O(4)-Mo(4)-O(12)	164.09(12)	C(10)-C(9)-N(1)	116.2(4)
O(16)-Mo(4)-O(12)	89.99(13)	C(9)-C(10)-C(11)	109.9(4)

O(21)-Mo(4)-O(12)	83.46(12)	C(12)-C(11)-C(10)	113.1(5)
O(11)-Mo(4)-O(12)	72.39(11)	C(14)-C(13)-N(1)	115.7(4)
O(26)-Mo(4)-O(12)	72.06(10)	C(13)-C(14)-C(15)	111.0(5)
O(4)-Mo(4)-Mo(2)	85.30(10)	C(16)-C(15)-C(14)	111.7(6)
O(16)-Mo(4)-Mo(2)	136.47(11)	C(18)-C(17)-N(2)	116.0(4)
O(21)-Mo(4)-Mo(2)	119.50(8)	C(17)-C(18)-C(19)	108.1(4)
O(11)-Mo(4)-Mo(2)	35.36(8)	C(20)-C(19)-C(18)	112.9(4)
O(26)-Mo(4)-Mo(2)	41.47(7)	C(22)-C(21)-N(2)	117.1(4)
O(12)-Mo(4)-Mo(2)	79.33(7)	C(21)-C(22)-C(23)	110.0(4)
O(4)-Mo(4)-K	25.52(10)	C(24)-C(23)-C(22)	113.9(4)
O(16)-Mo(4)-K	128.74(11)	N(2)-C(25)-C(26)	115.5(4)
O(21)-Mo(4)-K	88.35(9)	C(25)-C(26)-C(27)	109.7(4)
O(11)-Mo(4)-K	96.71(9)	C(28)-C(27)-C(26)	112.4(4)
O(26)-Mo(4)-K	69.21(8)	C(30)-C(29)-N(2)	116.9(4)
O(12)-Mo(4)-K	141.27(7)	C(29)-C(30)-C(31)	109.7(4)
Mo(2)-Mo(4)-K	72.07(2)	C(30)-C(31)-C(32)	112.9(5)
O(19)-Mo(5)-O(3)	105.11(16)	N(3)-C(33)-C(34)	179.6(6)
O(19)-Mo(5)-O(14)	102.11(13)	N(4)-C(35)-C(36)	178.2(6)
O(3)-Mo(5)-O(14)	97.63(13)		

Symmetry transformations used to generate equivalent atoms:

#1 $x, -y+3/2, z-1/2$ #2 $x, -y+3/2, z+1/2$

Ortep style representation of $((n\text{-C}_4\text{H}_9)_4\text{N})_{2n}[\text{KMo}_8\text{O}_{26}\text{Ag}(\text{CH}_3\text{CN})_2]_n$ (**8**): thermal ellipsoids at 50% probability, hydrogen atoms are omitted for clarity. Carbon atoms of counterion and acetonitrile not labelled, as well as nitrogen atoms of acetonitrile.



6.5 Crystal data for $(\text{Ph}_4\text{P})_2[\text{Ag}_2(\text{CH}_3\text{CN})_2\text{Mo}_8\text{O}_{26}]\cdot 2\text{CH}_3\text{CN}$ (10)

Empirical formula	$\text{C}_{56}\text{H}_{52}\text{Ag}_2\text{Mo}_8\text{N}_4\text{O}_{26}\text{P}_2$	
Crystal growth	Diffusion of diethyl ether, 3 days	
Crystal description	Colourless block crystals	
Crystal size	$0.10 \times 0.08 \times 0.08 \text{ mm}^3$	
Formula weight	2242.22	
Temperature	150(2) K	
Wavelength	0.71073 Å	
Crystal system	Triclinic	
Space group	$P\bar{1}$	
Unit cell dimensions	$a = 9.7210(3) \text{ Å}$	$\alpha = 85.561(2)^\circ$
	$b = 11.7984(5) \text{ Å}$	$\beta = 75.929(2)^\circ$
	$c = 16.0976(7) \text{ Å}$	$\gamma = 68.078(2)^\circ$
Volume	$1661.20(11) \text{ Å}^3$	
Z	1	
Density (calculated)	2.241 Mg/m^3	
Absorption coefficient	2.163 mm^{-1}	
$F(000)$	1084	
Theta range for data collection	1.86 to 26.00°	
Index ranges	$-11 \leq h \leq 11, -14 \leq k \leq 14, 0 \leq l \leq 19$	
Reflections collected/ unique	23586 / 6500 [$R(\text{int}) = 0.078$]	
Completeness to theta	26.00° 99.8 %	
Absorption correction	Analytical	
Max. and min. transmission	0.8460 and 0.8127	
Refinement method	Full-matrix least-squares on F^2	
Data / restraints / parameters	6500 / 0 / 444	
Goodness-of-fit on F^2	1.027	
Final R indices [$I > 2\sigma(I)$]	$R1 = 0.0450, wR2 = 0.0669$	
R indices (all data)	$R1 = 0.0893, wR2 = 0.0750$	
Extinction coefficient	None	
Largest diff. peak and hole	0.71 and -0.87 e.Å^{-3}	

Bond lengths [\AA] and angles [$^\circ$]

Ag-N(1)	2.197(5)	O(2)-Mo(2)-O(8)#1	91.36(16)
Ag-O(2)	2.321(4)	O(3)-Mo(2)-O(8)#1	78.56(15)
Ag-O(1)	2.515(4)	O(5)-Mo(2)-O(8)#1	73.13(14)
Mo(1)-O(1)	1.709(4)	O(7)#1-Mo(2)-O(8)#1	71.99(13)
Mo(1)-O(6)	1.728(4)	O(11)-Mo(3)-O(12)	105.57(19)
Mo(1)-O(5)	1.943(4)	O(11)-Mo(3)-O(10)	101.63(18)
Mo(1)-O(7)	1.949(4)	O(12)-Mo(3)-O(10)	100.92(19)
Mo(1)-O(8)#1	2.142(4)	O(11)-Mo(3)-O(7)	99.52(18)
Mo(1)-O(8)	2.327(3)	O(12)-Mo(3)-O(7)	96.18(17)
Mo(1)-Mo(3)	3.2111(8)	O(10)-Mo(3)-O(7)	147.99(15)
Mo(2)-O(4)	1.683(4)	O(11)-Mo(3)-O(8)#1	161.39(16)
Mo(2)-O(2)	1.722(4)	O(12)-Mo(3)-O(8)#1	92.49(16)
Mo(2)-O(3)	1.888(4)	O(10)-Mo(3)-O(8)#1	78.77(15)
Mo(2)-O(5)	1.999(4)	O(7)-Mo(3)-O(8)#1	73.61(15)
Mo(2)-O(7)#1	2.279(4)	O(11)-Mo(3)-O(5)#1	89.83(17)
Mo(2)-O(8)#1	2.311(4)	O(12)-Mo(3)-O(5)#1	161.91(16)
Mo(3)-O(11)	1.700(4)	O(10)-Mo(3)-O(5)#1	84.80(15)
Mo(3)-O(12)	1.703(4)	O(7)-Mo(3)-O(5)#1	71.48(14)
Mo(3)-O(10)	1.894(4)	O(8)#1-Mo(3)-O(5)#1	71.63(13)
Mo(3)-O(7)	2.012(4)	O(11)-Mo(3)-Mo(1)	134.61(15)
Mo(3)-O(8)#1	2.296(4)	O(12)-Mo(3)-Mo(1)	83.53(13)
Mo(3)-O(5)#1	2.304(4)	O(10)-Mo(3)-Mo(1)	120.53(12)
Mo(4)-O(9)	1.690(4)	O(7)-Mo(3)-Mo(1)	35.18(11)
Mo(4)-O(13)	1.706(4)	O(8)#1-Mo(3)-Mo(1)	41.78(10)
Mo(4)-O(10)	1.912(4)	O(5)#1-Mo(3)-Mo(1)	78.83(9)
Mo(4)-O(3)	1.915(4)	O(9)-Mo(4)-O(13)	105.1(2)
Mo(4)-O(6)#1	2.275(4)	O(9)-Mo(4)-O(10)	103.72(19)
Mo(4)-O(8)#1	2.495(4)	O(13)-Mo(4)-O(10)	97.83(18)
O(5)-Mo(3)#1	2.304(4)	O(9)-Mo(4)-O(3)	103.53(19)
O(6)-Mo(4)#1	2.275(4)	O(13)-Mo(4)-O(3)	97.77(18)
O(7)-Mo(2)#1	2.279(4)	O(10)-Mo(4)-O(3)	143.65(18)
O(8)-Mo(1)#1	2.142(4)	O(9)-Mo(4)-O(6)#1	94.60(17)
O(8)-Mo(3)#1	2.296(4)	O(13)-Mo(4)-O(6)#1	160.24(18)
O(8)-Mo(2)#1	2.311(4)	O(10)-Mo(4)-O(6)#1	77.34(15)
O(8)-Mo(4)#1	2.495(4)	O(3)-Mo(4)-O(6)#1	76.93(15)
P-C(1)	1.779(6)	O(9)-Mo(4)-O(8)#1	163.25(16)
P-C(7)	1.783(6)	O(13)-Mo(4)-O(8)#1	91.60(17)

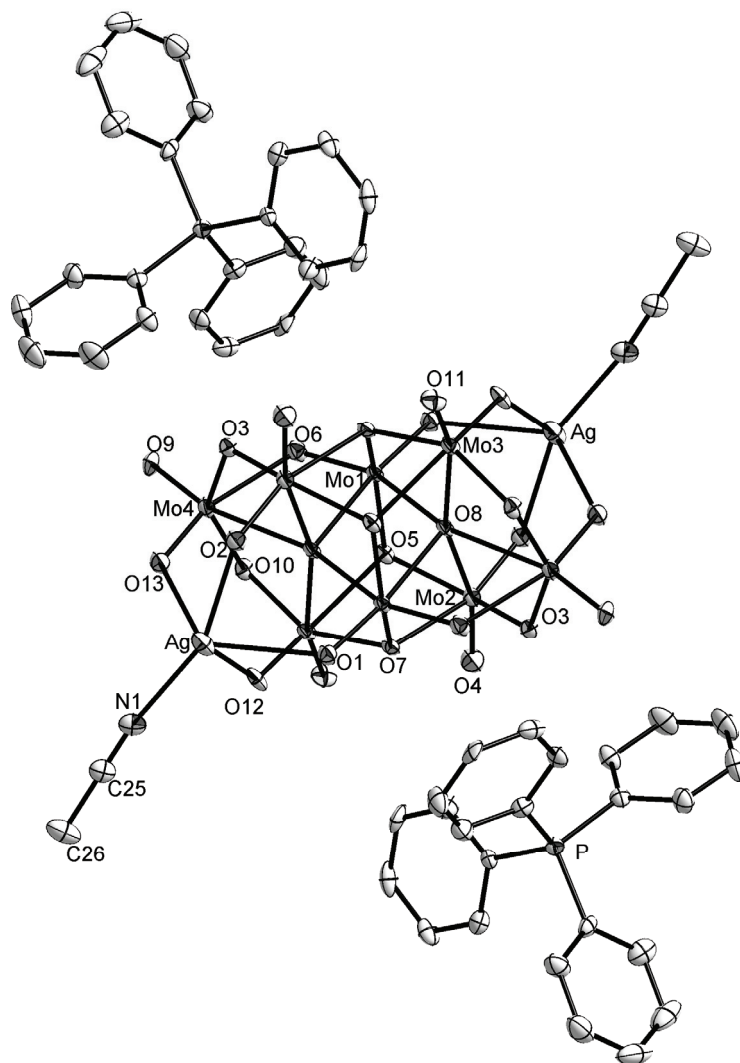
P-C(13)	1.787(6)	O(10)-Mo(4)-O(8)#1	73.46(15)
P-C(19)	1.797(6)	O(3)-Mo(4)-O(8)#1	73.48(15)
N(1)-C(25)	1.122(7)	O(6)#1-Mo(4)-O(8)#1	68.64(13)
N(2)-C(27)	1.124(9)	Mo(1)-O(1)-Ag	122.76(19)
C(1)-C(2)	1.389(8)	Mo(2)-O(2)-Ag	131.1(2)
C(1)-C(6)	1.390(8)	Mo(2)-O(3)-Mo(4)	117.3(2)
C(2)-C(3)	1.374(9)	Mo(1)-O(5)-Mo(2)	109.56(18)
C(3)-C(4)	1.366(9)	Mo(1)-O(5)-Mo(3)#1	109.80(17)
C(4)-C(5)	1.373(9)	Mo(2)-O(5)-Mo(3)#1	103.78(15)
C(5)-C(6)	1.385(8)	Mo(1)-O(6)-Mo(4)#1	118.28(19)
C(7)-C(8)	1.380(8)	Mo(1)-O(7)-Mo(3)	108.33(19)
C(7)-C(12)	1.388(9)	Mo(1)-O(7)-Mo(2)#1	110.21(16)
C(8)-C(9)	1.369(9)	Mo(3)-O(7)-Mo(2)#1	104.25(15)
C(9)-C(10)	1.389(10)	Mo(1)#1-O(8)-Mo(3)#1	92.65(15)
C(10)-C(11)	1.378(10)	Mo(1)#1-O(8)-Mo(2)#1	92.57(14)
C(11)-C(12)	1.379(9)	Mo(3)#1-O(8)-Mo(2)#1	162.54(18)
C(13)-C(18)	1.383(8)	Mo(1)#1-O(8)-Mo(1)	105.30(16)
C(13)-C(14)	1.395(9)	Mo(3)#1-O(8)-Mo(1)	97.69(14)
C(14)-C(15)	1.370(8)	Mo(2)#1-O(8)-Mo(1)	96.97(13)
C(15)-C(16)	1.389(9)	Mo(1)#1-O(8)-Mo(4)#1	163.49(17)
C(16)-C(17)	1.362(10)	Mo(3)#1-O(8)-Mo(4)#1	85.31(12)
C(17)-C(18)	1.388(9)	Mo(2)#1-O(8)-Mo(4)#1	84.96(13)
C(19)-C(20)	1.384(8)	Mo(1)-O(8)-Mo(4)#1	91.20(12)
C(19)-C(24)	1.385(9)	Mo(3)-O(10)-Mo(4)	117.21(19)
C(20)-C(21)	1.386(9)	C(1)-P-C(7)	107.1(3)
C(21)-C(22)	1.371(9)	C(1)-P-C(13)	111.7(3)
C(22)-C(23)	1.370(9)	C(7)-P-C(13)	108.8(3)
C(23)-C(24)	1.383(9)	C(1)-P-C(19)	109.2(3)
C(25)-C(26)	1.463(9)	C(7)-P-C(19)	110.3(3)
C(27)-C(28)	1.425(10)	C(13)-P-C(19)	109.8(3)
		C(25)-N(1)-Ag	171.4(5)
N(1)-Ag-O(2)	155.73(18)	C(2)-C(1)-C(6)	119.7(6)
N(1)-Ag-O(1)	126.02(17)	C(2)-C(1)-P	120.5(5)
O(2)-Ag-O(1)	76.45(14)	C(6)-C(1)-P	119.8(5)
O(1)-Mo(1)-O(6)	105.82(18)	C(3)-C(2)-C(1)	119.4(6)
O(1)-Mo(1)-O(5)	101.04(17)	C(4)-C(3)-C(2)	120.9(6)
O(6)-Mo(1)-O(5)	96.86(18)	C(3)-C(4)-C(5)	120.4(6)
O(1)-Mo(1)-O(7)	101.13(17)	C(4)-C(5)-C(6)	119.8(6)
O(6)-Mo(1)-O(7)	96.93(18)	C(5)-C(6)-C(1)	119.8(6)
O(5)-Mo(1)-O(7)	149.53(15)	C(8)-C(7)-C(12)	118.7(6)

O(1)-Mo(1)-O(8)#1	97.61(17)	C(8)-C(7)-P	120.8(5)
O(6)-Mo(1)-O(8)#1	156.57(16)	C(12)-C(7)-P	120.3(5)
O(5)-Mo(1)-O(8)#1	78.15(15)	C(9)-C(8)-C(7)	121.2(7)
O(7)-Mo(1)-O(8)#1	78.41(15)	C(8)-C(9)-C(10)	119.5(7)
O(1)-Mo(1)-O(8)	172.31(17)	C(11)-C(10)-C(9)	120.3(7)
O(6)-Mo(1)-O(8)	81.88(16)	C(10)-C(11)-C(12)	119.5(7)
O(5)-Mo(1)-O(8)	77.56(14)	C(11)-C(12)-C(7)	120.8(7)
O(7)-Mo(1)-O(8)	77.67(14)	C(18)-C(13)-C(14)	119.6(6)
O(8)#1-Mo(1)-O(8)	74.70(16)	C(18)-C(13)-P	121.9(5)
O(1)-Mo(1)-Mo(3)	89.22(13)	C(14)-C(13)-P	118.5(4)
O(6)-Mo(1)-Mo(3)	133.41(13)	C(15)-C(14)-C(13)	120.9(6)
O(5)-Mo(1)-Mo(3)	123.71(12)	C(14)-C(15)-C(16)	119.3(7)
O(7)-Mo(1)-Mo(3)	36.49(12)	C(17)-C(16)-C(15)	119.8(6)
O(8)#1-Mo(1)-Mo(3)	45.57(10)	C(16)-C(17)-C(18)	121.8(6)
O(8)-Mo(1)-Mo(3)	85.39(9)	C(13)-C(18)-C(17)	118.6(6)
O(4)-Mo(2)-O(2)	105.47(19)	C(20)-C(19)-C(24)	120.6(6)
O(4)-Mo(2)-O(3)	101.33(19)	C(20)-C(19)-P	120.7(5)
O(2)-Mo(2)-O(3)	101.01(18)	C(24)-C(19)-P	118.7(5)
O(4)-Mo(2)-O(5)	100.99(19)	C(19)-C(20)-C(21)	118.5(6)
O(2)-Mo(2)-O(5)	95.57(18)	C(22)-C(21)-C(20)	121.3(6)
O(3)-Mo(2)-O(5)	147.40(16)	C(23)-C(22)-C(21)	119.6(6)
O(4)-Mo(2)-O(7)#1	90.80(17)	C(22)-C(23)-C(24)	120.5(6)
O(2)-Mo(2)-O(7)#1	161.47(17)	C(23)-C(24)-C(19)	119.5(6)
O(3)-Mo(2)-O(7)#1	83.99(15)	N(1)-C(25)-C(26)	179.4(8)
O(5)-Mo(2)-O(7)#1	72.24(14)	N(2)-C(27)-C(28)	177.6(8)
O(4)-Mo(2)-O(8)#1	162.76(17)		

Symmetry transformations used to generate equivalent atoms:

#1 -x,-y+1,-z+1

Ortep style representation of $(\text{Ph}_4\text{P})_2[\text{Ag}_2(\text{CH}_3\text{CN})_2\text{Mo}_8\text{O}_{26}]\cdot 2\text{CH}_3\text{CN}$ (**10**): thermal ellipsoids at 50% probability, hydrogen atoms are omitted for clarity. Carbon atoms of counterions are not labelled.



6.6 Crystal data for $((n\text{-C}_4\text{H}_9)_4\text{N})_{2n}[\text{Ag}_2(\text{CH}_3\text{CN})_2\text{Mo}_8\text{O}_{26}]_n$ (11)

Empirical formula	$\text{C}_{36}\text{H}_{78}\text{Ag}_2\text{Mo}_8\text{N}_4\text{O}_{26}$	
Crystal growth	Evaporation over 24 hours	
Crystal description	Colourless block crystals	
Crystal size	$0.22 \times 0.14 \times 0.10 \text{ mm}^3$	
Formula weight	1966.28	
Temperature	150(2) K	
Wavelength	0.71073 Å	
Crystal system	Monoclinic	
Space group	$P2_1/n$	
Unit cell dimensions	$a = 10.4827(3) \text{ Å}$	$\alpha = 90^\circ$
	$b = 16.6484(4) \text{ Å}$	$\beta = 93.1440(10)^\circ$
	$c = 16.8280(4) \text{ Å}$	$\gamma = 90^\circ$
Volume	$2932.41(13) \text{ Å}^3$	
Z	2	
Density (calculated)	2.227 Mg/m^3	
Absorption coefficient	2.381 mm^{-1}	
$F(000)$	1920	
Theta range for data collection	2.24 to 26.00°	
Index ranges	$-12 \leq h \leq 12, 0 \leq k \leq 20, 0 \leq l \leq 20$	
Reflections collected/ unique	22362 / 5754 [$R(\text{int}) = 0.056$]	
Completeness to theta	26.00° 99.9 %	
Absorption correction	None	
Max. and min. transmission	0.7967 and 0.6224	
Refinement method	Full-matrix least-squares on F^2	
Data / restraints / parameters	5754 / 0 / 345	
Goodness-of-fit on F^2	1.024	
Final R indices [$I > 2\sigma(I)$]	$R1 = 0.0258, wR2 = 0.0546$	
R indices (all data)	$R1 = 0.0378, wR2 = 0.0582$	
Extinction coefficient	0.00040(6)	
Largest diff. peak and hole	0.57 and -0.60 e.Å^{-3}	

Bond lengths [\AA] and angles [$^\circ$]

Ag-N(1)	2.236(3)	O(5)-Mo(2)-O(9)	73.66(8)
Ag-O(11)	2.393(2)	O(4)-Mo(2)-O(9)	69.91(8)
Ag-O(10)	2.475(2)	O(3)-Mo(3)-O(12)	105.63(12)
Ag-O(12)	2.574(3)	O(3)-Mo(3)-O(6)	101.24(11)
Mo(1)-O(1)	1.692(2)	O(12)-Mo(3)-O(6)	101.02(11)
Mo(1)-O(10)	1.726(2)	O(3)-Mo(3)-O(7)#1	100.69(10)
Mo(1)-O(5)	1.891(2)	O(12)-Mo(3)-O(7)#1	96.20(11)
Mo(1)-O(8)	1.992(2)	O(6)-Mo(3)-O(7)#1	147.19(10)
Mo(1)-O(7)	2.309(2)	O(3)-Mo(3)-O(8)#1	90.22(10)
Mo(1)-O(9)	2.339(2)	O(12)-Mo(3)-O(8)#1	161.67(10)
Mo(2)-O(2)	1.694(2)	O(6)-Mo(3)-O(8)#1	84.41(9)
Mo(2)-O(11)	1.721(3)	O(7)#1-Mo(3)-O(8)#1	71.39(8)
Mo(2)-O(6)	1.924(2)	O(3)-Mo(3)-O(9)	161.80(11)
Mo(2)-O(5)	1.929(2)	O(12)-Mo(3)-O(9)	92.28(10)
Mo(2)-O(4)	2.285(2)	O(6)-Mo(3)-O(9)	77.96(9)
Mo(2)-O(9)	2.454(2)	O(7)#1-Mo(3)-O(9)	73.62(8)
Mo(3)-O(3)	1.701(2)	O(8)#1-Mo(3)-O(9)	71.58(8)
Mo(3)-O(12)	1.710(2)	O(3)-Mo(3)-Mo(4)	135.51(8)
Mo(3)-O(6)	1.905(2)	O(12)-Mo(3)-Mo(4)	83.73(8)
Mo(3)-O(7)#1	2.014(2)	O(6)-Mo(3)-Mo(4)	119.88(7)
Mo(3)-O(8)#1	2.313(2)	O(7)#1-Mo(3)-Mo(4)	34.89(6)
Mo(3)-O(9)	2.314(2)	O(8)#1-Mo(3)-Mo(4)	78.45(5)
Mo(3)-Mo(4)	3.2196(4)	O(9)-Mo(3)-Mo(4)	41.93(5)
Mo(4)-O(13)	1.692(2)	O(13)-Mo(4)-O(4)#1	105.07(11)
Mo(4)-O(4)#1	1.755(2)	O(13)-Mo(4)-O(7)#1	101.35(11)
Mo(4)-O(7)#1	1.945(2)	O(4)#1-Mo(4)-O(7)#1	96.88(10)
Mo(4)-O(8)	1.958(2)	O(13)-Mo(4)-O(8)	99.80(11)
Mo(4)-O(9)	2.153(2)	O(4)#1-Mo(4)-O(8)	97.14(10)
Mo(4)-O(9)#1	2.321(2)	O(7)#1-Mo(4)-O(8)	150.55(9)
O(4)-Mo(4)#1	1.755(2)	O(13)-Mo(4)-O(9)	96.57(10)
O(7)-Mo(4)#1	1.945(2)	O(4)#1-Mo(4)-O(9)	158.36(10)
O(7)-Mo(3)#1	2.014(2)	O(7)#1-Mo(4)-O(9)	78.73(9)
O(8)-Mo(3)#1	2.313(2)	O(8)-Mo(4)-O(9)	78.70(9)
O(9)-Mo(4)#1	2.321(2)	O(13)-Mo(4)-O(9)#1	172.44(10)
N(1)-C(1)	1.130(5)	O(4)#1-Mo(4)-O(9)#1	82.42(9)
N(2)-C(11)	1.519(4)	O(7)#1-Mo(4)-O(9)#1	78.41(9)
N(2)-C(15)	1.521(4)	O(8)-Mo(4)-O(9)#1	77.94(9)

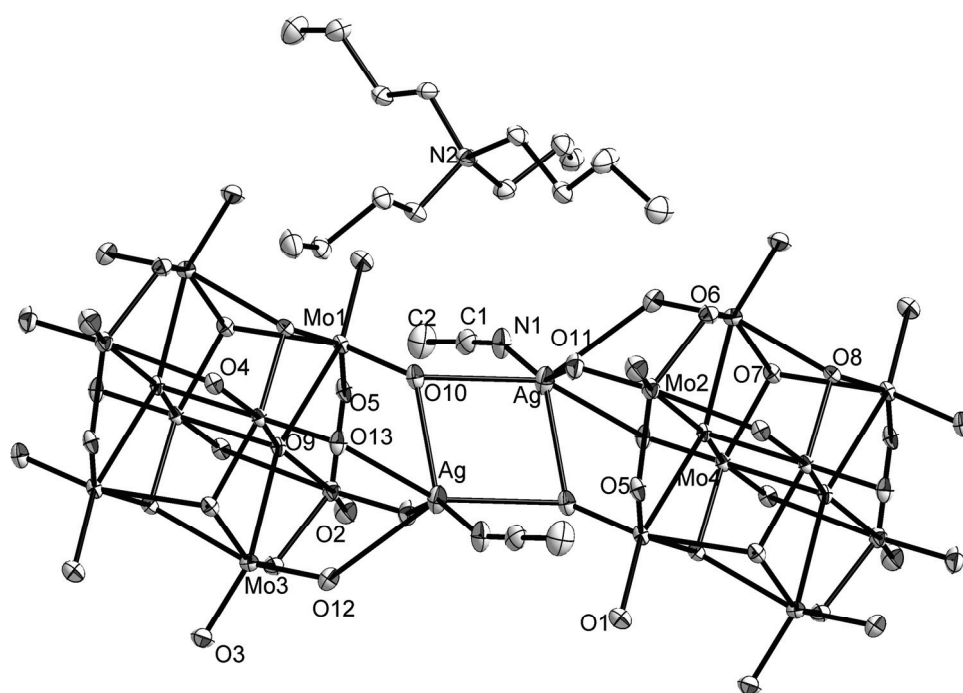
N(2)-C(23)	1.524(4)	O(9)-Mo(4)-O(9)#1	75.94(9)
N(2)-C(19)	1.525(4)	O(13)-Mo(4)-Mo(3)	89.08(8)
C(1)-C(2)	1.457(5)	O(4)#1-Mo(4)-Mo(3)	133.18(8)
C(11)-C(12)	1.514(5)	O(7)#1-Mo(4)-Mo(3)	36.31(7)
C(12)-C(13)	1.529(5)	O(8)-Mo(4)-Mo(3)	124.61(6)
C(13)-C(14)	1.522(5)	O(9)-Mo(4)-Mo(3)	45.92(6)
C(15)-C(16)	1.522(5)	O(9)#1-Mo(4)-Mo(3)	86.38(5)
C(16)-C(17)	1.530(5)	Mo(4)#1-O(4)-Mo(2)	115.74(11)
C(17)-C(18)	1.517(5)	Mo(1)-O(5)-Mo(2)	117.21(11)
C(19)-C(20)	1.524(5)	Mo(3)-O(6)-Mo(2)	116.51(11)
C(20)-C(21)	1.522(5)	Mo(4)#1-O(7)-Mo(3)#1	108.80(11)
C(21)-C(22)	1.509(6)	Mo(4)#1-O(7)-Mo(1)	110.27(10)
C(23)-C(24)	1.524(5)	Mo(3)#1-O(7)-Mo(1)	103.70(9)
C(24)-C(25)	1.524(5)	Mo(4)-O(8)-Mo(1)	109.38(10)
C(25)-C(26)	1.523(5)	Mo(4)-O(8)-Mo(3)#1	109.64(10)
		Mo(1)-O(8)-Mo(3)#1	104.28(9)
N(1)-Ag-O(11)	153.52(11)	Mo(4)-O(9)-Mo(3)	92.15(8)
N(1)-Ag-O(10)	127.69(10)	Mo(4)-O(9)-Mo(4)#1	104.06(9)
O(11)-Ag-O(10)	77.85(8)	Mo(3)-O(9)-Mo(4)#1	97.94(8)
N(1)-Ag-O(12)	94.37(10)	Mo(4)-O(9)-Mo(1)	91.63(8)
O(11)-Ag-O(12)	77.26(8)	Mo(3)-O(9)-Mo(1)	162.94(11)
O(10)-Ag-O(12)	115.58(8)	Mo(4)#1-O(9)-Mo(1)	97.26(8)
O(1)-Mo(1)-O(10)	104.81(12)	Mo(4)-O(9)-Mo(2)	164.01(11)
O(1)-Mo(1)-O(5)	102.10(10)	Mo(3)-O(9)-Mo(2)	86.09(7)
O(10)-Mo(1)-O(5)	101.02(11)	Mo(4)#1-O(9)-Mo(2)	91.92(7)
O(1)-Mo(1)-O(8)	100.50(10)	Mo(1)-O(9)-Mo(2)	85.70(7)
O(10)-Mo(1)-O(8)	97.52(10)	Mo(1)-O(10)-Ag	127.34(12)
O(5)-Mo(1)-O(8)	145.86(10)	Mo(2)-O(11)-Ag	129.17(13)
O(1)-Mo(1)-O(7)	91.22(10)	Mo(3)-O(12)-Ag	126.25(12)
O(10)-Mo(1)-O(7)	162.34(10)	C(1)-N(1)-Ag	158.4(3)
O(5)-Mo(1)-O(7)	82.40(9)	C(11)-N(2)-C(15)	111.2(3)
O(8)-Mo(1)-O(7)	71.83(9)	C(11)-N(2)-C(23)	110.7(3)
O(1)-Mo(1)-O(9)	162.59(10)	C(15)-N(2)-C(23)	107.1(3)
O(10)-Mo(1)-O(9)	92.32(10)	C(11)-N(2)-C(19)	106.2(3)
O(5)-Mo(1)-O(9)	77.15(9)	C(15)-N(2)-C(19)	110.7(3)
O(8)-Mo(1)-O(9)	73.67(8)	C(23)-N(2)-C(19)	110.9(3)
O(7)-Mo(1)-O(9)	71.40(8)	N(1)-C(1)-C(2)	179.1(5)
O(2)-Mo(2)-O(11)	105.48(12)	C(12)-C(11)-N(2)	116.9(3)
O(2)-Mo(2)-O(6)	104.48(11)	C(11)-C(12)-C(13)	108.0(3)
O(11)-Mo(2)-O(6)	97.98(11)	C(14)-C(13)-C(12)	114.2(3)

O(2)-Mo(2)-O(5)	101.56(11)	N(2)-C(15)-C(16)	116.2(3)
O(11)-Mo(2)-O(5)	98.19(11)	C(15)-C(16)-C(17)	109.7(3)
O(6)-Mo(2)-O(5)	144.26(10)	C(18)-C(17)-C(16)	113.3(3)
O(2)-Mo(2)-O(4)	92.69(11)	C(20)-C(19)-N(2)	116.6(3)
O(11)-Mo(2)-O(4)	161.80(10)	C(21)-C(20)-C(19)	110.0(3)
O(6)-Mo(2)-O(4)	78.00(9)	C(22)-C(21)-C(20)	112.7(3)
O(5)-Mo(2)-O(4)	76.73(9)	N(2)-C(23)-C(24)	115.2(3)
O(2)-Mo(2)-O(9)	162.54(11)	C(25)-C(24)-C(23)	111.3(3)
O(11)-Mo(2)-O(9)	91.90(10)	C(26)-C(25)-C(24)	111.7(3)
O(6)-Mo(2)-O(9)	74.15(8)		

Symmetry transformations used to generate equivalent atoms:

#1 -x+2,-y+2,-z

Ortep style representation of $((n\text{-C}_4\text{H}_9)_4\text{N})_{2n}[\text{Ag}_2(\text{CH}_3\text{CN})_2\text{Mo}_8\text{O}_{26}]_n$ (**11**): thermal ellipsoids at 50% probability, hydrogen atoms are omitted for clarity. Carbon atoms of counterion are not labelled.



6.7 Crystal data for

Empirical formula	$\text{C}_{26}\text{H}_{36}\text{N}_8\text{Ag}_4\text{Mo}_8\text{O}_{30}$	
Crystal growth	Diffusion of ethanol, 3 days	
Crystal description	Colourless block crystals	
Crystal size	$0.20 \times 0.12 \times 0.10 \text{ mm}^3$	
Formula weight	2139.63	
Temperature	150(2) K	
Wavelength	0.71073 Å	
Crystal system	Triclinic	
Space group	$P\bar{1}$	
Unit cell dimensions	$a = 9.6535(3) \text{ Å}$	$\alpha = 80.068(2)^\circ$
	$b = 10.8471(3) \text{ Å}$	$\beta = 82.5150(10)^\circ$
	$c = 12.1151(3) \text{ Å}$	$\gamma = 85.153(2)^\circ$
Volume	$1236.44(6) \text{ Å}^3$	
Z	1	
Density (calculated)	2.874 Mg/m^3	
Absorption coefficient	3.598 mm^{-1}	
$F(000)$	1012	
Theta range for data collection	2.13 to 25.99°	
Index ranges	$-11 \leq h \leq 11, -12 \leq k \leq 13, 0 \leq l \leq 14$	
Reflections collected/ unique	17497 / 4844 [$R(\text{int}) = 0.0377$]	
Completeness to theta	25.99° 99.8 %	
Absorption correction	Numerical	
Max. and min. transmission	0.7148 and 0.5330	
Refinement method	Full-matrix least-squares on F^2	
Data / restraints / parameters	4844 / 0 / 349	
Goodness-of-fit on F^2	1.081	
Final R indices [$I > 2\sigma(I)$]	$R1 = 0.0229, wR2 = 0.0538$	
R indices (all data)	$R1 = 0.0283, wR2 = 0.0556$	
Extinction coefficient	0.00147(14)	

Largest diff. peak and hole 0.65 and -0.71 e.Å⁻³

Bond lengths [Å] and angles [°]

Ag(1)-N(1)	2.219(4)	O(2)-Mo(2)-O(13)	93.43(10)
Ag(1)-O(1)	2.346(2)	O(11)-Mo(2)-O(13)	73.49(9)
Ag(1)-O(2)	2.510(3)	O(9)-Mo(2)-O(13)	72.87(9)
Ag(1)-Ag(1)#1	3.1811(6)	O(7)-Mo(2)-O(13)	69.47(8)
Ag(2)-N(2)	2.111(3)	O(3)-Mo(3)-O(7)#2	105.69(11)
Ag(2)-N(3)	2.180(3)	O(3)-Mo(3)-O(12)#2	102.76(10)
Mo(1)-O(5)	1.694(2)	O(7)#2-Mo(3)-O(12)#2	96.52(10)
Mo(1)-O(1)	1.737(2)	O(3)-Mo(3)-O(10)	100.45(10)
Mo(1)-O(9)	1.886(2)	O(7)#2-Mo(3)-O(10)	95.84(10)
Mo(1)-O(10)	1.996(2)	O(12)#2-Mo(3)-O(10)	149.58(9)
Mo(1)-O(12)	2.305(2)	O(3)-Mo(3)-O(13)	97.86(10)
Mo(1)-O(13)	2.308(2)	O(7)#2-Mo(3)-O(13)	156.44(9)
Mo(1)-Mo(3)	3.1960(4)	O(12)#2-Mo(3)-O(13)	78.76(9)
Mo(2)-O(6)	1.694(3)	O(10)-Mo(3)-O(13)	78.83(9)
Mo(2)-O(2)	1.718(2)	O(3)-Mo(3)-O(13)#2	173.01(10)
Mo(2)-O(11)	1.921(2)	O(7)#2-Mo(3)-O(13)#2	81.14(9)
Mo(2)-O(9)	1.937(2)	O(12)#2-Mo(3)-O(13)#2	77.53(8)
Mo(2)-O(7)	2.247(2)	O(10)-Mo(3)-O(13)#2	77.07(8)
Mo(2)-O(13)	2.494(2)	O(13)-Mo(3)-O(13)#2	75.29(9)
Mo(3)-O(3)	1.703(2)	O(3)-Mo(3)-Mo(1)	88.67(8)
Mo(3)-O(7)#2	1.753(2)	O(7)#2-Mo(3)-Mo(1)	132.24(8)
Mo(3)-O(12)#2	1.945(2)	O(12)#2-Mo(3)-Mo(1)	124.92(7)
Mo(3)-O(10)	1.951(2)	O(10)-Mo(3)-Mo(1)	36.39(7)
Mo(3)-O(13)	2.135(2)	O(13)-Mo(3)-Mo(1)	46.19(6)
Mo(3)-O(13)#2	2.353(2)	O(13)#2-Mo(3)-Mo(1)	85.53(5)
Mo(3)-Mo(4)	3.2184(4)	O(3)-Mo(3)-Mo(4)	90.39(8)
Mo(4)-O(8)	1.692(3)	O(7)#2-Mo(3)-Mo(4)	132.94(8)
Mo(4)-O(4)	1.715(2)	O(12)#2-Mo(3)-Mo(4)	36.42(7)
Mo(4)-O(11)	1.898(2)	O(10)-Mo(3)-Mo(4)	124.87(7)
Mo(4)-O(12)#2	2.017(2)	O(13)-Mo(3)-Mo(4)	46.07(6)
Mo(4)-O(10)#2	2.307(2)	O(13)#2-Mo(3)-Mo(4)	85.82(6)
Mo(4)-O(13)	2.320(2)	Mo(1)-Mo(3)-Mo(4)	91.029(10)
O(7)-Mo(3)#2	1.753(2)	O(8)-Mo(4)-O(4)	104.97(12)
O(10)-Mo(4)#2	2.307(2)	O(8)-Mo(4)-O(11)	102.84(11)

O(12)-Mo(3)#2	1.945(2)	O(4)-Mo(4)-O(11)	101.44(10)
O(12)-Mo(4)#2	2.017(2)	O(8)-Mo(4)-O(12)#2	99.51(11)
O(13)-Mo(3)#2	2.353(2)	O(4)-Mo(4)-O(12)#2	95.88(10)
O(14)-C(5)	1.428(4)	O(11)-Mo(4)-O(12)#2	146.95(10)
O(15)-C(11)	1.420(4)	O(8)-Mo(4)-O(10)#2	90.54(10)
N(1)-C(1)	1.139(5)	O(4)-Mo(4)-O(10)#2	161.61(10)
N(2)-C(3)	1.129(5)	O(11)-Mo(4)-O(10)#2	84.26(9)
N(3)-C(10)	1.342(5)	O(12)#2-Mo(4)-O(10)#2	71.43(8)
N(3)-C(6)	1.354(4)	O(8)-Mo(4)-O(13)	161.78(10)
N(4)-C(12)	1.128(11)	O(4)-Mo(4)-O(13)	92.49(10)
C(1)-C(2)	1.457(6)	O(11)-Mo(4)-O(13)	78.23(9)
C(3)-C(4)	1.453(5)	O(12)#2-Mo(4)-O(13)	73.06(9)
C(5)-C(6)	1.508(5)	O(10)#2-Mo(4)-O(13)	71.38(8)
C(6)-C(7)	1.390(5)	O(8)-Mo(4)-Mo(3)	134.32(9)
C(7)-C(8)	1.375(6)	O(4)-Mo(4)-Mo(3)	83.30(8)
C(8)-C(9)	1.386(5)	O(11)-Mo(4)-Mo(3)	119.72(7)
C(9)-C(10)	1.387(5)	O(12)#2-Mo(4)-Mo(3)	34.94(7)
C(10)-C(11)	1.506(5)	O(10)#2-Mo(4)-Mo(3)	78.74(6)
C(12)-C(13)	1.420(11)	O(13)-Mo(4)-Mo(3)	41.51(5)
		Mo(1)-O(1)-Ag(1)	132.97(13)
N(1)-Ag(1)-O(1)	169.84(11)	Mo(2)-O(2)-Ag(1)	128.20(13)
N(1)-Ag(1)-O(2)	98.35(11)	Mo(3)#2-O(7)-Mo(2)	118.68(11)
O(1)-Ag(1)-O(2)	78.59(8)	Mo(1)-O(9)-Mo(2)	117.58(12)
N(1)-Ag(1)-Ag(1)#1	120.74(9)	Mo(3)-O(10)-Mo(1)	108.15(11)
O(1)-Ag(1)-Ag(1)#1	61.13(6)	Mo(3)-O(10)-Mo(4)#2	111.06(10)
O(2)-Ag(1)-Ag(1)#1	139.61(6)	Mo(1)-O(10)-Mo(4)#2	104.36(9)
N(2)-Ag(2)-N(3)	166.60(11)	Mo(4)-O(11)-Mo(2)	118.08(12)
O(5)-Mo(1)-O(1)	106.14(12)	Mo(3)#2-O(12)-Mo(4)#2	108.64(10)
O(5)-Mo(1)-O(9)	102.05(11)	Mo(3)#2-O(12)-Mo(1)	110.53(10)
O(1)-Mo(1)-O(9)	100.65(11)	Mo(4)#2-O(12)-Mo(1)	103.77(9)
O(5)-Mo(1)-O(10)	99.16(11)	Mo(3)-O(13)-Mo(1)	91.92(8)
O(1)-Mo(1)-O(10)	97.44(10)	Mo(3)-O(13)-Mo(4)	92.41(8)
O(9)-Mo(1)-O(10)	146.92(10)	Mo(1)-O(13)-Mo(4)	162.88(11)
O(5)-Mo(1)-O(12)	90.60(10)	Mo(3)-O(13)-Mo(3)#2	104.71(9)
O(1)-Mo(1)-O(12)	161.60(10)	Mo(1)-O(13)-Mo(3)#2	97.29(8)
O(9)-Mo(1)-O(12)	82.80(9)	Mo(4)-O(13)-Mo(3)#2	97.61(8)
O(10)-Mo(1)-O(12)	71.84(8)	Mo(3)-O(13)-Mo(2)	164.59(10)
O(5)-Mo(1)-O(13)	162.44(10)	Mo(1)-O(13)-Mo(2)	85.77(7)
O(1)-Mo(1)-O(13)	90.89(10)	Mo(4)-O(13)-Mo(2)	85.66(7)
O(9)-Mo(1)-O(13)	78.36(9)	Mo(3)#2-O(13)-Mo(2)	90.70(7)

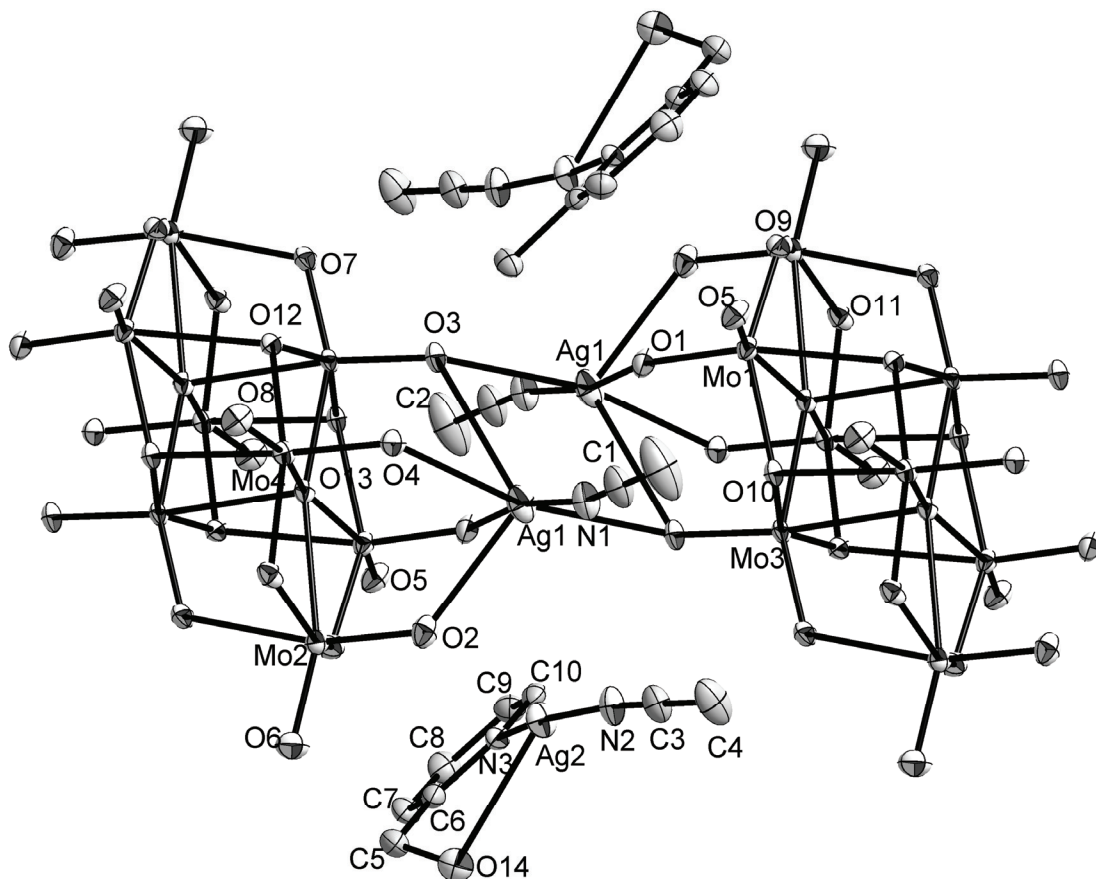
O(10)-Mo(1)-O(13)	73.87(9)	C(1)-N(1)-Ag(1)	170.2(4)
O(12)-Mo(1)-O(13)	71.97(8)	C(3)-N(2)-Ag(2)	172.9(3)
O(5)-Mo(1)-Mo(3)	134.44(8)	C(10)-N(3)-C(6)	119.3(3)
O(1)-Mo(1)-Mo(3)	83.26(8)	C(10)-N(3)-Ag(2)	121.4(2)
O(9)-Mo(1)-Mo(3)	120.24(7)	C(6)-N(3)-Ag(2)	119.3(2)
O(10)-Mo(1)-Mo(3)	35.45(7)	N(1)-C(1)-C(2)	179.1(5)
O(12)-Mo(1)-Mo(3)	79.47(5)	N(2)-C(3)-C(4)	179.4(4)
O(13)-Mo(1)-Mo(3)	41.88(5)	O(14)-C(5)-C(6)	113.1(3)
O(6)-Mo(2)-O(2)	105.03(12)	N(3)-C(6)-C(7)	120.7(3)
O(6)-Mo(2)-O(11)	104.39(12)	N(3)-C(6)-C(5)	118.2(3)
O(2)-Mo(2)-O(11)	98.57(11)	C(7)-C(6)-C(5)	121.1(3)
O(6)-Mo(2)-O(9)	103.23(12)	C(8)-C(7)-C(6)	119.8(3)
O(2)-Mo(2)-O(9)	96.37(11)	C(7)-C(8)-C(9)	119.3(4)
O(11)-Mo(2)-O(9)	143.81(10)	C(8)-C(9)-C(10)	118.5(4)
O(6)-Mo(2)-O(7)	92.05(10)	N(3)-C(10)-C(9)	122.2(3)
O(2)-Mo(2)-O(7)	162.83(10)	N(3)-C(10)-C(11)	115.9(3)
O(11)-Mo(2)-O(7)	78.49(9)	C(9)-C(10)-C(11)	121.8(3)
O(9)-Mo(2)-O(7)	77.60(9)	O(15)-C(11)-C(10)	110.5(3)
O(6)-Mo(2)-O(13)	161.50(10)	N(4)-C(12)-C(13)	177.1(9)

Symmetry transformations used to generate equivalent atoms:

#1 -x,-y+1,-z #2 -x+1,-y+1,-z

Ortep style representation of

$[\text{Ag}(\text{C}_7\text{H}_{12}\text{O}_2\text{N})(\text{CH}_3\text{CN})]_{2n}[(\text{Ag}(\text{CH}_3\text{CN}))_2\text{Mo}_8\text{O}_{26}]_n \cdot 2\text{CH}_3\text{CN}$ (**12**): thermal ellipsoids at 50% probability, hydrogen atoms are omitted for clarity.



6.8 Crystal data for $(\text{Ph}_4\text{P})_{2n}[\text{Ag}_2(\text{DMF})_2\text{Mo}_8\text{O}_{26}]_n \cdot 2\text{DMF}$ (13)

Empirical formula	$\text{C}_{60}\text{H}_{68}\text{Ag}_2\text{Mo}_8\text{N}_4\text{O}_{30}\text{P}_2$	
Crystal growth	Diffusion of diethyl ether over 3 days	
Crystal description	Colourless needle crystals	
Crystal size	$0.20 \times 0.07 \times 0.06 \text{ mm}^3$	
Formula weight	2370.38	
Temperature	150(2) K	
Wavelength	0.71073 Å	
Crystal system	Monoclinic	
Space group	$P2_1/n$	
Unit cell dimensions	$a = 17.1720(5) \text{ Å}$	$\alpha = 90^\circ$
	$b = 9.2312(3) \text{ Å}$	$\beta = 100.400(2)^\circ$
	$c = 24.0351(5) \text{ Å}$	$\gamma = 90^\circ$
Volume	$3747.41(18) \text{ Å}^3$	
Z	2	
Density (calculated)	2.101 Mg/m^3	
Absorption coefficient	1.928 mm^{-1}	
$F(000)$	2312	
Theta range for data collection	2.37 to 25.35°	
Index ranges	$-20 \leq h \leq 20, 0 \leq k \leq 11, 0 \leq l \leq 28$	
Reflections collected/ unique	22707 / 6845 [$R(\text{int}) = 0.0674$]	
Completeness to theta	25.35° 99.8 %	
Absorption correction	Gaussian	
Max. and min. transmission	0.894 and 0.752	
Refinement method	Full-matrix least-squares on F^2	
Data / restraints / parameters	6845 / 0 / 492	
Goodness-of-fit on F^2	1.016	
Final R indices [$I > 2\sigma(I)$]	$R1 = 0.0423, wR2 = 0.0772$	
R indices (all data)	$R1 = 0.0785, wR2 = 0.0865$	
Extinction coefficient	0.00018(4)	
Largest diff. peak and hole	0.76 and -0.65 e.Å ⁻³	

Bond lengths [\AA] and angles [$^\circ$]

Ag-O(1)	2.398(5)	O(5)-Mo(2)-O(8)#3	172.69(16)
Ag-O(3)#1	2.406(4)	O(11)-Mo(2)-O(8)#3	81.67(15)
Ag-O(15)#1	2.454(4)	O(9)-Mo(2)-O(8)#3	77.64(14)
Ag-O(4)	2.475(4)	O(10)-Mo(2)-O(8)#3	78.41(13)
Ag-O(5)	2.489(4)	O(8)-Mo(2)-O(8)#3	75.89(15)
Ag-Ag#2	3.1300(9)	O(14)-Mo(3)-O(15)	105.82(18)
Mo(1)-O(6)	1.695(3)	O(14)-Mo(3)-O(13)	100.82(17)
Mo(1)-O(4)	1.717(4)	O(15)-Mo(3)-O(13)	101.76(18)
Mo(1)-O(7)	1.880(4)	O(14)-Mo(3)-O(10)#3	101.04(16)
Mo(1)-O(9)	1.996(4)	O(15)-Mo(3)-O(10)#3	96.48(16)
Mo(1)-O(10)#3	2.293(4)	O(13)-Mo(3)-O(10)#3	146.36(14)
Mo(1)-O(8)	2.374(3)	O(14)-Mo(3)-O(9)	89.12(16)
Mo(2)-O(5)	1.698(4)	O(15)-Mo(3)-O(9)	162.31(14)
Mo(2)-O(11)	1.751(4)	O(13)-Mo(3)-O(9)	84.24(15)
Mo(2)-O(9)	1.949(3)	O(10)#3-Mo(3)-O(9)	70.88(13)
Mo(2)-O(10)	1.956(3)	O(14)-Mo(3)-O(8)#3	160.15(16)
Mo(2)-O(8)	2.134(4)	O(15)-Mo(3)-O(8)#3	93.79(14)
Mo(2)-O(8)#3	2.317(4)	O(13)-Mo(3)-O(8)#3	77.66(14)
Mo(3)-O(14)	1.698(4)	O(10)#3-Mo(3)-O(8)#3	73.11(13)
Mo(3)-O(15)	1.714(4)	O(9)-Mo(3)-O(8)#3	71.04(12)
Mo(3)-O(13)	1.889(4)	O(12)-Mo(4)-O(3)	105.1(2)
Mo(3)-O(10)#3	2.008(4)	O(12)-Mo(4)-O(7)#3	103.34(17)
Mo(3)-O(9)	2.305(4)	O(3)-Mo(4)-O(7)#3	96.84(17)
Mo(3)-O(8)#3	2.325(3)	O(12)-Mo(4)-O(13)	102.63(17)
Mo(4)-O(12)	1.696(4)	O(3)-Mo(4)-O(13)	98.21(17)
Mo(4)-O(3)	1.711(4)	O(7)#3-Mo(4)-O(13)	145.27(16)
Mo(4)-O(7)#3	1.929(3)	O(12)-Mo(4)-O(11)	93.73(18)
Mo(4)-O(13)	1.931(4)	O(3)-Mo(4)-O(11)	161.11(17)
Mo(4)-O(11)	2.261(4)	O(7)#3-Mo(4)-O(11)	77.66(14)
Mo(4)-O(8)#3	2.445(4)	O(13)-Mo(4)-O(11)	78.03(15)
O(1)-C(1)	1.247(10)	O(12)-Mo(4)-O(8)#3	163.42(17)
O(2)-C(4')	1.13(2)	O(3)-Mo(4)-O(8)#3	91.43(16)
O(2)-C(4)	1.183(11)	O(7)#3-Mo(4)-O(8)#3	74.54(14)
O(3)-Ag#4	2.406(4)	O(13)-Mo(4)-O(8)#3	73.96(13)
O(7)-Mo(4)#3	1.929(3)	O(11)-Mo(4)-O(8)#3	69.71(13)
O(8)-Mo(2)#3	2.317(4)	C(1)-O(1)-Ag	148.0(5)
O(8)-Mo(3)#3	2.325(3)	C(4')-O(2)-C(4)	58.3(13)

O(8)-Mo(4)#3	2.445(4)	Mo(4)-O(3)-Ag#4	133.5(2)
O(10)-Mo(3)#3	2.008(4)	Mo(1)-O(4)-Ag	135.7(2)
O(10)-Mo(1)#3	2.293(4)	Mo(2)-O(5)-Ag	129.50(18)
O(15)-Ag#4	2.454(4)	Mo(1)-O(7)-Mo(4)#3	117.88(19)
P-C(25)	1.789(6)	Mo(2)-O(8)-Mo(2)#3	104.11(14)
P-C(19)	1.792(5)	Mo(2)-O(8)-Mo(3)#3	92.62(13)
P-C(13)	1.799(6)	Mo(2)#3-O(8)-Mo(3)#3	97.85(13)
P-C(7)	1.800(5)	Mo(2)-O(8)-Mo(1)	91.83(13)
N(1)-C(1)	1.314(8)	Mo(2)#3-O(8)-Mo(1)	96.69(13)
N(1)-C(3)	1.463(10)	Mo(3)#3-O(8)-Mo(1)	163.26(17)
N(1)-C(2)	1.477(11)	Mo(2)-O(8)-Mo(4)#3	163.91(18)
N(2)-C(5')	1.35(3)	Mo(2)#3-O(8)-Mo(4)#3	91.95(13)
N(2)-C(4)	1.356(12)	Mo(3)#3-O(8)-Mo(4)#3	86.03(11)
N(2)-C(5)	1.380(13)	Mo(1)-O(8)-Mo(4)#3	85.24(12)
N(2)-C(4')	1.42(2)	Mo(2)-O(9)-Mo(1)	110.47(16)
N(2)-C(6)	1.465(13)	Mo(2)-O(9)-Mo(3)	110.42(16)
N(2)-C(6')	1.55(3)	Mo(1)-O(9)-Mo(3)	103.91(15)
C(7)-C(12)	1.392(8)	Mo(2)-O(10)-Mo(3)#3	108.97(17)
C(7)-C(8)	1.406(7)	Mo(2)-O(10)-Mo(1)#3	110.90(14)
C(8)-C(9)	1.378(8)	Mo(3)#3-O(10)-Mo(1)#3	103.98(15)
C(9)-C(10)	1.387(8)	Mo(2)-O(11)-Mo(4)	116.68(18)
C(10)-C(11)	1.374(8)	Mo(3)-O(13)-Mo(4)	116.92(18)
C(11)-C(12)	1.384(8)	Mo(3)-O(15)-Ag#4	129.73(18)
C(13)-C(18)	1.394(8)	C(25)-P-C(19)	109.8(3)
C(13)-C(14)	1.397(7)	C(25)-P-C(13)	110.4(3)
C(14)-C(15)	1.376(8)	C(19)-P-C(13)	109.5(3)
C(15)-C(16)	1.373(8)	C(25)-P-C(7)	108.0(3)
C(16)-C(17)	1.385(8)	C(19)-P-C(7)	110.1(3)
C(17)-C(18)	1.378(8)	C(13)-P-C(7)	109.1(2)
C(19)-C(24)	1.386(8)	C(1)-N(1)-C(3)	122.6(8)
C(19)-C(20)	1.392(8)	C(1)-N(1)-C(2)	123.3(8)
C(20)-C(21)	1.384(8)	C(3)-N(1)-C(2)	113.4(6)
C(21)-C(22)	1.368(10)	C(5')-N(2)-C(4)	79.6(15)
C(22)-C(23)	1.372(10)	C(5')-N(2)-C(5)	150.2(16)
C(23)-C(24)	1.386(8)	C(4)-N(2)-C(5)	122.7(9)
C(25)-C(30)	1.392(8)	C(5')-N(2)-C(4')	125.0(18)
C(25)-C(26)	1.397(8)	C(4)-N(2)-C(4')	47.8(10)
C(26)-C(27)	1.391(8)	C(5)-N(2)-C(4')	75.0(12)
C(27)-C(28)	1.396(9)	C(5')-N(2)-C(6)	44.6(13)
C(28)-C(29)	1.375(9)	C(4)-N(2)-C(6)	118.6(9)

C(29)-C(30)	1.376(8)	C(5)-N(2)-C(6)	118.7(10)
		C(4')-N(2)-C(6)	165.9(12)
O(1)-Ag-O(3)#1	76.92(15)	C(5')-N(2)-C(6')	121.1(18)
O(1)-Ag-O(15)#1	94.54(16)	C(4)-N(2)-C(6')	155.7(13)
O(3)#1-Ag-O(15)#1	80.33(13)	C(5)-N(2)-C(6')	44.7(11)
O(1)-Ag-O(4)	101.34(15)	C(4')-N(2)-C(6')	113.8(16)
O(3)#1-Ag-O(4)	177.65(13)	C(6)-N(2)-C(6')	77.7(13)
O(15)#1-Ag-O(4)	101.45(13)	O(1)-C(1)-N(1)	125.0(9)
O(1)-Ag-O(5)	86.71(16)	O(2)-C(4)-N(2)	126.7(10)
O(3)#1-Ag-O(5)	104.35(13)	O(2)-C(4')-N(2)	126(2)
O(15)#1-Ag-O(5)	175.31(13)	C(12)-C(7)-C(8)	119.0(5)
O(4)-Ag-O(5)	73.87(12)	C(12)-C(7)-P	121.6(4)
O(1)-Ag-Ag#2	144.10(14)	C(8)-C(7)-P	119.4(4)
O(3)#1-Ag-Ag#2	120.32(9)	C(9)-C(8)-C(7)	120.4(5)
O(15)#1-Ag-Ag#2	118.24(9)	C(8)-C(9)-C(10)	119.9(5)
O(4)-Ag-Ag#2	60.25(9)	C(11)-C(10)-C(9)	120.0(5)
O(5)-Ag-Ag#2	59.46(9)	C(10)-C(11)-C(12)	120.8(6)
O(6)-Mo(1)-O(4)	105.23(19)	C(11)-C(12)-C(7)	119.8(5)
O(6)-Mo(1)-O(7)	101.71(17)	C(18)-C(13)-C(14)	120.0(5)
O(4)-Mo(1)-O(7)	102.48(17)	C(18)-C(13)-P	120.3(4)
O(6)-Mo(1)-O(9)	102.70(16)	C(14)-C(13)-P	119.4(4)
O(4)-Mo(1)-O(9)	94.11(17)	C(15)-C(14)-C(13)	119.5(6)
O(7)-Mo(1)-O(9)	145.57(15)	C(16)-C(15)-C(14)	120.5(6)
O(6)-Mo(1)-O(10)#3	91.64(16)	C(15)-C(16)-C(17)	120.2(6)
O(4)-Mo(1)-O(10)#3	159.99(16)	C(18)-C(17)-C(16)	120.5(6)
O(7)-Mo(1)-O(10)#3	84.10(14)	C(17)-C(18)-C(13)	119.3(5)
O(9)-Mo(1)-O(10)#3	71.33(14)	C(24)-C(19)-C(20)	120.0(5)
O(6)-Mo(1)-O(8)	162.80(16)	C(24)-C(19)-P	118.5(5)
O(4)-Mo(1)-O(8)	91.67(15)	C(20)-C(19)-P	121.4(4)
O(7)-Mo(1)-O(8)	77.18(14)	C(21)-C(20)-C(19)	119.3(6)
O(9)-Mo(1)-O(8)	72.33(13)	C(22)-C(21)-C(20)	120.4(7)
O(10)#3-Mo(1)-O(8)	71.16(12)	C(21)-C(22)-C(23)	120.7(6)
O(5)-Mo(2)-O(11)	105.64(18)	C(22)-C(23)-C(24)	119.8(7)
O(5)-Mo(2)-O(9)	100.87(16)	C(23)-C(24)-C(19)	119.7(7)
O(11)-Mo(2)-O(9)	97.44(16)	C(30)-C(25)-C(26)	120.0(6)
O(5)-Mo(2)-O(10)	100.65(16)	C(30)-C(25)-P	119.2(4)
O(11)-Mo(2)-O(10)	96.13(16)	C(26)-C(25)-P	120.5(5)
O(9)-Mo(2)-O(10)	150.35(15)	C(27)-C(26)-C(25)	119.0(6)
O(5)-Mo(2)-O(8)	96.81(16)	C(26)-C(27)-C(28)	119.9(6)
O(11)-Mo(2)-O(8)	157.54(16)	C(29)-C(28)-C(27)	120.8(6)

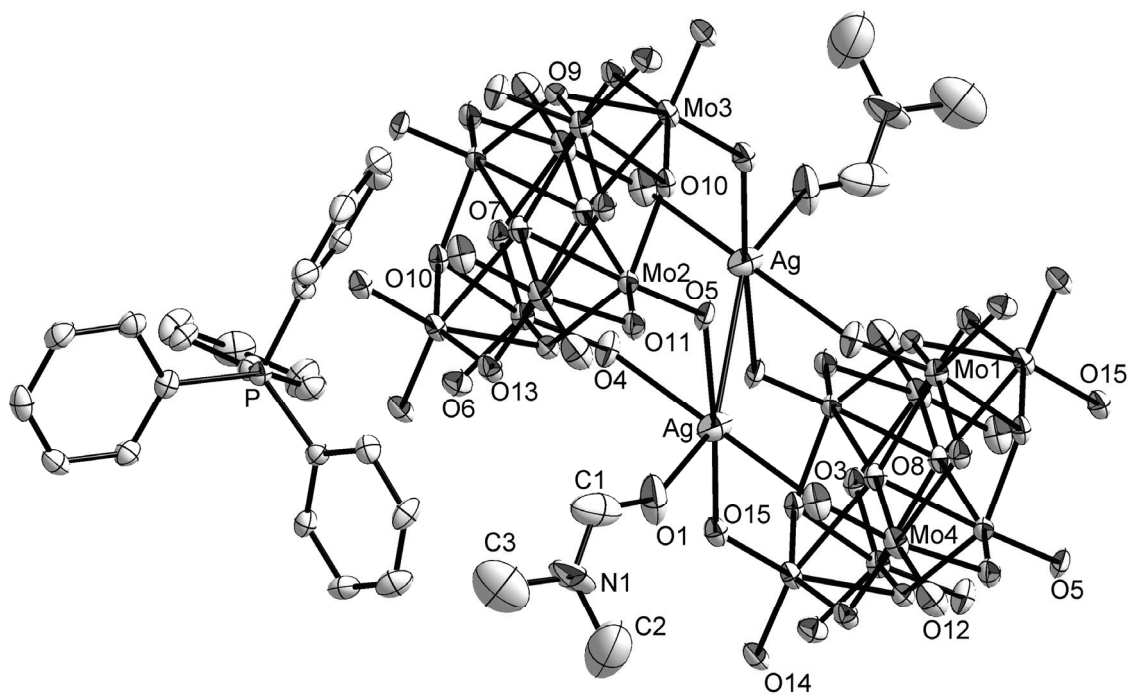
O(9)-Mo(2)-O(8)	78.84(14)	C(28)-C(29)-C(30)	119.5(6)
O(10)-Mo(2)-O(8)	78.57(14)	C(29)-C(30)-C(25)	120.7(6)

Symmetry transformations used to generate equivalent atoms:

#1 $x, y+1, z$ #2 $-x+1, -y+1, -z+1$ #3 $-x+1, -y, -z+1$

#4 $x, y-1, z$

Ortep style representation of $(\text{Ph}_4\text{P})_{2n}[\text{Ag}_2(\text{DMF})_2\text{Mo}_8\text{O}_{26}]_n \cdot 2\text{DMF}$ (**13**): thermal ellipsoids at 50% probability, hydrogen atoms are omitted for clarity. Not all carbon atoms labelled.



6.9 Crystal data for $(\text{H}_2\text{NMe}_2)_{2n}[\text{Ag}_2(\text{DMF})_2\text{Mo}_8\text{O}_{26}]_n \cdot 2\text{DMF}$ (14)

Empirical formula	$\text{C}_{16}\text{H}_{44}\text{Ag}_2\text{Mo}_8\text{N}_6\text{O}_{30}$	
Crystal growth	Diffusion of diethyl ether, 20 days	
Crystal description	Colourless block crystals	
Crystal size	$0.10 \times 0.04 \times 0.03 \text{ mm}^3$	
Formula weight	1783.83	
Temperature	150(2) K	
Wavelength	0.71073 Å	
Crystal system	Triclinic	
Space group	$P\bar{1}$	
Unit cell dimensions	$a = 10.0246(7) \text{ Å}$	$\alpha = 85.711(4)^\circ$
	$b = 10.5735(7) \text{ Å}$	$\beta = 65.494(4)^\circ$
	$c = 11.8724(6) \text{ Å}$	$\gamma = 69.821(3)^\circ$
Volume	$1071.33(12) \text{ Å}^3$	
Z	1	
Density (calculated)	2.765 Mg/m^3	
Absorption coefficient	3.251 mm^{-1}	
$F(000)$	852	
Theta range for data collection	1.89 to 25.99°	
Index ranges	$-10 \leq h \leq 12$, $-12 \leq k \leq 13$, $0 \leq l \leq 14$	
Reflections collected/ unique	15097 / 4195 [$R(\text{int}) = 0.0865$]	
Completeness to theta	25.99° 99.4 %	
Absorption correction	Gaussian	
Max. and min. transmission	0.911 and 0.725	
Refinement method	Full-matrix least-squares on F^2	
Data / restraints / parameters	4195 / 0 / 287	
Goodness-of-fit on F^2	0.991	
Final R indices [$I > 2\sigma(I)$]	$R1 = 0.0425$, $wR2 = 0.0729$	
R indices (all data)	$R1 = 0.0877$, $wR2 = 0.0828$	
Extinction coefficient	0.00040(11)	
Largest diff. peak and hole	0.88 and -0.92 e.Å^{-3}	

Bond lengths [Å] and angles [°]

Ag-O(9)#1	2.456(5)	O(12)-Mo(2)-O(6)	102.9(2)
Ag-O(1)	2.461(5)	O(9)-Mo(2)-O(6)	99.48(19)
Ag-O(10)#1	2.485(5)	O(12)-Mo(2)-O(11)	103.23(19)
Ag-O(14)	2.491(4)	O(9)-Mo(2)-O(11)	95.7(2)
Ag-O(2)	2.492(5)	O(6)-Mo(2)-O(11)	144.7(2)
Ag-Ag#1	3.0201(10)	O(12)-Mo(2)-O(5)#2	93.1(2)
Mo(1)-O(13)	1.697(4)	O(9)-Mo(2)-O(5)#2	160.74(18)
Mo(1)-O(10)	1.718(5)	O(6)-Mo(2)-O(5)#2	78.64(18)
Mo(1)-O(11)	1.890(4)	O(11)-Mo(2)-O(5)#2	76.67(17)
Mo(1)-O(8)	2.011(4)	O(12)-Mo(2)-O(7)	162.5(2)
Mo(1)-O(4)#2	2.323(5)	O(9)-Mo(2)-O(7)	91.62(17)
Mo(1)-O(7)	2.334(4)	O(6)-Mo(2)-O(7)	73.95(16)
Mo(2)-O(12)	1.690(4)	O(11)-Mo(2)-O(7)	73.95(15)
Mo(2)-O(9)	1.718(5)	O(5)#2-Mo(2)-O(7)	69.36(14)
Mo(2)-O(6)	1.927(4)	O(2)-Mo(3)-O(5)	104.4(2)
Mo(2)-O(11)	1.932(4)	O(2)-Mo(3)-O(8)	101.38(19)
Mo(2)-O(5)#2	2.252(5)	O(5)-Mo(3)-O(8)	96.50(18)
Mo(2)-O(7)	2.471(4)	O(2)-Mo(3)-O(4)	100.20(19)
Mo(3)-O(2)	1.701(5)	O(5)-Mo(3)-O(4)	96.37(18)
Mo(3)-O(5)	1.747(4)	O(8)-Mo(3)-O(4)	151.18(17)
Mo(3)-O(8)	1.950(4)	O(2)-Mo(3)-O(7)	98.62(19)
Mo(3)-O(4)	1.955(4)	O(5)-Mo(3)-O(7)	156.93(19)
Mo(3)-O(7)	2.111(4)	O(8)-Mo(3)-O(7)	79.13(16)
Mo(3)-O(7)#2	2.330(4)	O(4)-Mo(3)-O(7)	78.95(16)
Mo(4)-O(3)	1.699(4)	O(2)-Mo(3)-O(7)#2	174.16(18)
Mo(4)-O(1)	1.732(5)	O(5)-Mo(3)-O(7)#2	81.35(17)
Mo(4)-O(6)	1.882(4)	O(8)-Mo(3)-O(7)#2	78.47(16)
Mo(4)-O(4)	2.001(4)	O(4)-Mo(3)-O(7)#2	78.14(16)
Mo(4)-O(8)#2	2.339(4)	O(7)-Mo(3)-O(7)#2	75.58(18)
Mo(4)-O(7)	2.354(4)	O(3)-Mo(4)-O(1)	105.0(2)
O(4)-Mo(1)#2	2.323(5)	O(3)-Mo(4)-O(6)	103.08(19)
O(5)-Mo(2)#2	2.252(5)	O(1)-Mo(4)-O(6)	101.2(2)
O(7)-Mo(3)#2	2.330(4)	O(3)-Mo(4)-O(4)	100.31(19)
O(8)-Mo(4)#2	2.339(4)	O(1)-Mo(4)-O(4)	96.4(2)
O(9)-Ag#1	2.456(5)	O(6)-Mo(4)-O(4)	145.82(18)
O(10)-Ag#1	2.485(5)	O(3)-Mo(4)-O(8)#2	90.71(19)
O(14)-C(1)	1.241(8)	O(1)-Mo(4)-O(8)#2	161.71(19)

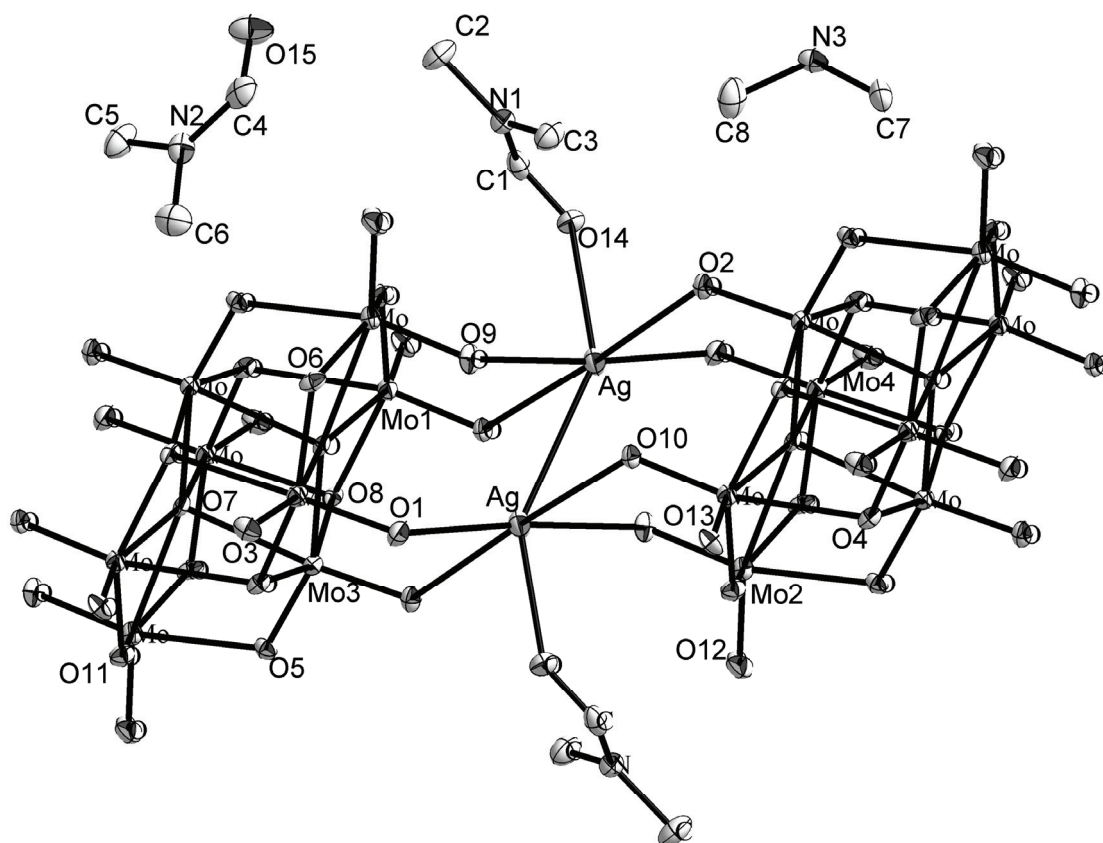
O(15)-C(4)	1.251(7)	O(6)-Mo(4)-O(8)#2	83.91(17)
N(1)-C(1)	1.323(8)	O(4)-Mo(4)-O(8)#2	71.16(16)
N(1)-C(3)	1.456(9)	O(3)-Mo(4)-O(7)	161.5(2)
N(1)-C(2)	1.474(8)	O(1)-Mo(4)-O(7)	92.83(18)
N(2)-C(4)	1.324(9)	O(6)-Mo(4)-O(7)	77.64(16)
N(2)-C(5)	1.445(9)	O(4)-Mo(4)-O(7)	72.40(14)
N(2)-C(6)	1.471(8)	O(8)#2-Mo(4)-O(7)	70.94(15)
N(3)-C(7)	1.455(9)	Mo(4)-O(1)-Ag	131.3(2)
N(3)-C(8)	1.469(9)	Mo(3)-O(2)-Ag	126.7(2)
		Mo(3)-O(4)-Mo(4)	109.36(19)
O(9)#1-Ag-O(1)	174.99(14)	Mo(3)-O(4)-Mo(1)#2	109.88(19)
O(9)#1-Ag-O(10)#1	74.36(15)	Mo(4)-O(4)-Mo(1)#2	104.59(17)
O(1)-Ag-O(10)#1	105.32(15)	Mo(3)-O(5)-Mo(2)#2	117.9(2)
O(9)#1-Ag-O(14)	95.67(14)	Mo(4)-O(6)-Mo(2)	118.2(2)
O(1)-Ag-O(14)	79.34(14)	Mo(3)-O(7)-Mo(3)#2	104.42(18)
O(10)#1-Ag-O(14)	93.67(15)	Mo(3)-O(7)-Mo(1)	92.77(16)
O(9)#1-Ag-O(2)	104.70(14)	Mo(3)#2-O(7)-Mo(1)	97.57(15)
O(1)-Ag-O(2)	75.39(15)	Mo(3)-O(7)-Mo(4)	92.44(14)
O(10)#1-Ag-O(2)	177.29(14)	Mo(3)#2-O(7)-Mo(4)	97.59(15)
O(14)-Ag-O(2)	83.87(14)	Mo(1)-O(7)-Mo(4)	162.2(2)
O(9)#1-Ag-Ag#1	61.04(9)	Mo(3)-O(7)-Mo(2)	164.2(2)
O(1)-Ag-Ag#1	123.29(10)	Mo(3)#2-O(7)-Mo(2)	91.36(13)
O(10)#1-Ag-Ag#1	59.50(9)	Mo(1)-O(7)-Mo(2)	85.13(12)
O(14)-Ag-Ag#1	147.25(12)	Mo(4)-O(7)-Mo(2)	85.24(14)
O(2)-Ag-Ag#1	122.41(10)	Mo(3)-O(8)-Mo(1)	108.8(2)
O(13)-Mo(1)-O(10)	105.6(2)	Mo(3)-O(8)-Mo(4)#2	110.16(19)
O(13)-Mo(1)-O(11)	101.31(19)	Mo(1)-O(8)-Mo(4)#2	103.70(16)
O(10)-Mo(1)-O(11)	100.5(2)	Mo(2)-O(9)-Ag#1	133.7(2)
O(13)-Mo(1)-O(8)	100.84(18)	Mo(1)-O(10)-Ag#1	128.3(2)
O(10)-Mo(1)-O(8)	98.17(18)	Mo(1)-O(11)-Mo(2)	116.61(18)
O(11)-Mo(1)-O(8)	145.85(18)	C(1)-O(14)-Ag	135.9(4)
O(13)-Mo(1)-O(4)#2	90.30(19)	C(1)-N(1)-C(3)	121.2(6)
O(10)-Mo(1)-O(4)#2	162.60(17)	C(1)-N(1)-C(2)	121.9(6)
O(11)-Mo(1)-O(4)#2	82.89(17)	C(3)-N(1)-C(2)	116.9(6)
O(8)-Mo(1)-O(4)#2	71.33(16)	C(4)-N(2)-C(5)	122.6(6)
O(13)-Mo(1)-O(7)	161.6(2)	C(4)-N(2)-C(6)	119.7(6)
O(10)-Mo(1)-O(7)	92.50(18)	C(5)-N(2)-C(6)	117.6(6)
O(11)-Mo(1)-O(7)	78.11(15)	C(7)-N(3)-C(8)	112.0(5)
O(8)-Mo(1)-O(7)	72.73(16)	O(14)-C(1)-N(1)	127.0(7)
O(4)#2-Mo(1)-O(7)	71.35(14)	O(15)-C(4)-N(2)	123.5(8)

O(12)-Mo(2)-O(9) 105.9(2) |

Symmetry transformations used to generate equivalent atoms:

#1 -x,-1,-y,-z+1 #2 -x,-y,-z+1

Ortep style representation of $(\text{H}_2\text{NMe}_2)_{2n}[\text{Ag}_2(\text{DMF})\text{Mo}_8\text{O}_{26}]_n \cdot 2\text{DMF}$ (**14**): thermal ellipsoids at 50% probability, hydrogen atoms are omitted for clarity.



6.10 Crystal data for $((n\text{-C}_4\text{H}_9)_4\text{N})_{2n}[\text{Ag}_2(\text{DMSO})_2\text{Mo}_8\text{O}_{26}]_n$ (15)

Empirical formula	$\text{C}_{36}\text{H}_{84}\text{Ag}_2\text{Mo}_8\text{N}_2\text{O}_{28}\text{S}_2$	
Crystal growth	Diffusion of ethanol, 14 days.	
Crystal description	Colourless block crystals	
Crystal size	$0.28 \times 0.18 \times 0.16 \text{ mm}^3$	
Formula weight	2040.43	
Temperature	120(2) K	
Wavelength	0.71073 Å	
Crystal system	Triclinic	
Space group	$P\bar{1}$	
Unit cell dimensions	$a = 12.9182(2) \text{ Å}$	$\alpha = 76.9880(10)^\circ$
	$b = 14.5922(3) \text{ Å}$	$\beta = 86.3660(10)^\circ$
	$c = 16.9871(3) \text{ Å}$	$\gamma = 83.7840(10)^\circ$
Volume	$3099.07(10) \text{ Å}^3$	
Z	2	
Density (calculated)	2.187 Mg/m^3	
Absorption coefficient	2.323 mm^{-1}	
$F(000)$	2000	
Theta range for data collection	1.68 to 26.00°	
Index ranges	$-15 \leq h \leq 15, -17 \leq k \leq 17, 0 \leq l \leq 20$	
Reflections collected/ unique	49689 / 12158 [$R(\text{int}) = 0.0342$]	
Completeness to theta	26.00° 99.9 %	
Absorption correction	Empirical	
Max. and min. transmission	0.730 and 0.627	
Refinement method	Full-matrix least-squares on F^2	
Data / restraints / parameters	12158 / 8 / 746	
Goodness-of-fit on F^2	1.041	
Final R indices [$I > 2\sigma(I)$]	$R1 = 0.0289, wR2 = 0.0698$	
R indices (all data)	$R1 = 0.0345, wR2 = 0.0723$	
Extinction coefficient	0.00012(4)	
Largest diff. peak and hole	1.17 and -1.27 e.Å^{-3}	

Bond lengths [Å] and angles [°]

Ag(1)-O(1)#1	2.366(3)	O(25)-Mo(3)-Mo(7)	83.40(9)
Ag(1)-O(6)	2.480(3)	O(21)-Mo(3)-Mo(7)	120.22(8)
Ag(1)-O(1)	2.495(3)	O(28)-Mo(3)-Mo(7)	34.85(7)
Ag(1)-O(5)	2.507(3)	O(20)-Mo(3)-Mo(7)	41.83(6)
Ag(1)-O(3)	2.564(3)	O(18)-Mo(3)-Mo(7)	79.38(6)
Ag(2)-Ag(2')	0.7853(15)	O(14)-Mo(4)-O(5)	104.61(13)
Ag(2)-O(2)	2.247(6)	O(14)-Mo(4)-O(12)	101.68(12)
Ag(2)-O(24)	2.364(3)	O(5)-Mo(4)-O(12)	101.54(12)
Ag(2)-O(16)	2.394(3)	O(14)-Mo(4)-O(7)#2	100.46(12)
Ag(2)-O(25)	2.417(3)	O(5)-Mo(4)-O(7)#2	97.00(11)
Ag(2')-O(2)	1.896(6)	O(12)-Mo(4)-O(7)#2	146.34(10)
Ag(2')-O(16)	2.345(3)	O(14)-Mo(4)-O(9)	162.26(11)
Ag(2')-O(24)	2.406(3)	O(5)-Mo(4)-O(9)	92.81(11)
Mo(1)-O(4)	1.703(2)	O(12)-Mo(4)-O(9)	77.56(10)
Mo(1)-O(8)#2	1.749(3)	O(7)#2-Mo(4)-O(9)	73.67(9)
Mo(1)-O(15)	1.951(2)	O(14)-Mo(4)-O(15)#2	90.41(11)
Mo(1)-O(7)#2	1.963(2)	O(5)-Mo(4)-O(15)#2	163.03(11)
Mo(1)-O(9)	2.139(2)	O(12)-Mo(4)-O(15)#2	82.68(10)
Mo(1)-O(9)#2	2.338(2)	O(7)#2-Mo(4)-O(15)#2	72.11(9)
Mo(1)-Mo(2)	3.2162(4)	O(9)-Mo(4)-O(15)#2	71.88(8)
Mo(1)-Mo(4)	3.2169(4)	O(14)-Mo(4)-Mo(1)	135.69(9)
Mo(2)-O(10)	1.697(3)	O(5)-Mo(4)-Mo(1)	84.35(9)
Mo(2)-O(3)	1.711(3)	O(12)-Mo(4)-Mo(1)	119.20(8)
Mo(2)-O(11)	1.896(3)	O(7)#2-Mo(4)-Mo(1)	35.34(7)
Mo(2)-O(15)	2.010(3)	O(9)-Mo(4)-Mo(1)	41.64(6)
Mo(2)-O(9)	2.323(2)	O(15)#2-Mo(4)-Mo(1)	79.32(6)
Mo(2)-O(7)	2.326(2)	O(13)-Mo(5)-O(6)	105.53(14)
Mo(3)-O(23)	1.701(3)	O(13)-Mo(5)-O(11)	103.84(12)
Mo(3)-O(25)	1.718(3)	O(6)-Mo(5)-O(11)	98.49(12)
Mo(3)-O(21)	1.891(3)	O(13)-Mo(5)-O(12)	103.65(12)
Mo(3)-O(28)	2.003(3)	O(6)-Mo(5)-O(12)	97.54(12)
Mo(3)-O(20)	2.305(2)	O(11)-Mo(5)-O(12)	142.97(11)
Mo(3)-O(18)	2.326(3)	O(13)-Mo(5)-O(8)	93.04(12)
Mo(3)-Mo(7)	3.2175(4)	O(6)-Mo(5)-O(8)	161.42(12)
Mo(4)-O(14)	1.707(3)	O(11)-Mo(5)-O(8)	77.35(10)
Mo(4)-O(5)	1.715(3)	O(12)-Mo(5)-O(8)	76.87(10)
Mo(4)-O(12)	1.885(3)	O(13)-Mo(5)-O(9)	162.51(12)

Mo(4)-O(7)#2	1.999(2)	O(6)-Mo(5)-O(9)	91.95(11)
Mo(4)-O(9)	2.321(2)	O(11)-Mo(5)-O(9)	73.63(9)
Mo(4)-O(15)#2	2.321(2)	O(12)-Mo(5)-O(9)	72.66(9)
Mo(5)-O(13)	1.695(3)	O(8)-Mo(5)-O(9)	69.48(8)
Mo(5)-O(6)	1.717(3)	O(22)-Mo(6)-O(16)	104.91(14)
Mo(5)-O(11)	1.919(3)	O(22)-Mo(6)-O(17)	101.32(12)
Mo(5)-O(12)	1.934(3)	O(16)-Mo(6)-O(17)	100.41(13)
Mo(5)-O(8)	2.284(3)	O(22)-Mo(6)-O(18)#3	100.19(12)
Mo(5)-O(9)	2.485(2)	O(16)-Mo(6)-O(18)#3	96.54(12)
Mo(6)-O(22)	1.701(3)	O(17)-Mo(6)-O(18)#3	148.04(11)
Mo(6)-O(16)	1.719(3)	O(22)-Mo(6)-O(28)#3	90.98(12)
Mo(6)-O(17)	1.892(3)	O(16)-Mo(6)-O(28)#3	162.06(11)
Mo(6)-O(18)#3	2.010(2)	O(17)-Mo(6)-O(28)#3	84.19(11)
Mo(6)-O(28)#3	2.289(3)	O(18)#3-Mo(6)-O(28)#3	72.06(9)
Mo(6)-O(20)	2.304(2)	O(22)-Mo(6)-O(20)	162.72(12)
Mo(6)-Mo(7)	3.2141(4)	O(16)-Mo(6)-O(20)	92.03(11)
Mo(7)-O(26)	1.699(3)	O(17)-Mo(6)-O(20)	78.48(10)
Mo(7)-O(27)	1.745(3)	O(18)#3-Mo(6)-O(20)	74.01(9)
Mo(7)-O(28)	1.946(3)	O(28)#3-Mo(6)-O(20)	71.76(9)
Mo(7)-O(18)#3	1.953(2)	O(22)-Mo(6)-Mo(7)	135.31(9)
Mo(7)-O(20)	2.148(2)	O(16)-Mo(6)-Mo(7)	83.99(9)
Mo(7)-O(20)#3	2.348(3)	O(17)-Mo(6)-Mo(7)	120.36(8)
Mo(8)-O(19)	1.696(3)	O(18)#3-Mo(6)-Mo(7)	35.22(7)
Mo(8)-O(24)	1.723(3)	O(28)#3-Mo(6)-Mo(7)	78.79(6)
Mo(8)-O(21)	1.917(3)	O(20)-Mo(6)-Mo(7)	41.88(6)
Mo(8)-O(17)	1.926(3)	O(26)-Mo(7)-O(27)	104.99(13)
Mo(8)-O(27)#3	2.269(3)	O(26)-Mo(7)-O(28)	101.78(12)
Mo(8)-O(20)	2.509(2)	O(27)-Mo(7)-O(28)	96.59(11)
S(1)-O(1)	1.504(3)	O(26)-Mo(7)-O(18)#3	101.00(12)
S(1)-C(2)	1.769(6)	O(27)-Mo(7)-O(18)#3	96.96(11)
S(1)-C(1)	1.798(5)	O(28)-Mo(7)-O(18)#3	149.40(10)
S(2)-O(2)	1.510(7)	O(26)-Mo(7)-O(20)	98.37(12)
S(2)-C(3)	1.700(7)	O(27)-Mo(7)-O(20)	156.63(12)
S(2)-C(4)	1.786(7)	O(28)-Mo(7)-O(20)	77.90(10)
O(1)-Ag(1)#1	2.366(3)	O(18)#3-Mo(7)-O(20)	78.81(10)
S(2')-O(2')	1.508(9)	O(26)-Mo(7)-O(20)#3	173.42(11)
O(7)-Mo(1)#2	1.963(2)	O(27)-Mo(7)-O(20)#3	81.59(11)
O(7)-Mo(4)#2	1.999(2)	O(28)-Mo(7)-O(20)#3	77.04(10)
O(8)-Mo(1)#2	1.749(3)	O(18)#3-Mo(7)-O(20)#3	77.99(10)
O(9)-Mo(1)#2	2.338(2)	O(20)-Mo(7)-O(20)#3	75.05(10)

O(15)-Mo(4)#2	2.321(2)	O(26)-Mo(7)-Mo(6)	90.12(10)
O(18)-Mo(7)#3	1.953(2)	O(27)-Mo(7)-Mo(6)	133.35(9)
O(18)-Mo(6)#3	2.010(2)	O(28)-Mo(7)-Mo(6)	123.61(7)
O(20)-Mo(7)#3	2.348(3)	O(18)#3-Mo(7)-Mo(6)	36.41(7)
O(27)-Mo(8)#3	2.269(3)	O(20)-Mo(7)-Mo(6)	45.75(7)
O(28)-Mo(6)#3	2.289(3)	O(20)#3-Mo(7)-Mo(6)	85.27(6)
N(1)-C(11)	1.522(5)	O(26)-Mo(7)-Mo(3)	89.79(9)
N(1)-C(23)	1.524(5)	O(27)-Mo(7)-Mo(3)	132.63(9)
N(1)-C(15)	1.525(6)	O(28)-Mo(7)-Mo(3)	36.04(7)
N(1)-C(19)	1.528(6)	O(18)#3-Mo(7)-Mo(3)	124.51(7)
N(2)-C(27)	1.514(5)	O(20)-Mo(7)-Mo(3)	45.71(7)
N(2)-C(31)	1.522(5)	O(20)#3-Mo(7)-Mo(3)	85.54(6)
N(2)-C(35)	1.525(5)	Mo(6)-Mo(7)-Mo(3)	90.235(11)
N(2)-C(39)	1.525(5)	O(19)-Mo(8)-O(24)	105.19(15)
C(11)-C(12)	1.519(6)	O(19)-Mo(8)-O(21)	105.35(13)
C(12)-C(13)	1.525(6)	O(24)-Mo(8)-O(21)	98.41(13)
C(13)-C(14)	1.523(7)	O(19)-Mo(8)-O(17)	102.89(13)
C(15)-C(16)	1.696(12)	O(24)-Mo(8)-O(17)	96.98(13)
C(16)-C(17)	1.430(15)	O(21)-Mo(8)-O(17)	142.83(11)
C(17)-C(18)	1.378(14)	O(19)-Mo(8)-O(27)#3	93.19(13)
C(16')-C(16'')	0.89(3)	O(24)-Mo(8)-O(27)#3	161.54(12)
C(16')-C(17'')	1.07(3)	O(21)-Mo(8)-O(27)#3	77.97(10)
C(16')-C(17')	1.55(3)	O(17)-Mo(8)-O(27)#3	76.80(11)
C(17')-C(16'')	0.90(3)	O(19)-Mo(8)-O(20)	162.12(12)
C(17')-C(17'')	1.69(3)	O(24)-Mo(8)-O(20)	92.62(11)
C(16'')-C(17'')	1.58(3)	O(21)-Mo(8)-O(20)	72.87(9)
C(19)-C(20)	1.516(7)	O(17)-Mo(8)-O(20)	72.81(10)
C(20)-C(21)	1.532(7)	O(27)#3-Mo(8)-O(20)	68.97(9)
C(21)-C(22)	1.536(11)	O(1)-S(1)-C(2)	105.5(3)
C(23)-C(24)	1.517(6)	O(1)-S(1)-C(1)	105.2(2)
C(24)-C(25)	1.517(6)	C(2)-S(1)-C(1)	96.9(3)
C(25)-C(26)	1.509(6)	O(2)-S(2)-C(3)	108.5(4)
C(27)-C(28)	1.524(5)	O(2)-S(2)-C(4)	97.4(4)
C(28)-C(29)	1.532(6)	C(3)-S(2)-C(4)	93.7(4)
C(29)-C(30)	1.524(6)	S(1)-O(1)-Ag(1)#1	135.96(17)
C(31)-C(32)	1.523(5)	S(1)-O(1)-Ag(1)	117.27(16)
C(32)-C(33)	1.524(6)	Ag(1)#1-O(1)-Ag(1)	106.27(11)
C(33)-C(34)	1.527(6)	S(2)-O(2)-Ag(2')	140.9(4)
C(35)-C(36)	1.516(6)	S(2)-O(2)-Ag(2)	121.4(4)
C(36)-C(37)	1.525(6)	Ag(2')-O(2)-Ag(2)	19.58(8)

C(37)-C(38)	1.530(8)	Mo(2)-O(3)-Ag(1)	126.96(13)
C(39)-C(40)	1.515(6)	Mo(4)-O(5)-Ag(1)	127.49(13)
C(40)-C(41)	1.570(7)	Mo(5)-O(6)-Ag(1)	128.63(14)
C(41)-C(42)	1.518(7)	Mo(1)#2-O(7)-Mo(4)#2	108.57(12)
C(41')-C(42')	1.487(17)	Mo(1)#2-O(7)-Mo(2)	110.03(10)
		Mo(4)#2-O(7)-Mo(2)	103.99(10)
O(1)#1-Ag(1)-O(6)	139.03(11)	Mo(1)#2-O(8)-Mo(5)	117.03(12)
O(1)#1-Ag(1)-O(1)	73.73(11)	Mo(1)-O(9)-Mo(4)	92.23(9)
O(6)-Ag(1)-O(1)	86.98(9)	Mo(1)-O(9)-Mo(2)	92.14(9)
O(1)#1-Ag(1)-O(5)	136.58(10)	Mo(4)-O(9)-Mo(2)	162.28(12)
O(6)-Ag(1)-O(5)	76.76(9)	Mo(1)-O(9)-Mo(1)#2	104.92(10)
O(1)-Ag(1)-O(5)	88.70(9)	Mo(4)-O(9)-Mo(1)#2	97.35(9)
O(1)#1-Ag(1)-O(3)	100.21(9)	Mo(2)-O(9)-Mo(1)#2	98.09(9)
O(6)-Ag(1)-O(3)	76.29(9)	Mo(1)-O(9)-Mo(5)	163.77(12)
O(1)-Ag(1)-O(3)	146.37(10)	Mo(4)-O(9)-Mo(5)	85.78(8)
O(5)-Ag(1)-O(3)	114.78(8)	Mo(2)-O(9)-Mo(5)	85.23(8)
Ag(2')-Ag(2)-O(2)	54.00(19)	Mo(1)#2-O(9)-Mo(5)	91.31(8)
Ag(2')-Ag(2)-O(24)	83.55(14)	Mo(2)-O(11)-Mo(5)	117.28(13)
O(2)-Ag(2)-O(24)	119.88(18)	Mo(4)-O(12)-Mo(5)	117.97(13)
Ag(2')-Ag(2)-O(16)	76.96(14)	Mo(1)-O(15)-Mo(2)	108.59(11)
O(2)-Ag(2)-O(16)	119.83(18)	Mo(1)-O(15)-Mo(4)#2	109.64(11)
O(24)-Ag(2)-O(16)	81.15(10)	Mo(2)-O(15)-Mo(4)#2	103.79(10)
Ag(2')-Ag(2)-O(25)	153.23(12)	Mo(6)-O(16)-Ag(2')	137.73(16)
O(2)-Ag(2)-O(25)	115.37(18)	Mo(6)-O(16)-Ag(2)	123.24(14)
O(24)-Ag(2)-O(25)	82.88(10)	Ag(2')-O(16)-Ag(2)	19.04(4)
O(16)-Ag(2)-O(25)	123.26(11)	Mo(6)-O(17)-Mo(8)	117.89(14)
Ag(2)-Ag(2')-O(2)	106.4(2)	Mo(7)#3-O(18)-Mo(6)#3	108.38(12)
Ag(2)-Ag(2')-O(16)	84.00(16)	Mo(7)#3-O(18)-Mo(3)	109.47(11)
O(2)-Ag(2')-O(16)	142.37(19)	Mo(6)#3-O(18)-Mo(3)	103.42(10)
Ag(2)-Ag(2')-O(24)	77.53(15)	Mo(7)-O(20)-Mo(6)	92.36(9)
O(2)-Ag(2')-O(24)	135.92(19)	Mo(7)-O(20)-Mo(3)	92.46(9)
O(16)-Ag(2')-O(24)	81.28(11)	Mo(6)-O(20)-Mo(3)	162.70(13)
O(4)-Mo(1)-O(8)#2	105.33(12)	Mo(7)-O(20)-Mo(7)#3	104.95(10)
O(4)-Mo(1)-O(15)	101.39(11)	Mo(6)-O(20)-Mo(7)#3	97.21(9)
O(8)#2-Mo(1)-O(15)	97.32(11)	Mo(3)-O(20)-Mo(7)#3	97.57(9)
O(4)-Mo(1)-O(7)#2	100.22(11)	Mo(7)-O(20)-Mo(8)	164.20(13)
O(8)#2-Mo(1)-O(7)#2	96.02(11)	Mo(6)-O(20)-Mo(8)	85.49(8)
O(15)-Mo(1)-O(7)#2	150.53(10)	Mo(3)-O(20)-Mo(8)	85.35(8)
O(4)-Mo(1)-O(9)	97.39(11)	Mo(7)#3-O(20)-Mo(8)	90.85(8)
O(8)#2-Mo(1)-O(9)	157.25(10)	Mo(3)-O(21)-Mo(8)	118.18(13)

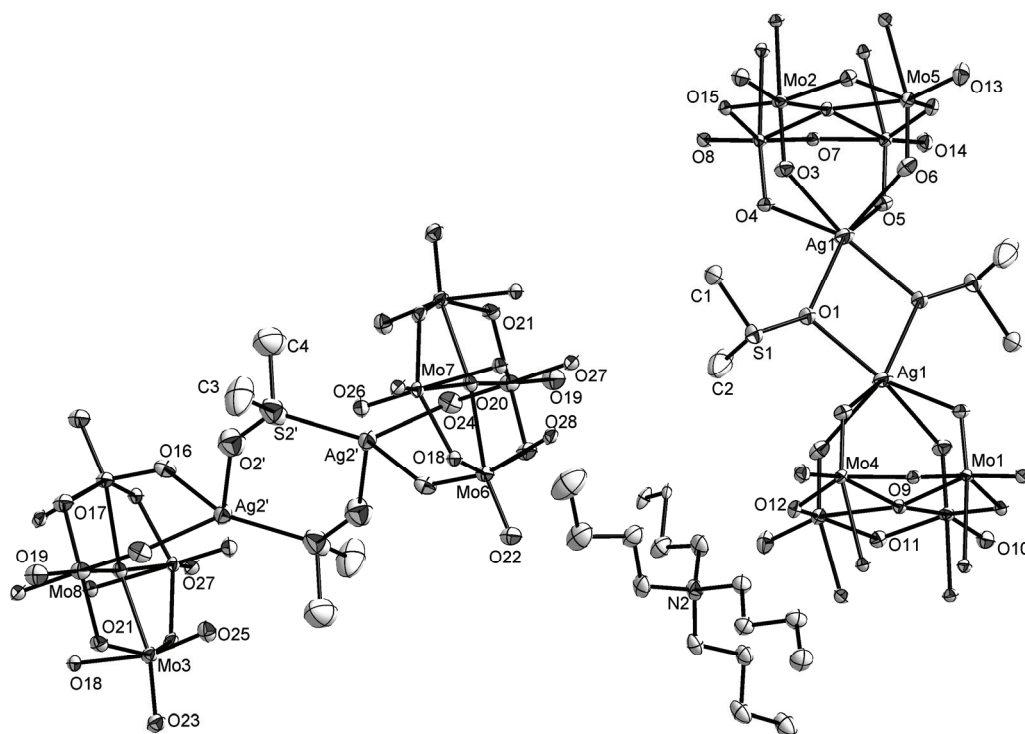
O(15)-Mo(1)-O(9)	78.92(10)	Mo(8)-O(24)-Ag(2)	122.63(15)
O(7)#2-Mo(1)-O(9)	78.64(10)	Mo(8)-O(24)-Ag(2')	136.44(16)
O(4)-Mo(1)-O(9)#2	172.42(11)	Ag(2)-O(24)-Ag(2')	18.92(4)
O(8)#2-Mo(1)-O(9)#2	82.18(10)	Mo(3)-O(25)-Ag(2)	122.27(14)
O(15)-Mo(1)-O(9)#2	78.32(9)	Mo(7)-O(27)-Mo(8)#3	118.58(13)
O(7)#2-Mo(1)-O(9)#2	77.62(9)	Mo(7)-O(28)-Mo(3)	109.11(12)
O(9)-Mo(1)-O(9)#2	75.08(10)	Mo(7)-O(28)-Mo(6)#3	110.73(11)
O(4)-Mo(1)-Mo(2)	89.39(9)	Mo(3)-O(28)-Mo(6)#3	104.96(11)
O(8)#2-Mo(1)-Mo(2)	133.64(8)	C(11)-N(1)-C(23)	106.4(3)
O(15)-Mo(1)-Mo(2)	36.32(7)	C(11)-N(1)-C(15)	110.8(4)
O(7)#2-Mo(1)-Mo(2)	124.83(7)	C(23)-N(1)-C(15)	110.4(3)
O(9)-Mo(1)-Mo(2)	46.20(6)	C(11)-N(1)-C(19)	111.1(3)
O(9)#2-Mo(1)-Mo(2)	86.01(6)	C(23)-N(1)-C(19)	110.3(3)
O(4)-Mo(1)-Mo(4)	88.59(9)	C(15)-N(1)-C(19)	107.8(4)
O(8)#2-Mo(1)-Mo(4)	132.11(8)	C(27)-N(2)-C(31)	110.6(3)
O(15)-Mo(1)-Mo(4)	125.04(7)	C(27)-N(2)-C(35)	111.7(3)
O(7)#2-Mo(1)-Mo(4)	36.09(7)	C(31)-N(2)-C(35)	107.0(3)
O(9)-Mo(1)-Mo(4)	46.13(6)	C(27)-N(2)-C(39)	106.3(3)
O(9)#2-Mo(1)-Mo(4)	85.48(6)	C(31)-N(2)-C(39)	110.5(3)
Mo(2)-Mo(1)-Mo(4)	90.997(11)	C(35)-N(2)-C(39)	110.7(3)
O(10)-Mo(2)-O(3)	105.50(13)	C(12)-C(11)-N(1)	115.5(3)
O(10)-Mo(2)-O(11)	101.84(12)	C(11)-C(12)-C(13)	109.7(4)
O(3)-Mo(2)-O(11)	101.85(12)	C(14)-C(13)-C(12)	112.9(4)
O(10)-Mo(2)-O(15)	99.84(12)	N(1)-C(15)-C(16)	109.9(5)
O(3)-Mo(2)-O(15)	96.15(12)	C(17)-C(16)-C(15)	116.6(9)
O(11)-Mo(2)-O(15)	146.81(10)	C(18)-C(17)-C(16)	111.5(11)
O(10)-Mo(2)-O(9)	161.50(11)	C(16'')-C(16')-C(17'')	108(2)
O(3)-Mo(2)-O(9)	92.49(11)	C(16'')-C(16')-C(17')	30.4(18)
O(11)-Mo(2)-O(9)	78.09(10)	C(17'')-C(16')-C(17')	78.0(17)
O(15)-Mo(2)-O(9)	73.46(9)	C(16'')-C(17')-C(16')	29.8(17)
O(10)-Mo(2)-O(7)	90.21(11)	C(16'')-C(17')-C(17'')	68(2)
O(3)-Mo(2)-O(7)	161.88(11)	C(16')-C(17')-C(17'')	38.3(10)
O(11)-Mo(2)-O(7)	83.22(10)	C(16')-C(16'')-C(17')	120(3)
O(15)-Mo(2)-O(7)	71.84(9)	C(16')-C(16'')-C(17'')	39.9(17)
O(9)-Mo(2)-O(7)	71.35(8)	C(17'')-C(16'')-C(17'')	80(2)
O(10)-Mo(2)-Mo(1)	134.85(10)	C(16')-C(17'')-C(16'')	32.1(13)
O(3)-Mo(2)-Mo(1)	83.65(9)	C(16')-C(17'')-C(17')	63.7(15)
O(11)-Mo(2)-Mo(1)	119.74(8)	C(16'')-C(17'')-C(17')	31.8(10)
O(15)-Mo(2)-Mo(1)	35.09(7)	C(20)-C(19)-N(1)	115.0(4)
O(9)-Mo(2)-Mo(1)	41.66(6)	C(19)-C(20)-C(21)	111.6(5)

O(7)-Mo(2)-Mo(1)	78.80(6)	C(20)-C(21)-C(22)	111.3(6)
O(23)-Mo(3)-O(25)	105.10(13)	C(24)-C(23)-N(1)	116.0(3)
O(23)-Mo(3)-O(21)	101.76(12)	C(25)-C(24)-C(23)	110.1(3)
O(25)-Mo(3)-O(21)	101.59(13)	C(26)-C(25)-C(24)	113.5(4)
O(23)-Mo(3)-O(28)	100.12(12)	N(2)-C(27)-C(28)	115.5(3)
O(25)-Mo(3)-O(28)	96.50(12)	C(27)-C(28)-C(29)	110.1(3)
O(21)-Mo(3)-O(28)	146.73(11)	C(30)-C(29)-C(28)	112.4(4)
O(23)-Mo(3)-O(20)	161.96(12)	N(2)-C(31)-C(32)	115.5(3)
O(25)-Mo(3)-O(20)	92.42(11)	C(31)-C(32)-C(33)	109.5(3)
O(21)-Mo(3)-O(20)	78.40(10)	C(32)-C(33)-C(34)	113.3(3)
O(28)-Mo(3)-O(20)	73.12(9)	C(36)-C(35)-N(2)	115.9(3)
O(23)-Mo(3)-O(18)	89.99(11)	C(35)-C(36)-C(37)	111.5(4)
O(25)-Mo(3)-O(18)	162.33(11)	C(36)-C(37)-C(38)	112.3(5)
O(21)-Mo(3)-O(18)	83.86(10)	C(40)-C(39)-N(2)	116.0(3)
O(28)-Mo(3)-O(18)	71.37(9)	C(39)-C(40)-C(41)	106.5(4)
O(20)-Mo(3)-O(18)	72.04(9)	C(42)-C(41)-C(40)	108.4(5)
O(23)-Mo(3)-Mo(7)	134.81(9)		

Symmetry transformations used to generate equivalent atoms:

#1 -x+1,-y+1,-z #2 -x,-y+1,-z #3 -x+1,-y+2,-z+1

Ortep style representation of $((n\text{-C}_4\text{H}_9)_4\text{N})_{2n}[\text{Ag}_2(\text{DMSO})_2\text{Mo}_8\text{O}_{26}]_n$ (**15**): thermal ellipsoids at 50% probability, hydrogen atoms are omitted for clarity. Not all carbon atoms are labelled and only one counterion shown for clarity.



6.11 Crystal data for (HDMF)_n[Ag₃(DMF)₄Mo₈O₂₆]_n (16)

Empirical formula	C ₁₅ H ₃₆ Ag ₃ Mo ₈ N ₅ O ₃₁	
Crystal growth	Diffusion of acetone , 21 days	
Crystal description	Colourless block crystals	
Crystal size	0.16 × 0.09 × 0.06 mm ³	
Formula weight	1873.62	
Temperature	150(2) K	
Wavelength	0.71073 Å	
Crystal system	Triclinic	
Space group	<i>P</i> -1	
Unit cell dimensions	<i>a</i> = 9.9458(4) Å	<i>α</i> = 62.938(2)°
	<i>b</i> = 10.8856(3) Å	<i>β</i> = 73.481(2)°
	<i>c</i> = 11.7553(5) Å	<i>γ</i> = 83.657(2)°
Volume	1086.31(7) Å ³	
<i>Z</i>	1	
Density (calculated)	2.864 Mg/m ³	
Absorption coefficient	3.644 mm ⁻¹	
<i>F</i> (000)	886	
Theta range for data collection	2.02 to 25.99°	
Index ranges	-11 ≤ <i>h</i> ≤ 12, -11 ≤ <i>k</i> ≤ 13, 0 ≤ <i>l</i> ≤ 14	
Reflections collected/ unique	15718 / 4260 [<i>R</i> (int) = 0.0431]	
Completeness to theta	25.99° 99.7 %	
Absorption correction	Gaussian	
Max. and min. transmission	0.8322 and 0.5866	
Refinement method	Full-matrix least-squares on <i>F</i> ²	
Data / restraints / parameters	4260 / 4 / 290	
Goodness-of-fit on <i>F</i> ²	1.054	
Final <i>R</i> indices [<i>I</i> > 2σ(<i>I</i>)]	<i>R</i> 1 = 0.0209, w <i>R</i> 2 = 0.0468	
<i>R</i> indices (all data)	<i>R</i> 1 = 0.0266, w <i>R</i> 2 = 0.0486	
Extinction coefficient	0.00115(9)	
Largest diff. peak and hole	0.80 and -0.64 e.Å ⁻³	

Bond lengths [Å] and angles [°]

Mo(1)-O(1)	1.716(2)	O(9)#1-Mo(3)-O(8)	157.45(10)
Mo(1)-O(5)	1.702(2)	O(10)#1-Mo(3)-O(8)	78.07(9)
Mo(1)-O(6)	2.004(2)	O(6)-Mo(3)-O(8)	78.36(9)
Mo(1)-O(7)	1.885(2)	O(3)-Mo(3)-O(8)#1	172.32(10)
Mo(1)-O(8)	2.316(2)	O(9)#1-Mo(3)-O(8)#1	82.11(9)
Mo(1)-O(10)	2.305(2)	O(10)#1-Mo(3)-O(8)#1	78.00(8)
Mo(2)-O(2)	1.723(2)	O(6)-Mo(3)-O(8)#1	77.95(8)
Mo(2)-O(7)	1.926(2)	O(8)-Mo(3)-O(8)#1	75.33(9)
Mo(2)-O(8)	2.460(2)	O(11)-Mo(4)-O(4)	105.17(12)
Mo(2)-O(9)	2.292(2)	O(11)-Mo(4)-O(12)#1	101.82(11)
Mo(2)-O(12)	1.926(2)	O(4)-Mo(4)-O(12)#1	100.45(11)
Mo(2)-O(13)	1.691(2)	O(11)-Mo(4)-O(10)	100.14(10)
Mo(3)-O(3)	1.703(2)	O(4)-Mo(4)-O(10)	96.48(11)
Mo(3)-O(9)#1	1.751(2)	O(12)#1-Mo(4)-O(10)	147.55(9)
Mo(3)-O(10)#1	1.946(2)	O(11)-Mo(4)-O(6)	90.02(10)
Mo(3)-O(6)	1.949(2)	O(4)-Mo(4)-O(6)	162.41(10)
Mo(3)-O(8)	2.165(2)	O(12)#1-Mo(4)-O(6)	84.68(9)
Mo(3)-O(8)#1	2.322(2)	O(10)-Mo(4)-O(6)	71.69(8)
Mo(4)-O(4)	1.708(2)	O(11)-Mo(4)-O(8)#1	161.53(10)
Mo(4)-O(6)	2.307(2)	O(4)-Mo(4)-O(8)#1	92.86(10)
Mo(4)-O(8)#1	2.315(2)	O(12)#1-Mo(4)-O(8)#1	78.31(9)
Mo(4)-O(10)	2.008(2)	O(10)-Mo(4)-O(8)#1	73.36(8)
Mo(4)-O(11)	1.703(2)	O(6)-Mo(4)-O(8)#1	71.55(8)
Mo(4)-O(12)#1	1.893(2)	O(1)-Ag(1)-O(4)#3	104.17(8)
Ag(1)-O(1)	2.393(2)	O(1)-Ag(1)-O(2)	78.62(8)
Ag(1)-O(2)	2.418(2)	O(4)#3-Ag(1)-O(2)	176.61(8)
Ag(1)-O(3)#2	2.436(2)	O(1)-Ag(1)-O(3)#2	176.98(8)
Ag(1)-O(4)#3	2.404(2)	O(4)#3-Ag(1)-O(3)#2	77.36(8)
Ag(1)-O(14)	2.442(3)	O(2)-Ag(1)-O(3)#2	99.77(8)
Ag(1)-Ag(1)#2	3.1475(6)	O(1)-Ag(1)-O(14)	94.20(9)
Ag(2)-O(5)	2.460(2)	O(4)#3-Ag(1)-O(14)	85.72(8)
Ag(2)-O(5)#4	2.460(2)	O(2)-Ag(1)-O(14)	96.05(9)
Ag(2)-O(11)	2.497(2)	O(3)#2-Ag(1)-O(14)	88.50(8)
Ag(2)-O(11)#4	2.497(2)	O(1)-Ag(1)-Ag(1)#2	65.46(6)
Ag(2)-O(15)#4	2.327(3)	O(4)#3-Ag(1)-Ag(1)#2	114.19(6)
Ag(2)-O(15)	2.327(3)	O(2)-Ag(1)-Ag(1)#2	65.04(6)
O(3)-Ag(1)#2	2.436(2)	O(3)#2-Ag(1)-Ag(1)#2	111.56(6)

O(4)-Ag(1)#5	2.404(2)	O(14)-Ag(1)-Ag(1)#2	153.85(6)
O(8)-Mo(4)#1	2.315(2)	O(15)#4-Ag(2)-O(15)	180
O(8)-Mo(3)#1	2.322(2)	O(15)#4-Ag(2)-O(5)	95.79(11)
O(9)-Mo(3)#1	1.751(2)	O(15)-Ag(2)-O(5)	84.21(10)
O(10)-Mo(3)#1	1.946(2)	O(15)#4-Ag(2)-O(5)#4	84.21(11)
O(12)-Mo(4)#1	1.893(2)	O(15)-Ag(2)-O(5)#4	95.79(10)
O(14)-C(1)	1.237(5)	O(5)-Ag(2)-O(5)#4	180
O(15)-C(4)	1.220(5)	O(15)#4-Ag(2)-O(11)	84.76(10)
N(1)-C(1)	1.320(5)	O(15)-Ag(2)-O(11)	95.24(10)
N(1)-C(3)	1.459(5)	O(5)-Ag(2)-O(11)	73.45(8)
N(1)-C(2)	1.462(5)	O(5)#4-Ag(2)-O(11)	106.55(8)
N(2)-C(4)	1.322(5)	O(15)#4-Ag(2)-O(11)#4	95.24(10)
N(2)-C(5)	1.451(5)	O(15)-Ag(2)-O(11)#4	84.76(10)
N(2)-C(6)	1.454(5)	O(5)-Ag(2)-O(11)#4	106.55(8)
N(3)-N(3)#6	1.086(15)	O(5)#4-Ag(2)-O(11)#4	73.45(8)
N(3)-C(8)	1.556(10)	O(11)-Ag(2)-O(11)#4	180
N(3)-C(7)	1.571(11)	Mo(1)-O(1)-Ag(1)	128.83(13)
C(9)-O(16)	1.340(14)	Mo(2)-O(2)-Ag(1)	131.95(13)
C(9)-O(16')	1.396(13)	Mo(3)-O(3)-Ag(1)#2	133.29(13)
C(9)-C(9)#6	1.64(3)	Mo(4)-O(4)-Ag(1)#5	137.96(13)
		Mo(1)-O(5)-Ag(2)	145.49(13)
O(5)-Mo(1)-O(1)	105.60(12)	Mo(3)-O(6)-Mo(1)	109.29(11)
O(5)-Mo(1)-O(7)	101.05(11)	Mo(3)-O(6)-Mo(4)	109.83(9)
O(1)-Mo(1)-O(7)	101.13(11)	Mo(1)-O(6)-Mo(4)	103.97(10)
O(5)-Mo(1)-O(6)	100.16(11)	Mo(1)-O(7)-Mo(2)	116.67(11)
O(1)-Mo(1)-O(6)	97.02(10)	Mo(3)-O(8)-Mo(4)#1	92.28(8)
O(7)-Mo(1)-O(6)	147.09(9)	Mo(3)-O(8)-Mo(1)	91.98(8)
O(5)-Mo(1)-O(10)	89.10(10)	Mo(4)#1-O(8)-Mo(1)	162.79(11)
O(1)-Mo(1)-O(10)	163.15(10)	Mo(3)-O(8)-Mo(3)#1	104.67(9)
O(7)-Mo(1)-O(10)	83.67(9)	Mo(4)#1-O(8)-Mo(3)#1	97.58(8)
O(6)-Mo(1)-O(10)	71.80(8)	Mo(1)-O(8)-Mo(3)#1	97.46(8)
O(5)-Mo(1)-O(8)	160.65(10)	Mo(3)-O(8)-Mo(2)	163.16(11)
O(1)-Mo(1)-O(8)	93.47(10)	Mo(4)#1-O(8)-Mo(2)	85.60(7)
O(7)-Mo(1)-O(8)	77.93(9)	Mo(1)-O(8)-Mo(2)	85.51(7)
O(6)-Mo(1)-O(8)	73.76(8)	Mo(3)#1-O(8)-Mo(2)	92.17(8)
O(10)-Mo(1)-O(8)	71.56(8)	Mo(3)#1-O(9)-Mo(2)	116.28(11)
O(13)-Mo(2)-O(2)	105.60(12)	Mo(3)#1-O(10)-Mo(4)	109.64(10)
O(13)-Mo(2)-O(12)	102.99(11)	Mo(3)#1-O(10)-Mo(1)	109.89(10)
O(2)-Mo(2)-O(12)	99.55(10)	Mo(4)-O(10)-Mo(1)	103.90(10)
O(13)-Mo(2)-O(7)	102.75(11)	Mo(4)-O(11)-Ag(2)	148.93(13)

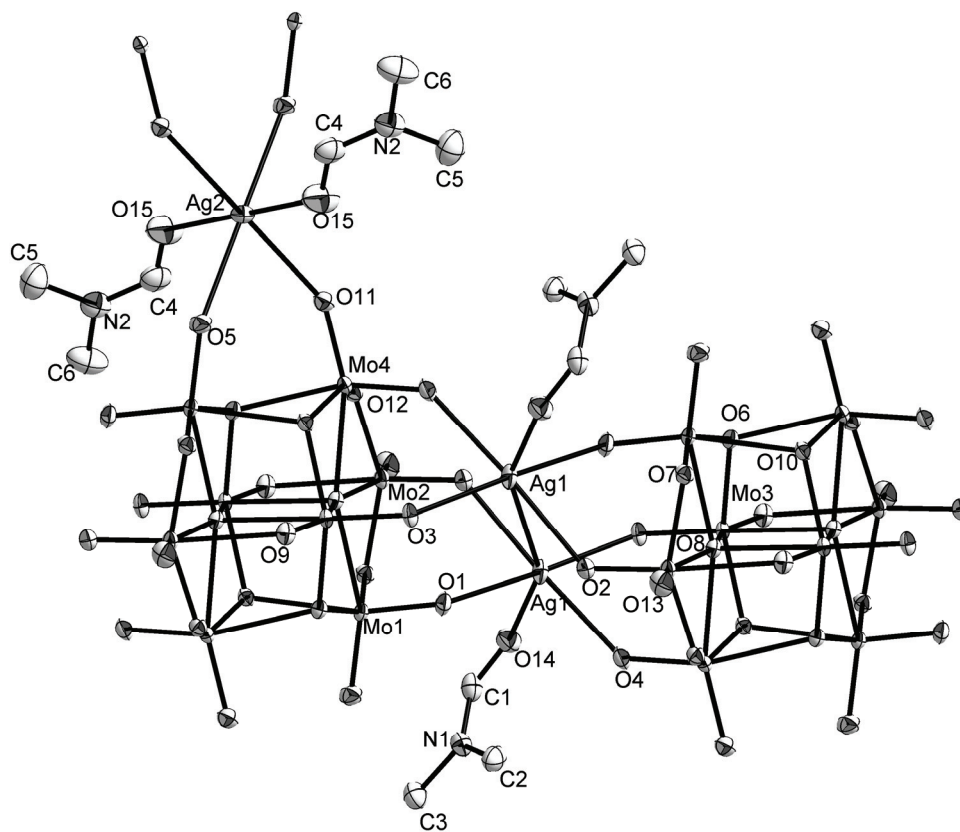
O(2)-Mo(2)-O(7)	97.28(11)	Mo(4)#1-O(12)-Mo(2)	116.44(12)
O(12)-Mo(2)-O(7)	144.01(10)	C(1)-O(14)-Ag(1)	143.1(3)
O(13)-Mo(2)-O(9)	92.72(11)	C(4)-O(15)-Ag(2)	130.9(3)
O(2)-Mo(2)-O(9)	161.61(11)	C(1)-N(1)-C(3)	121.0(3)
O(12)-Mo(2)-O(9)	77.41(9)	C(1)-N(1)-C(2)	121.8(3)
O(7)-Mo(2)-O(9)	76.65(9)	C(3)-N(1)-C(2)	117.2(3)
O(13)-Mo(2)-O(8)	162.15(10)	C(4)-N(2)-C(5)	121.9(4)
O(2)-Mo(2)-O(8)	92.24(10)	C(4)-N(2)-C(6)	121.7(4)
O(12)-Mo(2)-O(8)	74.13(8)	C(5)-N(2)-C(6)	116.4(4)
O(7)-Mo(2)-O(8)	73.64(8)	O(14)-C(1)-N(1)	126.5(4)
O(9)-Mo(2)-O(8)	69.43(8)	O(15)-C(4)-N(2)	124.2(4)
O(3)-Mo(3)-O(9)#1	105.57(11)	N(3)#6-N(3)-C(8)	121.3(10)
O(3)-Mo(3)-O(10)#1	100.42(10)	N(3)#6-N(3)-C(7)	127.4(10)
O(9)#1-Mo(3)-O(10)#1	97.42(10)	C(8)-N(3)-C(7)	111.3(8)
O(3)-Mo(3)-O(6)	100.96(10)	O(16)-C(9)-O(16')	128.0(13)
O(9)#1-Mo(3)-O(6)	97.12(10)	O(16)-C(9)-C(9)#6	114.9(13)
O(10)#1-Mo(3)-O(6)	149.79(9)	O(16')-C(9)-C(9)#6	117.1(12)
O(3)-Mo(3)-O(8)	96.99(10)		

Symmetry transformations used to generate equivalent atoms:

#1 $-x+2, -y, -z+2$ #2 $-x+1, -y, -z+2$ #3 $x-1, y, z$

#4 $-x+2, -y+1, -z+1$ #5 $x+1, y, z$ #6 $-x+2, -y+1, -z$

Ortep style representation of $(\text{HDMF})_n[\text{Ag}_3(\text{DMF})_4\text{Mo}_8\text{O}_{26}]_n$ (**16**): thermal ellipsoids at 50% probability, hydrogen atoms and counterions are omitted for clarity.



6.12 Crystal data for [(Ag(DMF))₂(Ag(DMF))₂Mo₈O₂₆]_n (17)

Empirical formula	C ₁₈ H ₄₂ Ag ₄ Mo ₈ N ₆ O ₃₂	
Crystal growth	Diffusion of diethyl ether, 5 days	
Crystal description	Colourless block crystals	
Crystal size	0.34 × 0.18 × 0.12 mm ³	
Formula weight	2053.58	
Temperature	150(2) K	
Wavelength	0.71073 Å	
Crystal system	Triclinic	
Space group	<i>P</i> -1	
Unit cell dimensions	<i>a</i> = 10.1101(2) Å	<i>α</i> = 63.312(1)°
	<i>b</i> = 11.4232(3) Å	<i>β</i> = 76.600(2)°
	<i>c</i> = 11.5474(3) Å	<i>γ</i> = 88.951(1)°
Volume	1153.43(5) Å ³	
<i>Z</i>	1	
Density (calculated)	2.956 Mg/m ³	
Absorption coefficient	3.852 mm ⁻¹	
<i>F</i> (000)	972	
Theta range for data collection	2.08 to 25.98°	
Index ranges	-12 ≤ <i>h</i> ≤ 12, -12 ≤ <i>k</i> ≤ 14, 0 ≤ <i>l</i> ≤ 14	
Reflections collected/ unique	15599 / 4455 [<i>R</i> (int) = 0.0383]	
Completeness to theta	25.98° 98.3 %	
Absorption correction	Gaussian	
Max. and min. transmission	0.681 and 0.278	
Refinement method	Full-matrix least-squares on <i>F</i> ²	
Data / restraints / parameters	4455 / 0 / 314	
Goodness-of-fit on <i>F</i> ²	1.091	
Final <i>R</i> indices [<i>I</i> > 2σ(<i>I</i>)]	<i>R</i> 1 = 0.0225, w <i>R</i> 2 = 0.0514	
<i>R</i> indices (all data)	<i>R</i> 1 = 0.0255, w <i>R</i> 2 = 0.0525	
Extinction coefficient	0.0044(2)	
Largest diff. peak and hole	1.12 and -1.11 e.Å ⁻³	

Bond lengths [\AA] and angles [$^\circ$]

Ag(1)-O(4)#1	2.399(2)	O(6)-Mo(1)-O(13)	75.30(8)
Ag(1)-O(1)	2.441(2)	O(12)-Mo(1)-O(13)	74.56(9)
Ag(1)-O(14)	2.461(2)	O(9)-Mo(1)-O(13)	69.72(8)
Ag(1)-O(2)	2.565(2)	O(7)-Mo(2)-O(2)	105.31(12)
Ag(1)-O(3)#1	2.592(2)	O(7)-Mo(2)-O(6)	102.12(11)
Ag(1)-Ag(1)#1	3.0549(5)	O(2)-Mo(2)-O(6)	99.48(11)
Ag(2)-O(15)	2.302(3)	O(7)-Mo(2)-O(8)#3	101.45(11)
Ag(2)-O(16)	2.302(3)	O(2)-Mo(2)-O(8)#3	98.10(10)
Ag(2)-O(14)#2	2.395(2)	O(6)-Mo(2)-O(8)#3	145.56(10)
Ag(2)-O(5)	2.531(2)	O(7)-Mo(2)-O(10)#3	91.41(11)
Mo(1)-O(5)	1.695(2)	O(2)-Mo(2)-O(10)#3	162.12(10)
Mo(1)-O(1)	1.726(2)	O(6)-Mo(2)-O(10)#3	82.76(9)
Mo(1)-O(6)	1.918(2)	O(8)#3-Mo(2)-O(10)#3	71.90(8)
Mo(1)-O(12)	1.925(2)	O(7)-Mo(2)-O(13)	162.72(11)
Mo(1)-O(9)	2.271(2)	O(2)-Mo(2)-O(13)	91.74(10)
Mo(1)-O(13)	2.425(2)	O(6)-Mo(2)-O(13)	77.31(9)
Mo(2)-O(7)	1.698(2)	O(8)#3-Mo(2)-O(13)	72.77(8)
Mo(2)-O(2)	1.724(2)	O(10)#3-Mo(2)-O(13)	71.34(8)
Mo(2)-O(6)	1.888(2)	O(3)-Mo(3)-O(9)#3	105.79(11)
Mo(2)-O(8)#3	1.993(2)	O(3)-Mo(3)-O(10)	102.56(11)
Mo(2)-O(10)#3	2.309(2)	O(9)#3-Mo(3)-O(10)	97.46(10)
Mo(2)-O(13)	2.366(2)	O(3)-Mo(3)-O(8)#3	99.99(11)
Mo(3)-O(3)	1.701(2)	O(9)#3-Mo(3)-O(8)#3	95.49(10)
Mo(3)-O(9)#3	1.748(2)	O(10)-Mo(3)-O(8)#3	149.76(9)
Mo(3)-O(10)	1.946(2)	O(3)-Mo(3)-O(13)	98.31(10)
Mo(3)-O(8)#3	1.961(2)	O(9)#3-Mo(3)-O(13)	155.86(10)
Mo(3)-O(13)	2.143(2)	O(10)-Mo(3)-O(13)	78.43(9)
Mo(3)-O(13)#3	2.351(2)	O(8)#3-Mo(3)-O(13)	78.60(9)
Mo(4)-O(11)	1.695(2)	O(3)-Mo(3)-O(13)#3	173.44(9)
Mo(4)-O(4)	1.718(2)	O(9)#3-Mo(3)-O(13)#3	80.48(9)
Mo(4)-O(12)	1.898(2)	O(10)-Mo(3)-O(13)#3	78.15(9)
Mo(4)-O(10)	2.005(2)	O(8)#3-Mo(3)-O(13)#3	77.21(9)
Mo(4)-O(8)	2.306(2)	O(13)-Mo(3)-O(13)#3	75.39(9)
Mo(4)-O(13)	2.314(2)	O(11)-Mo(4)-O(4)	104.94(12)
O(3)-Ag(1)#1	2.592(2)	O(11)-Mo(4)-O(12)	101.41(11)
O(4)-Ag(1)#1	2.399(2)	O(4)-Mo(4)-O(12)	99.83(11)
O(8)-Mo(3)#3	1.961(2)	O(11)-Mo(4)-O(10)	101.31(10)

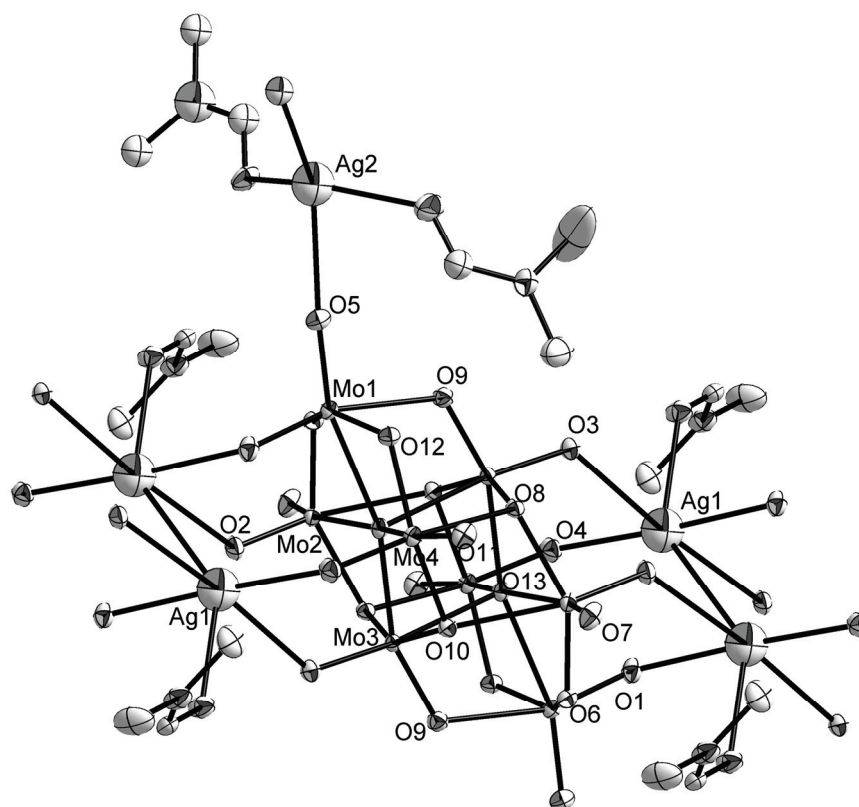
O(8)-Mo(2)#3	1.993(2)	O(4)-Mo(4)-O(10)	96.19(10)
O(9)-Mo(3)#3	1.748(2)	O(12)-Mo(4)-O(10)	147.66(10)
O(10)-Mo(2)#3	2.309(2)	O(11)-Mo(4)-O(8)	89.44(10)
O(13)-Mo(3)#3	2.351(2)	O(4)-Mo(4)-O(8)	163.05(10)
O(14)-C(1)	1.247(5)	O(12)-Mo(4)-O(8)	85.74(9)
O(14)-Ag(2)#2	2.395(2)	O(10)-Mo(4)-O(8)	71.78(8)
O(15)-C(4)	1.239(4)	O(11)-Mo(4)-O(13)	161.18(10)
O(16)-C(7)	1.222(5)	O(4)-Mo(4)-O(13)	93.65(10)
N(1)-C(1)	1.329(5)	O(12)-Mo(4)-O(13)	77.81(9)
N(1)-C(3)	1.447(5)	O(10)-Mo(4)-O(13)	73.28(8)
N(1)-C(2)	1.461(5)	O(8)-Mo(4)-O(13)	71.74(8)
N(2)-C(4)	1.331(5)	Mo(1)-O(1)-Ag(1)	132.58(13)
N(2)-C(5)	1.448(5)	Mo(2)-O(2)-Ag(1)	129.08(12)
N(2)-C(6)	1.459(5)	Mo(3)-O(3)-Ag(1)#1	125.23(12)
N(3)-C(7)	1.294(5)	Mo(4)-O(4)-Ag(1)#1	132.33(13)
N(3)-C(8)	1.427(7)	Mo(1)-O(5)-Ag(2)	174.81(15)
N(3)-C(9)	1.462(5)	Mo(2)-O(6)-Mo(1)	116.18(11)
		Mo(3)#3-O(8)-Mo(2)#3	110.17(10)
O(4)#1-Ag(1)-O(1)	176.85(8)	Mo(3)#3-O(8)-Mo(4)	110.44(10)
O(4)#1-Ag(1)-O(14)	90.91(8)	Mo(2)#3-O(8)-Mo(4)	103.61(9)
O(1)-Ag(1)-O(14)	85.94(9)	Mo(3)#3-O(9)-Mo(1)	117.40(11)
O(4)#1-Ag(1)-O(2)	108.07(8)	Mo(3)-O(10)-Mo(4)	109.20(10)
O(1)-Ag(1)-O(2)	72.52(8)	Mo(3)-O(10)-Mo(2)#3	111.24(10)
O(14)-Ag(1)-O(2)	99.06(8)	Mo(4)-O(10)-Mo(2)#3	103.12(9)
O(4)#1-Ag(1)-O(3)#1	76.34(8)	Mo(4)-O(12)-Mo(1)	116.45(12)
O(1)-Ag(1)-O(3)#1	102.94(8)	Mo(3)-O(13)-Mo(4)	92.44(8)
O(14)-Ag(1)-O(3)#1	78.12(8)	Mo(3)-O(13)-Mo(3)#3	104.61(9)
O(2)-Ag(1)-O(3)#1	174.92(7)	Mo(4)-O(13)-Mo(3)#3	97.61(8)
O(4)#1-Ag(1)-Ag(1)#1	126.06(6)	Mo(3)-O(13)-Mo(2)	91.83(8)
O(1)-Ag(1)-Ag(1)#1	57.03(6)	Mo(4)-O(13)-Mo(2)	163.76(11)
O(14)-Ag(1)-Ag(1)#1	141.19(6)	Mo(3)#3-O(13)-Mo(2)	96.46(8)
O(2)-Ag(1)-Ag(1)#1	61.51(6)	Mo(3)-O(13)-Mo(1)	163.02(11)
O(3)#1-Ag(1)-Ag(1)#1	118.23(5)	Mo(4)-O(13)-Mo(1)	86.55(7)
O(15)-Ag(2)-O(16)	141.35(11)	Mo(3)#3-O(13)-Mo(1)	92.32(8)
O(15)-Ag(2)-O(14)#2	111.97(9)	Mo(2)-O(13)-Mo(1)	84.81(7)
O(16)-Ag(2)-O(14)#2	99.47(10)	C(1)-O(14)-Ag(2)#2	117.8(2)
O(15)-Ag(2)-O(5)	84.77(8)	C(1)-O(14)-Ag(1)	132.7(2)
O(16)-Ag(2)-O(5)	80.80(9)	Ag(2)#2-O(14)-Ag(1)	107.72(10)
O(14)#2-Ag(2)-O(5)	146.29(8)	C(4)-O(15)-Ag(2)	116.5(2)
O(5)-Mo(1)-O(1)	105.48(12)	C(7)-O(16)-Ag(2)	130.3(3)

O(5)-Mo(1)-O(6)	102.21(11)	C(1)-N(1)-C(3)	120.5(3)
O(1)-Mo(1)-O(6)	97.83(11)	C(1)-N(1)-C(2)	121.8(4)
O(5)-Mo(1)-O(12)	101.88(11)	C(3)-N(1)-C(2)	117.7(3)
O(1)-Mo(1)-O(12)	98.60(11)	C(4)-N(2)-C(5)	121.3(3)
O(6)-Mo(1)-O(12)	145.89(10)	C(4)-N(2)-C(6)	121.1(3)
O(5)-Mo(1)-O(9)	93.18(10)	C(5)-N(2)-C(6)	117.5(3)
O(1)-Mo(1)-O(9)	161.34(10)	C(7)-N(3)-C(8)	120.8(4)
O(6)-Mo(1)-O(9)	77.56(9)	C(7)-N(3)-C(9)	123.4(4)
O(12)-Mo(1)-O(9)	77.33(9)	C(8)-N(3)-C(9)	115.7(4)
O(5)-Mo(1)-O(13)	162.90(10)	O(14)-C(1)-N(1)	124.9(4)
O(1)-Mo(1)-O(13)	91.62(10)	O(15)-C(4)-N(2)	123.9(3)
		O(16)-C(7)-N(3)	127.4(4)

Symmetry transformations used to generate equivalent atoms:

#1 $-x+2, -y+1, -z+1$ #2 $-x+2, -y, -z+1$ #3 $-x+1, -y+1, -z+1$

Ortep style representation of $[(\text{Ag}(\text{DMF}))_2(\text{Ag}(\text{DMF})_2)_2\text{Mo}_8\text{O}_{26}]_n$ (**17**): thermal ellipsoids at 50% probability, hydrogen atoms are omitted for clarity. Carbon, nitrogen and oxygen atoms of DMF are not labelled.



6.13 Crystal data for $[(\text{Ag}(\text{CH}_3\text{CN})_3)_2(\text{Ag}(\text{CH}_3\text{CN})_2)\text{AgMo}_8\text{O}_{26}]_n$ (18)

Empirical formula	$\text{C}_{16}\text{H}_{24}\text{Ag}_4\text{Mo}_8\text{N}_8\text{O}_{26}$
Crystal growth	Diffusion of diethyl ether, 4 days
Crystal description	Colourless block crystals
Crystal size	$0.20 \times 0.10 \times 0.10 \text{ mm}^3$
Formula weight	1943.43
Temperature	120(2) K
Wavelength	0.71073 Å
Crystal system	Triclinic
Space group	<i>P</i> -1
Unit cell dimensions	$a = 11.0978(2) \text{ Å}$ $\alpha = 97.212(2)^\circ$ $b = 12.7612(3) \text{ Å}$ $\beta = 97.158(2)^\circ$ $c = 15.6460(3) \text{ Å}$ $\gamma = 99.247(2)^\circ$
Volume	$2145.86(8) \text{ Å}^3$
<i>Z</i>	2
Density (calculated)	3.008 Mg/m^3
Absorption coefficient	4.123 mm^{-1}
<i>F</i> (000)	1816
Theta range for data collection	1.88 to 26.00°
Index ranges	$-13 \leq h \leq 13$, $-15 \leq k \leq 15$, $-19 \leq l \leq 19$
Reflections collected/ unique	35450 / 8435 [<i>R</i> (int) = 0.0384]
Completeness to theta	26.00° 99.8 %
Absorption correction	Empirical
Max. and min. transmission	0.6832 and 0.4927
Refinement method	Full-matrix least-squares on F^2
Data / restraints / parameters	8435 / 0 / 568
Goodness-of-fit on F^2	1.060
Final <i>R</i> indices [<i>I</i> > 2σ(<i>I</i>)]	<i>R</i> 1 = 0.0230, w <i>R</i> 2 = 0.0387
<i>R</i> indices (all data)	<i>R</i> 1 = 0.0394, w <i>R</i> 2 = 0.0419
Extinction coefficient	0.00022(2)
Largest diff. peak and hole	0.57 and -0.67 e.Å ⁻³

Bond lengths [Å] and angles [°]

Ag(1)-O(2)	2.395(2)	O(13)-Mo(3)-O(4)	80.98(9)
Ag(1)-O(14)	2.437(2)	O(6)#1-Mo(3)-O(4)	77.25(8)
Ag(1)-O(1)	2.498(2)	O(11)-Mo(3)-O(4)	77.76(8)
Ag(1)-O(15)	2.509(2)	O(4)#1-Mo(3)-O(4)	75.32(9)
Ag(2)-N(2)	2.167(3)	O(3)-Mo(4)-O(9)#1	105.48(11)
Ag(2)-N(1)	2.173(3)	O(3)-Mo(4)-O(8)	100.82(10)
Ag(2)-O(7)	2.532(2)	O(9)#1-Mo(4)-O(8)	101.44(11)
Ag(2)-O(9)	2.546(2)	O(3)-Mo(4)-O(11)#1	95.97(10)
Ag(3)-N(3)	2.223(4)	O(9)#1-Mo(4)-O(11)#1	99.85(10)
Ag(3)-N(5)	2.233(4)	O(8)-Mo(4)-O(11)#1	148.15(9)
Ag(3)-N(4)	2.243(4)	O(3)-Mo(4)-O(6)#1	161.98(9)
Ag(3)-O(17)	2.590(2)	O(9)#1-Mo(4)-O(6)#1	89.87(9)
Ag(4)-N(6)	2.179(3)	O(8)-Mo(4)-O(6)#1	84.93(9)
Ag(4)-N(8)	2.215(3)	O(11)#1-Mo(4)-O(6)#1	71.68(8)
Ag(4)-N(7)	2.225(4)	O(3)-Mo(4)-O(4)	92.34(10)
Mo(1)-O(10)	1.701(2)	O(9)#1-Mo(4)-O(4)	161.71(9)
Mo(1)-O(1)	1.709(2)	O(8)-Mo(4)-O(4)	78.70(9)
Mo(1)-O(5)	1.923(2)	O(11)#1-Mo(4)-O(4)	73.73(8)
Mo(1)-O(8)	1.927(2)	O(6)#1-Mo(4)-O(4)	71.88(8)
Mo(1)-O(13)	2.268(2)	O(17)-Mo(5)-O(15)	106.08(11)
Mo(1)-O(4)	2.449(2)	O(17)-Mo(5)-O(18)	102.16(10)
Mo(2)-O(2)	1.713(2)	O(15)-Mo(5)-O(18)	97.97(10)
Mo(2)-O(7)	1.714(2)	O(17)-Mo(5)-O(21)	102.35(11)
Mo(2)-O(5)	1.885(2)	O(15)-Mo(5)-O(21)	96.92(10)
Mo(2)-O(6)	1.999(2)	O(18)-Mo(5)-O(21)	146.41(9)
Mo(2)-O(11)	2.297(2)	O(17)-Mo(5)-O(23)	94.10(9)
Mo(2)-O(4)	2.322(2)	O(15)-Mo(5)-O(23)	159.80(10)
Mo(3)-O(12)	1.693(2)	O(18)-Mo(5)-O(23)	78.17(8)
Mo(3)-O(13)	1.748(2)	O(21)-Mo(5)-O(23)	77.49(8)
Mo(3)-O(6)#1	1.950(2)	O(17)-Mo(5)-O(22)	164.40(9)
Mo(3)-O(11)	1.957(2)	O(15)-Mo(5)-O(22)	89.51(9)
Mo(3)-O(4)#1	2.157(2)	O(18)-Mo(5)-O(22)	75.03(8)
Mo(3)-O(4)	2.345(2)	O(21)-Mo(5)-O(22)	75.17(8)
Mo(4)-O(3)	1.704(2)	O(23)-Mo(5)-O(22)	70.30(8)
Mo(4)-O(9)#1	1.715(2)	O(25)-Mo(6)-O(14)	105.25(11)
Mo(4)-O(8)	1.893(2)	O(25)-Mo(6)-O(21)	103.13(10)
Mo(4)-O(11)#1	2.011(2)	O(14)-Mo(6)-O(21)	101.26(10)

Mo(4)-O(6)#1	2.289(2)	O(25)-Mo(6)-O(24)	99.93(10)
Mo(4)-O(4)	2.309(2)	O(14)-Mo(6)-O(24)	95.62(10)
Mo(5)-O(17)	1.704(2)	O(21)-Mo(6)-O(24)	146.54(9)
Mo(5)-O(15)	1.709(2)	O(25)-Mo(6)-O(20)	91.75(9)
Mo(5)-O(18)	1.925(2)	O(14)-Mo(6)-O(20)	160.73(10)
Mo(5)-O(21)	1.932(2)	O(21)-Mo(6)-O(20)	83.22(8)
Mo(5)-O(23)	2.257(2)	O(24)-Mo(6)-O(20)	72.10(8)
Mo(5)-O(22)	2.422(2)	O(25)-Mo(6)-O(22)	163.13(9)
Mo(6)-O(25)	1.700(2)	O(14)-Mo(6)-O(22)	90.93(9)
Mo(6)-O(14)	1.714(2)	O(21)-Mo(6)-O(22)	77.80(9)
Mo(6)-O(21)	1.890(2)	O(24)-Mo(6)-O(22)	73.21(8)
Mo(6)-O(24)	2.006(2)	O(20)-Mo(6)-O(22)	71.54(7)
Mo(6)-O(20)	2.297(2)	O(19)-Mo(7)-O(16)	104.82(11)
Mo(6)-O(22)	2.347(2)	O(19)-Mo(7)-O(18)	101.09(11)
Mo(7)-O(19)	1.705(2)	O(16)-Mo(7)-O(18)	100.39(10)
Mo(7)-O(16)	1.711(2)	O(19)-Mo(7)-O(20)#2	101.13(10)
Mo(7)-O(18)	1.898(2)	O(16)-Mo(7)-O(20)#2	97.13(10)
Mo(7)-O(20)#2	1.997(2)	O(18)-Mo(7)-O(20)#2	147.01(9)
Mo(7)-O(24)#2	2.320(2)	O(19)-Mo(7)-O(24)#2	90.59(9)
Mo(7)-O(22)	2.327(2)	O(16)-Mo(7)-O(24)#2	162.70(9)
Mo(7)-Mo(8)#2	3.2176(4)	O(18)-Mo(7)-O(24)#2	83.96(8)
Mo(8)-O(26)	1.688(2)	O(20)#2-Mo(7)-O(24)#2	71.74(8)
Mo(8)-O(23)	1.757(2)	O(19)-Mo(7)-O(22)	161.85(9)
Mo(8)-O(24)#2	1.954(2)	O(16)-Mo(7)-O(22)	93.12(9)
Mo(8)-O(20)	1.958(2)	O(18)-Mo(7)-O(22)	77.90(9)
Mo(8)-O(22)#2	2.139(2)	O(20)#2-Mo(7)-O(22)	73.41(8)
Mo(8)-O(22)	2.330(2)	O(24)#2-Mo(7)-O(22)	71.26(7)
Mo(8)-Mo(7)#2	3.2176(4)	O(19)-Mo(7)-Mo(8)#2	136.20(8)
O(4)-Mo(3)#1	2.157(2)	O(16)-Mo(7)-Mo(8)#2	84.52(8)
O(6)-Mo(3)#1	1.950(2)	O(18)-Mo(7)-Mo(8)#2	119.51(7)
O(6)-Mo(4)#1	2.289(2)	O(20)#2-Mo(7)-Mo(8)#2	35.15(6)
O(9)-Mo(4)#1	1.715(2)	O(24)#2-Mo(7)-Mo(8)#2	78.83(5)
O(11)-Mo(4)#1	2.011(2)	O(22)-Mo(7)-Mo(8)#2	41.63(6)
O(20)-Mo(7)#2	1.997(2)	O(26)-Mo(8)-O(23)	105.65(11)
O(22)-Mo(8)#2	2.139(2)	O(26)-Mo(8)-O(24)#2	101.24(10)
O(24)-Mo(8)#2	1.954(2)	O(23)-Mo(8)-O(24)#2	95.97(10)
O(24)-Mo(7)#2	2.320(2)	O(26)-Mo(8)-O(20)	100.65(10)
N(1)-C(1)	1.137(5)	O(23)-Mo(8)-O(20)	96.91(10)
N(2)-C(3)	1.127(5)	O(24)#2-Mo(8)-O(20)	150.50(9)
N(3)-C(5)	1.130(5)	O(26)-Mo(8)-O(22)#2	97.70(10)

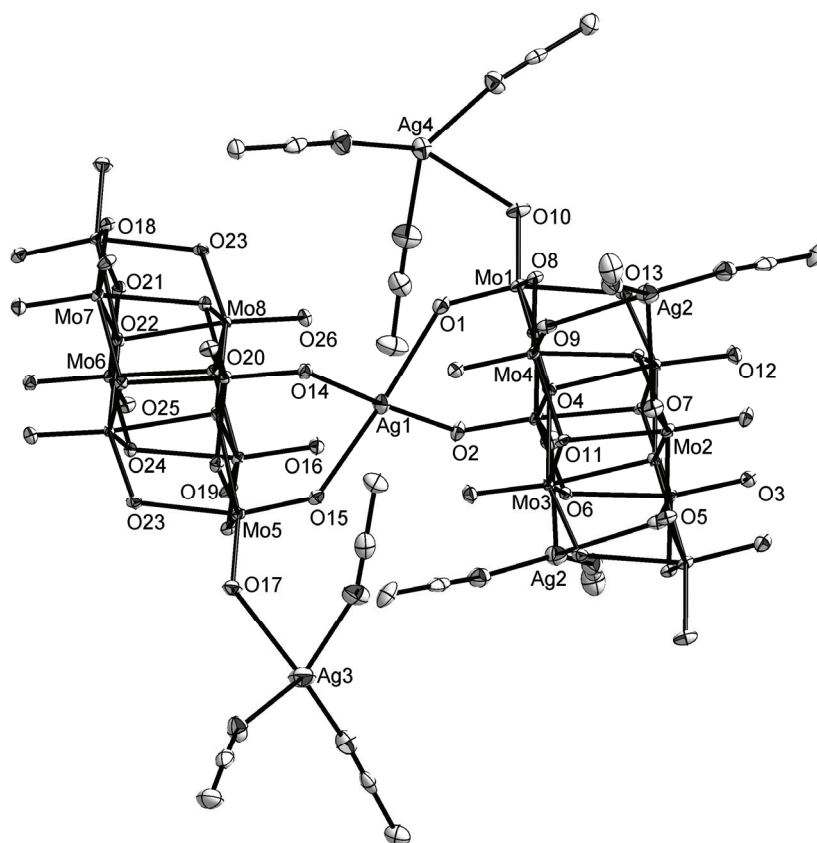
N(4)-C(7)	1.138(5)	O(23)-Mo(8)-O(22)#2	156.65(9)
N(5)-C(9)	1.126(5)	O(24)#2-Mo(8)-O(22)#2	79.10(9)
N(6)-C(11)	1.128(4)	O(20)-Mo(8)-O(22)#2	78.59(9)
N(7)-C(13)	1.142(5)	O(26)-Mo(8)-O(22)	173.03(10)
N(8)-C(15)	1.137(4)	O(23)-Mo(8)-O(22)	81.31(9)
C(1)-C(2)	1.449(5)	O(24)#2-Mo(8)-O(22)	77.83(8)
C(3)-C(4)	1.459(5)	O(20)-Mo(8)-O(22)	78.04(8)
C(5)-C(6)	1.462(5)	O(22)#2-Mo(8)-O(22)	75.34(9)
C(7)-C(8)	1.441(6)	O(26)-Mo(8)-Mo(7)#2	88.93(8)
C(9)-C(10)	1.467(6)	O(23)-Mo(8)-Mo(7)#2	132.88(7)
C(11)-C(12)	1.463(5)	O(24)#2-Mo(8)-Mo(7)#2	125.37(7)
C(13)-C(14)	1.437(6)	O(20)-Mo(8)-Mo(7)#2	35.97(7)
C(15)-C(16)	1.452(5)	O(22)#2-Mo(8)-Mo(7)#2	46.28(6)
		O(22)-Mo(8)-Mo(7)#2	86.09(5)
O(2)-Ag(1)-O(14)	177.13(8)	Mo(1)-O(1)-Ag(1)	135.82(12)
O(2)-Ag(1)-O(1)	77.83(8)	Mo(2)-O(2)-Ag(1)	136.06(12)
O(14)-Ag(1)-O(1)	99.34(7)	Mo(3)#1-O(4)-Mo(4)	92.53(9)
O(2)-Ag(1)-O(15)	109.27(8)	Mo(3)#1-O(4)-Mo(2)	92.11(8)
O(14)-Ag(1)-O(15)	73.57(7)	Mo(4)-O(4)-Mo(2)	163.54(10)
O(1)-Ag(1)-O(15)	172.41(7)	Mo(3)#1-O(4)-Mo(3)	104.68(9)
N(2)-Ag(2)-N(1)	144.47(12)	Mo(4)-O(4)-Mo(3)	97.10(8)
N(2)-Ag(2)-O(7)	107.94(10)	Mo(2)-O(4)-Mo(3)	96.98(8)
N(1)-Ag(2)-O(7)	93.05(10)	Mo(3)#1-O(4)-Mo(1)	163.47(10)
N(2)-Ag(2)-O(9)	98.60(10)	Mo(4)-O(4)-Mo(1)	85.63(7)
N(1)-Ag(2)-O(9)	115.48(10)	Mo(2)-O(4)-Mo(1)	85.44(8)
O(7)-Ag(2)-O(9)	71.07(7)	Mo(3)-O(4)-Mo(1)	91.84(8)
N(3)-Ag(3)-N(5)	119.02(12)	Mo(2)-O(5)-Mo(1)	116.52(12)
N(3)-Ag(3)-N(4)	110.64(12)	Mo(3)#1-O(6)-Mo(2)	109.62(10)
N(5)-Ag(3)-N(4)	121.18(13)	Mo(3)#1-O(6)-Mo(4)#1	110.53(10)
N(3)-Ag(3)-O(17)	119.55(11)	Mo(2)-O(6)-Mo(4)#1	104.32(9)
N(5)-Ag(3)-O(17)	79.01(10)	Mo(2)-O(7)-Ag(2)	119.00(12)
N(4)-Ag(3)-O(17)	102.78(10)	Mo(4)-O(8)-Mo(1)	115.73(11)
N(6)-Ag(4)-N(8)	131.25(12)	Mo(4)#1-O(9)-Ag(2)	130.90(11)
N(6)-Ag(4)-N(7)	122.31(12)	Mo(3)-O(11)-Mo(4)#1	108.90(11)
N(8)-Ag(4)-N(7)	105.79(12)	Mo(3)-O(11)-Mo(2)	110.21(9)
O(10)-Mo(1)-O(1)	105.46(12)	Mo(4)#1-O(11)-Mo(2)	103.63(9)
O(10)-Mo(1)-O(5)	102.92(11)	Mo(3)-O(13)-Mo(1)	117.56(11)
O(1)-Mo(1)-O(5)	98.69(10)	Mo(6)-O(14)-Ag(1)	135.11(12)
O(10)-Mo(1)-O(8)	102.54(11)	Mo(5)-O(15)-Ag(1)	135.76(12)
O(1)-Mo(1)-O(8)	96.93(10)	Mo(5)-O(17)-Ag(3)	140.39(12)

O(5)-Mo(1)-O(8)	145.21(9)	Mo(7)-O(18)-Mo(5)	115.85(11)
O(10)-Mo(1)-O(13)	94.39(10)	Mo(8)-O(20)-Mo(7)#2	108.88(11)
O(1)-Mo(1)-O(13)	160.14(10)	Mo(8)-O(20)-Mo(6)	110.57(9)
O(5)-Mo(1)-O(13)	77.15(9)	Mo(7)#2-O(20)-Mo(6)	104.09(9)
O(8)-Mo(1)-O(13)	77.64(8)	Mo(6)-O(21)-Mo(5)	115.62(12)
O(10)-Mo(1)-O(4)	164.00(9)	Mo(8)#2-O(22)-Mo(7)	92.09(8)
O(1)-Mo(1)-O(4)	90.54(10)	Mo(8)#2-O(22)-Mo(8)	104.66(9)
O(5)-Mo(1)-O(4)	74.39(9)	Mo(7)-O(22)-Mo(8)	97.95(8)
O(8)-Mo(1)-O(4)	74.58(8)	Mo(8)#2-O(22)-Mo(6)	91.96(8)
O(13)-Mo(1)-O(4)	69.61(8)	Mo(7)-O(22)-Mo(6)	162.97(10)
O(2)-Mo(2)-O(7)	105.23(11)	Mo(8)-O(22)-Mo(6)	97.01(8)
O(2)-Mo(2)-O(5)	101.20(11)	Mo(8)#2-O(22)-Mo(5)	163.28(10)
O(7)-Mo(2)-O(5)	102.42(11)	Mo(7)-O(22)-Mo(5)	85.98(7)
O(2)-Mo(2)-O(6)	95.84(10)	Mo(8)-O(22)-Mo(5)	92.05(8)
O(7)-Mo(2)-O(6)	99.81(10)	Mo(6)-O(22)-Mo(5)	85.39(7)
O(5)-Mo(2)-O(6)	147.19(9)	Mo(8)-O(23)-Mo(5)	116.32(11)
O(2)-Mo(2)-O(11)	161.88(10)	Mo(8)#2-O(24)-Mo(6)	109.21(10)
O(7)-Mo(2)-O(11)	90.15(9)	Mo(8)#2-O(24)-Mo(7)#2	110.27(9)
O(5)-Mo(2)-O(11)	84.37(9)	Mo(6)-O(24)-Mo(7)#2	102.99(9)
O(6)-Mo(2)-O(11)	71.69(8)	C(1)-N(1)-Ag(2)	174.7(3)
O(2)-Mo(2)-O(4)	92.04(9)	C(3)-N(2)-Ag(2)	160.2(3)
O(7)-Mo(2)-O(4)	162.11(9)	C(5)-N(3)-Ag(3)	168.7(3)
O(5)-Mo(2)-O(4)	78.23(9)	C(7)-N(4)-Ag(3)	155.7(3)
O(6)-Mo(2)-O(4)	73.31(8)	C(9)-N(5)-Ag(3)	158.9(3)
O(11)-Mo(2)-O(4)	72.06(7)	C(11)-N(6)-Ag(4)	166.7(3)
O(12)-Mo(3)-O(13)	105.85(11)	C(13)-N(7)-Ag(4)	171.6(4)
O(12)-Mo(3)-O(6)#1	101.04(10)	C(15)-N(8)-Ag(4)	168.7(3)
O(13)-Mo(3)-O(6)#1	97.35(10)	N(1)-C(1)-C(2)	179.2(4)
O(12)-Mo(3)-O(11)	101.62(10)	N(2)-C(3)-C(4)	179.1(4)
O(13)-Mo(3)-O(11)	96.26(10)	N(3)-C(5)-C(6)	179.1(4)
O(6)#1-Mo(3)-O(11)	149.18(9)	N(4)-C(7)-C(8)	178.7(4)
O(12)-Mo(3)-O(4)#1	97.85(10)	N(5)-C(9)-C(10)	179.0(5)
O(13)-Mo(3)-O(4)#1	156.30(9)	N(6)-C(11)-C(12)	177.8(4)
O(6)#1-Mo(3)-O(4)#1	78.13(9)	N(7)-C(13)-C(14)	179.1(5)
O(11)-Mo(3)-O(4)#1	78.32(9)	N(8)-C(15)-C(16)	178.8(4)
O(12)-Mo(3)-O(4)	173.15(10)		

Symmetry transformations used to generate equivalent atoms:

#1 -x+1,-y+1,-z+1 #2 -x+1,-y,-z

Ortep style representation of $[(\text{Ag}(\text{CH}_3\text{CN})_3)_2(\text{Ag}(\text{CH}_3\text{CN}))_2\text{AgMo}_8\text{O}_{26}]_n$ (**18**): thermal ellipsoids at 50% probability, hydrogen atoms are omitted for clarity. Carbon and nitrogen atoms of acetonitrile not labelled.



6.14 Crystal data for [(Ag(CH₃CN))₂(Ag(CH₃CN))₂Mo₈O₂₆]_n (19)

Empirical formula	C ₁₂ H ₁₈ Ag ₄ Mo ₈ N ₆ O ₂₆	
Crystal growth	Diffusion of diethyl ether, 4 days	
Crystal description	Colourless block crystals	
Crystal size	0.18 × 0.18 × 0.06 mm ³	
Formula weight	1861.32	
Temperature	150(2) K	
Wavelength	0.71073 Å	
Crystal system	Monoclinic	
Space group	<i>P</i> 2 ₁ / <i>n</i>	
Unit cell dimensions	<i>a</i> = 10.6524(5) Å	<i>α</i> = 90°
	<i>b</i> = 13.4553(6) Å	<i>β</i> = 103.579(3)°
	<i>c</i> = 13.2691(3) Å	<i>γ</i> = 90°
Volume	1848.71(13) Å ³	
<i>Z</i>	2	
Density (calculated)	3.344 Mg/m ³	
Absorption coefficient	4.776 mm ⁻¹	
<i>F</i> (000)	1728	
Theta range for data collection	2.21 to 25.98°	
Index ranges	-13 ≤ <i>h</i> ≤ 12, 0 ≤ <i>k</i> ≤ 16, 0 ≤ <i>l</i> ≤ 16	
Reflections collected/ unique	17507 / 3614 [<i>R</i> (int) = 0.0455]	
Completeness to theta	25.98° 99.6 %	
Absorption correction	Gaussian	
Max. and min. transmission	0.808 and 0.469	
Refinement method	Full-matrix least-squares on <i>F</i> ²	
Data / restraints / parameters	3614 / 0 / 257	
Goodness-of-fit on <i>F</i> ²	1.045	
Final <i>R</i> indices [<i>I</i> > 2σ(<i>I</i>)]	<i>R</i> 1 = 0.0267, <i>wR</i> 2 = 0.0613	
<i>R</i> indices (all data)	<i>R</i> 1 = 0.0372, <i>wR</i> 2 = 0.0646	
Extinction coefficient	0.00063(7)	
Largest diff. peak and hole	0.95 and -1.04 e.Å ⁻³	

Bond lengths [Å] and angles [°]

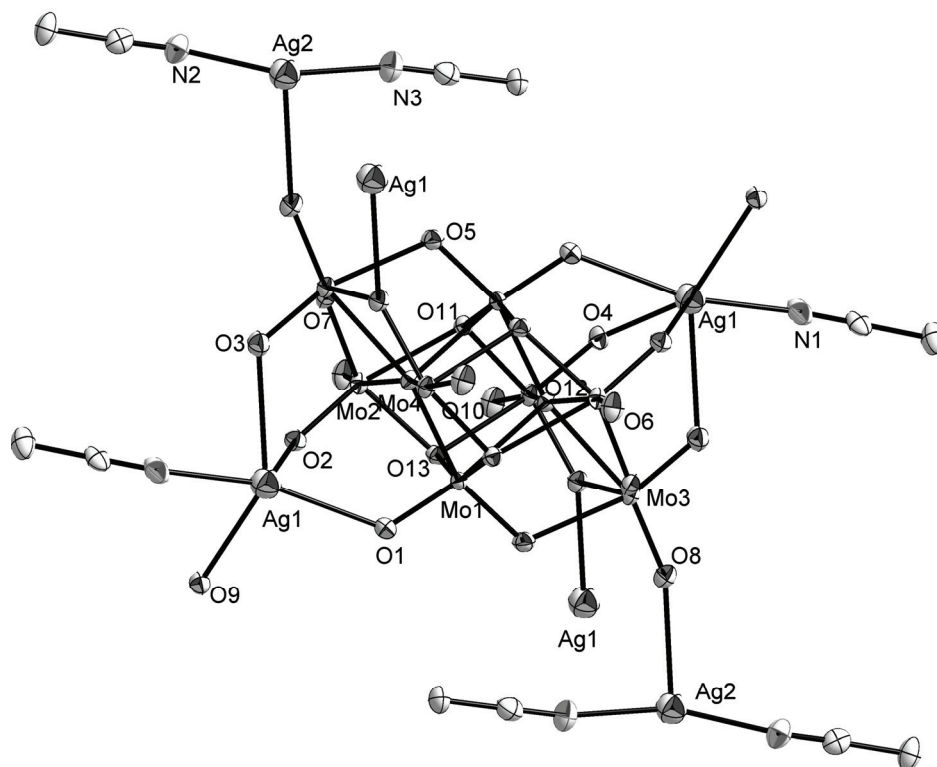
Ag(1)-N(1)	2.233(4)	O(7)-Mo(2)-O(13)#1	146.73(12)
Ag(1)-O(2)	2.420(3)	O(6)-Mo(2)-O(11)#1	92.80(14)
Ag(1)-O(1)	2.493(3)	O(2)-Mo(2)-O(11)#1	159.95(13)
Ag(2)-N(2)	2.112(4)	O(7)-Mo(2)-O(11)#1	83.79(12)
Ag(2)-N(3)	2.124(4)	O(13)#1-Mo(2)-O(11)#1	71.76(11)
Ag(2)-O(8)	2.583(3)	O(6)-Mo(2)-O(12)	163.84(13)
Mo(1)-O(1)	1.713(3)	O(2)-Mo(2)-O(12)	90.98(13)
Mo(1)-O(5)	1.742(3)	O(7)-Mo(2)-O(12)	77.22(11)
Mo(1)-O(13)#1	1.941(3)	O(13)#1-Mo(2)-O(12)	73.74(11)
Mo(1)-O(11)	1.947(3)	O(11)#1-Mo(2)-O(12)	71.05(10)
Mo(1)-O(12)	2.173(3)	O(8)-Mo(3)-O(3)	105.39(15)
Mo(1)-O(12)#1	2.300(3)	O(8)-Mo(3)-O(7)	103.06(14)
Mo(2)-O(6)	1.695(3)	O(3)-Mo(3)-O(7)	97.56(14)
Mo(2)-O(2)	1.721(3)	O(8)-Mo(3)-O(9)	102.27(14)
Mo(2)-O(7)	1.893(3)	O(3)-Mo(3)-O(9)	97.87(14)
Mo(2)-O(13)#1	2.012(3)	O(7)-Mo(3)-O(9)	145.50(12)
Mo(2)-O(11)#1	2.283(3)	O(8)-Mo(3)-O(5)#1	91.04(13)
Mo(2)-O(12)	2.344(3)	O(3)-Mo(3)-O(5)#1	163.57(13)
Mo(3)-O(8)	1.700(3)	O(7)-Mo(3)-O(5)#1	77.78(12)
Mo(3)-O(3)	1.713(3)	O(9)-Mo(3)-O(5)#1	78.73(12)
Mo(3)-O(7)	1.926(3)	O(8)-Mo(3)-O(12)	160.75(13)
Mo(3)-O(9)	1.934(3)	O(3)-Mo(3)-O(12)	93.86(13)
Mo(3)-O(5)#1	2.300(3)	O(7)-Mo(3)-O(12)	74.34(11)
Mo(3)-O(12)	2.438(3)	O(9)-Mo(3)-O(12)	74.00(11)
Mo(4)-O(10)	1.695(3)	O(5)#1-Mo(3)-O(12)	69.72(10)
Mo(4)-O(4)	1.719(3)	O(10)-Mo(4)-O(4)	105.82(16)
Mo(4)-O(9)	1.896(3)	O(10)-Mo(4)-O(9)	102.53(15)
Mo(4)-O(11)	2.015(3)	O(4)-Mo(4)-O(9)	101.86(14)
Mo(4)-O(12)	2.312(3)	O(10)-Mo(4)-O(11)	99.17(14)
Mo(4)-O(13)	2.314(3)	O(4)-Mo(4)-O(11)	95.84(14)
O(5)-Mo(3)#1	2.300(3)	O(9)-Mo(4)-O(11)	146.89(12)
O(11)-Mo(2)#1	2.283(3)	O(10)-Mo(4)-O(12)	161.11(13)
O(12)-Mo(1)#1	2.300(3)	O(4)-Mo(4)-O(12)	92.44(13)
O(13)-Mo(1)#1	1.941(3)	O(9)-Mo(4)-O(12)	77.77(12)
O(13)-Mo(2)#1	2.012(3)	O(11)-Mo(4)-O(12)	73.69(11)
N(1)-C(1)	1.148(6)	O(10)-Mo(4)-O(13)	90.44(13)
N(2)-C(3)	1.135(6)	O(4)-Mo(4)-O(13)	160.79(13)

N(3)-C(5)	1.141(6)	O(9)-Mo(4)-O(13)	84.02(12)
C(1)-C(2)	1.447(7)	O(11)-Mo(4)-O(13)	71.04(11)
C(3)-C(4)	1.445(7)	O(12)-Mo(4)-O(13)	70.73(10)
C(5)-C(6)	1.445(7)	Mo(1)-O(1)-Ag(1)	127.60(16)
		Mo(2)-O(2)-Ag(1)	132.26(16)
N(1)-Ag(1)-O(2)	119.27(14)	Mo(1)-O(5)-Mo(3)#1	114.90(14)
N(1)-Ag(1)-O(1)	164.86(14)	Mo(2)-O(7)-Mo(3)	117.10(15)
O(2)-Ag(1)-O(1)	73.13(10)	Mo(3)-O(8)-Ag(2)	159.60(17)
N(2)-Ag(2)-N(3)	159.91(18)	Mo(4)-O(9)-Mo(3)	116.46(16)
N(2)-Ag(2)-O(8)	106.82(14)	Mo(1)-O(11)-Mo(4)	108.87(14)
N(3)-Ag(2)-O(8)	87.38(14)	Mo(1)-O(11)-Mo(2)#1	110.87(13)
O(1)-Mo(1)-O(5)	105.76(14)	Mo(4)-O(11)-Mo(2)#1	104.50(13)
O(1)-Mo(1)-O(13)#1	100.51(14)	Mo(1)-O(12)-Mo(1)#1	104.01(12)
O(5)-Mo(1)-O(13)#1	97.25(13)	Mo(1)-O(12)-Mo(4)	91.82(11)
O(1)-Mo(1)-O(11)	100.68(14)	Mo(1)#1-O(12)-Mo(4)	98.62(11)
O(5)-Mo(1)-O(11)	96.89(13)	Mo(1)-O(12)-Mo(2)	91.04(11)
O(13)#1-Mo(1)-O(11)	150.20(12)	Mo(1)#1-O(12)-Mo(2)	97.36(11)
O(1)-Mo(1)-O(12)	95.28(13)	Mo(4)-O(12)-Mo(2)	162.56(14)
O(5)-Mo(1)-O(12)	158.95(13)	Mo(1)-O(12)-Mo(3)	163.56(15)
O(13)#1-Mo(1)-O(12)	79.16(12)	Mo(1)#1-O(12)-Mo(3)	92.40(10)
O(11)-Mo(1)-O(12)	78.24(12)	Mo(4)-O(12)-Mo(3)	86.53(10)
O(1)-Mo(1)-O(12)#1	171.26(13)	Mo(2)-O(12)-Mo(3)	85.87(9)
O(5)-Mo(1)-O(12)#1	82.98(12)	Mo(1)#1-O(13)-Mo(2)#1	109.35(14)
O(13)#1-Mo(1)-O(12)#1	77.79(11)	Mo(1)#1-O(13)-Mo(4)	110.27(13)
O(11)-Mo(1)-O(12)#1	78.08(11)	Mo(2)#1-O(13)-Mo(4)	103.48(12)
O(12)-Mo(1)-O(12)#1	75.99(12)	C(1)-N(1)-Ag(1)	161.6(4)
O(6)-Mo(2)-O(2)	104.85(16)	C(3)-N(2)-Ag(2)	171.4(4)
O(6)-Mo(2)-O(7)	102.29(15)	C(5)-N(3)-Ag(2)	169.0(4)
O(2)-Mo(2)-O(7)	101.28(14)	N(1)-C(1)-C(2)	179.0(5)
O(6)-Mo(2)-O(13)#1	101.13(14)	N(2)-C(3)-C(4)	178.3(6)
O(2)-Mo(2)-O(13)#1	95.15(13)	N(3)-C(5)-C(6)	179.6(6)

Symmetry transformations used to generate equivalent atoms:

#1 -x,-y+1,-z

Ortep style representation of $[(\text{Ag}(\text{CH}_3\text{CN}))_2(\text{Ag}(\text{CH}_3\text{CN})_2)_2\text{Mo}_8\text{O}_{26}]_n$ (**19**): thermal ellipsoids at 50% probability, hydrogen atoms are omitted for clarity. Not all carbon and nitrogen atoms of acetonitrile labelled.



6.15 Crystal data for [(Ag(CH₃CN)₂)₂Ag₂Mo₈O₂₆]_n (20)

Empirical formula	C ₈ H ₁₂ Ag ₄ Mo ₈ N ₄ O ₂₆	
Crystal growth	Diffusion of diethyl ether, 4 days	
Crystal description	Colourless block crystals	
Crystal size	0.24 × 0.08 × 0.02 mm ³	
Formula weight	1779.22	
Temperature	150(2) K	
Wavelength	0.71073 Å	
Crystal system	Triclinic	
Space group	<i>P</i> -1	
Unit cell dimensions	<i>a</i> = 7.7079(3) Å	<i>α</i> = 71.733(2)°
	<i>b</i> = 9.8937(4) Å	<i>β</i> = 75.067(2)°
	<i>c</i> = 11.0988(5) Å	<i>γ</i> = 77.256(3)°
Volume	767.52(6) Å ³	
<i>Z</i>	1	
Density (calculated)	3.849 Mg/m ³	
Absorption coefficient	5.741 mm ⁻¹	
<i>F</i> (000)	820	
Theta range for data collection	1.97 to 26.00°	
Index ranges	-8 ≤ <i>h</i> ≤ 9, -11 ≤ <i>k</i> ≤ 12, 0 ≤ <i>l</i> ≤ 13	
Reflections collected/ unique	10779 / 3015 [<i>R</i> (int) = 0.049]	
Completeness to theta	26.00° 99.7 %	
Absorption correction	Gaussian	
Max. and min. transmission	0.8938 and 0.3395	
Refinement method	Full-matrix least-squares on <i>F</i> ²	
Data / restraints / parameters	3015 / 0 / 229	
Goodness-of-fit on <i>F</i> ²	1.053	
Final <i>R</i> indices [<i>I</i> > 2σ(<i>I</i>)]	<i>R</i> 1 = 0.0224, w <i>R</i> 2 = 0.0505	
<i>R</i> indices (all data)	<i>R</i> 1 = 0.0301, w <i>R</i> 2 = 0.0524	
Extinction coefficient	0.00168(13)	
Largest diff. peak and hole	0.75 and -0.64 e.Å ⁻³	

Bond lengths [\AA] and angles [$^\circ$]

Ag(1)-O(2)#1	2.377(3)	O(10)#3-Mo(1)-O(8)	71.61(10)
Ag(1)-O(3)	2.397(3)	O(7)-Mo(2)-O(1)	104.98(14)
Ag(1)-O(4)	2.426(3)	O(7)-Mo(2)-O(6)	103.90(13)
Ag(1)-O(1)#1	2.468(3)	O(1)-Mo(2)-O(6)	96.12(13)
Ag(1)-O(7)#2	2.527(3)	O(7)-Mo(2)-O(9)	103.51(13)
Ag(1)-Ag(1)#1	3.0176(7)	O(1)-Mo(2)-O(9)	98.05(13)
Ag(2)-N(1)	2.136(4)	O(6)-Mo(2)-O(9)	144.56(11)
Ag(2)-N(2)	2.147(4)	O(7)-Mo(2)-O(12)	95.06(12)
Mo(1)-O(5)	1.701(3)	O(1)-Mo(2)-O(12)	159.95(12)
Mo(1)-O(2)	1.715(3)	O(6)-Mo(2)-O(12)	78.18(12)
Mo(1)-O(6)	1.886(3)	O(9)-Mo(2)-O(12)	77.42(11)
Mo(1)-O(13)#3	1.991(3)	O(7)-Mo(2)-O(8)	164.75(12)
Mo(1)-O(10)#3	2.294(3)	O(1)-Mo(2)-O(8)	90.26(12)
Mo(1)-O(8)	2.349(3)	O(6)-Mo(2)-O(8)	74.35(10)
Mo(2)-O(7)	1.706(3)	O(9)-Mo(2)-O(8)	73.27(10)
Mo(2)-O(1)	1.721(3)	O(12)-Mo(2)-O(8)	69.70(9)
Mo(2)-O(6)	1.922(3)	O(4)-Mo(3)-O(12)#3	106.13(13)
Mo(2)-O(9)	1.934(3)	O(4)-Mo(3)-O(10)	102.35(13)
Mo(2)-O(12)	2.248(3)	O(12)#3-Mo(3)-O(10)	98.48(12)
Mo(2)-O(8)	2.463(3)	O(4)-Mo(3)-O(13)#3	98.80(13)
Mo(3)-O(4)	1.699(3)	O(12)#3-Mo(3)-O(13)#3	95.31(12)
Mo(3)-O(12)#3	1.755(3)	O(10)-Mo(3)-O(13)#3	150.35(11)
Mo(3)-O(10)	1.946(3)	O(4)-Mo(3)-O(8)	96.59(12)
Mo(3)-O(13)#3	1.965(3)	O(12)#3-Mo(3)-O(8)	157.20(12)
Mo(3)-O(8)	2.150(3)	O(10)-Mo(3)-O(8)	78.08(11)
Mo(3)-O(8)#3	2.313(3)	O(13)#3-Mo(3)-O(8)	79.07(11)
Mo(4)-O(11)	1.697(3)	O(4)-Mo(3)-O(8)#3	171.58(11)
Mo(4)-O(3)	1.716(3)	O(12)#3-Mo(3)-O(8)#3	81.84(11)
Mo(4)-O(9)	1.891(3)	O(10)-Mo(3)-O(8)#3	78.74(11)
Mo(4)-O(10)	2.014(3)	O(13)#3-Mo(3)-O(8)#3	77.41(11)
Mo(4)-O(8)	2.299(3)	O(8)-Mo(3)-O(8)#3	75.38(11)
Mo(4)-O(13)	2.311(3)	O(11)-Mo(4)-O(3)	104.81(14)
O(1)-Ag(1)#1	2.468(3)	O(11)-Mo(4)-O(9)	101.88(13)
O(2)-Ag(1)#1	2.377(3)	O(3)-Mo(4)-O(9)	101.72(13)
O(7)-Ag(1)#4	2.527(3)	O(11)-Mo(4)-O(10)	99.78(12)
O(8)-Mo(3)#3	2.313(3)	O(3)-Mo(4)-O(10)	95.94(13)
O(10)-Mo(1)#3	2.294(3)	O(9)-Mo(4)-O(10)	147.37(12)

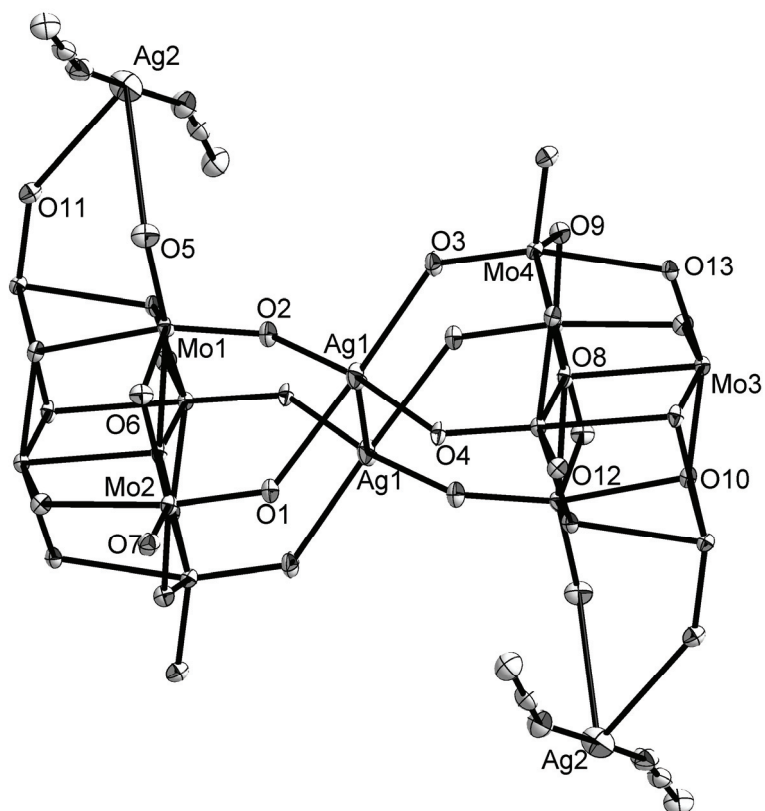
O(12)-Mo(3)#3	1.755(3)	O(11)-Mo(4)-O(8)	160.03(12)
O(13)-Mo(3)#3	1.965(3)	O(3)-Mo(4)-O(8)	94.64(12)
O(13)-Mo(1)#3	1.991(3)	O(9)-Mo(4)-O(8)	78.07(11)
N(1)-C(1)	1.129(5)	O(10)-Mo(4)-O(8)	73.30(10)
N(2)-C(3)	1.134(6)	O(11)-Mo(4)-O(13)	88.71(12)
C(1)-C(2)	1.466(6)	O(3)-Mo(4)-O(13)	163.05(12)
C(3)-C(4)	1.458(6)	O(9)-Mo(4)-O(13)	85.04(11)
		O(10)-Mo(4)-O(13)	71.31(10)
O(2)#1-Ag(1)-O(3)	108.25(10)	O(8)-Mo(4)-O(13)	71.34(10)
O(2)#1-Ag(1)-O(4)	173.15(10)	Mo(2)-O(1)-Ag(1)#1	133.28(15)
O(3)-Ag(1)-O(4)	78.54(10)	Mo(1)-O(2)-Ag(1)#1	130.81(15)
O(2)#1-Ag(1)-O(1)#1	73.59(10)	Mo(4)-O(3)-Ag(1)	130.86(15)
O(3)-Ag(1)-O(1)#1	174.48(9)	Mo(3)-O(4)-Ag(1)	129.00(14)
O(4)-Ag(1)-O(1)#1	99.57(10)	Mo(1)-O(6)-Mo(2)	116.78(14)
O(2)#1-Ag(1)-O(7)#2	98.94(10)	Mo(2)-O(7)-Ag(1)#4	135.14(15)
O(3)-Ag(1)-O(7)#2	80.47(10)	Mo(3)-O(8)-Mo(4)	92.76(10)
O(4)-Ag(1)-O(7)#2	81.06(9)	Mo(3)-O(8)-Mo(3)#3	104.62(11)
O(1)#1-Ag(1)-O(7)#2	94.14(10)	Mo(4)-O(8)-Mo(3)#3	98.67(11)
O(2)#1-Ag(1)-Ag(1)#1	60.87(7)	Mo(3)-O(8)-Mo(1)	91.40(10)
O(3)-Ag(1)-Ag(1)#1	124.34(7)	Mo(4)-O(8)-Mo(1)	162.54(14)
O(4)-Ag(1)-Ag(1)#1	116.37(7)	Mo(3)#3-O(8)-Mo(1)	96.66(10)
O(1)#1-Ag(1)-Ag(1)#1	61.16(7)	Mo(3)-O(8)-Mo(2)	163.83(14)
O(7)#2-Ag(1)-Ag(1)#1	150.73(7)	Mo(4)-O(8)-Mo(2)	86.59(9)
N(1)-Ag(2)-N(2)	174.47(15)	Mo(3)#3-O(8)-Mo(2)	91.43(9)
O(5)-Mo(1)-O(2)	105.13(15)	Mo(1)-O(8)-Mo(2)	84.73(8)
O(5)-Mo(1)-O(6)	102.24(13)	Mo(4)-O(9)-Mo(2)	117.39(14)
O(2)-Mo(1)-O(6)	99.71(13)	Mo(3)-O(10)-Mo(4)	108.92(13)
O(5)-Mo(1)-O(13)#3	100.50(13)	Mo(3)-O(10)-Mo(1)#3	110.15(12)
O(2)-Mo(1)-O(13)#3	97.62(12)	Mo(4)-O(10)-Mo(1)#3	103.96(12)
O(6)-Mo(1)-O(13)#3	146.56(12)	Mo(3)#3-O(12)-Mo(2)	116.88(14)
O(5)-Mo(1)-O(10)#3	93.21(13)	Mo(3)#3-O(13)-Mo(1)#3	109.11(13)
O(2)-Mo(1)-O(10)#3	160.50(12)	Mo(3)#3-O(13)-Mo(4)	109.55(12)
O(6)-Mo(1)-O(10)#3	82.46(11)	Mo(1)#3-O(13)-Mo(4)	104.10(11)
O(13)#3-Mo(1)-O(10)#3	72.07(10)	C(1)-N(1)-Ag(2)	168.5(4)
O(5)-Mo(1)-O(8)	164.74(13)	C(3)-N(2)-Ag(2)	160.7(4)
O(2)-Mo(1)-O(8)	89.80(12)	N(1)-C(1)-C(2)	179.3(5)
O(6)-Mo(1)-O(8)	77.83(11)	N(2)-C(3)-C(4)	179.3(5)
O(13)#3-Mo(1)-O(8)	73.86(10)		

Symmetry transformations used to generate equivalent atoms:

#1 $-x+1, -y+1, -z+1$ #2 $x+1, y, z$ #3 $-x+1, -y, -z+1$

#4 $x-1, y, z$

Ortep style representation of $[(\text{Ag}(\text{CH}_3\text{CN})_2)_2\text{Ag}_2\text{Mo}_8\text{O}_{26}]_n$ (**20**): thermal ellipsoids at 50% probability, hydrogen atoms are omitted for clarity. Carbon and nitrogen atoms of acetonitrile not labelled.



6.16 Crystal data for $[\text{Ag}_4(\text{DMSO})_6(\text{OC}(\text{CH}_3)_2)_2\text{Mo}_8\text{O}_{26}]_n$ (21)

Empirical formula	$\text{C}_{18}\text{H}_{48}\text{Ag}_4\text{Mo}_8\text{O}_{34}\text{S}_6$	
Crystal growth	Diffusion of acetone, 2 months	
Crystal description	Colourless block crystals	
Crystal size	$0.18 \times 0.12 \times 0.12 \text{ mm}^3$	
Formula weight	2199.92	
Temperature	150(2) K	
Wavelength	0.71073 Å	
Crystal system	Orthorhombic	
Space group	<i>Pbca</i>	
Unit cell dimensions	$a = 14.7008(5) \text{ Å}$	$\alpha = 90^\circ$
	$b = 18.6995(7) \text{ Å}$	$\beta = 90^\circ$
	$c = 19.1703(4) \text{ Å}$	$\gamma = 90^\circ$
Volume	$5269.9(3) \text{ Å}^3$	
<i>Z</i>	4	
Density (calculated)	2.773 Mg/m^3	
Absorption coefficient	3.611 mm^{-1}	
<i>F</i> (000)	4192	
Theta range for data collection	2.12 to 26.00°	
Index ranges	$0 \leq h \leq 18, 0 \leq k \leq 23, 0 \leq l \leq 23$	
Reflections collected/ unique	23170/ 5144 [<i>R</i> (int) = 0.0562]	
Completeness to theta	26.00° 99.5 %	
Absorption correction	Gaussian	
Max. and min. transmission	0.679 and 0.607	
Refinement method	Full-matrix least-squares on F^2	
Data / restraints / parameters	5144 / 0 / 335	
Goodness-of-fit on F^2	1.025	
Final <i>R</i> indices [<i>I</i> > 2σ(<i>I</i>)]	<i>R</i> 1 = 0.0345, w <i>R</i> 2 = 0.0639	
<i>R</i> indices (all data)	<i>R</i> 1 = 0.0566, w <i>R</i> 2 = 0.0694	
Extinction coefficient	0.000125(15)	
Largest diff. peak and hole	0.84 and -1.00 e.Å ⁻³	

Bond lengths [\AA] and angles [$^{\circ}$]

Ag(1)-O(1)	2.449(3)	O(11)-Mo(2)-O(10)	104.21(16)
Ag(1)-O(3)	2.501(4)	O(5)-Mo(2)-O(10)	98.17(15)
Ag(1)-O(6)	2.518(3)	O(11)-Mo(2)-O(15)	103.15(15)
Ag(1)-O(2)	2.523(3)	O(5)-Mo(2)-O(15)	96.39(16)
Ag(1)-O(5)	2.599(4)	O(10)-Mo(2)-O(15)	144.08(14)
Ag(1)-Ag(2)	3.2796(6)	O(11)-Mo(2)-O(12)	93.99(15)
Ag(2)-O(13)#1	2.329(3)	O(5)-Mo(2)-O(12)	160.32(15)
Ag(2)-O(3)	2.364(4)	O(10)-Mo(2)-O(12)	78.03(13)
Ag(2)-O(1)	2.423(3)	O(15)-Mo(2)-O(12)	77.28(13)
Ag(2)-O(4)	2.472(4)	O(11)-Mo(2)-O(7)	163.76(15)
Ag(2)-O(2)	2.579(4)	O(5)-Mo(2)-O(7)	90.57(14)
Mo(1)-O(6)	1.703(3)	O(10)-Mo(2)-O(7)	73.90(12)
Mo(1)-O(9)	1.706(3)	O(15)-Mo(2)-O(7)	73.30(12)
Mo(1)-O(10)	1.893(3)	O(12)-Mo(2)-O(7)	69.78(11)
Mo(1)-O(14)	2.000(3)	O(16)-Mo(3)-O(13)	105.04(17)
Mo(1)-O(17)	2.331(3)	O(16)-Mo(3)-O(15)#2	101.95(15)
Mo(1)-O(7)	2.337(3)	O(13)-Mo(3)-O(15)#2	101.41(15)
Mo(2)-O(11)	1.688(4)	O(16)-Mo(3)-O(17)	96.19(14)
Mo(2)-O(5)	1.708(3)	O(13)-Mo(3)-O(17)	99.07(14)
Mo(2)-O(10)	1.920(3)	O(15)#2-Mo(3)-O(17)	147.94(14)
Mo(2)-O(15)	1.936(3)	O(16)-Mo(3)-O(7)#2	92.64(14)
Mo(2)-O(12)	2.274(3)	O(13)-Mo(3)-O(7)#2	161.73(14)
Mo(2)-O(7)	2.472(3)	O(15)#2-Mo(3)-O(7)#2	78.91(13)
Mo(3)-O(16)	1.704(3)	O(17)-Mo(3)-O(7)#2	74.01(12)
Mo(3)-O(13)	1.709(3)	O(16)-Mo(3)-O(14)	162.30(14)
Mo(3)-O(15)#2	1.888(3)	O(13)-Mo(3)-O(14)	89.87(14)
Mo(3)-O(17)	2.009(3)	O(15)#2-Mo(3)-O(14)	83.97(13)
Mo(3)-O(7)#2	2.281(3)	O(17)-Mo(3)-O(14)	71.64(12)
Mo(3)-O(14)	2.313(3)	O(7)#2-Mo(3)-O(14)	71.94(11)
Mo(3)-Mo(4)	3.2060(6)	O(16)-Mo(3)-Mo(4)	83.82(12)
Mo(4)-O(8)	1.703(3)	O(13)-Mo(3)-Mo(4)	134.02(12)
Mo(4)-O(12)	1.749(3)	O(15)#2-Mo(3)-Mo(4)	121.12(10)
Mo(4)-O(17)	1.941(3)	O(17)-Mo(3)-Mo(4)	35.05(8)
Mo(4)-O(14)#2	1.946(3)	O(7)#2-Mo(3)-Mo(4)	42.21(8)
Mo(4)-O(7)#2	2.156(3)	O(14)-Mo(3)-Mo(4)	78.90(8)
Mo(4)-O(7)	2.326(3)	O(8)-Mo(4)-O(12)	104.79(16)
S(1)-O(1)	1.525(4)	O(8)-Mo(4)-O(17)	101.04(15)

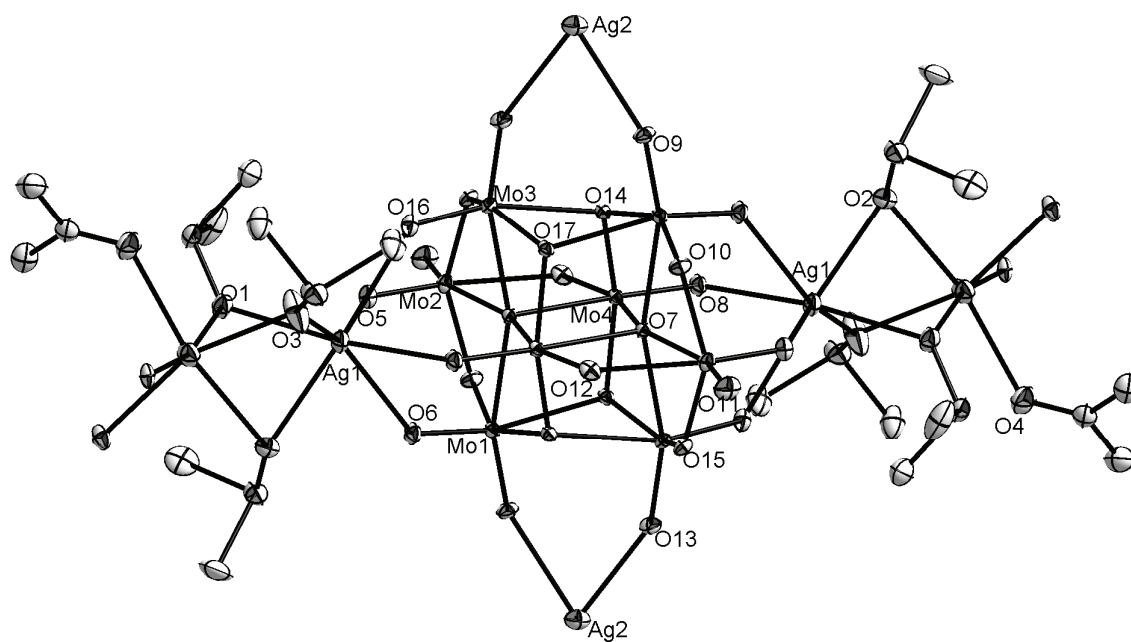
S(1)-C(1)	1.781(5)	O(12)-Mo(4)-O(17)	97.08(14)
S(1)-C(2)	1.788(6)	O(8)-Mo(4)-O(14)#2	100.43(14)
S(2)-O(2)	1.509(4)	O(12)-Mo(4)-O(14)#2	97.34(14)
S(2)-C(3)	1.774(6)	O(17)-Mo(4)-O(14)#2	150.05(14)
S(2)-C(4)	1.789(5)	O(8)-Mo(4)-O(7)#2	97.30(14)
S(3)-O(3)	1.503(4)	O(12)-Mo(4)-O(7)#2	157.91(14)
S(3)-C(6)	1.771(6)	O(17)-Mo(4)-O(7)#2	78.27(13)
S(3)-C(5)	1.778(5)	O(14)#2-Mo(4)-O(7)#2	78.51(13)
O(4)-C(7)	1.222(6)	O(8)-Mo(4)-O(7)	172.76(14)
C(7)-C(9)	1.477(8)	O(12)-Mo(4)-O(7)	82.43(13)
C(7)-C(8)	1.499(7)	O(17)-Mo(4)-O(7)	78.27(12)
O(7)-Mo(4)#2	2.156(3)	O(14)#2-Mo(4)-O(7)	77.79(12)
O(7)-Mo(3)#2	2.281(3)	O(7)#2-Mo(4)-O(7)	75.48(13)
O(13)-Ag(2)#3	2.329(3)	O(8)-Mo(4)-Mo(3)	89.25(11)
O(14)-Mo(4)#2	1.946(3)	O(12)-Mo(4)-Mo(3)	133.55(10)
O(15)-Mo(3)#2	1.888(3)	O(17)-Mo(4)-Mo(3)	36.46(10)
		O(14)#2-Mo(4)-Mo(3)	123.80(10)
O(1)-Ag(1)-O(3)	82.42(14)	O(7)#2-Mo(4)-Mo(3)	45.30(8)
O(1)-Ag(1)-O(6)	126.23(12)	O(7)-Mo(4)-Mo(3)	86.01(8)
O(3)-Ag(1)-O(6)	138.52(14)	O(1)-S(1)-C(1)	105.5(2)
O(1)-Ag(1)-O(2)	76.05(11)	O(1)-S(1)-C(2)	105.2(3)
O(3)-Ag(1)-O(2)	81.03(12)	C(1)-S(1)-C(2)	98.4(3)
O(6)-Ag(1)-O(2)	78.77(11)	S(1)-O(1)-Ag(2)	117.6(2)
O(1)-Ag(1)-O(5)	81.59(11)	S(1)-O(1)-Ag(1)	132.09(18)
O(3)-Ag(1)-O(5)	146.56(14)	Ag(2)-O(1)-Ag(1)	84.61(11)
O(6)-Ag(1)-O(5)	73.53(11)	O(2)-S(2)-C(3)	107.0(2)
O(2)-Ag(1)-O(5)	122.75(11)	O(2)-S(2)-C(4)	105.8(3)
O(1)-Ag(1)-Ag(2)	47.36(8)	C(3)-S(2)-C(4)	97.1(3)
O(3)-Ag(1)-Ag(2)	45.88(8)	S(2)-O(2)-Ag(1)	115.29(19)
O(6)-Ag(1)-Ag(2)	129.49(7)	S(2)-O(2)-Ag(2)	130.8(2)
O(2)-Ag(1)-Ag(2)	50.76(8)	Ag(1)-O(2)-Ag(2)	79.99(10)
O(5)-Ag(1)-Ag(2)	128.81(8)	O(3)-S(3)-C(6)	106.3(3)
O(13)#1-Ag(2)-O(3)	153.23(15)	O(3)-S(3)-C(5)	104.8(3)
O(13)#1-Ag(2)-O(1)	113.96(12)	C(6)-S(3)-C(5)	97.6(3)
O(3)-Ag(2)-O(1)	85.88(13)	S(3)-O(3)-Ag(2)	127.0(2)
O(13)#1-Ag(2)-O(4)	105.06(12)	S(3)-O(3)-Ag(1)	146.9(2)
O(3)-Ag(2)-O(4)	91.59(14)	Ag(2)-O(3)-Ag(1)	84.71(12)
O(1)-Ag(2)-O(4)	91.33(13)	C(7)-O(4)-Ag(2)	129.4(4)
O(13)#1-Ag(2)-O(2)	85.33(11)	O(4)-C(7)-C(9)	121.5(5)
O(3)-Ag(2)-O(2)	82.52(12)	O(4)-C(7)-C(8)	120.8(5)

O(1)-Ag(2)-O(2)	75.45(12)	C(9)-C(7)-C(8)	117.7(5)
O(4)-Ag(2)-O(2)	165.83(12)	Mo(2)-O(5)-Ag(1)	131.10(18)
O(13)#1-Ag(2)-Ag(1)	131.91(9)	Mo(1)-O(6)-Ag(1)	131.15(17)
O(3)-Ag(2)-Ag(1)	49.42(10)	Mo(4)#2-O(7)-Mo(3)#2	92.49(12)
O(1)-Ag(2)-Ag(1)	48.03(8)	Mo(4)#2-O(7)-Mo(4)	104.52(13)
O(4)-Ag(2)-Ag(1)	117.68(9)	Mo(3)#2-O(7)-Mo(4)	98.00(11)
O(2)-Ag(2)-Ag(1)	49.26(7)	Mo(4)#2-O(7)-Mo(1)	91.65(11)
O(6)-Mo(1)-O(9)	105.49(16)	Mo(3)#2-O(7)-Mo(1)	162.18(15)
O(6)-Mo(1)-O(10)	100.74(15)	Mo(4)-O(7)-Mo(1)	97.71(12)
O(9)-Mo(1)-O(10)	102.62(15)	Mo(4)#2-O(7)-Mo(2)	164.15(15)
O(6)-Mo(1)-O(14)	97.42(15)	Mo(3)#2-O(7)-Mo(2)	86.03(10)
O(9)-Mo(1)-O(14)	99.71(14)	Mo(4)-O(7)-Mo(2)	91.30(11)
O(10)-Mo(1)-O(14)	146.12(13)	Mo(1)-O(7)-Mo(2)	85.27(10)
O(6)-Mo(1)-O(17)	161.60(14)	Mo(1)-O(10)-Mo(2)	117.41(17)
O(9)-Mo(1)-O(17)	91.06(14)	Mo(4)-O(12)-Mo(2)	116.48(16)
O(10)-Mo(1)-O(17)	83.00(13)	Mo(3)-O(13)-Ag(2)#3	150.66(19)
O(14)-Mo(1)-O(17)	71.38(12)	Mo(4)#2-O(14)-Mo(1)	109.62(15)
O(6)-Mo(1)-O(7)	92.07(14)	Mo(4)#2-O(14)-Mo(3)	109.16(13)
O(9)-Mo(1)-O(7)	161.92(14)	Mo(1)-O(14)-Mo(3)	104.80(14)
O(10)-Mo(1)-O(7)	77.74(12)	Mo(3)#2-O(15)-Mo(2)	116.13(16)
O(14)-Mo(1)-O(7)	73.23(12)	Mo(4)-O(17)-Mo(3)	108.49(14)
O(17)-Mo(1)-O(7)	70.96(11)	Mo(4)-O(17)-Mo(1)	110.18(15)
O(11)-Mo(2)-O(5)	105.64(17)	Mo(3)-O(17)-Mo(1)	103.83(13)

Symmetry transformations used to generate equivalent atoms:

#1 $-x+2, y+1/2, -z+1/2$ #2 $-x+2, -y, -z+1$ #3 $-x+2, y-1/2, -z+1/2$

Ortep style representation of $[\text{Ag}_4(\text{DMSO})_6(\text{OC}(\text{CH}_3)_2)_2\text{Mo}_8\text{O}_{26}]_n$ (**21**): thermal ellipsoids at 50% probability, hydrogen atoms are omitted for clarity. Carbon, sulphur and oxygen atoms of DMSO not labelled.



6.17 Crystal data for [Ag₄(DMSO)₈Mo₈O₂₆]_n (22)

Empirical formula	C ₁₆ H ₄₈ Ag ₄ Mo ₈ O ₃₄ S ₈	
Crystal growth	Diffusion of ethanol, 10 days	
Crystal description	Colourless block crystals	
Crystal size	0.14 × 0.07 × 0.07 mm ³	
Formula weight	2240.02	
Temperature	150(2) K	
Wavelength	0.71073 Å	
Crystal system	Triclinic	
Space group	<i>P</i> -1	
Unit cell dimensions	<i>a</i> = 10.8053(3) Å	<i>α</i> = 97.200(2)°
	<i>b</i> = 11.1381(3) Å	<i>β</i> = 113.4870(10)°
	<i>c</i> = 13.3396(3) Å	<i>γ</i> = 108.7740(10)°
Volume	1333.30(6) Å ³	
<i>Z</i>	1	
Density (calculated)	2.790 Mg/m ³	
Absorption coefficient	3.646 mm ⁻¹	
<i>F</i> (000)	1068	
Theta range for data collection	1.74 to 26.00°	
Index ranges	-13 ≤ <i>h</i> ≤ 11, -13 ≤ <i>k</i> ≤ 13, 0 ≤ <i>l</i> ≤ 16	
Reflections collected/ unique	20196 / 5239 [<i>R</i> (int) = 0.050]	
Completeness to theta	26.00° 99.9 %	
Absorption correction	Numerical	
Max. and min. transmission	0.784 and 0.629	
Refinement method	Full-matrix least-squares on <i>F</i> ²	
Data / restraints / parameters	5239 / 0 / 317	
Goodness-of-fit on <i>F</i> ²	1.070	
Final <i>R</i> indices [<i>I</i> > 2σ(<i>I</i>)]	<i>R</i> 1 = 0.0215, <i>wR</i> 2 = 0.0414	
<i>R</i> indices (all data)	<i>R</i> 1 = 0.0377, <i>wR</i> 2 = 0.0441	
Extinction coefficient	0.00196(8)	
Largest diff. peak and hole	0.53 and -0.62 e.Å ⁻³	

Bond lengths [Å] and angles [°]

Ag(1)-O(1)	2.296(3)	O(10)-Mo(2)-O(14)	76.80(8)
Ag(1)-O(5)	2.406(2)	O(15)-Mo(2)-O(12)	163.37(9)
Ag(1)-O(3)	2.540(3)	O(16)-Mo(2)-O(12)	91.64(9)
Ag(1)-O(16)	2.581(2)	O(17)-Mo(2)-O(12)	74.11(8)
Ag(2)-O(4)	2.343(2)	O(10)-Mo(2)-O(12)	73.57(8)
Ag(2)-O(6)#1	2.421(2)	O(14)-Mo(2)-O(12)	69.21(7)
Ag(2)-O(2)	2.449(2)	O(6)-Mo(3)-O(5)	105.42(11)
Ag(2)-S(4)	2.6289(9)	O(6)-Mo(3)-O(17)	101.75(10)
Ag(2)-S(3)	2.8077(9)	O(5)-Mo(3)-O(17)	101.07(10)
Mo(1)-O(9)	1.703(2)	O(6)-Mo(3)-O(7)	99.90(10)
Mo(1)-O(11)	1.714(2)	O(5)-Mo(3)-O(7)	95.55(10)
Mo(1)-O(10)#2	1.896(2)	O(17)-Mo(3)-O(7)	147.98(9)
Mo(1)-O(8)	2.013(2)	O(6)-Mo(3)-O(8)	92.10(9)
Mo(1)-O(7)	2.294(2)	O(5)-Mo(3)-O(8)	160.29(9)
Mo(1)-O(12)#2	2.300(2)	O(17)-Mo(3)-O(8)	83.71(8)
Mo(2)-O(15)	1.696(2)	O(7)-Mo(3)-O(8)	72.15(8)
Mo(2)-O(16)	1.715(2)	O(6)-Mo(3)-O(12)	164.04(9)
Mo(2)-O(17)	1.928(2)	O(5)-Mo(3)-O(12)	89.99(9)
Mo(2)-O(10)	1.929(2)	O(17)-Mo(3)-O(12)	78.82(8)
Mo(2)-O(14)	2.287(2)	O(7)-Mo(3)-O(12)	73.97(8)
Mo(2)-O(12)	2.474(2)	O(8)-Mo(3)-O(12)	72.04(7)
Mo(3)-O(6)	1.704(2)	O(6)-Mo(3)-Mo(4)	134.68(8)
Mo(3)-O(5)	1.706(2)	O(5)-Mo(3)-Mo(4)	82.09(7)
Mo(3)-O(17)	1.889(2)	O(17)-Mo(3)-Mo(4)	120.94(7)
Mo(3)-O(7)	2.013(2)	O(7)-Mo(3)-Mo(4)	35.00(6)
Mo(3)-O(8)	2.288(2)	O(8)-Mo(3)-Mo(4)	79.12(5)
Mo(3)-O(12)	2.313(2)	O(12)-Mo(3)-Mo(4)	42.11(5)
Mo(3)-Mo(4)	3.2153(4)	O(13)-Mo(4)-O(14)#2	105.16(10)
Mo(4)-O(13)	1.700(2)	O(13)-Mo(4)-O(7)	101.02(10)
Mo(4)-O(14)#2	1.748(2)	O(14)#2-Mo(4)-O(7)	96.76(10)
Mo(4)-O(7)	1.946(2)	O(13)-Mo(4)-O(8)#2	101.04(10)
Mo(4)-O(8)#2	1.956(2)	O(14)#2-Mo(4)-O(8)#2	96.94(9)
Mo(4)-O(12)	2.157(2)	O(7)-Mo(4)-O(8)#2	149.92(9)
Mo(4)-O(12)#2	2.327(2)	O(13)-Mo(4)-O(12)	97.70(9)
S(1)-O(1)	1.519(3)	O(14)#2-Mo(4)-O(12)	157.14(9)
S(1)-C(2)	1.783(4)	O(7)-Mo(4)-O(12)	78.95(8)
S(1)-C(1)	1.786(4)	O(8)#2-Mo(4)-O(12)	78.05(8)

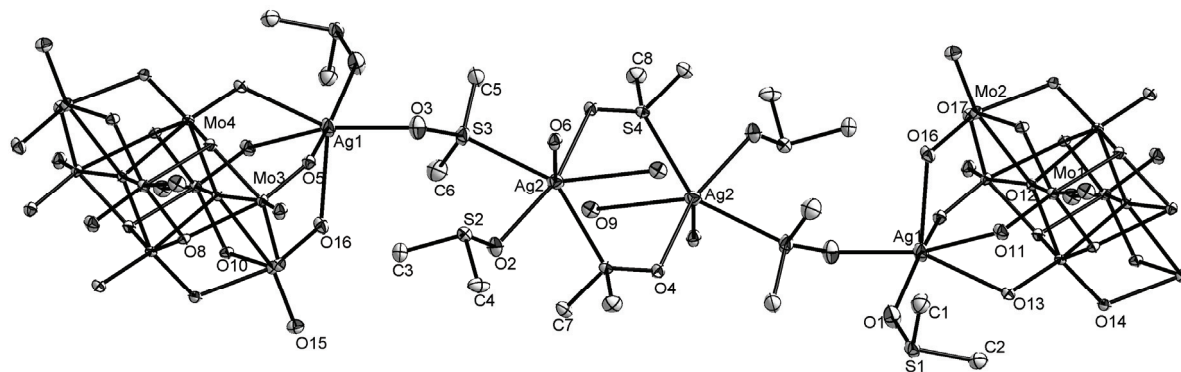
S(2)-O(2)	1.525(3)	O(13)-Mo(4)-O(12)#2	172.88(9)
S(2)-C(3)	1.784(3)	O(14)#2-Mo(4)-O(12)#2	81.97(9)
S(2)-C(4)	1.787(4)	O(7)-Mo(4)-O(12)#2	77.75(8)
S(3)-O(3)	1.504(3)	O(8)#2-Mo(4)-O(12)#2	77.82(8)
S(3)-C(5)	1.778(4)	O(12)-Mo(4)-O(12)#2	75.17(8)
S(3)-C(6)	1.779(4)	O(13)-Mo(4)-Mo(3)	89.62(8)
S(4)-O(4)#3	1.507(2)	O(14)#2-Mo(4)-Mo(3)	133.15(7)
S(4)-C(7)	1.780(3)	O(7)-Mo(4)-Mo(3)	36.40(6)
S(4)-C(8)	1.788(3)	O(8)#2-Mo(4)-Mo(3)	124.00(6)
O(6)-Ag(2)#1	2.421(2)	O(12)-Mo(4)-Mo(3)	45.97(6)
O(8)-Mo(4)#2	1.956(2)	O(12)#2-Mo(4)-Mo(3)	85.31(5)
O(10)-Mo(1)#2	1.896(2)	O(1)-S(1)-C(2)	105.27(16)
O(12)-Mo(1)#2	2.300(2)	O(1)-S(1)-C(1)	105.71(18)
O(12)-Mo(4)#2	2.327(2)	C(2)-S(1)-C(1)	99.20(18)
O(14)-Mo(4)#2	1.748(2)	O(2)-S(2)-C(3)	105.41(17)
O(4)-S(4)#3	1.507(2)	O(2)-S(2)-C(4)	105.06(17)
O(1)-Ag(1)-O(5)	151.89(9)	C(3)-S(2)-C(4)	97.75(18)
O(1)-Ag(1)-O(3)	86.40(8)	O(3)-S(3)-C(5)	108.34(18)
O(5)-Ag(1)-O(3)	80.51(7)	O(3)-S(3)-C(6)	104.94(17)
O(1)-Ag(1)-O(16)	132.39(9)	C(5)-S(3)-C(6)	98.9(2)
O(5)-Ag(1)-O(16)	74.15(7)	O(3)-S(3)-Ag(2)	123.95(11)
O(3)-Ag(1)-O(16)	96.44(8)	C(5)-S(3)-Ag(2)	109.03(13)
O(4)-Ag(2)-O(6)#1	93.07(8)	C(6)-S(3)-Ag(2)	108.73(14)
O(4)-Ag(2)-O(2)	163.18(8)	O(4)#3-S(4)-C(7)	107.25(16)
O(6)#1-Ag(2)-O(2)	89.80(8)	O(4)#3-S(4)-C(8)	105.34(15)
O(4)-Ag(2)-S(4)	115.49(6)	C(7)-S(4)-C(8)	98.56(17)
O(6)#1-Ag(2)-S(4)	119.56(6)	O(4)#3-S(4)-Ag(2)	123.78(10)
O(2)-Ag(2)-S(4)	76.96(6)	C(7)-S(4)-Ag(2)	106.33(12)
O(4)-Ag(2)-S(3)	82.64(6)	C(8)-S(4)-Ag(2)	112.60(13)
O(6)#1-Ag(2)-S(3)	93.70(6)	S(1)-O(1)-Ag(1)	137.95(15)
O(2)-Ag(2)-S(3)	80.64(6)	S(2)-O(2)-Ag(2)	117.52(14)
S(4)-Ag(2)-S(3)	139.26(3)	S(3)-O(3)-Ag(1)	118.49(14)
O(9)-Mo(1)-O(11)	104.94(11)	Mo(3)-O(5)-Ag(1)	135.45(11)
O(9)-Mo(1)-O(10)#2	100.92(10)	Mo(3)-O(6)-Ag(2)#1	141.85(13)
O(11)-Mo(1)-O(10)#2	101.29(10)	Mo(4)-O(7)-Mo(3)	108.60(10)
O(9)-Mo(1)-O(8)	100.51(10)	Mo(4)-O(7)-Mo(1)	109.89(9)
O(11)-Mo(1)-O(8)	96.02(10)	Mo(3)-O(7)-Mo(1)	103.74(9)
O(10)#2-Mo(1)-O(8)	147.83(9)	Mo(4)#2-O(8)-Mo(1)	108.86(10)
O(9)-Mo(1)-O(7)	89.56(9)	Mo(4)#2-O(8)-Mo(3)	109.92(9)
O(11)-Mo(1)-O(7)	162.89(9)	Mo(1)-O(8)-Mo(3)	103.96(9)

O(10)#2-Mo(1)-O(7)	84.44(8)	Mo(1)#2-O(10)-Mo(2)	116.59(11)
O(8)-Mo(1)-O(7)	72.01(8)	Mo(4)-O(12)-Mo(1)#2	92.77(8)
O(9)-Mo(1)-O(12)#2	161.47(9)	Mo(4)-O(12)-Mo(3)	91.92(8)
O(11)-Mo(1)-O(12)#2	93.26(9)	Mo(1)#2-O(12)-Mo(3)	162.97(10)
O(10)#2-Mo(1)-O(12)#2	78.47(8)	Mo(4)-O(12)-Mo(4)#2	104.83(8)
O(8)-Mo(1)-O(12)#2	73.63(8)	Mo(1)#2-O(12)-Mo(4)#2	97.42(8)
O(7)-Mo(1)-O(12)#2	71.93(7)	Mo(3)-O(12)-Mo(4)#2	97.18(8)
O(15)-Mo(2)-O(16)	104.98(11)	Mo(4)-O(12)-Mo(2)	163.27(10)
O(15)-Mo(2)-O(17)	102.42(11)	Mo(1)#2-O(12)-Mo(2)	85.85(7)
O(16)-Mo(2)-O(17)	98.68(10)	Mo(3)-O(12)-Mo(2)	84.96(7)
O(15)-Mo(2)-O(10)	103.82(10)	Mo(4)#2-O(12)-Mo(2)	91.88(7)
O(16)-Mo(2)-O(10)	98.21(10)	Mo(4)#2-O(14)-Mo(2)	116.94(10)
O(17)-Mo(2)-O(10)	143.76(9)	Mo(2)-O(16)-Ag(1)	130.19(12)
O(15)-Mo(2)-O(14)	94.17(10)	Mo(3)-O(17)-Mo(2)	115.90(11)
O(16)-Mo(2)-O(14)	160.86(10)	S(4)#3-O(4)-Ag(2)	120.30(13)
O(17)-Mo(2)-O(14)	76.76(8)		

Symmetry transformations used to generate equivalent atoms:

#1 $-x+1, -y+1, -z$ #2 $-x+2, -y+2, -z+1$ #3 $-x+1, -y+1, -z-1$

Ortep style representation of $[\text{Ag}_4(\text{DMSO})_8\text{Mo}_8\text{O}_{26}]_n$ (**22**): thermal ellipsoids at 50% probability, hydrogen atoms are omitted for clarity.



6.18 Crystal data for $((n\text{-C}_4\text{H}_9)_4\text{N})_{2n}[\text{K}_2(\text{DMSO})_3\text{Mo}_8\text{O}_{26}]_n$ (23)

Empirical formula	$\text{C}_{38}\text{H}_{90}\text{K}_2\text{Mo}_8\text{N}_2\text{O}_{29}\text{S}_3$	
Crystal growth	Diffusion of ethanol, 14 days	
Crystal description	Colourless block crystals	
Crystal size	$0.16 \times 0.16 \times 0.15 \text{ mm}^3$	
Formula weight	1981.02	
Temperature	150(2) K	
Wavelength	0.71073 Å	
Crystal system	Triclinic	
Space group	$P\bar{1}$	
Unit cell dimensions	$a = 13.9729(4) \text{ Å}$	$\alpha = 76.311(2)^\circ$
	$b = 14.1830(5) \text{ Å}$	$\beta = 86.084(2)^\circ$
	$c = 17.3775(5) \text{ Å}$	$\gamma = 83.630(2)^\circ$
Volume	$3322.20(18) \text{ Å}^3$	
Z	2	
Density (calculated)	1.980 Mg/m^3	
Absorption coefficient	1.756 mm^{-1}	
$F(000)$	1972	
Theta range for data collection	1.94 to 25.98°	
Index ranges	$-17 \leq h \leq 17, -16 \leq k \leq 17, 0 \leq l \leq 21$	
Reflections collected/ unique	48424 / 12950 [$R(\text{int}) = 0.0584$]	
Completeness to theta	25.98° 99.3 %	
Absorption correction	Gaussian	
Max. and min. transmission	0.82 and 0.73	
Refinement method	Full-matrix least-squares on F^2	
Data / restraints / parameters	12950 / 0 / 753	
Goodness-of-fit on F^2	1.053	
Final R indices [$I > 2\sigma(I)$]	$R1 = 0.0381, wR2 = 0.0688$	
R indices (all data)	$R1 = 0.0691, wR2 = 0.0757$	
Extinction coefficient	None	
Largest diff. peak and hole	0.93 and -0.69 e.Å^{-3}	

Bond lengths [Å] and angles [°]

Mo(1)-O(8)	1.697(3)	O(29)-Mo(6)-K(2)	63.38(7)
Mo(1)-O(4)	1.713(3)	O(23)-Mo(7)-O(19)	104.79(14)
Mo(1)-O(15)	1.889(3)	O(23)-Mo(7)-O(26)	102.28(14)
Mo(1)-O(12)	1.986(3)	O(19)-Mo(7)-O(26)	99.56(14)
Mo(1)-O(16)	2.330(3)	O(23)-Mo(7)-O(27)	101.25(13)
Mo(1)-O(13)	2.363(3)	O(19)-Mo(7)-O(27)	98.00(14)
Mo(1)-Mo(2)	3.2123(5)	O(26)-Mo(7)-O(27)	145.81(12)
Mo(2)-O(6)	1.697(3)	O(23)-Mo(7)-O(28)#2	91.50(12)
Mo(2)-O(9)	1.750(3)	O(19)-Mo(7)-O(28)#2	162.64(13)
Mo(2)-O(12)	1.944(3)	O(26)-Mo(7)-O(28)#2	82.45(11)
Mo(2)-O(13)#1	1.948(3)	O(27)-Mo(7)-O(28)#2	72.46(11)
Mo(2)-O(16)	2.141(3)	O(23)-Mo(7)-O(29)	163.17(13)
Mo(2)-O(16)#1	2.361(3)	O(19)-Mo(7)-O(29)	91.81(12)
Mo(2)-Mo(3)	3.2087(5)	O(26)-Mo(7)-O(29)	77.19(11)
Mo(3)-O(10)	1.702(3)	O(27)-Mo(7)-O(29)	73.14(11)
Mo(3)-O(7)	1.710(3)	O(28)#2-Mo(7)-O(29)	71.71(10)
Mo(3)-O(14)	1.896(3)	O(23)-Mo(7)-K(2)	133.39(10)
Mo(3)-O(13)#1	2.000(3)	O(19)-Mo(7)-K(2)	28.64(10)
Mo(3)-O(16)	2.313(3)	O(26)-Mo(7)-K(2)	90.03(9)
Mo(3)-O(12)#1	2.343(3)	O(27)-Mo(7)-K(2)	91.55(9)
Mo(4)-O(11)	1.703(3)	O(28)#2-Mo(7)-K(2)	134.93(7)
Mo(4)-O(5)	1.711(3)	O(29)-Mo(7)-K(2)	63.30(7)
Mo(4)-O(14)	1.926(3)	O(20)-Mo(8)-O(24)	105.65(14)
Mo(4)-O(15)	1.933(3)	O(20)-Mo(8)-O(28)	101.36(13)
Mo(4)-O(9)#1	2.276(3)	O(24)-Mo(8)-O(28)	97.46(13)
Mo(4)-O(16)	2.464(3)	O(20)-Mo(8)-O(27)	99.89(13)
Mo(5)-O(21)	1.699(3)	O(24)-Mo(8)-O(27)	96.24(13)
Mo(5)-O(17)	1.714(3)	O(28)-Mo(8)-O(27)	150.50(12)
Mo(5)-O(25)	1.893(3)	O(20)-Mo(8)-O(29)	96.81(13)
Mo(5)-O(28)	2.021(3)	O(24)-Mo(8)-O(29)	157.51(12)
Mo(5)-O(29)	2.322(3)	O(28)-Mo(8)-O(29)	78.94(11)
Mo(5)-O(27)#2	2.326(3)	O(27)-Mo(8)-O(29)	78.44(11)
Mo(5)-K(2)	4.0928(11)	O(20)-Mo(8)-O(29)#2	172.12(13)
Mo(6)-O(22)	1.697(3)	O(24)-Mo(8)-O(29)#2	82.16(12)
Mo(6)-O(18)	1.718(3)	O(28)-Mo(8)-O(29)#2	78.29(11)
Mo(6)-O(26)	1.920(3)	O(27)-Mo(8)-O(29)#2	77.86(11)
Mo(6)-O(25)	1.928(3)	O(29)-Mo(8)-O(29)#2	75.36(12)

Mo(6)-O(24)#2	2.296(3)	O(20)-Mo(8)-K(2)	31.88(10)
Mo(6)-O(29)	2.474(3)	O(24)-Mo(8)-K(2)	137.53(10)
Mo(6)-K(2)	4.0946(11)	O(28)-Mo(8)-K(2)	93.89(9)
Mo(7)-O(23)	1.701(3)	O(27)-Mo(8)-K(2)	93.44(8)
Mo(7)-O(19)	1.711(3)	O(29)-Mo(8)-K(2)	64.94(8)
Mo(7)-O(26)	1.890(3)	O(29)#2-Mo(8)-K(2)	140.30(8)
Mo(7)-O(27)	1.994(3)	O(2A)#3-K(1)-O(2A)	72.30(11)
Mo(7)-O(28)#2	2.303(3)	O(2A)#3-K(1)-O(5)	146.80(10)
Mo(7)-O(29)	2.347(3)	O(2A)-K(1)-O(5)	125.47(10)
Mo(7)-K(2)	4.1224(11)	O(2A)#3-K(1)-O(1)	93.89(10)
Mo(8)-O(20)	1.696(3)	O(2A)-K(1)-O(1)	79.80(10)
Mo(8)-O(24)	1.749(3)	O(5)-K(1)-O(1)	66.23(10)
Mo(8)-O(28)	1.956(3)	O(2A)#3-K(1)-O(4)	88.92(9)
Mo(8)-O(27)	1.961(3)	O(2A)-K(1)-O(4)	160.55(10)
Mo(8)-O(29)	2.148(3)	O(5)-K(1)-O(4)	68.72(9)
Mo(8)-O(29)#2	2.334(3)	O(1)-K(1)-O(4)	96.95(10)
Mo(8)-K(2)	4.0757(11)	O(2A)#3-K(1)-O(7)	146.32(10)
K(1)-O(2A)#3	2.752(3)	O(2A)-K(1)-O(7)	101.77(9)
K(1)-O(2A)	2.767(3)	O(5)-K(1)-O(7)	63.74(9)
K(1)-O(5)	2.808(3)	O(1)-K(1)-O(7)	118.15(10)
K(1)-O(1)	2.820(3)	O(4)-K(1)-O(7)	96.67(9)
K(1)-O(4)	2.832(3)	O(2A)#3-K(1)-O(6)	92.99(9)
K(1)-O(7)	2.930(3)	O(2A)-K(1)-O(6)	122.05(10)
K(1)-O(6)	3.049(3)	O(5)-K(1)-O(6)	97.51(9)
K(1)-S(2)	3.6456(16)	O(1)-K(1)-O(6)	158.15(10)
K(1)-K(1)#3	4.457(2)	O(4)-K(1)-O(6)	62.46(8)
K(2)-O(3A)#4	2.702(3)	O(7)-K(1)-O(6)	61.37(8)
K(2)-O(19)	2.746(3)	O(2A)#3-K(1)-S(2)	93.42(7)
K(2)-O(18)	2.749(3)	O(2A)-K(1)-S(2)	22.11(7)
K(2)-O(3A)	2.753(3)	O(5)-K(1)-S(2)	103.88(7)
K(2)-O(17)	2.765(3)	O(1)-K(1)-S(2)	71.20(8)
K(2)-O(20)	2.784(3)	O(4)-K(1)-S(2)	168.04(7)
K(2)-S(3)	3.6782(17)	O(7)-K(1)-S(2)	87.87(6)
K(2)-K(2)#4	4.331(2)	O(6)-K(1)-S(2)	129.01(7)
S(1)-O(1)	1.505(4)	O(2A)#3-K(1)-K(1)#3	36.26(7)
S(1)-C(2)	1.775(5)	O(2A)-K(1)-K(1)#3	36.03(7)
S(1)-C(1)	1.790(5)	O(5)-K(1)-K(1)#3	151.28(8)
S(2)-O(2A)	1.502(3)	O(1)-K(1)-K(1)#3	86.09(8)
S(2)-C(4)	1.778(5)	O(4)-K(1)-K(1)#3	125.02(7)
S(2)-C(3)	1.789(5)	O(7)-K(1)-K(1)#3	129.83(7)

S(3)-O(3A)	1.507(3)	O(6)-K(1)-K(1)#3	111.20(7)
S(3)-C(5)	1.772(5)	S(2)-K(1)-K(1)#3	57.43(3)
S(3)-C(6)	1.780(5)	O(3A)#4-K(2)-O(19)	152.81(10)
O(2A)-K(1)#3	2.752(3)	O(3A)#4-K(2)-O(18)	134.62(10)
O(3A)-K(2)#4	2.702(3)	O(19)-K(2)-O(18)	67.52(9)
O(9)-Mo(4)#1	2.276(3)	O(3A)#4-K(2)-O(3A)	74.89(11)
O(12)-Mo(3)#1	2.343(3)	O(19)-K(2)-O(3A)	89.07(10)
O(13)-Mo(2)#1	1.948(3)	O(18)-K(2)-O(3A)	95.30(10)
O(13)-Mo(3)#1	2.000(3)	O(3A)#4-K(2)-O(17)	99.17(10)
O(16)-Mo(2)#1	2.361(3)	O(19)-K(2)-O(17)	103.97(9)
O(24)-Mo(6)#2	2.296(3)	O(18)-K(2)-O(17)	71.98(9)
O(27)-Mo(5)#2	2.326(3)	O(3A)-K(2)-O(17)	155.91(10)
O(28)-Mo(7)#2	2.303(3)	O(3A)#4-K(2)-O(20)	111.33(10)
O(29)-Mo(8)#2	2.334(3)	O(19)-K(2)-O(20)	66.86(9)
N(1)-C(7)	1.519(5)	O(18)-K(2)-O(20)	105.16(9)
N(1)-C(19)	1.528(5)	O(3A)-K(2)-O(20)	138.21(10)
N(1)-C(11)	1.532(6)	O(17)-K(2)-O(20)	65.85(9)
N(1)-C(15)	1.533(6)	O(3A)#4-K(2)-S(3)	96.24(8)
N(2)-C(23)	1.514(6)	O(19)-K(2)-S(3)	70.54(7)
N(2)-C(31)	1.521(6)	O(18)-K(2)-S(3)	78.20(7)
N(2)-C(27)	1.524(6)	O(3A)-K(2)-S(3)	21.53(7)
N(2)-C(35)	1.527(6)	O(17)-K(2)-S(3)	149.21(8)
C(7)-C(8)	1.516(6)	O(20)-K(2)-S(3)	131.42(7)
C(8)-C(9)	1.520(6)	O(3A)#4-K(2)-Mo(8)	127.15(8)
C(9)-C(10)	1.518(6)	O(19)-K(2)-Mo(8)	58.47(7)
C(11)-C(12)	1.520(6)	O(18)-K(2)-Mo(8)	86.41(7)
C(12)-C(13)	1.516(7)	O(3A)-K(2)-Mo(8)	144.10(8)
C(13)-C(14)	1.516(7)	O(17)-K(2)-Mo(8)	57.49(6)
C(15)-C(16)	1.526(6)	O(20)-K(2)-Mo(8)	18.77(6)
C(16)-C(17)	1.527(6)	S(3)-K(2)-Mo(8)	128.79(3)
C(17)-C(18)	1.507(7)	O(3A)#4-K(2)-Mo(5)	117.67(7)
C(19)-C(20)	1.515(6)	O(19)-K(2)-Mo(5)	85.77(6)
C(20)-C(21)	1.530(6)	O(18)-K(2)-Mo(5)	60.62(7)
C(21)-C(22)	1.517(6)	O(3A)-K(2)-Mo(5)	155.47(8)
C(23)-C(24)	1.509(6)	O(17)-K(2)-Mo(5)	18.53(6)
C(24)-C(25)	1.531(6)	O(20)-K(2)-Mo(5)	60.02(6)
C(25)-C(26)	1.504(7)	S(3)-K(2)-Mo(5)	138.06(4)
C(27)-C(28)	1.512(6)	Mo(8)-K(2)-Mo(5)	46.515(14)
C(28)-C(29)	1.518(6)	O(3A)#4-K(2)-Mo(6)	146.86(8)
C(29)-C(30)	1.523(7)	O(19)-K(2)-Mo(6)	59.34(6)

C(31)-C(32)	1.519(6)	O(18)-K(2)-Mo(6)	18.33(6)
C(32)-C(33)	1.523(7)	O(3A)-K(2)-Mo(6)	110.39(7)
C(33)-C(34)	1.506(7)	O(17)-K(2)-Mo(6)	62.16(7)
C(35)-C(36)	1.528(6)	O(20)-K(2)-Mo(6)	86.86(7)
C(36)-C(37)	1.504(6)	S(3)-K(2)-Mo(6)	90.96(3)
C(37)-C(38)	1.509(7)	Mo(8)-K(2)-Mo(6)	68.102(18)
		Mo(5)-K(2)-Mo(6)	47.149(14)
O(8)-Mo(1)-O(4)	104.93(14)	O(3A)#4-K(2)-Mo(7)	166.03(8)
O(8)-Mo(1)-O(15)	101.88(13)	O(19)-K(2)-Mo(7)	17.37(6)
O(4)-Mo(1)-O(15)	100.89(13)	O(18)-K(2)-Mo(7)	59.25(7)
O(8)-Mo(1)-O(12)	100.35(13)	O(3A)-K(2)-Mo(7)	104.65(7)
O(4)-Mo(1)-O(12)	97.58(13)	O(17)-K(2)-Mo(7)	86.67(7)
O(15)-Mo(1)-O(12)	146.19(12)	O(20)-K(2)-Mo(7)	59.47(6)
O(8)-Mo(1)-O(16)	160.54(12)	S(3)-K(2)-Mo(7)	84.63(3)
O(4)-Mo(1)-O(16)	94.16(12)	Mo(8)-K(2)-Mo(7)	46.534(14)
O(15)-Mo(1)-O(16)	77.65(11)	Mo(5)-K(2)-Mo(7)	68.406(18)
O(12)-Mo(1)-O(16)	72.96(10)	Mo(6)-K(2)-Mo(7)	46.785(14)
O(8)-Mo(1)-O(13)	88.96(12)	O(3A)#4-K(2)-K(2)#4	37.85(7)
O(4)-Mo(1)-O(13)	163.96(12)	O(19)-K(2)-K(2)#4	123.00(7)
O(15)-Mo(1)-O(13)	83.66(11)	O(18)-K(2)-K(2)#4	119.80(8)
O(12)-Mo(1)-O(13)	71.59(11)	O(3A)-K(2)-K(2)#4	37.04(7)
O(16)-Mo(1)-O(13)	71.62(10)	O(17)-K(2)-K(2)#4	132.82(8)
O(8)-Mo(1)-Mo(2)	135.03(10)	O(20)-K(2)-K(2)#4	134.49(8)
O(4)-Mo(1)-Mo(2)	85.13(10)	S(3)-K(2)-K(2)#4	58.43(3)
O(15)-Mo(1)-Mo(2)	119.39(9)	Mo(8)-K(2)-K(2)#4	153.08(4)
O(12)-Mo(1)-Mo(2)	34.75(8)	Mo(5)-K(2)-K(2)#4	150.22(4)
O(16)-Mo(1)-Mo(2)	41.77(7)	Mo(6)-K(2)-K(2)#4	138.06(4)
O(13)-Mo(1)-Mo(2)	79.29(7)	Mo(7)-K(2)-K(2)#4	140.02(4)
O(6)-Mo(2)-O(9)	104.59(14)	O(1)-S(1)-C(2)	107.0(3)
O(6)-Mo(2)-O(12)	101.20(13)	O(1)-S(1)-C(1)	105.0(2)
O(9)-Mo(2)-O(12)	97.21(12)	C(2)-S(1)-C(1)	96.4(3)
O(6)-Mo(2)-O(13)#1	101.09(13)	O(2A)-S(2)-C(4)	106.1(2)
O(9)-Mo(2)-O(13)#1	96.34(12)	O(2A)-S(2)-C(3)	106.6(2)
O(12)-Mo(2)-O(13)#1	149.99(12)	C(4)-S(2)-C(3)	98.2(3)
O(6)-Mo(2)-O(16)	98.75(13)	O(2A)-S(2)-K(1)	43.91(13)
O(9)-Mo(2)-O(16)	156.66(13)	C(4)-S(2)-K(1)	110.31(18)
O(12)-Mo(2)-O(16)	78.23(11)	C(3)-S(2)-K(1)	143.14(17)
O(13)#1-Mo(2)-O(16)	78.74(11)	O(3A)-S(3)-C(5)	105.9(2)
O(6)-Mo(2)-O(16)#1	173.88(12)	O(3A)-S(3)-C(6)	105.9(2)
O(9)-Mo(2)-O(16)#1	81.49(12)	C(5)-S(3)-C(6)	98.4(3)

O(12)-Mo(2)-O(16)#1	77.17(11)	O(3A)-S(3)-K(2)	42.12(13)
O(13)#1-Mo(2)-O(16)#1	78.53(11)	C(5)-S(3)-K(2)	94.59(19)
O(16)-Mo(2)-O(16)#1	75.17(11)	C(6)-S(3)-K(2)	147.99(19)
O(6)-Mo(2)-Mo(3)	90.09(10)	S(1)-O(1)-K(1)	125.15(19)
O(9)-Mo(2)-Mo(3)	132.52(9)	S(2)-O(2A)-K(1)#3	134.84(18)
O(12)-Mo(2)-Mo(3)	124.30(8)	S(2)-O(2A)-K(1)	113.98(18)
O(13)#1-Mo(2)-Mo(3)	36.18(8)	K(1)#3-O(2A)-K(1)	107.70(11)
O(16)-Mo(2)-Mo(3)	46.08(7)	S(3)-O(3A)-K(2)#4	137.87(18)
O(16)#1-Mo(2)-Mo(3)	86.08(7)	S(3)-O(3A)-K(2)	116.34(17)
O(6)-Mo(2)-Mo(1)	89.58(10)	K(2)#4-O(3A)-K(2)	105.11(11)
O(9)-Mo(2)-Mo(1)	132.83(9)	Mo(1)-O(4)-K(1)	135.60(15)
O(12)-Mo(2)-Mo(1)	35.62(8)	Mo(4)-O(5)-K(1)	138.26(15)
O(13)#1-Mo(2)-Mo(1)	125.22(9)	Mo(2)-O(6)-K(1)	129.02(15)
O(16)-Mo(2)-Mo(1)	46.48(7)	Mo(3)-O(7)-K(1)	135.92(15)
O(16)#1-Mo(2)-Mo(1)	85.74(7)	Mo(2)-O(9)-Mo(4)#1	117.29(15)
Mo(3)-Mo(2)-Mo(1)	91.195(14)	Mo(2)-O(12)-Mo(1)	109.63(13)
O(10)-Mo(3)-O(7)	104.66(14)	Mo(2)-O(12)-Mo(3)#1	110.63(12)
O(10)-Mo(3)-O(14)	101.05(13)	Mo(1)-O(12)-Mo(3)#1	104.51(12)
O(7)-Mo(3)-O(14)	101.12(14)	Mo(2)#1-O(13)-Mo(3)#1	108.70(13)
O(10)-Mo(3)-O(13)#1	100.34(13)	Mo(2)#1-O(13)-Mo(1)	109.57(12)
O(7)-Mo(3)-O(13)#1	97.41(13)	Mo(3)#1-O(13)-Mo(1)	103.35(12)
O(14)-Mo(3)-O(13)#1	147.00(12)	Mo(3)-O(14)-Mo(4)	116.09(14)
O(10)-Mo(3)-O(16)	162.39(13)	Mo(1)-O(15)-Mo(4)	117.83(15)
O(7)-Mo(3)-O(16)	92.63(12)	Mo(2)-O(16)-Mo(3)	92.10(11)
O(14)-Mo(3)-O(16)	78.38(11)	Mo(2)-O(16)-Mo(1)	91.76(10)
O(13)#1-Mo(3)-O(16)	73.69(10)	Mo(3)-O(16)-Mo(1)	162.20(13)
O(10)-Mo(3)-O(12)#1	91.40(12)	Mo(2)-O(16)-Mo(2)#1	104.83(11)
O(7)-Mo(3)-O(12)#1	162.23(12)	Mo(3)-O(16)-Mo(2)#1	98.17(10)
O(14)-Mo(3)-O(12)#1	82.81(11)	Mo(1)-O(16)-Mo(2)#1	97.62(10)
O(13)#1-Mo(3)-O(12)#1	71.82(11)	Mo(2)-O(16)-Mo(4)	163.94(14)
O(16)-Mo(3)-O(12)#1	71.03(10)	Mo(3)-O(16)-Mo(4)	85.44(9)
O(10)-Mo(3)-Mo(2)	135.35(10)	Mo(1)-O(16)-Mo(4)	86.06(9)
O(7)-Mo(3)-Mo(2)	84.65(10)	Mo(2)#1-O(16)-Mo(4)	91.23(10)
O(14)-Mo(3)-Mo(2)	120.20(8)	Mo(5)-O(17)-K(2)	130.63(15)
O(13)#1-Mo(3)-Mo(2)	35.11(8)	Mo(6)-O(18)-K(2)	131.46(15)
O(16)-Mo(3)-Mo(2)	41.82(7)	Mo(7)-O(19)-K(2)	133.99(15)
O(12)#1-Mo(3)-Mo(2)	78.50(7)	Mo(8)-O(20)-K(2)	129.35(15)
O(11)-Mo(4)-O(5)	104.92(15)	Mo(8)-O(24)-Mo(6)#2	116.64(14)
O(11)-Mo(4)-O(14)	103.07(14)	Mo(5)-O(25)-Mo(6)	117.97(14)
O(5)-Mo(4)-O(14)	96.63(14)	Mo(7)-O(26)-Mo(6)	117.76(15)

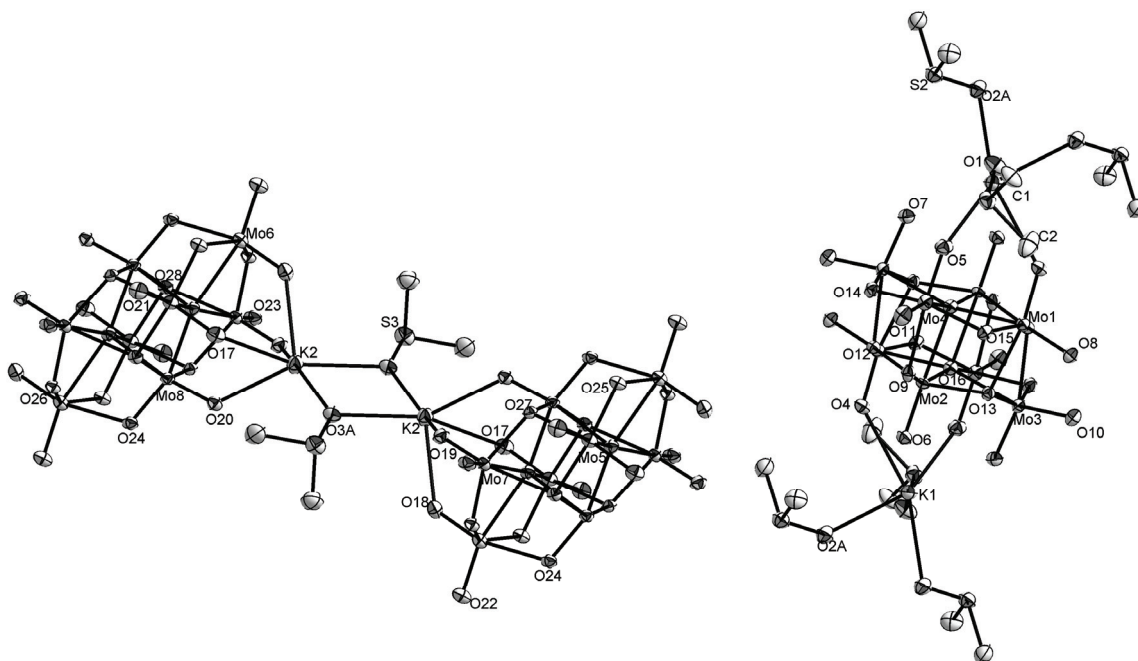
O(11)-Mo(4)-O(15)	103.71(14)	Mo(8)-O(27)-Mo(7)	109.94(13)
O(5)-Mo(4)-O(15)	98.11(14)	Mo(8)-O(27)-Mo(5)#2	109.70(12)
O(14)-Mo(4)-O(15)	144.79(12)	Mo(7)-O(27)-Mo(5)#2	103.62(12)
O(11)-Mo(4)-O(9)#1	92.94(13)	Mo(8)-O(28)-Mo(5)	108.42(13)
O(5)-Mo(4)-O(9)#1	162.12(13)	Mo(8)-O(28)-Mo(7)#2	110.40(13)
O(14)-Mo(4)-O(9)#1	78.04(11)	Mo(5)-O(28)-Mo(7)#2	103.57(12)
O(15)-Mo(4)-O(9)#1	78.17(11)	Mo(8)-O(29)-Mo(5)	92.29(11)
O(11)-Mo(4)-O(16)	162.92(13)	Mo(8)-O(29)-Mo(8)#2	104.64(12)
O(5)-Mo(4)-O(16)	92.16(12)	Mo(5)-O(29)-Mo(8)#2	97.91(10)
O(14)-Mo(4)-O(16)	74.08(10)	Mo(8)-O(29)-Mo(7)	92.09(10)
O(15)-Mo(4)-O(16)	73.58(11)	Mo(5)-O(29)-Mo(7)	163.00(14)
O(9)#1-Mo(4)-O(16)	69.98(10)	Mo(8)#2-O(29)-Mo(7)	96.86(11)
O(21)-Mo(5)-O(17)	105.12(15)	Mo(8)-O(29)-Mo(6)	163.57(14)
O(21)-Mo(5)-O(25)	101.29(14)	Mo(5)-O(29)-Mo(6)	86.05(9)
O(17)-Mo(5)-O(25)	102.18(14)	Mo(8)#2-O(29)-Mo(6)	91.78(10)
O(21)-Mo(5)-O(28)	100.60(13)	Mo(7)-O(29)-Mo(6)	85.12(10)
O(17)-Mo(5)-O(28)	94.90(13)	C(7)-N(1)-C(19)	107.2(3)
O(25)-Mo(5)-O(28)	147.52(12)	C(7)-N(1)-C(11)	110.8(3)
O(21)-Mo(5)-O(29)	160.47(13)	C(19)-N(1)-C(11)	110.1(3)
O(17)-Mo(5)-O(29)	94.05(12)	C(7)-N(1)-C(15)	110.9(3)
O(25)-Mo(5)-O(29)	77.77(11)	C(19)-N(1)-C(15)	111.0(3)
O(28)-Mo(5)-O(29)	73.60(11)	C(11)-N(1)-C(15)	106.9(3)
O(21)-Mo(5)-O(27)#2	89.01(13)	C(23)-N(2)-C(31)	110.8(4)
O(17)-Mo(5)-O(27)#2	162.21(12)	C(23)-N(2)-C(27)	110.2(4)
O(25)-Mo(5)-O(27)#2	85.17(12)	C(31)-N(2)-C(27)	107.0(3)
O(28)-Mo(5)-O(27)#2	71.51(11)	C(23)-N(2)-C(35)	107.3(3)
O(29)-Mo(5)-O(27)#2	71.46(10)	C(31)-N(2)-C(35)	111.0(4)
O(21)-Mo(5)-K(2)	135.48(11)	C(27)-N(2)-C(35)	110.6(3)
O(17)-Mo(5)-K(2)	30.84(10)	C(8)-C(7)-N(1)	115.1(4)
O(25)-Mo(5)-K(2)	88.61(9)	C(7)-C(8)-C(9)	109.7(4)
O(28)-Mo(5)-K(2)	92.37(8)	C(10)-C(9)-C(8)	112.1(4)
O(29)-Mo(5)-K(2)	63.99(7)	C(12)-C(11)-N(1)	114.5(4)
O(27)#2-Mo(5)-K(2)	135.33(7)	C(13)-C(12)-C(11)	111.8(4)
O(22)-Mo(6)-O(18)	105.03(15)	C(12)-C(13)-C(14)	111.7(4)
O(22)-Mo(6)-O(26)	102.59(14)	C(16)-C(15)-N(1)	114.9(4)
O(18)-Mo(6)-O(26)	98.64(13)	C(15)-C(16)-C(17)	111.4(4)
O(22)-Mo(6)-O(25)	103.85(14)	C(18)-C(17)-C(16)	114.1(4)
O(18)-Mo(6)-O(25)	98.14(14)	C(20)-C(19)-N(1)	116.0(4)
O(26)-Mo(6)-O(25)	143.62(12)	C(19)-C(20)-C(21)	110.1(4)
O(22)-Mo(6)-O(24)#2	92.02(13)	C(22)-C(21)-C(20)	112.2(4)

O(18)-Mo(6)-O(24)#2	162.95(13)	C(24)-C(23)-N(2)	115.6(4)
O(26)-Mo(6)-O(24)#2	77.00(11)	C(23)-C(24)-C(25)	111.0(4)
O(25)-Mo(6)-O(24)#2	77.54(11)	C(26)-C(25)-C(24)	113.7(4)
O(22)-Mo(6)-O(29)	161.39(13)	C(28)-C(27)-N(2)	115.4(4)
O(18)-Mo(6)-O(29)	93.57(12)	C(27)-C(28)-C(29)	110.5(4)
O(26)-Mo(6)-O(29)	73.53(11)	C(28)-C(29)-C(30)	112.2(4)
O(25)-Mo(6)-O(29)	73.41(11)	C(32)-C(31)-N(2)	115.7(4)
O(24)#2-Mo(6)-O(29)	69.38(10)	C(31)-C(32)-C(33)	110.4(4)
O(22)-Mo(6)-K(2)	135.23(11)	C(34)-C(33)-C(32)	112.5(4)
O(18)-Mo(6)-K(2)	30.21(11)	N(2)-C(35)-C(36)	114.2(4)
O(26)-Mo(6)-K(2)	90.44(9)	C(37)-C(36)-C(35)	111.3(4)
O(25)-Mo(6)-K(2)	88.10(9)	C(36)-C(37)-C(38)	111.7(4)
O(24)#2-Mo(6)-K(2)	132.75(8)		

Symmetry transformations used to generate equivalent atoms:

#1 -x,-y,-z #2 -x+1,-y+1,-z+1 #3 -x,-y+1,-z

Ortep style representation of $((n\text{-C}_4\text{H}_9)_4\text{N})_{2n}[\text{K}_2(\text{DMSO})_3\text{Mo}_8\text{O}_{26}]_n$ (**23**): thermal ellipsoids at 50% probability, hydrogen atoms and counterions are omitted for clarity. Not all carbon, sulphur and oxygen atoms of DMSO are labelled.



6.19 Crystal data for $((n\text{-C}_4\text{H}_9)_4\text{N})_n(\text{H}_2\text{NMe}_2)_n[\text{K}_2(\text{DMF})\text{Mo}_8\text{O}_{26}]_n \cdot \text{DMF}$ (24)

Empirical formula	$\text{C}_{24}\text{H}_{58}\text{K}_2\text{Mo}_8\text{N}_4\text{O}_{28}$	
Crystal growth	Diffusion of diethyl ether, 4 days	
Crystal description	Colourless block crystals	
Crystal size	$0.10 \times 0.10 \times 0.06 \text{ mm}^3$	
Formula weight	1696.46	
Temperature	150(2) K	
Wavelength	0.71073 Å	
Crystal system	Monoclinic	
Space group	$P2_1$	
Unit cell dimensions	$a = 11.7040(4) \text{ Å}$	$\alpha = 90^\circ$
	$b = 15.4744(7) \text{ Å}$	$\beta = 111.800(2)^\circ$
	$c = 15.0085(6) \text{ Å}$	$\gamma = 90^\circ$
Volume	$2523.83(18) \text{ Å}^3$	
Z	2	
Density (calculated)	2.232 Mg/m^3	
Absorption coefficient	2.171 mm^{-1}	
$F(000)$	1656	
Theta range for data collection	1.87 to 25.50°	
Index ranges	$-14 \leq h \leq 13, -16 \leq k \leq 18, 0 \leq l \leq 18$	
Reflections collected/ unique	14991 / 7702 [$R(\text{int}) = 0.0687$]	
Completeness to theta	25.50° 99.8 %	
Absorption correction	Gaussian	
Max. and min. transmission	0.884 and 0.788	
Refinement method	Full-matrix least-squares on F^2	
Data / restraints / parameters	7702 / 2 / 542	
Goodness-of-fit on F^2	1.016	
Final R indices [$I > 2\sigma(I)$]	$R1 = 0.0545, wR2 = 0.0776$	
R indices (all data)	$R1 = 0.1037, wR2 = 0.0910$	
Extinction coefficient	0.00022(4)	

Largest diff. peak and hole

0.99 and -1.03 e.Å⁻³

Bond lengths [Å] and angles [°]

Mo(1)-O(4)	1.706(12)	O(8)-Mo(6)-O(5)	83.9(4)
Mo(1)-O(23)	1.723(10)	O(20)-Mo(6)-O(5)	70.4(4)
Mo(1)-O(22)	1.875(10)	O(2)-Mo(6)-O(21)	93.3(5)
Mo(1)-O(5)	1.997(9)	O(17)-Mo(6)-O(21)	161.7(5)
Mo(1)-O(20)	2.287(11)	O(8)-Mo(6)-O(21)	77.3(4)
Mo(1)-O(24)	2.313(10)	O(20)-Mo(6)-O(21)	73.0(4)
Mo(1)-K(1)	4.037(4)	O(5)-Mo(6)-O(21)	71.2(3)
Mo(2)-O(26)	1.703(11)	O(2)-Mo(6)-K(2)#1	30.8(4)
Mo(2)-O(10)	1.710(11)	O(17)-Mo(6)-K(2)#1	135.3(4)
Mo(2)-O(18)	1.900(11)	O(8)-Mo(6)-K(2)#1	90.3(4)
Mo(2)-O(9)	2.016(10)	O(20)-Mo(6)-K(2)#1	91.3(3)
Mo(2)-O(21)	2.306(11)	O(5)-Mo(6)-K(2)#1	133.7(3)
Mo(2)-O(7)	2.342(12)	O(21)-Mo(6)-K(2)#1	62.8(3)
Mo(2)-K(2)#1	4.019(4)	O(19)-Mo(7)-O(1)	105.4(5)
Mo(3)-O(12)	1.685(12)	O(19)-Mo(7)-O(11)	102.1(5)
Mo(3)-O(25)	1.757(10)	O(1)-Mo(7)-O(11)	101.7(5)
Mo(3)-O(9)	1.941(9)	O(19)-Mo(7)-O(7)	99.7(5)
Mo(3)-O(20)	1.952(10)	O(1)-Mo(7)-O(7)	95.6(5)
Mo(3)-O(21)	2.157(9)	O(11)-Mo(7)-O(7)	147.3(4)
Mo(3)-O(24)	2.361(10)	O(19)-Mo(7)-O(9)	89.8(5)
Mo(3)-K(2)#1	3.971(4)	O(1)-Mo(7)-O(9)	161.8(5)
Mo(4)-O(15)	1.681(9)	O(11)-Mo(7)-O(9)	84.3(4)
Mo(4)-O(3)	1.729(12)	O(7)-Mo(7)-O(9)	71.6(4)
Mo(4)-O(8)	1.902(10)	O(19)-Mo(7)-O(24)	161.3(5)
Mo(4)-O(18)	1.917(11)	O(1)-Mo(7)-O(24)	92.5(4)
Mo(4)-O(14)	2.290(10)	O(11)-Mo(7)-O(24)	79.0(4)
Mo(4)-O(21)	2.473(10)	O(7)-Mo(7)-O(24)	72.7(4)
Mo(4)-K(2)#1	4.085(4)	O(9)-Mo(7)-O(24)	71.6(3)
Mo(5)-O(13)	1.715(11)	O(16)-Mo(8)-O(6)	105.9(6)
Mo(5)-O(14)	1.750(10)	O(16)-Mo(8)-O(22)	103.6(5)
Mo(5)-O(5)	1.934(9)	O(6)-Mo(8)-O(22)	97.7(5)
Mo(5)-O(7)	1.965(11)	O(16)-Mo(8)-O(11)	102.7(5)
Mo(5)-O(24)	2.110(9)	O(6)-Mo(8)-O(11)	97.7(5)
Mo(5)-O(21)	2.357(11)	O(22)-Mo(8)-O(11)	144.5(4)

Mo(5)-K(1)	4.052(4)	O(16)-Mo(8)-O(25)	92.7(5)
Mo(6)-O(2)	1.711(13)	O(6)-Mo(8)-O(25)	161.4(4)
Mo(6)-O(17)	1.715(11)	O(22)-Mo(8)-O(25)	77.7(4)
Mo(6)-O(8)	1.881(9)	O(11)-Mo(8)-O(25)	77.5(4)
Mo(6)-O(20)	2.018(10)	O(16)-Mo(8)-O(24)	162.4(5)
Mo(6)-O(5)	2.329(10)	O(6)-Mo(8)-O(24)	91.7(4)
Mo(6)-O(21)	2.336(11)	O(22)-Mo(8)-O(24)	73.7(4)
Mo(6)-K(2)#1	4.018(5)	O(11)-Mo(8)-O(24)	74.1(4)
Mo(7)-O(19)	1.703(12)	O(25)-Mo(8)-O(24)	69.8(3)
Mo(7)-O(1)	1.726(12)	O(16)-Mo(8)-K(1)	135.2(4)
Mo(7)-O(11)	1.877(9)	O(6)-Mo(8)-K(1)	29.4(4)
Mo(7)-O(7)	1.992(10)	O(22)-Mo(8)-K(1)	86.8(3)
Mo(7)-O(9)	2.307(10)	O(11)-Mo(8)-K(1)	91.2(3)
Mo(7)-O(24)	2.348(10)	O(25)-Mo(8)-K(1)	132.1(3)
Mo(8)-O(16)	1.690(10)	O(24)-Mo(8)-K(1)	62.4(2)
Mo(8)-O(6)	1.711(12)	O(26)#2-K(1)-O(4)	156.3(4)
Mo(8)-O(22)	1.946(10)	O(26)#2-K(1)-O(6)	97.2(4)
Mo(8)-O(11)	1.950(10)	O(4)-K(1)-O(6)	71.0(3)
Mo(8)-O(25)	2.250(11)	O(26)#2-K(1)-O(13)	135.4(3)
Mo(8)-O(24)	2.496(9)	O(4)-K(1)-O(13)	68.3(3)
Mo(8)-K(1)	4.116(4)	O(6)-K(1)-O(13)	104.9(4)
K(1)-O(26)#2	2.621(12)	O(26)#2-K(1)-O(19)#2	66.7(4)
K(1)-O(4)	2.661(11)	O(4)-K(1)-O(19)#2	114.7(4)
K(1)-O(6)	2.756(12)	O(6)-K(1)-O(19)#2	152.4(4)
K(1)-O(13)	2.762(12)	O(13)-K(1)-O(19)#2	102.1(3)
K(1)-O(19)#2	2.814(12)	O(26)#2-K(1)-O(1)	89.5(3)
K(1)-O(1)	2.870(13)	O(4)-K(1)-O(1)	103.9(4)
K(1)-O(27)	2.993(12)	O(6)-K(1)-O(1)	67.5(3)
K(2)-O(23)	2.642(12)	O(13)-K(1)-O(1)	65.1(3)
K(2)-O(17)	2.673(12)	O(19)#2-K(1)-O(1)	131.1(3)
K(2)-O(10)#3	2.681(11)	O(26)#2-K(1)-O(27)	88.6(3)
K(2)-O(2)#3	2.694(14)	O(4)-K(1)-O(27)	72.0(3)
K(2)-O(12)#3	2.741(12)	O(6)-K(1)-O(27)	92.8(3)
K(2)-O(3)#3	2.788(11)	O(13)-K(1)-O(27)	127.6(3)
K(2)-Mo(3)#3	3.971(4)	O(19)#2-K(1)-O(27)	65.8(3)
K(2)-Mo(6)#3	4.018(5)	O(1)-K(1)-O(27)	159.7(3)
K(2)-Mo(2)#3	4.019(4)	O(26)#2-K(1)-Mo(1)	157.1(3)
K(2)-Mo(4)#3	4.085(4)	O(4)-K(1)-Mo(1)	17.7(3)
O(2)-K(2)#1	2.694(14)	O(6)-K(1)-Mo(1)	60.6(2)
O(3)-K(2)#1	2.788(11)	O(13)-K(1)-Mo(1)	61.7(2)

O(10)-K(2)#1	2.681(11)	O(19)#2-K(1)-Mo(1)	130.9(3)
O(12)-K(2)#1	2.741(12)	O(1)-K(1)-Mo(1)	86.4(2)
O(19)-K(1)#4	2.814(12)	O(27)-K(1)-Mo(1)	87.5(2)
O(26)-K(1)#4	2.621(12)	O(26)#2-K(1)-Mo(5)	143.5(3)
O(27)-C(17)	1.240(19)	O(4)-K(1)-Mo(5)	58.1(3)
O(28)-C(20)	1.24(2)	O(6)-K(1)-Mo(5)	85.6(3)
N(1)-C(1)	1.504(17)	O(13)-K(1)-Mo(5)	19.4(2)
N(1)-C(9)	1.524(18)	O(19)#2-K(1)-Mo(5)	120.9(2)
N(1)-C(5)	1.527(16)	O(1)-K(1)-Mo(5)	57.9(2)
N(1)-C(13)	1.545(15)	O(27)-K(1)-Mo(5)	127.8(2)
N(2)-C(17)	1.291(19)	Mo(1)-K(1)-Mo(5)	46.98(5)
N(2)-C(19)	1.454(18)	O(26)#2-K(1)-Mo(8)	112.1(3)
N(2)-C(18)	1.456(17)	O(4)-K(1)-Mo(8)	61.0(3)
N(3)-C(20)	1.33(2)	O(6)-K(1)-Mo(8)	17.7(3)
N(3)-C(21)	1.42(2)	O(13)-K(1)-Mo(8)	87.3(2)
N(3)-C(22)	1.463(19)	O(19)#2-K(1)-Mo(8)	167.6(3)
N(4)-C(23)	1.47(2)	O(1)-K(1)-Mo(8)	60.26(19)
N(4)-C(24)	1.476(19)	O(27)-K(1)-Mo(8)	102.0(2)
C(1)-C(2)	1.513(19)	Mo(1)-K(1)-Mo(8)	47.10(5)
C(2)-C(3)	1.52(2)	Mo(5)-K(1)-Mo(8)	67.94(7)
C(3)-C(4)	1.533(15)	O(23)-K(2)-O(17)	67.9(4)
C(5)-C(6)	1.525(17)	O(23)-K(2)-O(10)#3	140.8(4)
C(6)-C(7)	1.49(2)	O(17)-K(2)-O(10)#3	106.7(4)
C(7)-C(8)	1.49(2)	O(23)-K(2)-O(2)#3	94.3(4)
C(9)-C(10)	1.51(2)	O(17)-K(2)-O(2)#3	142.8(3)
C(10)-C(11)	1.52(2)	O(10)#3-K(2)-O(2)#3	107.2(4)
C(11)-C(12)	1.48(3)	O(23)-K(2)-O(12)#3	150.8(4)
C(13)-C(14)	1.555(18)	O(17)-K(2)-O(12)#3	110.2(3)
C(14)-C(15)	1.532(17)	O(10)#3-K(2)-O(12)#3	68.3(3)
C(15)-C(16)	1.548(18)	O(2)#3-K(2)-O(12)#3	69.5(4)
		O(23)-K(2)-O(3)#3	86.8(3)
O(4)-Mo(1)-O(23)	104.1(6)	O(17)-K(2)-O(3)#3	135.9(4)
O(4)-Mo(1)-O(22)	101.0(5)	O(10)#3-K(2)-O(3)#3	70.7(3)
O(23)-Mo(1)-O(22)	102.1(5)	O(2)#3-K(2)-O(3)#3	71.0(3)
O(4)-Mo(1)-O(5)	95.5(5)	O(12)#3-K(2)-O(3)#3	109.1(4)
O(23)-Mo(1)-O(5)	100.6(5)	O(23)-K(2)-Mo(3)#3	154.3(3)
O(22)-Mo(1)-O(5)	147.6(5)	O(17)-K(2)-Mo(3)#3	128.9(3)
O(4)-Mo(1)-O(20)	162.1(4)	O(10)#3-K(2)-Mo(3)#3	59.6(3)
O(23)-Mo(1)-O(20)	90.8(5)	O(2)#3-K(2)-Mo(3)#3	60.4(2)
O(22)-Mo(1)-O(20)	85.1(4)	O(12)#3-K(2)-Mo(3)#3	20.1(2)

O(5)-Mo(1)-O(20)	71.7(4)	O(3)#3-K(2)-Mo(3)#3	89.0(3)
O(4)-Mo(1)-O(24)	92.5(5)	O(23)-K(2)-Mo(6)#3	108.9(3)
O(23)-Mo(1)-O(24)	162.5(5)	O(17)-K(2)-Mo(6)#3	159.9(2)
O(22)-Mo(1)-O(24)	79.5(4)	O(10)#3-K(2)-Mo(6)#3	88.3(3)
O(5)-Mo(1)-O(24)	72.0(4)	O(2)#3-K(2)-Mo(6)#3	19.0(2)
O(20)-Mo(1)-O(24)	71.9(3)	O(12)#3-K(2)-Mo(6)#3	62.2(3)
O(4)-Mo(1)-K(1)	28.3(4)	O(3)#3-K(2)-Mo(6)#3	61.4(3)
O(23)-Mo(1)-K(1)	132.3(4)	Mo(3)#3-K(2)-Mo(6)#3	47.89(6)
O(22)-Mo(1)-K(1)	90.2(3)	O(23)-K(2)-Mo(2)#3	144.6(2)
O(5)-Mo(1)-K(1)	91.4(3)	O(17)-K(2)-Mo(2)#3	125.1(3)
O(20)-Mo(1)-K(1)	136.4(2)	O(10)#3-K(2)-Mo(2)#3	18.7(2)
O(24)-Mo(1)-K(1)	64.7(3)	O(2)#3-K(2)-Mo(2)#3	88.6(2)
O(26)-Mo(2)-O(10)	105.9(5)	O(12)#3-K(2)-Mo(2)#3	61.8(2)
O(26)-Mo(2)-O(18)	101.0(5)	O(3)#3-K(2)-Mo(2)#3	60.9(2)
O(10)-Mo(2)-O(18)	101.9(5)	Mo(3)#3-K(2)-Mo(2)#3	47.64(5)
O(26)-Mo(2)-O(9)	100.8(5)	Mo(6)#3-K(2)-Mo(2)#3	69.68(7)
O(10)-Mo(2)-O(9)	96.4(5)	O(23)-K(2)-Mo(4)#3	104.2(3)
O(18)-Mo(2)-O(9)	146.4(5)	O(17)-K(2)-Mo(4)#3	152.2(2)
O(26)-Mo(2)-O(21)	161.2(5)	O(10)#3-K(2)-Mo(4)#3	61.7(2)
O(10)-Mo(2)-O(21)	92.6(4)	O(2)#3-K(2)-Mo(4)#3	61.6(2)
O(18)-Mo(2)-O(21)	78.0(4)	O(12)#3-K(2)-Mo(4)#3	89.6(2)
O(9)-Mo(2)-O(21)	73.2(4)	O(3)#3-K(2)-Mo(4)#3	19.5(3)
O(26)-Mo(2)-O(7)	88.8(5)	Mo(3)#3-K(2)-Mo(4)#3	69.48(7)
O(10)-Mo(2)-O(7)	162.2(4)	Mo(6)#3-K(2)-Mo(4)#3	47.37(5)
O(18)-Mo(2)-O(7)	84.7(4)	Mo(2)#3-K(2)-Mo(4)#3	47.46(5)
O(9)-Mo(2)-O(7)	70.5(4)	Mo(7)-O(1)-K(1)	130.1(5)
O(21)-Mo(2)-O(7)	72.4(4)	Mo(6)-O(2)-K(2)#1	130.2(5)
O(26)-Mo(2)-K(2)#1	135.9(4)	Mo(4)-O(3)-K(2)#1	127.9(6)
O(10)-Mo(2)-K(2)#1	30.1(4)	Mo(1)-O(4)-K(1)	134.0(6)
O(18)-Mo(2)-K(2)#1	90.5(3)	Mo(5)-O(5)-Mo(1)	110.2(5)
O(9)-Mo(2)-K(2)#1	91.4(3)	Mo(5)-O(5)-Mo(6)	110.8(5)
O(21)-Mo(2)-K(2)#1	62.8(3)	Mo(1)-O(5)-Mo(6)	103.7(4)
O(7)-Mo(2)-K(2)#1	135.0(3)	Mo(8)-O(6)-K(1)	132.9(6)
O(12)-Mo(3)-O(25)	105.1(5)	Mo(5)-O(7)-Mo(7)	109.6(5)
O(12)-Mo(3)-O(9)	101.3(5)	Mo(5)-O(7)-Mo(2)	108.6(4)
O(25)-Mo(3)-O(9)	97.6(4)	Mo(7)-O(7)-Mo(2)	104.4(4)
O(12)-Mo(3)-O(20)	101.8(5)	Mo(6)-O(8)-Mo(4)	118.8(6)
O(25)-Mo(3)-O(20)	96.0(5)	Mo(3)-O(9)-Mo(2)	109.3(5)
O(9)-Mo(3)-O(20)	149.0(4)	Mo(3)-O(9)-Mo(7)	110.8(5)
O(12)-Mo(3)-O(21)	98.3(5)	Mo(2)-O(9)-Mo(7)	104.9(4)

O(25)-Mo(3)-O(21)	156.6(5)	Mo(2)-O(10)-K(2)#1	131.2(6)
O(9)-Mo(3)-O(21)	78.1(4)	Mo(7)-O(11)-Mo(8)	117.0(6)
O(20)-Mo(3)-O(21)	78.4(4)	Mo(3)-O(12)-K(2)#1	125.9(5)
O(12)-Mo(3)-O(24)	173.6(4)	Mo(5)-O(13)-K(1)	128.1(5)
O(25)-Mo(3)-O(24)	81.3(4)	Mo(5)-O(14)-Mo(4)	116.8(5)
O(9)-Mo(3)-O(24)	77.9(4)	Mo(6)-O(17)-K(2)	151.8(6)
O(20)-Mo(3)-O(24)	76.9(4)	Mo(2)-O(18)-Mo(4)	117.4(4)
O(21)-Mo(3)-O(24)	75.3(3)	Mo(7)-O(19)-K(1)#4	149.4(6)
O(12)-Mo(3)-K(2)#1	34.0(4)	Mo(3)-O(20)-Mo(6)	109.5(5)
O(25)-Mo(3)-K(2)#1	139.1(4)	Mo(3)-O(20)-Mo(1)	111.0(4)
O(9)-Mo(3)-K(2)#1	94.0(3)	Mo(6)-O(20)-Mo(1)	104.4(4)
O(20)-Mo(3)-K(2)#1	93.7(3)	Mo(3)-O(21)-Mo(2)	92.6(4)
O(21)-Mo(3)-K(2)#1	64.3(3)	Mo(3)-O(21)-Mo(6)	92.3(3)
O(24)-Mo(3)-K(2)#1	139.6(2)	Mo(2)-O(21)-Mo(6)	163.1(5)
O(15)-Mo(4)-O(3)	104.4(6)	Mo(3)-O(21)-Mo(5)	103.6(4)
O(15)-Mo(4)-O(8)	103.9(5)	Mo(2)-O(21)-Mo(5)	97.5(3)
O(3)-Mo(4)-O(8)	98.6(5)	Mo(6)-O(21)-Mo(5)	97.1(4)
O(15)-Mo(4)-O(18)	103.0(5)	Mo(3)-O(21)-Mo(4)	165.2(5)
O(3)-Mo(4)-O(18)	97.3(5)	Mo(2)-O(21)-Mo(4)	86.0(3)
O(8)-Mo(4)-O(18)	144.1(5)	Mo(6)-O(21)-Mo(4)	85.2(4)
O(15)-Mo(4)-O(14)	92.1(5)	Mo(5)-O(21)-Mo(4)	91.2(3)
O(3)-Mo(4)-O(14)	163.5(4)	Mo(1)-O(22)-Mo(8)	117.0(4)
O(8)-Mo(4)-O(14)	78.2(4)	Mo(1)-O(23)-K(2)	146.4(6)
O(18)-Mo(4)-O(14)	77.4(4)	Mo(5)-O(24)-Mo(1)	93.4(4)
O(15)-Mo(4)-O(21)	162.0(5)	Mo(5)-O(24)-Mo(7)	92.9(3)
O(3)-Mo(4)-O(21)	93.6(4)	Mo(1)-O(24)-Mo(7)	163.5(5)
O(8)-Mo(4)-O(21)	73.5(4)	Mo(5)-O(24)-Mo(3)	104.9(4)
O(18)-Mo(4)-O(21)	73.5(4)	Mo(1)-O(24)-Mo(3)	96.9(3)
O(14)-Mo(4)-O(21)	69.9(3)	Mo(7)-O(24)-Mo(3)	96.1(4)
O(15)-Mo(4)-K(2)#1	137.0(4)	Mo(5)-O(24)-Mo(8)	164.5(5)
O(3)-Mo(4)-K(2)#1	32.6(4)	Mo(1)-O(24)-Mo(8)	85.2(3)
O(8)-Mo(4)-K(2)#1	88.0(3)	Mo(7)-O(24)-Mo(8)	84.7(3)
O(18)-Mo(4)-K(2)#1	88.3(3)	Mo(3)-O(24)-Mo(8)	90.5(3)
O(14)-Mo(4)-K(2)#1	130.9(2)	Mo(3)-O(25)-Mo(8)	118.4(5)
O(21)-Mo(4)-K(2)#1	61.0(2)	Mo(2)-O(26)-K(1)#4	155.0(6)
O(13)-Mo(5)-O(14)	104.4(5)	C(17)-O(27)-K(1)	104.1(10)
O(13)-Mo(5)-O(5)	101.7(5)	C(1)-N(1)-C(9)	108.7(11)
O(14)-Mo(5)-O(5)	97.3(4)	C(1)-N(1)-C(5)	109.1(10)
O(13)-Mo(5)-O(7)	100.0(5)	C(9)-N(1)-C(5)	109.8(11)
O(14)-Mo(5)-O(7)	97.2(5)	C(1)-N(1)-C(13)	112.7(10)

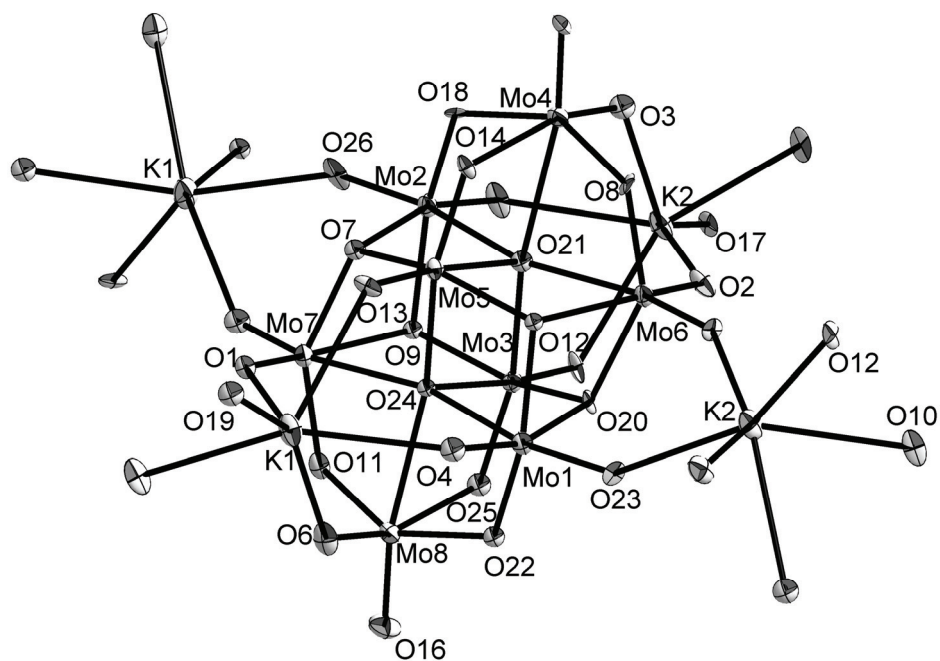
O(5)-Mo(5)-O(7)	149.9(4)	C(9)-N(1)-C(13)	107.1(11)
O(13)-Mo(5)-O(24)	97.4(4)	C(5)-N(1)-C(13)	109.5(9)
O(14)-Mo(5)-O(24)	158.2(5)	C(17)-N(2)-C(19)	123.0(14)
O(5)-Mo(5)-O(24)	78.0(4)	C(17)-N(2)-C(18)	119.6(14)
O(7)-Mo(5)-O(24)	78.8(4)	C(19)-N(2)-C(18)	117.4(14)
O(13)-Mo(5)-O(21)	173.6(4)	C(20)-N(3)-C(21)	122.8(15)
O(14)-Mo(5)-O(21)	82.0(4)	C(20)-N(3)-C(22)	118.9(14)
O(5)-Mo(5)-O(21)	77.8(4)	C(21)-N(3)-C(22)	117.7(15)
O(7)-Mo(5)-O(21)	78.3(4)	C(23)-N(4)-C(24)	113.3(13)
O(24)-Mo(5)-O(21)	76.2(3)	N(1)-C(1)-C(2)	116.1(11)
O(13)-Mo(5)-K(1)	32.4(3)	C(1)-C(2)-C(3)	111.1(12)
O(14)-Mo(5)-K(1)	136.7(3)	C(2)-C(3)-C(4)	113.0(14)
O(5)-Mo(5)-K(1)	91.9(3)	C(6)-C(5)-N(1)	115.1(11)
O(7)-Mo(5)-K(1)	95.3(3)	C(7)-C(6)-C(5)	113.1(13)
O(24)-Mo(5)-K(1)	65.1(3)	C(6)-C(7)-C(8)	112.8(14)
O(21)-Mo(5)-K(1)	141.2(2)	C(10)-C(9)-N(1)	117.8(13)
O(2)-Mo(6)-O(17)	104.6(5)	C(9)-C(10)-C(11)	111.8(14)
O(2)-Mo(6)-O(8)	101.5(5)	C(12)-C(11)-C(10)	110.7(14)
O(17)-Mo(6)-O(8)	102.4(5)	N(1)-C(13)-C(14)	113.7(11)
O(2)-Mo(6)-O(20)	97.2(5)	C(15)-C(14)-C(13)	105.7(11)
O(17)-Mo(6)-O(20)	100.4(5)	C(14)-C(15)-C(16)	113.5(13)
O(8)-Mo(6)-O(20)	145.5(4)	O(27)-C(17)-N(2)	129.0(16)
O(2)-Mo(6)-O(5)	162.3(5)	O(28)-C(20)-N(3)	128.5(15)
O(17)-Mo(6)-O(5)	90.5(4)		

Symmetry transformations used to generate equivalent atoms:

#1 $-x+2, y+1/2, -z+2$ #2 $-x+1, y-1/2, -z+1$ #3 $-x+2, y-1/2, -z+2$

#4 $-x+1, y+1/2, -z+1$

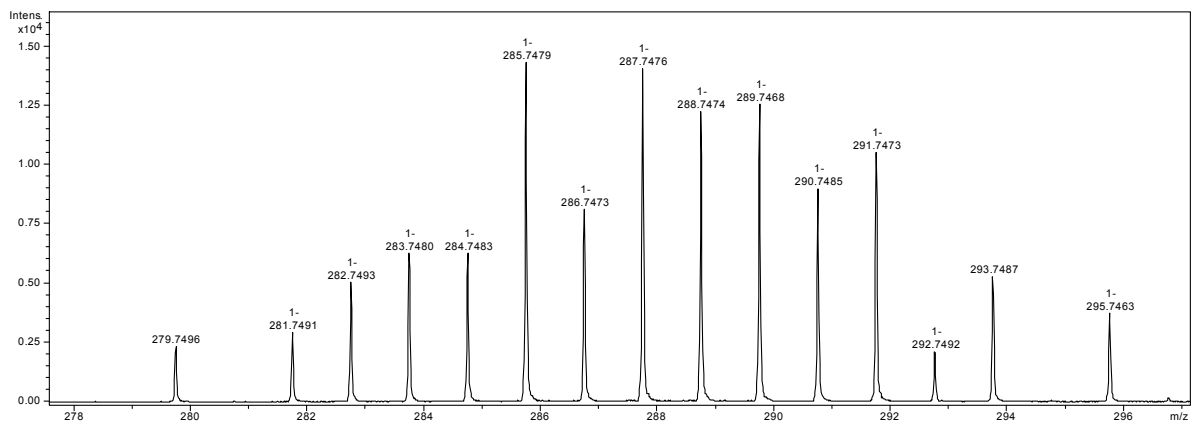
Ortep style representation of $((n\text{-C}_4\text{H}_9)_4\text{N})_n(\text{H}_2\text{NMe}_2)_n[\text{K}_2(\text{DMF})_2\text{Mo}_8\text{O}_{26}]_n \cdot \text{DMF}$ (**24**): thermal ellipsoids at 50% probability, hydrogen atoms and counterions are omitted for clarity.



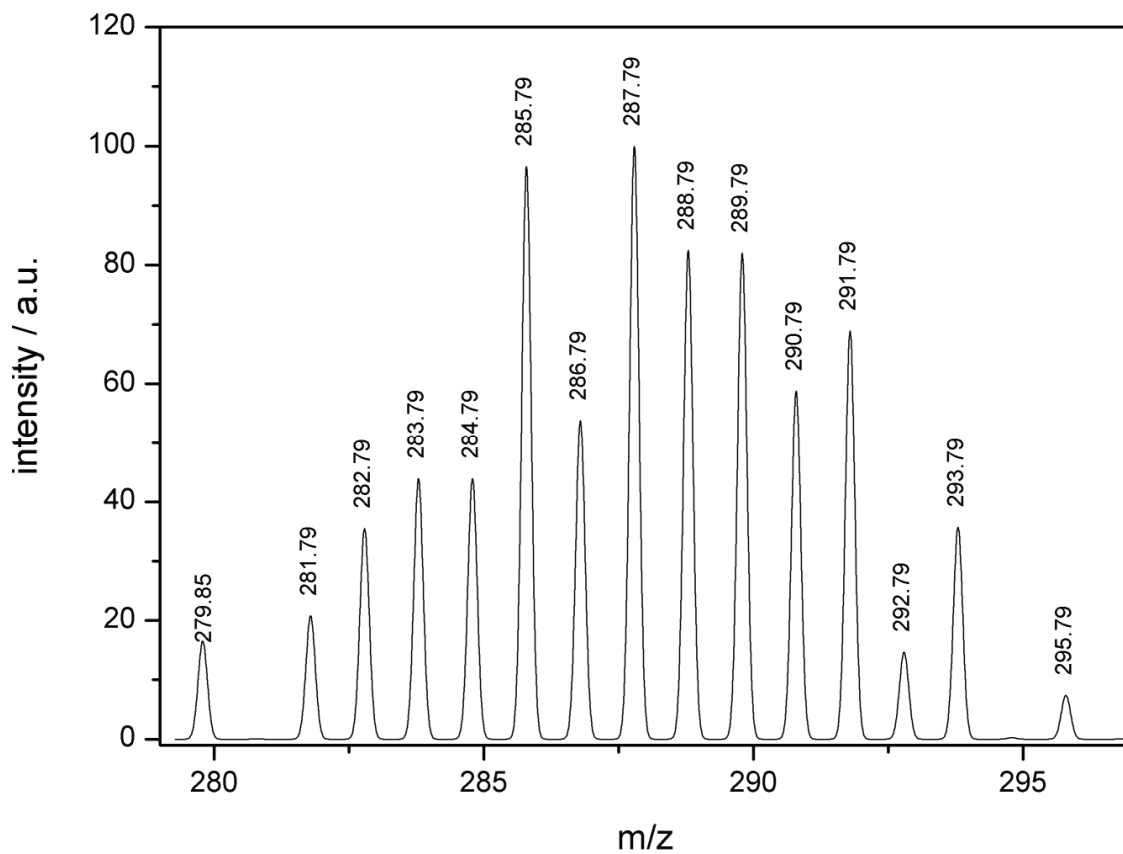
7 SUPPLEMENTARY DATA

7.1 Mass Spectrum for $[\text{Mo}^{\text{VI}}\text{Mo}^{\text{V}}\text{O}_6]^{1-}$

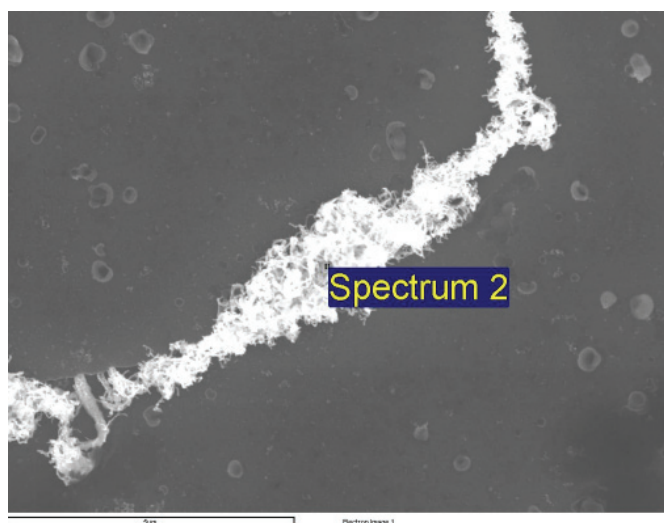
Observed



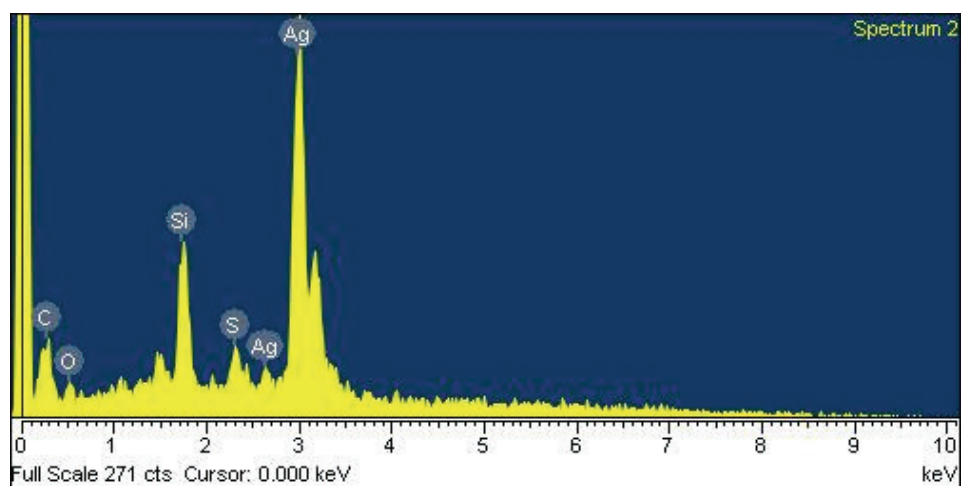
Simulated



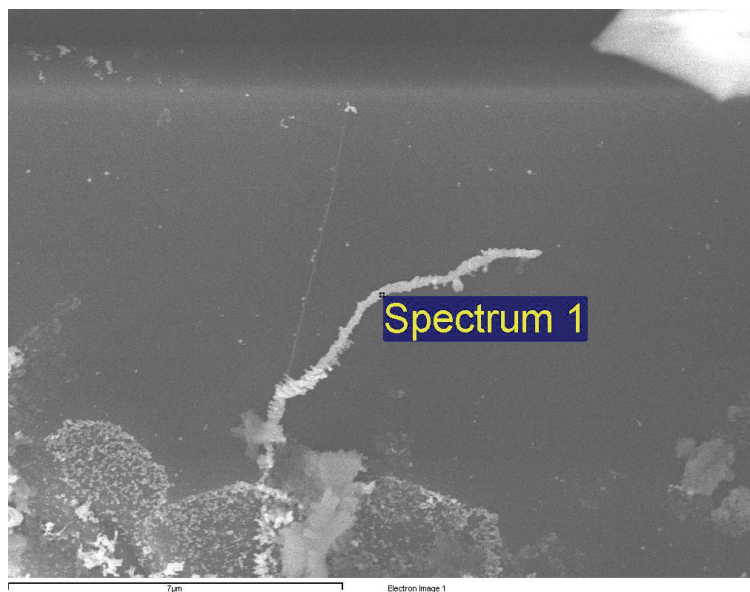
7.2 EDX Data for Wire Material



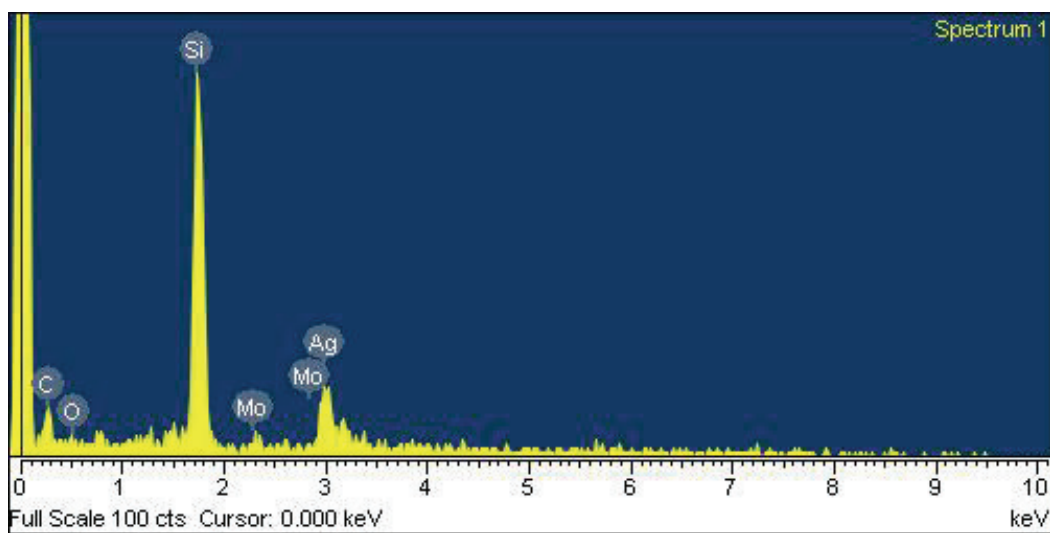
Sample	Ratio Ag	Ratio O
Wires	53	14

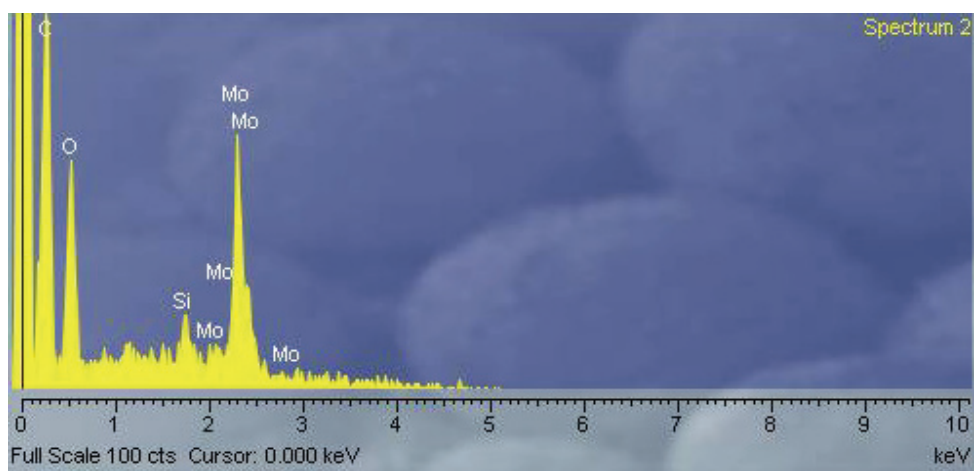
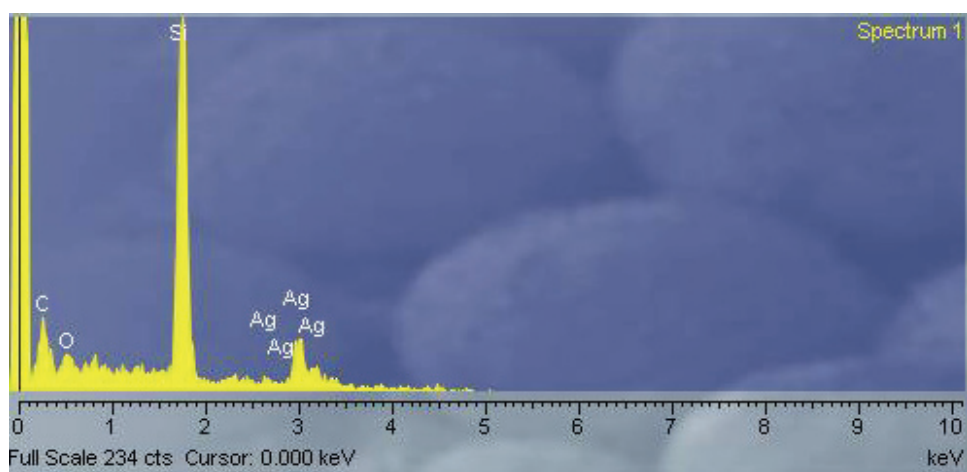
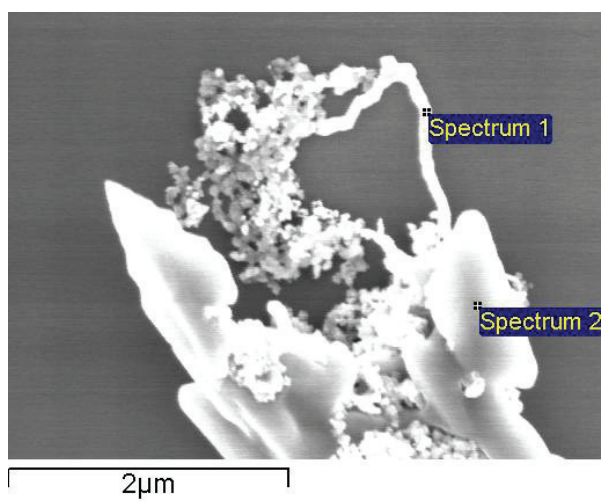


7.3 EDX Data for Wires/Fibres Obtained from Powder Material



Sample	Ratio Ag	Ratio Mo	Ratio O
Wire	10	0	0



7.4 EDX Data for $((n\text{-C}_4\text{H}_9)_4\text{N})_{2n}[\text{Ag}_2(\text{DMSO})_2\text{Mo}_8\text{O}_{26}]_n$ (15)

8 REFERENCES

1. M. T. Pope, A. Müller, *Angew. Chem., Int. Ed.* **1991**, *30*, 34.
2. N. Glezos, P. Argitis, D. Velessiotis, C. D. Diakoumakos, *App. Phys. Lett.* **2003**, *83*, 488.
3. I. M. Mbomekalle, B. Keita, Y. W. Lu, L. Nadjo, R. Contant, N. Belai, M. T. Pope, *Eur. J. Inorg. Chem.* **2004**, 276.
4. D. Gatteschi, L. Pardi, A. L. Barra, A. Müller, J. Doring, *Nature* **1991**, *354*, 463.
5. T. Yamase, *Chem. Rev.* **1998**, *98*, 307.
6. L. Cronin, in *Comprehensive Coordination Chemistry II, Vol. 7*, Elsevier, Amsterdam, **2004**, pp. 1.
7. J. F. Keggin, *Nature* **1933**, *132*, 351.
8. A. Müller, C. Serain, *Acc. Chem. Res.* **2000**, *33*, 2.
9. D. L. Long, L. Cronin, *Chem. Eur. J.* **2006**, *12*, 3699.
10. M. I. Khan, E. Yohannes, R. J. Doedens, *Angew. Chem., Int. Ed.* **1999**, *38*, 1292.
11. A. Müller, S. Roy, *Coord. Chem. Rev.* **2003**, *245*, 153.
12. L. Cronin, P. Kögerler, A. Müller, *J. Solid State Chem.* **2000**, *152*, 57.
13. A. Müller, P. Kögerler, C. Kuhlmann, *Chem. Commun.* **1999**, 1347.
14. A. Müller, E. Krickemeyer, J. Meyer, H. Bögge, F. Peters, W. Plass, E. Diemann, S. Dillinger, F. Nonnenbruch, M. Randerath, C. Menke, *Angew. Chem., Int. Ed.* **1995**, *34*, 2122.
15. G. J. T. Cooper, PhD Thesis, University of Glasgow (Glasgow), **2005**.
16. A. Müller, E. Krickemeyer, H. Bögge, M. Schmidtman, C. Beugholt, P. Kögerler, C. Z. Lu, *Angew. Chem., Int. Ed.* **1998**, *37*, 1220.
17. A. Müller, S. Q. N. Shah, H. Bögge, M. Schmidtman, *Nature* **1999**, *397*, 48.
18. A. Müller, E. Beckmann, H. Bögge, M. Schmidtman, A. Dress, *Angew. Chem., Int. Ed.* **2002**, *41*, 1162.
19. L. Cronin, (Ed.: D. N. G. Meyer, L. Wesemann), Wiley-VCH, Weinheim, **2002**, pp. 113.
20. Q. H. Luo, R. C. Howell, J. Bartis, M. Dankova, W. D. Horrocks, A. L. Rheingold, L. C. Francesconi, *Inorg. Chem.* **2002**, *41*, 6112.
21. K. Wassermann, M. H. Dickman, M. T. Pope, *Angew. Chem., Int. Ed.* **1997**, *36*, 1445.

22. D. L. Long, H. Abbas, P. Kögerler, L. Cronin, *J. Am. Chem. Soc.* **2004**, *126*, 13880.
23. D. L. Long, O. Brucher, C. Streb, L. Cronin, *Dalton Trans.* **2006**, 2852.
24. D. R. Xiao, Y. Xu, Y. Hou, E. B. Wang, S. T. Wang, Y. G. Li, L. Xu, C. W. Hu, *Eur. J. Inorg. Chem.* **2004**, 1385.
25. Y. P. Jeannin, *Chem. Rev.* **1998**, *98*, 51.
26. D. L. Long, D. Orr, G. Seeber, P. Kögerler, L. J. Farrugia, L. Cronin, *J. Cluster Sci.* **2003**, *14*, 313.
27. I. S. Tidmarsh, R. H. Laye, P. R. Brearley, M. Shanmugam, E. C. Sanudo, L. Sorace, A. Caneschi, E. J. L. McInnes, *Chem. Commun.* **2006**, 2560.
28. M. J. Manos, A. L. Tasiopoulos, E. L. Tolis, N. Lalioti, J. D. Woollins, A. M. Z. Slawin, M. P. Sigalas, T. A. Kabanos, *Chem. Eur. J.* **2003**, *9*, 695.
29. L. Chen, F. L. Jiang, Z. Z. Lin, Y. F. Zhou, C. Y. Yue, M. C. Hong, *J. Am. Chem. Soc.* **2005**, *127*, 8588.
30. A. Müller, R. Rohlfing, J. Doring, M. Penk, *Angew. Chem., Int. Ed.* **1991**, *30*, 588.
31. I. V. Kozhevnikov, *Chem. Rev.* **1998**, *98*, 171.
32. M. V. Vasylyev, R. Neumann, *J. Am. Chem. Soc.* **2004**, *126*, 884.
33. C. L. Hill, C. M. Prosser-McCartha, *Coord. Chem. Rev.* **1995**, *143*, 407.
34. J. M. Clemente-Juan, E. Coronado, *Coord. Chem. Rev.* **1999**, *195*, 361.
35. J. M. Clemente-Juan, E. Coronado, J. R. Galan-Mascaros, C. J. Gómez-García, *Inorg. Chem.* **1999**, *38*, 55.
36. M. Clemente-León, E. Coronado, J. R. Galan-Mascaros, C. J. Gómez-García, C. Rovira, V. N. Lauhkin, *Synth. Metals* **1999**, *103*, 2339.
37. J. T. Rhule, C. L. Hill, D. A. Judd, *Chem. Rev.* **1998**, *98*, 327.
38. S. Polarz, B. Smarsly, C. Goltner, M. Antonietti, *Adv. Matr.* **2000**, *12*, 1503.
39. F. Caruso, D. G. Kurth, D. Volkmer, M. J. Koop, A. Muller, *Langmuir* **1998**, *14*, 3462.
40. U. Kortz, C. Holzapfel, M. Reicke, *J. Mol. Struct.* **2003**, *656*, 93.
41. M. Clemente-León, E. Coronado, C. J. Gómez-García, E. Martínez-Ferrero, *J. Cluster Sci.* **2002**, *13*, 381.
42. E. K. Zueva, H. Chermette, S. A. Borshch, *Inorg. Chem.* **2004**, *43*, 2834.
43. J. M. Clemente-Juan, E. Coronado, A. Forment-Aliaga, J. R. Galan-Mascaros, C. Gimenez-Saiz, C. J. Gómez-García, *Inorg. Chem.* **2004**, *43*, 2689.

44. B. Godin, J. Vaissermann, P. Herson, L. Ruhlmann, M. Verdaguer, P. Gouzerh, *Chem. Commun.* **2005**, 5624.
45. M. S. Balula, J. A. Gamelas, H. M. Carapuca, A. M. V. Cavaleiro, W. Schlindwein, *Eur. J. Inorg. Chem.* **2004**, 619.
46. L. H. Bi, U. Kortz, B. Keita, L. Nadjo, *Dalton Trans.* **2004**, 3184.
47. M. D. Ritorto, T. M. Anderson, W. A. Neiwert, C. L. Hill, *Inorg. Chem.* **2004**, *43*, 44.
48. U. Kortz, S. S. Hamzeh, N. A. Nasser, *Chem. Eur. J.* **2003**, *9*, 2945.
49. F. Hussain, B. S. Bassil, L. H. Bi, M. Reicke, U. Kortz, *Angew. Chem., Int. Ed.* **2004**, *43*, 3485.
50. C. N. Kato, A. Shinohara, N. Moriya, K. Nomiya, *Catal. Commun.* **2006**, *7*, 413.
51. A. R. Howells, A. Sankarraj, C. Shannon, *J. Am. Chem. Soc.* **2004**, *126*, 12258.
52. Y. Matsumoto, M. Asami, M. Hashimoto, M. Misono, *J. Mol. Catal. A - Chemical* **1996**, *114*, 161.
53. D. L. Long, P. Kögerler, L. Cronin, *Angew. Chem., Int. Ed.* **2004**, *43*, 1817.
54. D. L. Long, H. Abbas, P. Kögerler, L. Cronin, *Angew. Chem., Int. Ed.* **2005**, *44*, 3415.
55. C. R. Kagan, D. B. Mitzi, C. D. Dimitrakopoulos, *Science* **1999**, *286*, 945.
56. M. Lu, Y. G. Wei, B. B. Xu, C. F. C. Cheung, Z. H. Peng, D. R. Powell, *Angew. Chem., Int. Ed.* **2002**, *41*, 1566.
57. J. B. Strong, G. P. A. Yap, R. Ostrander, L. M. Liable-Sands, A. L. Rheingold, R. Thouvenot, P. Gouzerh, E. A. Maatta, *J. Am. Chem. Soc.* **2000**, *122*, 639.
58. W. Clegg, R. J. Errington, K. A. Fraser, S. A. Holmes, A. Schafer, *J. Chem. Soc., Chem. Commun.* **1995**, 455.
59. J. Kang, B. B. Xu, Z. H. Peng, X. D. Zhu, Y. G. Wei, D. R. Powell, *Angew. Chem., Int. Ed.* **2005**, *44*, 6902.
60. I. Bar-Nahum, K. V. Narasimhulu, L. Weiner, R. Neumann, *Inorg. Chem.* **2005**, *44*, 4900.
61. C. Sanchez, G. J. D. A. Soler-Illia, F. Ribot, T. Lalot, C. R. Mayer, V. Cabuil, *Chem. Matr.* **2001**, *13*, 3061.
62. H. D. Zeng, G. R. Newkome, C. L. Hill, *Angew. Chem., Int. Ed.* **2000**, *39*, 1772.
63. C. R. Mayer, C. Roch-Marchal, H. Lavanant, R. Thouvenot, N. Sellier, J. C. Blais, F. Sécheresse, *Chem. Eur. J.* **2004**, *10*, 5517.

64. B. J. S. Johnson, R. C. Schroden, C. C. Zhu, V. G. Young, A. Stein, *Inorg. Chem.* **2002**, *41*, 2213.
65. B. B. Xu, Z. H. Peng, Y. G. Wei, D. R. Powell, *Chem. Commun.* **2003**, 2562.
66. M. Vasylyev, R. Popovitz-Biro, L. J. W. Shimon, R. Neumann, *J. Mol. Struct.* **2003**, *656*, 27.
67. D. L. Long, P. Kögerler, L. J. Farrugia, L. Cronin, *Angew. Chem., Int. Ed.* **2003**, *42*, 4180.
68. D. L. Long, P. Kögerler, L. J. Farrugia, L. Cronin, *Dalton Trans.* **2005**, 1372.
69. J. M. Knaust, C. Inman, S. W. Keller, *Chem. Commun.* **2004**, 492.
70. C. Inman, J. M. Knaust, S. W. Keller, *Chem. Commun.* **2002**, 156.
71. Y. Ishii, Y. Takenaka, K. Konishi, *Angew. Chem., Int. Ed.* **2004**, *43*, 2702.
72. X. Wang, Y. Guo, Y. Li, E. Wang, C. Hu, N. Hu, *Inorg. Chem.* **2003**, *42*, 4135.
73. P. J. Hagrman, D. Hagrman, J. Zubieta, *Angew. Chem., Int. Ed.* **1999**, *38*, 2639.
74. B. J. S. Johnson, R. C. Schroden, C. C. Zhu, A. Stein, *Inorg. Chem.* **2001**, *40*, 5972.
75. E. Burkholder, J. Zubieta, *Solid State Sciences* **2004**, *6*, 1421.
76. E. Burkholder, J. Zubieta, *Chem. Commun.* **2001**, 2056.
77. L. Lisnard, A. Dolbecq, P. Mialane, J. Marrot, F. Sécheresse, *Inorg. Chim. Acta.* **2004**, *357*, 845.
78. J. P. Wang, J. W. Zhao, J. Y. Niu, *J. Mol. Struct.* **2004**, *697*, 191.
79. C. Qin, X. L. Wang, Y. F. Qi, E. B. Wang, C. W. Hu, L. Xu, *J. Solid State Chem.* **2004**, *177*, 3263.
80. V. Shivaiah, S. Hajeebu, S. K. Das, *Inorg. Chem. Commun.* **2002**, *5*, 996.
81. N. Belai, M. T. Pope, *Chem. Commun.* **2005**, 5760.
82. C. Ritchie, E. Burkholder, P. Kögerler, L. Cronin, *Dalton Trans.* **2006**, 1712.
83. Y. H. Sun, X. B. Cui, G. H. Li, J. Q. Xu, T. G. Wang, W. Xu, L. Y. Pan, Q. X. Yang, *J. Coord. Chem.* **2005**, *58*, 1561.
84. J. Y. Niu, D. J. Guo, J. W. Zhao, J. P. Wang, *New J. Chem.* **2004**, *28*, 980.
85. M. Yuan, Y. G. Li, E. B. Wang, C. G. Tian, L. Wang, C. W. Hu, N. H. Hu, H. Q. Jia, *Inorg. Chem.* **2003**, *42*, 3670.
86. J. P. Wang, J. W. Zhao, X. Y. Duan, J. Y. Niu, *Crystal Growth & Design* **2006**, *6*, 507.
87. V. Shivaiah, M. Nagaraju, S. K. Das, *Inorg. Chem.* **2003**, *42*, 6604.
88. J. J. Lu, Y. Xu, N. K. Goh, L. S. Chia, *Chem. Commun.* **1998**, 2733.

-
89. M. I. Khan, E. Yohannes, R. J. Doedens, *Inorg. Chem.* **2003**, *42*, 3125.
90. L. Lisnard, A. Dolbecq, P. Mialane, J. Marrot, E. Codjovi, F. Sécheresse, *Dalton Trans.* **2005**, 3913.
91. S. T. Zheng, Y. M. Chen, J. Zhang, J. Q. Xu, G. Y. Yang, *Eur. J. Inorg. Chem.* **2006**, 397.
92. H. Y. An, Y. G. Li, D. R. Xiao, E. B. Wang, C. Y. Sun, *Crystal Growth & Design* **2006**, *6*, 1107.
93. C. Lei, J. G. Mao, Y. Q. Sun, J. L. Song, *Inorg. Chem.* **2004**, *43*, 1964.
94. A. Dolbecq, P. Mialane, L. Lisnard, J. Marrot, F. Sécheresse, *Chem. Eur. J.* **2003**, *9*, 2914.
95. H. Jin, C. Qin, Y.G. Li, E. B. Wang, *Inorg. Chem. Commun.* **2006**, *9*, 482.
96. N. G. Armatas, E. Burkholder, J. Zubieta, *J. Solid State Chem.* **2005**, *178*, 2430.
97. H. Y. An, D. R. Xiao, E. B. Wang, C. Y. Sun, L. Xu, *J. Mol. Struct.* **2005**, *743*, 117.
98. M. Ruben, J. Rojo, F. J. Romero-Salguero, L. H. Uppadine, J. M. Lehn, *Angew. Chem., Int. Ed.* **2004**, *43*, 3644.
99. N. Robertson, C. A. McGowan, *Chem. Soc. Rev.* **2003**, *32*, 96.
100. D. Appell, *Nature* **2002**, *419*, 553.
101. D. H. Cobden, *Nature* **2001**, *409*, 32.
102. C. Joachim, J. K. Gimzewski, A. Aviram, *Nature* **2000**, *408*, 541.
103. J. R. Heath, M. A. Ratner, *Physics Today* **2003**, *56*, 43.
104. R. F. Service, *Science* **2002**, *295*, 2398.
105. X. Wang, Y. Li, *Angew. Chem., Int. Ed.* **2002**, *41*, 4790.
106. S. H. Sun, G. W. Meng, M. A. Zhang, Y. F. Hao, X. R. Zhang, L. D. Zhang, *J. Phys. Chem. B* **2003**, *107*, 13029.
107. J. H. Song, Y. Y. Wu, B. Messer, H. Kind, P. D. Yang, *J. Am. Chem. Soc.* **2001**, *123*, 10397.
108. J. D. Holmes, K. P. Johnston, R. C. Doty, B. A. Korgel, *Science* **2000**, *287*, 1471.
109. Y. N. Xia, P. D. Yang, Y. G. Sun, Y. Y. Wu, B. Mayers, B. Gates, Y. D. Yin, F. Kim, Y. Q. Yan, *Adv. Matr.* **2003**, *15*, 353.
110. M. P. Zach, K. H. Ng, R. M. Penner, *Science* **2000**, *290*, 2120.
111. M. J. Edmondson, W. Z. Zhou, S. A. Sieber, I. P. Jones, I. Gameson, P. A. Anderson, P. P. Edwards, *Adv. Matr.* **2001**, *13*, 1608.

112. J. Sloan, D. M. Wright, H. G. Woo, S. Bailey, G. Brown, A. P. E. York, K. S. Coleman, J. L. Hutchison, M. L. H. Green, *Chem. Commun.* **1999**, 699.
113. M. Reches, E. Gazit, *Science* **2003**, *300*, 625.
114. G. A. Ozin, A. C. Arsenault, *Nanochemistry- A Chemical Approach to Nanomaterials*, The Royal Society of Chemistry, Cambridge, **2005**.
115. B. H. Hong, S. C. Bae, C. W. Lee, S. Jeong, K. S. Kim, *Science* **2001**, *294*, 348.
116. Y. G. Sun, B. Mayers, T. Herricks, Y. N. Xia, *Nano Letters* **2003**, *3*, 955.
117. C. Li, X. G. Yang, B. J. Yang, Y. Yan, Y. T. Qian, *Materials Letters* **2005**, *59*, 1409.
118. D. Wang, F. Qian, C. Yang, Z. H. Zhong, C. M. Lieber, *Nano Letters* **2004**, *4*, 871.
119. S. Jin, D. M. Whang, M. C. McAlpine, R. S. Friedman, Y. Wu, C. M. Lieber, *Nano Letters* **2004**, *4*, 915.
120. A. Müller, P. Kögerler, *Coord. Chem. Rev.* **1999**, *182*, 3.
121. D. Hagrman, P. J. Zapf, J. Zubieta, *Chem. Commun.* **1998**, 1283.
122. Y. Q. Guo, X. L. Wang, Y. G. Li, E. B. Wang, L. Xu, C. W. Hu, *J. Coord. Chem.* **2004**, *57*, 445.
123. H. Fang, Y. Wu, J. H. Zhao, J. Zhu, *Nanotechnology* **2006**, *17*, 3768.
124. S. Q. Liu, T. Kuroda-Sowa, H. Konaka, Y. Suenaga, M. Maekawa, T. Mizutani, G. L. Ning, M. Munakata, *Inorg. Chem.* **2005**, *44*, 1031.
125. V. J. Catalano, H. M. Kar, J. Garnas, *Angew. Chem., Int. Ed.* **1999**, *38*, 1979.
126. A. L. Pickering, PhD Thesis, University of Glasgow (Glasgow), **2004**.
127. B. M. Gatehouse, P. Leverett, *J. Chem. Soc., Dalton Trans.* **1976**, 1316.
128. S. M. Chen, C. Z. Lu, Y. Q. Yu, Q. Z. Zhang, X. He, *Inorg. Chem. Commun.* **2004**, *7*, 1041.
129. L. Xu, M. Lu, B. B. Xu, Y. G. Wei, Z. H. Peng, D. R. Powell, *Angew. Chem., Int. Ed.* **2002**, *41*, 4129.
130. V. W. Day, M. F. Fredrich, W. G. Klemperer, W. Shum, *J. Am. Chem. Soc.* **1977**, *99*, 6146.
131. E. C. Alyea, D. Craig, I. Dance, K. Fisher, G. Willett, M. Scudder, *Crystengcomm* **2005**, *7*, 491.
132. W. J. Wang, L. Xu, Y. G. Wei, F. Y. Li, G. G. Gao, E. B. Wang, *J. Solid State Chem.* **2005**, *178*, 608.

133. H. Y. An, Y. G. Li, E. B. Wang, D. R. Xiao, C. Y. Sun, L. Xu, *Inorg. Chem.* **2005**, *44*, 6062.
134. R. Villanneau, A. Proust, F. Robert, P. Gouzerh, *Chem. Commun.* **1998**, 1491.
135. G. Y. Luan, Y. G. Li, S. T. Wang, E. B. Wang, Z. B. Han, C. W. Hu, N. H. Hu, H. Q. Jia, *Dalton Trans.* **2003**, 233.
136. K. Singh, J. R. Long, P. Stavropoulos, *J. Am. Chem. Soc.* **1997**, *119*, 2942.
137. H. Abbas, A. L. Pickering, D. L. Long, P. Kögerler, L. Cronin, *Chem. Eur. J.* **2005**, *11*, 1071.
138. U. Lee, H.-C. Joo, M.-A. Chob, *Acta Cryst. E* **2002**, *58*, 599.
139. Q. Wang, X. Xu, X. Wang, *Acta Cryst. C* **1993**, *C49*, 464.
140. Z. G. Han, Y. L. Zhao, J. Peng, H. Y. Ma, Q. Liu, E. B. Wang, N. H. Hu, H. Q. Jia, *Eur. J. Inorg. Chem.* **2005**, 264.
141. Z. Y. Shi, X. J. Gu, J. Peng, Z. F. Xin, *Eur. J. Inorg. Chem.* **2005**, 3811.
142. J. T. Rhule, W. A. Neiwert, K. I. Hardcastle, B. T. Do, C. L. Hill, *J. Am. Chem. Soc.* **2001**, *123*, 12101.
143. J. X. Chen, T. Y. Lan, Y. B. Huang, C. X. Wei, Z. S. Li, Z. C. Zhang, *J. Solid State Chem.* **2006**, *179*, 1904.
144. A. Michailovski, F. Krumeich, G. R. Patzke, *Chem. Matr.* **2004**, *16*, 1433.
145. Z. H. Kang, E. Wang, M. Jiang, S. Y. Lian, *Nanotechnology* **2004**, *15*, 55.
146. Z. H. Kang, E. B. Wang, M. Jiang, S. Y. Lian, Y. G. Li, C. W. Hu, *Eur. J. Inorg. Chem.* **2003**, 370.
147. R. Y. Wang, D. Z. Jia, L. Zhang, L. Liu, Z. P. Guo, B. Q. Li, J. X. Wang, *Advanced Functional Materials* **2006**, *16*, 687.
148. B. Liu, H. C. Zeng, *J. Am. Chem. Soc.* **2004**, *126*, 8124.
149. X. Bao, M. Muhler, B. Pettinger, R. Schlogl, G. Ertl, *Catalysis Letters* **1993**, *22*, 215.
150. G. J. Millar, J. B. Metson, G. A. Bowmaker, R. P. Cooney, *J. Chem. Soc., Chem. Commun.* **1994**, 1717.
151. L. Kvitek, R. Prucek, A. Panacek, R. Novotny, J. Hrbac, R. Zboril, *J. Matr. Chem.* **2005**, *15*, 1099.
152. C. Korzeniewski, C. L. Childers, *J. Phys. Chem. B* **1998**, *102*, 489.
153. R. Kong, Q. Yang, K. Tang, *Chem. Lett.* **2006**, *35*, 402.
154. M. W. Barsoum, L. Farber, *Science* **1999**, *284*, 937.

-
155. L. M. Worboys, P. P. Edwards, P. A. Anderson, *Chem. Commun.* **2002**, 2894.
 156. L. Sun, F. Banhart, A. V. Krashennnikov, J. A. Rodriguez-Manzo, M. Terrones, P. M. Ajayan, *Science* **2006**, *312*, 1199.
 157. H. Chun, D. N. Dybtsev, H. Kim, K. Kim, *Chem. Eur. J.* **2005**, *11*, 3521.
 158. D. N. Dybtsev, H. Chun, K. Kim, *Angew. Chem., Int. Ed.* **2004**, *43*, 5033.
 159. M. Filowitz, R. K. C. Ho, W. G. Klemperer, W. Shum, *Inorg. Chem.* **1979**, *18*, 93.
 160. G. M. Sheldrick, *Acta Cryst. A* **1997**, *A46*, 467.
 161. A. Altomare, G. Cascarano, C. Giacovazzo, A. Guagliardi, *J. Appl. Cryst.* **1993**, *26*, 343.
 162. L. J. Farrugia, *J. Appl. Cryst.* **1999**, *32*, 837.